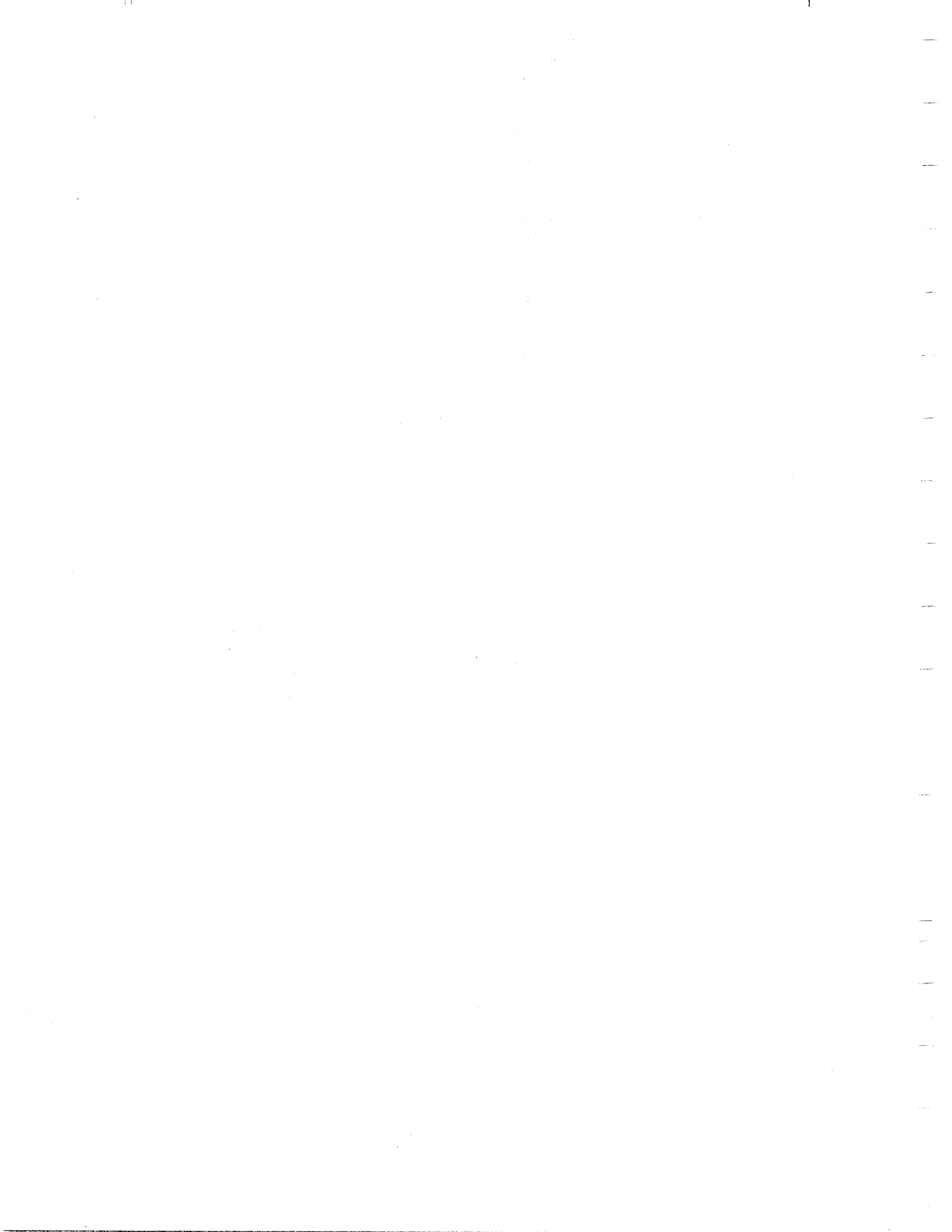


Plasma Fusion Center  
Massachusetts Institute of Technology  
167 Albany Street  
Cambridge, MA 02139

MHD Magnet Technology  
Development Program Summary  
September 1982

Prepared for  
U.S. Department of Energy  
Office of Fossil Energy  
MHD Division

Published  
November 1983



### Foreword

This report is issued by the MHD Magnet Group of the Plasma Fusion Center (PFC), Massachusetts Institute of Technology (MIT). Up to the time of its transfer to PFC in May 1982, the MHD Magnet Group was part of the Francis Bitter National Magnet Laboratory (FBNML), MIT.

The work reported herein has been carried out by the Francis Bitter National Magnet Laboratory, the Plasma Fusion Center and selected subcontractors in performance of Task 3 of Department of Energy (DOE) Contract EX-76-A-01-2295.

The following staff members of the MHD Magnet Group have contributed to this program:

B.M. Bailey	P.G. Marston
H.D. Becker	A.G. Montgomery
E.S. Bobrov	D.B. Montgomery
J. Davin	H. Nomura
A.M. Dawson	M. Olmstead
N. Diatchenko	R.D. Pillsbury, Jr.
E.A. Erez	A.D. Rabasco
E. Etienne	S.R. Shanfield
R.B. Frankel	R.H. Shaw
A.M. Hatch	M. Sinclair
M.O. Hoenig	D.J. Sliski
Y. Iwasa	J.M. Tarrh
R.S. Kensley	R.J. Thome
W.G. Langton	J.B. Thompson
M.J. Leupold	J.E.C. Williams
J.F. Maguire	M.N. Wilson



## Table of Contents

		<u>Page</u>
	ABSTRACT	1
1.0	INTRODUCTION	1
2.0	GENERAL STRATEGY AND APPROACH	2
3.0	OVERALL RESULTS AND RECOMMENDATIONS	7
3.1	Results	7
3.2	Recommendations	9
4.0	SUMMARY OF WORK ACCOMPLISHED	9
4.1	Analysis, Research And Development	12
4.1.1	Compilation and Analysis of Data Base from Previous Superconducting Magnet Experience	12
4.1.2	Construction and Operation of In-House Test Facility at FBNML	12
4.1.3	Upgrading of Analytical Tools	14
4.1.4	Stability Testing and Analysis of Pool-Cooled Conductor	17
4.1.5	Development of High Current Conductor, Pool-Cooled	17
4.1.5.1	Design Studies by Conductor Manufacturers	17
4.1.5.2	Manufacturing and Cost Investigation of Separated Substrate Conductors	19
4.1.5.3	Development of High Current Cable-Type Conductor, Pool-Cooled	27
4.1.6	Development of Internally-Cooled Cable Superconductor	28
4.1.7	Analysis and Development of Superstructure	41
4.1.8	Substructure and Winding Development	42
4.1.8.1	GE Substructure and Winding Studies	42
4.1.8.2	MCA Substructure and Winding Studies	44
4.1.8.3	GD Substructure and Winding Studies	52
4.1.9	Study of Impact of High Current Operation	66
4.1.10	Stability Analysis of High Current Conductors	66
4.1.10.1	Conductor Analysis for Large Scale Superconducting MHD Magnets (MEA)	71
4.1.10.2	Stability Analysis and Evaluation of Composite Conductors for MHD Magnets (Hilal)	71
4.1.11	Testing of Materials for Main Structure	77
4.1.12	Testing of Materials for Substructure	85
4.1.12.1	Choice of Material	85
4.1.12.2	Compressive Testing of G-10 Specimens	87
4.1.12.3	Tensile Testing of G-10 Specimens	87
4.1.12.4	Interlaminar Shear Testing	87
4.1.12.5	Structural Tooth Testing	87



	<u>Page</u>	
4.3.2	Stanford Test Facility Superconducting Magnet, SSM	299
4.3.2.1	Summary	299
4.3.2.2	Description	311
4.3.3	U-25 Superconducting MHD Magnet, U.S. SCMS	319
4.3.3.1	Summary	319
4.3.3.2	Description	325
4.3.4	Coal-Fired Flow Facility Superconducting Magnet, CFFF/SM	333
4.3.4.1	Summary	333
4.3.4.2	Description	333
4.3.5	The CDIF Conventional Water-Cooled Magnet, CDIF/CM	342
4.3.5.1	Summary	342
4.3.5.2	Description	342
4.3.5.3	Comparative Evaluation, CDIF/CM and AVCO/CM	350
4.3.6	The AVCO Mk VI-II Conventional Water-Cooled Magnet, AVCO/CM	350
4.3.6.1	Summary	350
4.3.6.2	Description	350
5.0	REFERENCES	357
6.0	SUPPLEMENTARY BIBLIOGRAPHY	364
	Appendices:	
A	Lists of Major Subcontractors and Bidders	A-1
B	Data Tables, Large Magnet Systems from Other Programs	B-1
C	Method of Calculating Magnet Size Index, $VB^2$	C-1
D	FBNML Specification No. A4442 Rev D, Interim Criteria for Personnel and Equipment Exposure to Magnetic Fields	D-1

## List of Figures

<u>Fig. No.</u>	<u>Title</u>	<u>Page</u>
2A	MHD Magnet Program Approach	4
2B	MHD Magnet Program Overall Strategy	5
2C	Proposed Approach to Design Freeze of Commercial-Scale MHD Magnet	6
4.1.2A	Layout of MHD Magnet Component Test Facility at MIT	13
4.1.2B	Cutaway View of Component Test Facility 6 T Racetrack Magnet (TFM) and Dewar at MIT	16
4.1.5A	Typical Integrated-Substrate Conductor - Aluminum-Stabilized NbTi, Soldered Cable	20
4.1.5B	Typical Integrated-Substrate Conductor - Aluminum-Stabilized NbTi, Wrapped Substrate (Soldered)	21
4.1.5C	Typical Integrated-Substrate Conductor - Copper-Stabilized NbTi, Wrapped Substrate	22
4.1.5D	Typical Separated-Substrate Conductor - Copper-Stabilized NbTi, Grooved Copper Substrate (Multiple Channels)	23
4.1.5E	Typical Separated-Substrate Conductor - Copper-Stabilized NbTi, Grooved Copper Substrate, Multiple Cables, Single Channel, Soldered	24
4.1.5F	Typical Separated-Substrate Conductor - Copper-Stabilized NbTi, Grooved Copper Substrate, Single Cable, Soldered	25
4.1.5G	Cable-Type NbTi Copper Composite Conductor Proposed for CSM Commercial-Scale Magnet	29
4.1.6A	Cross Section of Internally-Cooled Superconductor of Type Developed by CERN	30
4.1.6B	Cross Section of Internally-Cooled Superconductor of Type Developed by MIT	31
4.1.6C	Diagram of Test Apparatus for Simulated Internally-Cooled Cable Conductor	32
4.1.6D	Plots of Experimental and Computer-Predicted Results in Internally-Cooled Superconductor Investigation	34
4.1.6E	Photograph of Apparatus for Testing Small Coils of ICCS	35
4.1.6F	Plot of Recovery Current at 8 T as a Function of Flow Rate for a Given Pulse Energy Input	36
4.1.6G	Photograph of One Meter-Scale ICCS Test Coil Mounted in Test Support Frame	37
4.1.6H	Plot of Critical Pulse Energy vs. Flow for Small Nb <sub>3</sub> Sn ICCS Test Coil	38
4.1.6J	Photograph of Cross Section of 2 × 2 cm 486 Strand Nb <sub>3</sub> Sn ICCS	39
4.1.6K	Sketch of ICCS "Football" Coil	40
4.1.8A	Baseline Concept for Substructure and Winding Development, Circular Saddle MHD Magnet	43
4.1.8.2A	MCA Flat-Sided Shell Substructure and Winding Concept. Subassembly of Seven Shells Forming Saddle Magnet Half	45
4.1.8.2B	Single Half-Shell with Typical Slots for Conductor	46
4.1.8.2C	MCA Force Containment Structure Concept Consisting of Frames and Tie Plates for Support of Windings and Shells	47
4.1.8.2D	MCA Flat Plate Racetrack and Rectangular Saddle Concept, Coil Locations	48
4.1.8.2E	Exploded View of MCA Conductor and Support Channel (Substructure)	49
4.1.8.2F	Midplane Section of MCA Racetrack and Saddle Concept Showing Superstructure	50
4.1.8.2G	MCA Separated-Substrate 50 kA Single Insert Conductor Design	51
4.1.8.2H	MCA Integral-Substrate 50 kA Solder Filled "Bicable" Conductor Design	53
4.1.8.2J	MCA Integral-Substrate 50 kA Solder Filled "Tricable" Conductor Design	54
4.1.8.2K	MCA Proposed Winding Model Magnet Design	55



<u>Fig. No.</u>	<u>Title</u>	<u>Page</u>
4.1.8.3A	Sketch Showing Machining of Mated Pair of Substructure Shell Sections	56
4.1.8.3B	Typical Mechanical Joint for Joining Conical Support Shell Sections	57
4.1.8.3C	Sketch of Fixture for Subshell Assembly, Winding and Final Assembly with Superstructure	59
4.1.8.3D	Flat Pattern Layout of Typical Combined Tension and Support Plate, Rectangular Saddle Concept	60
4.1.8.3E	Assembly of Wound Support Plate Around Core Tube, Rectangular Saddle Concept	61
4.1.8.3F	CASK Magnet Design Concept	62
4.1.8.3G	Stack of Separated-Substrate Conductors Installed in CASK Substructure	63
4.1.8.3H	GD Winding Model Magnet Design	64
4.1.8.3J	Conductor Substrate Design for GD Magnet	65
4.1.9A	Curves of Estimated Component Costs and Total Cost vs. Magnet Current for Nested Shell Concept with Semifluted Conductor and $0.6 \text{ W/cm}^2$ Heat Flux	70
4.1.10.1A	Schematic Diagram of a 50 kA Conductor Considered in Stability Analysis	73
4.1.10.1B	Typical Plot of Limiting Currents for a Large Built-Up Copper Plus NbTi Conductor Cooled by Liquid Helium (The anticipated operating point is indicated by the circled dot)	74
4.1.10.2A	Conductor Model Used to Determine Recovery Length. Composite Conductor with Delaminated Length, $l$	75
4.1.10.2B	Curves Showing Allowable Dimensionless Delaminated Length, $x_m/T_b$ , for $A_2/A_0 = 0.1$ ( $\delta^2 = \text{heat removed/heat generated}$ )	76
4.1.10.2C	Curve of MPZ Energy ( $\Delta E$ ) vs. Fraction of Composite in Contact ( $f$ ) for Composite Conductor with Thermal Contact Resistance $\beta = 0.5$	84
4.1.12A	Stack of Model Subplates for Compression Testing at Room Temperature and 77 K	86
4.1.12B	Polar Diagram of Edgewise Compressive Strength of G-10 as a Function of Fiber Direction	88
4.1.12C	Curves of Effect of Specimen Size on Compressive Strength of G-10 at RT and 77 K	89
4.1.12D	Plot of Tensile and Compressive Strength of the Same Sheet of G-10 at RT and 77 K	90
4.1.12E	Polar Diagram of the Interlaminar Shear Strength of G-10 Specimens as a Function of Fiber Orientation	91
4.1.12F	Diagram of Structural Test Fixture for G-10 Tooth Push-Off Test	92
4.1.12G	Sketch of Structural Tooth Specimen, $W = 1.27 \text{ cm}$	95
4.1.12H	Polar Diagram of Breaking Force in Tooth Test	96
4.1.12J	Plot of Variation of Breaking Force with Changes of Groove Radius in Tooth Test	97
4.1.17A	Diagram Showing Interim Limits for Personnel Exposure to the Fringe Magnetic Field of the 6 T Magnet in the ETF 200 MWe Power Plant Conceptual Design	105
4.1.18A	Block Diagram Flow Sheet for Typical MHD Magnet Cryogenic System	106
4.1.19A	Simplified Schematic Diagram of MHD Magnet Power Supply System (a) Charging and Maintaining Magnet Current, $i_m$ (b) Discharge Through Dump Resistor	111
4.1.20A	Diagrams of Cross Sections of Magnet Warm Bores with Various Channel/Bore Configurations	115
4.1.20B	Sketch Showing Fixed Magnet and Roll-Aside Diffuser to Facilitate Channel Changeout	117
4.1.20C	Sketch Showing Magnet on Turntable to Facilitate Channel Changeout	118
4.1.20D	Sketch Showing Roll-Aside Magnet to Facilitate Channel Changeout	119

<u>Fig. No.</u>	<u>Title</u>	<u>Page</u>
4.1.20E	Sketch Showing Roll-Apart Magnet to Facilitate Channel Changeout	120
4.1.20F	Sketch Showing Dolly Used for Insertion and Removal of Channel from Magnet	121
4.1.22A	Curve of Estimated MHD Magnet System Cost vs Size Index ( $VB^2$ )	124
4.1.22B	Curve of Estimated Magnet System Cost vs MHD Power Output	125
4.1.22C	Bar Chart Showing Relationship of Magnet System Cost Elements ("First Unit" Baseload Magnet)	126
4.1.22D	Bar Chart Showing Comparative Costs of MHD Magnet Components (Fabricated)	127
4.2.2A	Axial Field Profile for MCA 6 T Baseload Magnet Reference Design	137
4.2.2B	Diagram of MCA Baseload Magnet Winding Configuration	138
4.2.2C	Typical Winding Cross Section Showing Conductor and Internal Winding Structural Details for the MCA Baseload Magnet	139
4.2.2D	Cross Section Diagrams of Conductor for MCA Baseload MHD Magnet	140
4.2.2E	MCA Baseload Magnet Assembly Drawing, Inlet End and Partial Section Views	141
4.2.2F	MCA Baseload Magnet Assembly Drawing, Section at Midplane and Top View	142
4.2.2G	Block Diagram of MCA Baseload Magnet Accessory Subsystems	145
4.2.3A	Curve of On-Axis Magnetic Field vs Distance Along Axis for AVCO Baseload Magnet Design BL6-P1 (Circular Saddle)	150
4.2.3B	Diagram of Winding Configuration, AVCO Baseload Magnet Design BL6-P1 (Circular Saddle). One half of Winding is Shown	151
4.2.3C	Detail of Winding (Module Cross Section) AVCO Baseload Circular Saddle Magnet Design BL6-P1	152
4.2.3D	Cross Section of Rectangular Cable Type Conductor for AVCO Baseload Circular Saddle Magnet Design BL6-P1	153
4.2.3E	Assembly Layout (Cutaway) AVCO 6 T Baseload Circular Saddle MHD Magnet Design BL6-P1	154
4.2.3F	Block Diagram, Electrical System AVCO 6 T Baseload Circular Saddle Magnet Design BL6-P1	159
4.2.4A	Curve of On-Axis Magnetic Field vs Distance Along Axis for AVCO Baseload Magnet Design BL6-P2 (Rectangular Saddle)	164
4.2.4B	Diagram of Winding Configuration, AVCO Baseload Magnet Design BL6-P2 (Rectangular Saddle). One Quadrant Only is Shown	165
4.2.4C	Detail of Winding (Module Cross Section) AVCO Baseload Rectangular Saddle Magnet Design BL6-P1	166
4.2.4D	Assembly Layout (Cutaway) AVCO 6 T Baseload Rectangular Saddle MHD Magnet, Design BL6-P2	167
4.2.5A	Cutaway View of CASK 6 T Baseload MHD Magnet Conceptual Design	173
4.2.5B	Principal Dimensions of CASK Baseload MHD Magnet	174
4.2.5C	Curve of On-Axis Magnetic Field vs Distance Along Axis for CASK Baseload MHD Magnet Design	175

<u>Fig. No.</u>	<u>Title</u>	<u>Page</u>
4.2.5D	Cross Section of 50 kA Conductor for CASK Baseload MHD Magnet	176
4.2.5E	Layout, Conductor Corner Piece, CASK Baseload MHD Magnet	177
4.2.5F	Conductor/Electrical Insulation Arrangement, CASK Baseload MHD Magnet	179
4.2.5G	Diagram of Winding Configuration, CASK Baseload MHD Magnet	180
4.2.5H	Sketch Showing Midplane Cross Section of Winding of CASK Magnet	181
4.2.5J	Cutaway View of Winding/Substructure Assembly Showing End Block and Shell-to-Shell Shear Plate, CASK Baseload MHD Magnet	182
4.2.5K	Sketch, Crescent Girder Superstructure, CASK Baseload MHD Magnet	183
4.2.5L	Portion of Manufacturing Flow Chart, CASK Baseload MHD Magnet	184
4.2.5M	Sketch of Assembly Fixture, CASK Baseload MHD Magnet	189
4.2.5N	Exploded View of Winding, Substructure and Superstructure, CASK Baseload MHD Magnet	190
4.2.5P	Estimated Schedule, Design and Construction of CASK Magnet	191
4.2.6A	Elevation View of Magnet Assembly, CSM Design	196
4.2.6B	Plan View of Magnet Assembly, CSM Design	197
4.2.6C	Inlet and Exit Views of Magnet Assembly, CSM Design	198
4.2.6D	Elevation and End View of Vacuum Vessel, CSM Design	199
4.2.6E	Curve of On-Axis Field vs Distance Along Axis for CSM Design	200
4.2.6F	Diagram Showing Conductor Configuration for SM Design (Grade A)	201
4.2.6G	Sketch Showing Cable Conductor Turns Individually Supported in Insulating Substructure, CSM	202
4.2.6H	Diagram Showing Overall Winding Configuration, One Half CSM Design	203
4.2.6J	Layout Showing Cross Section of Coil Bundle of One Winding Half, CSM Design	204
4.2.6K	Layout Drawing of Coil Container Weldment, CSM	205
4.2.6L	Layout Drawing Showing Alternative Main Structural Support System, CSM Design	207
4.2.7A	Cutaway View of Advanced Design Commercial Size MHD Magnet, ICCS/SM	213
4.2.7B	Elevation View of Advanced Design Magnet Assembly, ICCS/SM	214
4.2.7C	Plan View of Advanced Design Magnet Assembly, ICCS/SM	215
4.2.7D	Inlet and Outlet Views of Advanced Design Magnet, ICCS/SM	216
4.2.7E	Curve of On-Axis Field vs Distance Along Axis for Advanced Design Magnet, ICCS/SM	217
4.2.7F	Conductor-Insulation Arrangement in Winding, ICCS/SM	218
4.2.9A	Curve of On-Axis Field vs Distance Along Axis for MCA ETF Magnet Design	226
4.2.9B	Diagram Showing Magnet Winding Configuration, MCA ETF Magnet Design	227
4.2.9C	Elevation View, MCA ETF Magnet Assembly	228
4.2.9D	Outlet End View, MCA ETF Magnet Assembly	229
4.2.9E	Power Supply and Discharge Subsystem, MCA ETF Magnet	230
4.2.10A	Curve of On-Axis Field vs Distance Along Axis for AVCO ETF Magnet, ETF6-P1	236
4.2.10B	Diagram Showing Coil Configuration, AVCO ETF Magnet, ETF6-P1 (circular saddle) and ETF6-P2 (rectangular saddle)	237
4.2.10C	Typical Winding Cross Section (One Quadrant) AVCO ETF Magnet, ETF6-P1	238
4.2.10D	Elevation and End View of Magnet Assembly, AVCO ETF Magnet, ETF6-P1	239
4.2.10E	Diagram, Electrical System, AVCO ETF Magnet, ETF6-P1	243

<u>Fig. No.</u>	<u>Title</u>	<u>Page</u>
4.2.11A	Curve of On-Axis Field vs Distance Along Axis for AVCO ETF Magnet Assembly, ETF6-2	248
4.2.11B	Cutaway View of AVCO ETF Magnet Assembly, ETF6-2	249
4.2.12A	Curve of On-Axis Field vs Distance Along Axis for AVCO ETF Alternative Design Magnet	255
4.2.12B	Sketch Showing Winding Configuration in End Turn Region, AVCO ETF Alternative Design Magnet	256
4.2.12C	Sketch of Typical Winding Cross Section Showing Modular Construction, AVCO ETF Alternative Design Magnet	257
4.2.12D	Plan View of Magnet Assembly, AVCO ETF Alternative Design Magnet	258
4.2.12E	Cross Section View of Magnet Assembly, AVCO ETF Alternative Design Magnet	259
4.2.13A	Curve of On-Axis Field vs Distance Along Axis for MIT ETF 6 T Magnet (Principal Design)	268
4.2.13B	Curve of On-Axis Field vs Distance Along Axis for MIT ETF 4 T Magnet (Alternative Design)	269
4.2.13C	Diagram Showing Cable Conductor Cross Section for MIT ETF 6 T Magnet (Principal Design)	270
4.2.13D	Diagram Showing Winding Configuration, MIT ETF 6 T Magnet (Principal Design)	271
4.2.13E	Sketch Showing Typical Winding Cross Section for MIT ETF 6 T Magnet (Principal Design)	272
4.2.13F	Outline Drawing of MIT ETF 6 T Magnet (Principal Design)	273
4.2.13G	Elevation View, Magnet Assembly, MIT ETF 6 T Magnet (Principal Design)	274
4.2.13H	Plan View, Magnet Assembly, MIT ETF 6 T Magnet (Principal Design)	275
4.2.13J	End View, Magnet Assembly, MIT ETF 6 T Magnet (Principal Design)	276
4.2.13K	Outline Drawing of MIT ETF 4 T Magnet (Alternative Design)	277
4.2.13L	Plan and Elevation Views of Magnet System Including Accessories, MIT ETF 6 T Magnet (Principal Design)	278
4.2.13M	Diagram of Helium (Cryogenic) System, MIT ETF 6 T Magnet	279
4.2.13N	Diagram of Nitrogen (Cryogenic) System, MIT ETF 6 T Magnet	280
4.2.13P	Diagram of Electrical System, MIT ETF 6 T Magnet	281
4.2.14A	Artist's Conception of Single Coil Solenoid Disk Magnet Design	283
4.2.14B	Diagram Showing Single Solenoid Disk Magnets and Split Pair Magnets Compared	284
4.2.15A	Cutaway Plan View (Conceptual) of Baseload Size 6 T Circular Saddle Magnet with I-Beam Ring Girders, Design BL6-1	285
4.2.15B	Cutaway Plan View (Conceptual) of Baseload Size 6 T Circular Saddle Magnet with Solid Ring Girders, Design BL6-2	286
4.2.15C	Cutaway Plan View and End View (Conceptual) of Baseload Size 6 T Rectangular Saddle Magnet, Design BL6-3	287
4.2.15D	Cutaway Plan View (Conceptual) of Baseload Size 5 T Circular Saddle Magnet, Design BL5-1	288
4.2.15E	Cutaway Plan View (Conceptual) of Baseload Size 7 T Circular Saddle Magnet, Design BL7-1	289
4.2.15F	Graph of Estimated Weights and Stored Energies of Conceptual Design Magnets	290
4.2.15G	Bar Chart - Normalized Weights of Major Components of Conceptual Design Magnets	291
4.2.17A	Network Diagram, Commercial-Scale MHD Magnet Design Selection	295
4.2.17B	Network Diagram, Commercial-Scale MHD Magnet Supporting Investigations	296

<u>Fig. No.</u>	<u>Title</u>	<u>Page</u>
4.3.1A	Curve of On-Axis Field vs Distance Along Axis for CDIF Superconducting Magnet (CDIF/SM)	303
4.3.1B	Diagram Showing Coil Configuration, CDIF Superconducting Magnet (CDIF/SM)	304
4.3.1C	Sketch Showing Typical Winding Cross Section, CDIF Superconducting Magnet (CDIF/SM)	305
4.3.1D	Sketch Showing Conductor, CDIF Superconducting Magnet (CDIF/SM)	306
4.3.1E	Layout Showing Cold Mass Assembly, CDIF Superconducting Magnet (CDIF/SM)	307
4.3.1F	Cutaway View of Magnet and Vacuum Jacket Assembly, CDIF Superconducting Magnet (CDIF/SM)	308
4.3.1G	Diagram, Cryogenic Subsystem and Power Supply Subsystem, CDIF Superconducting Magnet (CDIF/SM)	309
4.3.2A	Curve of On-Axis Field vs Distance Along Axis for Stanford Superconducting Magnet	316
4.3.2B	Diagram Showing Winding Configuration, Stanford Superconducting Magnet	316
4.3.2C	Sketch of Conductor, Stanford Superconducting Magnet	317
4.3.2D	Elevation and End Views of Magnet Assembly, Stanford Superconducting Magnet	318
4.3.2E	Cross Section of Stanford Alternative Design (CMPS) Magnet Winding and Substructure	320
4.3.2F	Layout of Ring Girder for Stanford Alternative Design (CMPS) Magnet	321
4.3.2G	Sketch of Conductor for Stanford Alternative Design (CMPS) Magnet	322
4.3.2H	Layout Showing Cold Mass Support Links for Stanford Alternative Design (CMPS) Magnet	323
4.3.2J	Cutaway View of Stanford Alternative Design (CMPS) Magnet Assembly	324
4.3.3A	Curve of On-Axis Field vs Distance Along Axis for U25 Superconducting Magnet (U.S. SCM)	329
4.3.3B	Cutaway View of Magnet and Cryostat, U25 Superconducting Magnet (U.S. SCM)	330
4.3.3C	Diagram of Cryogenic Subsystem, U25 Superconducting Magnet (U.S. SCM)	331
4.3.3D	Photograph of U25 Superconducting Magnet (U.S. SCM)	332
4.3.4A	Curve of On-Axis Field vs Distance Along Axis, Coal-Fired Flow Facility Magnet (CFFF/SM)	337
4.3.4B	Diagram Showing Winding Configuration and Conductor and Insulation System for Coal-Fired Flow Facility Magnet (CFFF/SM)	338
4.3.4C	Sketch Showing Structural Core Tube and Cross Section of Winding and Main Structure Consisting of Ring Girders and Tie Plates, Coal-Fired Flow Facility Magnet (CFFF/SM)	339
4.3.4D	Cutaway View of Magnet and Cryostat Assembly, Coal-Fired Flow Facility Magnet (CFFF/SM)	340
4.3.4E	Diagram of Cryogenic Subsystem, Coal-Fired Flow Facility Magnet (CFFF/SM)	341
4.3.5A	Curve of On-Axis Field vs Distance Along Axis, CDIF Conventional Magnet (CDIF/CM)	344
4.3.5B	Exploded View of CDIF Conventional Magnet Coils, Yokes and Pole Pieces (CDIF/CM)	345
4.3.5C	Elevation, Plan and End Views of CDIF Conventional Magnet (CDIF/CM)	346
4.3.5D	Coil Outline, One Half of Winding, CDIF Conventional Magnet (CDIF/CM)	347
4.3.5E	Artist's Sketch of CDIF Conventional Magnet Assembly	348
4.3.5F	Photograph of Completed CDIF Conventional Magnet (CDIF/CM)	349
4.3.6A	Curve of On-Axis Field vs Distance Along Axis, AVCO Conventional Magnet (AVCO/CM)	353
4.3.6B	Elevation, Plan and End Views of AVCO Conventional Magnet (AVCO/CM)	354
4.3.6C	Sketch Showing Coil Outline (One Half of Winding), and Coil Cross Section, AVCO Conventional Magnet (AVCO/CM)	355
4.3.6D	Photograph of Completed AVCO Conventional Magnet (AVCO/CM)	356

## List of Abbreviations

AEDC	Arnold Engineering Development Center (Tullahoma Tenn) (Also see ARO)
AIRCO	Air Reduction Corp.
ALCOA	Aluminum Company of America
ANL	Argonne National Laboratory
ARO	Arnold Research Organization
ASME	American Society of Mechanical Engineers
ASTM	American Society for Testing and Materials
AVCO (AERL)	Avco Everett Research Laboratory Inc.
CASK	Designation for a particular magnet design concept originated by GD and MEA
CBI	Chicago Bridge & Iron
CCM	Critical Current Margin
CDER	Conceptual Design Engineering Report prepared for MHD Engineering Test Facility 200 MWe Power PLant
CDIF	Component Development and Integration Facility (as used herein it refers to the MHD Component and Integration Test Facility established by DOE at Butte, Montana)
CDP	Commercial Demonstration Plant
CE	Combustion Engineering
CEC	Cryogenic Engineering Conference
CFFF	Coal Fired Flow Facility (MHD), University of Tennessee Space Center, Tullahoma TN
CM	Conventional (water-cooled) magnet
CMP	Cask Magnet Prototype
CMPS	Cask Magnet Prototype System, a Designation Applied to the Stanford Magnet Alternative Design
CSM	Designation for a particular magnet design concept at MIT (commercial size magnet design)
DOE	U.S. Department of Energy
ECAS	Energy Conversion Alternatives Study (conducted for ERDA by NASA LeRC)
ERDA	U.S. Energy Research and Development Administration (superseded by U.S. Department of Energy circa 1978)
ETF	Engineering Test Facility (as used herein, it refers to the MHD Engineering Test Facility planned by DOE)
FBNML	Francis Bitter National Magnet Laboratory, Massachusetts Institute of Technology
G-10	Designation for a particular grade of fiberglass-epoxy laminate
G-10CR	cryogenic grade of G-10 fiberglass-epoxy laminate
GA	General Atomics (now GA Technologies, Inc.)
GD	General Dynamics Convair Division
GE	General Electric Co.
GRP	Glass-reinforced plastic
HPDE	High Performance Demonstration Experiment
ICCS	Internally-cooled cable superconductor
IEEE	Institute of Electrical and Electronic Engineers
IGC	Intermagnetics General Corp., Guildersland, NY
ILSS	Interlaminar shear strength

JACSAD	Designation of computer program for saddle coil field and force calculations
MCA	Magnetic Corp. of America, Waltham, MA
MEA	Magnetic Engineering Associates, Cambridge, MA
MEPPSCO	MEPPSCO, Inc., Boston, MA
MHD	Magnetohydrodynamic(s)
MIT	Massachusetts Institute of Technology
MPZ	Minimum propagating zone
MTBF	Mean time between failures
MVU	Magnetic volume utilization
MWe	Megawatts of electrical power
NASA LeRC	National Aeronautics and Space Administration, Lewis Research Center
NBS	National Bureau of Standards, National Engineering Laboratory, Boulder, CO
NMLMAP	Designation of computer program for analyzing penetration of magnetic fields
PAFEC	Designation of computer program for finite element computation of stresses, deflections, dynamic response, heat transfer, etc.
PENFLD	Designation of computer subprogram, a part of NMLMAP
PFC	Plasma Fusion Center, Massachusetts Institute of Technology
PSPEC	Parametric Study of Potential Early Commercial MHD Power Plants (ERDA-sponsored)
RFP	Request for Proposal
ROM	Rough order of magnitude
RT	Room temperature
SDD	System design description
SSM	Stanford Superconducting Magnet (for MHD testing)
TFM	Test Facility Magnet (6 T racetrack pair superconducting magnet at MIT)
U25B	Designation of bypass test loop at USSR U25 MHD Test Facility at the Institute for High Temperatures in Moscow





## List of Tables

<u>Table No.</u>	<u>Title</u>	<u>Page</u>
2-1	MHD Magnet Program - Technology Base Development	3
3.2-I	List of Recommended Tasks, Analysis, Research and Development	10
3.2-II	List of Recommended Tasks, Magnet System Design Studies	11
4.1.2-I	Characteristics of MIT Test Facility Racetrack Magnet (ITFM)	15
4.1.5-I	High Current Conductor Specifications (for Use in Development of Conductor Designs)	18
4.1.5-II	Comparison of Baseline Design CASK CIDP Magnet Conductor and Scaled-Up CFFF (UTSI) Magnet Conductor	26
4.1.9-I	Estimated Magnet System Capital Cost Breakdown and Integration (\$10 <sup>6</sup> ) (based on channel and plate concept using semifluted conductor at $\dot{q} = 0.6 \text{ W/cm}^2$ )	67
4.1.9-II	Estimated Cost for Magnet System Based on Ten-Year Operation (magnet incorporating channel and plate concept)	68
4.1.9-III	Magnet System Estimated Costs (based on nested shell concept using semifluted conductor at $\dot{q} = 0.6 \text{ W/cm}^2$ )	69
4.1.10.1-I	Initial Conductor Specifications (for Use in Stability Analysis)	72
4.1.10.2-I	CIDF Conductor Allowable Delamination Length Assuming End Cooling but No Composite Cooling	78
4.1.10.2-II	CIDF Conductor Allowable Delamination Length, Determined by Computer Program, Assuming Different Values of $S_2/S_0$	79
4.1.10.2-III	MPZ Data for 40 kA CASK Type Conductor	80
4.1.10.2-IV	CASK Type Conductor Dimensions for Absolute Cryogenic Stability	81
4.1.10.2-V	Allowable Delamination Length for 40 kA CASK Type Conductor	82
4.1.10.2-VI	A.C. Losses for 40 kA CASK Type Conductor	83
4.1.12-I	Interlaminar Shear Strength of G-10 Samples at 77 K after Thermal and Load Cycling	94
4.1.13-I	Typical Material Choices for MHD Magnet Designs	99
4.1.13-II	Proposed Program of Low Temperature Materials Research for MHD Magnets	100
4.1.18-I	Cryogenic Characteristics of Baseline Design MHD Magnet Systems	108
4.1.18-II	Expected Minimum Mean Time Between Failures (MTBF) for Components of the Cryogenic System	109
4.1.18-III	Cost Estimate Breakdown for 100 Liter/Hour Refrigerator/Liquefier System	110
4.1.19-I	Power Supply and Dump Circuit Design Characteristics - Magnet Current Selected Independently	113
4.1.19-II	Breakdown of Estimated Costs for a 50 kA, 2.65 MW Magnet Power Supply	114
4.2.1-I	Major Design Characteristics of Commercial-Scale Magnet Reference and Conceptual Designs	130
4.2.2-I	Design Criteria for a Baseload-Scale MHD Magnet: Estimated MHD Power, 600 MWe	133
4.2.2-II	Design Characteristics, Baseload MHD Magnet Design BL-MCA, Magnetic Corporation of America	134
4.2.2-III	Baseload MHD Magnet System Cost Estimates, BL-MCA (1977 dollars)	144

<u>Table No.</u>	<u>Title</u>	<u>Page</u>
4.2.3-I	Design Characteristics, Baseload MHD Magnet Design BL.6-P1, (AVCO)	147
4.2.3-II	Summary, Estimated Component Costs and Assembly Labor, 6 T Baseload Circular Saddle Magnet Design BL.6-P1 (AVCO)	156
4.2.3-III	Summary, Estimated Cost of Installed Magnet System, First Unit 6 T Baseload Circular Saddle Magnet Design BL.6-P1 (AVCO)	158
4.2.4-I	Design Characteristics, Baseload MHD Magnet Design BL.6-P2, (AVCO)	161
4.2.5-I	Design Criteria for a Commercial Demonstration Plant (CDP) MHD Magnet, Estimated MHD Power 250 MWe	169
4.2.5-II	Design Characteristics, Commercial-Scale MHD Magnet Design CASK (General Dynamics, Convair Division)	170
4.2.5-III	Typical Work Breakdown Sheets Used in Estimating Cost of CASK Magnet, One Unit Basis	186
4.2.5-IV	Commercial-Scale MHD Magnet Design CASK, Cost Estimates	188
4.2.6-I	Design Characteristics, Commercial-Scale MHD Magnet Design CSM (MIT)	193
4.2.7-I	Design Characteristics, Commercial-Scale MHD Magnet Advanced Design, ICCSM (MIT)	210
4.2.8-I	Major Characteristics of ETF-Scale Magnet Reference and Conceptual Designs	219
4.2.9-I	Design Criteria for ETF-Scale MHD Magnet Reference Designs (MCA & AVCO 1977 Designs)	222
4.2.9-II	Design Characteristics, ETF MHD Magnet Design ETF-MCA	223
4.2.9-III	ETF Magnet System Cost Estimates, ETF-MCA	232
4.2.10-I	Design Characteristics, ETF MHD Magnet Design ETF6-P1 (AVCO)	233
4.2.10-II	Summary, Estimated Component Costs and Assembly Labor, 6 T ETF-Size Magnet Design ETF6-P1	241
4.2.10-III	Summary, Estimated Cost of Installed Magnet System, 6 T ETF-Size Circular Saddle Magnet Design ETF6-P1 (AVCO)	242
4.2.11-I	Design Characteristics, ETF MHD Magnet Design ETF6-P2 (AVCO)	245
4.2.12-I	Design Characteristics, ETF MHD Magnet Design AVCO-3 (AVCO)	251
4.2.12-II	Summary, Estimated Cost of Installed Magnet System, Alternative ETF 6 T Magnet Design, AVCO-3	254
4.2.13-I	Design Characteristics, 6 T and 4 T ETF MHD Magnet Designs CSM Scaledown (MIT) (Magnets for NASA LeRC Conceptual Design MHD ETF 200 MWe Power Plant)	261
4.2.13-II	Summary, Estimated Cost of Installed Magnet System 6 T Magnet for MHD ETF 200 MWe Power Plant	264
4.2.13-III	Summary, Estimated Cost of Installed Magnet System, 4 T Magnet Design for MHD ETF 200 MWe Power Plant	266

<u>Table No.</u>	<u>Title</u>	<u>Page</u>
4.3.1-I	Design Criteria, CDIF Superconducting Magnet	298
4.3.1-II	Design Characteristics, CDIF Superconducting Magnet	300
4.3.2-I	Design Criteria, Stanford 7 T Superconducting Magnet	310
4.3.2-II	Design Characteristics, Stanford 7 T Superconducting Magnet Alternative Designs	312
4.3.3-I	Design Characteristics, U25 Superconducting Magnet	326
4.3.4-I	Design Characteristics, Coal-Fired Flow Facility Superconducting Magnet	334
4.3.5-I	Magnet System Design Characteristics, CDIF/CM	343
4.3.6-I	Magnet System Design Characteristics, AVCO/CM	352



### Abstract

The program of MHD magnet technology development conducted for the U.S. Department of Energy by the Massachusetts Institute of Technology during the past five years is summarized. The general strategy is explained, the various parts of the program are described and the results are discussed. Subjects covered include component analysis, research and development aimed at improving the technology base, preparation of reference designs for commercial-scale magnets with associated design evaluations, manufacturability studies and cost estimations, the detail design and procurement of MHD test facility magnets involving transfer of technology to industry, investigations of accessory subsystem characteristics and magnet-flow-train interfacing considerations and the establishment of tentative recommendations for design standards, quality assurance procedures and safety procedures.

A systematic approach (framework) developed to aid in the selection of the most suitable commercial-scale magnet designs is presented and the program status as of September 1982 is reported. Recommendations are made for future work needed to complete the design evaluation and selection process and to provide a sound technological base for the detail design and construction of commercial-scale MHD magnets.

### 1.0 Introduction

A program to develop superconducting magnets for commercial magnetohydrodynamic (MHD) power generation plants, initiated in 1976, is being carried out by the Massachusetts Institute of Technology under the sponsorship of the U.S. Department of Energy (DOE), Office of Fossil Energy, MHD Division. Overviews of MHD magnet technology status and technology development planning are contained in References 1 through 15.

The overall objective of the program is to prepare the technological and industrial base required for minimum time, cost and risk implementation of superconducting magnets for MHD. It is planned that this will be achieved through a parallel effort of technology development and magnet construction yielding successive generations of magnet systems of increasing size. The near-term goal is to freeze the design concept for a commercial-scale MHD magnet system by the late 1980's.

The program has an intentional orientation toward increased industry and utility participation. This has initiated a dialogue which will expand in the future to assure proper consideration of cost effective techniques for large-scale component or subassembly fabrication and shipment, as well as proper interfacing of the magnet with the other components of the MHD system and balance of plant.

The purpose of this report is to summarize the work accomplished in the period from 1976 through 1982, to evaluate the results achieved and to make recommendations for future work needed to ensure the meeting of the overall objective of the program. Although considerable progress has been made, as reflected in this report, a substantial further effort will be required to complete the program.

## 2.0 General Strategy and Approach

The foundation for the program, as illustrated in Fig. 2.A, was experience generated in the design, construction and operation of large magnets in the past. This includes information for magnets which have been operated in MHD facilities as well as magnets constructed for use in other areas. The program grows from this initial data base through phases involving 1) component and system analysis, research and development, 2) preparation of reference designs for full-scale MHD magnet systems, concept evaluation, cost-risk assessment and verification testing, and 3) design and construction of magnets for Government-sponsored MHD test facilities (CDIF, CFFF, Stanford, Avco).

Supporting investigations including magnet/power train interfacing studies, manufacturability studies, accessory system studies and development of design and safety standards are a part of the overall effort. Two major themes are carried throughout the program. One involves technology development and the other the design and construction of successively larger magnet systems. The present generation of this family of magnets is outlined in Fig. 2.A. The overall strategy for the program is shown in Fig. 2.B.

The technology base is intended to provide information to support both the design and construction of magnets now being procured and the design of the magnet for a near-commercial-scale MHD Engineering Test Facility (ETF). It includes the generation and extension of a design data base, development of improved analytical techniques and tools, production of reference designs for early identification of potential problem areas, interface requirement definition, and the construction of models for test and evaluation. The effort carried out in technology base development includes both basic and applied programs. Typical areas of interest are outlined in Table 2.1. The reference for the technology and design studies is a 1000 MW<sub>e</sub> plant (500 MW<sub>e</sub> MHD and 500 MW<sub>e</sub> steam turbine). The ETF magnet will be a direct scale-down from this commercial-scale reference design and will thus implement the concepts most suitable for commercial-scale systems.

The magnet procurement plan provides that alternative design concepts (CDIF, CFFF, Stanford) will receive the ultimate test of fabrication and operation. These magnets are intended for use in MHD component test facilities. Their procurement, therefore, also begins to establish the interface requirements between the magnet and other components of the flow train and the facility itself. Magnet design, construction, and installation as well as much of the technology development effort is subcontracted to industry. (A list of subcontracts is contained in Appendix A.) This creates the strong industrial base necessary for commercialization of MHD and also allows the program to have the advantage of existing industrial expertise in specific areas of design and fabrication. A continued interaction with utilities and utility equipment manufacturers is essential to assure that design concepts evolve which are consistent with fabrication capability, material availability, and interface requirements within the plants where MHD generating systems are to be installed.

Scenarios must be evaluated to select a cost effective sequence for module fabrication, shipment, and site assembly. This will have a major effect on cost and feasibility. The spectrum of possibilities for consideration range from the shipment of a complete magnet in Dewar to the opposite extreme in which all parts are shipped unassembled to the site. A mid-range approach is probably most efficient at the ETF scale or larger, but requires definition. This will provide input for production of the necessary cost estimates, trade-off and freeze of the ETF design concept.

The general approach to the design freeze for the commercial-scale reference design is illustrated in Fig. 2.C, which is a simplified version of a complex network analysis developed for the magnet program (see Section 4.2.17). Following definition of the flow train and facility requirements for the system, a set of alternative system concepts is defined based on past experience (a more extensive discussion of the alternatives will be given later). In the approach toward a commercial-scale design freeze, the alternatives provide the immediate basis

**Table 2-I**

**MHD Magnet Program  
Technology Base Development**

**Typical Basic Programs**

- Stability Analysis, Superconducting Windings
- Sources of Instability
- Normal Front Propagation
- Heat Transfer
- Low Temperature Properties of Materials
- Sensors and Diagnostics
- Advanced Concepts and Analytical Tools

**Typical Applied Programs**

- High Current Conductor Fabrication
- Evaluation of System Protection Methods
- Fabrication of Structural Models
- Development of Structural and Safety Standards
- Reference Designs of Commercial-Scale Magnet Systems

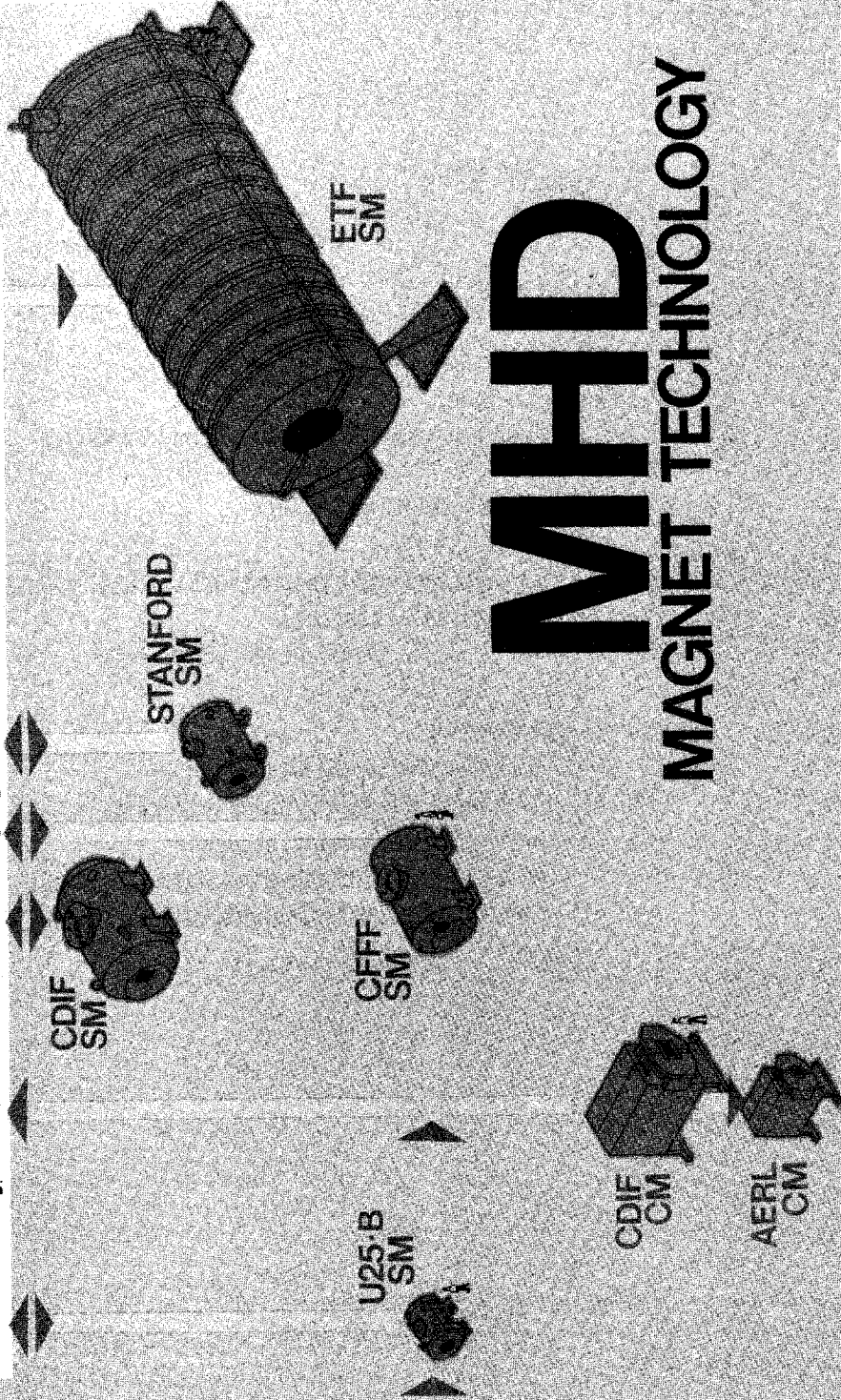
**BACKGROUND**

HIGH ENERGY PHYSICS  
 Bubble Chambers  
 Beam Transport  
 SC ACCELERATORS  
 ENERGY STORAGE  
 LINE FEEDS  
 FUSION  
 ACO MHD  
 ACO MHD  
 SO/IE MHD  
 AIRCRAFT MHD  
 ACO FIDE  
 BASELOAD STUDIES

**CONCEPTS - EXPERIMENTS    COST/RISK - VERIFICATION TESTS    DETAIL DESIGN & FABRICATION**

**MHD SUPERCONDUCTING MAGNET TECHNOLOGY DEVELOPMENT**

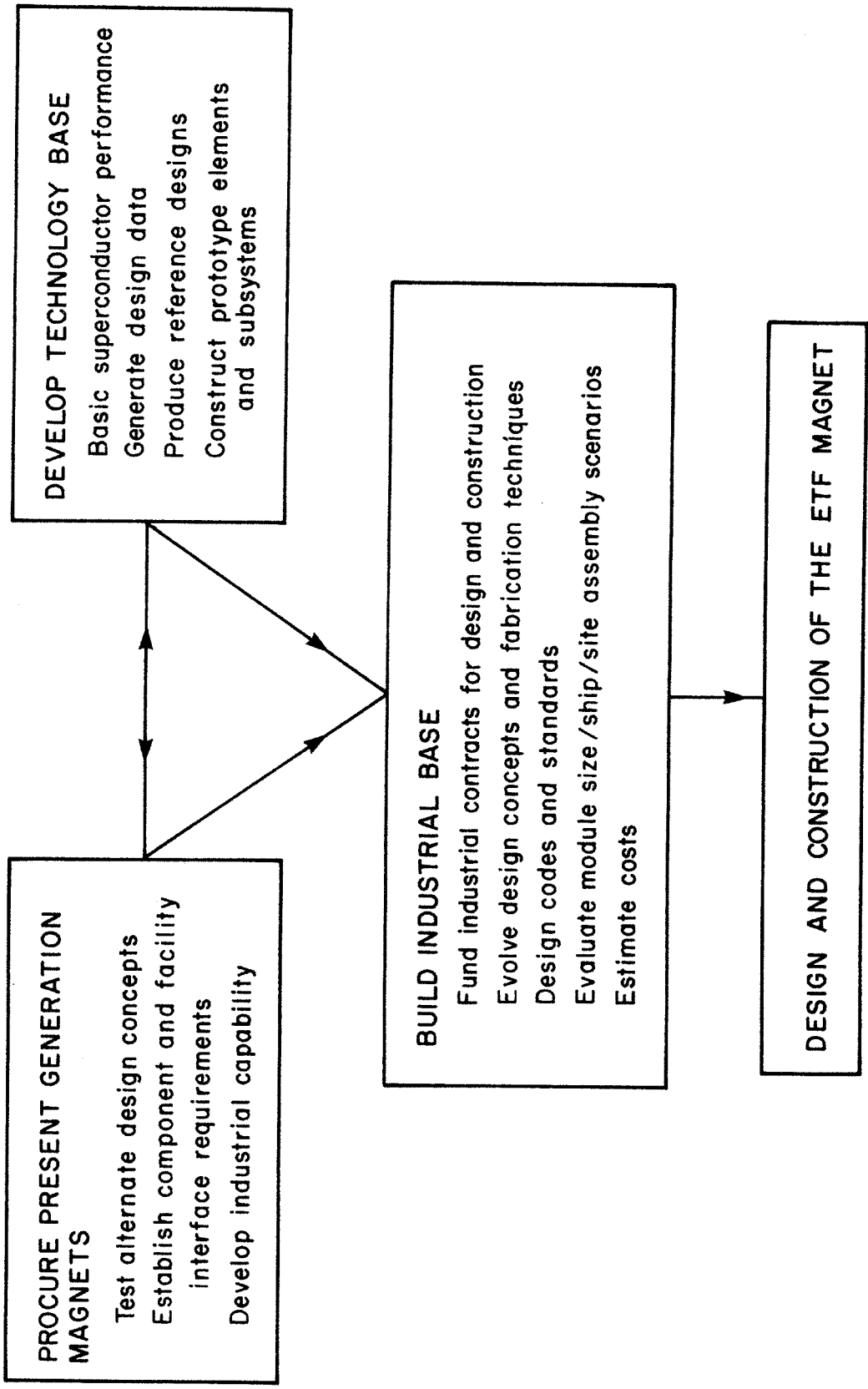
test facility · conductor · structure · cryogenics · control · protection · publications

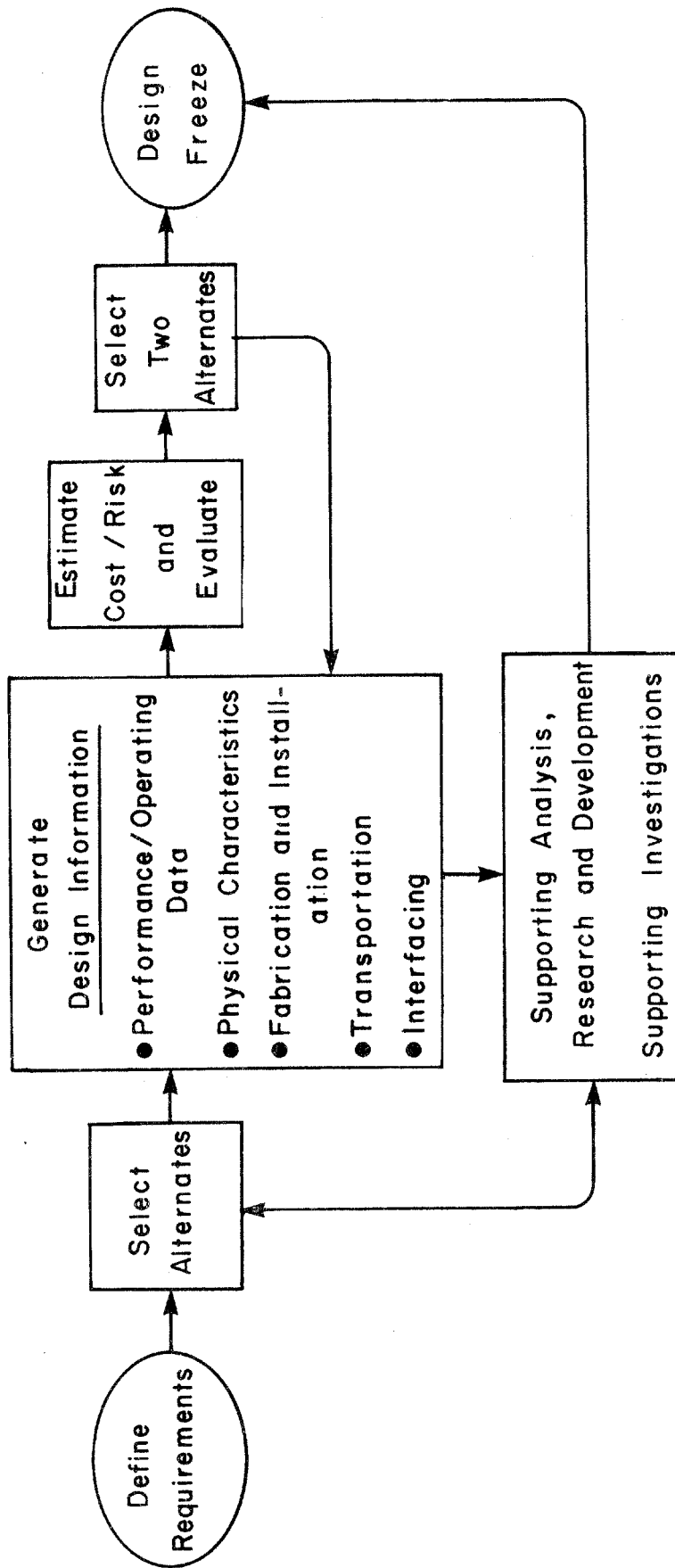


**MHD**  
**MAGNET TECHNOLOGY**

1911 - 1976    77    78    79    80    81    82    83    84    85    86    87    88







for identification of the areas for supporting investigations in technology development. Design information is generated for each alternative to define its physical characteristics and, more importantly, to allow its evaluation from the viewpoints of fabrication, assembly, quality control and its implications concerning shipment of sub-assemblies and installation of the system. The design information provides input for cost/risk estimation for each design alternative and identifies additional areas for supporting development in both basic and applied programs. After cost/risk evaluation, it is expected that two designs will be selected and carried through a more detailed design concept.

As of the date of this report, several alternative reference designs have been prepared and are in the process of evaluation and upgrading. More work is required before final design selection can be made.

### **3.0 Overall Results and Recommendations**

The program described in this report is a very broad one, covering aspects of magnet technology ranging from theory and analysis through engineering investigations and the procurement of test facility magnets, to manufacturing, planning and cost predictions for future large magnet systems.

The program is not yet complete. It was anticipated at the start that the program would require at least seven years, continuing through calendar year 1983. While much has already been accomplished, the level of effort (due to funding limitations) has been below that originally planned and there is a large amount of work still to be done before the final design and construction of commercial-scale MHD magnets can be undertaken with confidence. It is therefore recommended, as discussed in more detail below, that planning of future steps toward the commercialization of MHD include a continuation of the magnet development program at a level consistent with the importance of the magnet in the overall system.

### **3.1 Results**

As a result of the work done to date, the data base for the design and manufacture of large superconducting MHD magnets has been greatly improved and extended over that which existed at the start, as evidenced by this report and the large volume of technical information referenced herein.

Industry has been brought into the MHD magnet engineering and manufacturing areas to a much greater extent than was the case before.

Conceptual designs have been developed for five alternative commercial-scale magnet systems and are entering the evaluation stage to determine which is most suitable for use in early commercial MHD power generators.

Two large conventional, water-cooled magnets [16] have been completed and are installed and operating in their respective test facilities. These are the CDIF/CM, manufactured by MCA and the AVCO/CM, manufactured by Everson and Bethlehem Corp. A large superconducting magnet intended for use in the CFFF [17] has been completed and successfully tested by ANL, but is not yet installed due to lack of funds. The large superconducting magnets under construction for Stanford [18] (by GD) and for the CDIF [19] (by GE) have both been halted due to lack of funds. A 6 T test facility magnet, [20] prototypical of the CDIF/SM design concept has been installed and operated in numerous tests at MIT.

Specific results which are of particular interest to the long range MHD magnet program are:

- Application of the minimum propagating zone and critical current margin theories in analyzing superconductor stability [21].
- Development of analytical and design data on high current superconductors for MHD magnets [22].

- Development of internally-cooled cable superconductors (ICCS) [23].
- Analysis of details of various aspects of coil protection [24].
- Test data on mechanical properties of glass-reinforced plastic (G-10) at conditions simulating those to which superconducting magnet insulators and substructures are subjected (information not previously available) [25].
  - Test data on relationship of acoustic emissions during charging to stability of superconducting coils [26].
  - Development of analytical tools, including computer programs for calculating magnetic fields, forces and stresses in MHD magnets [27].
    - Construction of a test facility for testing large magnet components (conductors, insulators, substructure elements, power leads) with high background field, high current and low temperature [20].
    - Identification of superstructure and substructure design concepts [28].
    - Development of the CSM (CDIF scaleup) winding/substructure design concept in which individual conductors are supported in a modular substructure in such a manner that the conductors are not subjected to accumulated magnetic forces (improved stability; ease of manufacture) [28, 29].
    - Development of the "CASK" winding/substructure design concept in which bundles of conductors are supported in a modular substructure in such a manner that the bundles are not subjected to accumulated magnetic forces and the total accumulated longitudinal magnetic forces are carried by substructural elements themselves, eliminating the need for external longitudinal superstructure (improved stability; ease of manufacture) [30].
      - Development of the "momentless" winding/structure design concept, in which outward magnetic forces are carried by a band-type, all tension superstructure (reduced superstructure weight; lower cost) [31].
      - Development of preliminary standards for MHD magnet structures and for superconductors of the type used in MHD magnets [32].
      - Quantification of the effect of careful MHD channel packaging and channel/magnet interfacing in reducing magnet size and cost in a specific MHD system [33].
      - Identification of the transportation options and associated costs for carrying large magnet components from manufacturing plant to power plant site [34].
      - Identification of design characteristics and estimated costs of cryogenic support systems for large MHD magnets [35].
      - Identification of design characteristics and estimated costs of power supply and discharge systems for large MHD magnets [36].
      - Development of progressively improved procedures for estimating costs of large MHD magnet component and system costs [37].
      - Availability of a data base for the development of the ETF superconducting magnet conceptual design (implemented in 1981 by MIT under contract from NASA LeRC) for the MHD ETF 200 MWe Power Plant [38].

### **3.2 Recommendations**

Although the basic technology is well understood and although there have been several recent successful demonstrations of large superconducting magnets in the MHD, fusion and high energy physics communities, it is worth noting that those successes have been within large and experienced national laboratories and were based principally on the specific experience of a very few key individuals. It is also worth noting that there have been several recent serious and costly failures.

The most important consideration relative to assessing the status of superconducting magnet technology for MHD is the recognition of the huge difference in the cost/risk assessment of the magnet as compared to other flow train components. Magnets either work or they don't. There is no opportunity for operation at reduced output or reduced life or for modest turn-around time and cost for repair or replacement. If the first commercial magnet does not work, a several hundred million dollar project, a billion dollar total investment and a valuable energy technology will be in serious jeopardy. A magnet technology development program must continue to be a part of the national MHD development program. It should be maintained at a level consistent with the importance of the magnet in the MHD system and on a schedule consistent with the planned schedule for commercialization of MHD. It should include the tasks listed in Tables 3.2-I and 3.2-II. Of the items listed, the most important are (1) the demonstration of the performance and manufacturing technology for superconductors capable of reliable operation at operating currents above 25 kA (at 7.5 T and 4.5 T) and (2) the development of a complete and detailed specification for the design and structural basis for large superconducting magnets including recommendations of a preliminary voluntary standard.

### **4.0 Summary of Work Accomplished**

The main categories of work performed under the program have been:

- **Analysis, Research and Development**  
(including reviews of past magnet experience, construction of in-house test facilities, laboratory testing and special investigations)
- **Design of Commercial-Scale and ETF Magnet Systems**  
(including manufacturing and cost studies)
- **Design and Construction Supervision of Magnets for Government-Sponsored MHD Test Facilities**  
(CDIF, CFFF, Stanford, AVCO)

Summaries of the work accomplished in each of the major subtasks under the above-listed categories are given in the sections which follow. Where appropriate, references containing more detailed information are cited and/or detailed data compilations are included as appendices to this report.

**Table 3.2-I**  
**Analysis, Research and Development**  
**List of Recommended Tasks**

- **Compilation and Analysis of Data Base from Recent Superconducting Magnet Experience**
- **Operation of In-House Test Facility at FBNML**
- **Continued Upgrading of Analytical Tools (3-D, Transient, Finite Element)**
- **Continued Stability Testing and Analysis of Pool-Cooled Conductor**
- **Development of High Current Cable Superconductor, Pool-Cooled**
- **Development of Internally-Cooled Cable Superconductor**
- **Demonstration of Performance and Manufacturing Technology for Superconductors for Operation Above 25 kA**
- **Continued Analysis and Development of Superstructure**
- **Development of Complete and Detailed Structural Basis for MHD Magnets**
- **Continued Development of Superconductor Standards**
- **Continued Investigation of Safety and Quench Protection**
- **Continued Investigation of Effects of Fringe Fields on Personnel and Equipment**
- **Interfacing (Packaging) Studies**
- **Upgrading of Cost Estimating Procedure**
- **Study of Impact of Current Density on Magnet Cost**
- **Investigation of Modular Design for Large Magnets**

**Table 3.2-II**  
**Magnet System Design Studies**  
**List of Recommended Tasks**

- **Evaluation of Recent Commercial-Scale Magnet System Designs**
- **Upgrading of Magnet System Designs and Cost Estimates**
- **Selection of Preferred Design using Matrix/Framework Approach**
- **Investigation of Special Magnet System Designs (Roll-Apart, Roll-Aside)**
- **Disk Generator Magnet System Design Studies**
- **Magnet Subsystem Design Studies**

## **4.1 Analysis, Research and Development**

Analysis, research and development were carried out in a number of areas for the purposes of verifying existing theories relating to superconductor stability and quench phenomena, improving analytical techniques, developing improved components and generally filling out and strengthening the technology base for commercial-size MHD magnets.

Substantial progress was made during the report period. Highlights were the pioneering of the minimum propagating zone and critical current margin concepts in analyzing conductor stability, the development of new design approaches for high current conductors, both pool-cooled and internally-cooled types, the construction and operation of a new in-house component test facility, the development of new concepts for large winding and substructure systems (CASK and CSM), the testing of structural materials, the compilation of tentative structural standards for MHD magnets and the issuance of reports on a number of special investigations ranging from magnet system (electrical) protection to transportation of large magnet components.

Tasks accomplished are described in more detail in the following subsections.

### **4.1.1 Compilation and Analysis of Data Base from Previous Superconducting Magnet Experience**

Technical data, construction information and test results from other superconducting magnet programs, both past and current, have been gathered, recorded and analyzed for use as a base for the magnet designs and investigations reported herein. In particular, magnet data from the following sources have been compiled and analyzed: AVCO MHD programs, ECAS and PSPEC studies, Japanese MHD program, ANL-U25-B magnet project, AEDC MHD project, large bubble chamber programs, both U.S. and European, and fusion power generation programs. Tables of data obtained from these sources are contained in Appendix B.

### **4.1.2 Construction and Operation of In-House Test Facility at MIT**

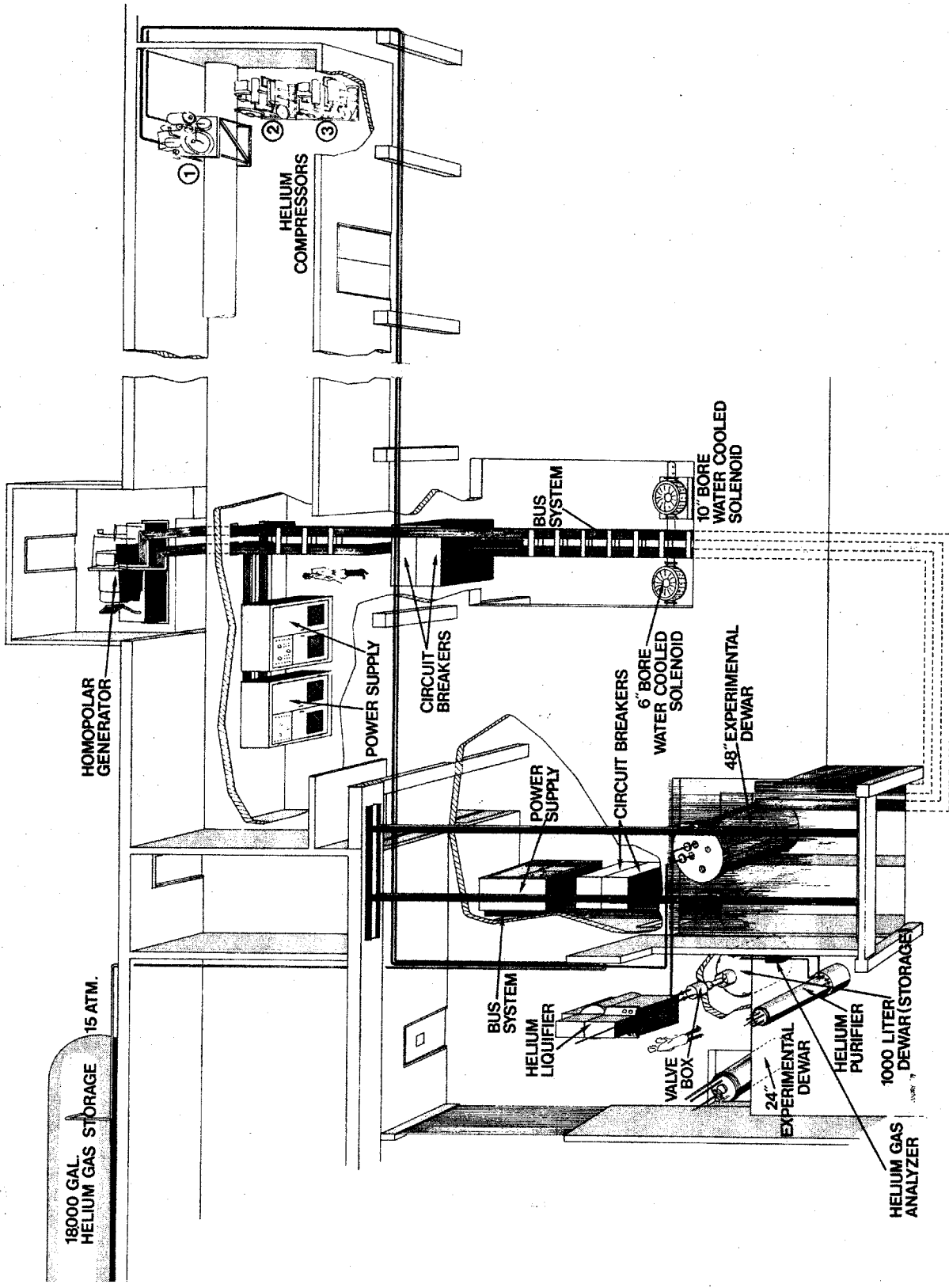
The in-house test facility, a dedicated facility for testing MHD magnet conductor and winding components, was constructed early in the report period and commissioned in 1978. It provides three essential environments for the operation of large-scale experiments in superconducting magnet technology. These environments are: (1) low (cryogenic) temperature, (2) high magnetic field, and (3) high current.

Figure 4.1.2A shows an overall layout of the facility. A helium liquefier and liquid storage Dewar provide liquid helium refrigerant to two experimental Dewars, one with 0.61 meter diameter test space and the other with a 1.22 meter diameter test space. To provide high magnetic field, there is a 7 T split-pair solenoid magnet mounted in the smaller Dewar and a 6 T split-pair racetrack magnet (TFM) mounted in the larger Dewar. In addition there are two water-cooled test solenoids, one providing 7 T in a 220 mm bore and the other providing 12 T in a 150 mm bore. High current (dc) is available from three sources, (1) a set of four 10 kA, 5 V rectified power supplies; (2) four Laboratory motor-generators capable of supplying up to 40 kA at 250 V; and (3) a 25 kA, 2 V homopolar generator.

The split-pair superconducting racetrack magnet (TFM), designed by the MHD Group and built under subcontract by GE during the report period, incorporates a new type of winding and substructure system similar to that being introduced in the CDIF/SM magnet.

Each racetrack coil is made up of 11 double pancakes, each pancake having a racetrack-shaped winding totaling 31 turns in a G-10 plate, 0.97 m wide, 1.85 m high, and 11 mm thick. A 4.7 mm square cross section copper composite NbTi conductor, wrapped with copper wires, is placed in grooves machined in each plate. A stainless steel structure surrounds the winding and G-10 substructure of each coil half. The characteristics of the





4.1.2A Layout of MHD Magnet Component Test Facility at MIT

magnet are listed in Table 4.1.2-I. A cutaway view of the magnet installed in the 1.22 m I.D. test Dewar is shown in Figure 4.1.2B.

Initial testing of the split-pair racetrack test magnet (TFM) was conducted in the latter part of 1980. The objectives of the initial testing were 1) to operate the test magnet (TFM) successfully and 2) to test three experimental coils placed in the gap of the test magnet, namely a double pancake coil wound with TFM conductor, a single pancake coil with CDIF/SM conductor in a CDIF-type subplate and a single pancake coil with cable conductor in a CDIF-type subplate.

Successful operation of the TFM at a field of 6 T was achieved after modifications were made to prevent premature dumping caused by the quench detector/dump system.

Tests were made on the experimental coils to evaluate stability and normal zone propagation characteristics. At 5.5 T, recovery current on the CDIF monolithic conductor was found to be 6000 A. On the cable conductor, recovery current was somewhat lower.

The results of the initial tests demonstrated the usefulness and versatility of the TFM.

Following initial testing, it was planned that the "football" coil, made of NbTi/Cu internally-cooled, cabled superconductor as described in Section 4.1.6, would be placed in the gap of the TFM and subjected to a series of tests to evaluate that type of conductor. This test series was held up due to lack of funds.

Further information on the in-house test facility is contained in References 20, 39 and 40.

#### 4.1.3 Upgrading of Analytical Tools

Analytical tools, including magnetic field and force "stick" programs and finite element analysis techniques, were upgraded progressively by FBNML during the course of the program, for use in analysis of the MHD magnets being designed.

Updating of the JACSAD stick program for computing fields and forces in circular-saddle coil magnets was accomplished by a subcontractor, Littleton Research.

NMLMAP (National Magnet Laboratory Magnet Analysis Program) was developed as a method to analyze the diffusion or penetration of the magnetic field in two-dimensional plane or axisymmetrical bodies. This finite element program consists of two distinct subprograms that share pre- and post- processing packages.

The first of these programs (EXTFLD) calculates the time-dependent magnetic field (and the attendant eddy currents in any conducting medium present) produced by a known current distribution acting in the direction perpendicular to the plane of the problem. The program has the capability of solving this problem in the presence of ferromagnetic materials.

The second program (PENFLD) was developed to solve a particular problem. The program calculates the magnetic field and current penetration in a fast discharging homopolar machine.

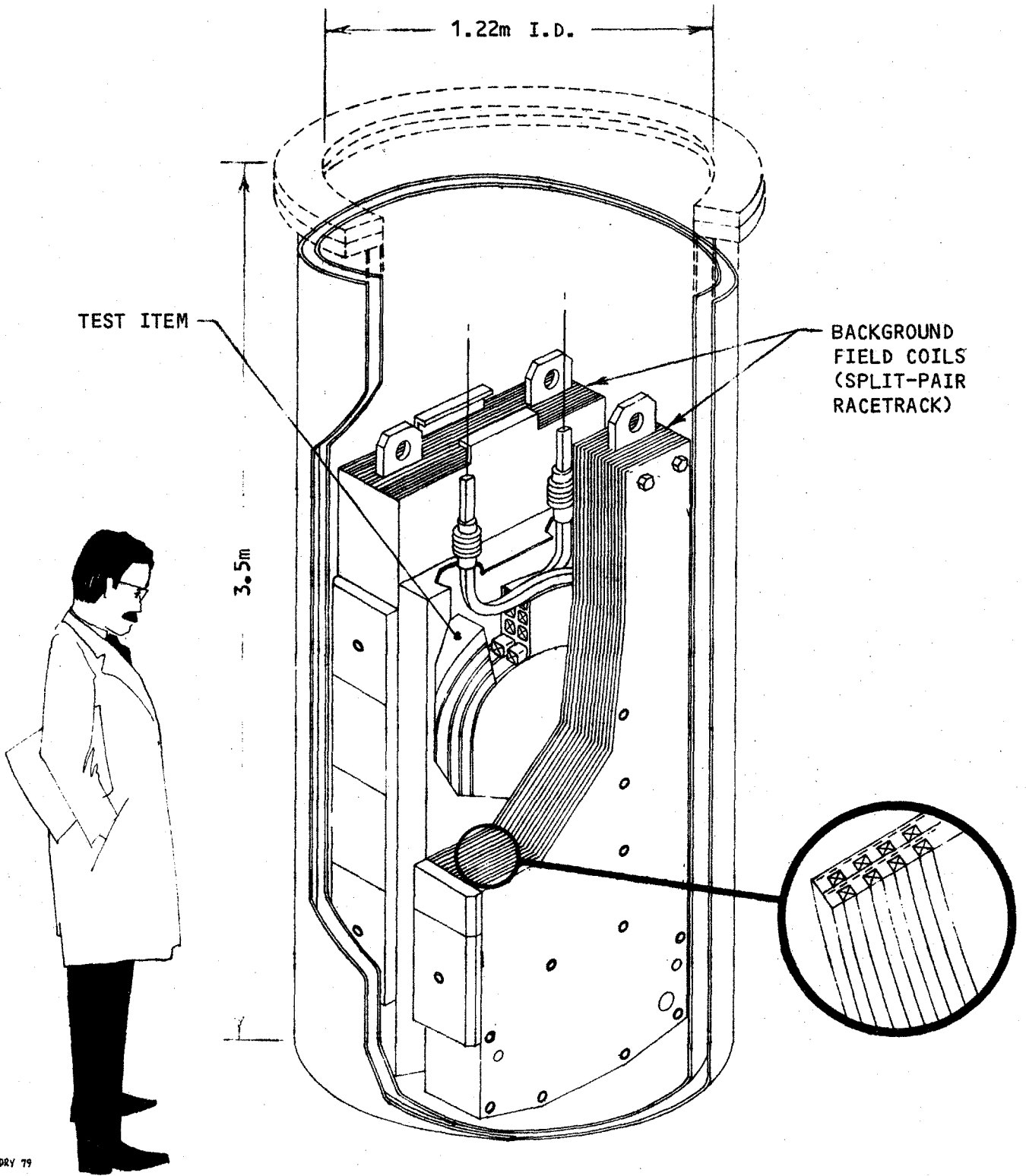
The PAFEC package (Program for Automatic Finite Element Calculations), developed at Nottingham University, UK, was purchased. This package greatly extends the group's internal capabilities in finite element analyses. The program is suitable for analyzing stresses, deflections, frequencies, dynamic response, creep, plasticity and heat transfer. Since structural analysis for all superconductive magnet systems is complex and of tremendous importance for a magnet's success, this package is a powerful tool for our structural analysts and designers.

A program capable of analyzing the detailed thermodynamic response of ICCS conductors was developed by NBS.

Table 4.1.2-I

Characteristics of FBNML Test Facility Racetrack Magnet (TFM)

Operating current	4100 A
Maximum gap	100 mm
Peak field at maximum gap	6.0 T
Current density in winding	3600 A cm <sup>-2</sup>
Normal state heat flux	2.2 W cm <sup>-2</sup>
Inductance with 100 mm gap	1.3 H
Stored energy	11 MJ
Magnet weight	3700 kg



4.1.2B Cutaway View of Component Test Facility 6 T Racetrack Magnet (TFM) and Dewar at MIT

#### 4.1.4 Stability Testing and Analysis of Pool-Cooled Conductor

Stability testing and analysis involving types of NbTi composite conductor planned for use in pool-cooled windings of MHD magnets were the focus of an extensive test program conducted in the FBNML in-house test facility. In 1976 samples of conductor for the U25-B magnet then under construction at Argonne National Laboratory (ANL) were tested with instrumentation to analyze transient effects and investigate minimum propagating zone phenomena. Higher-current conductors including samples of the conductor being manufactured for the CDIF/SM and samples of cable conductor were also tested. The effect of mechanical disturbances (frictional heating) was analyzed and investigated in tests using acoustic emission detection techniques.

Tests determined the low temperature static and dynamic friction coefficients for a variety of material pairs suitable for use in superconducting magnets. The Lorentz compaction heating in an ICCS was also measured. Several subcontractors made analyses of the stability of high current conductors (50 kA rating) of a type intended for use in commercial-scale MHD magnets. This work is summarized in Section 4.1.10.

The stability testing work has resulted in a better understanding of transient phenomena and their effect on stability and a new approach to winding design, involving both the minimum propagating zone (MPZ) and the critical current margin concepts. [41].

#### 4.1.5 Development of High Current Conductor, Pool-Cooled

Early investigation [1] of magnets for baseload MHD generators determined that large (high current) conductors would be required to limit the voltage that would appear in the event of an emergency discharge of the magnet and to minimize the amount of labor needed for winding. These conclusions were confirmed by studies [42, 43, 44] summarized in Section 4.1.9 of this report.

Since no experience existed with the size and type of composite superconductor contemplated, conceptual designs were obtained from five superconductor manufacturers (MCA, IGC, Supercon, Airc0 and Alcoa) for 50 kA pool-cooled conductors. Out of this work came several alternative designs, including a new concept, the "separate substrate" conductor.

Investigation of manufacturing and cost aspects of the separate substrate type of conductor was performed by General Dynamics in connection with their work on the CASK magnet [45].

Design and testing of large pool-cooled cable-type conductors for use in the CSM and ETF magnet conceptual designs which were under development during 1980 and 1981 was also begun. The subsections which follow summarize these high-current, pool-cooled conductor developments.

##### 4.1.5.1 Design Studies by Conductor Manufacturers

Five conductor manufacturers were invited to submit proposed designs for high current conductors for MHD magnet applications, based on the conductor specifications listed in Table 4.1.5-I. It was suggested to each manufacturer that the magnet to consider would have a circular saddle shape which might be wound of a conductor based on a copper substrate of cross section 1 cm high by 10 cm wide.

Two basic approaches to conductor design resulted from the design studies. They are identified as the integrated substrate conductor concept and the separated substrate concept.

The integrated substrate conductor concept, which was the basic concept generally used in medium current conductors in the past, involves factory fabrication of the complete conductor (composite superconductor and stabilizing substrate) and shipment of the integrated conductor to the plant site on large spools holding lengths of 500 m to several kilometers. The length is limited primarily by the weight of material that can be processed

Table 4.1.5-I

High Current Conductor Specifications

Type	Cryostable
Critical current	55 kA at 4.5 K
Filament diameter	< 0.05 inch
Cooling geometry	66% of each of 2 exposed faces only
Maximum heat flux from any exposed face	0.6 W·cm <sup>-2</sup>
Conductor overall current density	6000 A·cm <sup>-2</sup>
Joint resistance	< 2 × 10 <sup>-11</sup> Ω

in a single lot. At the plant site the conductor is wound into the required saddle-shaped coils using bending and forming tools to shape the conductor to conform to the saddle coil topology.

Typical integrated substrate conductors are shown in Figures 4.1.5A, 4.1.5B and 4.1.5C.

The separated substrate conductor concept, a concept not previously used in superconducting magnets, involves factory prefabrication of the stabilizing substrate separately from the composite superconductor. The substrate, incorporating multiple grooves to receive the composite superconductor, is prefabricated in sections conforming in shape to the local topology of the substructure channels in which the windings are to be installed. The prefabricated substrate sections and the composite superconductor are shipped separately to the plant site. At the site, the substrate sections are welded or brazed end-to-end to form complete turns of final configuration. The composite superconductor is unreeled from the shipping spools, inserted into grooves in the substrate and soldered in place.

Typical separated substructure conductors are shown in Figures 4.1.5D, 4.1.5E and 4.1.5F.

In the concepts shown in Figures 4.1.5D and 4.1.5E the composite superconductor, a monolith or cable, is relatively small in cross section. This is because it is deployed in multiple parallel paths when installed in the substrate and each path is required to carry only a fraction of the total current. Therefore, the composite can be supplied in relatively long lengths, wound on spools. The total lengths (expected to be 10 km or more) are limited primarily by the weight of material that can be processed in a single lot. This represents an advantage over other concepts because splices in the composite superconductors can be staggered and will carry relatively low current per splice, thus enhancing overall reliability.

#### 4.1.5.2 Manufacturing and Cost Investigation of Separated Substrate Conductors

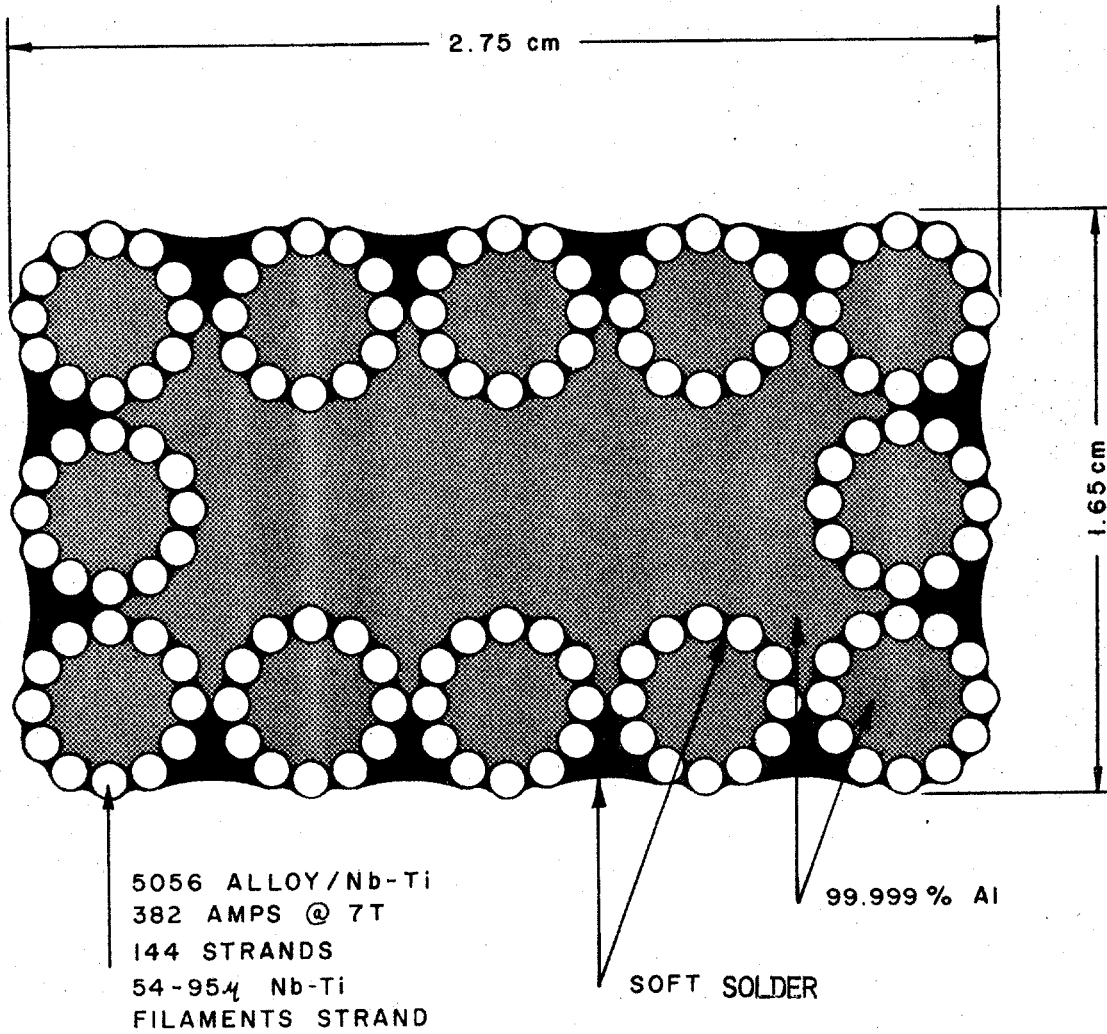
As part of the CASK commercial-size magnet design study (Section 4.2.5 of this report) the manufacturing aspects of separated substrate conductors were investigated and costs of fabrication and winding were estimated. Initially, two types of 50 kA conductor were compared for use in the CASK magnet. The baseline conductor considered was the separated substrate conductor shown in Figure 4.1.5E. The alternative was the separated substrate conductor shown in Figure 4.1.5F which is similar in geometry to the conductor used in the CFFF magnet (see Section 4.3.4 of this report).

Table 4.1.5-II contains a comparison of the two conductors. Supported by this comparison, the separated substrate conductor was selected as the preferred conductor. The General Dynamics engineers justified the

selection in the following excerpt from their report (Reference 30).

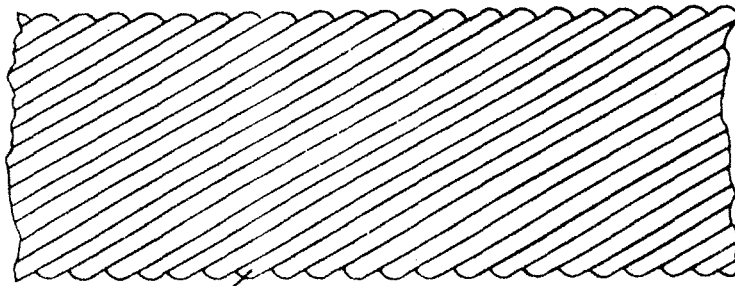
"The major disadvantage of the large version of the CFFF-type conductor was the difficulty to prepare edgewise bends. This conclusion was derived by actually handling an existing cabled conductor of comparable geometry. The other anticipated disadvantage is the large bulk of in situ soldering required to associate the cable into the substrate. A significant conclusion of this study, is that the true objective in selecting a conductor for a CDP magnet should be the ability to economically fabricate large quantities of reliable conductor. The baseline CASK conductor meets this objective. The CASK CDP conductor copper substrate will be reliably joined into long lengths by electron beam (EB) welding. The supplied lengths of monolithic superconducting core will be cold-welded together during conductor assembly and then subsequently placed and soldered into the machined grooves in the substrate. Using this approach, high reliability is achieved since the substrate provides full structural redundancy for every superconductor joint. Also, the superconductor core is essentially fully utilized since the supplied lengths are spliced into continuous lengths during conductor assembly."

The General Dynamics report covering their cost estimate of the CASK magnet [45] showed that the cost of the installed winding using the baseline conductor discussed above and including on-site assembly, soldering and insulation, was approximately  $\$26 \times 10^6$ , of which the composite superconductor itself, not including substrate, was  $\$8.7 \times 10^6$ . This represented the cost for the first unit, not including contingency and profit. Further information on costs of large magnet components is contained in Section 4.2.16.

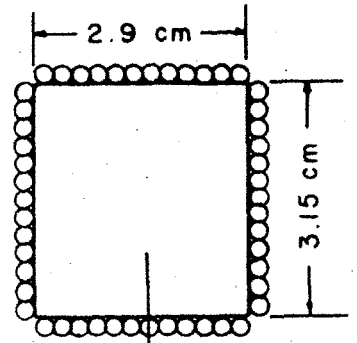


4.1.5A Typical Integrated Substrate Conductor - Aluminum Stabilized NbTi, Soldered Cable



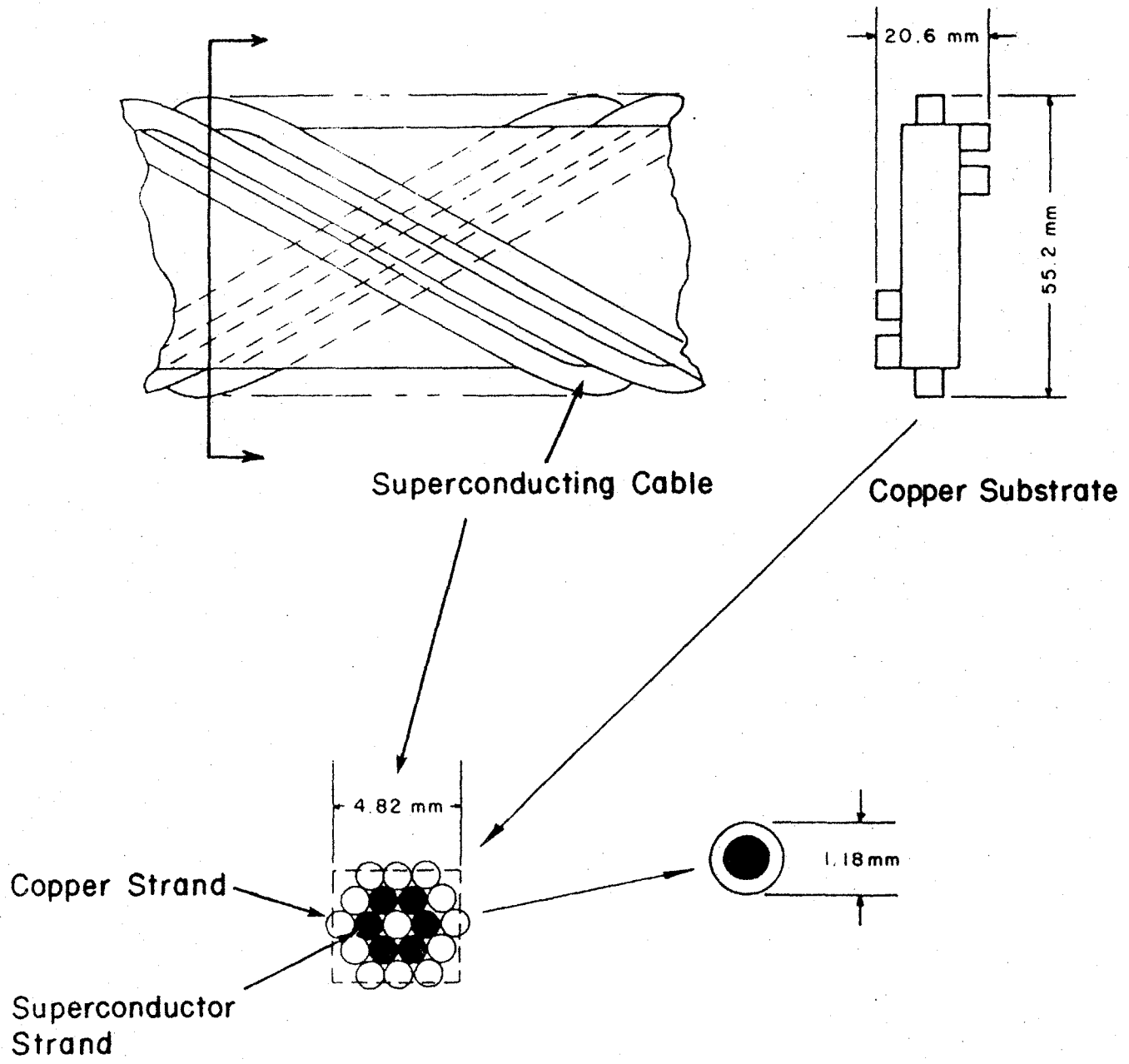


Superconductors Wrapped and Soldered around Substrate

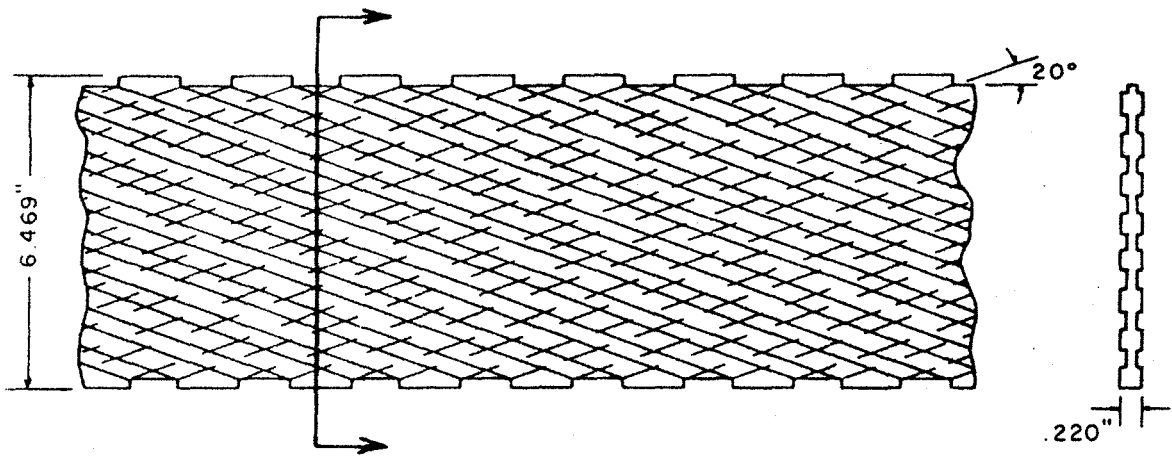


High Purity Aluminum Substrate

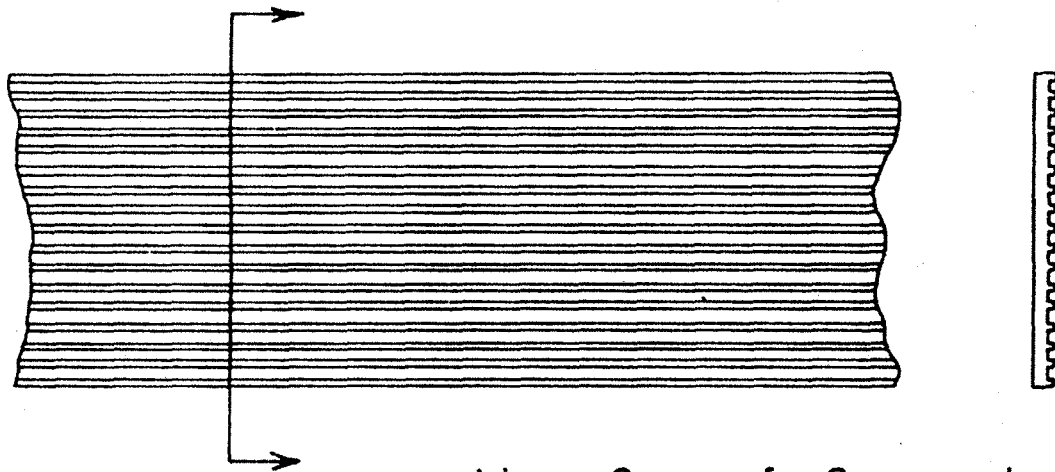
4.1.5B Typical Integrated-Substrate Conductor - Aluminum-Stabilized NbTi, Wrapped Substrate (Soldered)



4.1.5C Typical Integrated-Substrate Conductor - Copper-Stabilized NbTi, Wrapped Substrate

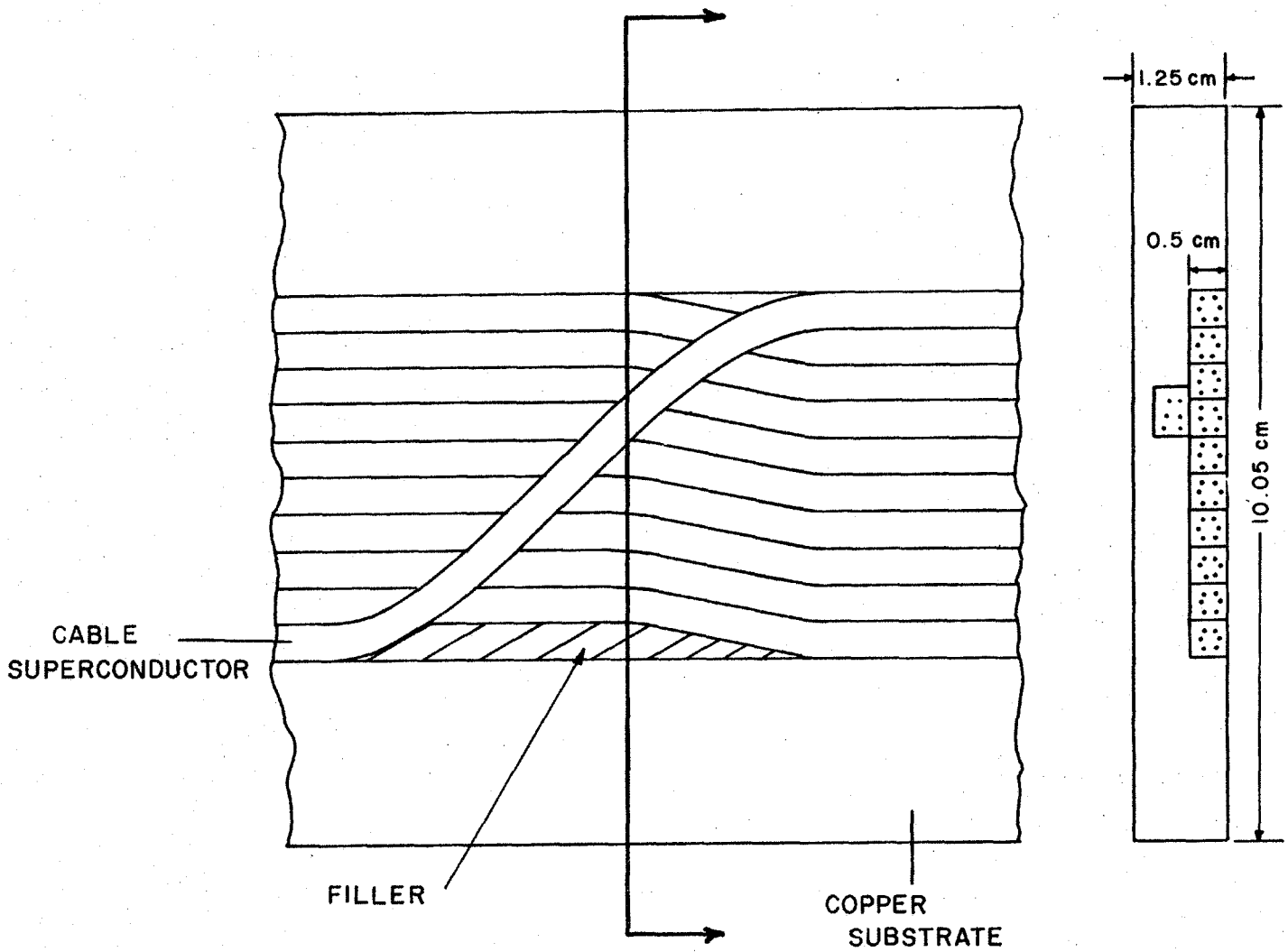


Angled Grooves for  
Transposed Superconductors

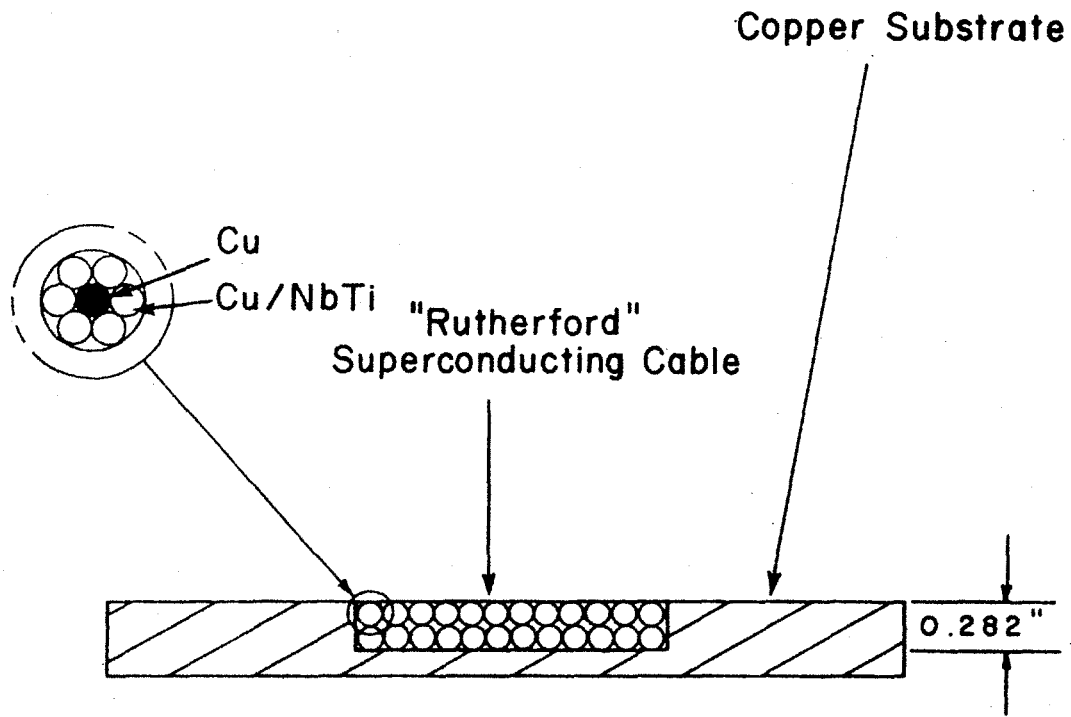


Linear Grooves for Superconductors  
Transposed only at ends

4.1.5D Typical Separated-Substrate Conductor - Copper-Stabilized NbTi, Grooved Copper Substrate (Multiple Channels)



4.1.5E Typical Separated-Substrate Conductor - Copper-Stabilized NbTi, Grooved Copper Substrate, Multiple Cables, Single Channel, Soldered



4.1.5F Typical Separated-Substrate Conductor - Copper-Stabilized NbTi, Grooved Copper Substrate, Single Cable, Soldered

Table 4.1.5-II

Comparison of Baseline Design CASK CDP Magnet Conductor and Scaled-Up CFFF Magnet Conductor

	Baseline (preferred)	Scaled-Up CFFF
Construction	10 - 5.13 mm Square Conductors Soldered in Individual Grooves on Broad Face of Nominal 25 mm × 100 mm Copper Bar. Transposition Occurs During Soldering.	50 - 2 mm Wire Cables Around 1 mm × 46 mm Copper Strip and Soldered in Groove on Broad Face of Nominal 25 mm × 100 mm Copper Bar.
Grading	Can be done by Leaving Out One or More Conductors.	Different Cables with Lesser Number of Superconducting Strands Needed
Joining	Cold Weld or Solder Can Locate Joints in Each Composite Randomly Through Coil	Entire Conductor Must be Done at One Place. Difficult to Stagger Joints Between Individual Wires
Bending	Easily Bent Around Proposed Radii.	Difficult to Bend Edgewise.
Soldering	Minumum Solder Required. More Easily Soldered	Critical - Minimum 5 × More Solder Required. More Difficult Configuration.
Repair	Damaged Pieces Can be Replaced Easily.	More Chance of Damage in Cabling. Difficult to Replace Strands.

#### 4.1.5.3 Development of High Current Cable-Type Conductor, Pool-Cooled

When high current (50 kA) conductor development was initiated in 1977, attention was focused mainly on conductors of the "built-up" type in which composite superconductors were bonded to large normal conducting substrates (copper or aluminum strip) with sufficient surface exposed in well-defined cooling channels to ensure stability. There had been satisfactory experience with this type of conductor in smaller versions [46, 47]. Furthermore, this type of conductor possessed mechanical properties which made it possible for bundles of conductors to withstand accumulated magnetic compression loading, which was not the case with the cable-type conductor.

The simple (unsoldered) cable conductor, while obviously easy to manufacture and wind into saddle shape, was given only secondary consideration because background experience was lacking, its ability to carry compressive loads was limited and its stability in large sizes (where outside surface-to-volume ratios would be low) was in question.

The cable as a pool-cooled high current conductor became the subject of more serious interest in 1979 and 1980, for reasons including the following:

1) A new type of substructure was developed in conjunction with the CDIF/SM and CSM magnet designs in which conductors were individually supported. This favored cable because cumulative loading was eliminated.

2) High current built-up types of conductors were expected to be relatively expensive to fabricate and wind.

3) During the development of internally-cooled cable superconductors (which was underway at MIT as reported in Section 4.1.6 of this report) it was found experimentally that a twisted cable of composite superconducting wires enclosed in a sheath would operate satisfactorily with much lower coolant flow velocities than originally predicted. Near maximum current-carrying capacity was demonstrated in the pool-cooled mode.

In 1980 and 1981, tests were run at MIT on a single turn of NbTi/copper composite cable superconductor in a background field, supported in a test fixture simulating the CDIF/SM substructure [48]. Results showed that recovery from disturbances occurred at heat fluxes on the order of  $0.1 \text{ W}\cdot\text{cm}^{-2}$  and that stability was a weak function of void fraction (ratio of liquid helium volume to conductor volume). Overall results indicated that high current cable conductor deserved further consideration.

Later in 1981, a larger cable conductor was tested as an alternative to the built-up conductor which had been established as the baseline conductor for the CDIF/SM magnet described in Section 4.3.1. A single-layer experimental coil of cable conductor was installed in the MHD test facility, mounted in the gap of the 6 T split-pair racetrack test magnet. Also mounted in the gap was a single-layer experimental coil of CDIF/SM built-up conductor. Both experimental coils had a copper-to-superconductor ratio of 9.2 and a current-carrying capacity of 9600 A at 7 T. It was found that the cable conductor would recover fully from a disturbance at a heat flux of  $0.025 \text{ W}\cdot\text{cm}^{-2}$  or lower with a current of 6250 A and 5.5 T. Tests at higher currents and heat fluxes showed partial recovery at 7050 A and  $0.03 \text{ W}\cdot\text{cm}^{-2}$  and normal zone propagation at 7280 A and  $0.034 \text{ W}\cdot\text{cm}^{-2}$ . Heat fluxes for the cable conductor were calculated based on 100 % surface cooling of each strand.

Test data on the CDIF/SM baseline conductor showed similar but somewhat superior performance as regards current levels for full recovery, partial recovery and propagation.

The tests on the CDIF/SM size cable confirmed that cable conductors are a viable option for large MHD magnets, although further work is needed to fully characterize cable performance.

Preliminary designs were prepared for cable conductors for the CSM baseload-scale magnet and the ETF 200 MW MHD Power Plant magnet. The CSM design called for a 52 kA cable, 4.4 cm in outside diameter as shown in Figure 4.1.5G. Design heat fluxes were in the neighborhood of  $0.03 \text{ W}\cdot\text{cm}^{-2}$ , assuming all strands are 100 % surface cooled. Most recent studies show that a slightly larger copper cross section may be necessary. These cable designs are described in more detail in Sections 4.2.6 and 4.2.12 of this report.

#### 4.1.6 Development of Internally-Cooled Cable Superconductor

Development of internally-cooled cable-type superconductor (ICCS) has been underway since 1974. Major emphasis has been placed on the concept in which state-of-the-art copper-stabilized niobium titanium and niobium tin superconductors in the form of conventional cables are enclosed in vacuum-tight metal conduits. Supercritical helium is circulated in the conduit to provide cooling of the cable.

The encapsulated conductors can be rolled to a square cross section, fully insulated on the outside and wound into coils in the manner of conventional hollow, water-cooled copper conductors. Internally-cooled conductors are considered advantageous for use in large, high-current coils including tokamak and mirror reactor magnets, MHD magnets and energy storage magnets.

Early in the program, two types of hollow conductor were considered. In the first, superconducting wires were wrapped around the outside of a metal tube containing helium and were cooled by conduction through the walls of the tube, as in the conductor developed at CERN (Reference 49). This type of conductor is shown in Figure 4.1.6A. In the second, a superconducting cable was enclosed in a metal conduit containing helium in intimate contact with the strands of the cable, as shown in Figure 4.1.6B.

Investigations showed that application of the first type to high current, high field magnets was not practical because with the limited heat transfer surface available, it was necessary to circulate helium at high velocity to ensure conductor stability. The fluid friction associated with the high velocity caused excessive pumping losses.

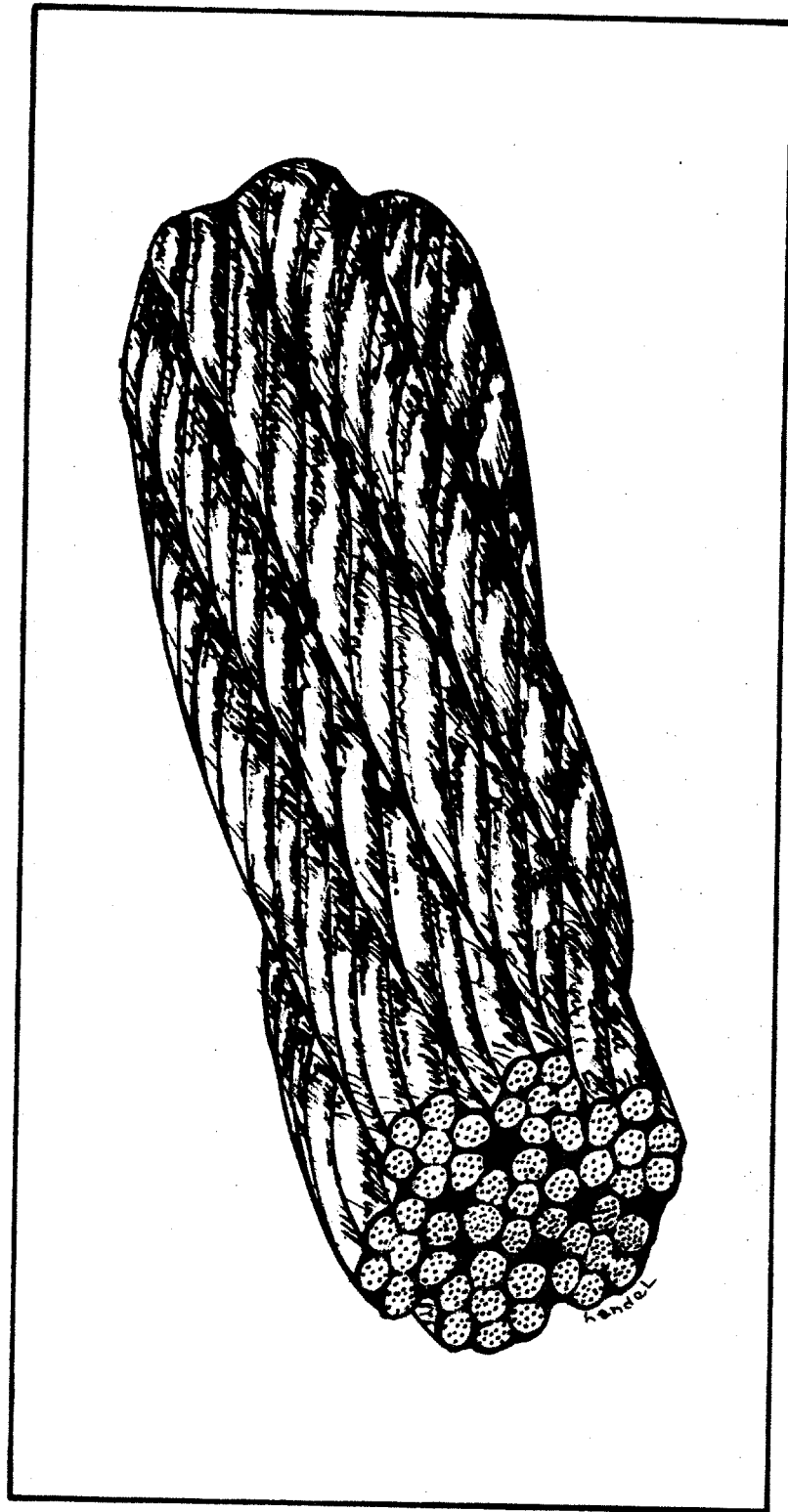
The second type was found to be practical, because the very large conductor surface area exposed to helium made it relatively easy to ensure conductor stability. It was also discovered that forced flow (pumped circulation) was not required to achieve high heat transfer coefficients required for good stability. It was first found experimentally and later proven analytically that local thermal perturbations create very high velocity pressure waves and local turbulence creating heat transfer coefficients comparable to those achieved with nucleate boiling. This very important discovery eliminated the major drawback of these conductors which was the anticipated large pumping power required for "forced flow." Another early concern was that a large amount of heat might be generated by the physical compaction of the cable under the influence of Lorentz forces. This Lorentz compaction heating was measured and found not only to be small but energizing rate dependent and therefore controllable (particularly for dc MHD applications). It was thus determined that only a modest amount of helium circulation would be required during energization of a large ICCS magnet and once at operating field, circulation could be virtually eliminated (assuming appropriate thermal intercepts for radiation heat loads). These findings together with the obviously good mechanical properties of the ICCS conductor make it a very promising candidate for large superconducting magnets.

An analytical model of the internally-cooled conductor was developed and programmed for computer analysis. Use of the program confirmed that the enclosed cable-type conductor was superior to the wrapped-tube type for large, high field magnets.

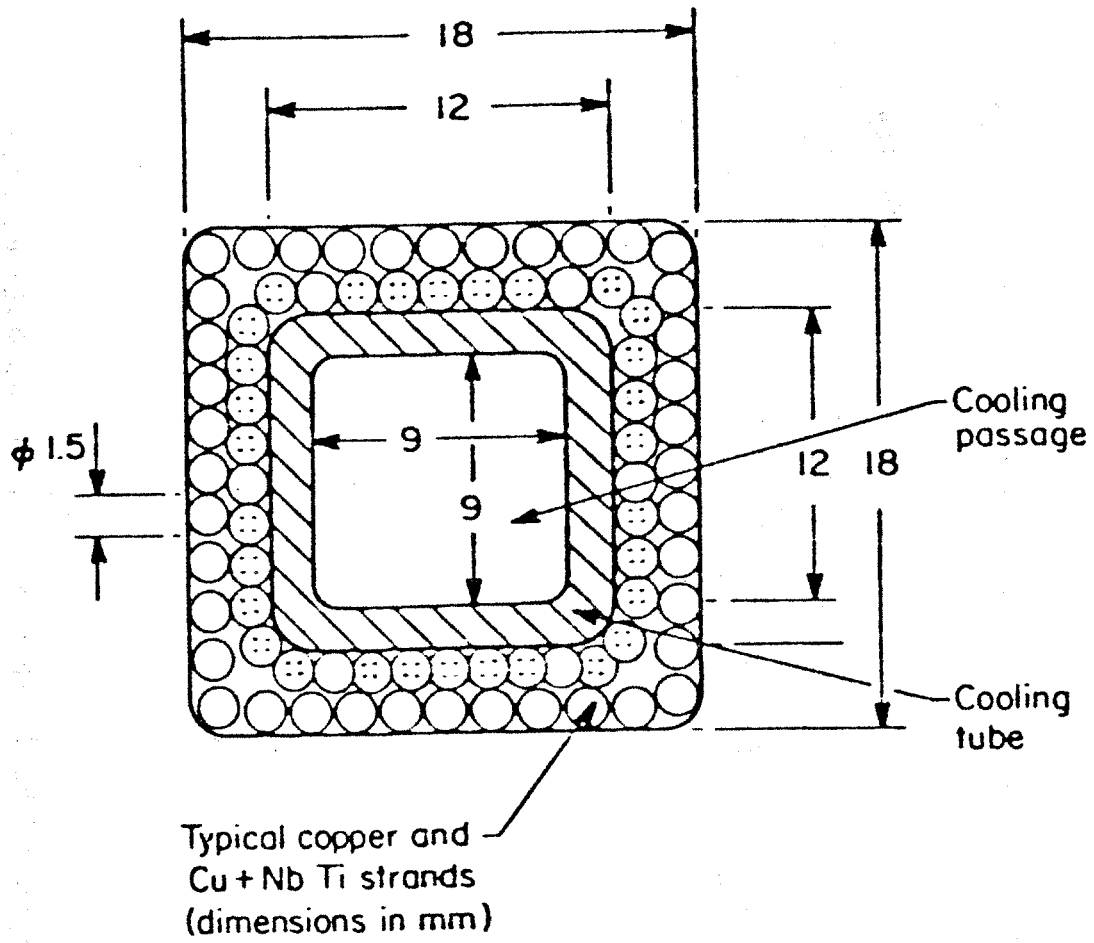
Experiments were performed with NbTi superconductors in a simulated cable configuration. The test apparatus is shown in Fig. 4.1.6C. Thirty 1 mm strands of Formvar-insulated copper-stabilized NbTi wire were wound into a rectangular helical groove machined into the surface of a mica cylinder. The strands were connected noninductively in series. A tightly fitting outer sheath was installed to enclose the helical cooling passage. The test specimen (1), enclosed in the liquid helium filled test dewar (2), was located in the bore of the 15 cm ID water-cooled 9 T Bitter magnet (3). Helium for force-flow cooling the test specimen was delivered from a standard pressure bottle (9) via a liquid nitrogen precooling bath (5), a coaxial transfer line (4) which acted as a counterflow heat exchanger to further precool the incoming helium and a heat exchanger (6) submerged in the 4.2 K liquid helium bath surrounding the test specimen.

In the experiment a large, square current pulse was introduced through the conductor strands. The pulse was followed by a predetermined current of a smaller amplitude and longer duration. The initial current pulse provided energy to raise the conductor temperature, intentionally causing a thermal instability. Flow through



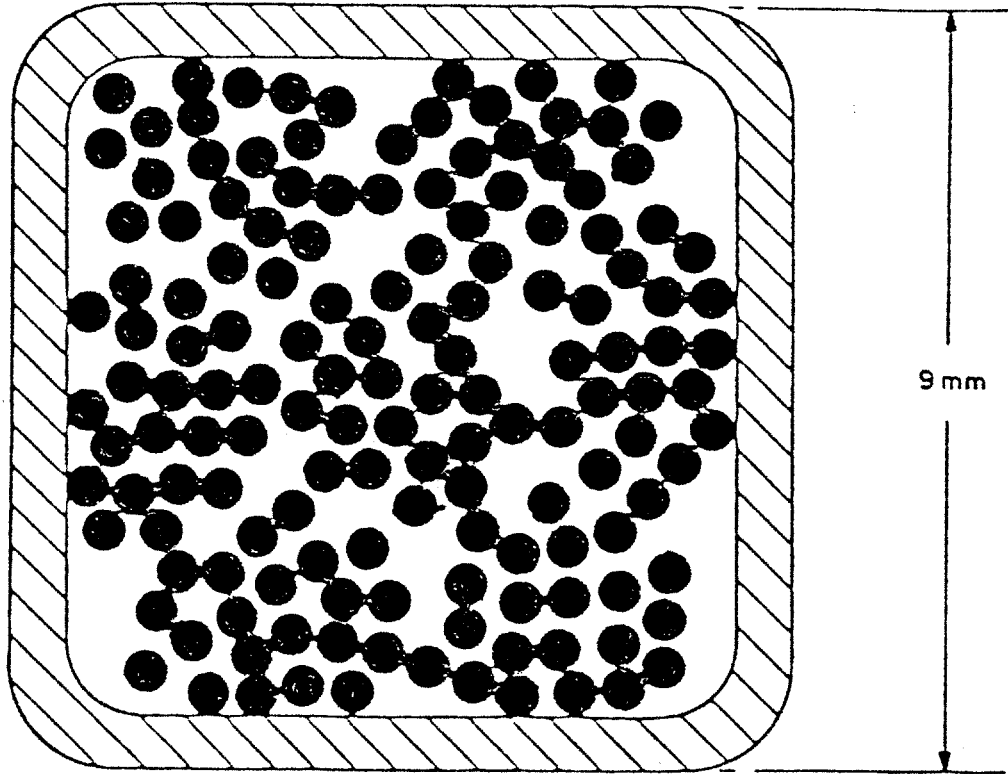


4.1.5A Typical Integrated-Substrate Conductor - Aluminum-Stabilized NbTi, Soldered Cable



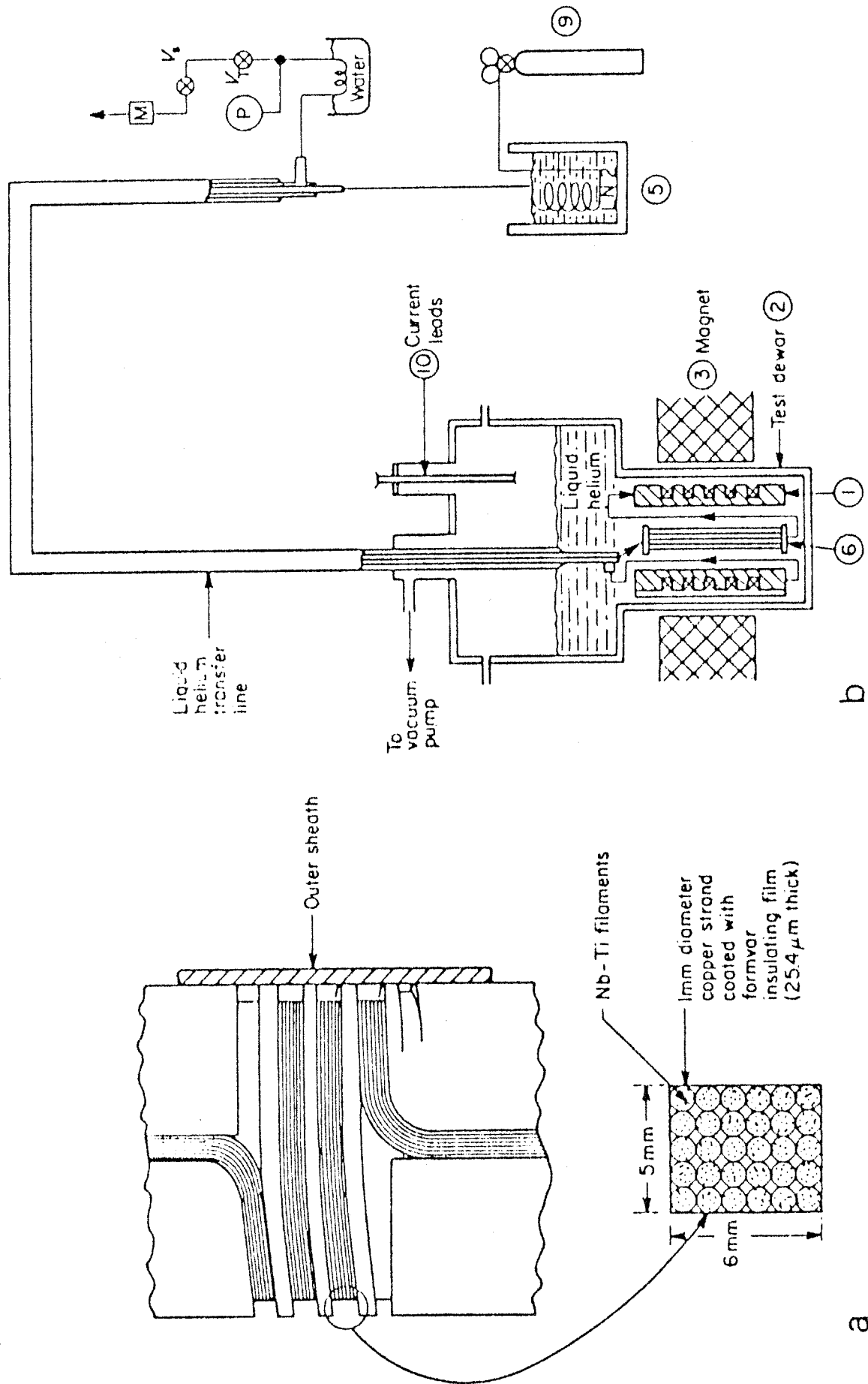
4.1.6A

Cross Section of Internally-Cooled Superconductor of Type Developed by CERN



4.1.6B Cross Section of Internally-Cooled Superconductor of Type Developed by MIT

4.1.6C Diagram of Test Apparatus for Simulated Internally-Cooled Cable Conductor



the conductor was initiated prior to the current onset. Data were taken at various flow rates and magnetic fields. Recovery, indicated by the voltage across the conductor dropping to zero, was found to be dependent on initial heating, flow rate and the second stage current amplitude.

All relevant experimental results have been plotted in Fig. 4.1.6D together with "short-sample" test data and computer-predicted recovery curves for given flow velocities. The experimental points indicated by squares are test recovery points. The experiments indicated a definite effect of flow on stability as well as a general agreement between experimental results and computer prediction.

Additional experiments were conducted using a closed loop helium system with bellows-type circulating pump, test coils made with NbTi/Cu cables encapsulated in round cross section metal tubes and a pulse coil to inductively heat the test coil. Figure 4.1.6E is a photograph of the test apparatus used for testing small coils of ICCS. Typical results are shown in Figure 4.1.6F. The conductor was a  $3 \times 19$  NbTi/Cu cable with 1.05 mm strand diameter enclosed in a 12 mm O.D. stainless steel tube.

A one-meter-scale test coil of internally-cooled conductor was made and tested with a background field of 8 T provided by a split-pair of superconducting solenoids. The test coil was wound using a 20 m length of 12 mm O.D. aluminum encapsulated NbTi/Cu cable,  $3 \times 19$ , with 1.05 mm strand diameter. The critical current rating of the conductor was 6800 A at 5 K and 7 T. Figure 4.1.6G is a photograph of the one-meter-scale test coil mounted in its test support frame with the split-pair background field solenoids.

Steady-state operations of the test coil were performed at 89% of its quench current of 6702 A (7 T) at a temperature of 5 K. The coil was operated at reduced helium velocity (6.6 vs 18  $\text{cm s}^{-1}$ ) to evaluate the effect of flow reduction. No change in stability was observed.

Development of internally-cooled cable superconductors using  $\text{Nb}_3\text{Sn}$  was started in 1976.

Small ICCS test coils similar to those used for NbTi tests (see Figure 4.1.6E) were fabricated. The conductor was copper matrix  $\text{Nb}_3\text{Sn}$  wire in a  $19 \times 3 \times 1.05$  mm cable configuration with 0.43 mm stainless steel tube. Critical current tests were conducted without flow.

Initial quench occurred at approximately 105% of short sample current. Operating conditions were 9.0 T, 4.2 K, 8000 A critical current. Stability tests were conducted at 5800 A, 9.0 T, initial pressure 3.0 atm, initial temperature 4.2 K, helium flow 0 to 36  $\text{g cm}^{-2}\text{s}^{-1}$ . Results are shown in a plot of critical pulse energy vs flow, Figure 4.1.6H.

A program to develop manufacturing technology for  $\text{Nb}_3\text{Sn}$  ICCS was carried out by MIT. Because activation of  $\text{Nb}_3\text{Sn}$  conductor (at temperatures of 700 to 800°C) after encapsulation is generally required, an aluminum alloy sheath is not practical. Manufacturing developments at Kabelmetal and at Airco, Inc. were undertaken to provide facilities for the continuous process encapsulation of  $\text{Nb}_3\text{Sn}$  cable in a stainless steel sheath. Airco's facility has demonstrated the capability to encapsulate and draw down a 2 cm diameter cable and square it to a  $2 \times 2$  cm product as shown in Figure 4.1.6J.

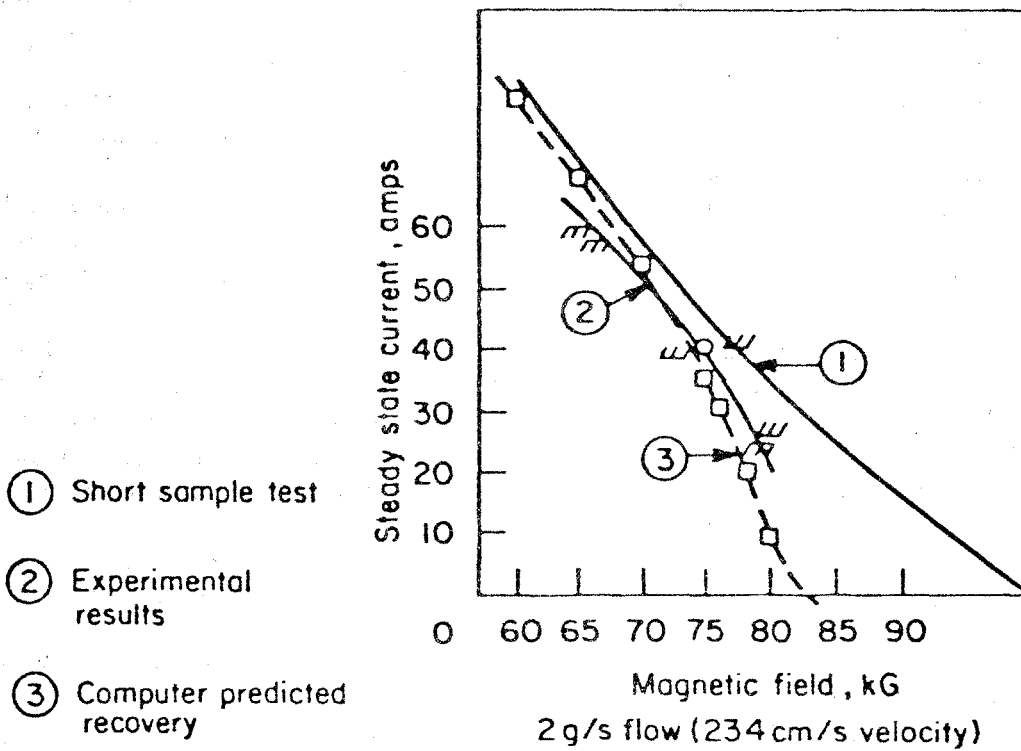
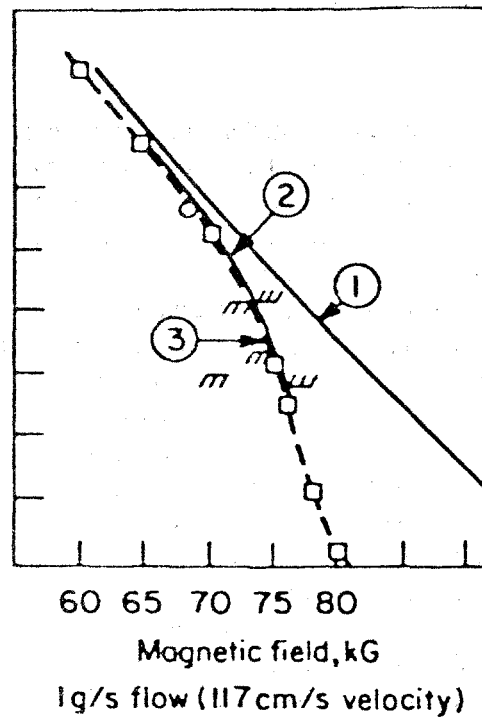
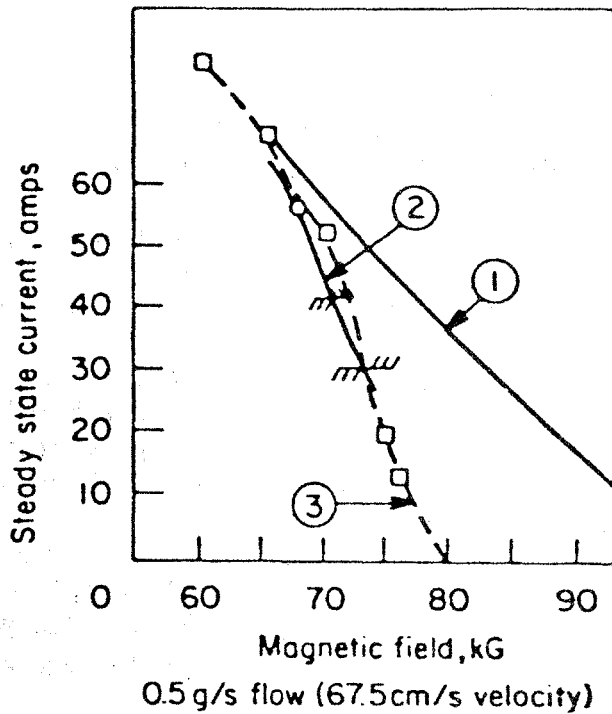
Problems of coil fabrication with  $\text{Nb}_3\text{Sn}$  ICCS have been investigated. Shear and compression tests have been performed on 2.54 cm square ICCS individual conductors and laminated arrays. Terminations for high current cable conductors are under development.

Under DOE auspices, starting in 1978, work has been sponsored on computer-aided analysis of stability and the quench phenomenon in ICCS.

An oval-shaped one-meter-scale test coil associated with the development of ICCS for large MHD magnets has been designed and fabricated. It is now nearly ready for test, but work is held up because of lack of funds. This coil, known as the "football" coil is shown in Figure 4.1.6K. It is a double pancake coil wound with a  $2 \times 2$  cm stainless-steel-sheathed NbTi ICCS and designed to demonstrate that heavily-sheathed ICCS is intrinsically self-supporting under magnetically-induced tension loading. Testing planned for this coil is described in Section 4.1.2.

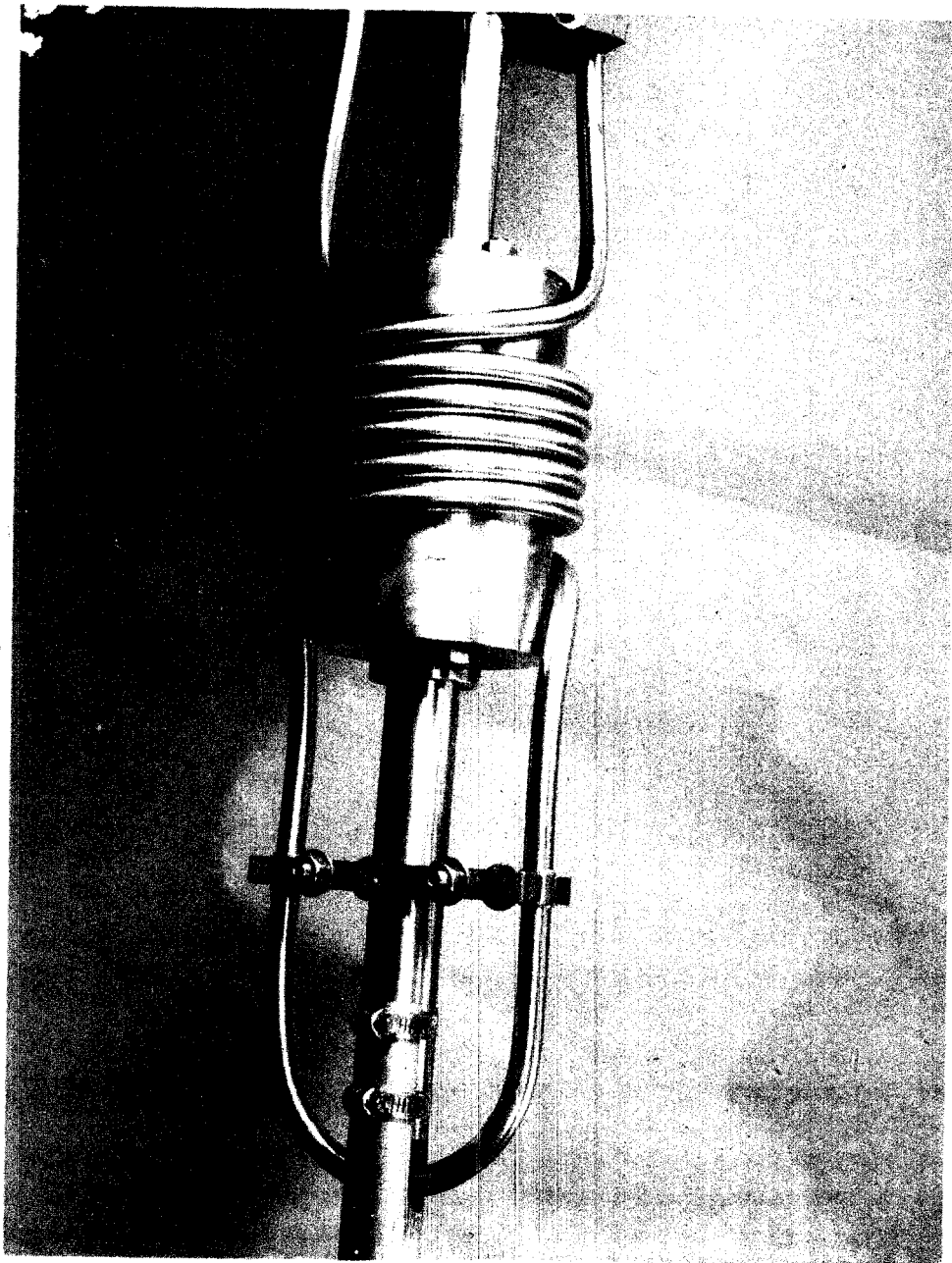
A 1 m diameter 15 kA solenoid is now being constructed under DOE Fusion sponsorship. It incorporates  $2 \times 2$  cm stainless-steel-sheathed  $\text{Nb}_3\text{Sn}$  ICCS and is designed to operate at 12 T.

Further information on ICCS is contained in Reference 23.

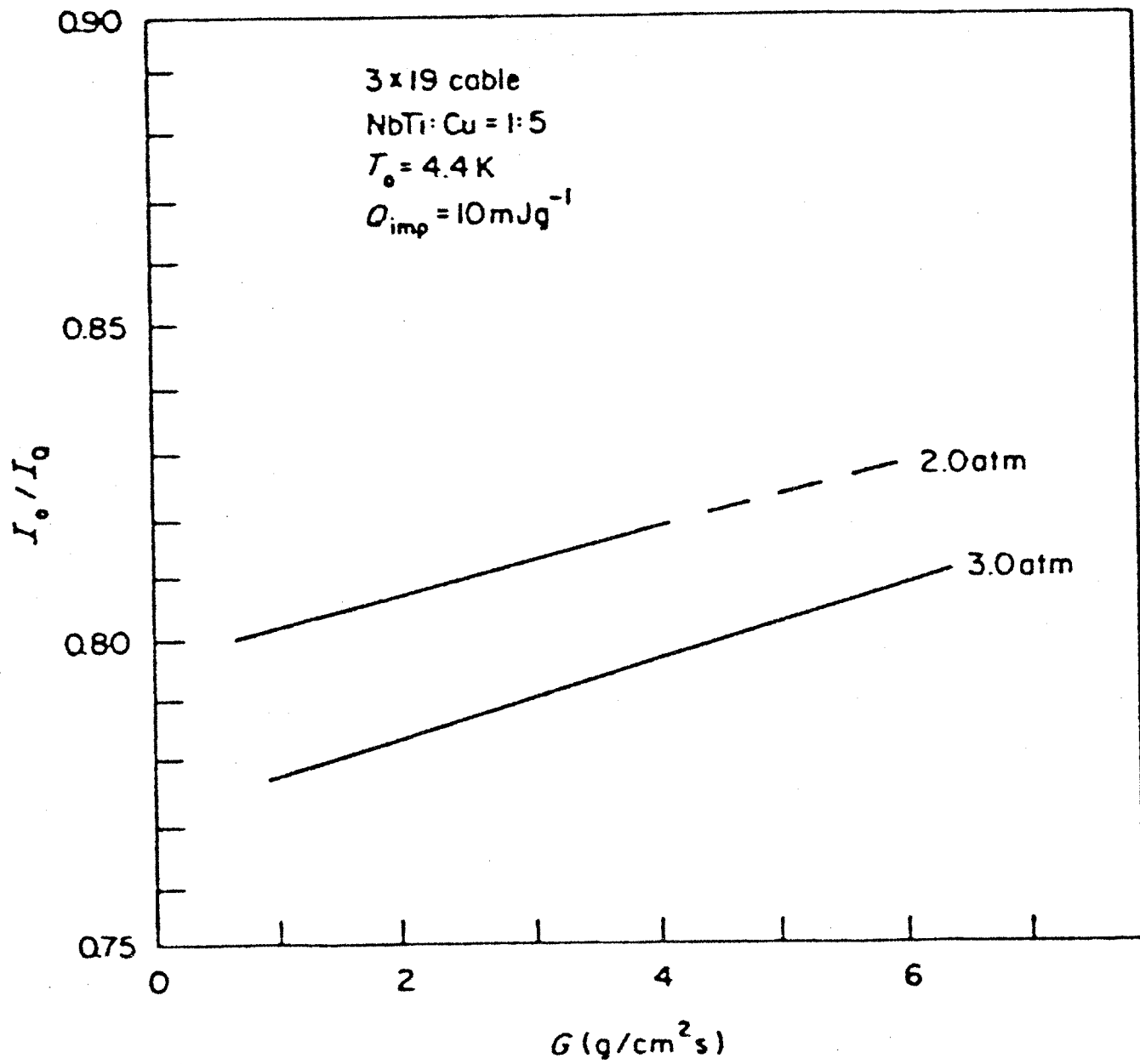


- ① Short sample test
- ② Experimental results
- ③ Computer predicted recovery

4.1.6D Plots of Experimental and Computer-Predicted Results in Internally-Cooled Superconductor Investigation

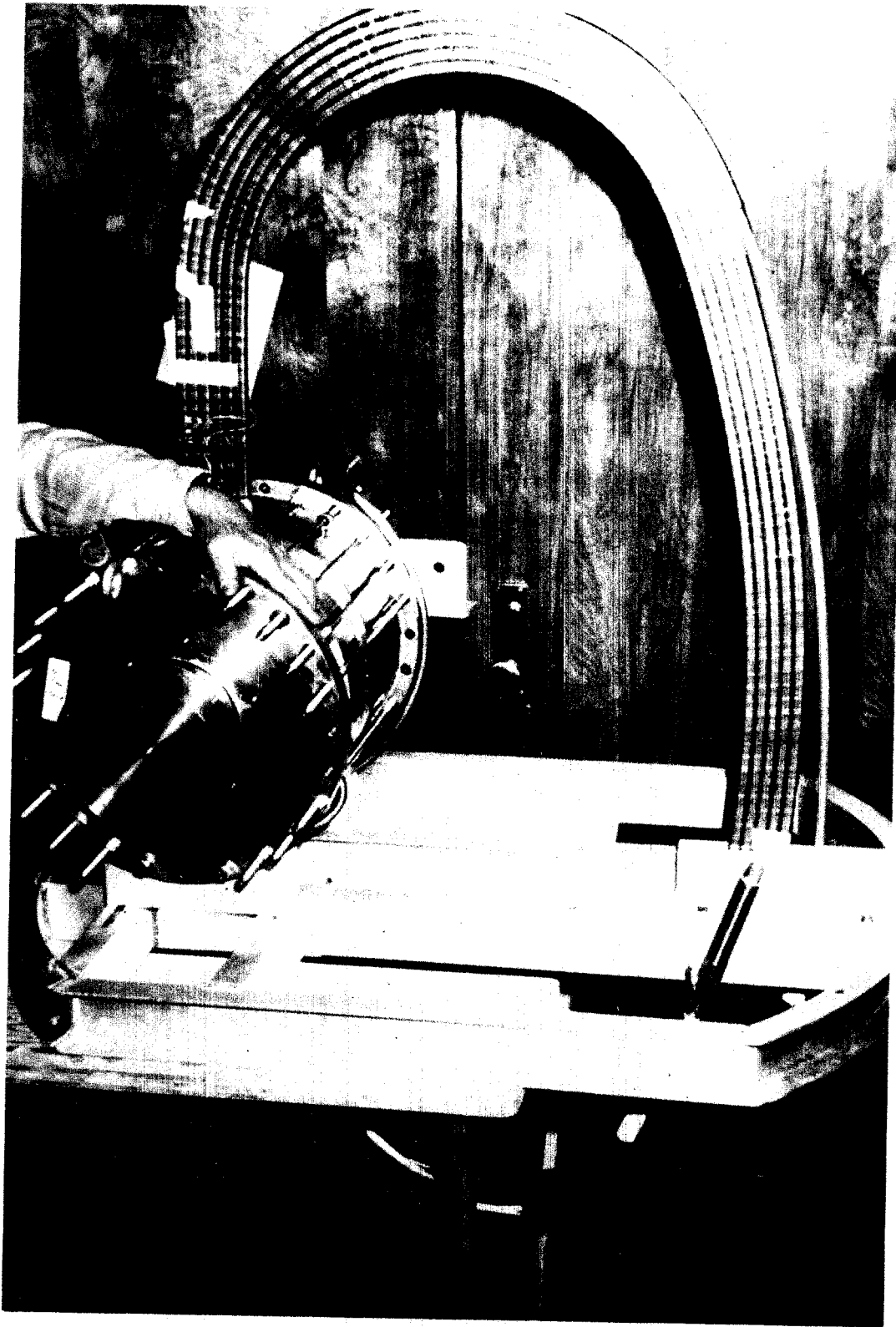


4.1.6E Photograph of Apparatus for Testing Small Coils of ICCS

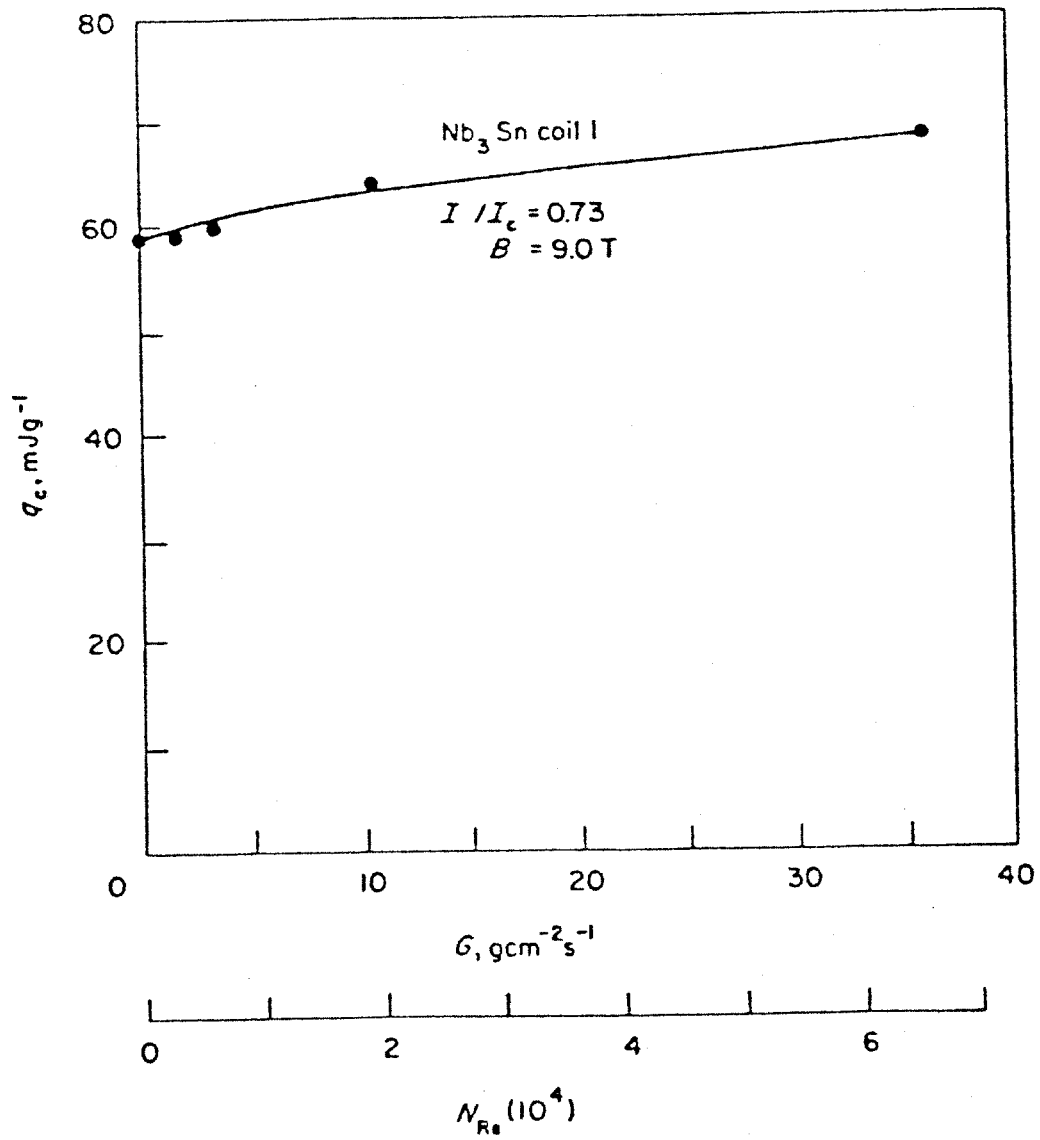


4.1.6F Plot of Recovery Current at 8 T as a Function of Flow Rate for a Given Pulse Energy Input

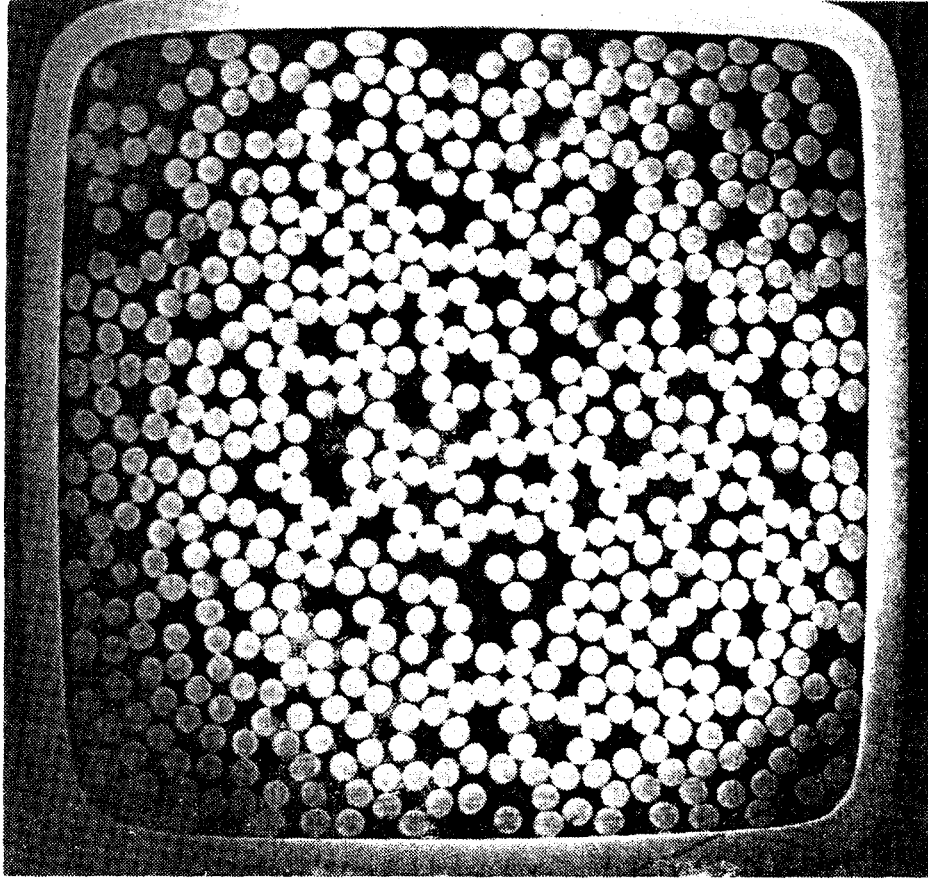




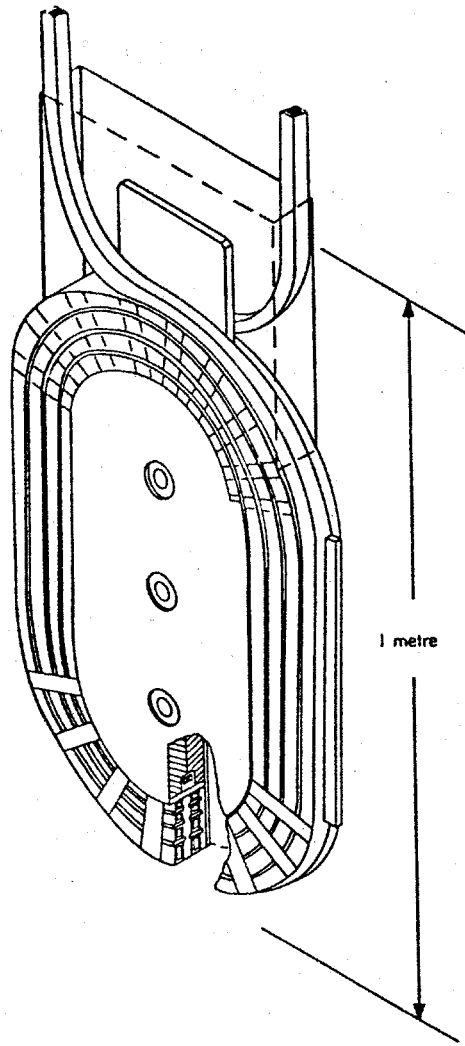
4.1.6G Photograph of One Meter-Scale ICCS Test Coil Mounted in Test Support Frame



4.1.6H Plot of Critical Pulse Energy vs. Flow for Small Nb<sub>3</sub>SN ICCS Test Coil



4.1.6J Photograph of Cross Section of  $2 \times 2$  cm 486 Strand  $\text{Nb}_3\text{Sn}$  ICCS



4.1.6K Sketch of ICCS "Football" Coil

#### 4.1.7 Analysis and Development of Superstructure

The structure required to support the winding of MHD magnets against magnetic forces, referred to here as superstructure, is a major component in the magnet system. Outward forces on coil bundles along the middle portion of a large MHD magnet are of the order of millions of kilograms per meter length. The superstructure as a whole is one of the largest system components in terms of weight and cost. It is also critical to safe operation and reliable performance of a magnet.

Conceptual designs for superstructure were investigated and analyzed from the start of the MHD magnet program. Much of this work was done in conjunction with investigations of winding configurations, because superstructure design concepts and winding shapes are closely interrelated. Winding/structure configurations considered included the following (References 44, 46, 50, 51, 52, 53, 54):

Circular saddle coils with ring girders

Circular saddle coils with crescent-shaped girders

Circular saddle coils with stiff central bore tube and tension banding around windings

Rectangular saddle coils with rectangular structural frames (beams and tension straps or tie rods)

Rectangular saddle coils with tension straps around winding

The above winding/structure configurations are incorporated in magnet designs described in Sections 4.2 and 4.3.

A study of MHD magnet structural optimization was made, considering typical structures (ring girders and rectangular frames) for both circular and rectangular saddle coil magnets (Reference 55). The possibility of developing an all-tension structure, more efficient than conventional "beam-type" structures, was explored. A subcontract was placed with Battelle Memorial Institute to analyse this approach, and a report was issued (Reference 56). The results of this study were embodied in the magnet conceptual design described in Section 4.2.7.

In an effort to obtain industry input in solving structural problems, an RFP for superstructure conceptual design and development was issued. Proposals were received from the following organizations:

Beech Aircraft Corp.

Littleton Research and Engineering Corp. with Sun Shipbuilding and Drydock Co.

Avco Everett Research Laboratory Inc. with Avco Systems Division

Magnetic Engineering Associates Inc. with Allis Chalmers Corp.

General Atomic Co.

Combustion Engineering Inc.

Chicago Bridge and Iron Co.

Westinghouse Electric Corp.

Several proposals contained innovative ideas for superstructure designs and for combination substructure/superstructure designs. Because of funding limitations, it was not possible to place contracts with any of the proposers.

Testing of materials for magnet superstructures is described in Section 4.1.11. A survey of materials for superconducting MHD magnets is discussed in Section 4.1.13 and the development of structural standards for MHD magnets is discussed in Section 4.1.14.

#### **4.1.8 Substructure and Winding Development**

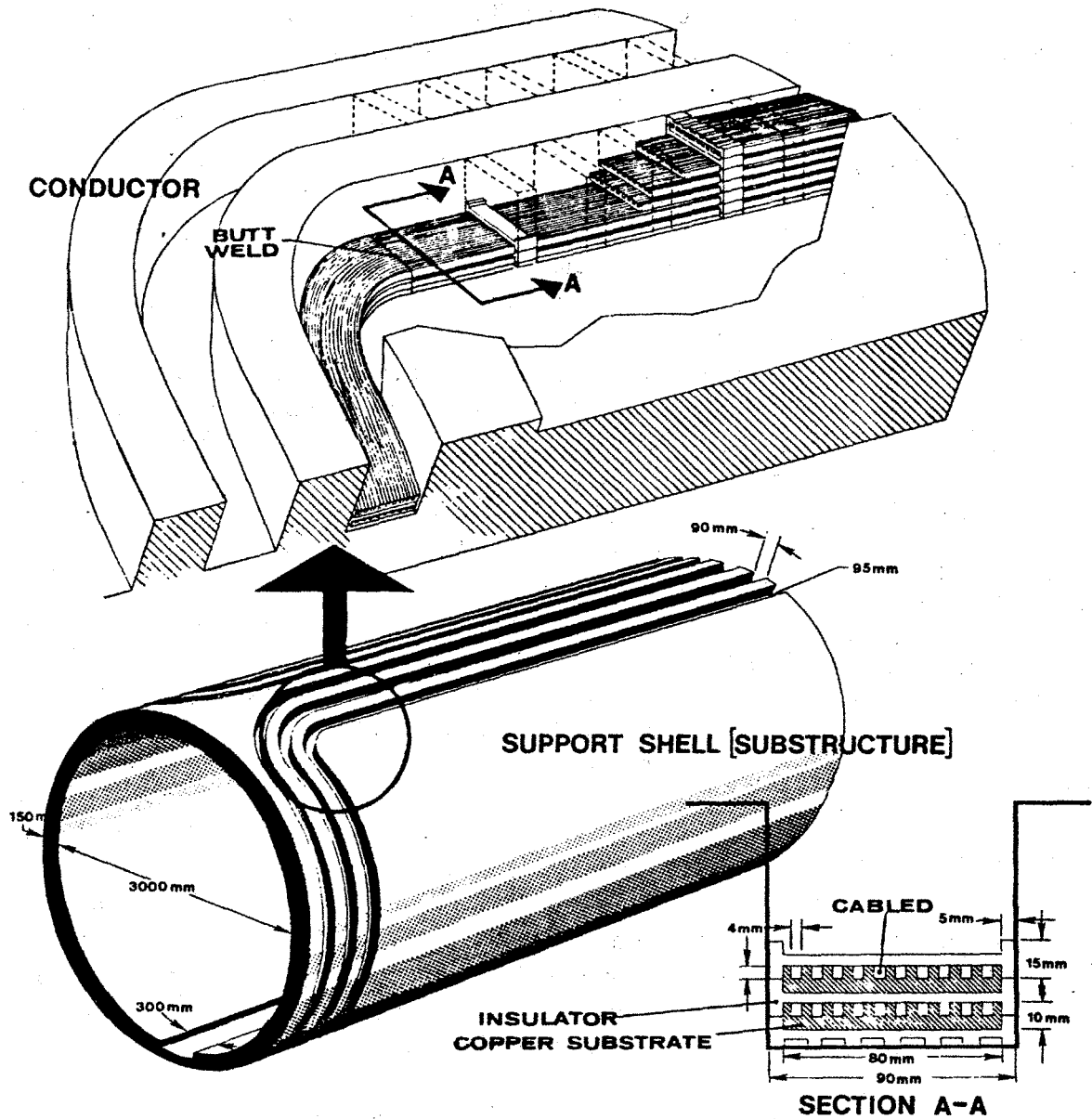
Substructure and winding development was carried out for both circular-saddle and rectangular-saddle configurations. The approach used was to examine the demands of baseload magnet construction, to review and evaluate existing baseload magnet reference designs [57, 58], to develop improved designs and winding methods and to propose means for proof-testing the concepts developed using partially-scaled models (winding model magnets). It was established at the outset that the development would be based on using 50 kA conductor wound into a substructure designed to support groups of conductors in such a manner that the groups would not be exposed to accumulated Lorentz loading from other groups.

Requests for proposal were issued to potential subcontractors for a three phase program. Phase I covered an evaluation of full scale magnet design concepts and winding methods and the conceptual design for the winding model magnet, Phase II the detailed design of the winding model magnet, and Phase III fabrication of a winding model magnet to be tested at MIT. The baseline concept issued by MIT with the request for proposal is shown in Figure 4.1.8A. Orders were placed with three subcontractor teams (GE/IGC, MCA/CE, GD/MEA) for Phase I studies. An extension was given to GD/MEA to further investigate their concept, called CASK, including preparation of a reference design for a full-scale magnet (see Section 4.2.5). No orders were placed for detail design and construction of circular-saddle winding model magnets (Phases II and III). The substructure and winding schemes which evolved under the subcontracted study programs are described in Subsections 4.1.8.1, 4.1.8.2 and 4.1.8.3.

For the rectangular-saddle configuration, a substructure and winding concept was developed at MIT, in which conductors are individually supported in a grooved substructure so designed that all magnetic loads are transmitted via substructure to the main force-containment structure without subjecting conductors to any accumulated loading. Alternate substructure materials, both metal and reinforced plastic, were considered. Testing was conducted to determine the mechanical properties of candidate reinforced plastic materials (see Section 4.1.12). A scaled-down version of this concept was tested successfully in the MIT Test Facility Magnet (see Section 4.1.2). The concept was incorporated in the CDIF/SM magnet described in Section 4.3.1, in the commercial scale magnet design (CSM) described in Section 4.2.6 and in the ETF magnet design described in Section 4.2.13.

##### **4.1.8.1 GE Substructure and Winding Studies**

The GE Phase I report focused on a conventional circular-saddle magnet configuration. The design recommended used a separated substrate conductor geometry with the conductor wound on forms and then placed in aluminum substructural shells. The concept proposed was considered by the MIT review board to be insufficiently innovative compared with those of other contractors (reported in Sections 4.1.8.2 and 4.1.8.3) to warrant further work.



4.1.8A Baseline Concept for Substructure and Winding Development, Circular Saddle MHD Magnet

#### 4.1.8.2 MCA Substructure and Winding Studies

In the report of the Phase I Study by MCA [59] two full-scale winding and structure concepts were described and compared, after which a winding model configuration was proposed for testing candidate conductor and insulation systems for use in the full-scale windings.

The first of the full-scale concepts was an innovative variation of the stacked shells circular-saddle concept used in AVCO's reference design described in Section 4.2.3. The MCA concept, sometimes referred to as the truncated shell concept, is illustrated in Figure 4.1.8.2A. The substructure consists of an array of flat-sided half-shells with arched crossovers nested together to form one half of the magnet winding. A single half-shell with typical slots for conductor is shown in Figure 4.1.8.2B, and the force containment structure concept is shown in Figure 4.1.8.2C. Stainless steel was the preferred material for both substructure and superstructure. A conductor and insulation system such as that shown in Figure 4.1.8A could be installed in the slots in the half-shells. A unique feature of the MCA scheme is that flat plates make up the entire straight section of the saddle winding substructure, instead of conical shells as shown in the AVCO design or cylindrical shells shown in Figure 4.1.8A. Curved (cylindrical) plates are used for the crossover segments at the ends of the winding only.

The MCA concept results in a substructure that should be much easier to fabricate and to assemble than the cylindrical or conical shell designs. It is easier to machine grooves in flat plates than in cylindrical or conical shells and it is easier to obtain close fits, shell to shell, when the shells are mainly flat surfaces rather than all curved surfaces. Material is saved in the MCA scheme by omitting the central portion of the substructure shells, and by providing a more efficient superstructure configuration in the middle portion of the winding (the configuration is more efficient because the beam span is smaller). A significant reduction in overall magnet cost is predicted for the MCA concept as compared to the cylindrical or conical shell concept.

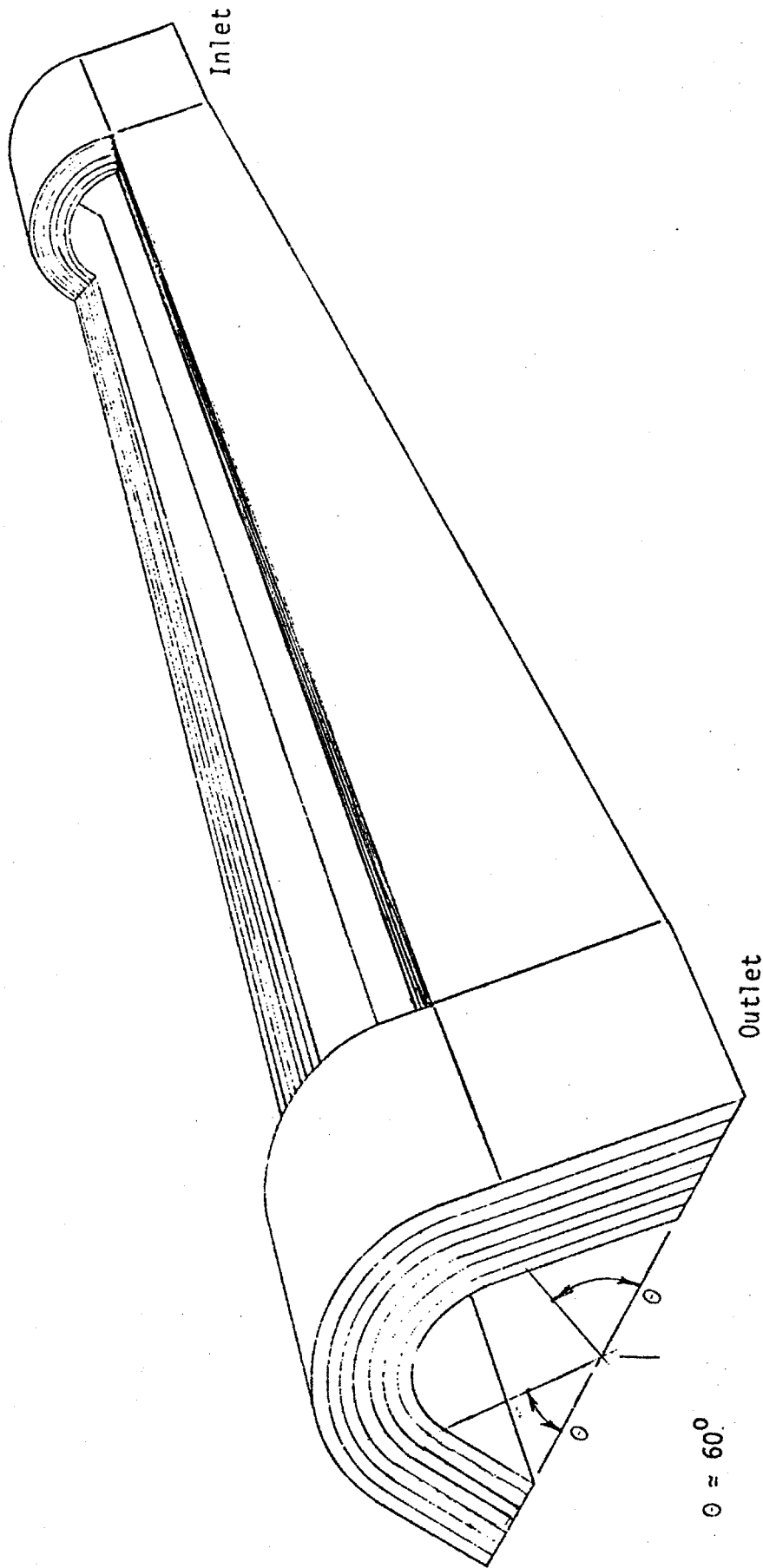
The second full-scale concept was the flat plate racetrack rectangular-saddle concept developed earlier by MCA as a part of the reference design program and described in more detail in Section 4.2.2. In this concept, the winding consists of six racetrack coils and two 90° saddle coils, each in its own close fitting stainless steel coil containment vessel, arranged as shown in Figure 4.1.8.2D. The proposed conductor and the stainless steel channel which encloses the conductor and forms the substructure are shown in Figure 4.1.8.2E. A midplane section depicting the coils supported in the flat plate stainless steel superstructure is shown in Figure 4.1.8.2F.

A comparison of the two concepts was made by MCA. It was concluded that both concepts were feasible from the manufacturing standpoint and both were viable from the shipping and handling standpoint. The estimated weight of superstructure and substructure was 1,556,000 kg for the flat plate concept and 4,976,000 kg for the modified circular-saddle concept (a factor of 3.2 higher). A part of the difference can be attributed to the larger bore of the modified circular-saddle concept, which was a circle 2.25 m in diameter at the inlet vs a square 1.59 m on the side for the flat plate concept. It is also important to note that while neither design was optimized, MCA had expended more design effort on the flat plate concept.

Consideration was given by MCA to aluminum alloy as an alternative to stainless steel in the modified circular-saddle design. Taking into account the thickness of plate required and the need for good weldability and good low temperature properties, alloy 5083-0 was chosen. It was noted that the yield strength of the aluminum alloy was 30.5 ksi compared to 112 ksi for annealed stainless steel (Type 310). Therefore, it was concluded that allowable (design) stresses for 5083-0 alloy would be too low to make the material an attractive alternative to stainless steel. Furthermore, it was determined that stainless steel was a much better match for the conductor than aluminum alloy from the standpoint of thermal stress.

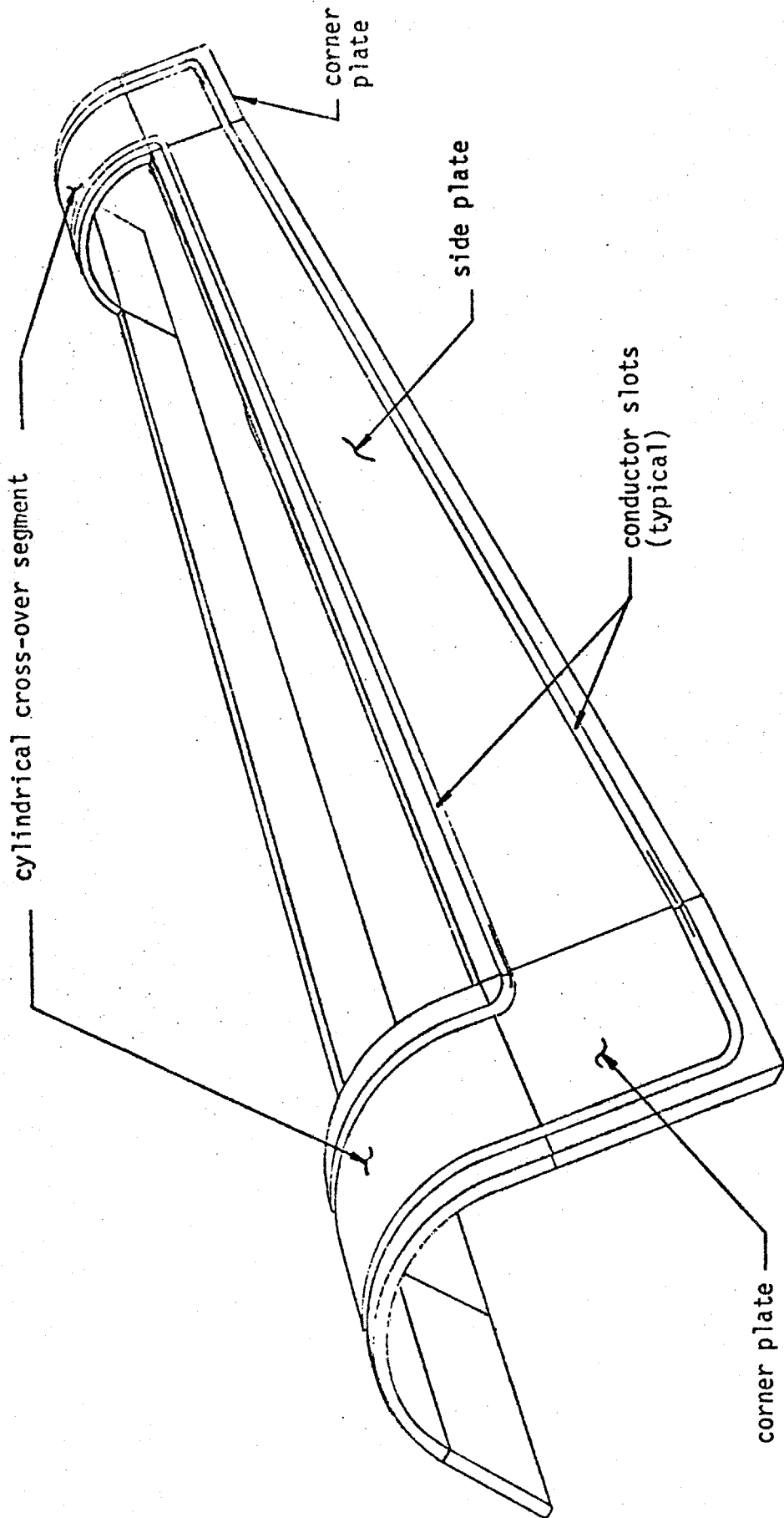
Three alternative conductors were proposed by MCA. The first was a separated substrate design shown in Figure 4.1.8.2G. The second and third were integral substrate designs called "bicable" and "tricable" as shown

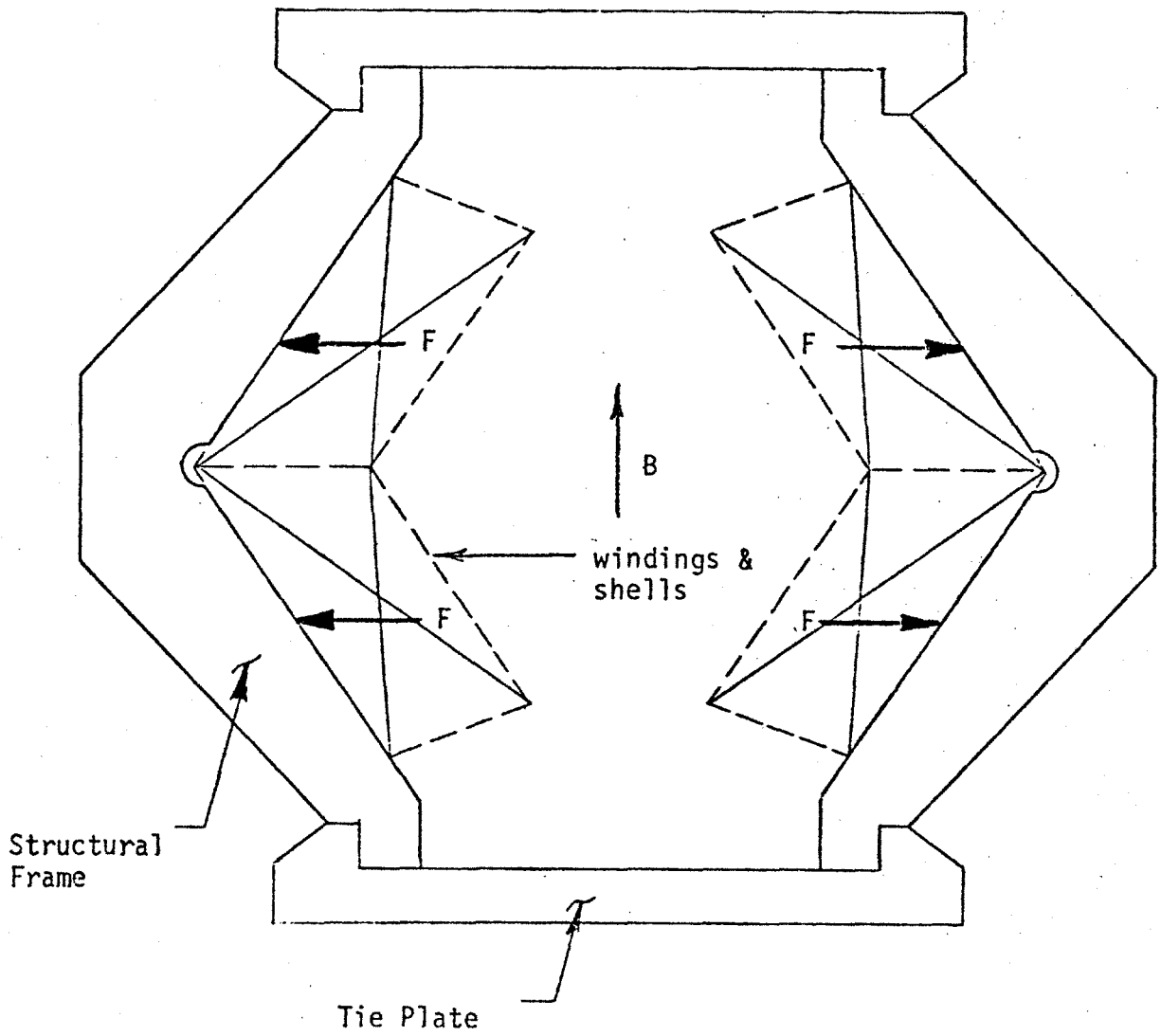




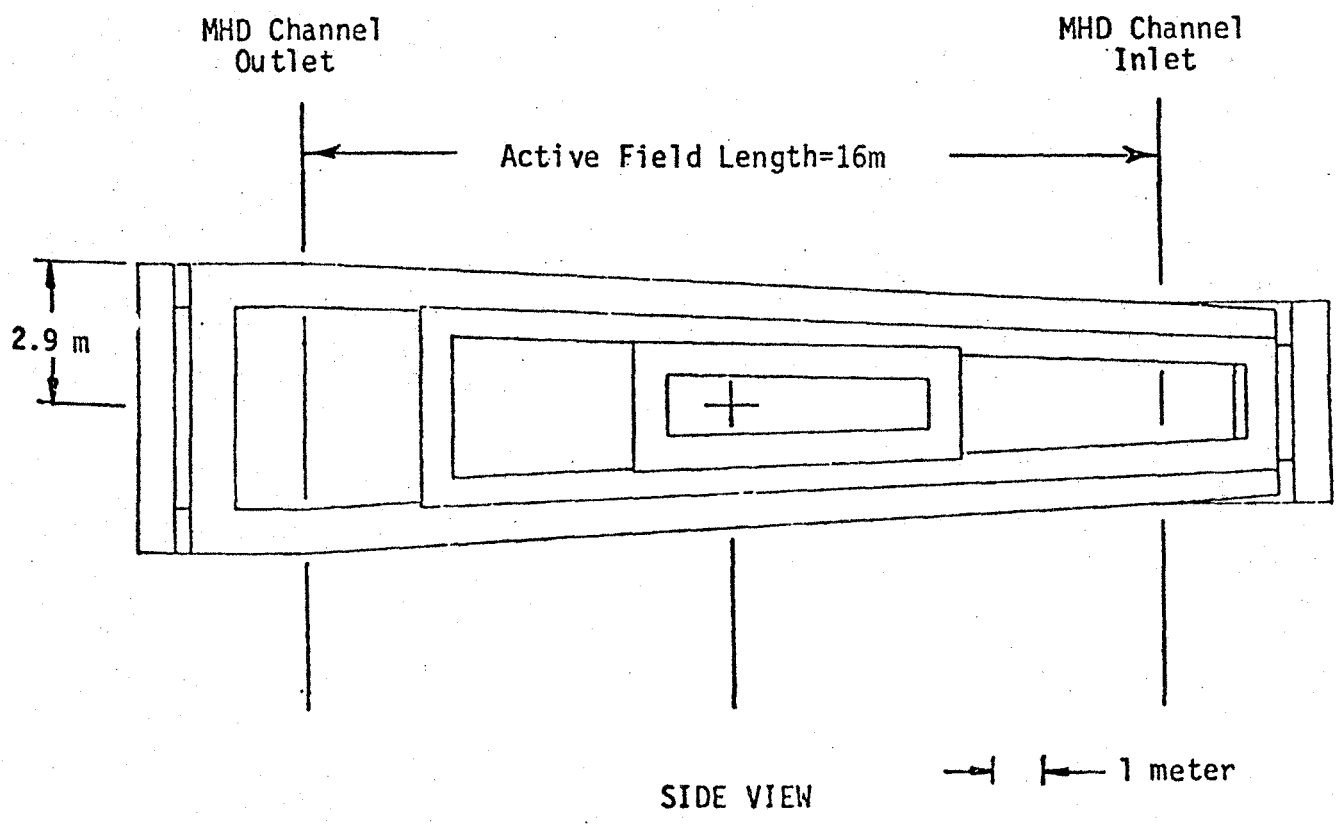
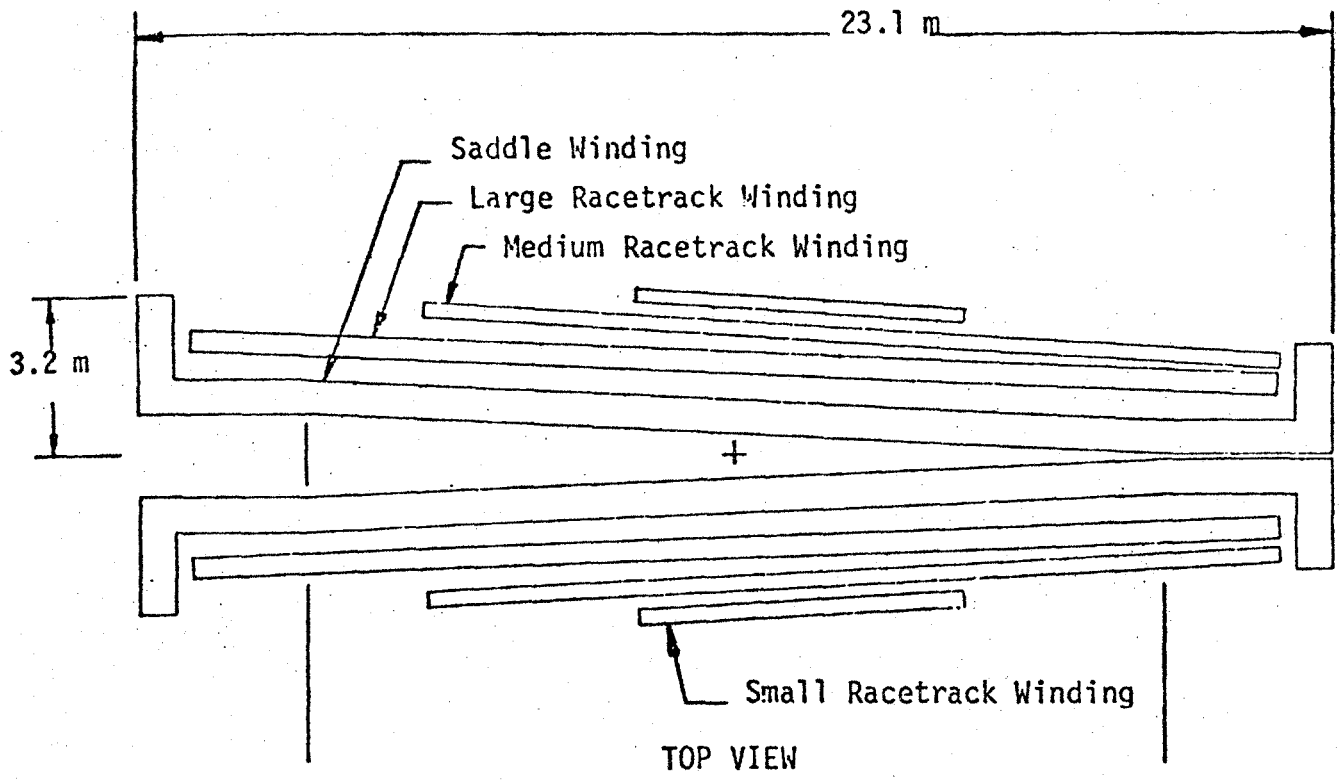
4.1.8.2A MCA Flat-Sided Shell Substructure and Winding Concept. Subassembly of Seven Shells Forming Saddle Magnet Half

4.1.8.2B Single Half-Shell with Typical Slots for Conductor

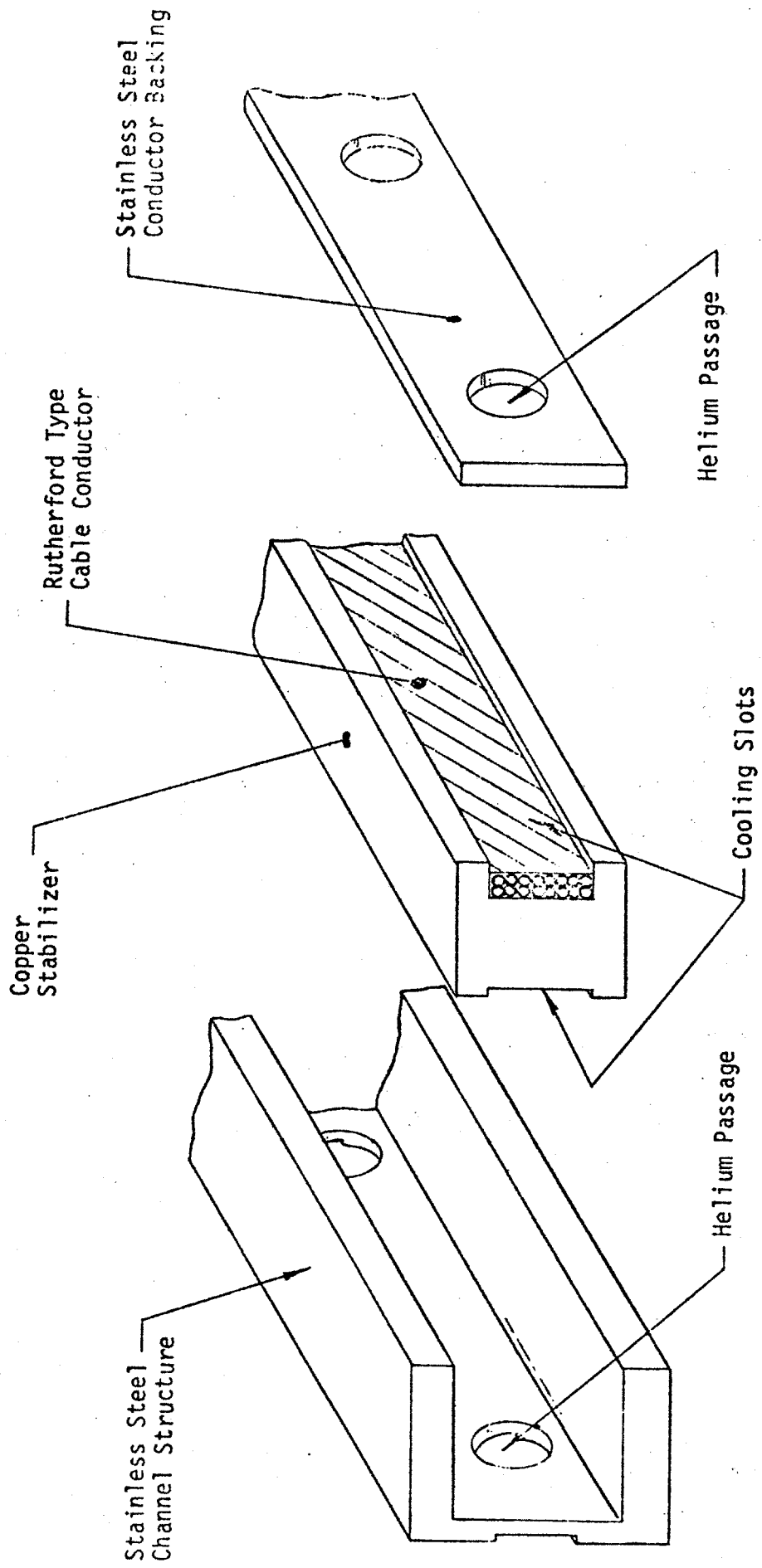




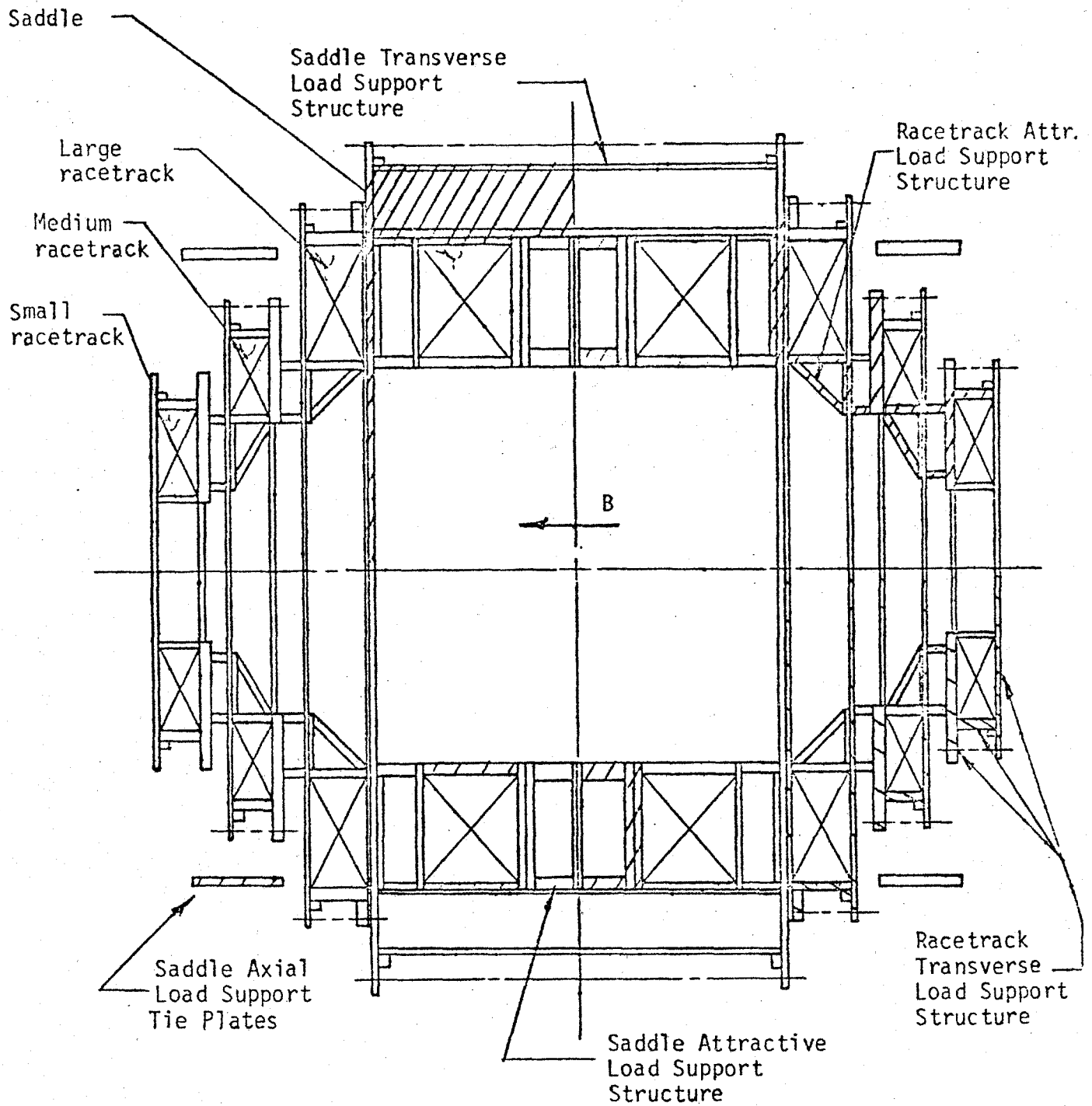
4.1.8.2C MCA Force Containment Structure Concept Consisting of Frames and Tie Plates for Support of Windings and Shells



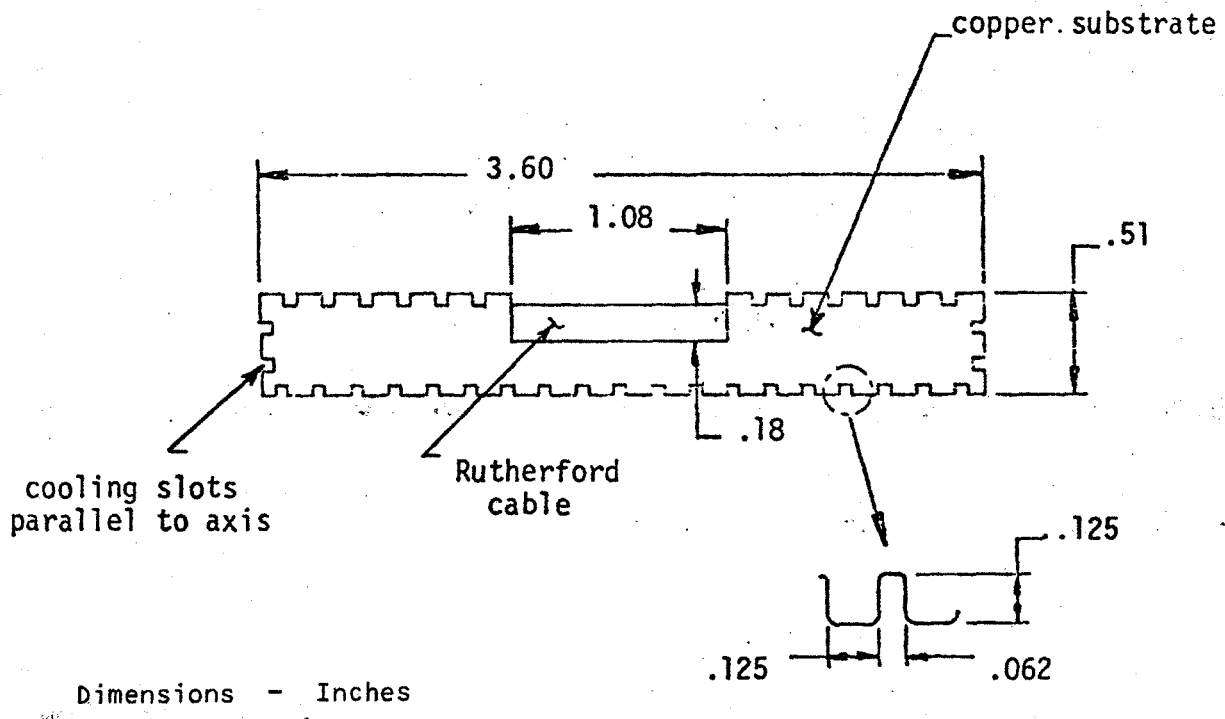
4.1.8.2D MCA Flat Plate Racetrack and Rectangular Saddle Concept, Coil Locations



4.1.8.2E Exploded View of MCA Conductor and Support Channel (Substructure)



4.1.8.2F Midplane Section of MCA Racetrack and Saddle Concept Showing Superstructure



4.1.8.2G MCA Separated-Substrate 50 kA Single Insert Conductor Design

in Figures 4.1.8.2H and 4.1.8.2J respectively.

A winding model magnet design was proposed as shown in Figure 4.1.8.2K. The winding forms are of 6061-T6 aluminum alloy. There is one winding groove in each half, each groove designed to accommodate a stack of six conductors. Support shells of aluminum alloy, not shown in Figure 4.1.8.2K, are assembled around the winding forms and bolted to them. A helium vessel made of stainless steel is then assembled around the entire winding and structure. It was proposed that the two halves be wound using different conductor and insulation alternatives. Several alternative conductor designs were proposed by MCA for testing. It was planned that the winding model magnet would be instrumented and assembled by the subcontractor and then delivered for installation and testing in a test Dewar at MIT.

The design characteristics of the MCA proposed winding model magnet, generally in accordance with the requirements of the request for proposal, are listed below:

Design current	50 kA
Critical current at 1.5 T and 4.2 K	55.6 kA
Ampere turns	$6 \times 10^5$ A
Central field	1.0 T
Maximum field in winding	1.5 T
Winding inside diameter	0.20 m
Winding outside diameter	0.31 m
Winding overall length	0.72 m

The MCA estimate for the weight of the winding model magnet including superstructure and helium vessel is 955 kg (2100 lbs).

It was considered that the MCA concept of a substructure incorporating flat inclined side plates was an innovative, cost effective structural design which warranted proceeding with Phases II and III of the investigation. However, limitation of funds prevented continuation of the project.

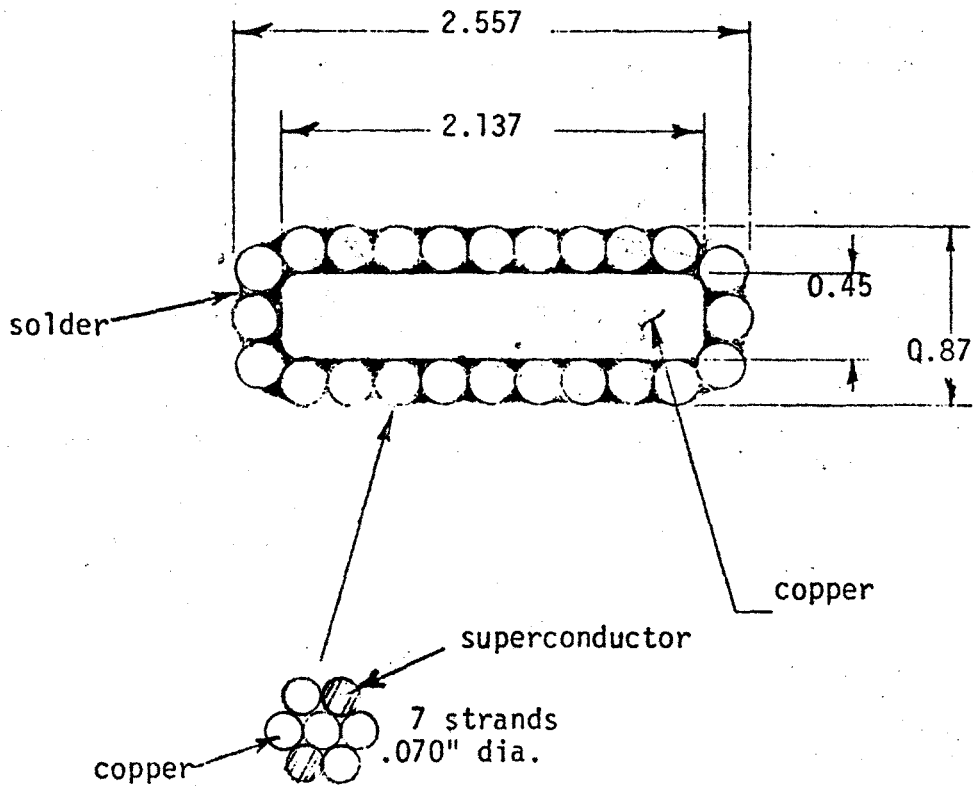
#### **4.1.8.3 GD Substructure and Winding Study**

At the beginning of the Phase I study by GD [60], two full-scale winding and structure concepts developed earlier by AVCO were analyzed and evaluated. The first was the circular-saddle configuration described in Section 4.2.3, and the second, the rectangular-saddle configuration described in Section 4.2.4. A third full-scale concept, referred to as the "CASK" circular-saddle design, was then developed by GD and evaluated in comparison with the other two. The "CASK" concept was considered to be the preferred concept. A winding model configuration incorporating features of the CASK concept was proposed.

As a part of GD's evaluation of the AVCO circular-saddle configuration, a manufacturing plan was developed in which the winding support shells (substructure modules) were constructed by assembling a number of short sections with bolted joints to form the full-length shell. The 180° sections, formed from aluminum alloy 5083 plate, were machined in mated pairs as shown in Figure 4.1.8.3A. Circumferential joints between sections were as shown in Figure 4.1.8.3B. The aluminum alloy core tube was made up of a number of 360° sections with circumferential bolted joints. The aluminum alloy outer helium vessel and end plates were made in sections and welded together at the plant site.

The alternative AVCO aluminum alloy ring girder designs, rectangular cross section and I cross section, were analyzed and both were found to be poor from the standpoint of manufacture. Further redesign effort was recommended. The separated substrate conductor was considered more suitable than the integrated substrate

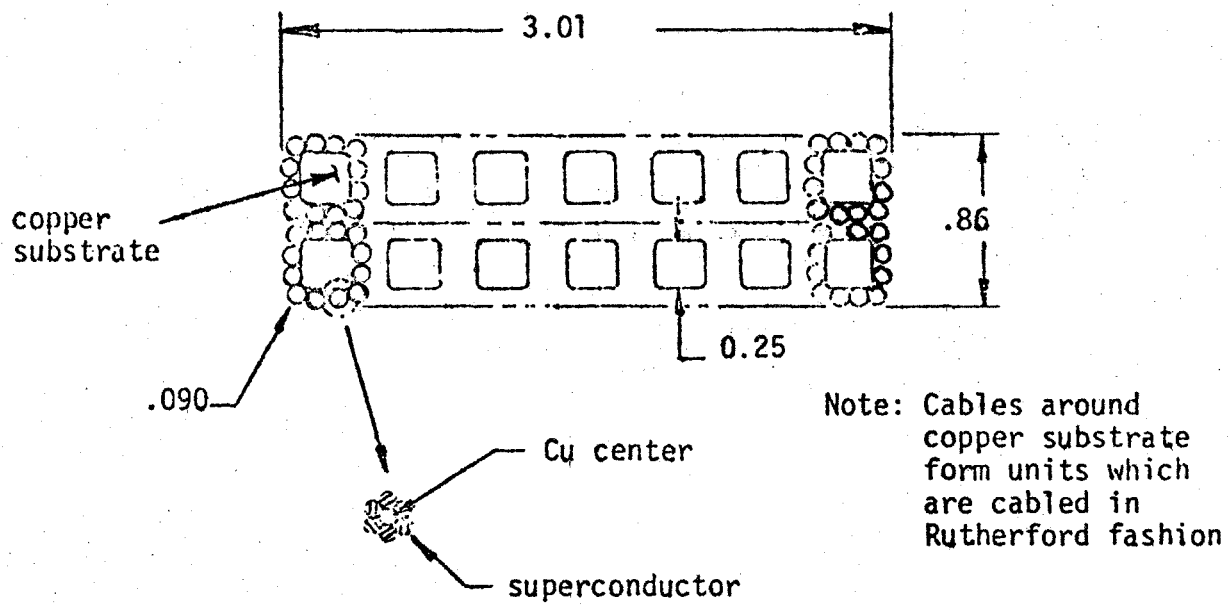




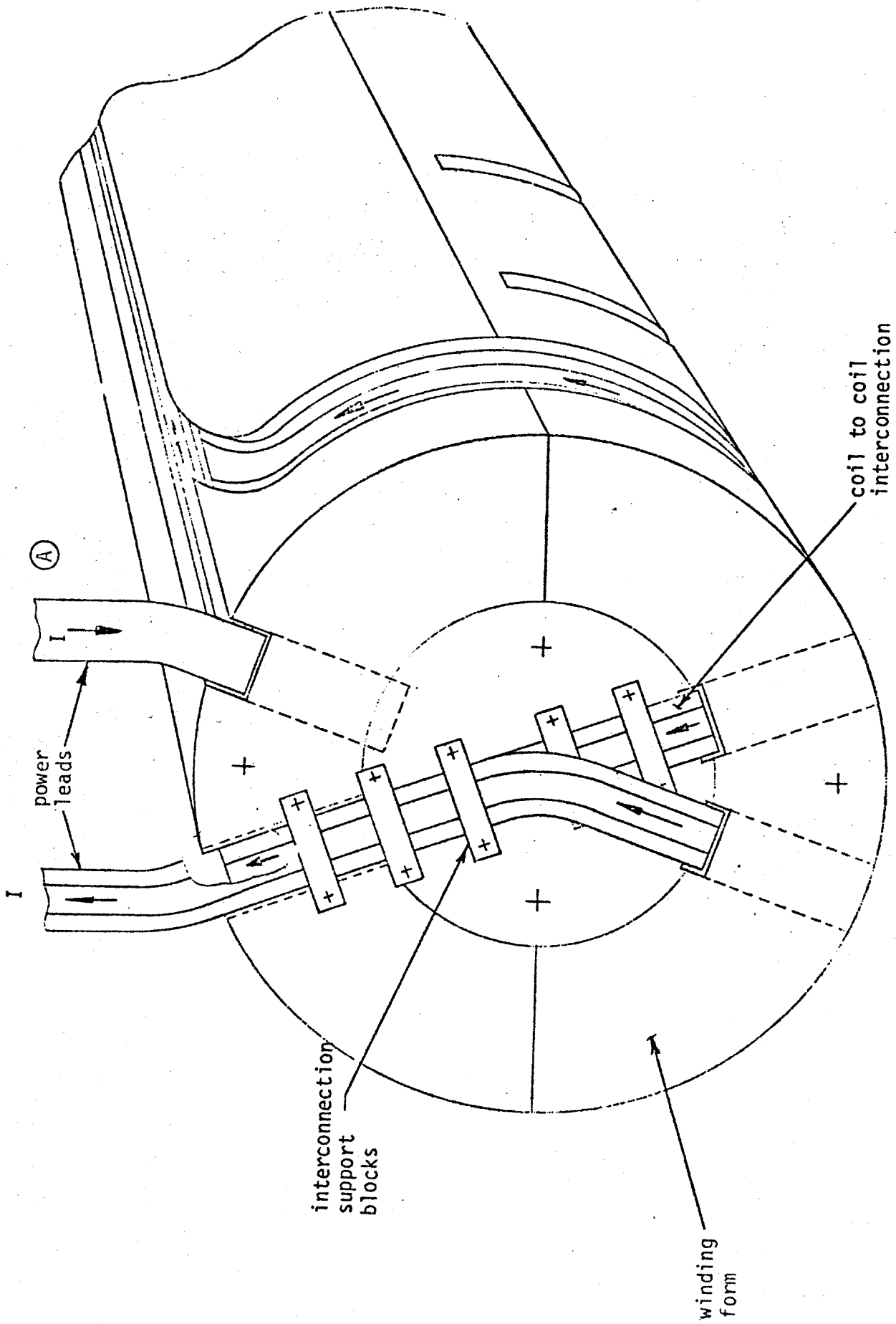
Note: 7-strand cables form units which are wrapped around central substrate in Rutherford cable fashion.

Dimensions - Inches

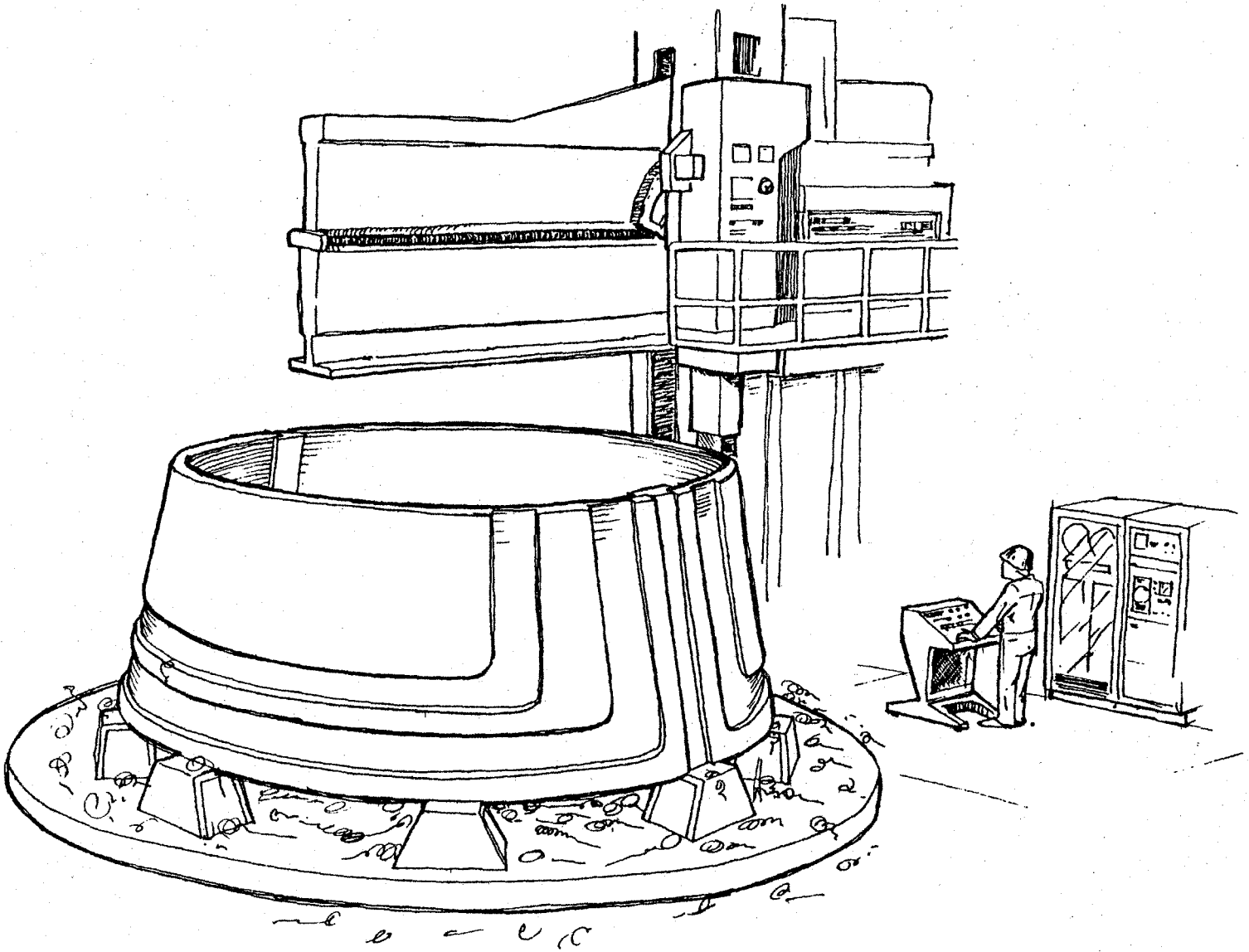
4.1.8.2H MCA Integral-Substrate 50 kA Solder Filled "Bicable" Conductor Design



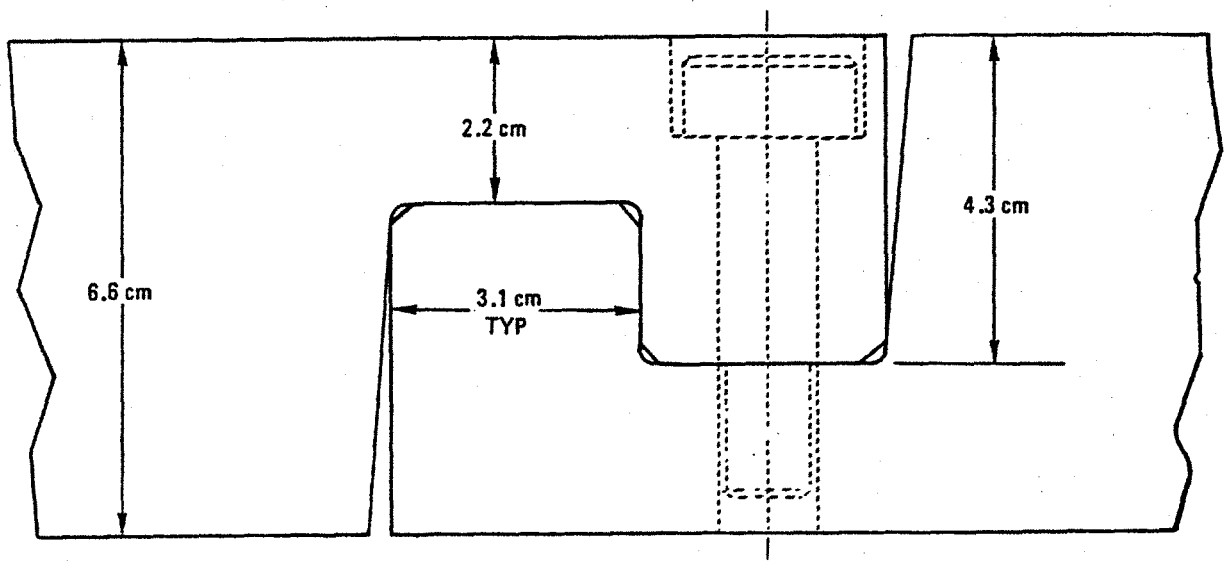
4.1.8.2I MCA Integral-Substrate 50 kA Solder Filled "Tricable" Conductor Design



4.1.8.2K MCA Proposed Winding Model Magnet Design



4.1.8.3A Sketch Showing Machining of Mated Pair of Substructure Shell Sections



4.1.8.3B Typical Mechanical Joint for Joining Conical Support Shell Sections

type. A final assembly fixture, as shown in Figure 4.1.8.3C, was proposed for use both in winding of conductor into support shell grooves and in assembling the subshells, helium vessel and superstructure.

As a part of GD's evaluation of the AVCO rectangular-saddle configuration, a manufacturing plan was also developed. In this plan, the aluminum alloy winding support plates were made up of a number of sections machined flat in a numerical controlled skin mill. Sections located at the end turn-up regions were brake formed to the required 90° angle after machining. The sections were then connected with bolted joints to form complete full length support plates. Figure 4.1.8.3D shows a flat pattern layout of a typical combined tension plate and support plate. It was planned that conductor would be installed in individual support plates in the horizontal position. The wound support plates would then be assembled around the core tube as shown in Figure 4.1.8.3E using an assembly fixture similar to that shown in Figure 4.1.8.3C.

The CASK magnet configuration, with the accompanying manufacturing plan, both developed by GD, were considered to represent an improved, easier-to-manufacture version of the circular-saddle magnet. The CASK design configuration is shown in Figure 4.1.8.3F.

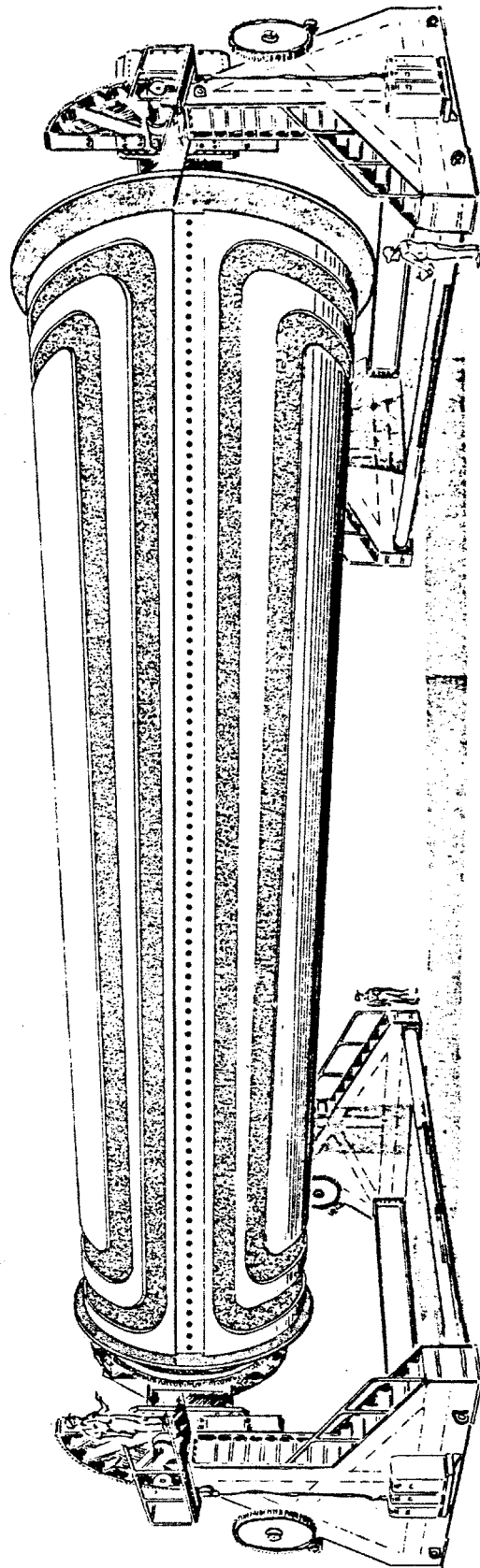
The basic concept of this design is the division of the circular section of the substructure into a number of staves, with each staff being fabricated independently. Thus, each staff becomes a long, high-quality, unwelded 2219-T87 aluminum alloy plate. These plates are designed to be machined easily at a central factory site and then transported on currently-available carriers to the baseload site for assembly. The structural and force resisting requirements of the overall magnet assembly are met in a unique way. The axial magnetic force, estimated at 27,000 tons, is directly contained by the tension generated in the 25 m long aluminum alloy staves. These are standard, commercially-available plates of material with a reported tensile yield strength of approximately 74,000 psi, and an elongation of 15% at 4 K temperature. The transverse (outward) magnetic forces are contained by fabricated aluminum alloy ring girders of I-beam cross section.

The contract extension given to GD for further work on the CASK concept resulted in a proposal for the preliminary design of a CASK baseload MHD superconducting magnet. A contract was placed and the preliminary design was completed as reported in Section 4.2.5. The preliminary design work resulted in some changes from the conceptual design described above; in particular, the material of the substructure and superstructure was changed from aluminum to stainless steel and the ring girders were changed from circular configuration to crescent configuration. The CASK concept is described in considerable detail in Section 4.2.5 and the GD report, Reference 30.

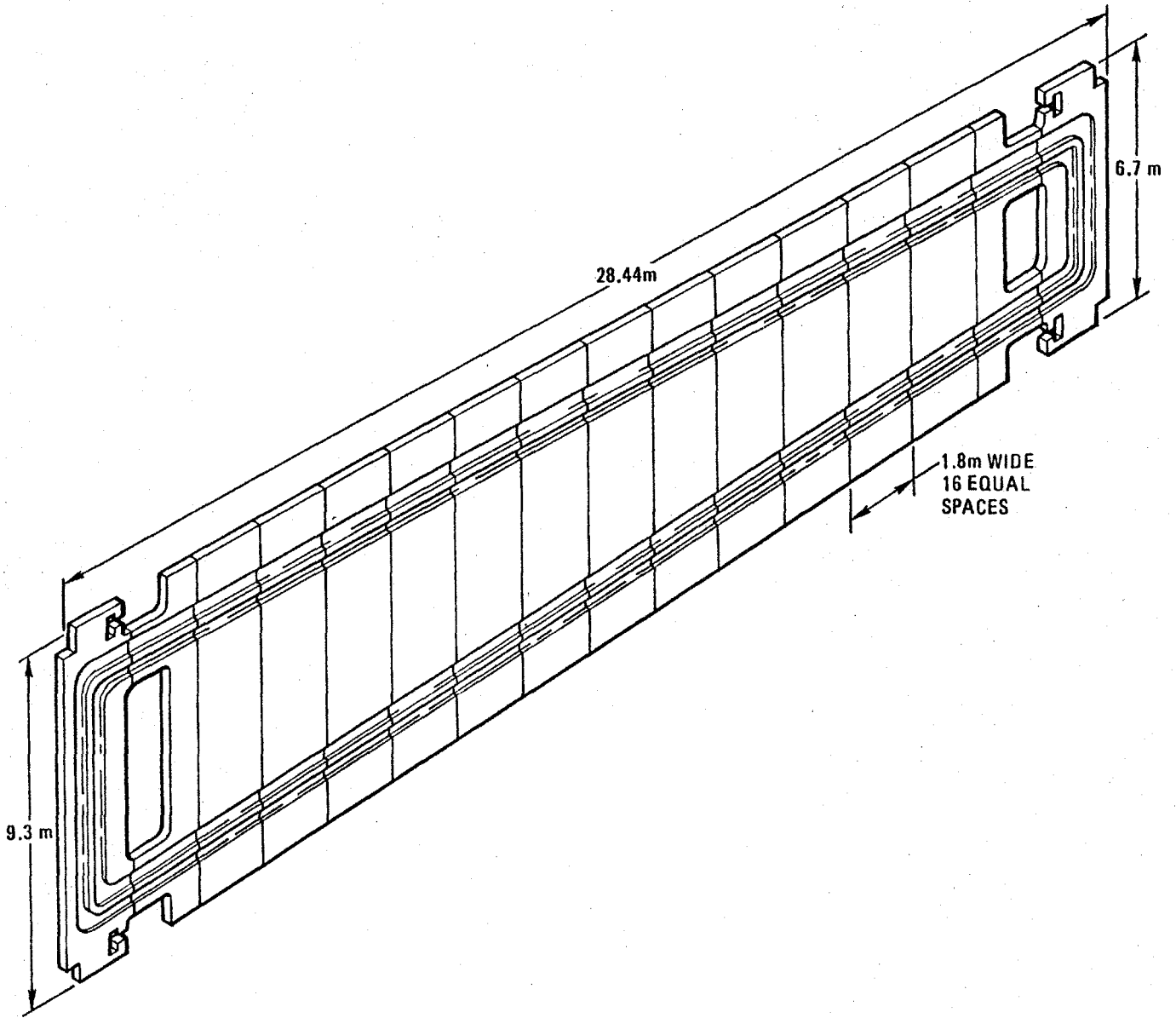
The preferred conductor for all winding designs studied by GD was the separated substrate type. Figure 4.1.8.3G shows a stack of separated-substrate conductors as installed in the CASK concept substructure.

After evaluating all three full-scale winding and substructure concepts, GD concluded that the CASK concept offers the best approach to an economical, practical design that can be built immediately with today's technology. The AVCO circular-saddle concept was rated second, and the AVCO rectangular-saddle concept third.

The winding model magnet (WMM) design developed by GD is shown in Figure 4.1.8.3H. It embodies the principal concepts of the cylindrical-saddle baseload design and incorporates many of the features of the CASK baseload design. The coils, made of 50 kA separated-substrate conductor, are supported in a substructure consisting of concentric aluminum alloy shells of "staff" configuration. The design of the conductor substrate is shown in Figure 4.1.8.3J. The conductor insert is a rectangular cross section NbTi/copper monolith. Turn-to-turn insulation is provided by G-10 clips fastened to the conductor. An aluminum alloy helium vessel surrounds the winding and aluminum alloy ring girders (superstructure) are clamped around the outside of the helium vessel.

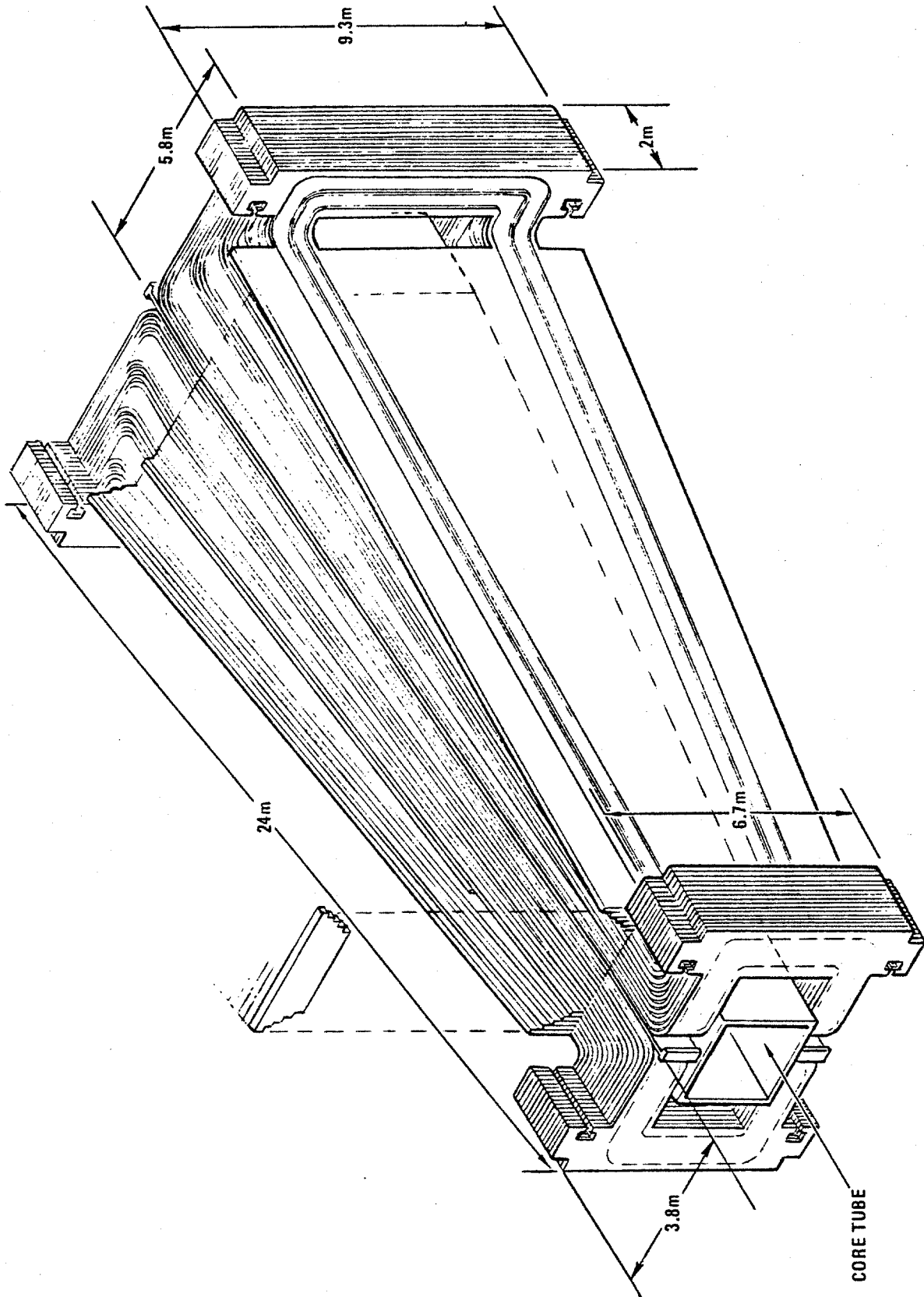


4.1.8.3C Sketch of Fixture for Subshell Assembly, Winding and Final Assembly with Superstructure

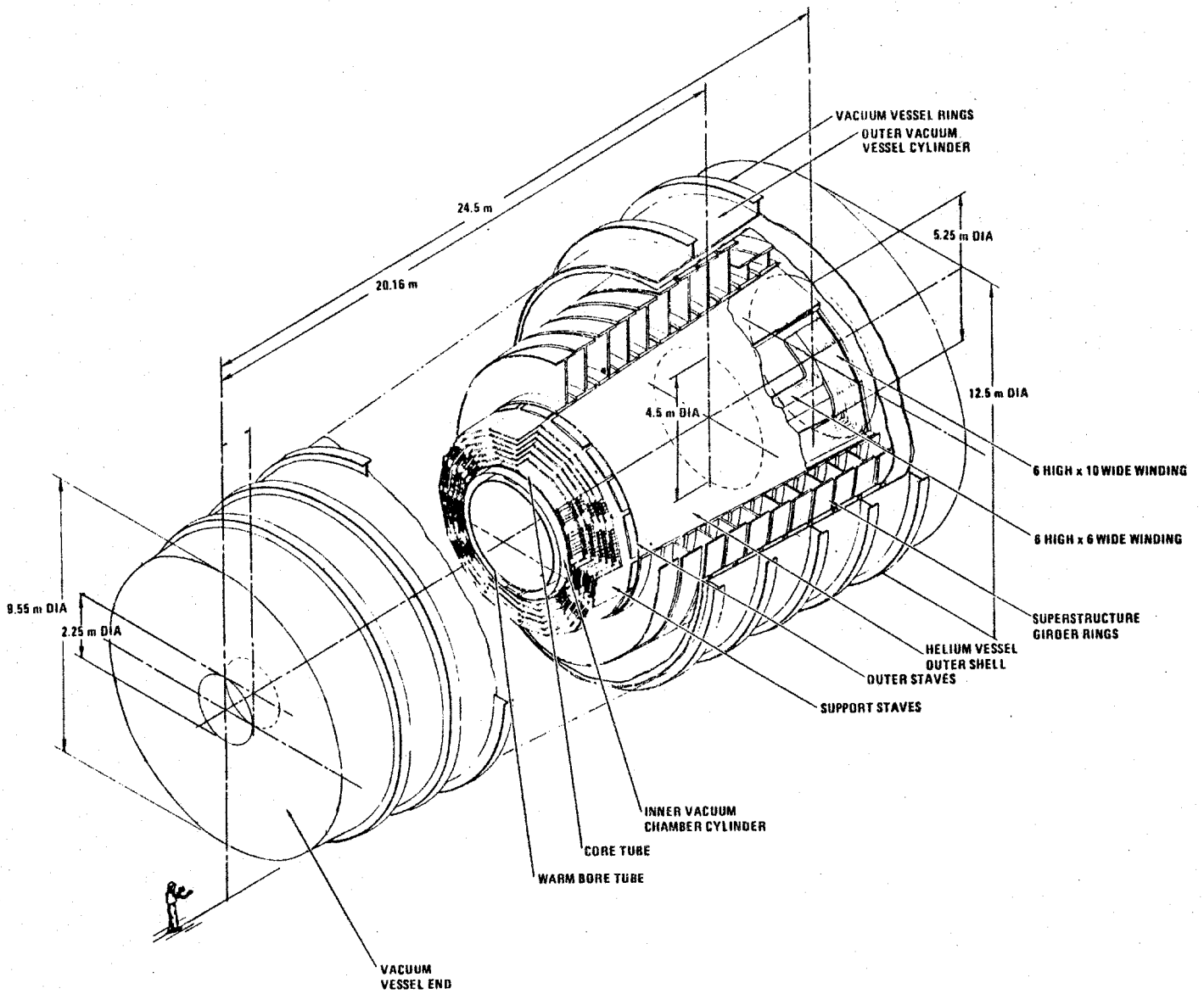


4.1.8.3D Flat Pattern Layout of Typical Combined Tension and Support Plate, Rectangular Saddle Concept

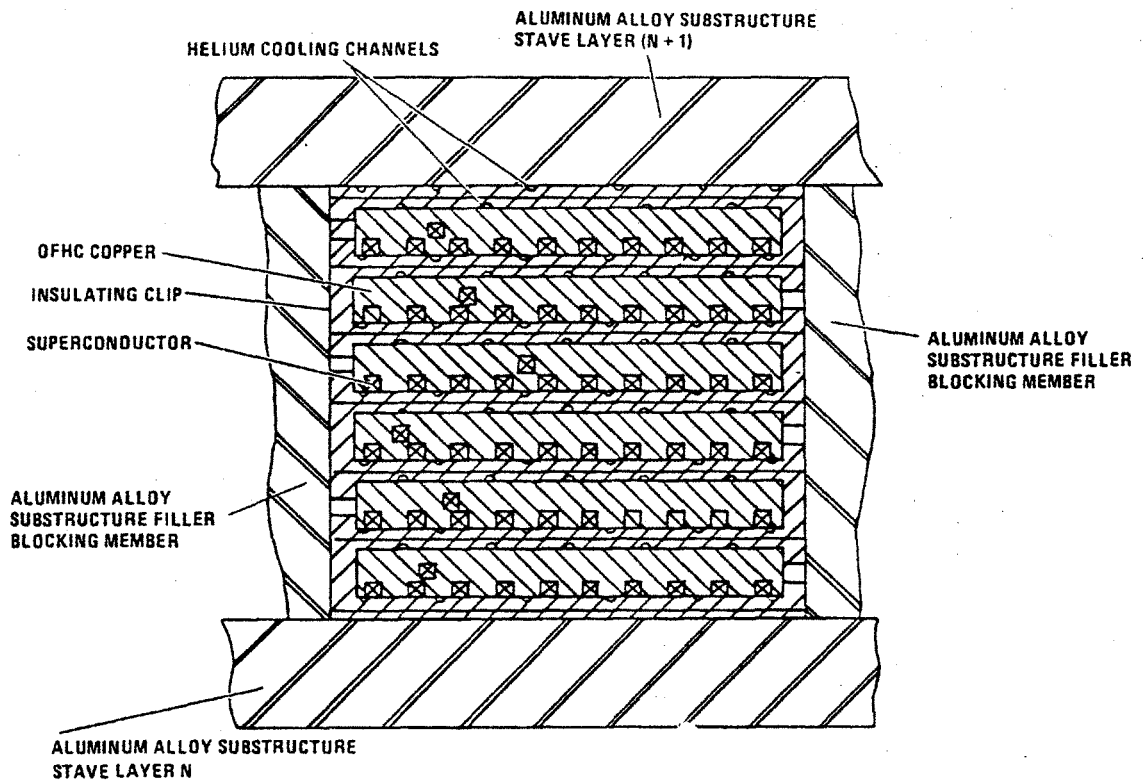




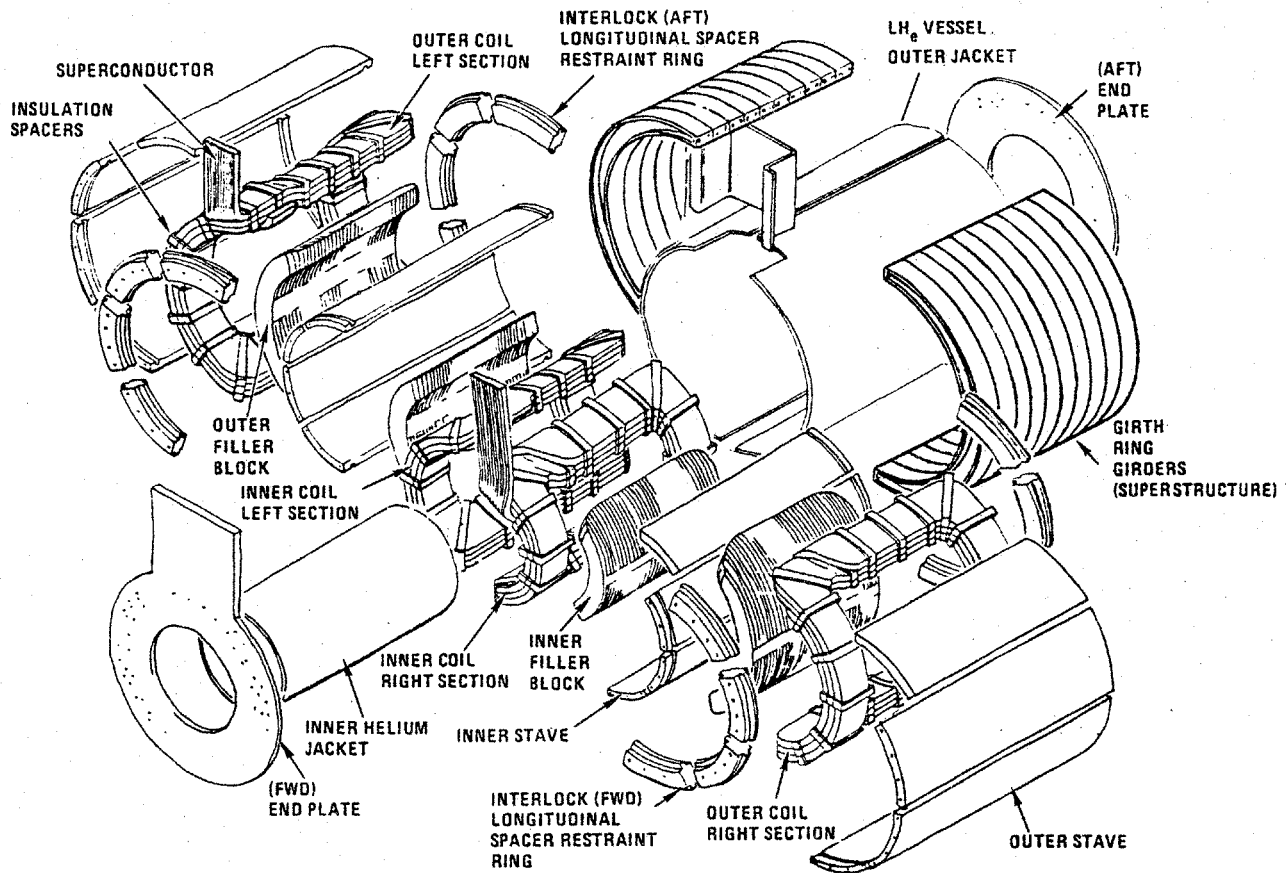
4.1.8.3E Assembly of Wound Support Plate Around Core Tube, Rectangular Saddle Concept



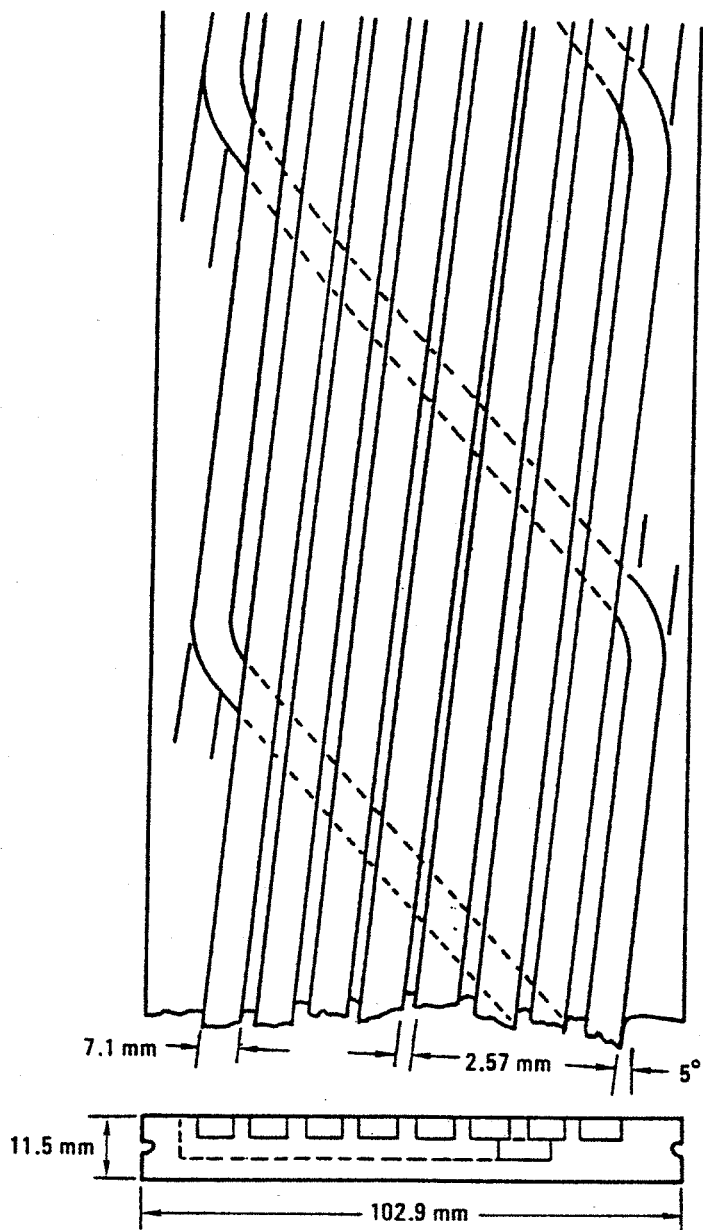
4.1.8.3F CASK Magnet Design Concept



4.1.8.3G Stack of Separated-Substrate Conductors Installed in CASK Substructure



4.1.8.3H GD Winding Model Magnet Design



4.1.8.3J Conductor Substrate Design for GD Magnet

The design characteristics of the GD winding model magnet are listed below:

Design current	50 kA
Ampere turns	$6 \times 10^5$ A
Maximum field in winding	1.75 T

#### 4.1.9 Study of Impact of High Current Operation on Magnet System Cost

The cost of many of the components, the cost of some of the steps in fabrication and the operating cost of a superconducting MHD magnet are all dependent on design operating current. A question naturally arises, therefore, as to what is the optimum current level from the cost standpoint. To investigate this question, a study of the impact of design operating current on magnet system cost was conducted by MCA under a series of subcontracts.

The approach taken was to develop a set of cost factors in the general areas of system components, fabrication and operation. Components considered included conductor, substructure, superstructure, Dewar, power supply subsystem and refrigerator/liquefier subsystem. Fabrication operations, including coil winding, magnet assembly and system installation were considered. Fabrication and quality control development were taken into account, as well as system operating expenses over a 10-year period. Three conductor configurations were selected and three values of surface heat flux were considered for the baseline conductor. The alternative conductor configurations were the fluted substrate, the semifluted substrate and the tricable type, as described in Section 4.1.8.2. The studies covered operating currents from 10 kA to 250 kA and involved two magnet design concepts, the first incorporating a stainless steel channel and plate substructure as described in Section 4.2.2, and the second an aluminum alloy, nested shell substructure, as described in Section 4.2.3.

Results indicated that overall cost for the channel and plate substructure concept was minimum in the vicinity of 100 kA and for the nested shell substructure concept, in the vicinity of 50 kA. The curves of cost vs current were relatively flat in the region of the minimum.

Table 4.1.9-I shows the estimated magnet system capital cost breakdown for the channel and plate concept with semi-fluted conductor and heat flux of  $0.6 \text{ W/cm}^2$  for the current range of 10 kA to 250 kA. Table 4.1.9-II shows the magnet system estimated total cost, including ten year power cost, for the channel and plate concept with three types of conductor and three heat fluxes. Table 4.1.9-III shows the estimated magnet system cost breakdown and total cost for the nested shell concept with semi-fluted conductor and heat flux of  $0.6 \text{ W/cm}^2$ , Figure 4.1.9A shows curves of estimated component costs and total cost vs magnet current for the nested shell concept with semi-fluted conductor and  $0.6 \text{ W/cm}^2$  heat flux.

Detailed information on the study is contained in References 42, 43 and 44.

#### 4.1.10 Stability Analysis of High Current Conductors

Since high current composite superconductors planned for commercial-scale MHD magnets are much larger than superconductors for which a background of stability testing and analysis exists today, it was considered important that stability analysis and conductor evaluation be performed specifically for conductors of sizes and types proposed for MHD magnets. Accordingly, subcontracts were placed with MEA and with Dr. M.A. Hilal, Michigan Technological University for studies in these areas. The analysis and evaluation work performed is summarized in the following subsections.

Table 4.1.9-I

Estimated Magnet System Capital Cost Breakdown  
And Integration (\$10<sup>6</sup>)

(based on channel and plate concept using semifluted conductor at  $\dot{q} = 0.6 \text{ W/cm}^2$ )

Current (kA)	10	25	50	100	150	200	250
Conductor	8.24	8.39	8.51	8.73	8.97	9.21	9.38
Substructure	0.403	0.613	0.895	1.63	2.40	3.17	4.09
Power Supply Subsystem	0.213	0.240	0.268	0.348	0.428	0.507	0.586
Refrigerator/Liquefier Subsystem	0.464	0.547	0.653	0.883	1.08	1.32	1.53
Superstructure	15.2	15.2	15.2	15.2	15.2	15.2	15.2
Dewar	2.51	2.51	2.51	2.51	2.51	2.51	2.51
Miscellaneous Components & Shipping <sup>1</sup>	4.05	4.13	4.21	4.39	4.59	4.79	4.99
Windings & Substructure Fabrication	18.8	12.6	9.56	6.76	5.64	5.24	5.36
Fabrication & Quality Control Development	0.675	0.738	0.800	1.05	1.34	1.69	2.00
Assembly to Super- structure, Dewar & Support Systems	5.92	5.92	5.92	5.92	5.92	5.92	5.92
Subtotal	56.5	50.9	48.5	47.4	48.1	49.6	51.6
Administrative Expenses <sup>2</sup>	16.9	15.3	14.6	14.2	14.4	14.9	15.4
<b>TOTAL COST<sup>3</sup></b>	<b>73.4</b>	<b>66.1</b>	<b>63.1</b>	<b>61.6</b>	<b>62.5</b>	<b>64.5</b>	<b>67.0</b>

1 Fifteen percent of total of previous six items

2 Thirty percent of Subtotal

3 Does not include design system quality assurance estimated at  $\$2.93 \times 10^6$ ;  
does not include design support development

Table 4.1.9-II

Estimated Cost for Magnet System Based on Ten-Year Operation  
(magnet incorporating channel and plate concept)

I (kA)	Annual Power Cost at 0.04 \$/kWh	10-Year Power Cost \$10 <sup>6</sup>	Semifluted $\dot{q}=0.6$ W/cm <sup>2</sup> \$10 <sup>6</sup>	Fully Fluted $\dot{q}=0.6$ W/cm <sup>2</sup> \$10 <sup>6</sup>	Total Cost Tricable $\dot{q}=0.6$ W/cm <sup>2</sup> \$10 <sup>6</sup>	Semifluted $\dot{q}=0.3$ W/cm <sup>2</sup> \$10 <sup>6</sup>	Semifluted $\dot{q}=0.9$ W/cm <sup>2</sup> \$10 <sup>6</sup>
	10	86	0.86	74.3	74.1	74.2	74.5
25	115	1.15	67.3	67.2	67.7	68.4	66.9
50	158	1.58	64.7	64.3	66.5	67.0	64.0
100	255	2.55	64.2	63.7	67.0	66.2	63.4
150	349	3.49	66.0	65.1	70.6	68.8	64.8
200	464	4.64	69.1	68.0	75.3	72.7	67.5
250	574	5.74	72.7	71.0	80.1	77.7	70.9

Notes:

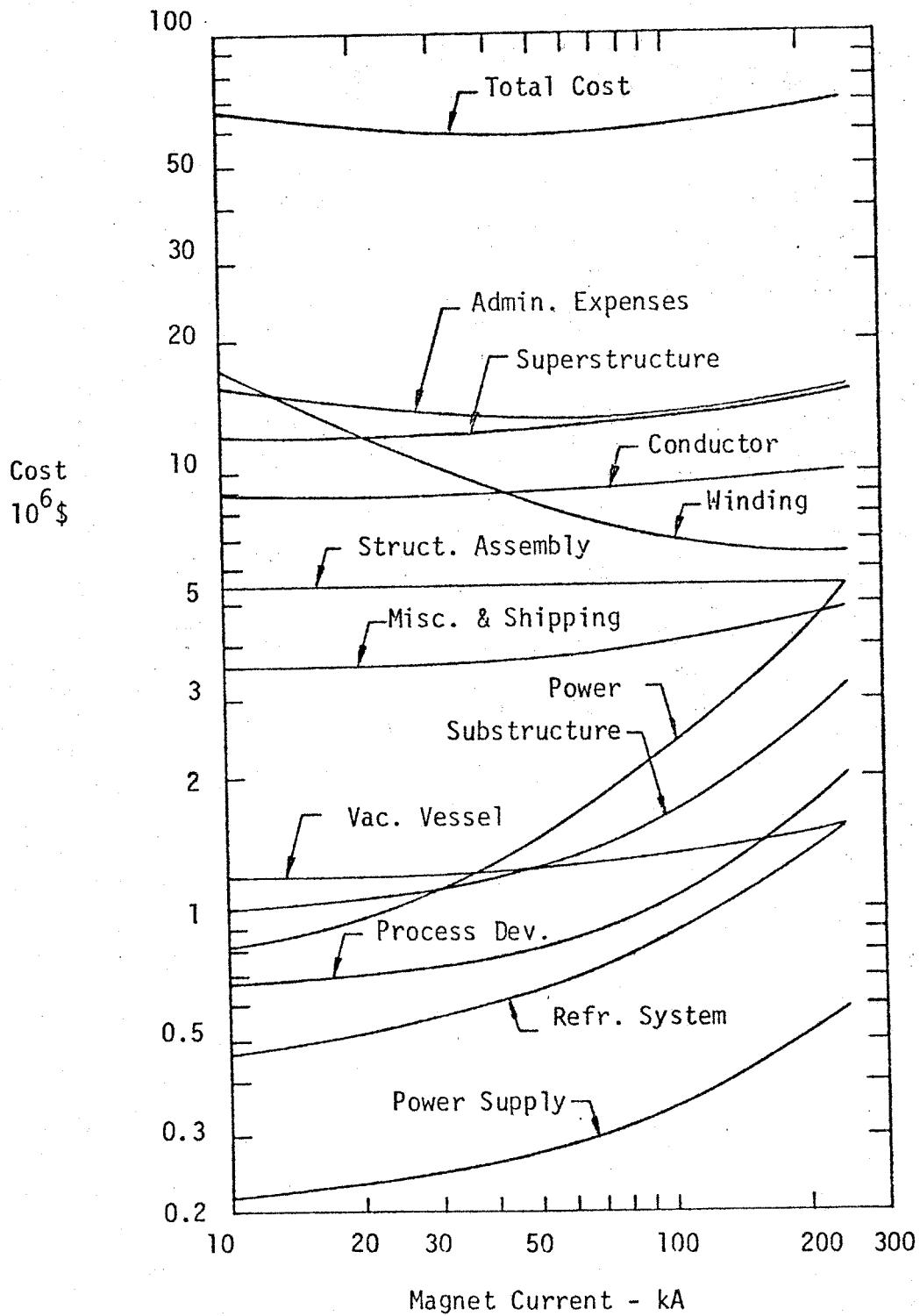
- Semifluted and fully-fluted conductors are both separate-substrate conductors with final assembly required at the winding facility.
- Tricable is a complex integral-substrate conductor; final assembly not required at winding facility.
- Cost difference between separate and integral-substrate conductors primarily due to complexity of the latter geometry and not the fact that it is integral in nature.



Table 4.1.9-III

Magnet System Estimated Costs  
(based on nested shell concept using semifluted conductor at  $\dot{q} = 0.6 \text{ W/cm}^2$ )

Current, kA	<u>10</u>	<u>25</u>	<u>50</u>	<u>100</u>	<u>150</u>	<u>200</u>	<u>250</u>
Costs, $10^6$ \$:							
Conductor	8.73	8.87	9.00	9.23	9.67	9.74	9.92
Substructure	1.04	1.21	1.30	1.62	2.99	2.41	3.21
Superstructure	12.14	12.31	12.37	13.59	14.73	14.02	15.26
Vacuum Vessel	1.21	1.23	1.23	1.36	1.48	1.41	1.54
Power Supply	.21	.24	.27	.35	.43	.51	.59
Refrig. System	<u>.47</u>	<u>.55</u>	<u>.65</u>	<u>.89</u>	<u>1.08</u>	<u>1.32</u>	<u>1.54</u>
Total Components	23.83	24.40	24.82	27.04	30.39	29.41	32.06
Misc. & Shipping, 15%	3.57	3.66	3.72	4.06	4.56	4.41	4.81
Winding Fab.	17.15	11.27	9.08	6.90	6.75	6.61	6.56
Process Develop.	.68	.74	.80	1.05	1.34	1.69	2.00
Structural Assembly	<u>5.50</u>	<u>5.50</u>	<u>5.50</u>	<u>5.50</u>	<u>5.50</u>	<u>5.50</u>	<u>5.50</u>
Total Cost	50.72	45.57	43.93	44.55	48.53	47.62	50.92
Admin. Expenses, 30%	<u>15.22</u>	<u>13.67</u>	<u>13.18</u>	<u>13.36</u>	<u>14.56</u>	<u>14.29</u>	<u>15.28</u>
Total Installed Cost	54.94	59.24	57.10	57.91	63.09	61.90	66.20
Power Cost	<u>.82</u>	<u>1.09</u>	<u>1.49</u>	<u>2.41</u>	<u>3.30</u>	<u>4.39</u>	<u>5.45</u>
GRAND TOTAL	66.76	60.32	58.60	60.32	66.39	66.29	71.65



4.1.9A

Curves of Estimated Component Costs and Total Cost vs. Magnet Current for Nested Shell Concept with Semifluted Conductor and  $0.6 \text{ W/cm}^2$  Heat Flux

#### 4.1.10.1 Conductor Analysis for Large Scale Superconducting MHD Magnets (MEA)

The work done by MEA was intended to supplement and extend the work on the development of high current conductors reported in Section 4.1.5.

The conductor specifications used as a basis for stability analysis, which were established by MIT as representative of large MHD magnet conductors, are listed in Table 4.1.10.1-I.

The investigation of stability in high current conductors performed by MEA consisted of an analytical study which took into account past analytical and experimental work on stability of smaller superconductors, and used computer techniques to support the investigation.

This study was limited to a coil design in which the conductor is cooled by liquid helium in open channels running transversely across the face of the conductor. The initial conductor configuration considered is illustrated schematically in Figure 4.1.10.1A. The overall objective of the study was to develop design criteria relevant to this type of high current conductor.

Because of the relatively large amount of copper in the conductor, it was decided at the outset of the study to place major emphasis on cold-end recovery for short normal zones. The relationship of the three possible modes of recovery is indicated in Figure 4.1.10.1B. Short zone cold-end recovery is the only mode of recovery possible when the operating current is above the limit specified by the equal area criterion given by Maddock, James and Norris, [60A]. When the current is above this limit, the maximum recovery current is directly related to the maximum energy the conductor can absorb and still recover. The unstable equilibrium state corresponding to this energy is called a minimum propagating zone (MPZ), and the theory which treats it is called the minimum propagating zone theory [60B]; [21].

Conclusions were that high current conductors should be designed such that (1) the superconducting to normal transition time is greater than 10 ms, (2) the thermal stability parameter  $\gamma$  (relating to transverse thermal gradients) is less than one, and (3) the stabilizer thickness is less than one centimeter.

More detailed information on the investigation of stability is contained in References 61 and 62.

#### 4.1.10.2 Stability Analysis and Evaluation of Composite Conductors for MHD Magnets (Hilal)

Dr. Hilal's studies included analysis of persistent resistive regions in composite conductors, including determinations of allowable delaminated length in CDIF/SM conductor, evaluation of various MHD magnet conductors and analysis of effects of electrical and thermal contact resistance.

Persistent resistive regions may develop in high current conductors 1) as a result of conductor delamination, or 2) as a result of degradation of cooling. Typical high current MHD magnet conductors consist of a copper/superconductor composite soldered or metallurgically bonded to a stabilizer substrate. Delamination cannot be eliminated in this type of conductor. Narrow channels along the conductor and/or long (insulating) spacers can result in cooling degradation.

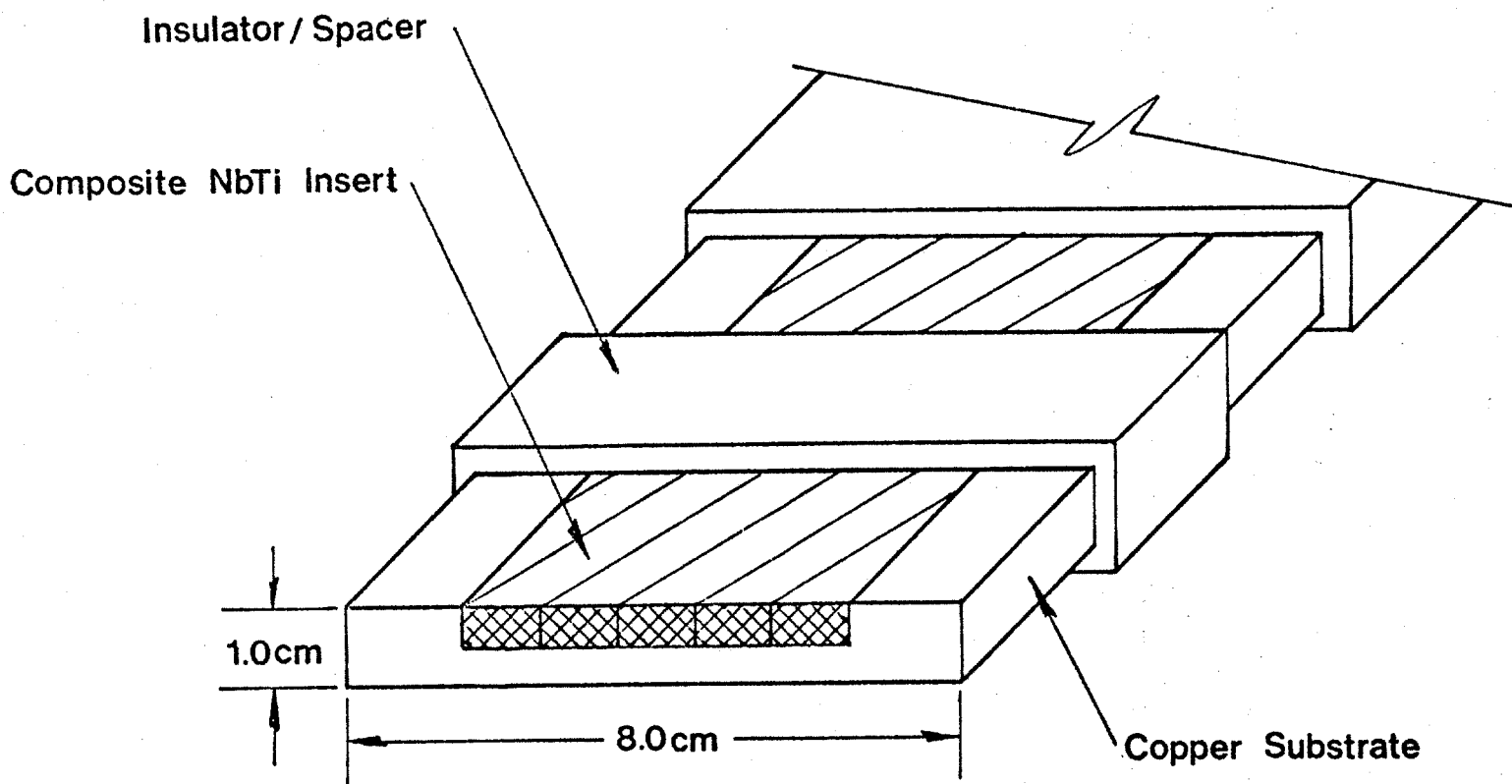
A model shown in Figure 4.1.10.2A was used to determine recovery length both analytically and numerically. Cases considered included 1) infinite end cooling and no composite cooling, 2) infinite end cooling and partial composite cooling, and 3) finite end cooling and no composite cooling. Using parameters for the CDIF/SM conductor, it was determined analytically that for Case 1,  $2\ell = 1.96$  cm where  $\ell =$  allowable delaminated length. Figure 4.1.10.2B contains a series of curves showing the allowable dimensionless delaminated length,  $\frac{X_m}{T_b}$ , versus  $\delta$  under conditions of Case 2, where

$$\delta = \left( \frac{\text{heat removed per unit length}}{\text{heat generated per unit length}} \right)^{\frac{1}{2}}$$

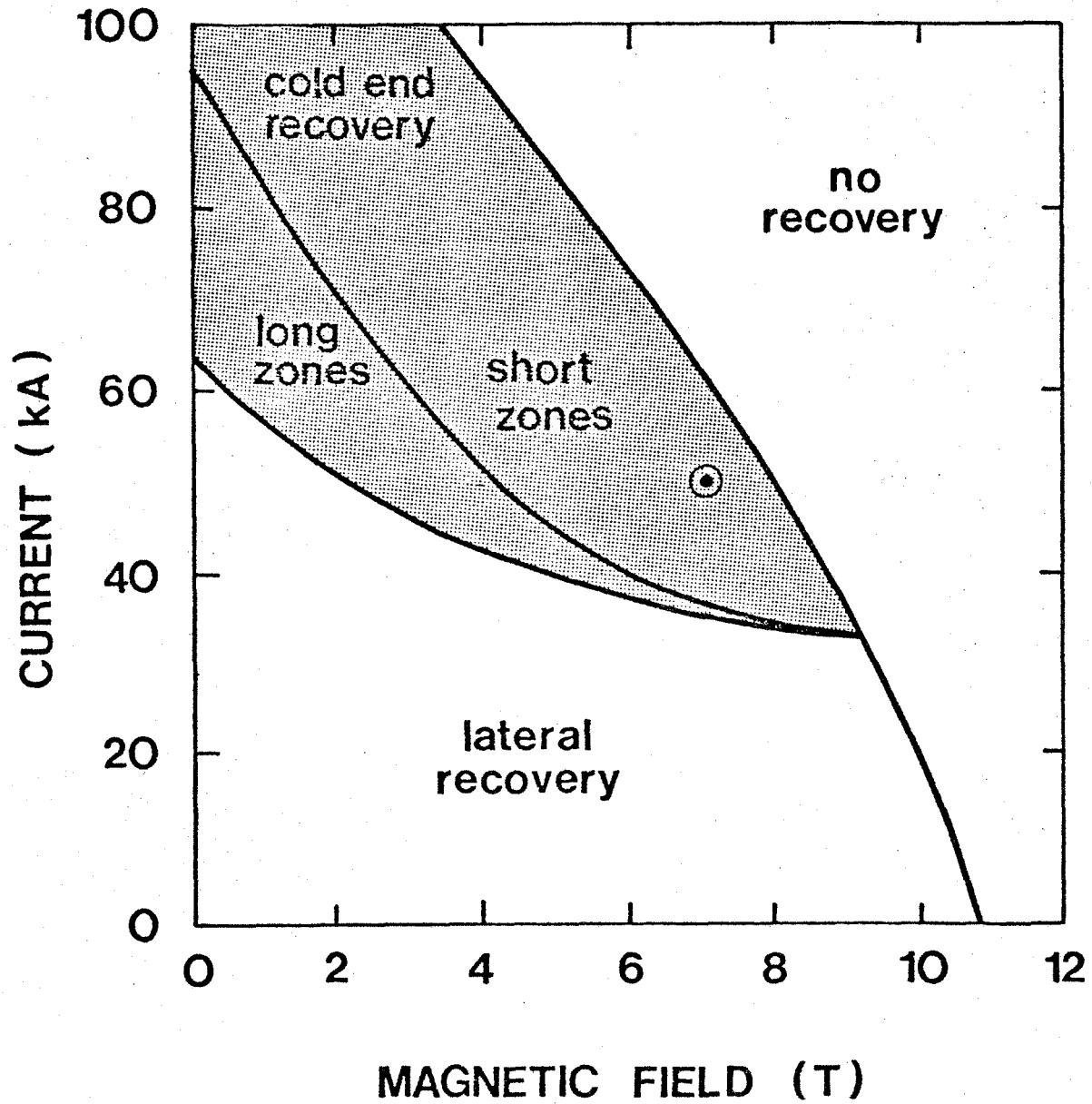
Table 4.1.10.1-I

Initial Conductor Specifications

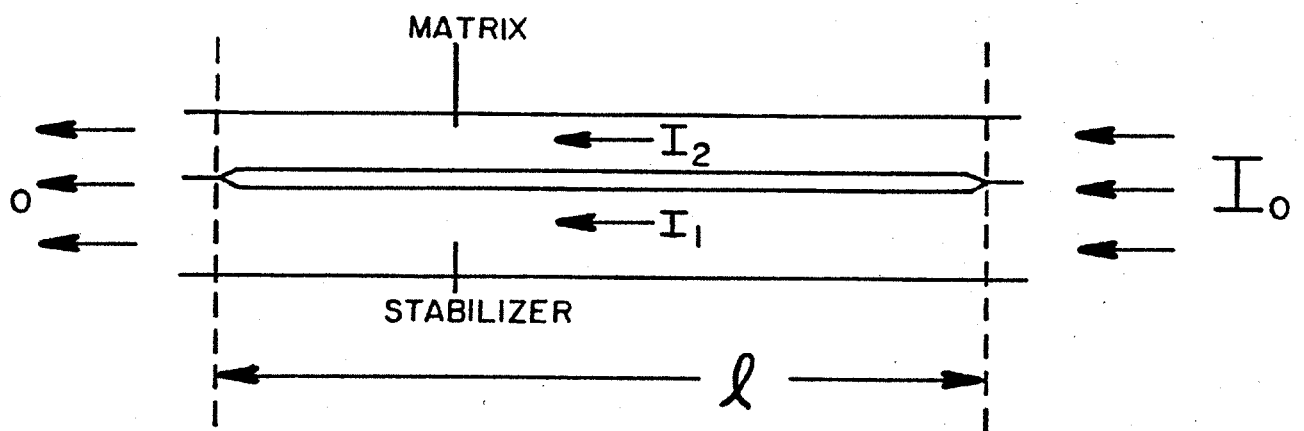
Conductor dimension	$1.0 \times 8.0 \text{ cm}^2$
Current rating (dc)	50 kA at 7 T
Channel size	$9.0 \times 9.0 \text{ cm}^2$
Angle of conductor face to horizontal	$16^\circ$
Material	NbTi-Cu



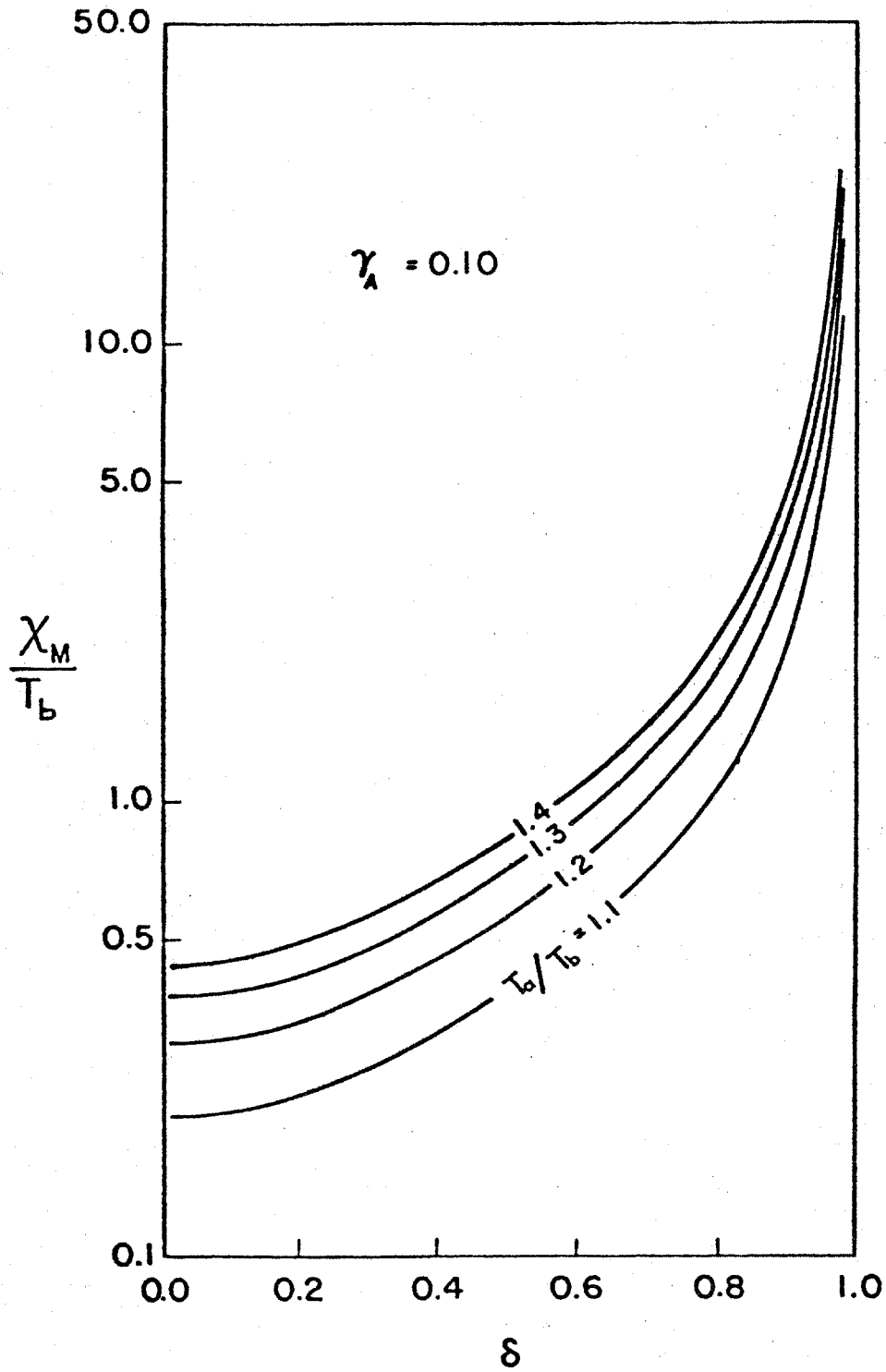
4.1.10.1A Schematic Diagram of a 50 kA Conductor Considered in Stability Analysis



4.1.10.1B Typical Plot of Limiting Currents for a Large Built-Up Copper Plus NbTi Conductor Cooled by Liquid Helium (The anticipated operating point is indicated by the circled dot)



4.1.10.2A Conductor Model Used to Determine Recovery Length. Composite Conductor with Delaminated Length,  $l$



4.1.10.2B Curves Showing Allowable Dimensionless Delaminated Length,  $x_m/T_b$ , for  $A_2/A_0 = 0.1$   
 ( $\delta^2 = \text{heat removed/heat generated}$ )



$$T_a = \frac{T_c + T_s}{2}$$

$T_c$  = critical temperature

$T_s$  = transition temperature

Table 4.1.10.2-I shows allowable delaminated lengths,  $\ell$ , for three assumed heat transfer coefficients determined analytically under conditions of Case 3.

Using parameters of the CDIF/SM conductor and with a numerical approach aided by a computer program, maximum allowable delamination lengths  $\ell$ , were determined as listed in Table 4.1.10.2-II where  $s_2$  = composite cooling surface area and  $s_0$  = conductor cooling surface.

Evaluation of MHD magnet conductors covered the following types of conductor, each sized for 20 kA, 40 kA and 60 kA:

CASK conductor (flat strip, multiple inserts)

Cable conductor (circular, twisted)

CFFF conductor (flat strip, Rutherford cable inserts)

CDIF conductor (square, monolith or cable insert)

Each conductor was analyzed in terms of stability based on minimum propagating zone (MPZ) energy and in terms of absolute cryogenic stability. Design charts were produced and conductor dimensions were determined using these charts. Delamination limits and ac losses were estimated.

MPZ calculations for the CDIF conductor at 6 kA determined MPZ energy per unit area,  $\Delta E = 15.5$  mJ/cm<sup>2</sup>. Typical data calculated for the CASK type full-scale conductor designed for 40 kA are listed in Table 4.1.10.2-III. Data calculated for the CASK type full-scale conductor designed for absolute cryogenic stability, using a heat flux of 0.18 W/cm<sup>2</sup>, are listed in Table 4.1.10.2-IV. Allowable delamination lengths calculated for the 40 kA CASK conductor are listed in Table 4.1.10.2-V. Calculated ac losses for this conductor are listed in Table 4.1.10.2-VI. Similar data were calculated for other sizes of CASK type conductor and for cable, CFFF and CDIF (full-scale) conductors.

The effects of electric and thermal contact resistance on the cryogenic stability of MHD magnets was investigated. Figure 4.1.10.2C shows MPZ energy,  $\Delta E$ , in K<sup>4</sup>, versus fraction of composite in contact,  $f$ , for a composite conductor simulating the CDIF conductor length exposed to coolant,  $\beta = 0.50$ . The figure shows that  $\Delta E$  decreases appreciably for  $f$  less than 0.55. Based on these data, it was recommended that the void ratio in the CDIF conductor be less than 0.4.

More detailed information on the stability analysis and evaluation of MHD magnet conductors is contained in References 63, 64 and 65.

#### 4.1.11 Testing of Materials for Main Structure

Testing of structural materials was conducted in conjunction with the CDIF/SM design and construction program (See Section 4.3.1). The CDIF/SM design incorporated a main structure of welded 304LN stainless steel. When the magnet is in service, the main structure operates at 4 K and is subjected to very large magnetic forces. Manufacturing plans called for final welding of the main structure to be done by GE.

In order to verify the expected tensile and fracture toughness properties of the structural welds, two sample weldments were tested by NBS. Both samples consisted of 304LN stainless steel base plates, submerged-arc welded by GE using 316L filler material. One sample contained approximately 5% delta-ferrite, the other approximately 9%.

Cross-weld and all-weld tensile specimens were tested at 295 K, 76 K and 4 K. Compact tension specimens were tested for fracture toughness and fatigue crack growth rate at 4 K. In the tensile tests, all ten specimens

Table 4.1.10.2-I

CDIF Conductor Allowable Delamination Length Assuming  
End Cooling But No Composite Cooling

	Heat Transfer Coefficient, W/m <sup>2</sup> K		
	10000	5000	1000
$g_1$	0.515	0.509	0.450
$T_e$ , end temperature, K	4.64	4.69	4.881
$I_2/I_0$	0.515	0.059	0.450
$\ell$ , allowable delaminated length, cm	1.84	1.60	1.59

Table 4.1.10.2-II

CDIF Conductor Allowable Delamination Length, Determined By  
Computer Program, Assuming Different Values of  $S_2/S_0$

	$S_2/S_0$			
	0	0.05	0.1	0.15
$I_2/I_0$	0.681	0.684	0.688	0.694
$T_m$ , maximum temperature, K	5.50	5.50	5.60	5.6
$T_e$ , end temperature, K	4.64	4.64	4.67	4.67
$\ell$ , maximum allowable delamination length, cm	2.03	2.14	2.24	2.35

Table 4.1.10.2-III

## MPZ Data for 40 kA CASK Type Conductor

	Overall Current Density, A/cm <sup>2</sup>			
	2000	4000	6000	8000
Copper cross section, cm <sup>2</sup>	19.4	9.37	6.03	4.37
S.C. cross section, cm <sup>2</sup>	0.635	0.635	0.635	0.635
Number of wires, cm	8	8	8	8
Conductor width, cm	6.8	6.8	6.8	6.8
Conductor height, cm	2.94	1.47	0.98	0.74
$\phi_{Cu}$ , m <sup>2</sup> K/s <sup>2</sup>	1.64	1.23	1.22	1.10
$\phi_{sc}$ , m <sup>2</sup> K/s <sup>2</sup>	18.32	14.13	12.75	11.35
$\phi_{He}$ , m <sup>2</sup> K/s <sup>2</sup>	$2.88 \times 10^4$	$1.11 \times 10^4$	$0.60 \times 10^4$	$0.42 \times 10^4$
$\gamma$	$1.32 \times 10^{-4}$	$0.56 \times 10^{-4}$	$0.34 \times 10^{-4}$	$0.24 \times 10^{-4}$
Maximum temperature, K	6.11	5.53	5.27	5.15
$\Delta E$ (MPZ), mJ	892.4	209.1	96.2	53.65
$\Delta e$ , mJ/cm <sup>2</sup>	44.62	20.91	14.44	10.73

Table 4.1.10.2-IV

## CASK Type Conductor Dimensions for Absolute Cryogenic Stability

	Wire Size	Current, kA		
	cm	20	40	60
Conductor width, cm	0.2	6.7	13.1	19.4
Conductor height, cm	0.2	1.5	1.7	1.8
Number of composite wires	0.2	17	33	49
Conductor width, cm	0.4	3.9	7.1	10.3
Conductor height, cm	0.4	3.2	4.3	4.9
Number of composite wires	0.4	5	9	13

Table 4.1.10.2-V

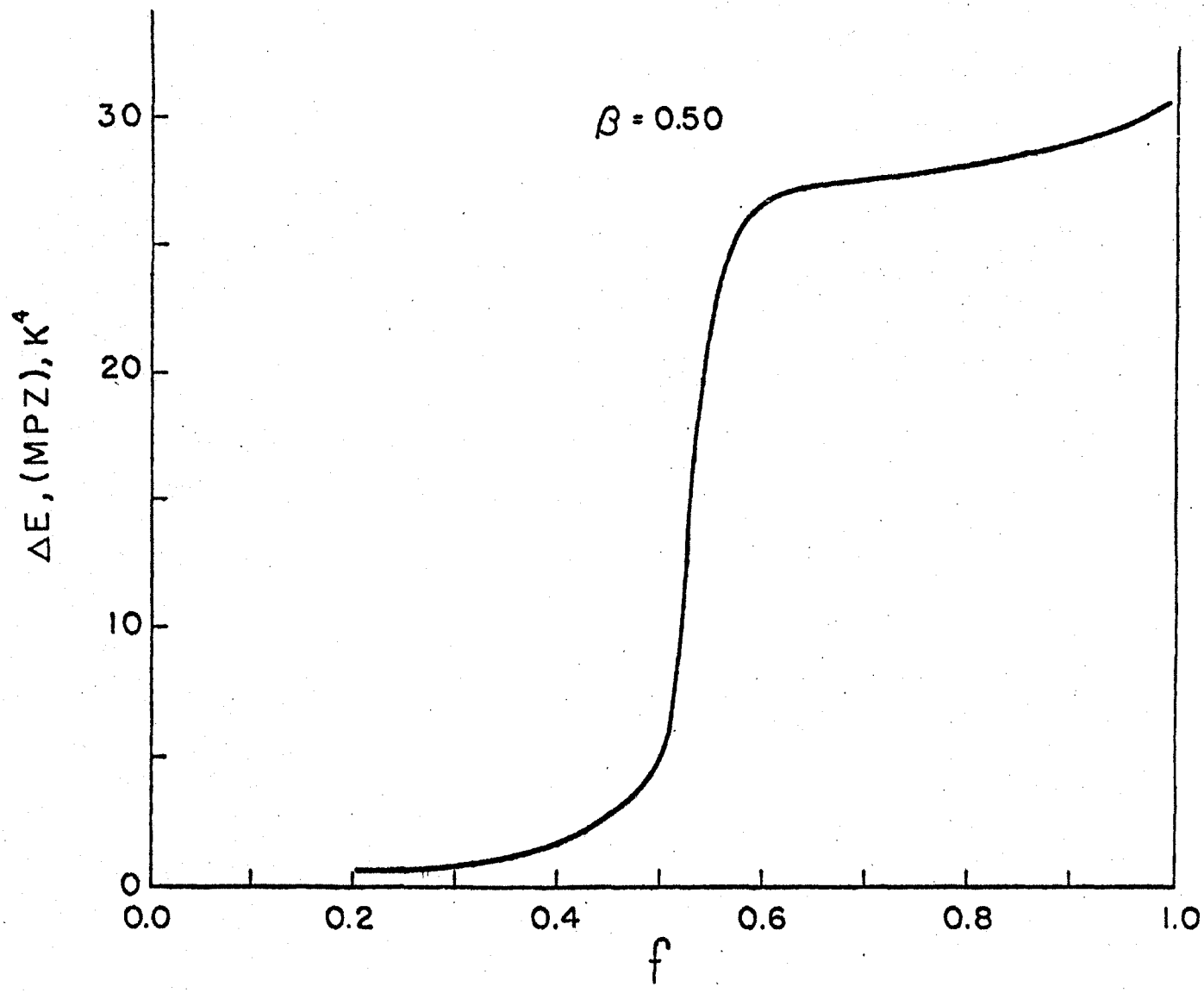
Allowable Delamination length for 40 kA CASK type conductor

	Current Density, A/cm <sup>2</sup>			
	2000	4000	6000	8000
$I_2/I_0$	0.412	0.548	0.671	0.777
$T_e$ , end temperature, K	4.77	4.85	4.80	4.76
$T_M$ , maximum temperature, K	5.82	5.62	5.46	5.33
$l$ , delamination length, cm	4.8	2.6	1.9	1.6

Table 4.1.10.2-VI

A.C. Losses for 40 kA CASK Type Conductor

	Current Density, A/cm <sup>2</sup>			
	2000	4000	6000	8000
$\lambda_c$ , twist length, cm	14.1	15.1	15.4	15.6
$t_c$ , charging time, s	1150.0	654.3	457.2	353.6
$P_t$ , twist losses, W/m	9.712	8.536	8.144	7.952
$P_d$ , eddy current losses, W/m	0.0658	0.0579	0.0552	0.0539



4.1.10.2C Curve of MPZ Energy ( $\Delta E$ ) vs. Fraction of Composite in Contact ( $f$ ) for Composite Conductor with Thermal Contact Resistance  $\beta = 0.5$



tested at 4 K showed yield strength and ultimate strength within expected limits. The minimum test yield was 721 MPa; the minimum test ultimate was 956 MPa. Eight of the 10 specimens had elongations within expected limits (minimum test elongation 20.4%) but two were abnormally low (6.7 % and 13.3%). The reason for the low elongation measurements on these two specimens appeared to be the presence of some microfissuring in the weldment.

More detailed information on testing of these two weldments is contained in Reference 66.

In order to verify the expected shear strength of the structural welds, three additional samples of 304-LN material with 316L welds were prepared at GE. The samples were then machined and tested at another subcontractor, Manlabs. The 316L weld shear sections tested were about 2.5 cm long by 0.5 cm thick. Testing was done at liquid nitrogen temperature (77.4 K).

Test results showed shear ultimate to be in the range of 897 to 945 MPa.

The weld design shear stress for the CDIF/SM at 4 K was 276 MPa. This is only 30% of the average ultimate shear stress observed on the tests. This margin was considered adequate.

Additional information on the shear testing performed is contained in Reference 66A.

#### 4.1.12 Testing of Materials for Substructure

The CDIF/SM design incorporated an insulating substructure made up of grooved plates of cloth-reinforced plastic laminate. Conductors were individually supported in the grooves. Since the substructure was thus required to transmit magnetic loads from the conductors to the surrounding superstructure, a material having high mechanical strength at cryogenic temperature was called for. It was found that adequate information on structural properties of candidate insulating materials was not available; therefore an extensive testing program was carried out by Manlabs Inc. to obtain data needed to verify the CDIF/SM substructure design.

The major areas of testing and their results are summarized below. More detailed information is contained in Reference 25.

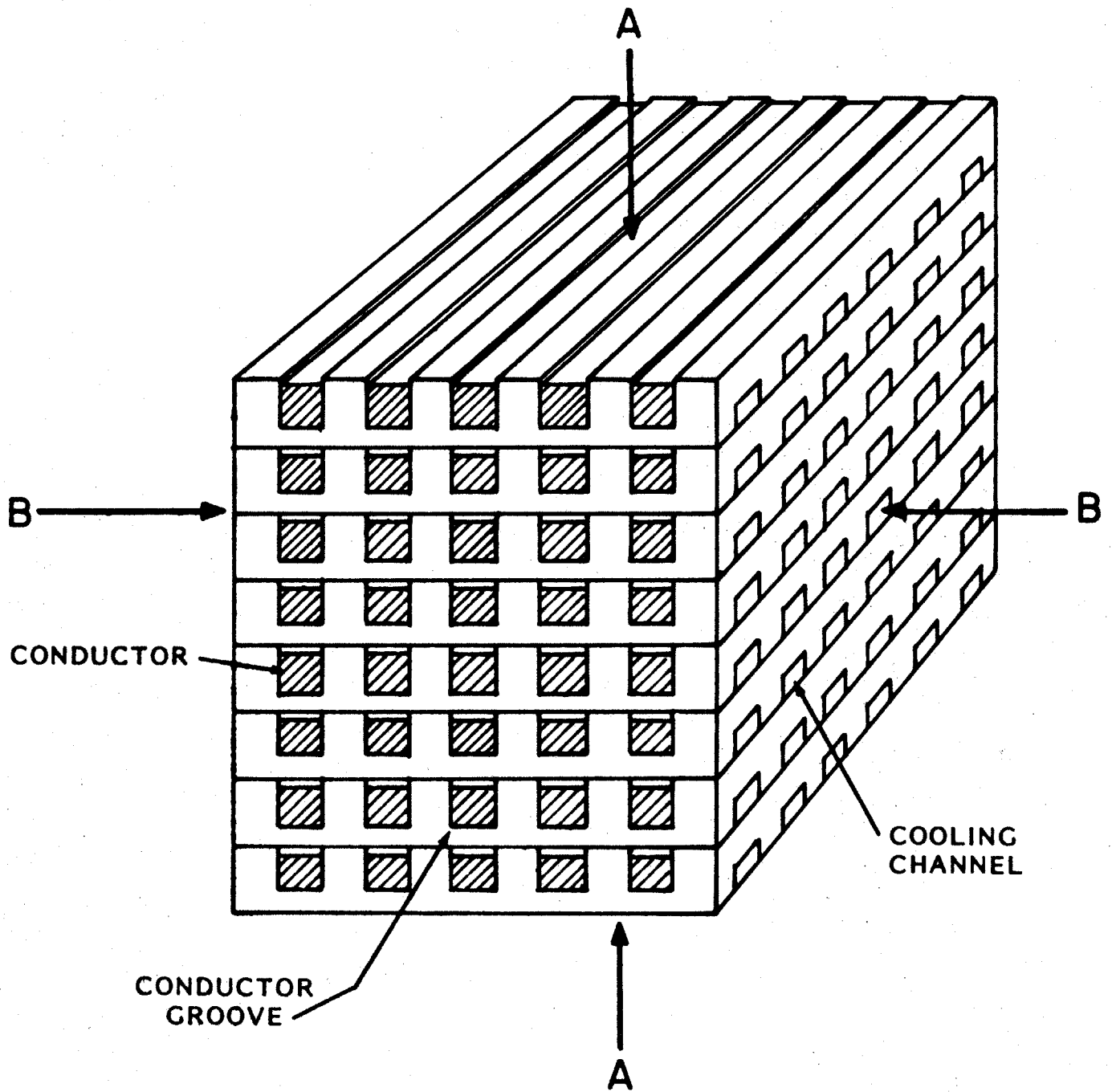
##### 4.1.12.1 Choice of Material

Two candidate materials were subjected to initial testing: linen-phenolic and epoxy-fiberglass (G-10). Compression stress-strain and creep tests were made on substructure models consisting of stacks of grooved plates with dummy conductors in the grooves. The stacks were cubes, 10 cm on a side, as shown in Fig. 4.1.12A. Tests were conducted at room temperature and at 77 K.

When tested at room temperature, the linen-phenolic stack failed under a pressure of 105 MPa in the A direction (indicated in Figure 4.1.12A), whereas the G-10 stack showed only barely detectable changes in surface texture at this pressure, which was the maximum applied. Stress-strain diagrams were plotted from tests at both room temperature and 77 K. The compressive elastic modulus of the linen-phenolic stack was about 1.1 GPa at room temperature and about 1.4 GPa at 77 K. The compressive modulus of the G-10 stack was about 1.9 GPa at room temperature and about 2 GPa at 77 K.

When tested for creep under pressure in the A direction at room temperature, the linen-phenolic stack showed a creep, after initial set, of about 0.35% in 10 hours with 28 MPa load, while the G-10 stack showed a creep of < 0.02% in 50 hours with 25 MPa load.

According to the literature [66B], epoxy composites such as G-10 have better mechanical properties at low temperature than other reinforced plastics employing different matrix systems. This information, together with the superior performance of the G-10 compared to linen-phenolic in tests on the 10 cm stacks described above, led to the selection of G-10 as the preferred substructure material.



4.1.12A Stack of Model Subplates for Compression Testing at Room Temperature and 77 K

Further testing was done on 10 cm G-10 stacks using different designs of conductor grooves and cooling channels. The B direction edgewise compressive modulus of elasticity of the stack of final design (with straight grooves containing wrapped superconductor) at room temperature was approximately 3 GPa; the A direction flatwise compressive modulus of the stack was approximately 4 GPa.

#### 4.1.12.2 Compressive Testing of G-10 Specimens

Since orientation of the Lorentz forces in the magnet winding is a function of all three coordinates, mechanical strength in relation to fiber direction is an important parameter. At the time the test program started, this information for G-10 at cryogenic temperature was not available from the literature.

Over 240 specimens of different sizes and various fiber directions from four suppliers were tested for compressive strength. Approximately half of all tests were conducted at RT, half at 77 K and a few at 4 K.

The effect of the fiber direction on edgewise compressive ultimate strength ( $\sigma_{cu}$ ) for specimens obtained from three different suppliers was measured at RT and 77 K (Figure 4.1.12B). Edgewise  $\sigma_{cu}$  at 45° to the fiber direction was found to be 50% and 67% of the edgewise  $\sigma_{cu}$  at 0° to the fiber direction, at RT and 77 K, respectively. Thus, in structural design analysis it is necessary to take into account the dependence of edgewise compressive strength on the fiber direction in G-10-type materials.

One of the problems in designing large structures from composite materials is extrapolating the strength data obtained in testing small size specimens to values appropriate for the large structures.

To study the effect of a specimen's size on the edgewise compressive strength, thirty specimens of G-10CR cut at 90° to fiber direction were tested, half at RT and the rest at 77 K. Proportional changes in specimen size were made by varying all three dimensions. Each data point represents the average of tests on five specimens.

Results of the tests (Figure 4.1.12C) at RT show no significant change in properties of specimens of different sizes, but at 77 K the  $\sigma_{cu}$  of the larger specimens is 20% lower than the  $\sigma_{cu}$  of the smaller specimens. This relative decrease is possibly due specifically, or principally to an increased brittleness of the material at lower temperatures.

#### 4.1.12.3 Tensile Testing of G-10 Specimens

Twelve specimens were tested for tensile ultimate strength ( $\sigma_{tu}$ ) at RT and 77 K. Half were tested at 0°, and the rest at 45° to fiber direction. No significant scatter was observed. Results show (Figure 4.1.12D) that the relation between  $\sigma_{tu}$  at 45° and 0° to fiber direction is similar to the relationship between edgewise  $\sigma_{cu}$  at 45° and 0° at both RT and 77 K.

Transverse tension tests were conducted with cylindrically-shaped specimens,  $d = 0.75$  cm at RT and 77 K. Transverse  $\sigma_{tu}$  is 39 MPa, and increases to 87 MPa at 77 K.

#### 4.1.12.4 Interlaminar Shear Testing

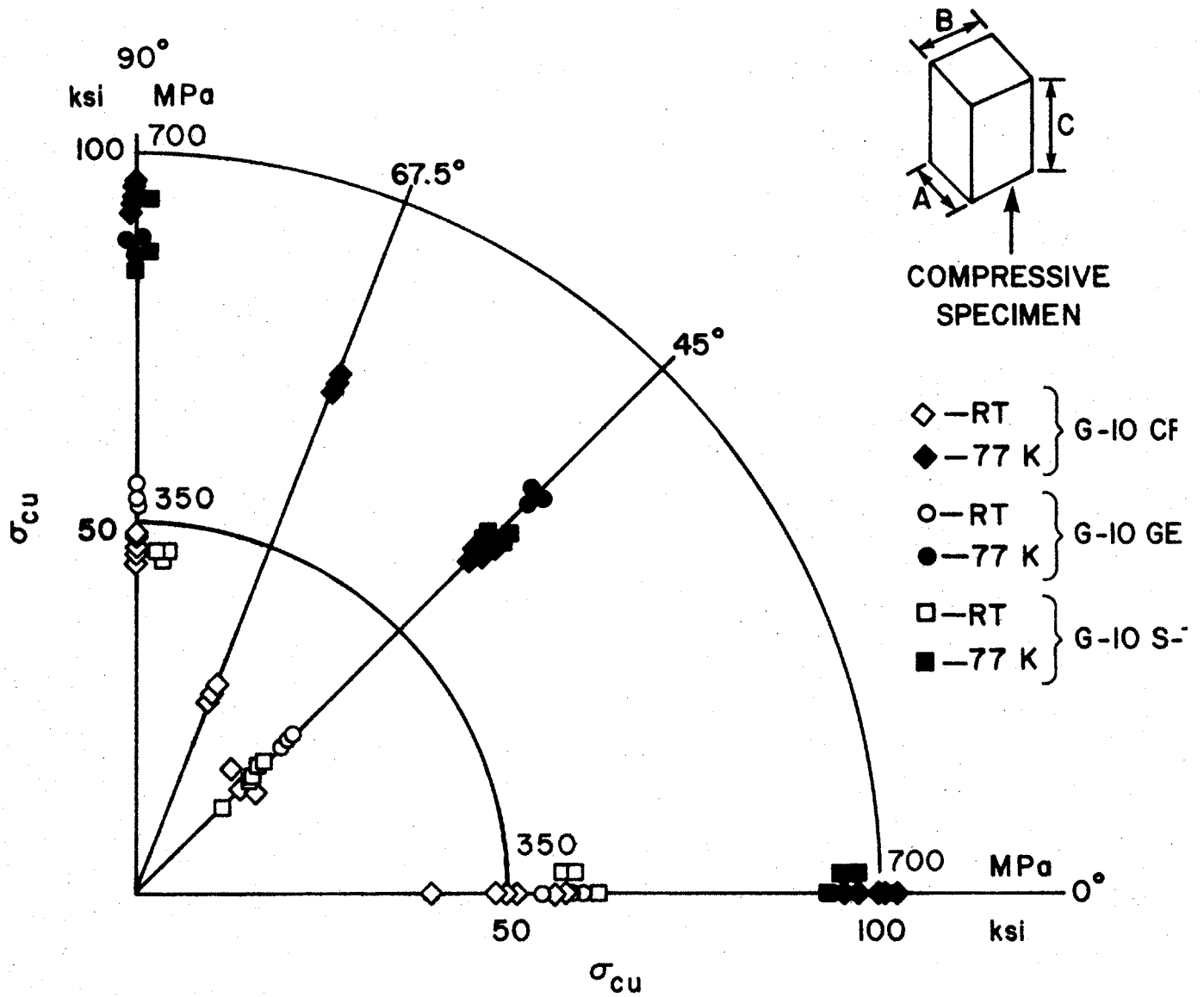
Interlaminar shear strength, (ILSS) plays an important role in subplate design. Over 260 guillotine test specimens from five different suppliers were tested at RT, 77 K, and a few at 4 K. Both standard grade material (G-10) and cryogenic grade material (G-10CR) were included.

The effect of sample orientation with respect to fiber direction is shown in Figure 4.1.12E. Interlaminar shear strength ( $\tau$ ) at 45° in comparison with 0° decreased about 34% at RT and about 13% at 77 K.

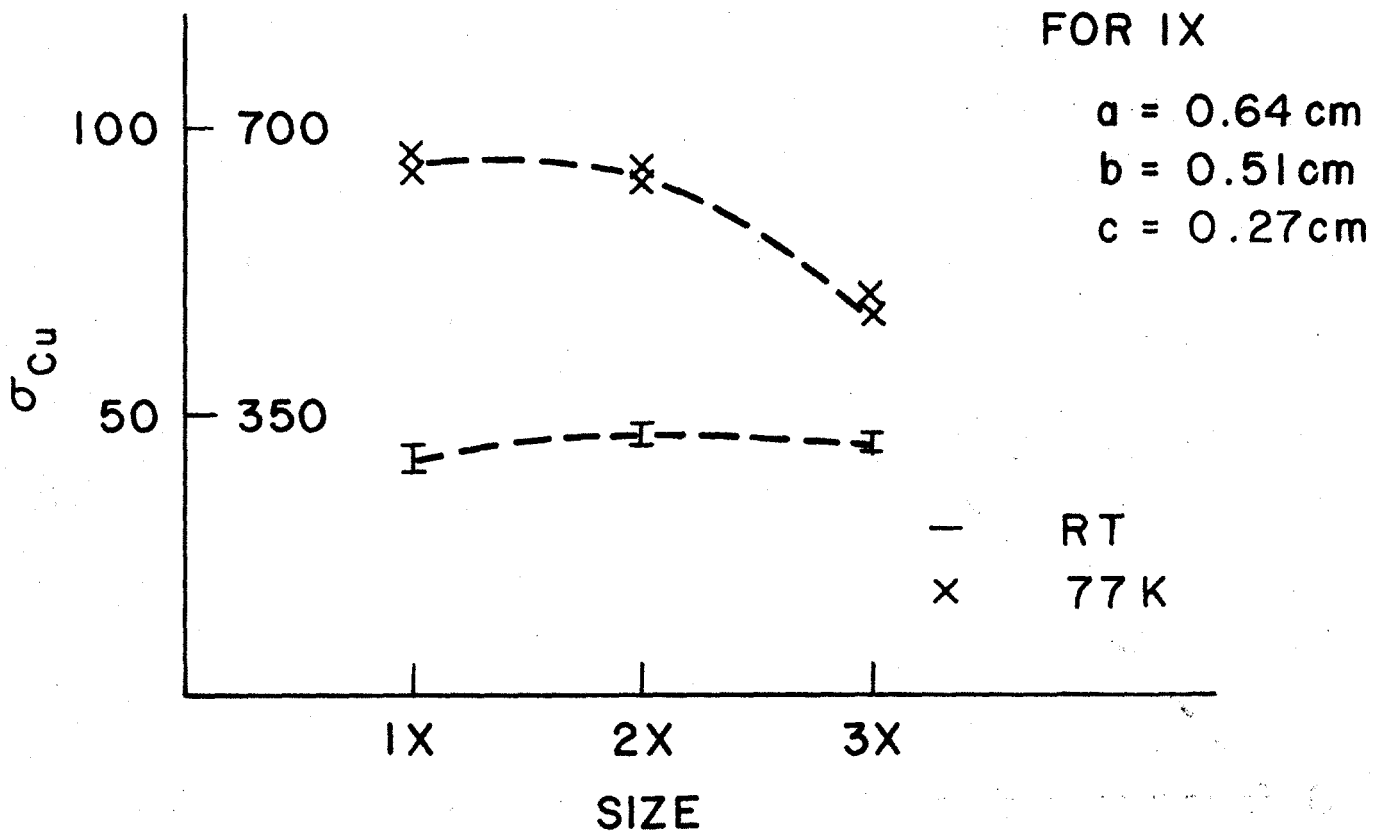
#### 4.1.12.5 Structural Tooth Testing

Most of the testing with GRP materials is carried out by uniaxial loading. However, the real structure is often stressed multiaxially and therefore a specific structural test with a load distributed simultaneously along different axes should be used.

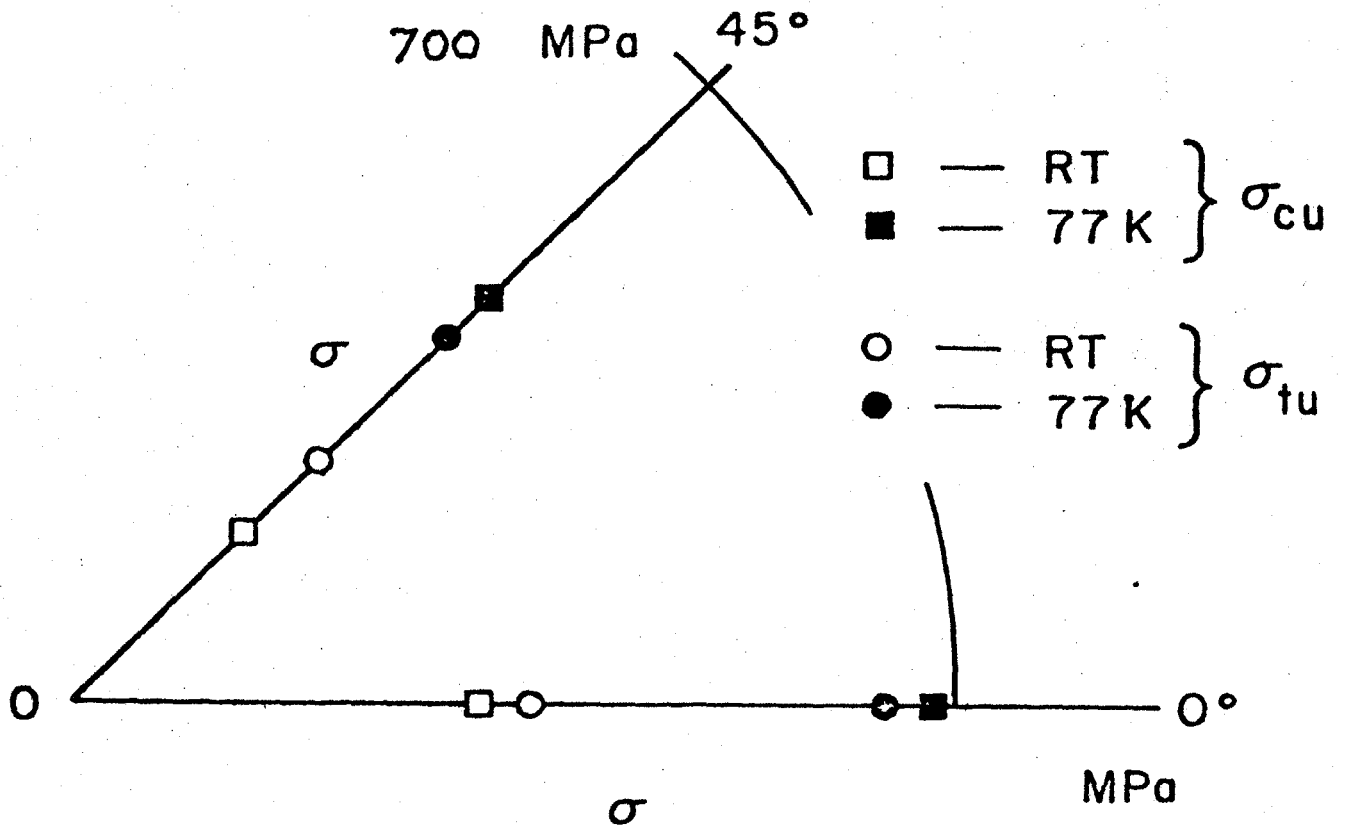
A structural test, tooth push-off, was conducted using a fixture which corresponds to the design of the CDIF magnet. A schematic drawing of this fixture is presented in Figure 4.1.12F. Side-plates allow one to model the influence of the actual plates in the magnet's design. A retention frame and preload screw permit



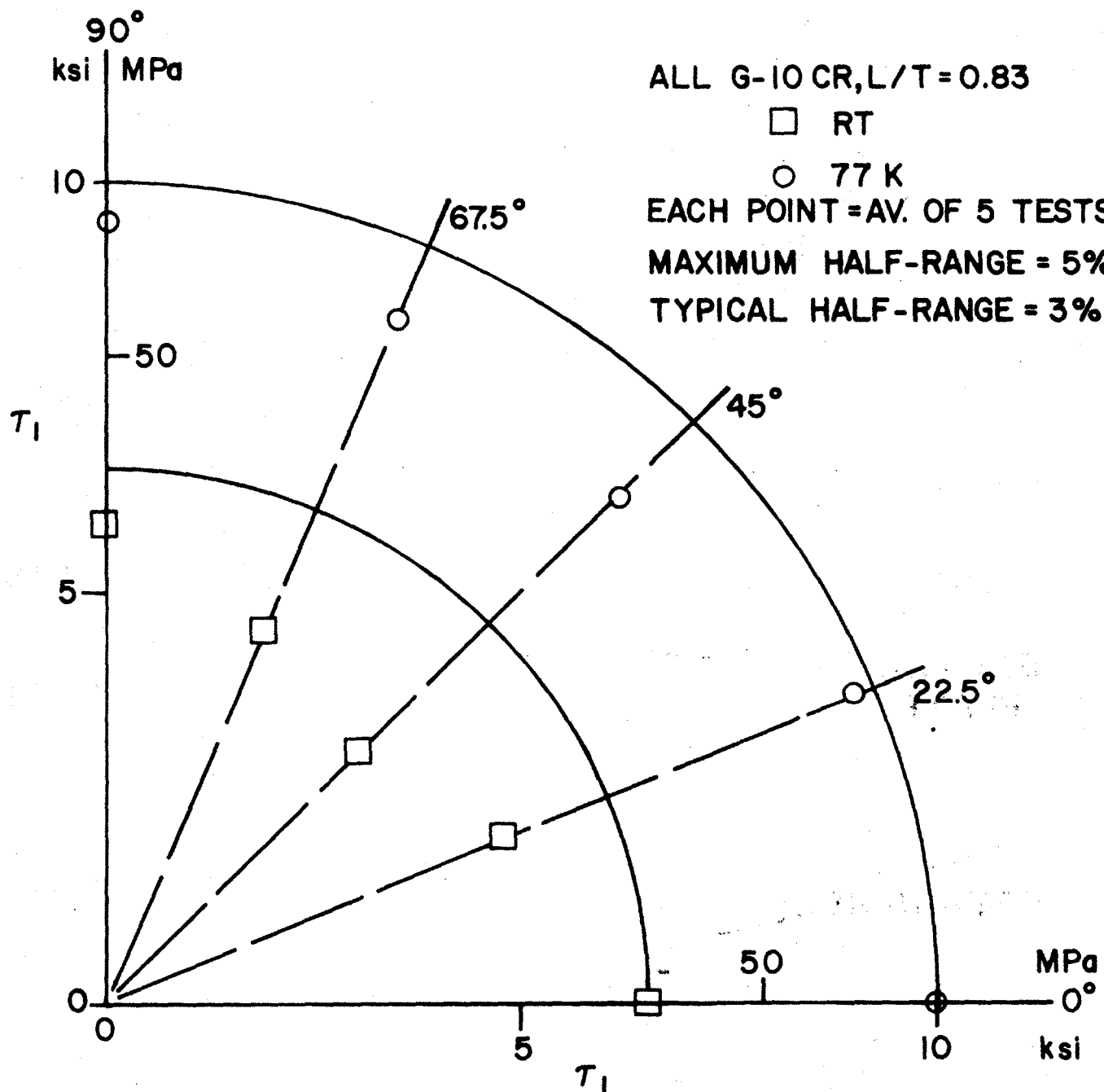
4.1.12B Polar Diagram of Edgewise Compressive Strength of G-10 as a Function of Fiber Direction



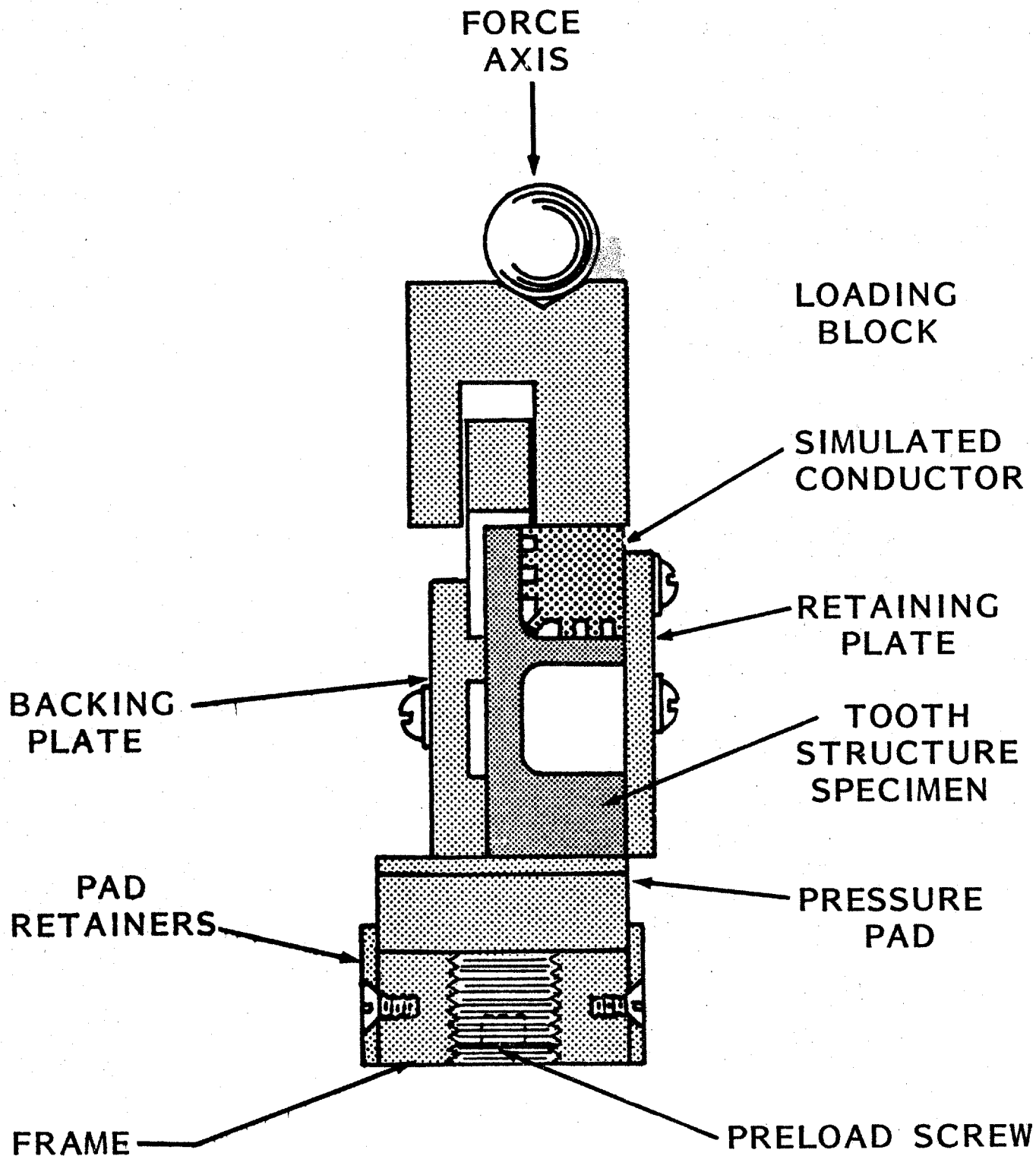
4.1.12C Curves of Effect of Specimen Size on Compressive Strength of G-10 at RT and 77 K



4.1.12D Plot of Tensile and Compressive Strength of the Same Sheet of G-10 at RT and 77 K



4.1.12E Polar Diagram of the Interlaminar Shear Strength of G-10 Specimens as a Function of Fiber Orientation



4.1.12F

Diagram of Structural Test Fixture for G-10 Tooth Push-Off Test



modeling of the cumulative compressive force. The simulated conductor is made from copper and grooved to model the actual design of the CDIF superconductor. The structural test specimen is shown schematically in Figure 4.1.12G.

The first thirty specimens were cut at  $0^\circ$ ,  $45^\circ$  and  $90^\circ$  to the fiber direction with two different tooth thicknesses ( $T = 0.64$  cm and  $T = 0.27$  cm) with radii of  $R = 0$  (Figure 4.1.12G). These were tested at RT and 77 K. The specimens with either tooth thickness cut at  $0^\circ$  to fiber direction are characterized by the lowest breaking force at both RT and 77 K (Figure 4.1.12H).

Therefore, the next tests were conducted only with specimens cut at  $0^\circ$  to the fiber direction. Specimens with a range of tooth thicknesses and different groove radii ( $R = 0; 0.08; 0.15; 0.23$  cm) were tested at RT and 77 K (Figure 4.1.12J). A radius of 0.23 cm satisfied the CDIF design requirements.

The combination of compressive forces from cumulative magnetic field loads, and the tooth breaking force was tested using a retention frame with a preload screw (Figure 4.1.12F) at RT and 77 K. With a rectangular cross section conductor model, an increase in breaking force was observed with increasing compressive forces at both RT and 77 K.

The presence of side-plates (backing plate and retaining plate as shown in Figure 4.1.12J) in tests conducted both at RT and 77 K leads to a significant increase in tooth breaking force.

#### 4.1.12.6 Thermal Cycling

As the CDIF magnet system will normally be operated at 4.5 K but will be brought to room temperature or to intermediate temperature occasionally, measurements were made of the ILSS at 77 K as a function of thermal cycling.

Specimens of G-10 laminates from two suppliers were tested (Table 4.1.12-I). Hundred-cycle tests from RT to 77 K and ten-cycle tests from RT to 4.2 K indicated no significant changes in ILSS at 77 K.

#### 4.1.12.7 Quality Control

Quality control in the fabrication of GRP materials is especially important when these composites have to serve at cryogenic temperatures.

Two sheets, #1 and #2, from different lots produced by one supplier were tested for ILSS at RT and 77 K. ILSS of sheet #1 was approximately 35% lower at RT and 52% lower at 77 K than were ILSS data for sheet #2 and for most of the other G-10 materials tested at NML. Structural tooth tests on these two sheets showed similar differences at 77 K.

Investigation of this phenomenon showed that both sheets have the same type of glass-cloth, and almost identical density and percent glass content. But micrographs and ultrasonic inspection indicated that distribution of resin within the composite in sheet #2 was more uniform than in sheet #1.

In discussion with the manufacturer, the conclusion was reached that the precise technological procedure used in manufacture was different for these two sheets. Therefore, when G-10 laminate is to be used at cryogenic temperature, special attention must be paid to follow stable manufacturing procedures.

#### 4.1.12.8 Cryogenic Grade G-10

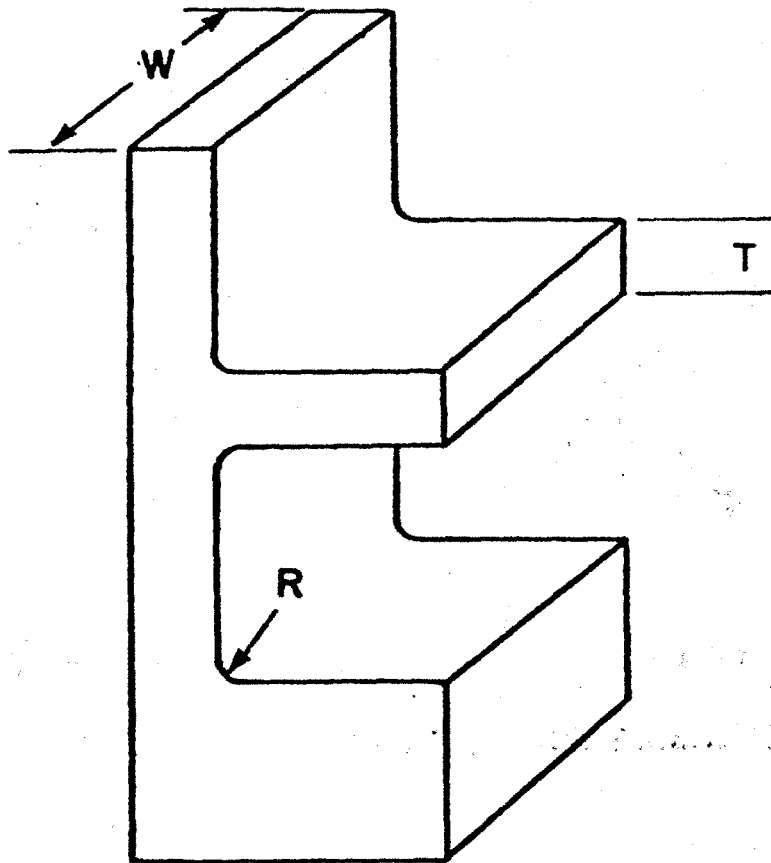
As a result of contacts with manufacturers of G-10 material during the testing program described above, interest in material for cryogenic applications was stimulated. As a result, considerable work was done by manufacturers themselves in developing a cryogenic grade of G-10, known as G-10CR. The objective was to establish controlled compositions and manufacturing procedures, generally within the constraints already established for G-10 electrical grade material, that would result in more uniformly good mechanical properties at cryogenic temperatures. Some of the material tested in the MHD program was cryogenic grade. More work should be done in the future involving cooperative effort of materials manufacturers and magnet designers.

**Table 4.1.12-I**  
**Interlaminar Shear Strength of G-10 Samples at 77 K After Thermal and Load Cycling**

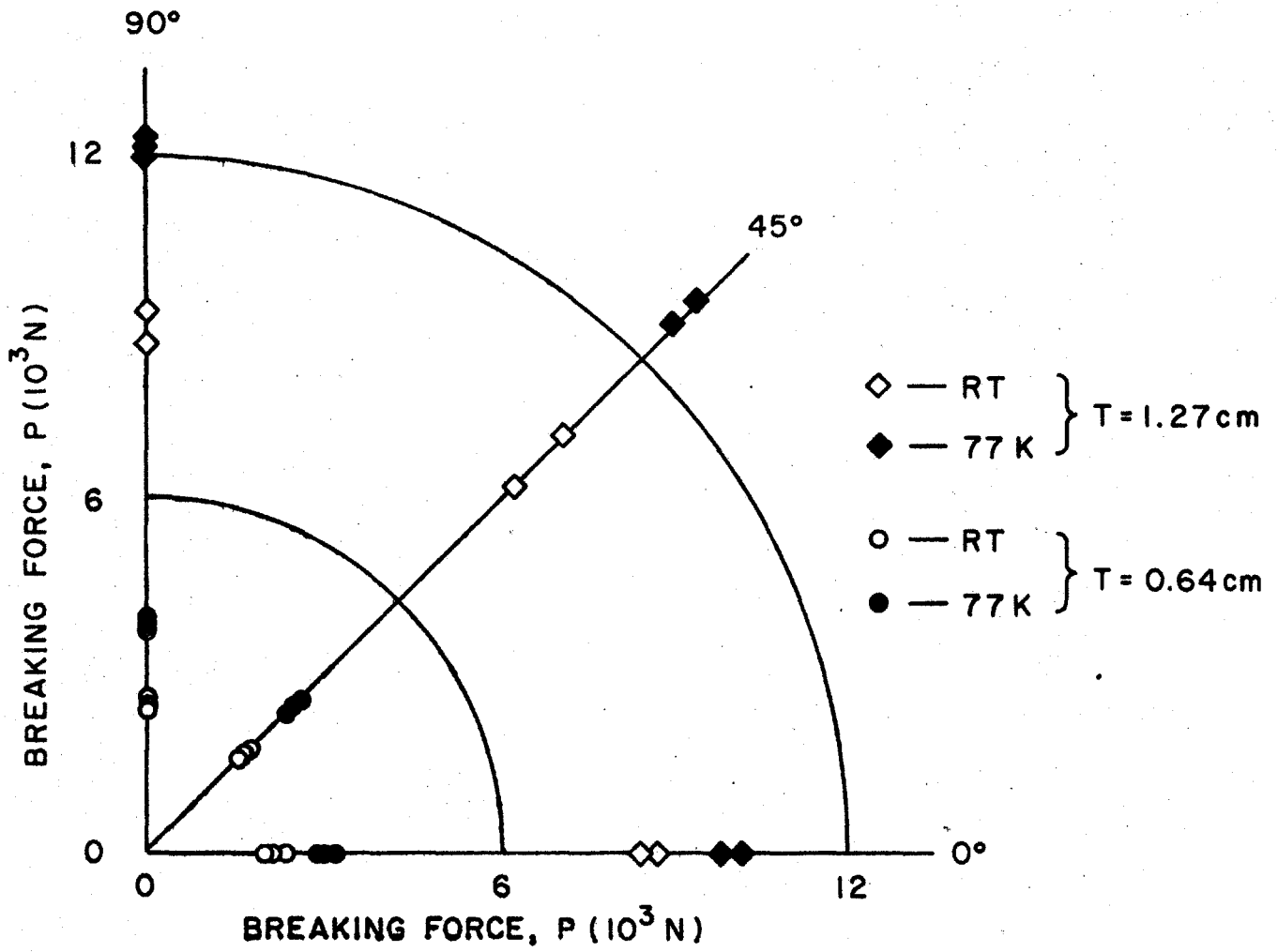
Number of Thermal Cycles		Number of Loading Cycles*	$\tau_I$ at 77 K (MPa)	
RT-77 K	RT-4.2 K		G-10GE $l/t=0.75$	G-10CR $l/t=0.6$
0	0	0	67.0	82.9
10	0	0	67.1	81.3
100	0	0	67.1	—
100	0	100	66.6	—
10	0	100	—	82.6
0	10	0	—	81.5
0	10	100	—	82.5

\*Range of load cycling  
G-10GE: 0-10.5 MPa  
G-10CR: 0-16.8 MPa

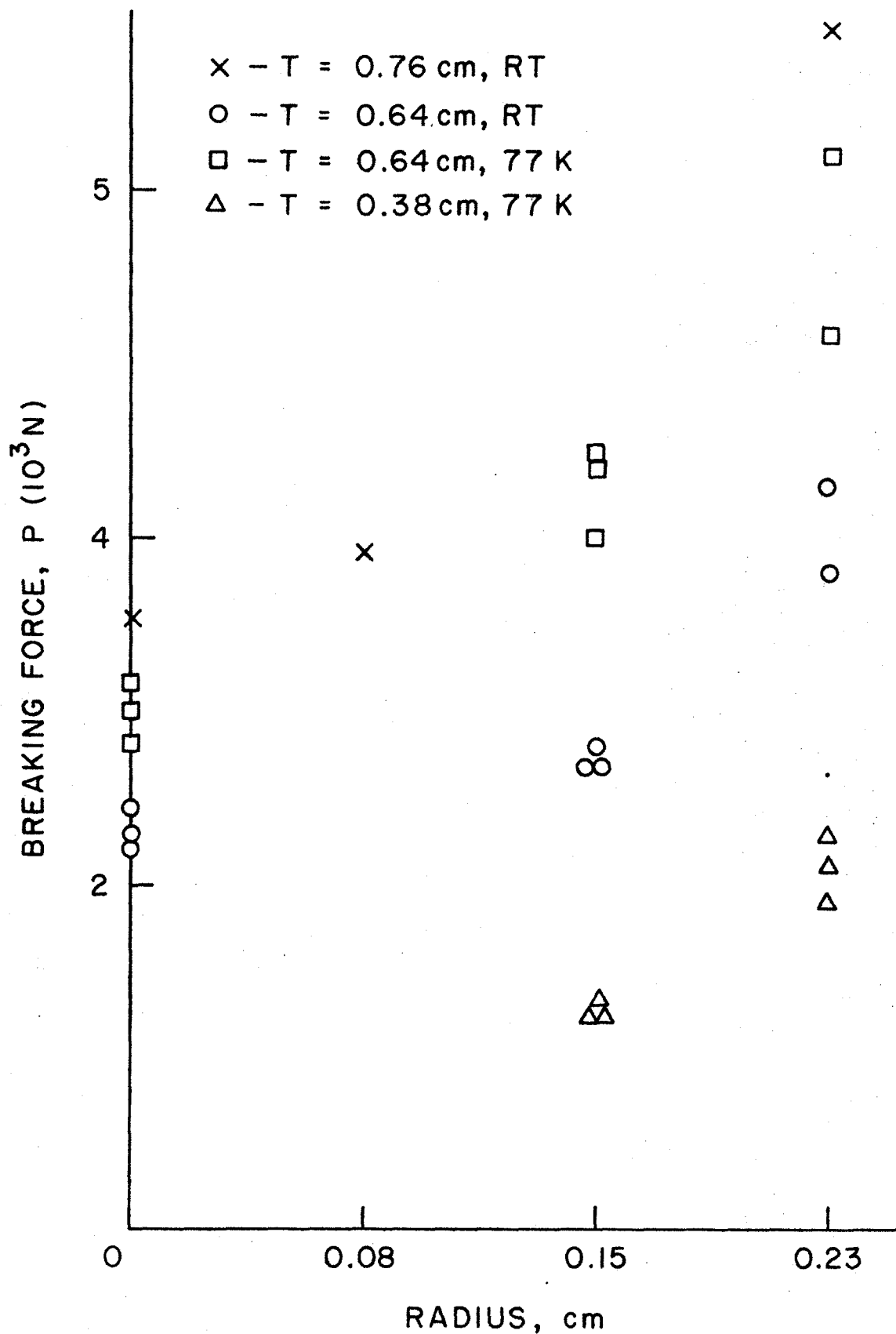
# BENDING - SHEAR SPECIMEN



4.1.12G Sketch of Structural Tooth Specimen,  $W = 1.27$  cm



4.1.12H Polar Diagram of Breaking Force in Tooth Test



4.1.12]

Plot of Variation of Breaking Force with Changes of Groove Radius in Tooth Test

#### **4.1.13 Survey of Materials for Superconducting MHD Magnets**

A preliminary survey of materials for superconducting MHD magnets was made and a proposed research program was outlined by the National Bureau of Standards under subcontract from MIT.

Materials chosen by designers for MHD magnets built or currently being designed, including those listed in Table 4.1.13-I, were reviewed.

Attention was called to the need for an adequate data base for MHD magnet materials, particularly for the structural materials used in the low temperature (4.5 K) portions of the magnet assemblies (cold bore tube, end flanges, girders, banding, substructure, insulation, cold mass supports and conductor substrate).

It was concluded by NBS that the data base as it exists today is barely adequate in a few instances and totally inadequate in most others.

A proposed program was generated by NBS, aimed at providing a suitable data base by the year 1985. This program, together with estimated costs, is outlined in Table 4.1.13-II.

The need for coordination of such a program with the Office of Fusion Energy Materials Program was pointed out.

The materials survey is reported in more detail in Reference 67.

#### **4.1.14 Structural Standards for MHD Magnets**

The windings of commercial-scale MHD magnets require very large, strong structures to support them against magnetic forces. The forces act outward from the magnet axis with a magnitude of millions of kilograms per meter of length along the axis. The magnetic energies which the structures must contain are in the range of 5,000 to 15,000 MJ. Cryogenic considerations dictate that the structures be at the same temperature as the windings (liquid helium temperature).

In view of the above, the force containment structure of the MHD magnet is a critical component. It must be designed to operate at relatively high stress in order to be cost effective, yet must safely contain the potentially dangerous energy of the charged windings.

When MHD becomes commercial, it will be necessary that magnets conform to rigorous safety standards. Codes and standards now in use, such as the ASME codes for boilers and pressure vessels, are not written to cover the force containment structures of magnets. It seemed reasonable, therefore, that the matter of codes and standards for MHD magnets be given preliminary consideration in the MHD magnet program, in parallel with the preparation of reference designs for commercial-scale magnet systems. Accordingly, a program to look into codes and standards was initiated. Since magnets for fusion power applications have similar characteristics and needs, the program was expanded to cover both MHD and fusion magnets.

The development of a tentative structural design code was started and an internal report [32] was issued in 1979. After further study, a tentative standard, "Structural Design Basis for Superconducting Magnets" [68] was issued early in 1980. The standard was sent to a number of laboratories and manufacturers for review and comments.

A Workshop on Structural Standards for Superconducting MHD and Fusion Magnets was conducted at MIT in October 1980 [69]. It was attended by representatives of industry and government. Discussions covered the general subject of codes and standards for magnets, as well as the proposed "Structural Design Basis for Superconducting Magnets" prepared by the MHD Group.

Conclusions derived from the workshop were: 1) there was little consensus among the participants on the need for structural design standards; 2) if standards are to be established, they should be developed in a

Table 4.1.13-I  
Typical Material Choices for MHD Magnet Designs

Magnet	U-25	Stanford	CFFF	CDIF
Stored Energy, MJ	20	79	168	200
Cold Bore Tube	AISI 316	5083 Al	316L	304LN
End Flanges	AISI 316	5083 Al	CF8M	304LN
Girders	—	2219-T87 Al (or T852) 304L Wedges	CF8M 2224-T81 Al	304LN
Banding	AISI 304	—	5052 Al	—
Substructure	Micarta Coil form	2219-T87 Al subplates	Micarta Coil forms	G-10 subplates
Vacuum Vessel	AISI 304	304L	304L	304
Radiation Shield	AISI 304 with copper	6061-T6 Al	304L with copper	304
Helium Vessel	AISI 316	5083 Al	304L	304LN
Turn-Turn Insulation	Polymer film	G-10CR	Pultruded Fiberglass and Polymer film	—
Layer-Layer Insulation	Pultruded Fiberglass	G-10CR	Pultruded Fiberglass and G-10	—
Conductor Stabilizer	copper	copper	copper	copper
Cold Mass Suspension	Fiberglass epoxy strap	Fiberglass epoxy strap	Fiberglass epoxy strap	Fiberglass epoxy bars

Table 4.1.13-II Sheet 1 of 2

## Proposed Program of Low Temperature Materials Research for MHD Magnets

<u>Program</u>	<u>Cost Per year (\$K)</u>	<u>Priority</u>
<u>Base Metal</u>		
Design Allowables at 4 K of Structural alloys:		
304 LN, 2219	400	I
304, 5083	200	III
Development of Weldable, High Strength Aluminum Alloy 7000 Series	75*	II
<u>Welding</u>		
Stainless Steel Welding Process & Filler Metal Development & Specifications		
Weldability	75*	I
Variability	75*	I
Characterization	75*	I
<u>Mechanical Fasteners</u>		
Tensile, Notch Tensile Characterization, 310S, A286	15	III
<u>Castings</u>		
Characterization of Stainless Steel Castings (CF3, CF8, CF3M, CF8M):		
Effects of N <sub>2</sub> Levels	75	II
Effects of Ferrite	75	II
Influence of Microstructural Instability	75	II
<u>Structural Composites</u>		
Variability of 4 K Properties of Commercial, High-Pressure Laminates	100	I
Low Pressure Resin Selection & Characterization	75	II
B-Stage Epoxy Selection & Characterization	75	II
Quality Assurance		
Inexpensive 77 K Test	75	I
Improved NDE	75	I



Table 4.1.13-II Sheet 2 of 2

<u>Program</u>	<u>Cost Per year (\$K)</u>			<u>Priority</u>	
<u>Conductors</u>					
Young's Modulus					
(1) Cold Worked & Processed Cu	20			II	
(2) Superconducting Composite	20			II	
Electrical Resistivity and Magnetoresistivity of Cold Worked Cu	50			II	
Strengthening of Conductor Composite	50			III	
Joining of Conductor Composite	50			III	
<u>Technology Transfer</u>					
Annual Workshops (w/OFE)	5			I	
Handbook (w/OFE)	40			I	
Annual Reports	10			I	
<u>Cost Per Year</u>	<u>FY80</u>	<u>FY81</u>	<u>FY82</u>	<u>FY83</u>	<u>FY84</u>
Priority I	630	630	605	680	605
Priority I & II	800	950	880	980	830
Priority I, II, & III	1000	1150	1095	1230	1080

\* Estimated on basis of probable industrial cost sharing.

step-by-step manner starting with the establishment of specifications and definitions and proceeding in a manner that will not hamper innovation in design; and 3) careful groundwork should be done by an informal group including broad community representation, before an effort is made to form a Standards Committee through a recognized organization such as IEEE or ASME.

Concerning certain detailed items discussed, there was no major disagreement with the proposals that magnet vacuum jackets be designed in accordance with ASME codes for unfired pressure vessels (pending establishment of specific standards) and that magnet force containment structures and associated parts be designed with factors of safety based on material properties at operating temperatures (cryogenic), rather than at room temperature.

The consensus of the overall discussions was that much additional work, including extensive testing of materials at low temperatures, is needed before a basis for structural standards can be developed.

#### 4.1.15 Superconductor Standards

There are as yet no large commercial uses for superconductors. They are currently produced by private industry in relatively small quantities without any widely-accepted, standardized procedure for assuring performance and quality.

In anticipation of future needs for large quantities of superconductor in the areas of fusion energy, high energy physics and magnetohydrodynamics, a program to develop standards for superconductors was initiated at NBS, National Engineering Laboratory, Boulder, Colorado, in 1979. This program was funded by DOE with part of the funding in FY 1979, 1980, and 1981 channeled through MIT. The program was conceived as a cooperative venture involving DOE, NBS and private industry. Its goal was to arrive at a set of useful voluntary standards for measurements on superconductors.

During the first year a great deal of work was done on standardization of terminology; a preliminary assessment of the current status of superconductor measurements around the country was made; an ASTM subcommittee on superconductors was formed; preliminary transient loss measurements were made; critical temperature measurements on practical materials were made; and, after evaluation, it was decided that specific standards for this parameter were not appropriate yet; extensive research on factors that influence the determination of critical current was done by NBS and the four wire manufacturers.

The second year's work concentrated heavily on the critical current measurement standard. The present state of measurement capability was evaluated by means of a survey that also determined presently-used criteria and precision and accuracy values for critical current measurements. Also, a round robin test of several superconducting materials was made among the wire manufacturers and NBS.

During the third year, a standard for critical current measurement up to 600 A was put in final form. The standard is currently in the ASTM voting process. Standard terminology was developed and is also currently in the voting process. The effect of current transfer on critical current measurement, determined to be more difficult to evaluate than originally expected, was further investigated. Work continued on standards for critical current measurements of 10 kA and above. Consideration is being given to making such standards recommended only, without obtaining ASTM acceptance at this time.

Work done in the first two years is reported in References 70 and 71. A report covering work in 1981 is in process.

#### 4.1.16 Investigation of Safety and Quench Protection

Safety and quench protection investigations have included preliminary quench analyses of the TFM and three test coils mounted in it, and planning of special quench and protection tests to be run in this facility. Instrumentation to detect quench and quench propagation has already been installed and initial test data have been obtained. Investigations of quench protection of baseload-scale MHD magnets, with particular attention to insulation and voltage breakdown levels have been conducted and reported on by a subcontractor, Underground Power Corp., Reference 72.

In addition, an analytical investigation concerned with the protection of large stable superconducting coils was conducted by another subcontractor, MCA. This investigation was planned as a three-phase effort, Phase I covering detailed analysis, Phase II, generation of computer programs and Phase III, use of computer programs to evaluate coil protection techniques and procedures. Phase I has been completed and is reported in Reference 24. Efforts during Phase I have resulted in a model of the quench behavior of fully-stabilized MHD coils that predicts considerably lower temperatures than would result from the simple assumption of adiabatic heating of the normal region. The impact on coil design is to allow discharge of the windings over a much longer time, thus resulting in lower discharge voltages.

The work done in Phase I includes the following:

##### Short Circuit Analysis

The general problem of charge and discharge of a coil with a single internal short of arbitrary resistance is considered. The results of the analysis are presented in graphical as well as tabular form and allow quick calculation of the individual currents as well as power dissipation in the short itself. The results are applied to a typical MHD superconducting magnet.

##### Thermal Diffusion During a Quench

The effects of thermal diffusion during the propagation of the normal region are considered. It is shown that the propagation of a normal region is qualitatively different for coils with significant amounts of helium present. Scaling relationships for quench characteristics are also discussed for coils which discharge into an external resistor, or which have only the internal normal region resistance.

##### The Superconducting to Normal Transition in a Fully Stabilized Winding

A model of the quench of a fully-stable superconducting coil is presented. The model is based on the assumption of a quasi-steady temperature distribution in the normal region which overestimates the existing temperatures. One of the main features of the model is that it takes into account the vaporization and flow of helium during the transient. Temperatures, voltages, and rate of drop of helium level are computed for three limiting cases of helium vapor interaction with the winding. It is shown that below a certain maximum critical temperature the windings are cooled by heat transfer to the helium liquid and vapor. Above this critical temperature the increase in conductor temperature is more rapid than the dissipation of heat energy to the helium.

##### Propagation of Normal Region - Variable Current

The results discussed above are extended to the case of time varying current. Both the internal resistance of the normal region as well as an external discharge resistor is taken into account. Conditions are derived relating the discharge conditions and coil design parameters required to maintain the winding temperature below the instability value discussed earlier.

#### 4.1.17 Investigation of Effects of Fringe Fields on Personnel and Equipment

The effects of high fringe magnetic fields (dc) have been the subject of preliminary investigations. A literature search and experiments on the effects of magnetic fields on small organisms have been initiated. Interim criteria for personnel and equipment exposure to magnetic fields in a power plant environment were prepared in connection with MIT work on the MHD ETF 200 MWe power plant magnet system conceptual design (References 73, 38). These criteria, in the form of a specification, are contained in Appendix D.

Fringe magnetic field zone boundaries and limits for personnel exposure, based on the interim criteria, in the vicinity of the 6 T magnet in the ETF 200 MWe power plant conceptual design are shown diagrammatically in Figure 4.1.17A.

The interim standards contained in Appendix D are based on recommended standards included in a letter from Dr. Edward L. Alpen, University of California, to Dr. Kenneth R. Baker, ERDA, dated July 23, 1979. They are intended to serve as preliminary guidelines during the ETF conceptual design stage and are subject to change as more information and experience are accumulated.

The standards are aimed at minimizing chances of future unforeseen adverse effects of long range personnel exposure to magnetic (fringe) fields, a subject about which very little is known at this time. Considerable expense will be involved in implementing this standard in the ETF.

Future research and development work on large superconducting magnet systems should include further study of the biological effects of magnetic fields. As such work proceeds, consideration should be given to whether or not the criteria for personnel exposure contained in Appendix D should be eased.

#### 4.1.18 Cryogenic Systems

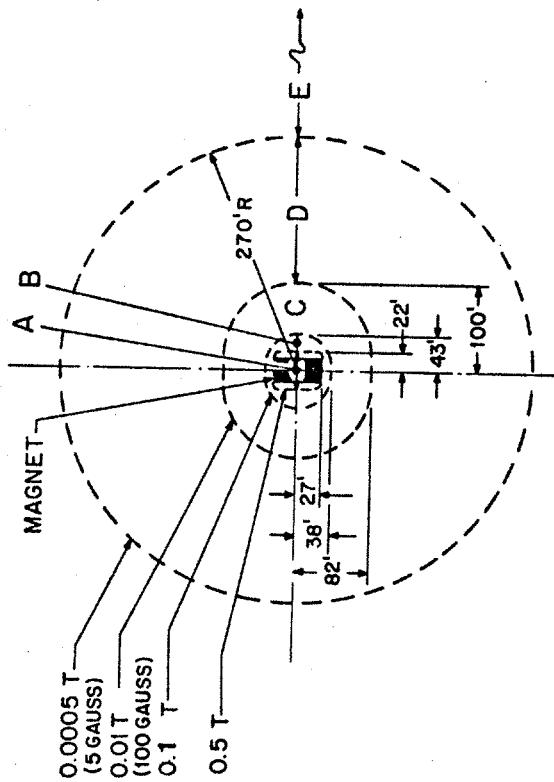
Commercial-scale MHD magnets require efficient, reliable cryogenic systems for magnet cool-down and warm-up and to maintain cryogenic conditions continually for long operating periods. The cryogenic system is considered to be a part of the overall magnet system.

Helium refrigerator/liquefiers and associated equipment required for such systems are commercially available. However, the cryogenic system for a particular size and type of magnet must be custom designed for that magnet. Characteristics and costs depend on the specific system design.

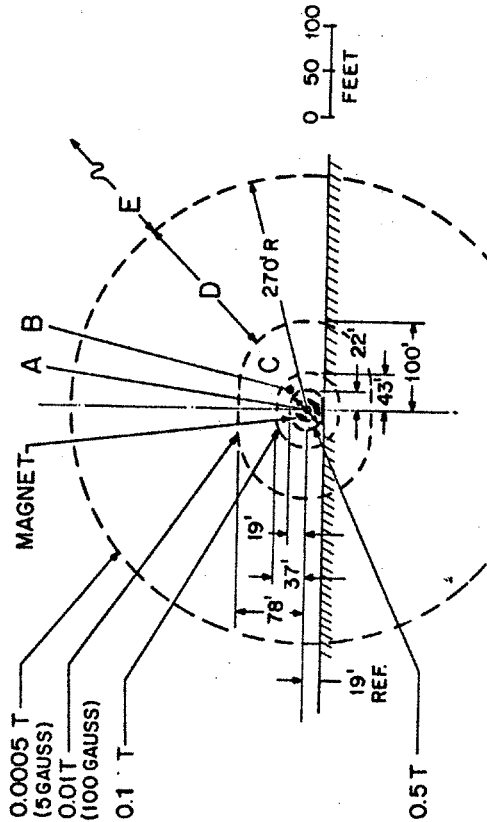
In support of the program task involving reference designs for full-scale magnet systems (see Section 4.2), it was considered desirable to obtain representative designs and estimated costs for cryogenics from an industrial source. Accordingly, a subcontract was placed with Cryogenic Consultants, Inc. to develop cryogenic system designs and provide engineering data and costs for systems for typical commercial-scale MHD magnets.

The results of the subcontractor's work are contained in a final report, Reference 35. The report contains system flow diagrams, lists of components, data on size, weight and cost of components, descriptions of start-up and operating procedures and discussions of safety, maintenance procedures and expected overhaul periods.

Figure 4.1.18A was prepared by Cryogenic Consultants to show a block diagram flow sheet for a typical MHD magnet cryogenic system. A helium refrigerator/liquefier supplies liquid helium to a storage tank from which the liquid is transferred automatically to the magnet to maintain the desired liquid level in the coil container. Part of the boil-off helium gas passes through the power leads to cool them and returns to the compressor. The remainder of the boil-off gas is returned cold to the refrigerator coldbox. Liquid nitrogen is used to cool the thermal radiation shield of the magnet and also for precooling in the refrigerator. While variations in this system may be introduced (for example, cooling to the magnet shield may be supplied by a secondary helium gas loop instead of by liquid nitrogen), the block diagram is sufficiently representative to



PLAN VIEW



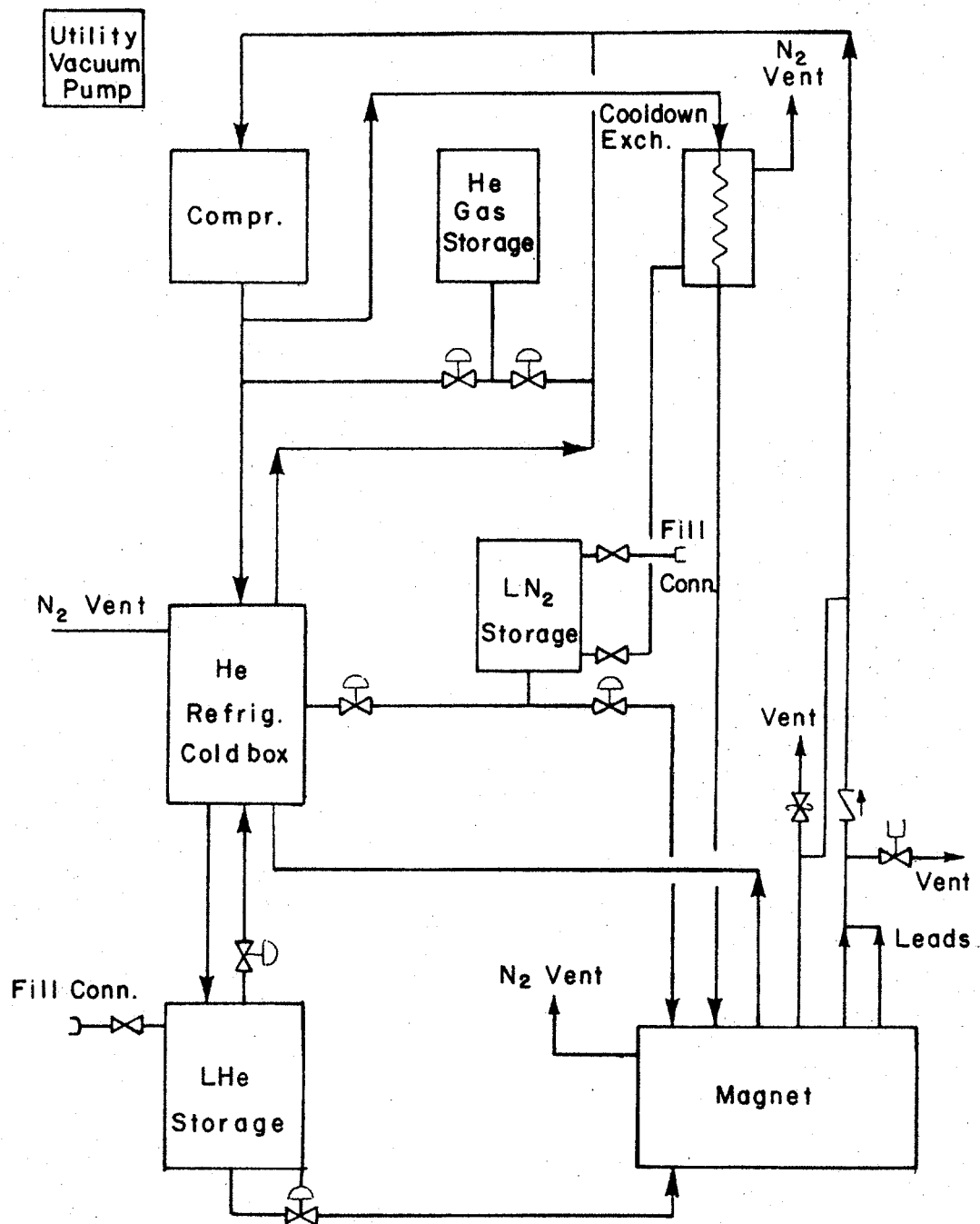
END VIEW

PERSONNEL EXPOSURE LIMITS (WHEN MAGNET IS CHARGED)

ZONE (See diagrams)	FIELD (T)	LIMITS (maximum exposure permitted, based on 8hr. work day, 5 days per week)
A	>0.5	0 exposure (no access to area)
B	0.1 to 0.5	10 min. per work day
C	0.01 to 0.1	1 hr. per work day
D	0.0005 to 0.01	8 hr. work day, 5 days per week
E	>0.0005	No limits, all personnel

NOTES:

1. Data are for FBNML-designed 6 T magnet in MHD ETF 200 MW Power Plant.
2. Lines of constant magnetic fringe field indicated by - - - - -.
3. Magnet is shown in operating position and will be charged only when in this position. It will be fully discharged when moved aside for channel changeout.
4. No limits when magnet fully discharged.
5. For definition of approved personnel, see FBNML Specification A 4442 (Appendix D of this report)



4.1.18A Block Diagram Flow Sheet for Typical MHD Magnet Cryogenic System

serve as a basis for the engineering and cost estimation of the cryogenic equipment required for MHD magnet systems.

Sizing of the components of a cryogenic system is based on the estimated heat loads of the magnet system. Table 4.1.18-I shows estimated heat loads of typical commercial size magnet systems with design operating currents of 5 kA, 10 kA and 50 kA. The estimated conductor splice heat load is conservatively high and subject to revision when more experience is obtained on splice losses in high current superconducting windings. It is concluded that a refrigerator with a 100  $\ell$ /hr liquid-generating capacity would be adequate for most commercial scale magnets.

Cool down of magnet from room temperature, required only occasionally during the life of the magnet, will be accomplished in two steps as follows: a) cool to 100 K by circulating helium gas cooled with bulk liquid nitrogen, and b) cool from 100 K to liquid helium temperature by circulating helium gas cooled by the refrigerator and adding liquid helium after temperature of cold mass is below 20 K. A refrigerator capable of generating 100  $\ell$ /hr of liquid helium is expected to cool 100 tons of mass from 100 K to 20 K in about 200 hours.

Reliability and failure modes for cryogenic system components are discussed. A mean time between failure (MTBF) of about 10,000 hours is considered reasonable for refrigerator heat exchangers, assuming care and good procedures. Screw compressors are expected to run 12,000 hours without down time. Turbo-expanders and reciprocating expanders should be accessible for repair and replacement of parts. Typical time allowance for parts replacement is from 4 to 8 hours. It is expected that magnet operation can continue using stored liquid helium for refrigeration during such periods when the refrigerator is down for repair of components. Expected minimum mean time between failures (MTBF) for cryogenic components is summarized in Table 4.1.18-II.

The Cryogenic Consultants, Inc. report includes outline specifications for cryogenic system components. It lists characteristics and prices of various manufacturers' products (liquid storage tanks, gas storage tanks, etc.), detailed flow sheets for typical systems and estimated system costs.

Table 4.1.18-III contains a cost estimate breakdown for a 100  $\ell$ /hr system.

#### 4.1.19 Power Supply and Discharge Systems

A power supply subsystem consisting of a dc power supply to charge the magnet, resistors to accomplish fast discharge of the magnet and the associated controls is considered to be a part of the overall magnet system in a commercial-scale MHD plant. As is the case for the cryogenic system, power supply system components are commercially available but the system must be custom-designed to fit the characteristics of the magnet.

In support of the magnet reference design program (Section 4.2) a subcontract was placed with Alexander Kusko, Inc. to provide engineering data and estimated costs for power supply subsystems for typical commercial-scale MHD magnets.

The results of the subcontractor's work are contained in a final report, Reference 74.

The investigation by Alexander Kusko, Inc. covered magnet power supply systems for generators ranging from 200 MWe to 1000 MWe MHD power with magnet currents from 20 kA to 100 kA and supply peak powers up to 10 MW.

A simplified schematic diagram of a magnet power supply is shown in Figure 4.1.19A. It consists of a rectifier power supply unit taking 3-phase ac power from the plant auxiliary power system and delivering dc power to the magnet via dc switches and an emergency dump resistor connected permanently across the magnet terminals. The necessary instrumentation is also part of a power supply system. The functions of the power supply system are to charge the magnet in a reasonable time (typically 60 minutes), to maintain the magnet at

Table 4.1.18-I

## Cryogenic Characteristics of Baseline Design MHD Magnet Systems

Electrical Leads	5 kA	1 kA	50 kA
4.5°K Flow g/s	.695	1.39	1.80
78°K Flow g/s	-	-	5.0
Heat Leak from Environment			
Radiation (2000 ft <sup>2</sup> )	8 W	8 W	8 W
Conduction	10 W	10 W	10 W
Heat Leak to Stack	5 W	5 W	5 W
Conductor Splices	12.5 W	50 W	1250 W
Total Heat Load	35.5 W	73 W	1273 W
Total Liquid Helium Consumption	20 l/hr	40 l/hr	52 l/hr



Table 4.1.18-II

Expected minimum mean time between failures (MTBF)  
for the components of the cryogenic system

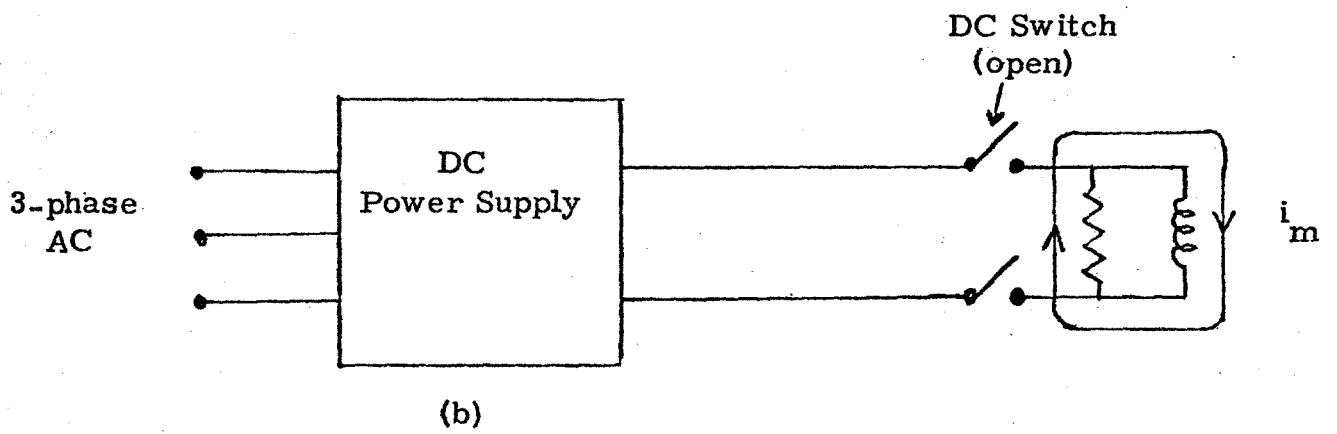
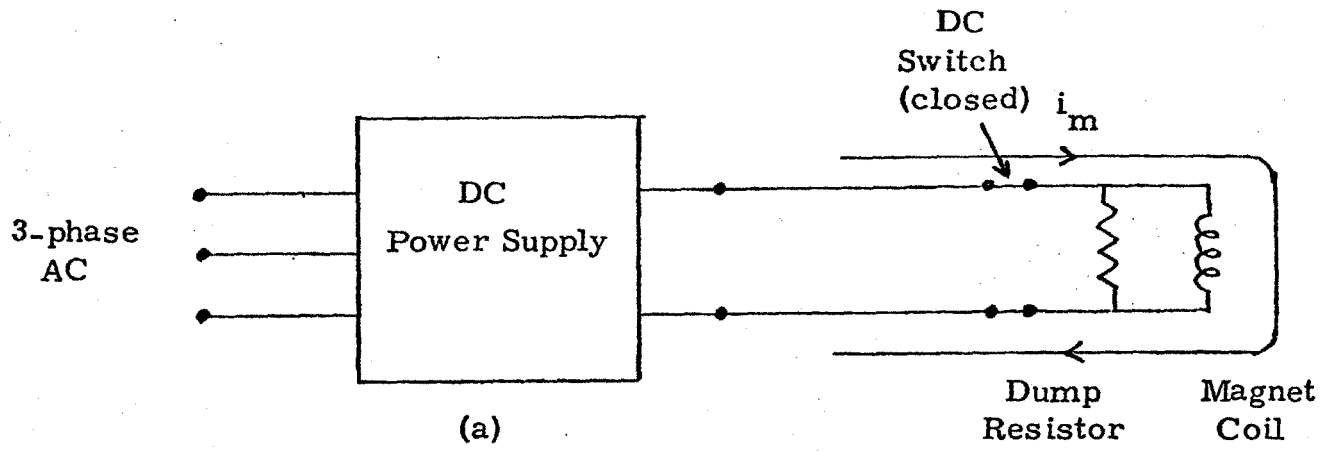
	<u>MTBF</u>
Compressor	12,000 hrs
Compressor Oil Removal System	12,000 hrs
Refrigerator Cold Box	
Heat Exchanger Plugging	20,000 hrs
Turbine	8,000 hrs
Reciprocating Expander	4,000 hrs
Insulating Vacuum	50,000 hrs
Valves	20,000 hrs
Liquid Helium Storage Vessel	50,000 hrs
Gaseous Helium Storage Vessel	50,000 hrs
Vacuum Jacketed Piping	50,000 hrs
Liquid Nitrogen Storage Tank	50,000 hrs
Warm Piping and Valves	50,000 hrs

Table 4.1.18-III

## Cost Estimate Breakdown for 100 Liter/Hour Refrigerator/Liquefier System

	<u>Cost</u>
Liquefier with compressor and oil removal system	\$360,000
Helium Dewar (Cryofab), 1000 liter capacity	12,000
Estimated neck tube modifications	2,000
Nitrogen Dewar (Process Engr.), 3125 gal. capacity	18,500
Estimated accessory cost	2,000
Gas storage tank (Riley Beard), 12,000 gal. capacity	10,000
Cooldown heat exchanger (spec item), estimated cost	10,000
Warmup heater (spec item), estimated cost	7,000
Transfer line components (spec items), consisting of:	
(1) Tee box	6,000
(2) Valve box	8,000
(3) Transfer line bayonet assembly	2,000
(4) Heat exchanger assembly (installed in line)	3,000
(5) 6 in. vacuum jacketed line (10 ft section)	2,000
(6) 6 in. "L" vacuum jacketed line (4 ft × 10 ft)	2,000
(7) 4 in. "L" vacuum jacketed line (9 ft × 26 ft) w/two bayonets	3,000
(8) Equipment "U" transfer line assemblies	8,000
(9) Misc. warm lines and valves for Item g)	<u>6,000</u>
<b>TOTAL SYSTEM COST</b>	<b>\$461,500</b>

Note: The installation of components and the engineering cost for custom made equipment and piping is not included in this cost.



4.1.19A Simplified Schematic Diagram of MHD Magnet Power Supply System

the desired steady state field for long periods of time, to accomplish normal discharge through the power supply unit (by inversion) and to accomplish emergency discharge by transferring stored magnetic energy to the dump resistor (by opening dc switches).

The subcontractor's report analyzes dc power supply requirements, reviews historical experience, describes characteristics of components, presents system baseline designs, outlines system and component specifications and provides information on costs of power supply equipment.

Characteristics of baseline designs are given in Table 4.1.19-I. A breakdown of estimated costs for a 50 kA, 2.65 MW magnet power supply is given in Table 4.1.19-II.

#### 4.1.20 Interfacing (Packaging) Study

In commercial-scale MHD generators the channel should be packaged inside the magnet bore with the most efficient space use practicable, in order to minimize the required bore size and thereby reduce the cost of the magnet, which is a major item in overall plant capital cost. To accomplish this successfully, the channel designer and magnet designer must work in close cooperation.

In addition to channel/magnet packaging, there are other important interfacing considerations that require careful attention. One example is that of supporting the power train (combustor, channel, diffuser) in relation to the magnet and the question of what forces the magnet must withstand as a result of thermal expansion of the power train. Another example is the provision for channel-changeout, and the question of whether a movable magnet (roll-aside, turntable mounted or roll-apart design) has overall advantages compared to the fixed magnet with movable diffuser.

A study was initiated in January 1980 to investigate channel/magnet packaging and to determine tentatively what packaging efficiencies may be expected in future commercial-scale MHD magnets. To provide channel technology input to the study, a contract was placed with MEPPSCO, Inc. for their engineering assistance, and help was also obtained from Avco Everett Research Laboratory, Inc. (AVCO).

The study showed that by careful packaging, the utilization factor (plasma volume/warm bore volume) could be increased from a value of about 0.25, associated with early reference designs, to 0.5 or higher. This means that the MHD power generated in a particular size magnet could be doubled, or for a given power, the size and cost of the magnet could be substantially decreased. Alternative channel/magnet bore configurations considered included those shown in Figure 4.1.20A.

Other conclusions derived from the study were, 1) a square-bore cross section is generally preferred over a round-bore cross section, from the channel packaging standpoint, 2) a rectangular bore with the long dimension parallel to the field lines is the most advantageous bore geometry for types of channels which require many power leads (because lead bundles can be located in the ends of the rectangle, allowing maximum use of the central high field region for power generation) and 3) power generated in a given magnet bore volume can be nearly as high with a supersonic channel and 4 T peak on-axis field as with a subsonic channel at 6 T peak on-axis field. (This leads to the conclusion that for a given MHD power output, the magnet cost would be substantially lower with a supersonic channel than with a subsonic channel).

The results of the study are reported in References 33, 75 and 76.

A Workshop on Magnet-Channel Interfacing was organized and held at M.I.T. on November 18, 1980. Attendees included representatives of NASA LeRC, AVCO, GE, GD, MEPPSCO, Rockwell International, Reynolds Metal Co., TRW Inc., and the Babcock and Wilcox Co.

Table 4.1.19-I

Power Supply and Dump Circuit Design Characteristics  
Magnet Current Selected Independently

Magnet Rating		Power Supply Rating $T_1 = 3600$ s			Dump Parameters $V_m = 1000$ V		Res. Energy Para. $T_2 = 900$ s $E_m = 0.05$ pu	
$E_m$	$I_m$	$L_m$	$V_{ps}$	$P_{ps}$	$R_d$	$T_m$	$E_m$	$T_2$
MJ	kA	H	V	MW	m $\Omega$	s	pu	s
6500	20	32.5	181	3.61	50	650	0.063	974
6500	50	5.2	72.2	3.61	20	260	$9.8 \times 10^{-4}$	390
6500	100	1.3	36.1	3.61	10	130	$9.7 \times 10^{-7}$	195
17000	20	85.0	472	9.44	50	1700	0.347	2545
17000	50	13.6	188.9	9.44	20	680	0.071	1020
17000	100	3.4	94.4	9.44	10	340	$5.0 \times 10^{-3}$	510

$E_m$  = Stored magnetic energy (rated)

$I_m$  = Magnet operating current (rated)

$L_m$  = Magnet inductance

$V_{ps}$  = Charging voltage (rated)

$P_{ps}$  = Power supply output power

$R_d$  = Dump resistor resistance

$T_m$  = Time constant, discharge circuit

$V_m$  = Magnet terminal voltage (max)

$T_1$  = Charging time

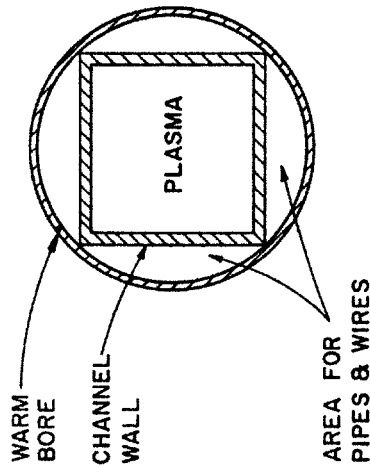
$T_2$  = Discharge period

Table 4.1.19-II

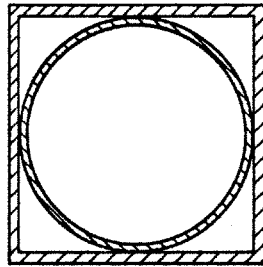
Breakdown of Estimated Costs for a 50 kA,  
2.65 MW Magnet Power Supply

<u>Transformers</u>	
Rating - 900 kVA, 4160/90/90 V	
Number - 2	
Unit Cost - \$20/kVA	
Total Cost	\$36,000
<u>Rectifiers (unit costs include fuses, heat sinks, etc.)</u>	
60 SCRs at \$600 each - \$36,000	
25 silicon diodes at \$300 each - \$7,500	
Total Cost	\$43,500
<u>Controls</u>	\$10,000
<u>DC Transductor and Interphase Transformers</u>	\$22,500
<u>Cabinets</u>	
32 ft at \$600/ft	\$19,200
<u>Bus Work</u>	
60 ft at \$400/ft	\$24,000
<u>AC Circuit Breaker</u>	
5 kV, 1200 A	\$20,000
<u>External Buswork</u>	
100 ft of 10 in <sup>2</sup> buswork at \$400/ft	\$40,000
<u>Dump Circuit</u>	
Dump resistor and water tank	\$25,000
Dump diodes, 50 diodes at \$300 each	\$15,000
<u>DC Switch</u>	
50 kA, 600 V, air circuit breaker	\$100,000
<u>Cooling Water System (pumps and piping)</u>	\$8,000
Total (Components and Labor) Cost	\$363,200
Purchase Price - 3 × \$363,200	\$1,089,600

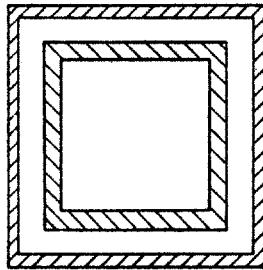
SQUARE WINDOW-  
FRAME CHANNEL  
IN ROUND BORE  
(MEPPSCO)



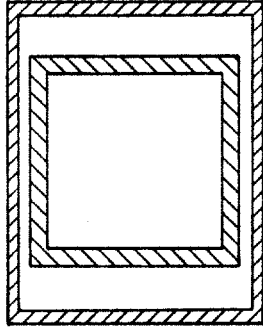
CIRCULAR WINDOW-  
FRAME CHANNEL  
IN SQUARE BORE  
(MEPPSCO)



INSULATING-WALL  
CHANNEL IN  
SQUARE BORE  
(AVCO)



INSULATING-WALL  
CHANNEL IN  
RECTANGULAR BORE  
(AVCO)



PLASMA AREA (m <sup>2</sup> )	7.9	9.6	6.8	10.0
WARM BORE AREA <sup>a</sup> (m <sup>2</sup> )	15.9	16.0	16.0	20.0
MVU <sup>b</sup>	0.50	0.60	0.42	0.50

<sup>a</sup> Warm bore areas are typical for early commercial scale magnets, exit end.

<sup>b</sup> MVU = magnetic volume utilization factor.

(a) Charging and Maintaining Magnet Current,  $i_m$ , (b) Discharge Through Dump Resistor  
Diagrams of Cross Sections of Magnet Warm Bores with  
Various Channel/Bore Configurations

The topics discussed included the following:

Channel/magnet packaging

Need for magnet warm bore liner

Effect on magnet of flow-train vibration

The CDIF-1B combustor, including flange connections, magnetic effects, and rapid shut-down

Motion of boiler and diffuser due to thermal expansion

Provisions for channel changeout, including roll-aside, rotatable and roll-apart magnet systems

Magnet fringe field effects

In connection with thermal expansion of flow train components and resulting loads on flanges, it is noted that the practice at MIT, in preparing commercial-scale MHD magnet reference designs, has been to make the warm bore and bore liner structurally capable of supporting only the weight of the channel and the seismic loading attributable to the channel. It has been assumed that flexible joints and/or other means are provided in the flow-train to ensure that loads from combustor, diffuser and boiler (gravity, seismic, thermal expansion) are not transmitted to the channel and magnet.

Attention is called to the above-mentioned practice because discussions at the November 18 meeting indicated that little or nothing has been done in MHD system designs to isolate the channel and magnet from heavy loads that may be imposed by adjacent equipment.

In discussing channel changeout, several schemes were considered, including the following:

1. Fixed magnet, roll-aside diffuser (Figure 4.1.20B)
2. Magnet on turn-table (Figure 4.1.20C)
3. Roll-aside magnet (Figure 4.1.20D)
4. Roll-apart magnet (Figure 4.1.20E)

In the first three schemes, the magnet is a single piece (nonsplit) assembly and the channel is installed and withdrawn through the large (exit) end of the warm bore with the aid of a dolly as shown in Figure 4.1.20F.

In the fourth scheme, the magnet is split along the vertical center plane and the two halves are arranged to roll apart. With the halves separated, the channel is installed and removed either by hoisting vertically or by being rolled aside on a dolly into space provided by extra side movement of one magnet half.

The consensus of the discussion seemed to be that the diffuser should be moved rather than the magnet, i.e., that Scheme 1 is preferred.

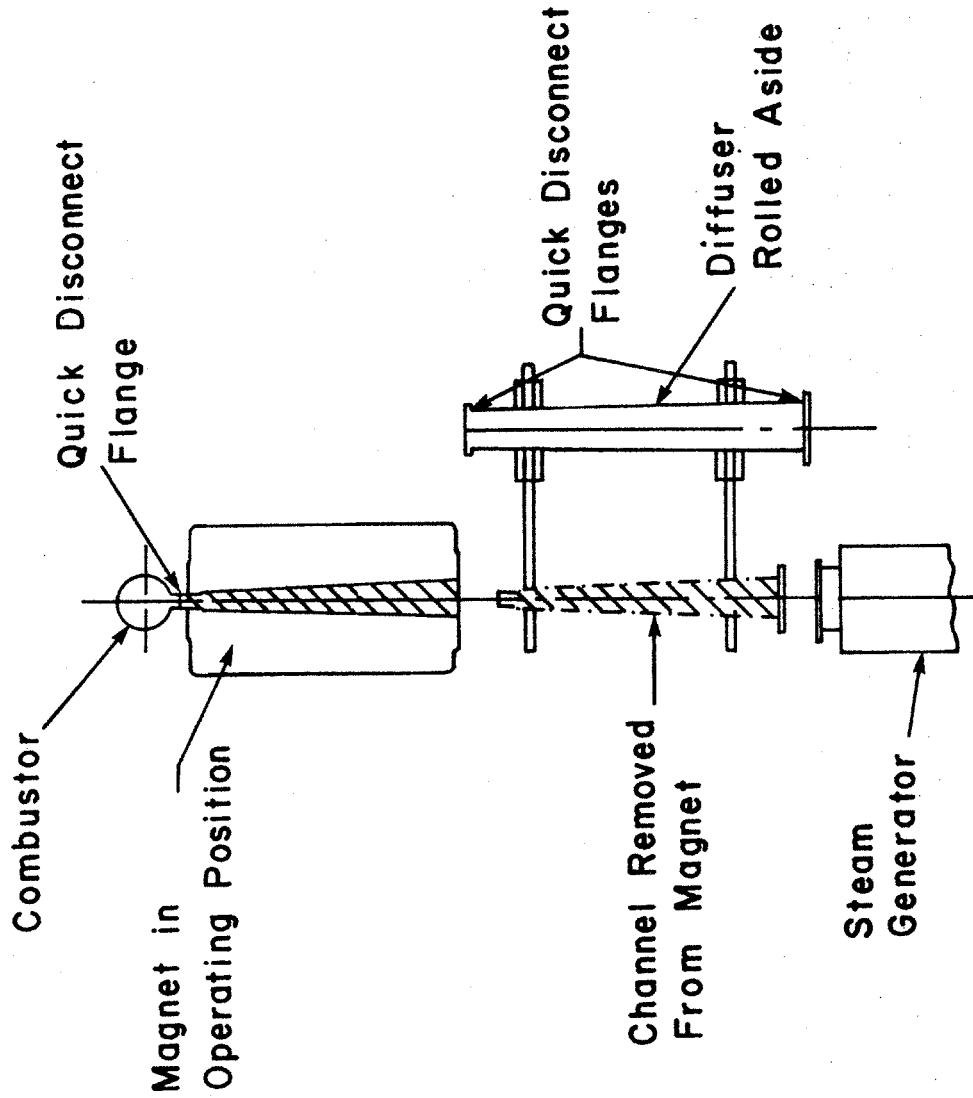
Further investigations of roll-aside and roll-apart magnet systems are reported in Section 4.2.16.

The meeting was useful in revealing issues needing resolution and areas needing further investigation. Loading on channel flanges was shown to be a major issue. Magnetic force on ferromagnetic combustor parts also was shown to be a major issue. The need for further investigation of the roll-aside magnet was emphasized, the objective being to estimate the overall cost-effectiveness of this concept as compared to the single-piece fixed-mount magnet. The need for another interfacing meeting among representatives of MHD component designers and manufacturers, power plant designers and possibly operating utilities was also emphasized. Sponsorship broader than the MIT MHD Magnet Group seemed desirable.

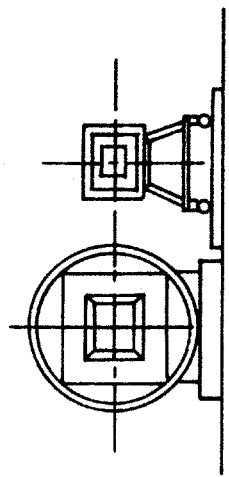
A summary of the November 18 meeting is contained in Reference 77.



PLAN VIEW

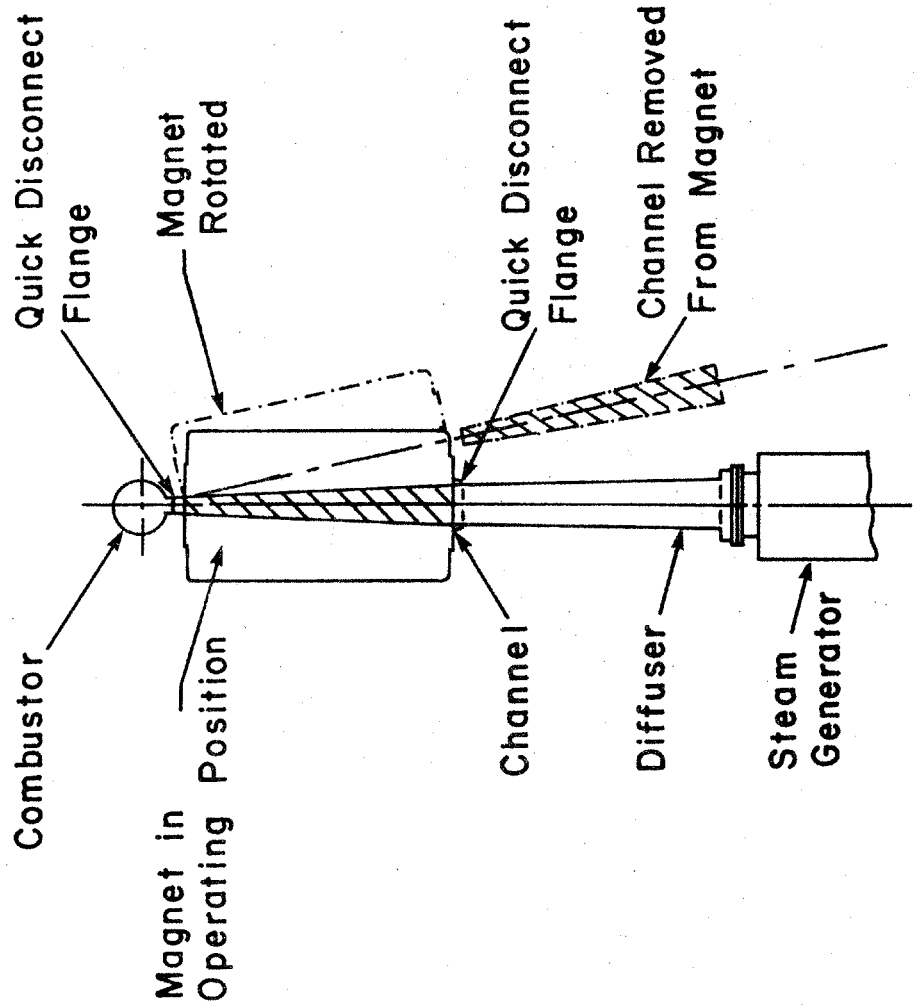


ELEVATION VIEW

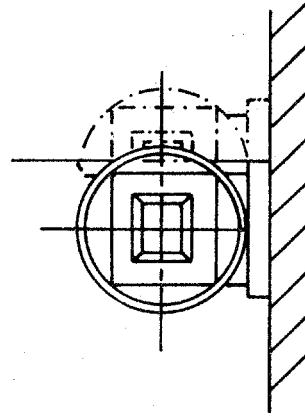


4.1.20C Sketch Showing Magnet on Turntable to Facilitate Channel Changeout

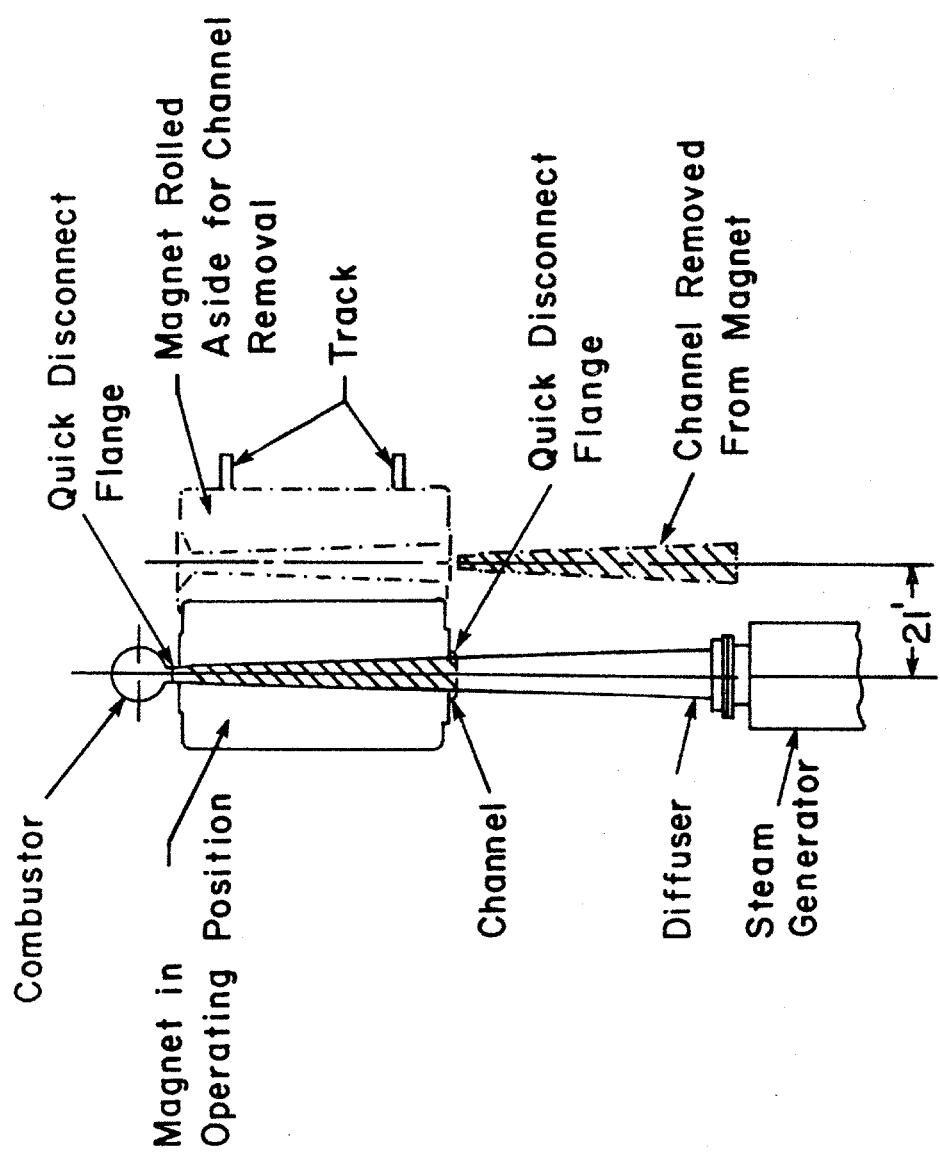
PLAN VIEW



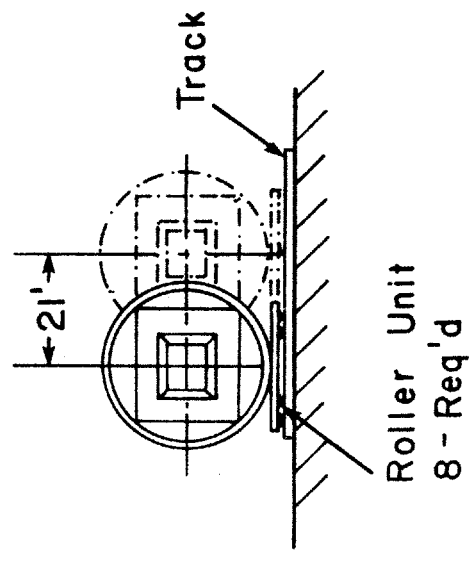
ELEVATION VIEW



PLAN VIEW

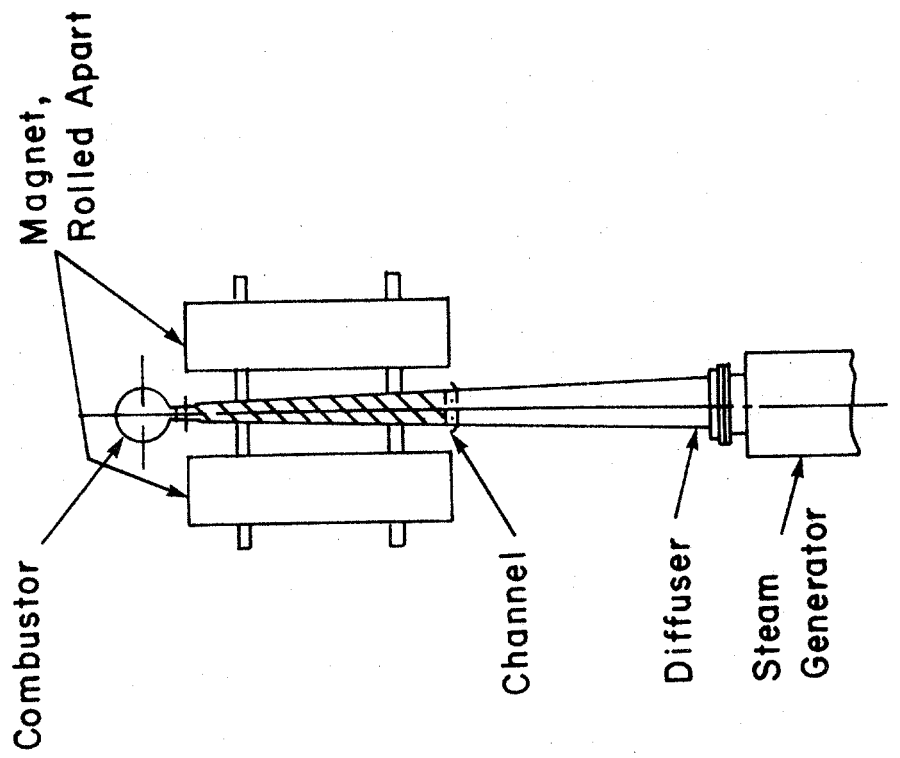


ELEVATION VIEW

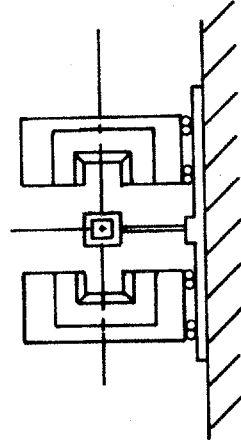


4.1.20E Sketch Showing Roll-Apart Magnet to Facilitate Channel Changeout

PLAN VIEW



ELEVATION VIEW



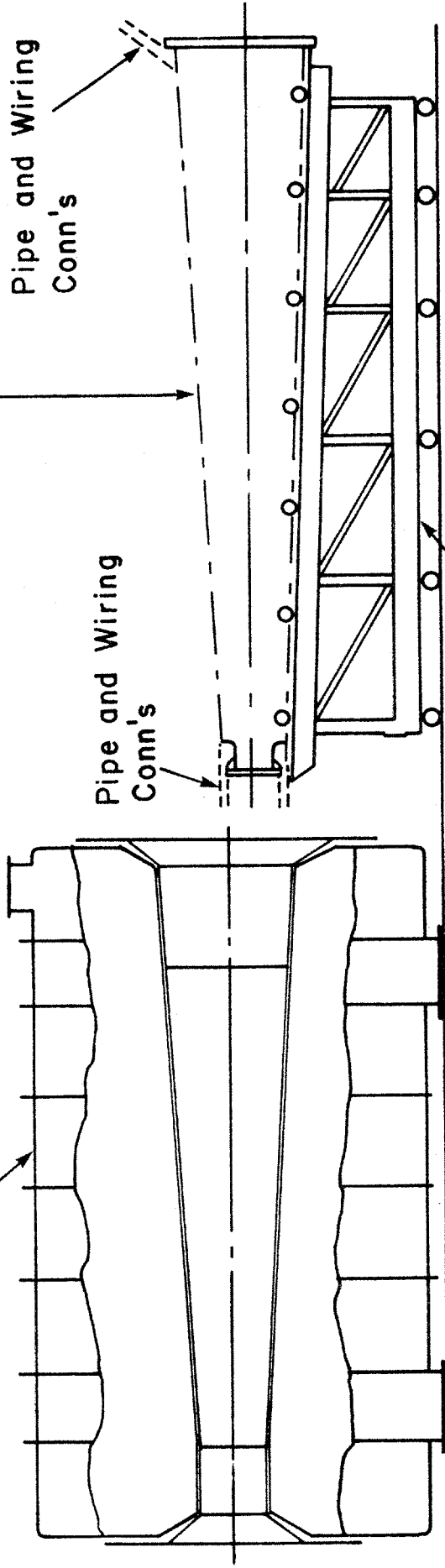
Channel Exterior.  
Envelope, Including  
Structure, Piping, Wiring

Pipe and Wiring  
Conn's

Pipe and Wiring  
Conn's

Dolly

Magnet



4.1.20F Sketch Showing Dolly Used for Insertion and Removal of Channel from Magnet

#### 4.1.21 Transportation Study

Commercial-scale MHD magnets are too large to be shipped in one piece from factory to plant site. In most cases, even the major components are too large to ship in single pieces. It is therefore necessary that some manufacturing operations and all final assembly work be performed at the plant site. Since factory work is less expensive, it is desirable to factory-fabricate magnet parts in modules as large as practical for shipping.

In preparing reference designs, manufacturing studies and cost estimates for full-scale MHD magnet systems, as described in Section 4.2, it was important to know shipping constraints and shipping costs applicable for very large component parts. Accordingly, a subcontract was placed with Belding Corporation, a company specializing in transportation of heavy equipment, for an investigation of current heavy equipment transportation methods applicable to MHD plant components.

The study was directed toward transportation of component parts for typical MHD magnets for 150, 250, 500 and 1,000 MWe (topping cycle) generators.

The study established size and weight-carrying capabilities of water, air and land transportation methods. The limits of water transportation (rivers, canals) within the United States were defined. Land transportation methods investigated included special rail transportation equipment (Schnabel Cars) and special overland transporters. Costs of various methods at various capacity levels were tabulated.

The results of the study are reported in Reference 34.

#### 4.1.22 Cost Analysis

The analysis of magnet costs and the development of procedures for estimating and scaling costs of large magnet systems has been underway at MIT since the start of the MHD magnet development program. The main objectives of this work have been:

- To generate progressively more reliable magnet cost estimates and cost scaling information as needed by DOE and other investigators for comparing and evaluating overall MHD power generating systems and in budgetary planning. (System sizes up to 2000 MWe)
- To identify, break down and analyze the various elements of magnet cost as a basis for improving the cost-effectiveness of overall magnet systems by improved design, better material selection, component and manufacturing development and careful interfacing.

As a guide for use in connection with preliminary estimating of the capital cost of MHD magnets, a curve of magnet system cost vs. magnet size was developed as shown in Fig. 4.1.22A. The curve represents the average of a number of magnet cost estimates (and actual costs for smaller magnets) obtained from both industry and government sources.

The measure of size,  $VB^2$ , used as the abscissa in the curve, is a parameter reflecting the magnet warm bore volume and the square of the magnetic field. (In the parameter  $VB^2$ :  $V = A \times L_a$ , where  $A$  is the magnet warm bore area at the plane of the channel inlet,  $L_a$  is the channel active length, and  $B$  is the peak on-axis magnetic field. The magnet size index is explained in more detail in Appendix A.) It is a convenient parameter to use in preliminary cost vs. size studies, since it is an approximate indication of the MHD power generating capacity in the active volume of the magnet. Estimated magnet capital cost plotted directly vs. MHD power instead of vs. magnet size ( $VB^2$ ), is shown in Figure 4.1.22B for MHD channel power outputs in the range of 200 to 1000 MWe. To arrive at this relationship, certain assumptions must be made about the MHD channel itself, because channel performance may be different for different channel designs. The assumptions made in this case concern the power density achieved in the plasma and the magnetic volume utilization (MVU), which is the ratio of

active plasma volume to magnet warm bore volume. As indicated in the figure, the assumed power density is 9 MW/m<sup>3</sup> and curves are presented for MVU's of 0.25, 0.35 and 0.50.

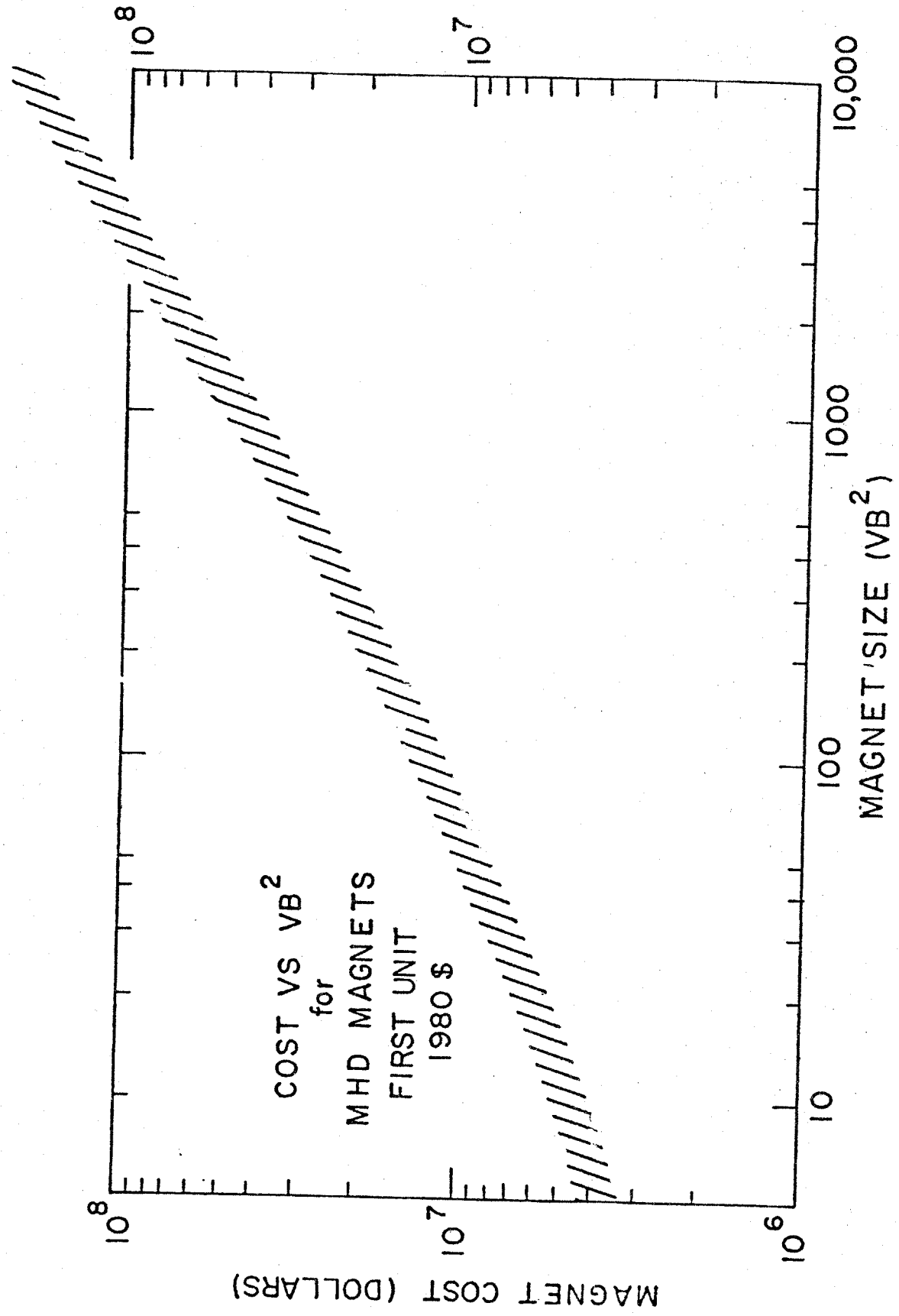
The data shown in Figures 4.1.22A and 4.1.22B are based on "first unit" estimates, with the entire cost of engineering analysis, design, tooling, etc., charged against the single magnet system. It is expected that when the technology has matured and multiple units are produced to a given design, engineering and tooling costs can be prorated over a number of magnets and unit costs will be lower. A preliminary estimate indicates that the unit cost for a lot of 10 large magnet systems might be about 25 % lower than the "first unit" costs shown in the curves, Figures 4.1.22A and 4.1.22B.

Analysis of commercial-scale magnet system "first unit" costs showed that the components of the magnet itself represent only about half of the total cost of the installed system. The balance of the total cost is made up of items such as design and analysis, project management, accessories, shipping and installation at plant site. A typical distribution of costs is shown in Fig. 4.1.22C.

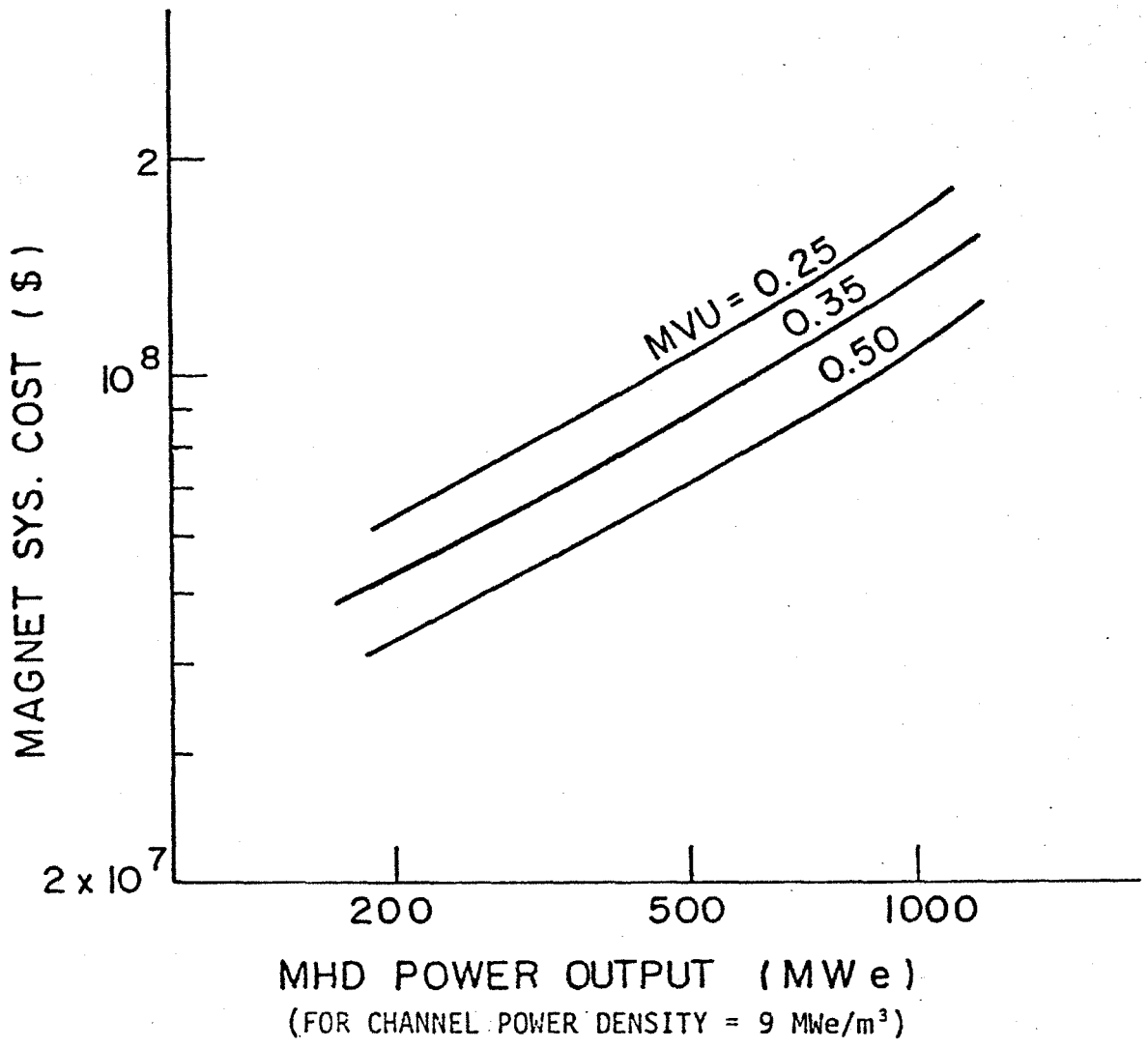
Within the magnet itself, each of the three major components, conductor, structure and cryostat, each represent roughly 1/3 of the total cost of components. However, scaling characteristics are such that, with increasing magnet size, the amount of conductor does not increase as rapidly as the amount of structure. For very large magnets, structure tends to predominate. This is shown in Fig 4.1.22D, a bar chart of component costs for magnets for various MHD power outputs.

Further information on cost estimating is contained in References 37, 45 and 78.

4.1.22A Curve of Estimated MHD Magnet System Cost vs Size Index (VB<sup>2</sup>)



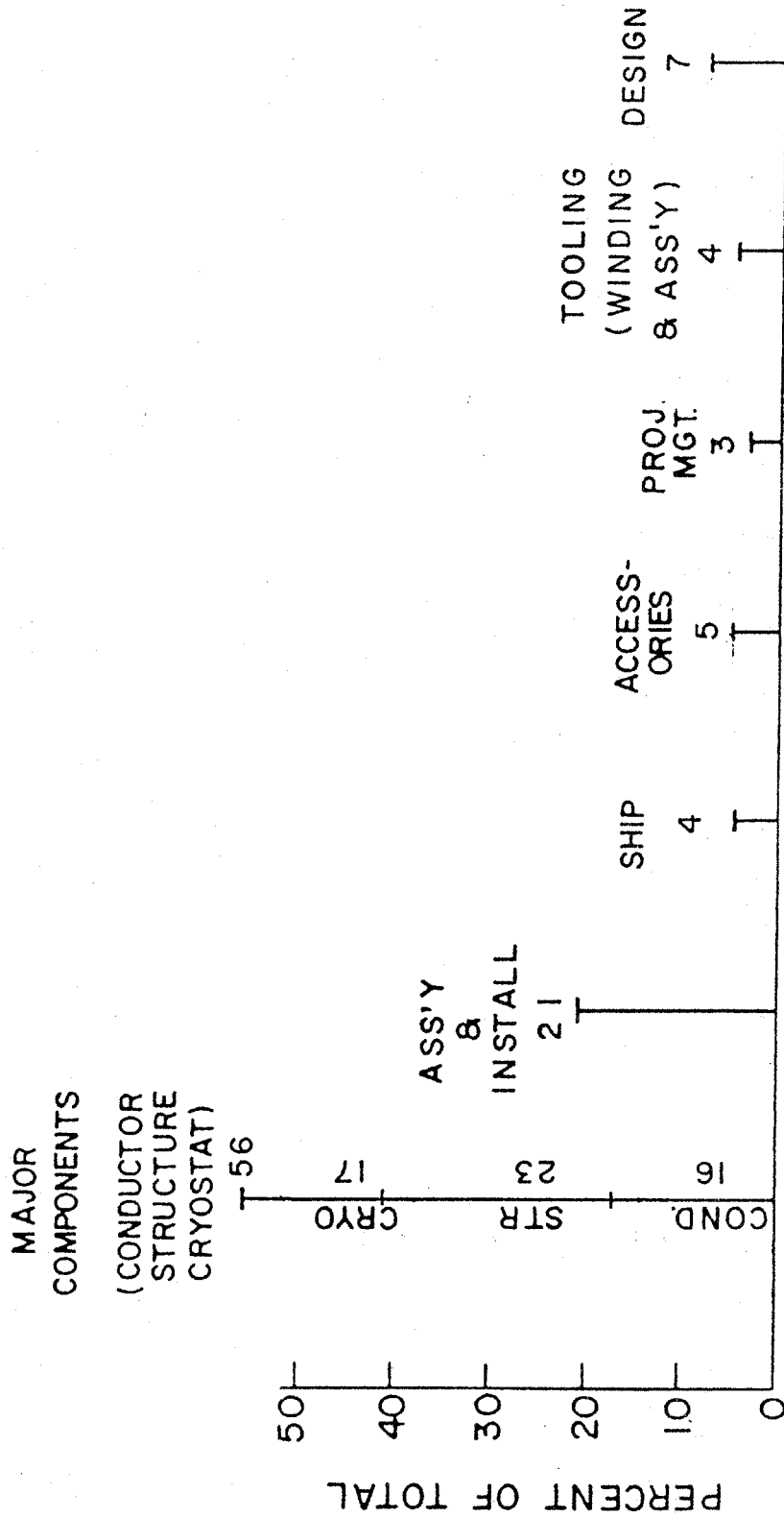


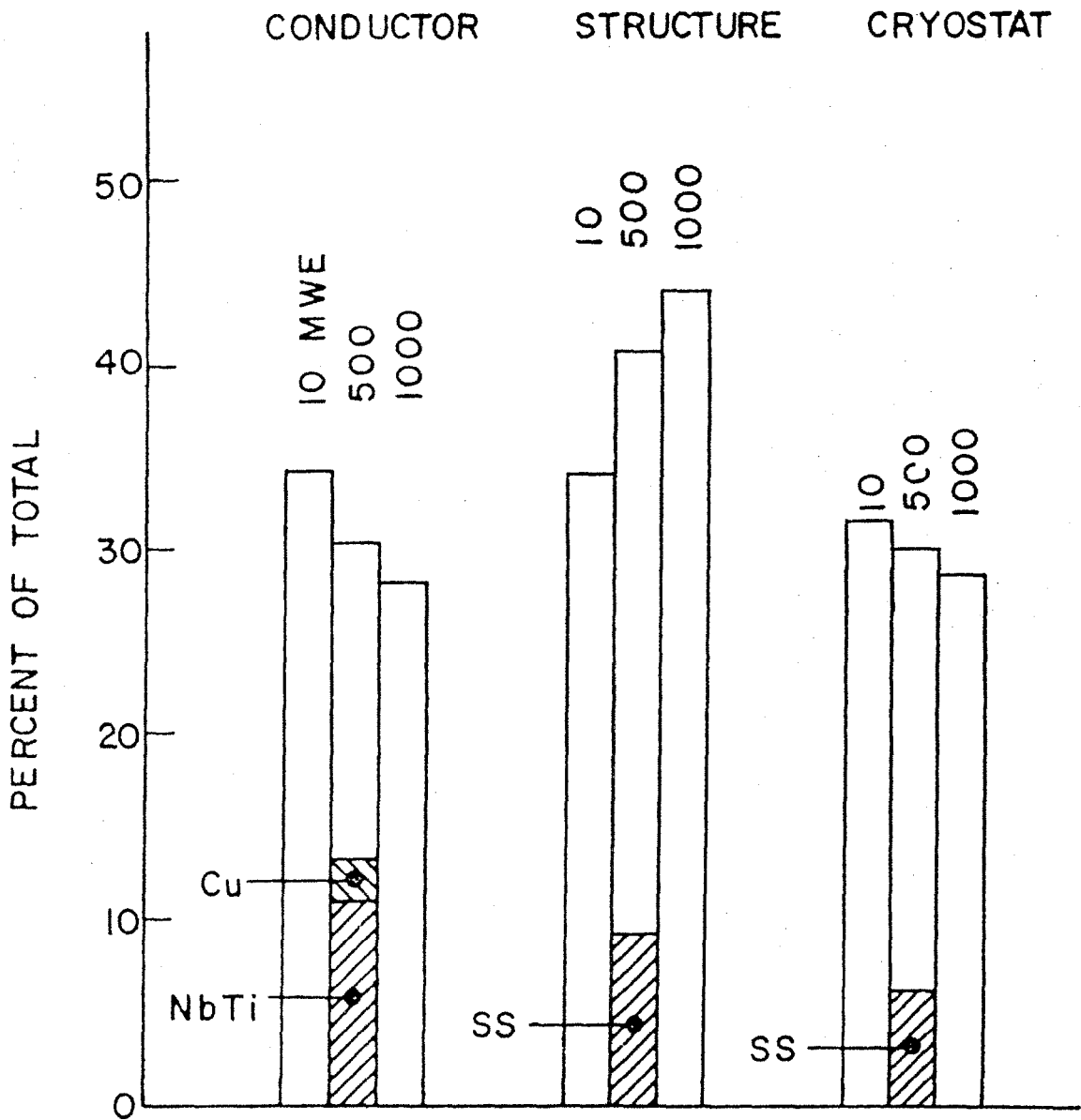


4.1.22B

Curve of Estimated Magnet System Cost vs MHD Power Output

4.1.22C Bar Chart Showing Relationship of Magnet System Cost Elements ("First Unit" Baseload Magnet)





NOTE: CROSS-HATCHED PORTION REPRESENTS RAW MATERIAL COST

4.1.22D Bar Chart Showing Comparative Costs of MHD Magnet Components (Fabricated)

## 4.2 Commercial-Scale and ETF Magnet System Designs

The development of commercial-scale and ETF magnet system (reference) designs is the second part of MIT's overall three-part MHD magnet technology program. It has been carried out in parallel with the first part, analysis, research and development summarized in Section 4.1.

Whereas the long range objective of the reference design work is to achieve a design freeze for the commercial-scale magnet, a more immediate objective is to identify areas where supporting analysis, research and technology development are most needed. The reference design program has been in progress for more than five years, and during the entire period up to the present, close coordination has been maintained between the design program and the analysis, research and development program.

At the outset, basic design concepts were reviewed and compared by MIT, assisted by inputs from the magnet community [1]. A series of reference (conceptual) design alternatives for commercial-size and ETF-size saddle coil magnets were then prepared, both in-house and by subcontractors.

A systematic procedure (framework) was developed to assist in evaluating the alternatives and selecting the design or designs most suitable to serve as a basis for future procurement of ETF and initial commercial-scale magnets (see Section 4.2.17). During the report period, six commercial-size and five ETF-size reference designs were investigated. Evaluations and comparisons of these designs and also of concepts incorporated in the U25-B/SM, CFFF/SM and the MCA truncated shell design (see Section 4.1.8.2) were initiated. A tentative selection was made early in 1980 of the most suitable design for the ETF magnet, this design to be incorporated in the Conceptual Design Engineering Report (CDER) for the Magnetohydrodynamic Engineering Test Facility 200 MWe Power Plant (MHD/ETF), issued in 1981 by NASA Lewis Research Center (NASA/LeRC). This was a 60° rectangular saddle magnet, representing a scale-down of the CSM commercial-size design.

Although substantial progress has been made toward final design selection, more work is required before the "framework" procedure can be completed and a well-supported final selection established. The work accomplished on MHD saddle-coil magnet design and magnet system studies is summarized in the sections which follow and in the references cited therein.

It will be noted that all the design alternatives mentioned here are basically saddle-coil magnets. The reason that this configuration is used and other configurations such as the racetrack or the split-pair solenoid are omitted from consideration is that studies [1] conducted under DOE (formerly ERDA) sponsorship prior to 1976 determined with reasonable certainty that for large size linear MHD systems the saddle configuration is superior in overall effectiveness to both the racetrack and split-pair solenoid (although a combination of saddle and racetrack is not ruled out).

An alternative to the linear MHD generator is the disk MHD generator. The disk generator has been under development in the MHD community for more than 10 years, in parallel with the development of linear generators. The disk generator has certain attractive features and is generally considered as a viable backup for the linear generator in the overall U.S. program to develop commercial-scale MHD power generators.

While the primary concern of the MHD magnet program has been magnets for linear MHD generators, a few preliminary studies were made of magnets for disk MHD generators, where solenoid magnets are most appropriate. These studies are summarized in Section 4.2.14.

#### 4.2.1 Summary of Commercial-Scale Magnet Reference Designs

The commercial-scale reference designs and conceptual designs prepared during the past five years were as follows:

<u>Type</u>	<u>Designer</u>	<u>Remarks</u>
Rectangular Saddle and Racetrack (MCSM)	MCA	Report June 1977 [57]. Concept still under evaluation
Circular Saddle, Conical-Shell Metal Substructure (BL6-P1)	AVCO	Report June 1977 [58]. Conical shell substructure difficult to make. Superseded by CASK concept
Rectangular Saddle, 90° Ends, Metal Substructure (BL6-P2)	AVCO	Report June 1977 [58]. Superstructure for crossovers difficult to make. Superseded by CSM
Circular Saddle, CASK-type Metal Substructure	GD	Report Dec 1979 [30]. Concept still under evaluation
Rectangular Saddle, 60° Ends, Nonmetal Substructure (CSM)	MIT	Initial version, 1980, now undergoing revisions to improve manufacturability. Concept still under evaluation
Rectangular Saddle, 45° Ends, Internally-Cooled Conductor	MIT	Initial version, 1980, not complete [79]. Represents advanced concept requiring considerable development. Evaluation to continue.

The major characteristics of the six designs are listed in Table 4.2.1-I. The designs are described in greater detail in Sections 4.2.2 through 4.2.7.

Further study and evaluation are required to make a final, well-supported selection among the candidate designs described above. It is recommended that, in the interest of successful commercialization of MHD, this work continue, the evaluation be expanded to include features of the U25-B/SM and CFFF/SM, and a report be prepared presenting the final selection and documenting the basis for the resultant choice.

In 1980 it was necessary to make a tentative selection of a preferred design concept for use in preparing a magnet system design description (SDD) for incorporation in the MHD/ETF 200 MWe Power Plant Conceptual Design Engineering Report [38] under preparation by NASA LeRC for DOE.

The CSM design concept was selected, based on data then available, as being most appropriate for scaling to the ETF application, particularly with respect to manufacturability. It was recognized that several features, in particular the large cable conductor which was an unproven item, required further verification before being

Table 4.2.1-I Sheet 1 of 2

## Major Design Characteristics of Commercial-Scale Magnet Reference and Conceptual Designs

Magnet designation	BL-MCA	BL6-P1	BL6-P2	CASK	CSM	ICCSM
Designer	MCA	AVCO	AVCO	GD	MIT	MIT
Date of Design	1977	1977	1977	1979	1980	1980
Magnet type	rect. sad. + racetr.	Circ. sad. Conical shell	90° rect. sad.	circ. sad. Conical stave	60° rect. sad.	45° rect. sad.
Superstructure type	Beam & tens. strap	Ring girder	Beam & tens. strap	Ring girder	Beam & tens. strap	Tens. band
Peak on-axis field (T)	6.0	6.0	6.0	6.0	6.0	6.0
Active field length (m) <sup>a</sup>	16(17.4)	16(17.4)	16(17.4)	14.5	14.5	14.5
Field at start of active length (T) <sup>a</sup>	6.0(4.8)	6.0(4.8)	6.0(4.8)	4.8	4.8	4.8
Field at end of active length (T)	3.5	3.4	3.3	3.6	3.6	3.6
Peak field in winding (T)	8.8	8.1	8.2	7.0	7.2	7.1
Aperture, start of active length, dimensions (m)	1.59 × 1.59	2.25 dia	2.94 × 2.94 <sup>b</sup>	3.28 dia <sup>c</sup>	2.2 × 2.8	2.2 × 2.2
Aperture, start of active length, area (m <sup>2</sup> )	2.53	3.98	8.64	8.45(4)	6.16	4.84
Aperture, end of active length, dimensions (m)	3.36 × 3.36	4.75 dia	4.42	4.5 dia	4.0 × 4.2	4.0 × 4.0
Aperture, end of active length, area (m <sup>2</sup> )	11.29	17.72	19.5	15.9	16.8	16.0
Warm bore (active) volume (m <sup>3</sup> )	103	160	219	133	162	143
Vacuum vessel overall length (m)	26.1	25	26.4	23.6	21.0	25.2
Vacuum vessel outside dimensions (m)	9.6	12.5	10.7 × 13.0	7.11	12.0	12.3

<sup>a</sup> Values in parentheses are adjusted values based on definition of active length as starting at 80% of peak field. Field profile is unchanged. After 1977, design characteristics for most large MHD magnet designs were consistent with this definition.

<sup>b</sup> Dimensions at inlet end of vacuum jacket are 1.99 m × 1.99 m (area 3.96 m<sup>2</sup>).

<sup>c</sup> Dimension at inlet end of vacuum jacket is 2.48 m dia. (area 4.83 m<sup>2</sup>).

Table 4.2.1-1 Sheet 2 of 2

Magnet Designation	BL-MCA	BL6-P1	BL6-P2	CASK	CSM	ICCSM
Conductor type <sup>a</sup>	Built-up (rect)	Built-up (rect)	Built-up (rect)	Built-up (rect)	Cable (round)	Sheathed cable(square)
Design current (kA)	20.0	14.5	14.5	50.0	52.2	20.0
Winding current density, average (Jλ)(10 <sup>7</sup> A/m <sup>2</sup> )	1.78	1.3	1.14	1.28	1.15	1.27
Conductor current density, (J)(10 <sup>7</sup> A/m <sup>2</sup> )	5.00	3.5	3.5	2.0	5.7	5.5
Copper-to-superconductor ratio, high field region	6.3	15	15	34	7.7	9.9
Heat flux (W/cm <sup>2</sup> )	1.0	0.40	0.41	0.4	0.07 <sup>d</sup>	0.03
Ampere turns (10 <sup>6</sup> A)	38	37	40.6	34.4	37.6	33.2
Ampere meters (10 <sup>8</sup> Am)	17.3	18.3	26.0	14.52	18.5	16.84
Inductance (H)	33.6	57	78	5	5.3	29
Stored energy (MJ)	6710	6100	8200	6300	7200	5800
Weight: conductor (tonnes)	324	477	678	552	300	269
substructure and insulation (tonnes)	450	556	40 <sup>b</sup>	719	155	277
superstructure (tonnes)	1106	1960	2220 <sup>c</sup>	689	—	269
helium vessel (tonnes)	incl. above	265	170	267		286
thermal shield, cold mass supports, etc. (tonnes)	incl. below	50	96	36	65	88
vacuum vessel (tonnes)	384	183	376	343	400	362
miscellaneous (tonnes)				38		3
total magnet (tonnes)	2264	3491	3580	2644	1850	1554
Superstructure material	SS 310S	Al 5083	Al 5083	SS 304LN	SS 304LN	SS 304LN
Design stress (MPa)	379	179	179	552	414	414

<sup>a</sup> All conductors are NbTi/Cu composite.

<sup>b</sup> Insulation only

<sup>c</sup> Superstructure and substructure

<sup>d</sup> Assumes all strands in cable are 100 % surface cooled

accepted for a detail design.

Descriptions of each of the commercial-scale reference designs are contained in the following sections, together with information concerning manufacturing studies and cost estimates, where applicable.

#### **4.2.2 Baseload MHD Magnet Design by MCA, Rectangular Saddle and Racetrack**

The baseload 6 T magnet reference design described below was started early in 1976 as part of an ERDA sponsored program at MCA which also included consideration of alternative magnet configurations, examination of the effect on the magnet system of variations in bore size and field strength, and development of an ETF magnet reference design (see Section 4.2.9).

The design criteria established by ERDA for the baseload magnet reference design are listed in Table 4.2.2-I. The same criteria were used as a basis for both the MCA design described below and the AVCO design described in Section 4.2.3.

The MCA magnet design incorporates a 20 kA copper-stabilized NbTi composite conductor built up with a readily available basic building block (Rutherford cable). The winding is made up of eight coils, including six racetrack coils and two coils of the 90° saddle type. The sides of the coils diverge from the magnet axis going toward the channel exit end in order to produce the desired tapered field profile. The coil containers and the major force containment structure surrounding them are of stainless steel. Separate coil containers enclose each coil and serve as liquid helium containment vessels.

The Dewar includes an aluminum alloy thermal radiation shield cooled by tracer tubes supplied with cold helium gas, a cylindrical outer vacuum shell and dished end covers (room temperature) of aluminum alloy and a square cross section, room temperature bore tube of aluminum alloy. The cold mass of the magnet is carried on four low heat leak columns which transmit the load to the magnet foundation.

The characteristics of the MCA baseload reference design are listed in Table 4.2.2-II. The calculated axial field profile is shown in Figure 4.2.2A, the coil configuration is shown in Figure 4.2.2B, a typical winding cross section is shown in Figure 4.2.2C, typical conductors are shown in Figure 4.2.2D and the magnet assembly is shown in Figures 4.2.2E and 4.2.2F.

A major effort was made to ensure that the design concept is well adapted to fabrication using present state-of-the-art capabilities. Many of the features of the design were generated and determined by consideration of fabrication, handling, shipping and on-site system assembly. The MCA fabrication study indicated that the major components of the system, i.e. the coil subassemblies, structural components and Dewar components could be fabricated, tested and preassembled off-site and then partially disassembled, shipped and assembled on-site. The two saddle coil and container assemblies are the largest single components to be transported. Each will be 23.3 m long by 6.2 m high by 4.0 m wide. Transportation of a unit of this size is nontrivial according to MCA's study, but is still within the present state of the art using existing equipment or equipment currently on the drawing boards.

It should be noted that the inside dimension of the bore tube in the MCA design is the inscribed square of the circular bore specified in the design criteria, Table 4.2.2-I. Thus, the MCA square bore volume is smaller than the specified circular bore volume by a factor of 0.64. This is important to keep in mind when comparing the MCA design with the AVCO baseload magnet designs described in Section 4.2.3. Both AVCO designs, circular-saddle and rectangular-saddle, represent larger magnets than the MCA design because they incorporate bore volumes equivalent to the full circular bore specified.



Table 4.2.2-I

Design Criteria For a Baseload Scale MHD Magnet:  
Estimated MHD Power, 600 MWe

	Principal Design	Variations
<b>Channel Inside Dimensions</b>		
Inlet	1.35 m × 1.35 m	0.95 m × 1.9 m
Exit	2.9 m × 2.9 m	2.05 m × 4.1 m
Active length	16 m	
<b>Magnetic Field</b>		
Inlet, Active Length	6.0 T	5.0 T, 7.0 T
Exit, Active Length	3.5 T	Same % taper as principal design
Magnet Field Uniformity	±5% across duct & deviation from linear taper	
<b>Warm Bore Dimensions</b>		
Inlet	2.25 m dia	1.6 m × 3.2 m
Exit	4.75 m dia	3.35 m × 6.7 m
Operating Temperature	4.5 K	4.5 K at 7.0 T

Table 4.2.2-II Sheet 1 of 3

Design Characteristics  
Baseload MHD Magnet Design BL-MCA  
Magnetic Corporation of America

Date of design		1977
MHD power train data		
MHD power output (estimated)	(MWe)	600
Channel inlet dimensions	(m)	1.35 × 1.35
Channel exit dimensions	(m)	2.9 × 2.9
Magnet data		
Magnet type	—	90° rect. sad. and racetracks
Warm bore liner?	—	No
Magnetic field:		
Peak on-axis field	(T)	6.0
Active field length <sup>a</sup>	(m)	16(17.7)
Field at start of active length <sup>a</sup>	(T)	6.0(4.8)
Field at end of active length	(T)	3.5
Area ratio, plasma c.s./warm bore, end of active length	—	0.7+
Peak field in winding	(T)	8.88
Dimensions:		
Aperture, warm bore inlet <sup>c</sup>	(m)	1.57 sq.
Aperture, start of active length <sup>c</sup>	(m)	1.57 sq.
Aperture, end of active length <sup>c</sup>	(m)	3.36 sq.
Aperture, warm bore exit <sup>c</sup>	(m)	3.36 sq.
Aperture area, start of active length <sup>c</sup>	(m <sup>2</sup> )	2.53
Aperture area, end of active length <sup>c</sup>	(m <sup>2</sup> )	11.29
Vacuum vessel overall length	(m)	26.1
Vacuum vessel outside dia.	(m)	9.6
Warm bore volume, active <sup>c</sup>	(m <sup>3</sup> )	112
MVU <sup>d</sup>	—	0.74

<sup>a</sup> Values in parentheses are adjusted values based on definition of active length as starting at 80% of peak field. Field profile is unchanged. After 1977, design characteristics for most large MHD magnet designs were consistent with this definition.

<sup>c</sup> Dimensions inside warm bore, without liner

<sup>d</sup> Ratio of channel volume to warm bore volume

Table 4.2.2-II Sheet 2 of 3

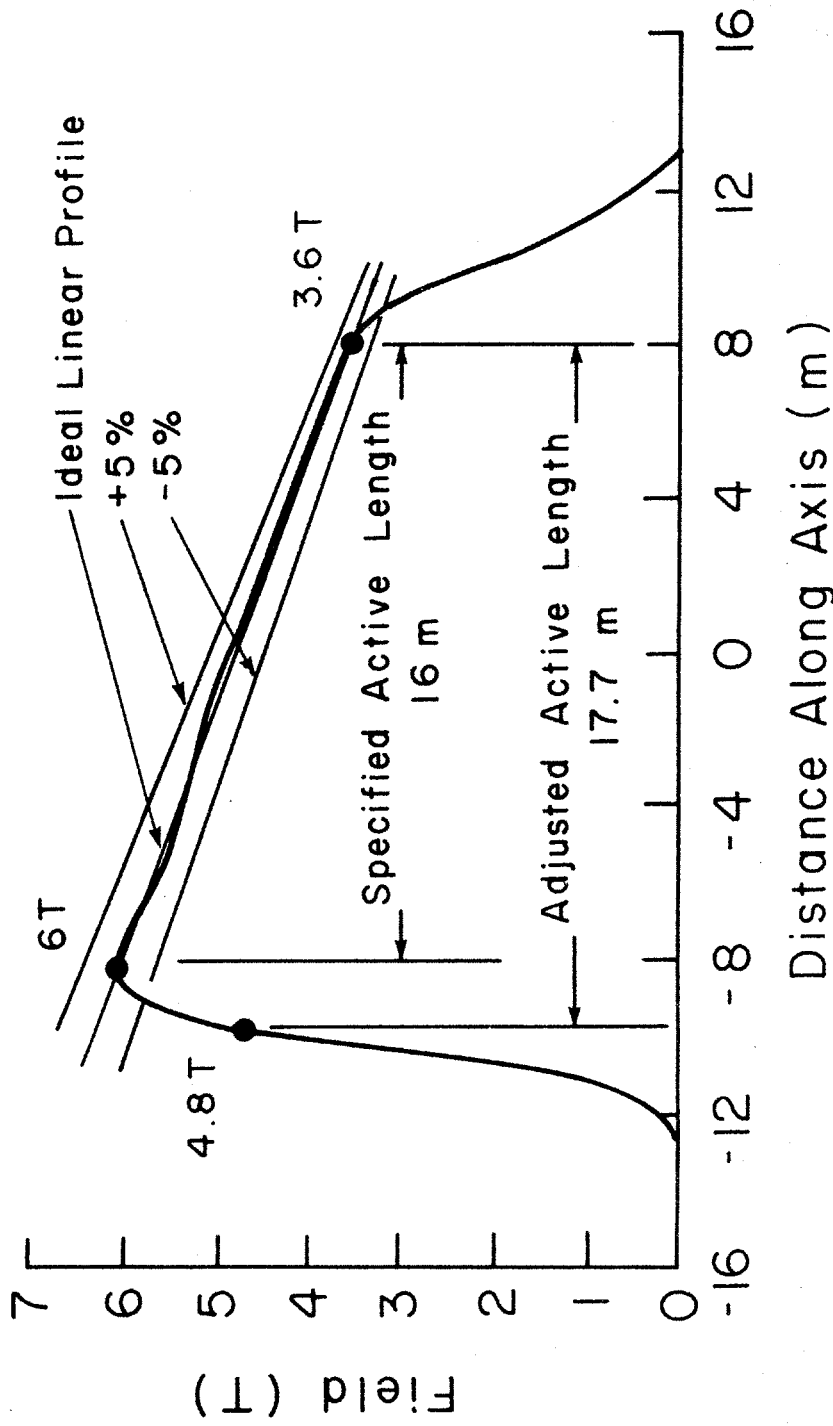
<b>Winding characteristics:</b>		
Build, winding cross section	(m)	0.77
Number of winding modules (or layers) per half	—	4
Design current, I	(kA)	20
Winding current density, average, $J\lambda^a$	( $10^7$ A/cm <sup>2</sup> )	1.78
Packing factor, $\lambda^a$	—	0.36
Conductor current density, $J^a$	( $10^7$ A/cm <sup>2</sup> )	5.0
Total number of turns, N	—	1884
Total length of conductor	(km)	86.7
Ampere turns, NI	( $10^6$ A)	38.0
Ampere meters	( $10^8$ Am)	17.3
Inductance	(H)	33.6
Stored energy	(MJ)	6710
Conductor type	—	Built-up
Conductor materials	—	NbTi-Cu
Conductor dimensions <sup>a</sup>	(cm)	3.81 × 1.25
Copper-to-superconductor ratio <sup>a</sup>	—	6.3
LHe to conductor ratio (vol.) <sup>a</sup>	—	0.19
Heat flux <sup>a</sup>	(W/cm <sup>2</sup> )	1.0
<b>Weights:</b>		
Conductor	(tonnes)	324
Insulation	(tonnes)	incl. below
Substructure	(tonnes)	450
Superstructure	(tonnes)	1106
Liquid He vessel	(tonnes)	incl. above
<b>Total cold mass</b>	(tonnes)	<b>1880</b>
Thermal shield, cold mass supports, etc	(tonnes)	incl. below
Vacuum vessel	(tonnes)	384
Miscellaneous	(tonnes)	0
<b>Total magnet weight</b>	(tonnes)	<b>2264</b>

<sup>a</sup> Where graded winding is incorporated, values listed are for high field region of winding.

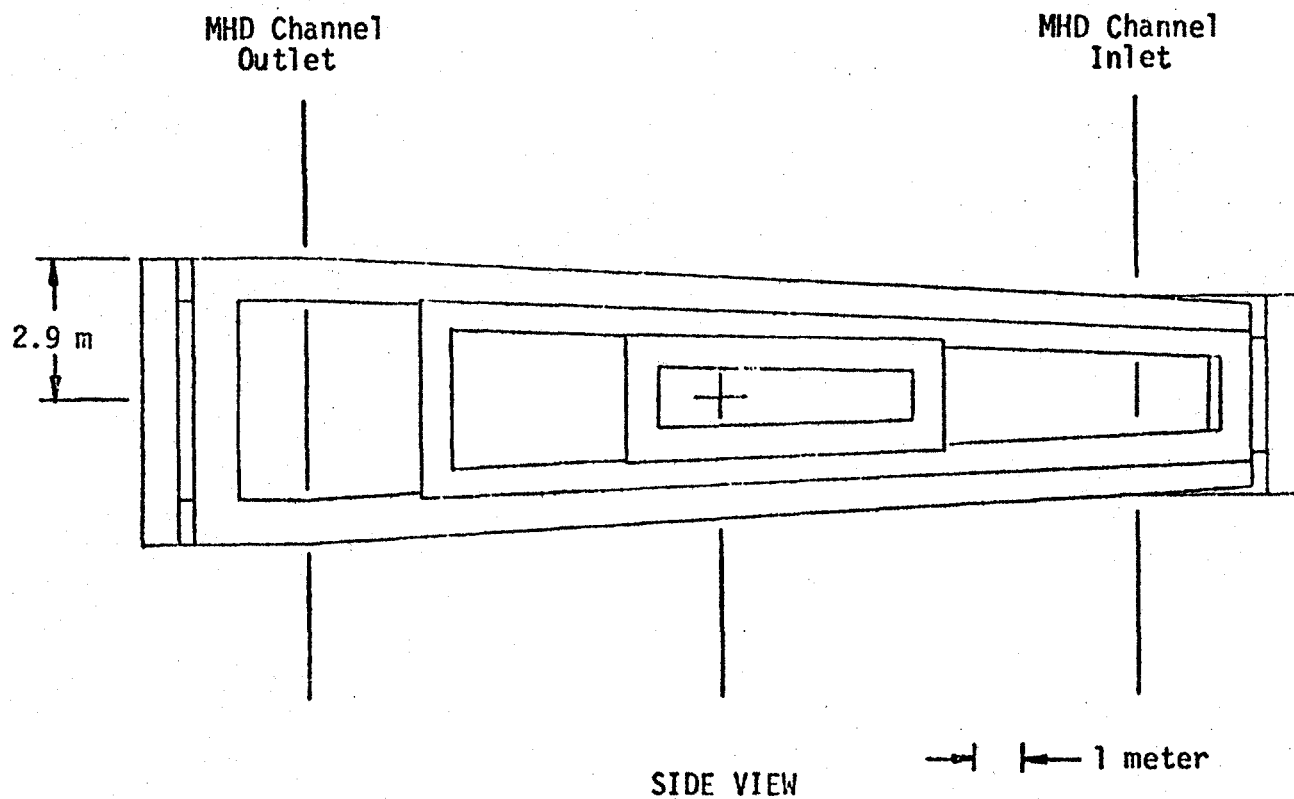
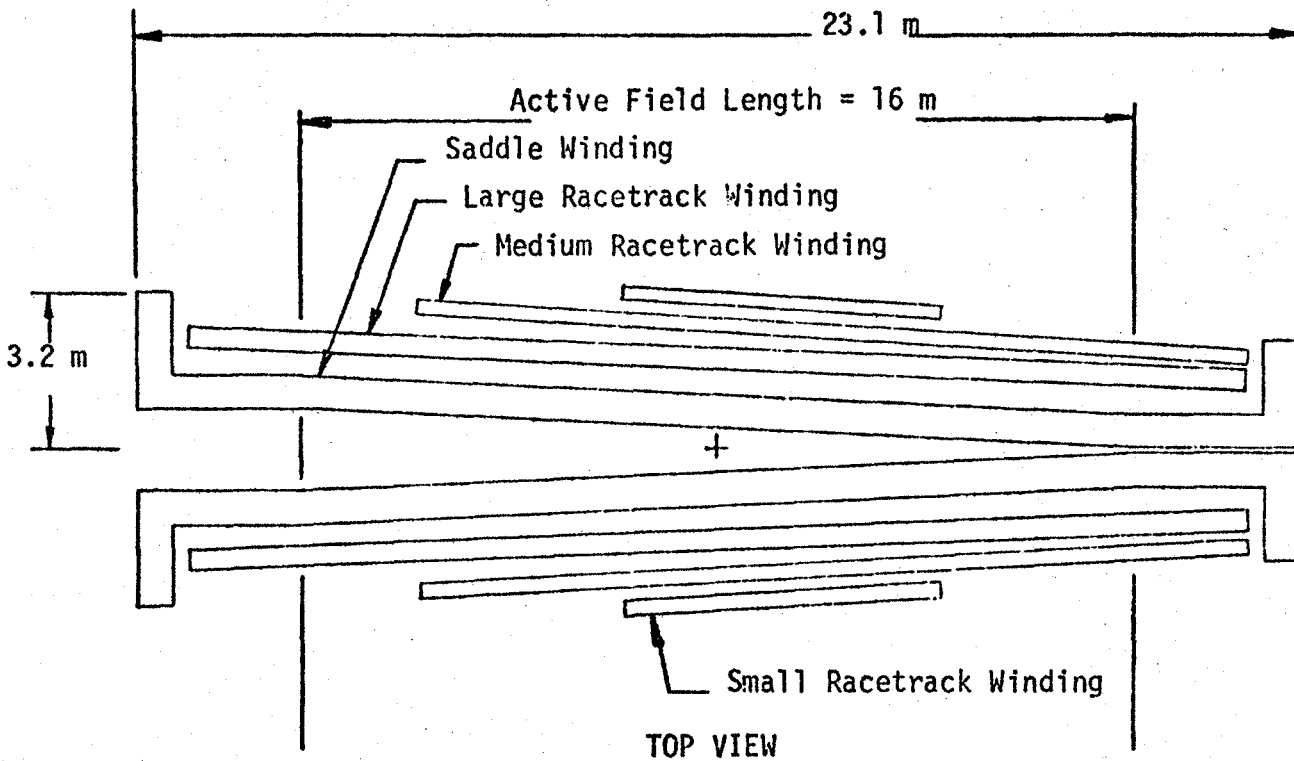
Table 4.2.2-II Sheet 3 of 3

Cryogenic data:		
Operating temperature at winding	(K)	4.5
Operating temperature, thermal shield	(K)	102
Thermal shield coolant	—	He gas
Heat load, LHe region, not incl. leads <sup>a</sup>	(W)	93
LHe for lead cooling at design current	(ℓ/hr)	60
Refrigerator/liquefier capacity	(ℓ/hr)	234
Power supply and discharge data:		
Number of current leads	—	2
Resistance, emergency dump resistor	(Ω)	0.0125
Emergency discharge time constant	(min)	45
Maximum discharge voltage, terminal	(V)	250
Materials of construction:		
Winding substructure	—	SS 310 S
Insulation	—	Epoxy/glass
Superstructure	—	SS 310 S
Liquid helium vessel	—	SS 310 S
Thermal shield	—	Al 5083
Vacuum vessel	—	Al 5083
Design stresses:		
Winding substructure	(MPa)	379
Superstructure	(MPa)	379 tens. 379 bend.
Pressure rating		
Liquid helium vessel		
Normal operating	(atm)	1.3

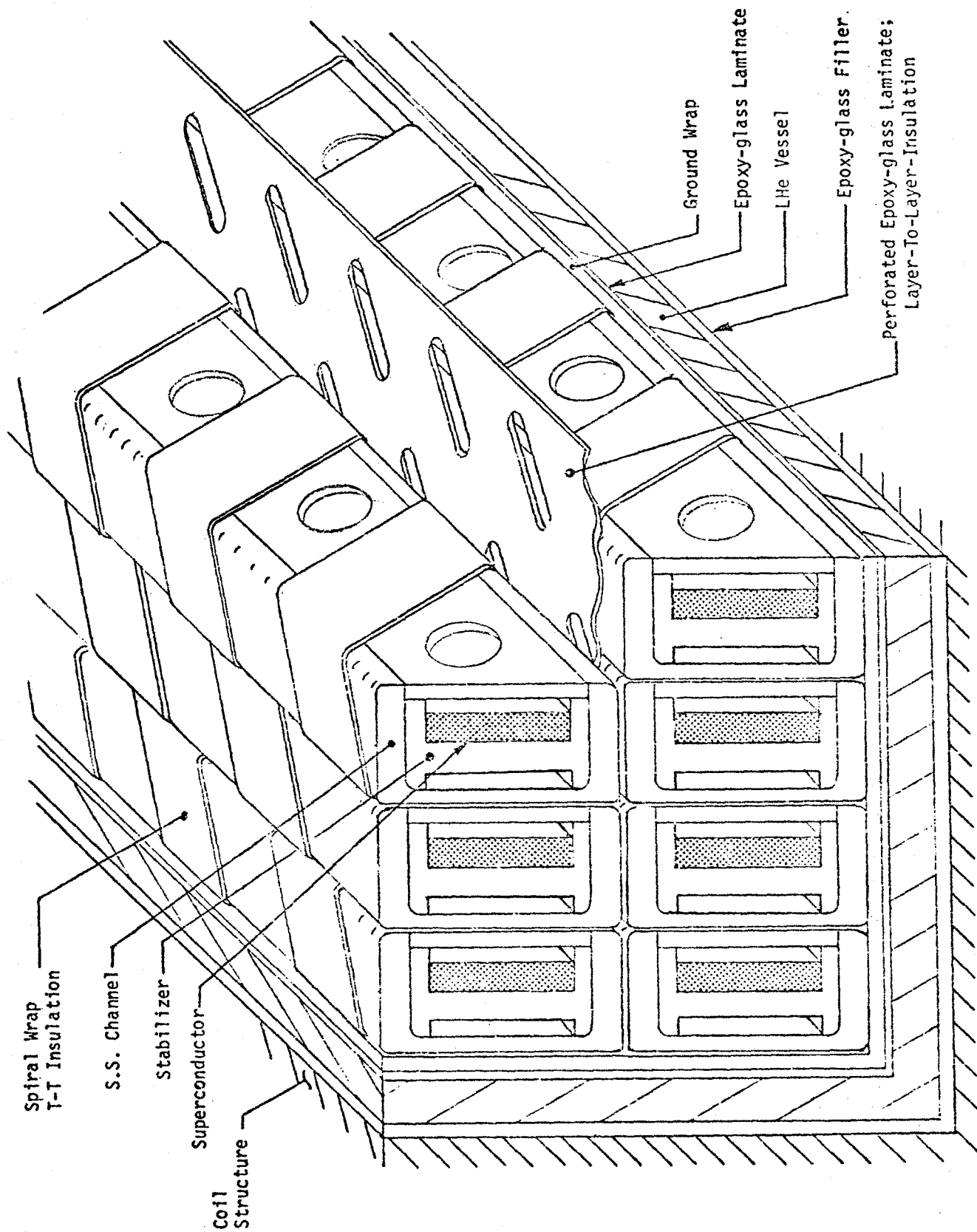
<sup>a</sup> Does not include conductor splice loss.



4.2.2A Axial Field Profile for MCA 6 T Baseload Magnet Reference Design

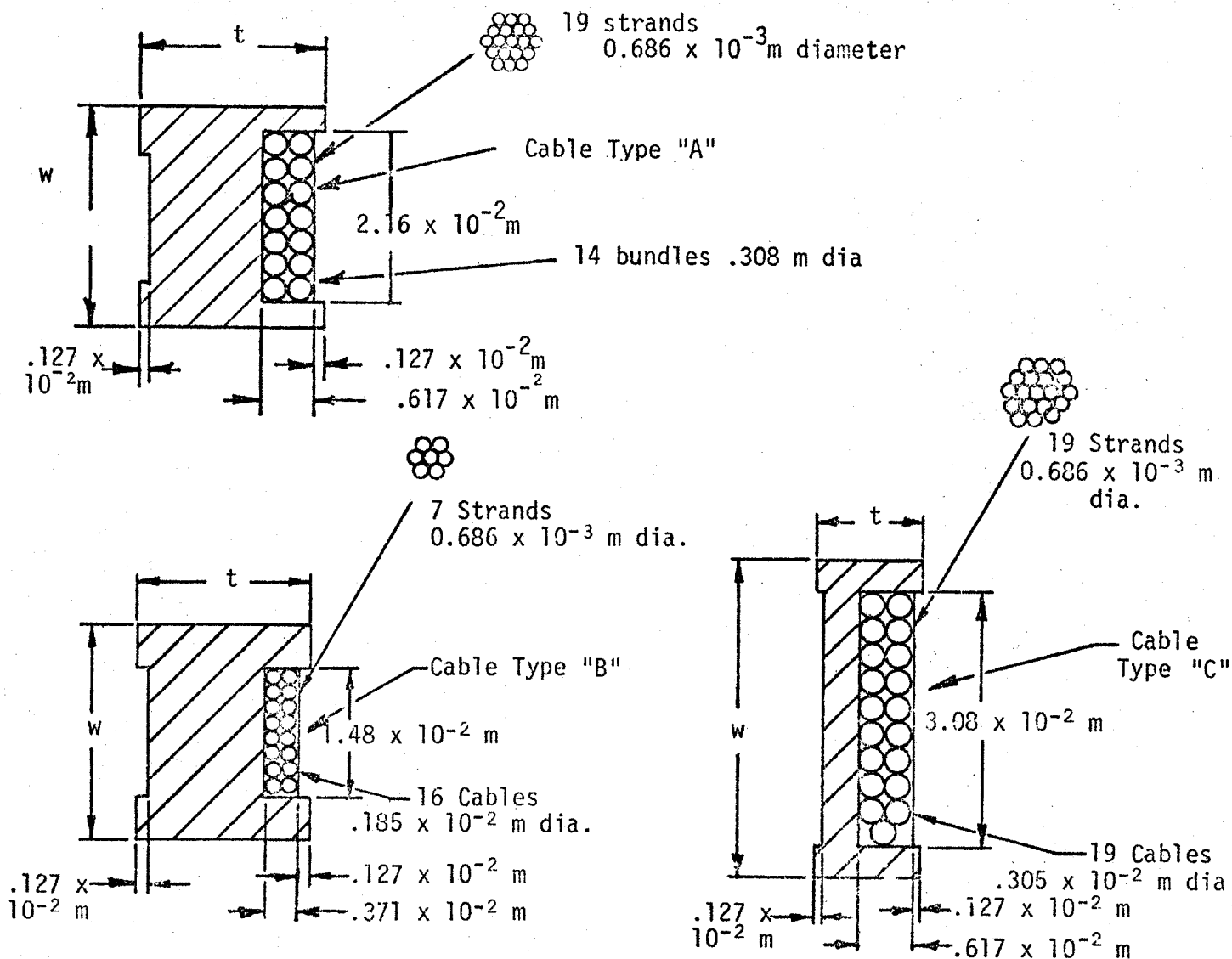


4.2.2B Diagram of MCA Baseload Magnet Winding Configuration



FA 4036

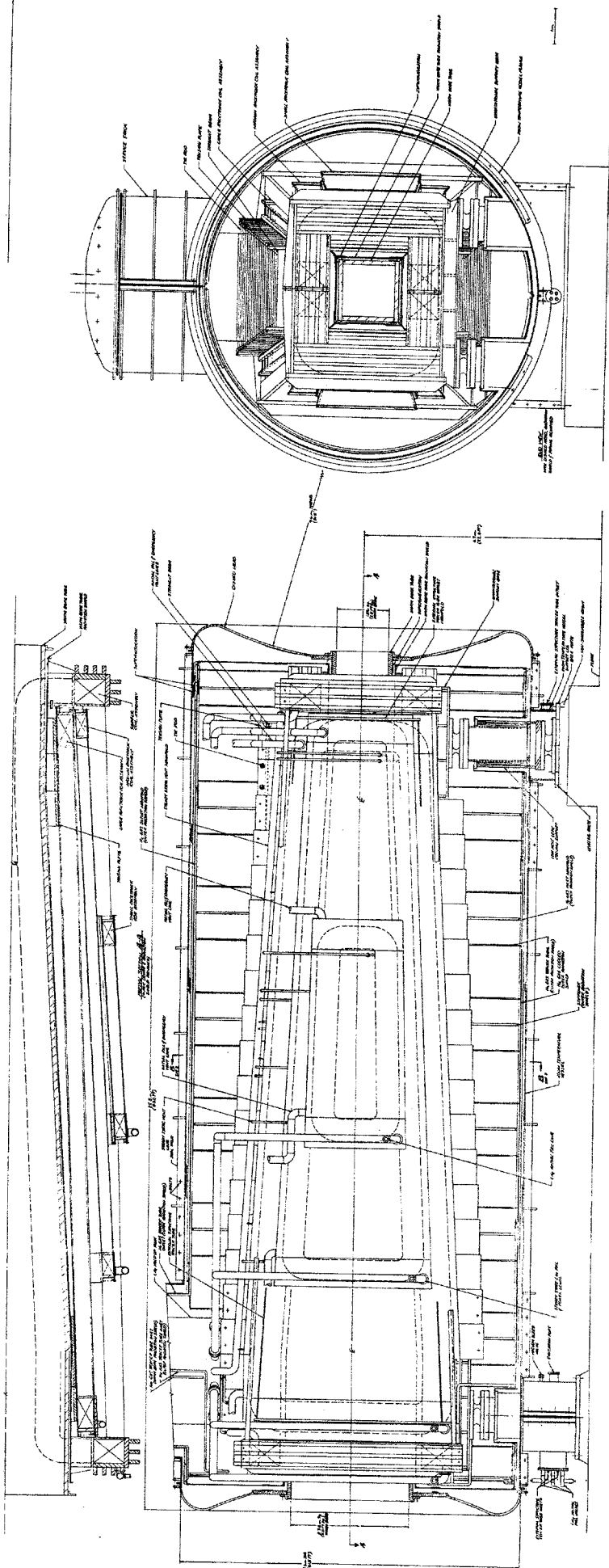
4.2.2C Typical Winding Cross Section Showing Conductor and Internal Winding Structural Details for the MCA Base-load Magnet



Conductor No.	Cable Type	w( $10^{-2}$ m)	t( $10^{-2}$ m)	$j_{cond}$ $10^7$ A/m <sup>2</sup>	$B_{peak}$ (T)	Location
1	A	2.54	2.12	4.14	8.00	Saddle
2	B	2.54	2.04	4.16	5.50	Saddle
3	B	2.54	1.78	4.82	4.50	Saddle
4	C	3.81	1.25	5.02	8.88	Racetrack
5	C	3.81	1.185	5.36	7.86	Racetrack
6	C	3.81	1.12	5.74	6.96	Racetrack

4.2.2D Cross Section Diagrams of Conductor for MCA Baseload MHD Magnet





4.2.2E MCA Base-load Magnet Assembly Drawing, Inlet End and Partial Section Views



The major accessory subsystems for the MCA baseload magnet are a cryogenic system for magnet cool-down, steady state operation and warmup, and a power supply system for magnet charging and discharging. These subsystems are shown diagrammatically in Figure 4.2.2G.

The cryogenic system includes a screw-type helium compressor, a helium liquefier using turbo-expanders, a liquid helium storage Dewar and a liquid nitrogen to helium gas heat exchanger for magnet cooldown. The recommended rated capacity for the liquefier is 25% greater than the estimated boil-off rate of 187 l/hr. The refrigerator provides a cold helium gas loop for maintaining the thermal radiation shield at cryogenic temperature. No liquid nitrogen precooling is required for refrigerator operation under steady state conditions. Liquid nitrogen is required only for magnet cooldown from room temperature.

The power supply system consists of a rectifier unit, a dump resistor and a dump switch. Voltage sensors in the magnet coil are arranged to detect a quench and automatically actuate the dump switch. When the switch is thus opened, the power supply is disconnected and the coil discharges through the dump resistor which is permanently connected across the coil terminals.

The fabrication plan envisions two off-site facilities, i.e., the coil fabrication and assembly facility and the Dewar fabrication facility.

In the coil facility, the composite superconductor in the form of Rutherford cable, the copper substrate and the stainless steel channel (see Figure 4.2.2C) are assembled together in a winding mandrel. In this process, the substrate and channel sections are bent together in the mandrel to conform to the coil shape; substrate sections are spliced by means of soldered, scarfed joints; the conductor is inserted and soldered into the groove in the substrate and cover strips and insulation are applied. The coil containers and structural components which are prefabricated elsewhere, are brought into the coil facility and assembled with the coils to form modules that are then shipped to the plant site.

In the Dewar fabrication facility, Dewar parts including coil containers and structural components are prefabricated. Parts required for the coil modules are shipped to the coil facility. The remaining parts are transported to the plant site in shippable modules.

At the plant site, the low heat leak columns are mounted on the foundation. The two saddle coil modules are mounted on the columns. Beams and tension plates are bolted in place and the racetrack modules are attached. Piping, thermal radiation shield components and warm bore tube are installed and the clam shell outer vacuum vessel and heads are put in place around the outside of the magnet assembly.

The estimated costs for one baseload magnet system are shown in Table 4.2.2-III. The total estimated installed cost is  $\$71.3 \times 10^6$ . The estimated schedule shows a four year program including an initial fifteen months of preliminary design and development. Completion of the magnet system occurs thirty-three months after the start of the final (Title II) design.

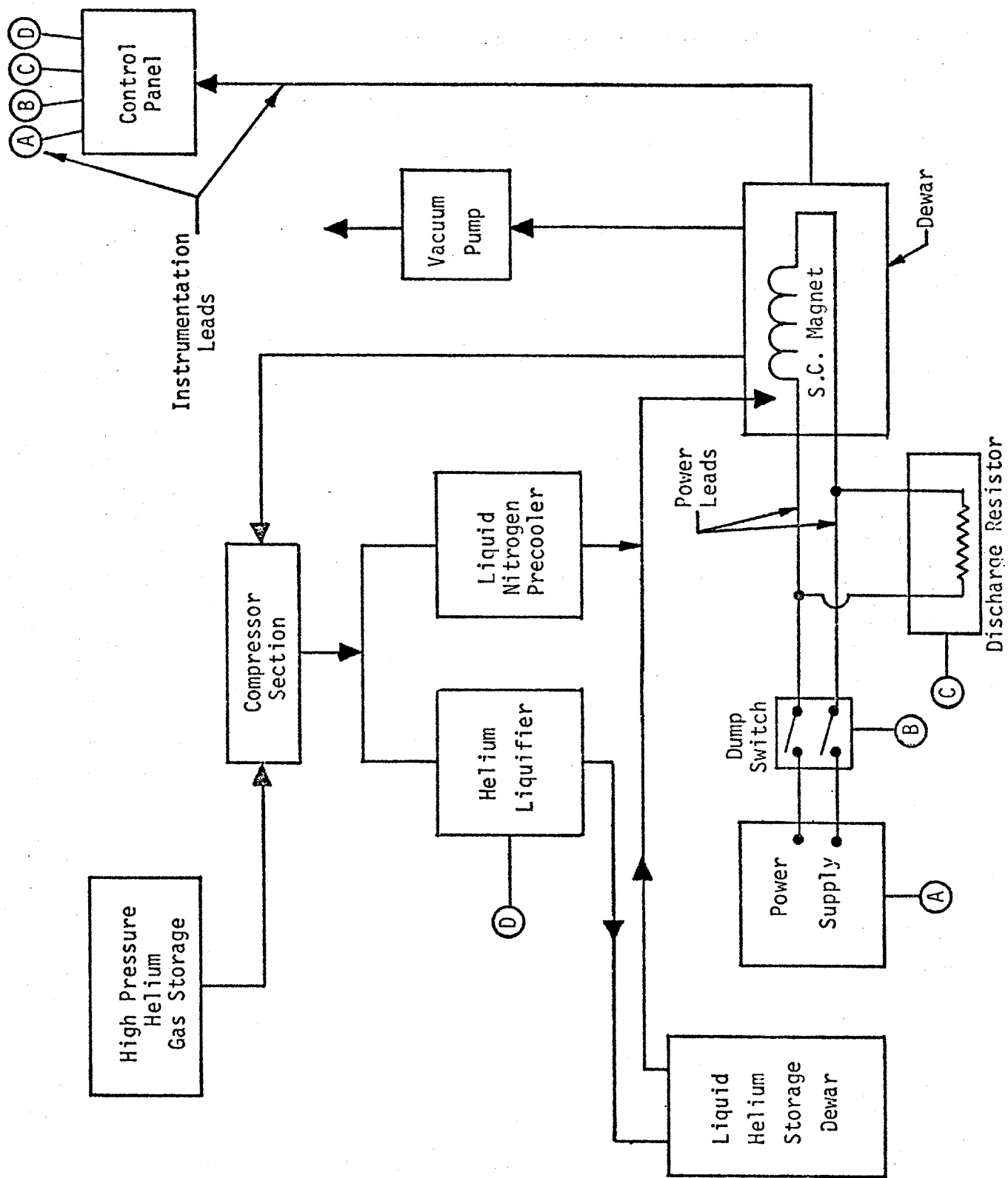
A number of potential areas for future research and development were pointed out. These included high current conductor fabrication and testing, study of the impact of high current conductor operation on magnet system cost, mock winding fabrication, development of joints in high current conductor, high current vapor-cooled lead design, further investigation of structural support of windings, further investigation of fault conditions, instrumentation, protection and controls, and further study of interface problems.

More detailed information on the MCA baseload magnet design is contained in Reference 57.

Table 4.2.2-III

Baseload System Cost Estimates, BL-MCA  
(1977 dollars)

Material Costs (\$10 <sup>6</sup> )	
Conductor	16.20
Structure	12.84
Dewar	2.32
Tooling	5.43
Misc. and Shipping	<u>5.52</u>
Subtotal	42.3
Administrative Expenses	<u>12.7</u>
Subtotal	55.0
Labor for Design and Fabrication (\$ × 10 <sup>6</sup> )	<u>16.3</u>
<b>TOTAL</b>	<b>71.3</b>



### 4.2.3 Baseload MHD Magnet Design by AVCO, Circular-Saddle, BL6-P1

The baseload 6 T magnet reference design BL6-P1 described in this section and the alternative (rectangular saddle) design described in the next section were both started at AVCO early in 1976 under ERDA sponsorship, and were carried out in parallel with the MCA design program described in Section 4.2.2. MEA and IGC, under subcontract to AVCO, assisted with both the principal reference design and the alternative reference design.

The design criteria for the AVCO reference designs were the same as for the MCA program (see Table 4.2.2-1). AVCO's program also included consideration of alternate magnet configurations and examination of the effects of variations in design criteria.

The AVCO design, designated BL6-P1, is a circular saddle coil magnet with a circular-cross-section warm bore. At the time their reference design program was completed (June 1977), AVCO considered this design to be superior to their alternative (90° rectangular saddle) design described in Section 4.2.4. A discussion concerning design preference appears at the beginning of that section.

The AVCO circular saddle design incorporates a 14.5 kA built-up copper and NbTi composite superconductor consisting of a rectangular-cross-section copper substrate with a spiral wrapping of composite wire soldered in place. The conductor components are readily available items. The winding is modular, with saddle-shaped winding layers installed in grooves in conical aluminum alloy structural shells which are stacked concentrically around a central core tube to make up the winding assembly. The shells form a substructure which supports groups of conductors and prevents the accumulation of magnetic loading on the conductor bundle as a whole. The shells themselves carry the axial magnetic load; they transmit radially outward loads to the surrounding superstructure.

The substructure shells are conical, so that the winding layers diverge from the magnet axis going toward the channel exit end, thus producing the desired tapered field profile. There are fourteen structural shells in each coil half, with two layers of conductor in each shell. The liquid helium containment vessel consists of a conical outer shell wrapped around the winding and substructure, a pair of end plates and the central core tube which forms the inner wall of the vessel. The entire vessel is of welded aluminum alloy construction. The major force containment structure (superstructure) is a series of aluminum alloy ring girders with bolted joints, assembled around the outer envelope of the winding assembly and liquid helium containment vessel.

The Dewar includes an aluminum alloy thermal radiation shield, cooled by tracer tubes supplied with cold helium gas, and an aluminum alloy room temperature vacuum jacket consisting of a conical outer shell, dished heads and a conical warm bore tube, all of welded construction. The cold mass of the magnet is supported by a system of low heat leak tubular struts of titanium alloy including four vertical struts, two transverse struts and one longitudinal strut.

Manufacturing, assembly and cost considerations were kept in mind throughout the design program. It was planned that the windings would be installed in their structural support shells at an off-site manufacturing facility. The largest single components to be shipped to the site would be the outer winding modules (wound structural support shells), each 23.1 m long by 7.6 m high by 3.8 m wide. It was anticipated that barges and/or special transporters would be required.

The characteristics of the AVCO baseload (BL6-P1) circular saddle reference design are listed in Table 4.2.3-1. The calculated axial field profile is shown in Figure 4.2.3A. The coil configuration is shown in Figure 4.2.3B. A typical winding cross section is shown in Figure 4.2.3C, a typical conductor in Figure 4.2.3D and the magnet assembly in Figure 4.2.3E.

The AVCO design anticipates that a cryogenic system including a closed-loop helium refrigerator of a type

Table 4.2.3-1 Sheet 1 of 3

Design Characteristics  
 Baseload MHD Magnet Design BL6-PI  
 (AVCO)

Date of design		1977
MHD power train data		
MHD power output (estimated)	(MWe)	600
Channel inlet dimensions	(m)	1.35 × 1.35
Channel exit dimensions	(m)	2.9 × 2.9
Magnet data		
Magnet type	—	Circ. sad.
Warm bore liner?	—	No
Magnetic field:		
Peak on-axis field	(T)	6.0
Active field length <sup>a</sup>	(m)	16(17.7)
Field at start of active length <sup>a</sup>	(T)	6.0(4.8)
Field at end of active length	(T)	3.4
Field uniformity at end of active length <sup>b</sup>	(%)	+2    -4
Area ratio, plasma c.s./warm bore, end of active length	—	0.46
Peak field in winding	(T)	8.0
Dimensions:		
Aperture, warm bore inlet <sup>c</sup>	(m)	2.25 dia.
Aperture, start of active length <sup>c</sup>	(m)	2.25 dia.
Aperture, end of active length <sup>c</sup>	(m)	4.84 dia.
Aperture, warm bore exit <sup>c</sup>	(m)	5.50 dia.
Aperture area, start of active length <sup>c</sup>	(m <sup>2</sup> )	3.98
Aperture area, end of active length <sup>c</sup>	(m <sup>2</sup> )	17.72
Distance, bore inlet to start of active length	(m)	4.14
Vacuum vessel overall length	(m)	25.0
Vacuum vessel outside dia.	(m)	12.5
Warm bore volume, active <sup>c</sup>	(m <sup>3</sup> )	183
MVU <sup>d</sup>	—	0.46

<sup>a</sup> Values in parentheses are adjusted values based on definition of active length as starting at 80% of peak field. Field profile is unchanged. After 1977, design characteristics for most large MHD magnet designs were consistent with this definition.

<sup>b</sup> Field uniformity is + and - variation from on-axis field, central 50% of warm bore cross section

<sup>c</sup> Dimensions inside warm bore, without liner

<sup>d</sup> Ratio of channel volume to warm bore volume

Table 4.2.3-I Sheet 2 of 3

Winding characteristics:		
Build, winding cross section	(m)	0.94
Number of winding modules (or layers) per half		14
Design current, I	(kA)	14.5
Winding current density, average, $J\lambda^a$	( $10^7 \text{ A/cm}^2$ )	1.21
Packing factor, $\lambda^a$	—	0.37
Conductor current density, $J^a$	( $10^7 \text{ A/cm}^2$ )	3.3
Total number of turns, N	—	2550
Total length of conductor	(km)	126.2
Ampere turns, NI	( $10^6 \text{ A}$ )	37.0
Ampere meters	( $10^8 \text{ Am}$ )	18.3
Inductance	(H)	57
Stored energy	(MJ)	6100
Conductor type	—	Built-up
Conductor materials	—	NbTi-Cu
Conductor dimensions <sup>a</sup>	(cm)	$3.49 \times 1.43$
Copper-to-superconductor ratio <sup>a</sup>	—	15
LHe to conductor ratio (vol.) <sup>a</sup>	—	0.4
Heat flux <sup>a</sup>	( $\text{W/cm}^2$ )	0.4
Weights:		
Conductor	(tonnes)	454
Insulation	(tonnes)	40
Substructure	(tonnes)	526
Superstructure	(tonnes)	1960
He vessel	(tonnes)	260
Total cold mass	(tonnes)	3240
Thermal shield, cold mass supports, etc	(tonnes)	60
Vacuum vessel	(tonnes)	183
Miscellaneous	(tonnes)	0
Total magnet weight	(tonnes)	3483

<sup>a</sup> Where graded winding is incorporated, values listed are for high field region of winding.

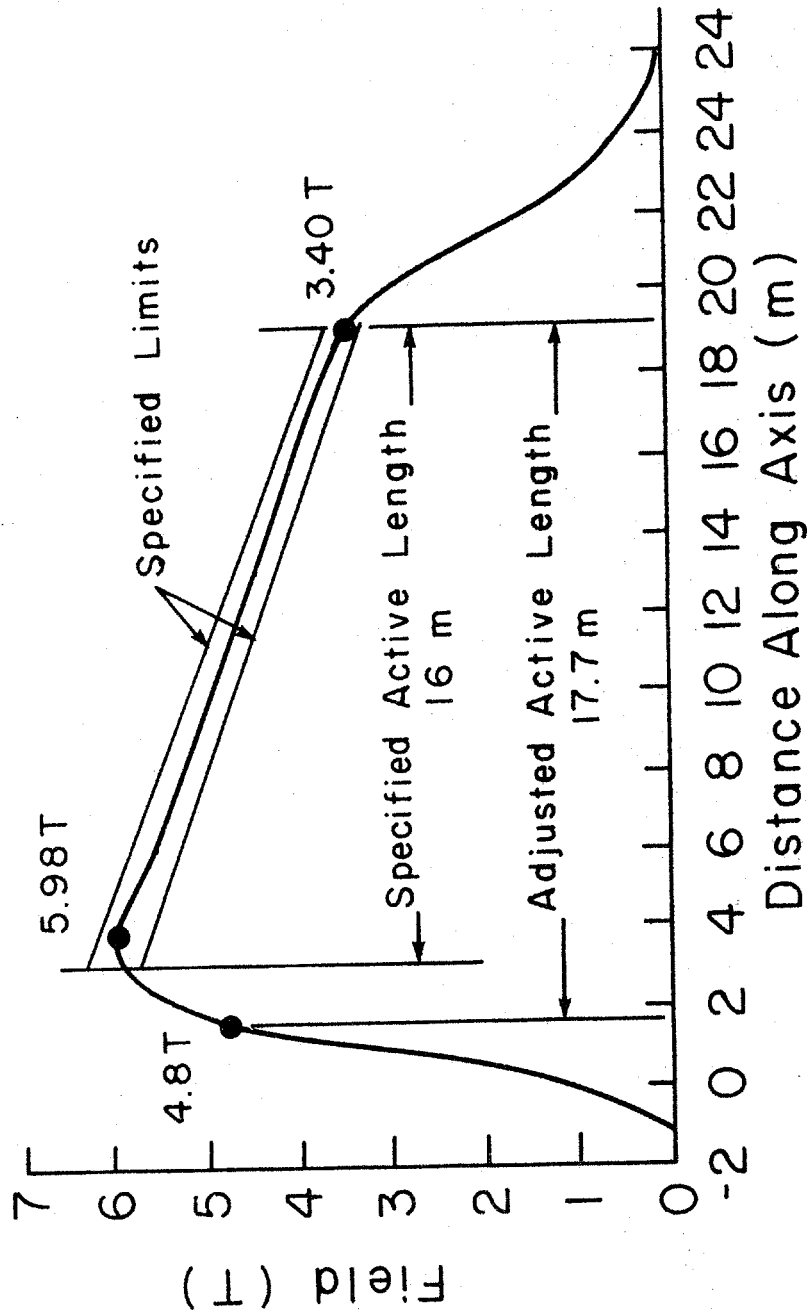


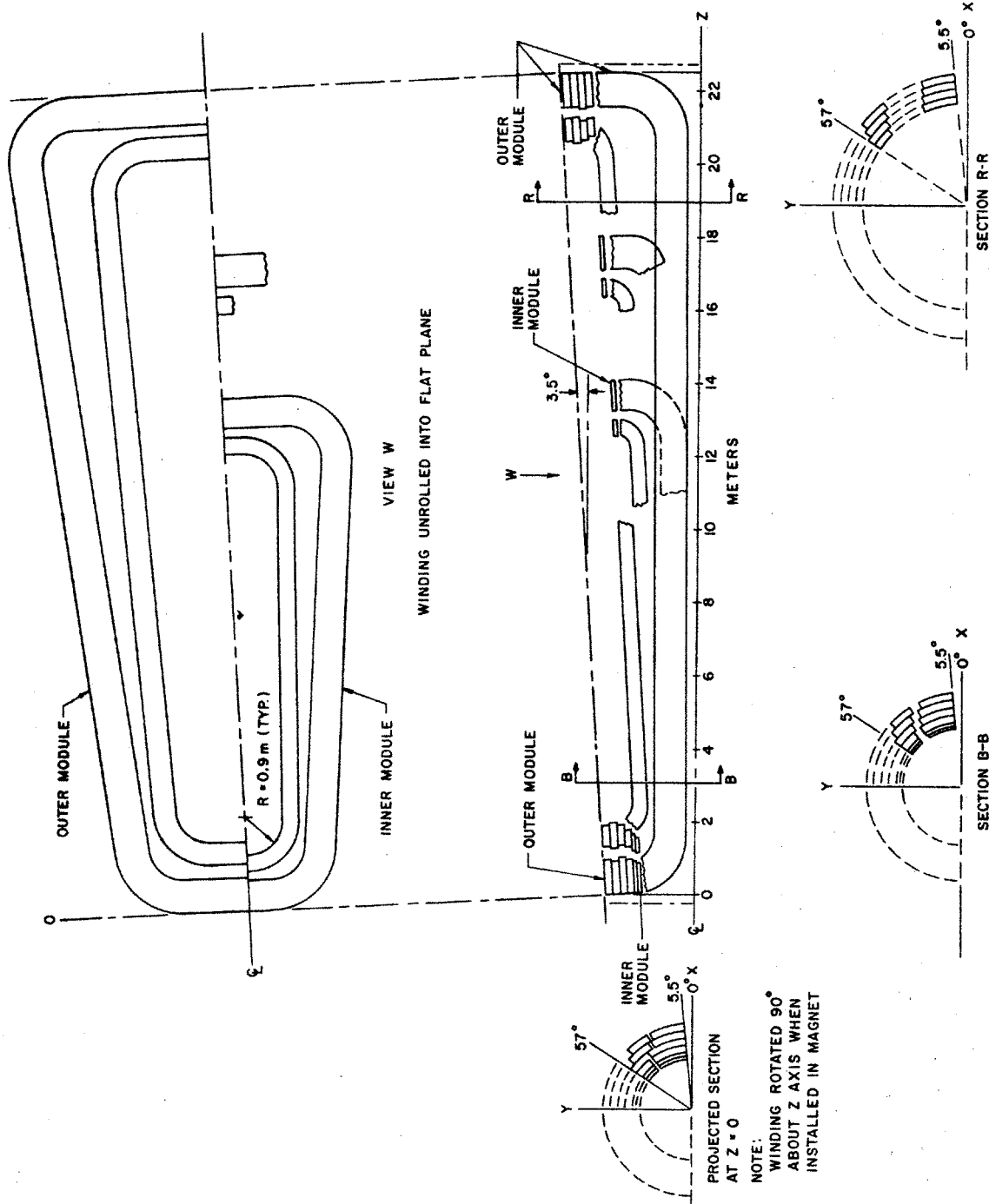
Table 4.2.3-1 Sheet 3 of 3

Cryogenic data:		
Operating temperature at winding	(K)	4.5
Thermal shield temperature	(K)	80
Thermal shield coolant	—	He gas
Heat load, LHe region, not incl. leads	(W)	265
LHe for lead cooling at design current	(ℓ/hr)	87
Power supply and discharge data:		
Number of current leads <sup>a</sup>	—	4
Rated voltage, power supply <sup>a</sup>	(V)	20
Minimum charge time	(hrs)	6
Resistance, emergency dump resistor <sup>a</sup>	(Ω)	0.05
Emergency discharge time constant	(min)	9.5
Maximum discharge voltage, terminal	(V)	725
Materials of construction:		
Winding substructure	—	Al 5083
Insulation	—	G-10
Superstructure	—	Al 6061
Liquid helium vessel	—	Al 5083
Thermal shield	—	Al 5083
Vacuum vessel	—	Al 5083
Design stresses:		
Conductor (compression)	(MPa)	79
Winding substructure (tension)	(MPa)	97
Insulation (compression)	(MPa)	97
Superstructure (bending)	(MPa)	179
Pressure rating		
Liquid helium vessel		
Normal operating	(atm)	1.3

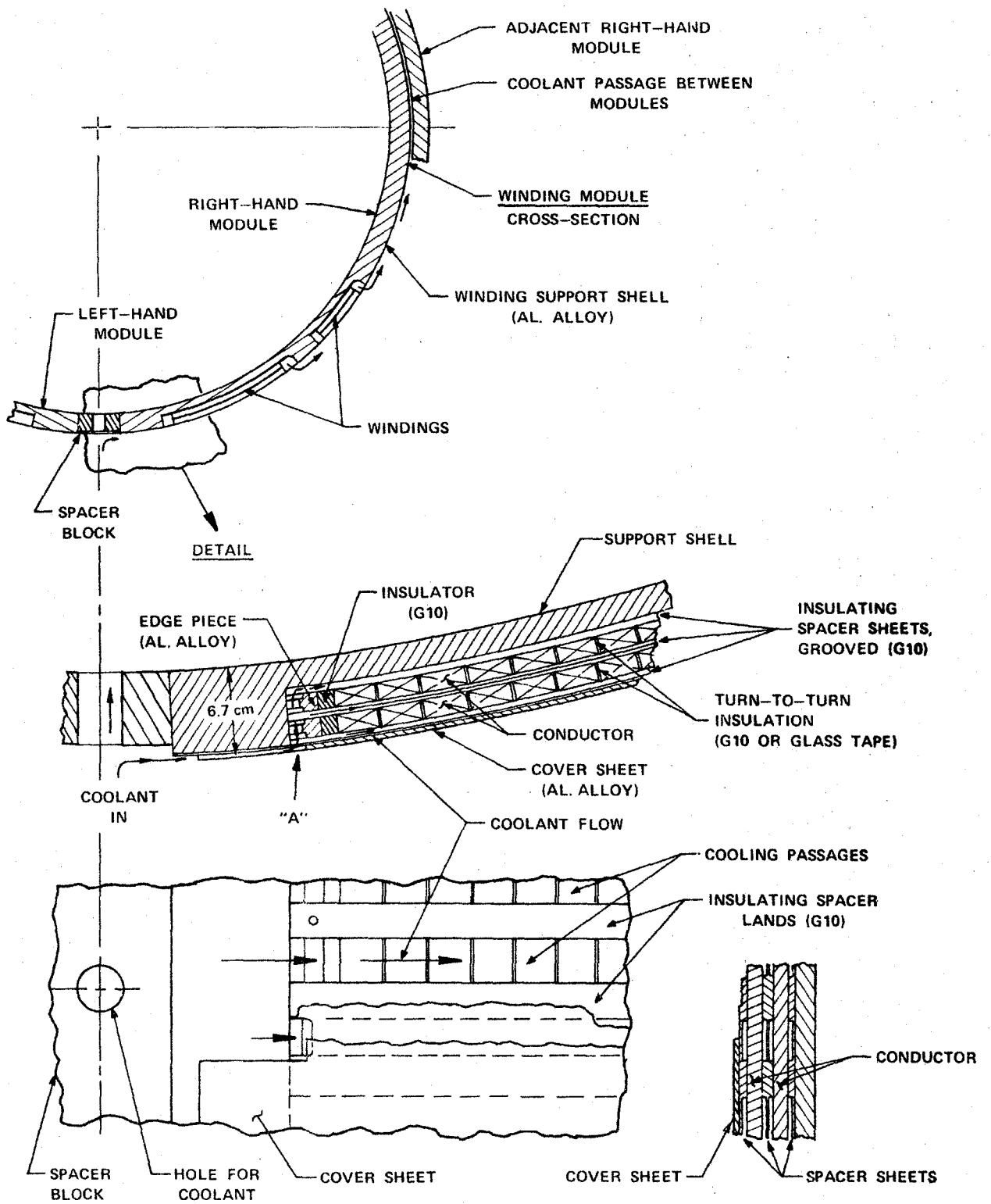
<sup>a</sup> Two parallel circuits, one for each half. Two power supply and discharge packages.

4.2.3A Curve of On-Axis Magnetic Field vs Distance Along Axis for AVCO  
 Baseload Magnet Design BL6-P1 (Circular Saddle)

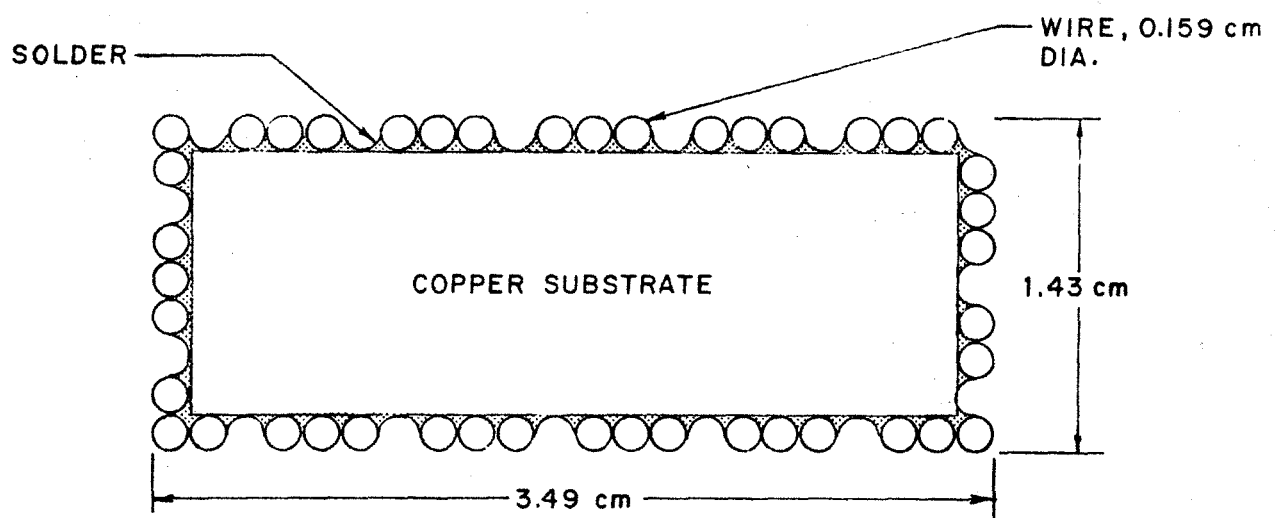




4.2.3B Diagram of Winding Configuration, AVCO Baseload Magnet Design BL6-PI (Circular Saddle). One half of Winding is Shown

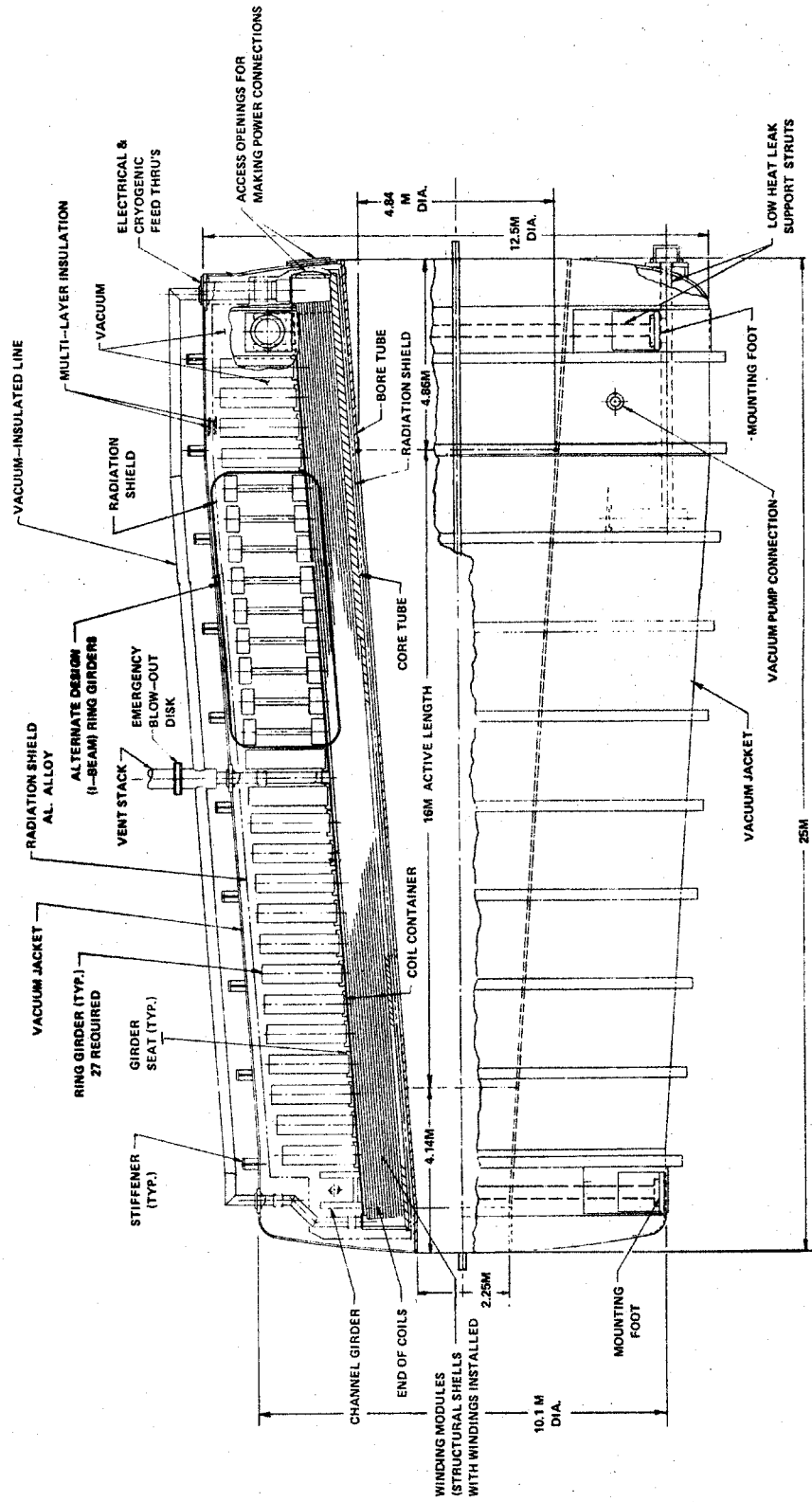


4.2.3C Detail of Winding (Module Cross Section) AVCO Baseload Circular Saddle Magnet Design BL6-P1



4.2.3D Cross Section of Rectangular Cable Type Conductor for AVCO Baseload Circular Saddle Magnet Design BL6-P1

4.2.3E Assembly Layout (Cutaway) AVCO 6 T Baseload Circular Saddle MHD Magnet Design BL6-P1



currently available would be used to cool down the magnet and maintain it at operating temperature.

A power supply subsystem is proposed as shown in Figure 4.2.3F. Two rectifier power supply units and two resistor and switch systems are provided, one set for each half of the winding. Four vapor-cooled power leads are required, two for each winding half. It is planned that a fault detecting system will be installed in the winding to operate the switches automatically (or after a warning and short time delay) and dump the energy from both winding halves into the emergency resistors which are connected across the terminals of each winding half.

In the manufacturing plan proposed by AVCO, the conductor will be shipped fully assembled from the superconductor manufacturer, in continuous lengths of up to 1830 m. It will be delivered to the (off-site) magnet fabricating facility where it will be wound into grooves in structural shells to form winding and substructure modules which will then be shipped to the plant site. The core tube, other coil container parts, main structural components and Dewar parts will be prefabricated at manufacturing facilities and shipped to the plant site.

At the plant site, assembly of the magnet will start with the core tube mounted on a special assembly fixture which is arranged to provide for rotation of the core tube and components assembled on it. The winding modules will be assembled around the core tube, one pair at a time, and bolted in place. After electrical connections and internal piping are installed, outer shells and end covers will be installed and seal-welded to complete the helium containment vessel. Ring girders will then be bolted around the containment vessel, support struts installed and the thermal radiation shield and room temperature Dewar parts, including warm bore tube, assembled to complete the enclosure of the magnet.

The estimated costs of the first unit and of one unit following the first lot of five prepared by AVCO are listed in Table 4.2.3-II. The estimated total cost of components for the first unit, not including coil winding and module assembly, is  $\$34 \times 10^6$ . To arrive at an estimated cost for the complete first magnet system, MIT added its own estimates of  $\$13 \times 10^6$  for winding and assembly labor and  $\$14 \times 10^6$  for other costs, including tooling, accessory subsystems, project management and design and analysis, for a total installed cost of  $\$61 \times 10^6$ . This estimate is shown in Table 4.2.3-III.

Estimated schedules for design, construction and installation were not included in the AVCO program results.

A list of twelve recommendations for future research, development and manufacturing were compiled by AVCO at the end of the program. Included in these recommendations were the proving of high current conductors and conductor splices, further research on the effects of motion and frictional heating on conductor stability, analyses and experiments to evaluate quench protection provisions, design and manufacture of winding models to develop and verify winding construction technology, and refinement of field, force and stress computation techniques.

More complete information on the AVCO baseload magnet design BL6-P1 is contained in Reference 58.

#### 4.2.4 Baseload MHD Magnet Alternative Design by AVCO, Rectangular Saddle, BL6-P2

The 6 T magnet design described below, designated BL6-P2, is an alternative to the design BL6-P1, described in Section 4.2.3. It is based on the same design criteria, Table 4.2.2-I, and was developed in parallel with the principal design. The major difference is that the alternative design incorporates the rectangular saddle winding configuration (with 90° turn-ups at ends), whereas the principal design incorporates the circular saddle winding configuration. MEA and IGC, under subcontract to AVCO, assisted in the preparation of this design. The alternative design was developed with the intent that when completed, it would be compared in detail with the principal design and a selection would be made. At the start of the AVCO program, a preliminary review

Table 4.2.3-II Sheet 1 of 2

Summary of Estimated Component Costs and Assembly Labor  
6 T Baseload Circular-Saddle Magnet Design BL6-P1 (AVCO)

<u>Components</u>	<u>Estimated Weight</u> 10 <sup>3</sup> kg	<u>First Unit</u>	<u>First Unit</u>	<u>Subsequent Units<sup>a</sup></u>
		<u>Cost/kg</u> \$	<u>Total Cost</u> \$ × 10 <sup>3</sup>	<u>Total Cost</u> \$ × 10 <sup>3</sup>
Conductor: Region A	123 <sup>b</sup>	22.60	2780	
Region B	211 <sup>b</sup>	17.90	3777	
Region C	143 <sup>b</sup>	14.30	2045	
Total Conductor	477 <sup>b</sup>		8602	7895
Insulating spacers, etc	30	10.00	300	
Core tube	133	8.40	1117	
Winding support shells	526	9.45	4971	
Outer shells	126	8.40	1058	
End plates	6	8.40	50	
Channel girders	60	8.40	50	
Main girders	1900	7.70	14630	
Total, cold structure			22630	19236
Radiation shield	40	8.40	336	
Thermal insulation and miscellaneous	4	35.00	140	
Vacuum jacket	183	8.60	1574	
Support posts, etc	6	33.00	198	
Leads, piping, etc	—		100	
Total radiation shield, vacuum jacket, etc			2348	2113
<b>Total components (f.o.b. factory)</b>			33580	29244
Miscellaneous materials and supplies (on site)			100	100
<b>Total component and material cost</b>			33680	29344

<sup>a</sup> Unit cost, lot of five

<sup>b</sup> Includes 5% margin over net calculated weights



Table 4.2.3-II Sheet 2 of 2

<u>Labor</u>	<u>Man Weeks</u>	<u>Man Weeks</u>
Coil winding and module assembly (factory)		
Assembly of magnet on plant site	4700	3700

Notes:

(1) Special tools and fixtures, factory and on-site, rough estimate 15% to 25% of total cost of first unit, or \$6,000,000 to \$10,000,000

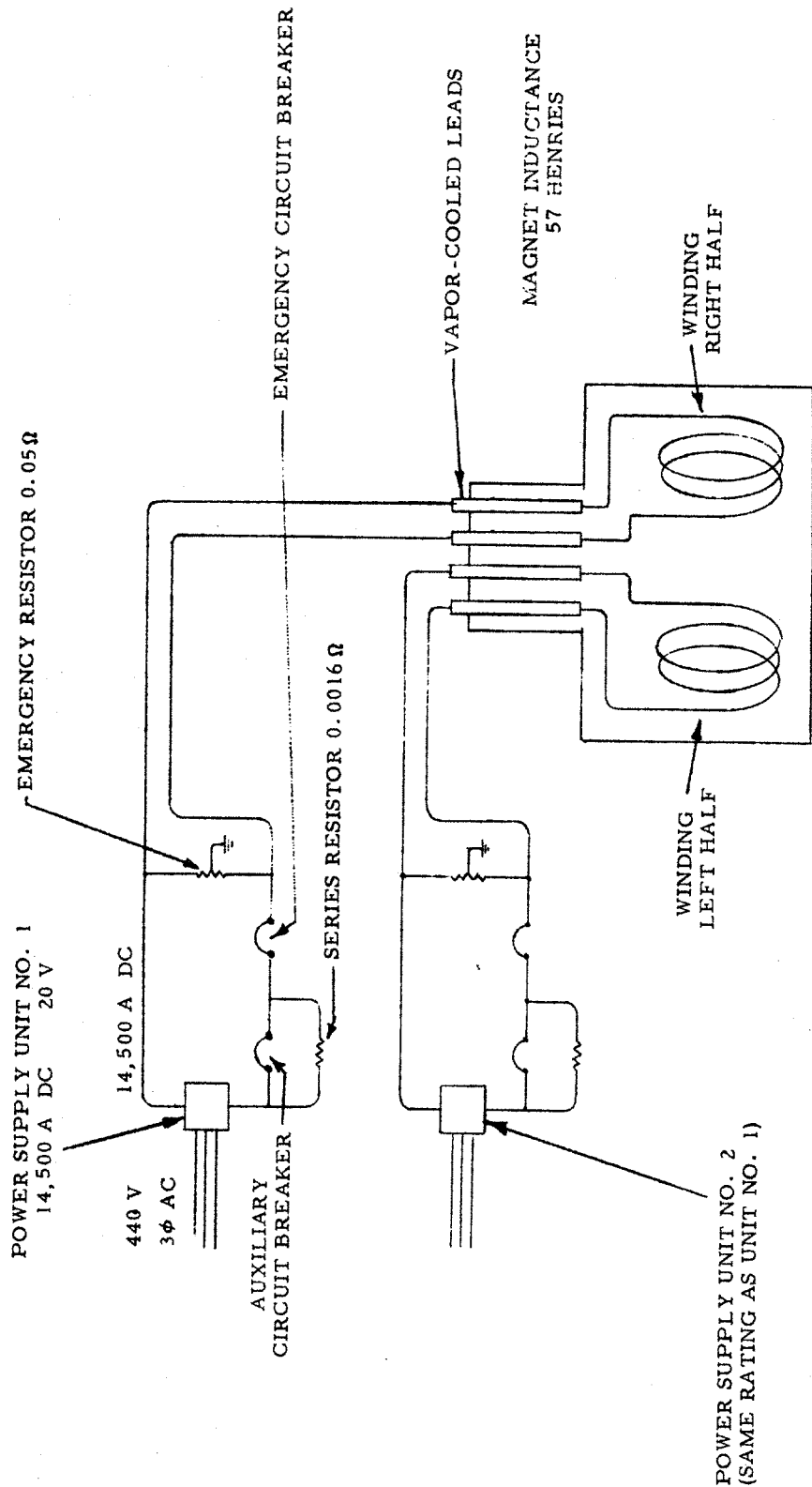
(2) The above cost estimate does not include development, design engineering, tool design, costs related to buildings, foundations, etc., transportation costs, refrigeration and power supply system, shakedown test and similar items

(3) Costs and labor for "Subsequent Units" are based on the assumption that at least five similar baseload size magnets have been built.

**Table 4.2.3-III**  
**Summary of Estimated Costs of Installed Magnet System,**  
**First Unit 6 T Baseload Circular Saddle Magnet Design BL6-P1 (AVCO)**

	<b>\$ × 10<sup>3</sup> (1977)</b>
Total, components and materials	33,680
Coil winding module assembly, etc. (factory)	
8000 man weeks at \$1000/wk <sup>a</sup>	8000
Magnet system assembly & installation (on site)	
4700 man weeks at \$1085/wk <sup>a</sup>	5100
Supervision, QA, etc.	Incl. in above
Tooling, facility modifications & other	7000 <sup>a</sup>
Accessory subsystems	3800 <sup>a</sup>
Design, analysis, engineering	<u>3300<sup>a</sup></u>
<b>Total</b>	<b>60,880</b>

<sup>a</sup> MIT estimate



4.2.3F Block Diagram, Electrical System AVCO 6 T Baseload Circular Saddle Magnet Design BL6-PI

of configurations led to the conclusion that the circular saddle configuration was more efficient in conductor use than other configurations, but that the rectangular configuration, while requiring somewhat more conductor, showed promise of being easier to manufacture. Since the trade-offs could not be evaluated without more detailed design information, it was decided to develop both designs in parallel.

At the end of the program, AVCO concluded that, contrary to early expectations, the alternative reference design did not appear to be easier to build or less expensive overall than the principal design. Structural support of the windings in the 90° end-turn portion of the magnet was difficult, and the solution which was developed involved rather elaborate superstructure which increased overall magnet weight and added to on-site assembly labor cost. The liquid helium containment vessel also was more elaborate and heavier than that in the principal design.

The baseload magnet alternative design, BL6-P2, incorporates not only a rectangular saddle coil, but also a square-cross-section warm bore. The dimensions of the bore are such that the cross-sectional areas are the same as those of the circular-cross-section bore specified in the design criteria, Table 4.2.2-1.

The alternative design uses the same type of conductor as the principal design (Section 2.2.3). It also incorporates a modular winding design in which conductor bundles are installed in grooves in flat plate substructure members made of aluminum alloy, turned up at the ends to form saddle-shaped modules which are then stacked to form the two winding halves. The sides of these modules diverge from the axis going toward the channel exit end and spacers between groups of modules become thicker toward the exit end, thus producing the desired tapered field profile. There are sixteen winding and substructure modules in each winding half, with four layers of conductor per module.

Outward acting magnetic forces in the "straight" portion of the magnet are resisted by rectangular frames consisting of beams and tie-plates, both of aluminum alloy. The plates and beams are fastened by mechanical joints at the corners to facilitate assembly and disassembly. Cross ties with mechanical joints connect the end turns of the coil halves to resist magnetic repulsion forces between crossovers. Yoke structures are provided at the coil ends to support the ends against longitudinal (outward) forces and carry this load into the substructure plates of the "straight" section. The overall structural design uses substructure plates as main structural members wherever possible.

The liquid helium containment vessel, made of aluminum alloy, fits closely around the winding modules and superstructure. The walls of the vessel are flat plates which are button-welded to the magnet winding structure to provide stiffness.

The Dewar includes an aluminum alloy thermal radiation shield, a rectangular-cross-section warm bore tube of aluminum alloy and a rectangular outer vacuum shell also of aluminum alloy, incorporating deep-section stiffeners to support the shell walls against atmospheric pressure. The cold mass of the magnet is carried on four low-heat-leak columns which transmit the load to the foundation.

Manufacturing, assembly and cost considerations influenced the design strongly. The use of flat plates for most of the substructure and superstructure was in the interest of ease of fabrication. The overall manufacturing plan was similar to that for the circular-saddle (principal) design, with modules wound at a manufacturing facility and then shipped to the site by special large-load transportation means. The largest modules to be shipped measure 24 m long by 9.3 m high by 5.8 m wide.

The characteristics of the AVCO baseload alternative design (BL6-P2) rectangular saddle magnet are listed in Table 4.2.4-1. The calculated axial field profile is shown in Figure 4.2.4A, the coil configuration in Figure 4.2.4B, a typical winding cross section in Figure 4.2.4C and the magnet assembly in Figure 4.2.4D.

Cryogenic and power supply systems are similar to those described in Section 4.2.3 for the principal design, except that the alternative design (rectangular saddle) magnet has each winding half divided into two

Table 4.2.4-I Sheet 1 of 3

Design Characteristics  
Baseload MHD Magnet Design BL6-P2  
AVCO Everett Research Laboratory, Inc.

Date of design		1977
MHD power train data		
MHD power output (estimated)	(MWe)	600
Channel inlet dimensions	(m)	1.35×1.35
Channel exit dimensions	(m)	2.9×2.9
Magnet data		
Magnet type	—	90° rect. sad.
Warm bore liner?	—	No
Magnetic field:		
Peak on-axis field	(T)	6.0
Active field length <sup>a</sup>	(m)	16(17.7)
Field at start of active length <sup>a</sup>	(T)	6.0(4.8)
Field at end of active length	(T)	3.3
Field uniformity at end of active length <sup>b</sup>	(%)	+4.1 —4.4
Area ratio, plasma c.s./warm bore, end of active length	—	0.46
Peak field in winding	(T)	8+
Dimensions:		
Aperture, warm bore inlet <sup>c</sup>	(m)	1.99×1.99
Aperture, start of active length <sup>c</sup>	(m)	2.94×2.94
Aperture, end of active length <sup>c</sup>	(m)	4.42×4.42
Aperture, warm bore exit <sup>c</sup>	(m)	5.30×5.30
Aperture area, start of active length <sup>c</sup>	(m <sup>2</sup> )	8.64
Aperture area, end of active length <sup>c</sup>	(m <sup>2</sup> )	19.5
Distance, bore inlet to start of active length	(m)	4.75
Vacuum vessel overall length	(m)	26.4
Vacuum vessel outside dims.	(m)	10.7×13.0
Warm bore volume, active <sup>c</sup>	(m <sup>3</sup> )	191
MVU <sup>d</sup>	—	0.44

<sup>a</sup> Values in parentheses are adjusted values based on definition of active length as starting at 80% of peak field. Field profile is unchanged. After 1977, design characteristics for most large MHD magnet designs were consistent with this definition.

<sup>b</sup> Field uniformity is + and - variation from on-axis field, central 50% of warm bore cross section

<sup>c</sup> Dimensions inside warm bore, without liner

<sup>d</sup> Ratio of channel volume to warm bore volume

Table 4.2.4-I Sheet 2 of 3

<b>Winding characteristics:</b>		
Build, winding cross section	(m)	0.87
Number of winding modules (or layers) per half	—	16
Design current, I	(kA)	14.5
Winding current density, average, $J\lambda^a$	( $10^7$ A/cm <sup>2</sup> )	1.14
Packing factor, $\lambda^a$	—	0.35
Conductor current density, $J^a$	( $10^7$ A/cm <sup>2</sup> )	3.3
Total number of turns, $N^b$	—	2820
Total length of conductor	(km)	350
Ampere turns, NI	( $10^6$ A)	40.6
Ampere meters	( $10^8$ Am)	26.0
Inductance	(H)	78
Stored energy	(MJ)	8150
Conductor type	—	Built-up
Conductor materials	—	NbTi-Cu
Conductor dimensions <sup>a</sup>	(cm)	$1.74 \times 1.43$
Copper-to-superconductor ratio <sup>a</sup>	—	15
LHe to conductor ratio (vol.) <sup>a</sup>	—	0.4
Heat flux <sup>a</sup>	(W/cm <sup>2</sup> )	0.41
<b>Weights:</b>		
Conductor	(tonnes)	678
Insulation	(tonnes)	40
Substructure	(tonnes)	incl. in superstr.
Superstructure	(tonnes)	2220
Liquid He vessel	(tonnes)	170
Total cold mass	(tonnes)	3108
Thermal shield, cold mass supports, etc	(tonnes)	76
Vacuum vessel	(tonnes)	376
Miscellaneous	(tonnes)	0
Total magnet weight	(tonnes)	3580

<sup>a</sup> Where graded winding is incorporated, values listed are for high field region of winding.

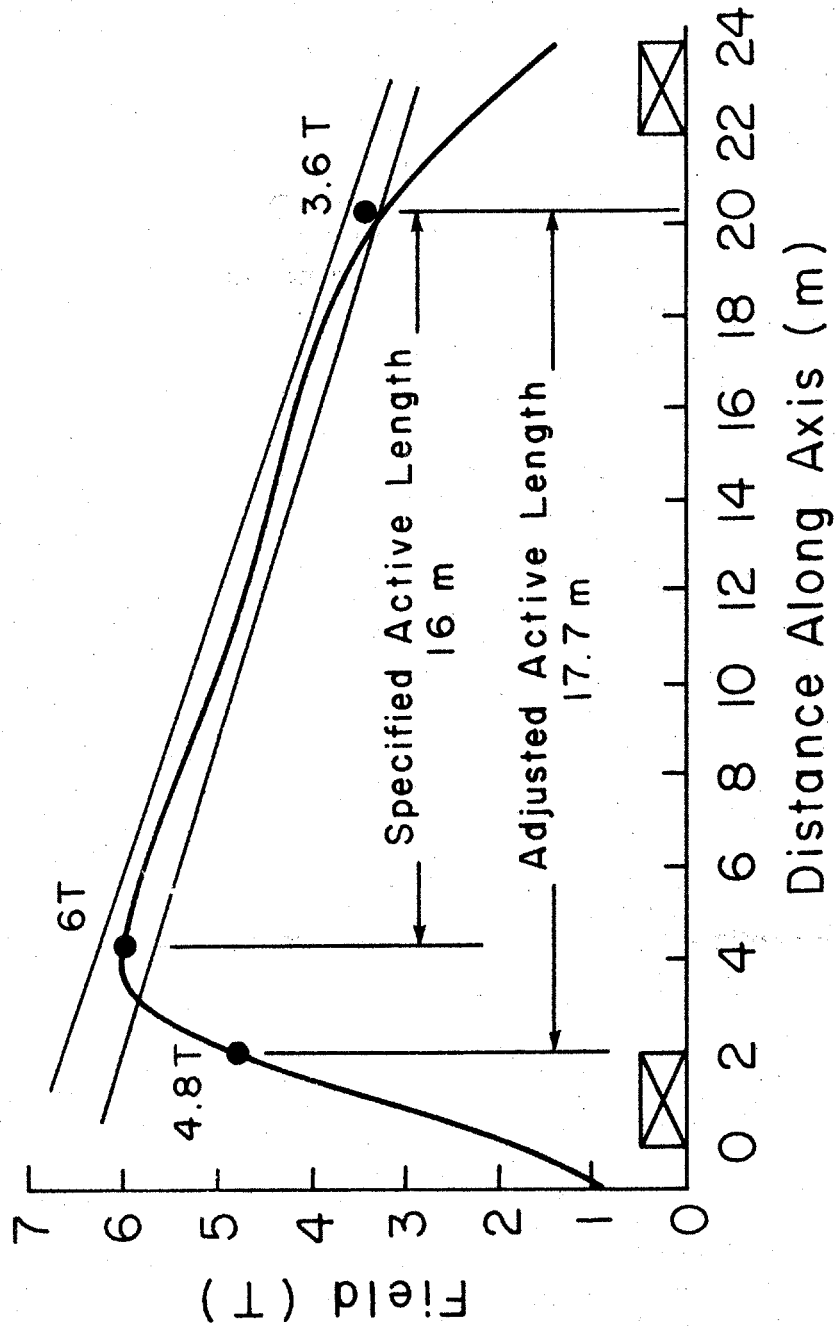
<sup>b</sup> Two conductors wound in parallel carry the total of 14.5 kA. One turn consists of 2 conductors.

Table 4.2.4-I Sheet 3 of 3

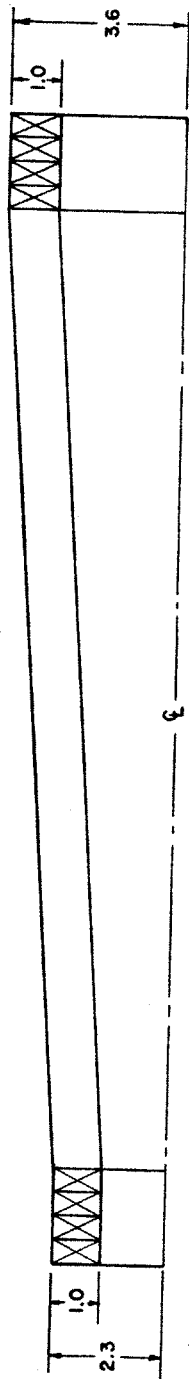
<b>Cryogenic data:</b>		
Operating temperature at winding	(K)	4.5
Operating temperature, thermal shield	(K)	80
Coolant, thermal shield	—	He gas
Heat load, LHe region, not incl. leads	(W)	288
LHe for lead cooling at design current	( $\ell$ /hr)	87
<b>Power supply and discharge data:</b>		
Number of current leads	—	8 <sup>a</sup>
Rated voltage, power supply	(V)	20 <sup>a</sup>
Minimum charge time	(hrs)	8.2
Resistance, emergency dump resistor	( $\Omega$ )	0.1 <sup>a</sup>
Emergency discharge time constant	(min)	4
Maximum discharge voltage, terminal	(V)	725 <sup>a</sup>
<b>Materials of construction:</b>		
Winding substructure	—	Al 5083
Insulation	—	G-10
Superstructure	—	Al 5083
Liquid helium vessel	—	Al 5083
Thermal shield	—	Al 5083
Vacuum vessel	—	Al 5083
<b>Design stresses:</b>		
Conductor	(MPa)	79 compr.
Winding substructure	(MPa)	179 tens.
Insulation (compressive)	(MPa)	79
Superstructure	(MPa)	179 bend.
<b>Pressure rating</b>		
Liquid helium vessel		
Normal operating	(atm)	1.3

<sup>a</sup> Four parallel circuits, two for each half. Four power supply and discharge packages.

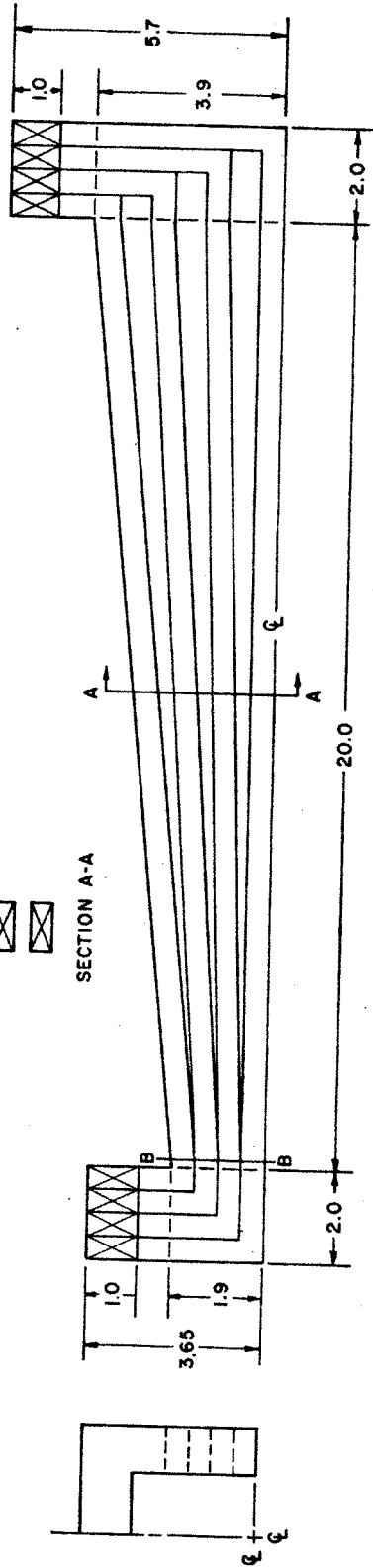
4.2.4A Curve of On-Axis Magnetic Field vs Distance Along Axis for AVCO  
 Baseload Magnct Design BL6-P2 (Rectangular Saddle)



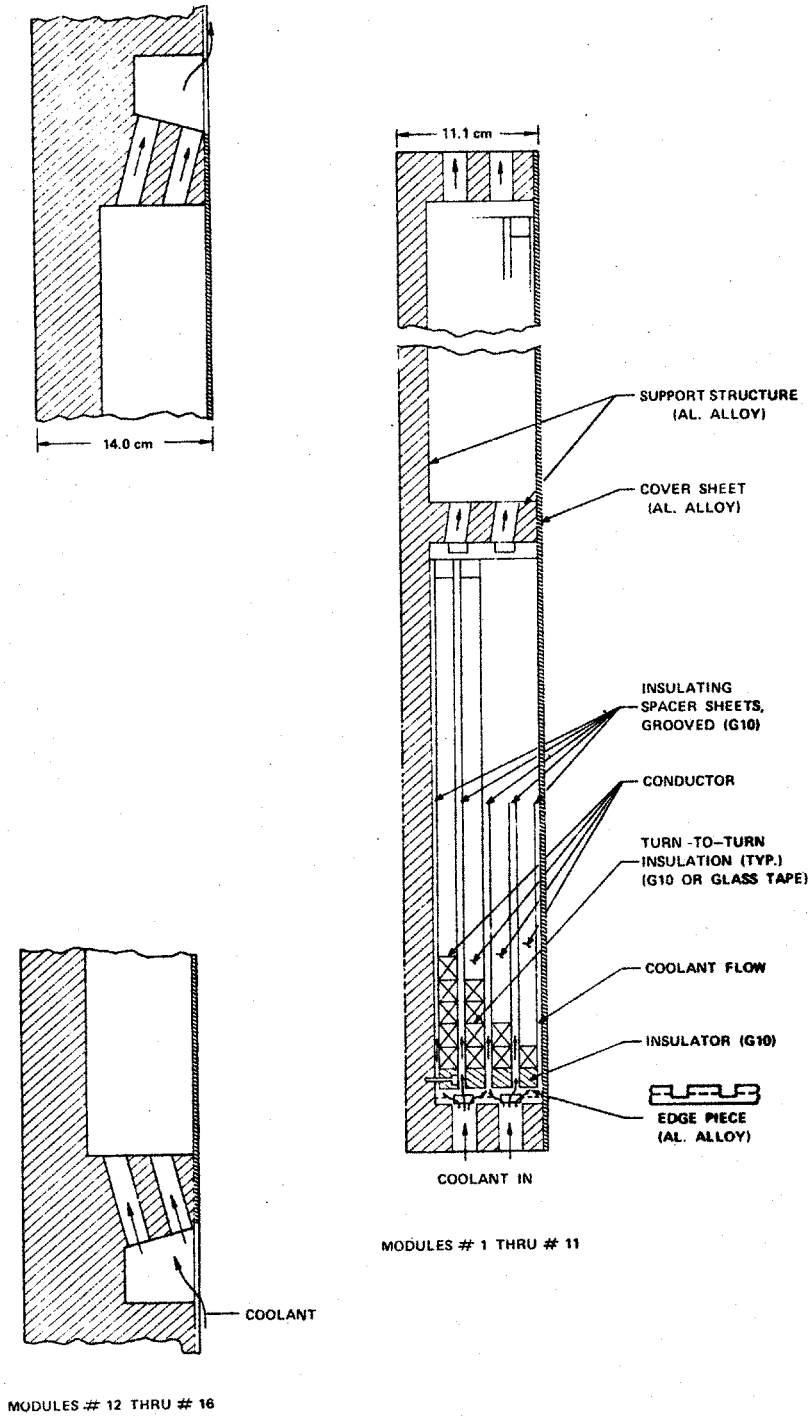




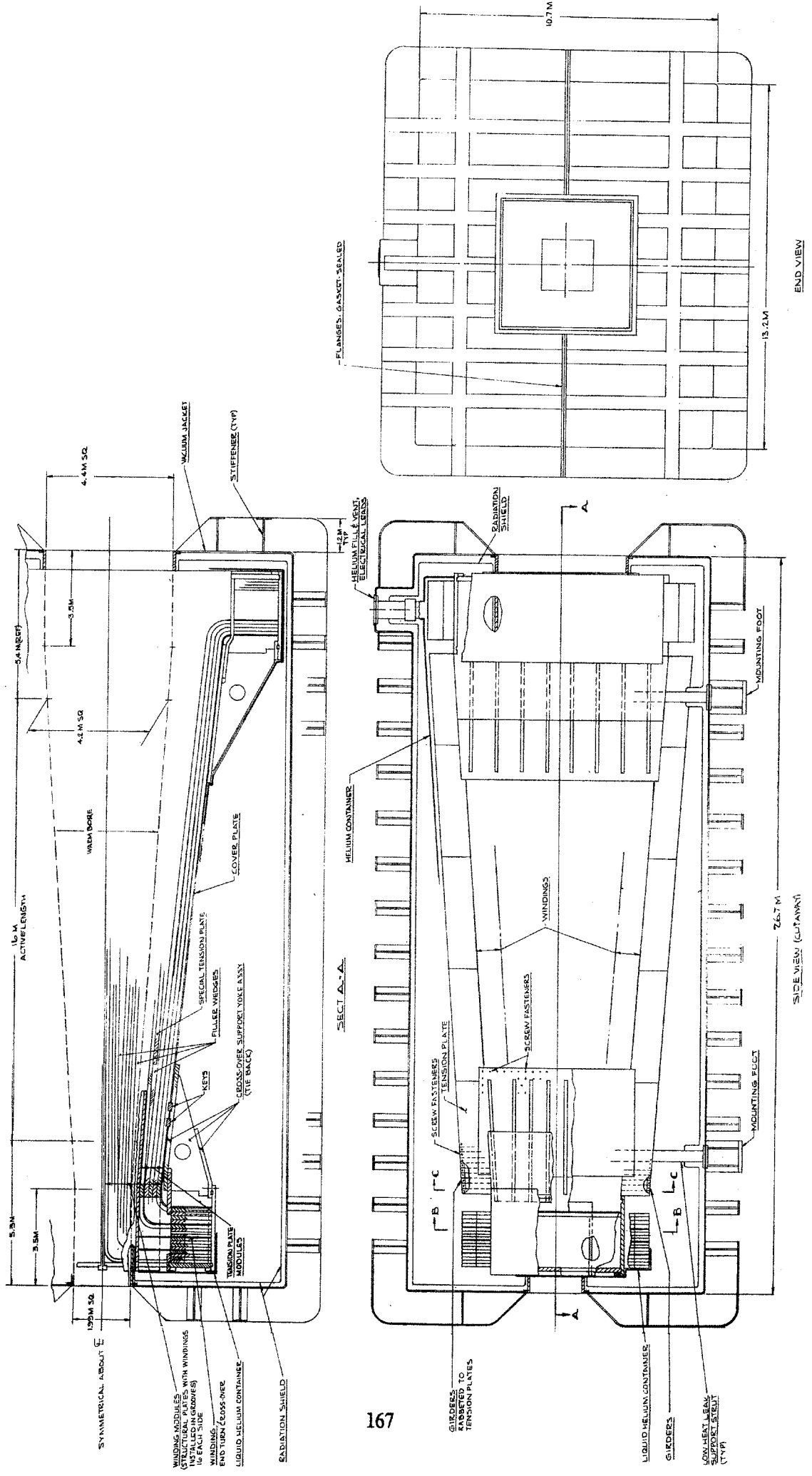
DIMENSIONS IN METERS



4.2.4B Diagram of Winding Configuration, AVCO Baseload Magnet Design BL6-P2 (Rectangular Saddle). One Quadrant Only is Shown



4.2.4C Detail of Winding (Module Cross Section) AVCO Baseload Rectangular Saddle Magnet Design BL6-P1



4.2.4D Assembly Layout (Cutaway) AVCO 6 T Baseload Rectangular Saddle MHD Magnet, Design BL6-P2

sections with separate vapor-cooled leads for each (8 leads total) and four rectifier power supply units and discharge resistor and switch systems.

Specific manufacturing plans and cost estimates were not prepared for the alternative design baseload magnet.

More complete design information on the alternative magnet, BL6-P2, is contained in Reference 58.

#### 4.2.5 Commercial-Scale MHD Magnet Design by GD, Modified Circular Saddle, CASK

The commercial-scale 6 T MHD magnet conceptual design designated CASK, described in this section, was developed by GD in 1979 under subcontract to MIT.

The CASK magnet incorporates an innovative approach to structural design which was conceived in the Winding Model Magnet (WMM) program carried out by GD in 1978 with assistance from MEA and Supercon (See Section 4.1.8). The overall winding configuration of CASK, i.e., circular saddle coil supported in conical structural shells, was derived from the AVCO BL6-P1 design (Section 4.2.3), but the CASK design is distinctly different in conductor configuration and in structural design. The CASK conductor is of the separated-substrate type described in Section 4.1.5; it is much larger and has a much higher operating current than the conductor used in BL6-P1 (50 kA vs 14.5 kA). The CASK substructure, a major innovation, involves the division of the conical substructure into a number of independently manufactured axial staves. These staves are nested together to form the shells which contain the distributed windings. Minimum welding of the winding support shell is required at the assembly site. Surrounding the assembly of the staves containing the coils are the superstructure hoops. Thus, this concept was designated "CASK" because of its similarity to barrel construction. Fundamentally, the staves (substructure) are designed to contain the  $276 \times 10^6$  newton ( $62 \times 10^6$  pounds) axial forces and tangential magnetic forces. The hoops (superstructure) are designed to contain 31 MPa (4500 psi) radial pressures. All components are thus reduced to manageable sizes that may be prefabricated at a central factory site and shipped to the commercial power plant site.

The objective of the GD 1979 program was to develop a conceptual design of a readily producible superconducting MHD magnet system of commercial demonstration plant size, embodying the CASK concept. It was planned that this design would be evaluated and compared with earlier baseload magnet reference designs and also with designs to be developed in the future, as a part of the overall program at MIT to implement a configuration selection and design freeze by the mid-1980's.

The design criteria established by MIT for commercial-scale (commercial demonstration plant "CDP") magnets are listed in Table 4.2.5-I. These criteria were used as a basis for the CASK conceptual design at GD and also for two in-house conceptual designs started at MIT in 1979 (see Sections 4.2.6 and 4.2.7). It will be noted that the CDP magnet requirements as listed in Table 4.2.5-I are similar to the baseload magnet requirements listed in Table 4.2.2-I (Section 4.2.2) with the major differences that the active length is shorter for the CDP magnet and bore divergence is less.

The CASK magnet conceptual design, with its modified circular saddle type winding and circular-cross-section warm bore, is shown in cutaway assembly drawing, Figure 4.2.5A. Principal dimensions are shown in Figure 4.2.5B. Design characteristics are listed in Table 4.2.5-II. The calculated field profile is shown in Figure 4.2.5C.

The design incorporates a 50 kA NbTi/copper conductor of the separated-substrate type, as shown in Figure 4.2.5D. A typical conductor corner piece is shown in Figure 4.2.5E. It is planned that the copper substrate sections, including corner pieces, will be prefabricated and grooved in the factory and then shipped to the plant site where they will be electron beam welded together and the inserts (composite superconductor)

Table 4.2.5-I

Design Criteria for a Commercial Demonstration Plant (CDP) MHD Magnet,  
Estimated MHD Power 250 MWe

Magnetic Field:

Peak on-axis field	(T)	6.0
Active Length	(m)	14.5
Field at start of active length	(m)	4.8
Field at end of active length	(m)	3.6

Warm Bore Dimensions:

Start of active length, diameter	(m)	2.48 <sup>a,b</sup>
End of active length, diameter	(m)	4.50 <sup>a</sup>

<sup>a</sup> The magnet warm bore is sized very conservatively for a 250 MWe channel. With careful channel packaging, the magnet should accommodate a 500 MWe channel.

<sup>b</sup> It is noted that in the GD CASK design, the actual warm bore diameter at start of active length is 3.28 m, see Fig. 4.2.5B. The diameter at bore inlet and for the first 1.55 m is 2.48 m.

Table 4.2.5-II Sheet 1 of 3

Design Characteristics  
Commercial-Scale MHD Magnet Design CASK  
General Dynamics - Convair Division

Date of design		1979
MHD power train data		
MHD power output (estimated)	(MWe)	250
Magnet data		
Magnet type	—	Mod. circ. sad.
Warm bore liner?	—	No
Magnetic field:		
Peak on-axis field	(T)	6.0
Active field length	(m)	14.5
Field at start of active length	(T)	4.8
Field at end of active length	(T)	3.6
Peak field in winding	(T)	7+
Dimensions:		
Aperture, warm bore inlet <sup>b</sup>	(m)	2.48 dia.
Aperture, start of active length <sup>b</sup>	(m)	3.28 dia.
Aperture, end of active length <sup>b</sup>	(m)	4.50 dia.
Aperture, warm bore exit <sup>b</sup>	(m)	5.03 dia.
Aperture area, start of active length <sup>b</sup>	(m <sup>2</sup> )	8.45
Aperture area, end of active length <sup>b</sup>	(m <sup>2</sup> )	15.9
Distance, bore inlet to start of active length	(m)	4.6
Warm bore length	(m)	23.6
Vacuum vessel overall length	(m)	23.6
Vacuum vessel O.D.	(m)	7.11
Warm bore volume, active <sup>b</sup>	(m <sup>3</sup> )	133

<sup>a</sup> Magnet bore sized very conservatively for 250 MWe channel. With careful channel packaging, magnet should accommodate 500 MWe channel.

<sup>b</sup> Dimensions inside warm bore, without liner

Table 4.2.5-II Sheet 2 of 3

## Winding characteristics:

Build, winding cross section	(m)	0.74
Winding volume, total	(m <sup>3</sup> )	101
Number of winding modules (or layers) per half	—	4
Design current, I	(kA)	50
Winding current density, average, $J\lambda^a$	(10 <sup>7</sup> A/cm <sup>2</sup> )	1.28
Packing factor, $\lambda^a$	—	0.58
Conductor current density, $J^a$	(10 <sup>7</sup> A/cm <sup>2</sup> )	2.2
Total number of turns, N	—	688
Total length of conductor	(km)	32.2
Ampere turns, NI	(10 <sup>6</sup> A)	34.4
Ampere meters	(10 <sup>8</sup> Am)	14.5
Inductance	(H)	5.04
Stored energy	(MJ)	6300
Conductor type	—	Built-up
Conductor materials	—	NbTi-Cu
Conductor dimensions <sup>a</sup>	(cm)	11.4 × 2.5
Copper-to-superconductor ratio <sup>a</sup>	—	34
LHe to conductor ratio (vol.) <sup>a</sup>	—	0.25
Heat flux <sup>a</sup>	(W/cm <sup>2</sup> )	0.27
<b>Weights:</b>		
Conductor	(tonnes)	552
Insulation	(tonnes)	55
Substructure	(tonnes)	664
Superstructure	(tonnes)	689
Liquid He vessel	(tonnes)	267
<b>Total cold mass</b>	(tonnes)	<b>2227</b>
Thermal shield, cold mass supports, etc	(tonnes)	36
Vacuum vessel	(tonnes)	343
Miscellaneous	(tonnes)	0
<b>Total magnet weight</b>	(tonnes)	<b>2644</b>

<sup>a</sup> Where graded winding is incorporated, values listed are for high field region of winding.

Table 4.2.5-II Sheet 3 of 3

## Cryogenic data:

Operating temperature at winding	(K)	4.5
Operating temperature, thermal shield	(K)	80
Coolant, thermal shield	—	LN <sub>2</sub>
Heat load, LHe region, not incl. leads	(W)	568
LHe for lead cooling at design current	(ℓ/hr)	140

## Materials of construction:

Winding substructure	—	SS 304 LN
Insulation	—	G-10 CR
Superstructure	—	SS 304 LN
Liquid helium vessel	—	SS 304 LN
Thermal shield	—	Al 6061
Vacuum vessel	—	SS 304 L

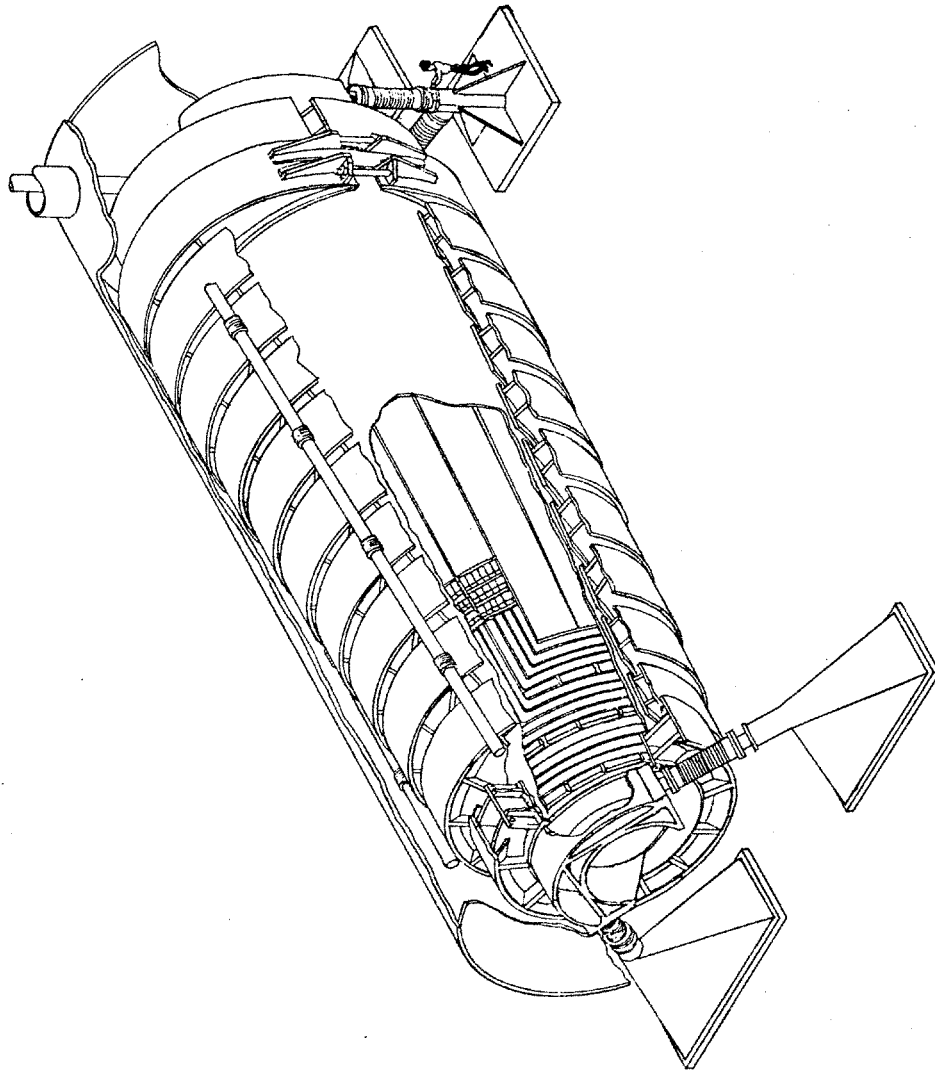
## Design stresses:

Conductor	(MPa)	130
Winding substructure (tension)	(MPa)	681
Insulation (compression)	(MPa)	94
Superstructure (tension)	(MPa)	552
Superstructure (bending)	(MPa)	448

## Pressure rating

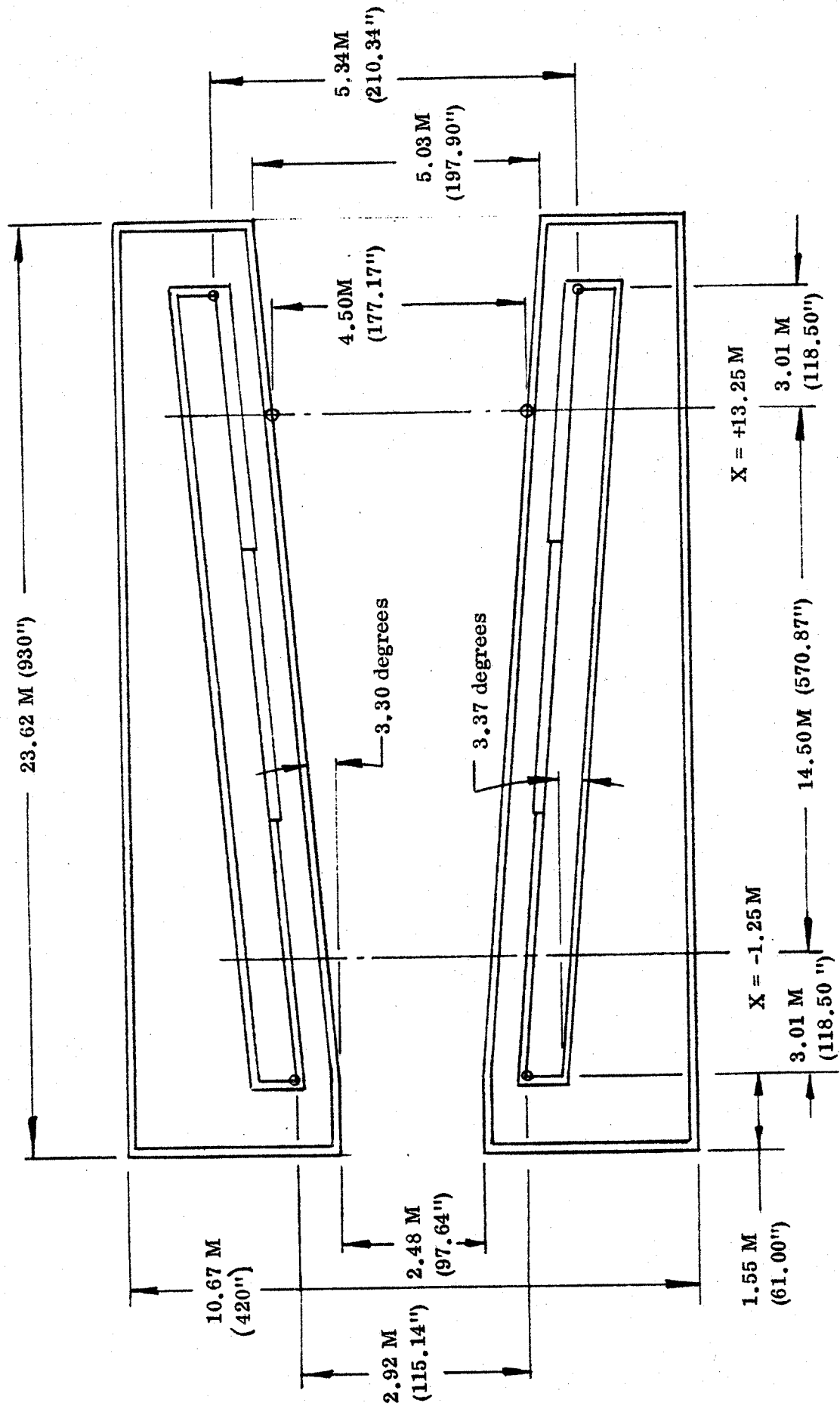
Liquid helium vessel		
Normal operating	(atm)	1.36
Maximum design	(atm)	6.8

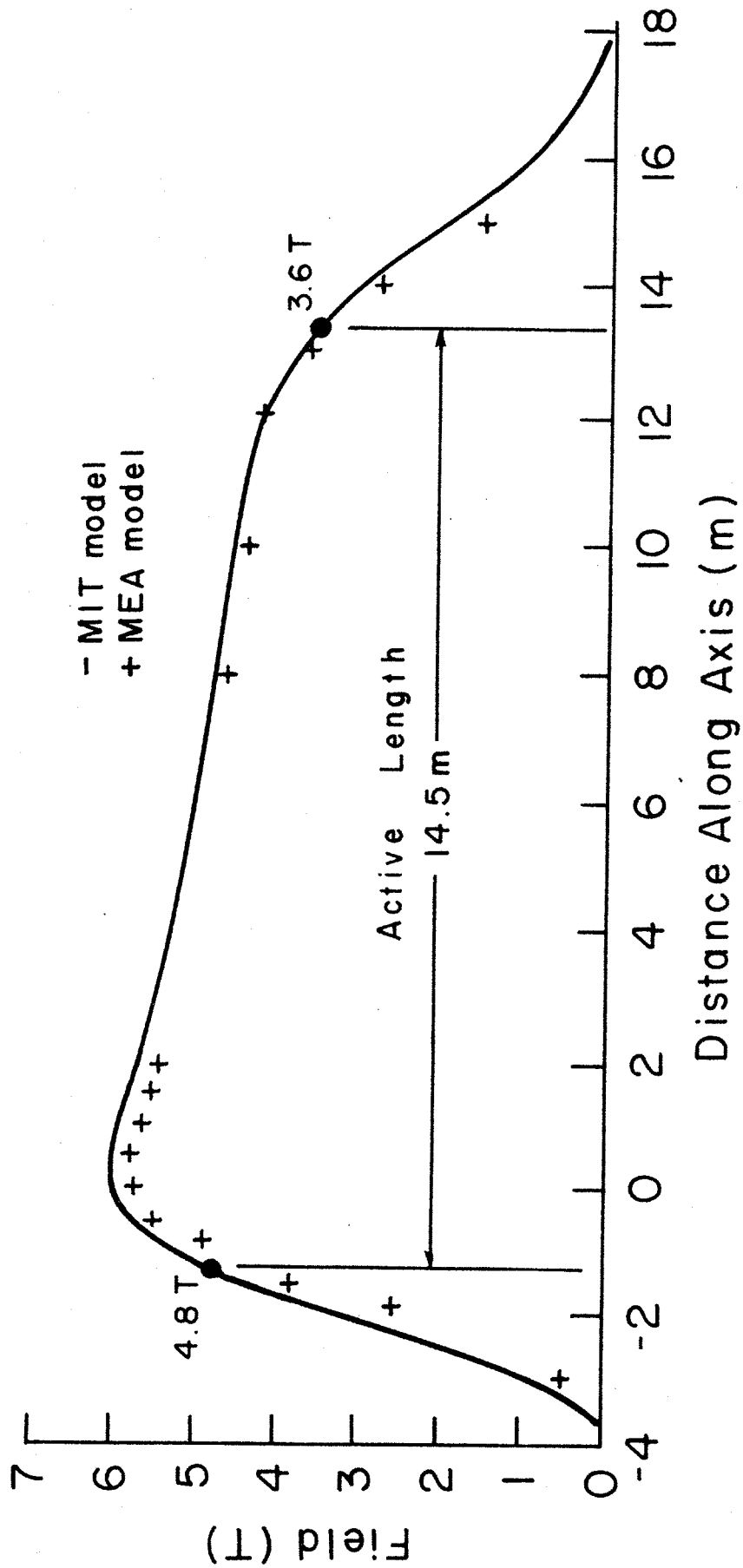




4.2.5A Cutaway View of CASK 6 T Baseload MHD Magnet Conceptual Design

4.2.5B Principal Dimensions of CASK Baseload MHD Magnet





4.2.5C Curve of On-Axis Magnetic Field vs Distance Along Axis for CASK  
 Baseload MHD Magnet Design

4.2.5D Cross Section of 50 kA Conductor for CASK Baseload MHD Magnet

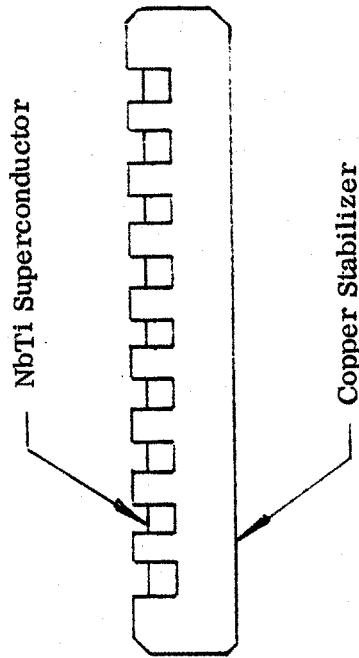
Substrate: Copper (CDA Alloy 101)  
 1/4 Hard, RRR @ (H=0)  $\geq 110$   
 Approximately 100 mm  $\times$  25 mm

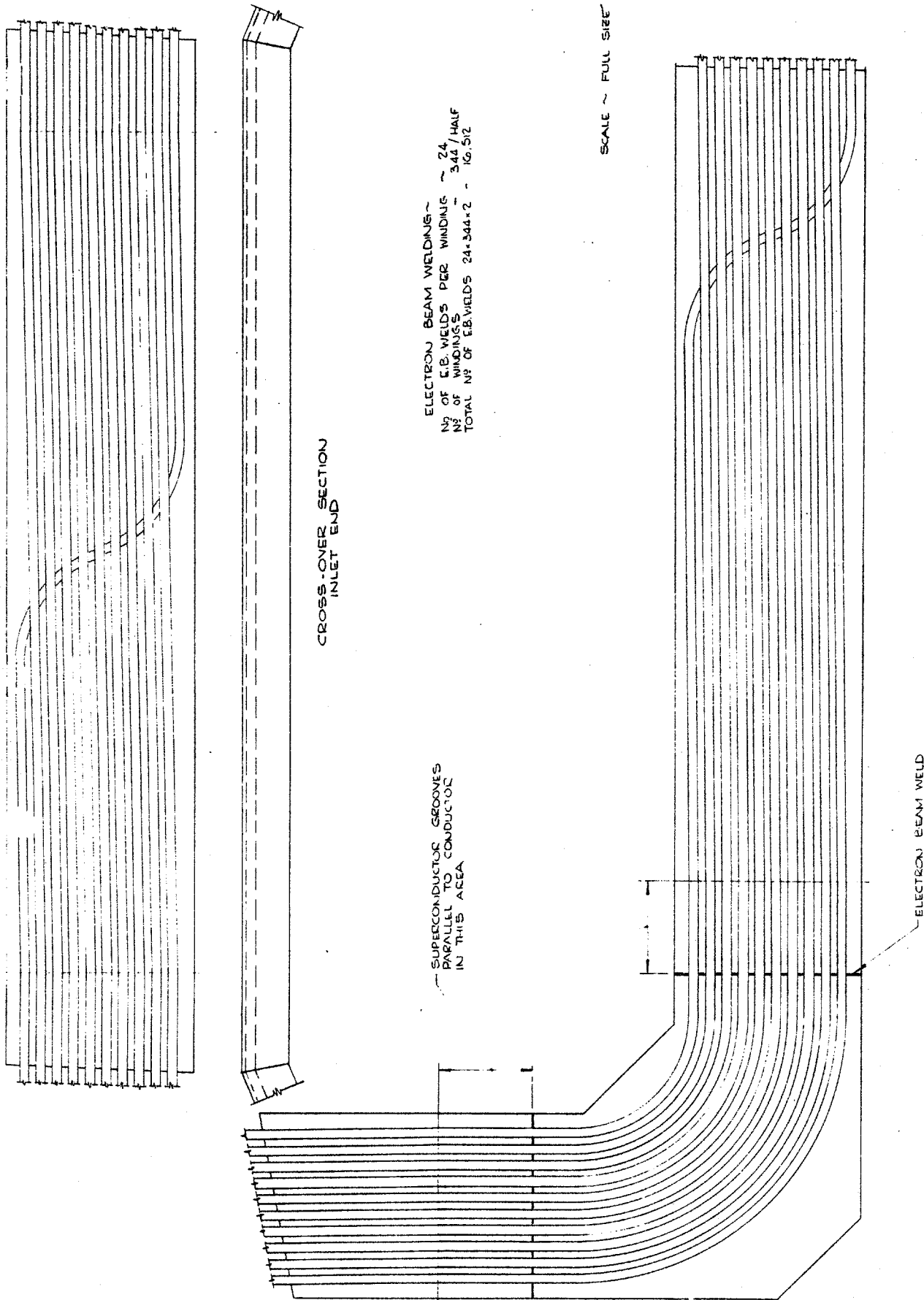
Insert: Composite; NbTi Filaments in Copper  
 (CDA Alloy 101), Matrix  
 5.13 mm Square  
 600 Filaments, 0.13 mm Diameter  
 100 mm Twist Pitch  
 Cu:SC = 2.0:1 (Insert)  
 = 32.0:1 (Overall)

$J_c$  (Filament) at 7T =  $6.0 \times 10^4$  A/cm<sup>2</sup>  
 $J_c$  (Insert) =  $2.0 \times 10^4$  A/cm<sup>2</sup>  
 $J_c$  (Conductor) =  $2.0 \times 10^3$  A/cm<sup>2</sup>

Up to 10 Inserts in Substrate

Conductor: Av. Xsectional Area 23 cm<sup>2</sup>  
 Av. Weight/Meter 20.5 kg/m  
 Substrate Length/Piece 10 m or greater  
 Insert Length/Piece 650 m





ELECTRON BEAM WELDING ~  
 NO OF E.B. WELDS PER WINDING ~ 24  
 NO OF WINDINGS ~ 344 / HALF  
 TOTAL NO OF E.B. WELDS 24 \* 344 \* 2 = 16,512

CROSS-OVER SECTION  
 INLET END

SUPERCONDUCTOR GROOVES  
 PARALLEL TO CONDUCTOR  
 IN THIS AREA

ELECTRON BEAM WELD

SCALE ~ FULL SIZE

soldered in place to make up the magnet winding. Winding bundles will be installed in the substructure with G-10CR insulation as shown in Figure 4.2.5F.

The overall coil configuration is shown in Figure 4.2.5G. The winding is modular, with four layers of coil bundles in each magnet half, as shown in Figure 4.2.5H, which shows a midplane cross section of winding, substructure and helium vessel perpendicular to the magnet axis.

The substructure in the midplane region consists of axial staves and corner blocks. Tangential magnetic forces from each coil bundle are transmitted via corner blocks to the staves. Radially outward magnetic forces from inner coil bundles are transmitted outward through staves and corner blocks to the outer helium vessel and thence to the main structural girders (ring girders) described below. With this arrangement, magnetic forces on each coil bundle are carried by structure and there is no accumulative loading on coil bundles.

In the end turn region of the windings, the substructure includes end blocks and shear plates which bridge across between staves as shown in Figure 4.2.5J. They resist the axial magnetic loading produced by the end turns and transmit it to the staves. The staves are continuous from end to end of the winding and thus form the main structural members holding the winding ends in place against axially outward forces.

The helium container consists of conical inner and outer shells (see Figure 4.2.5H), end plates welded to the shells at both ends and a service stack attached to the outer shell at the top, exit end.

All substructure and helium container parts are of 304LN stainless steel except the filler blocks at the horizontal centerline, which are of cast aluminum.

The main force containment structure (superstructure) consists of a set of twelve specially contoured 304LN stainless steel ring girders which are clamped tightly around the outer shell of the helium container. The central ten ring girders, which carry most of the magnetic loading, are constructed as shown in Figure 4.2.5K. Each consists of a pair of welded, crescent-shaped box beams which are clamped around the helium container with temporary studs and nuts and then welded together with link plates at the horizontal split line.

The Dewar consists of a liquid-nitrogen-cooled 6061-T6 aluminum alloy thermal radiation shield, multi-layer insulation blankets and a 304L stainless steel cylindrical outer vacuum vessel, conical warm bore tube and flat heads. The cold mass suspension system consists of low heat leak struts as shown in Figure 4.2.5A. The struts are made of stacks of fiberglass-epoxy disks.

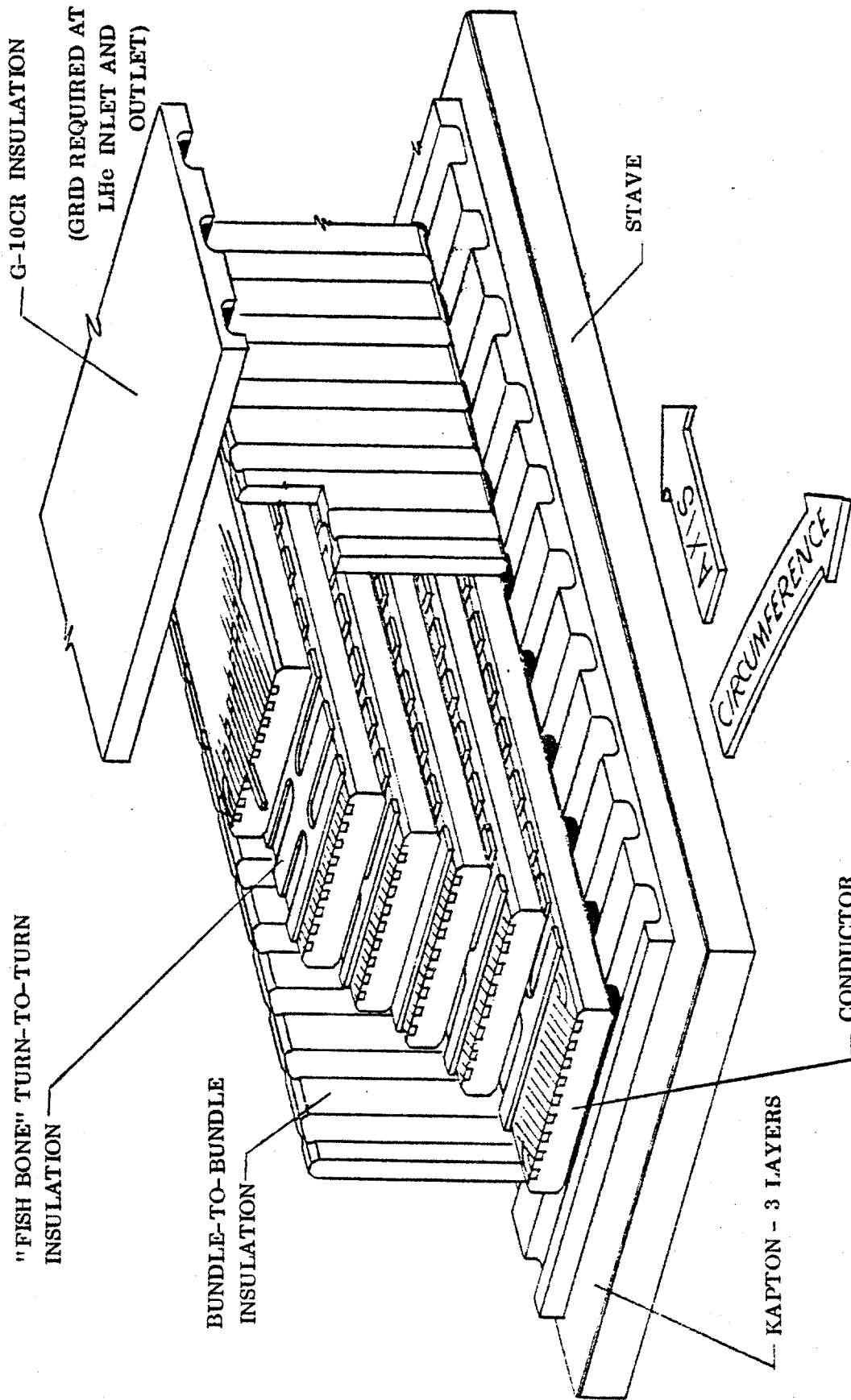
Accessory subsystems (cryogenic support system, power supply system, etc) were not included in the GD magnet design program.

Manufacturability received major emphasis in the GD program. Highlights of the manufacturing study included:

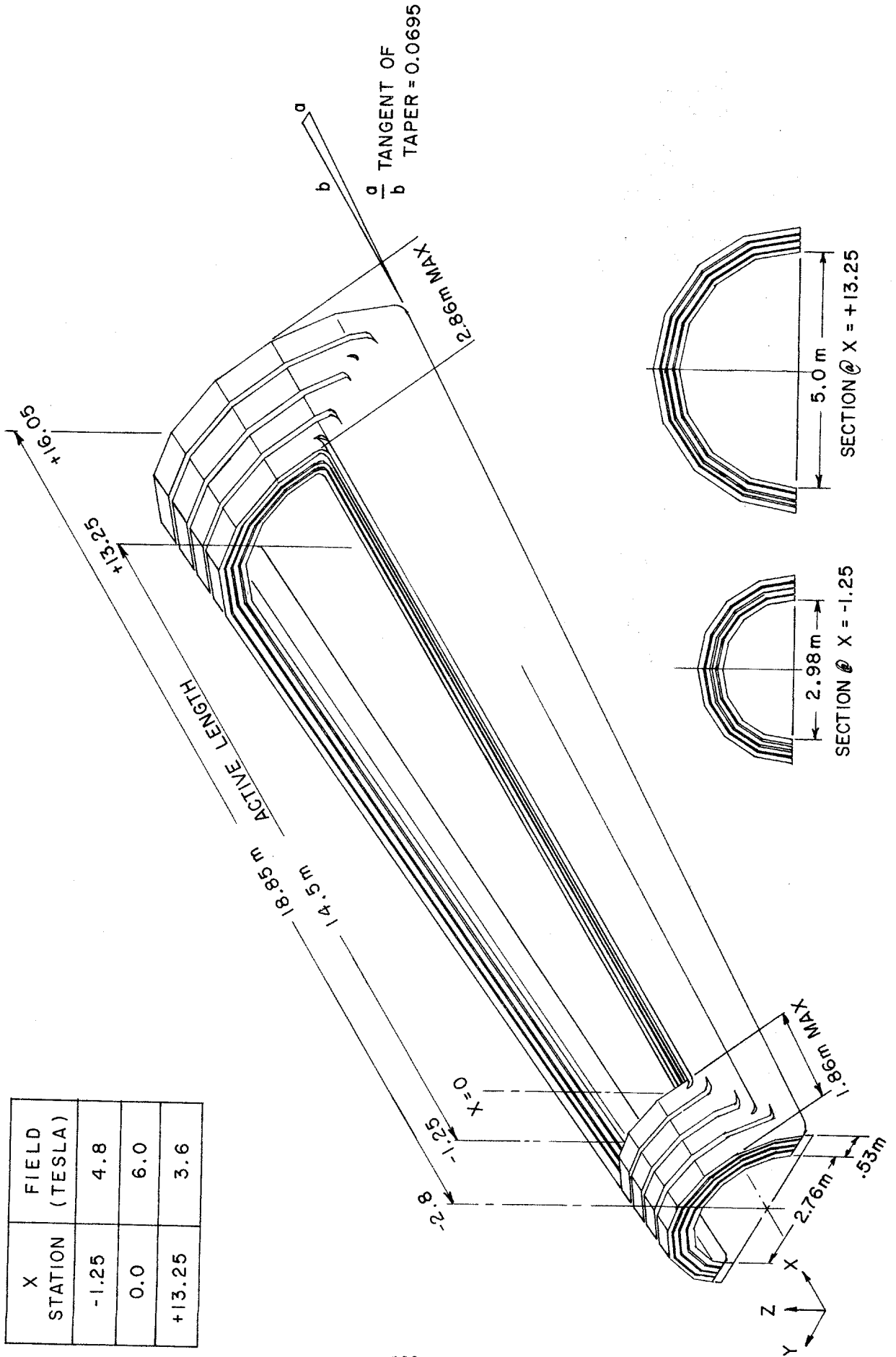
- Assistance in the development of an overall design that is functionally feasible, practical and economical to build
- Development of manufacturing plans for all major structural components
- Development of a preliminary manufacturing sequence and flow chart covering parts fabrication, on-site assembly and testing
- Development of a shipping plan
- Manufacturing analysis of various engineering concepts during initial design phase

A typical portion of the flow chart showing the sequence of operations on staves, inner helium vessel, end plates and outer helium vessel is shown in Figure 4.2.5L.

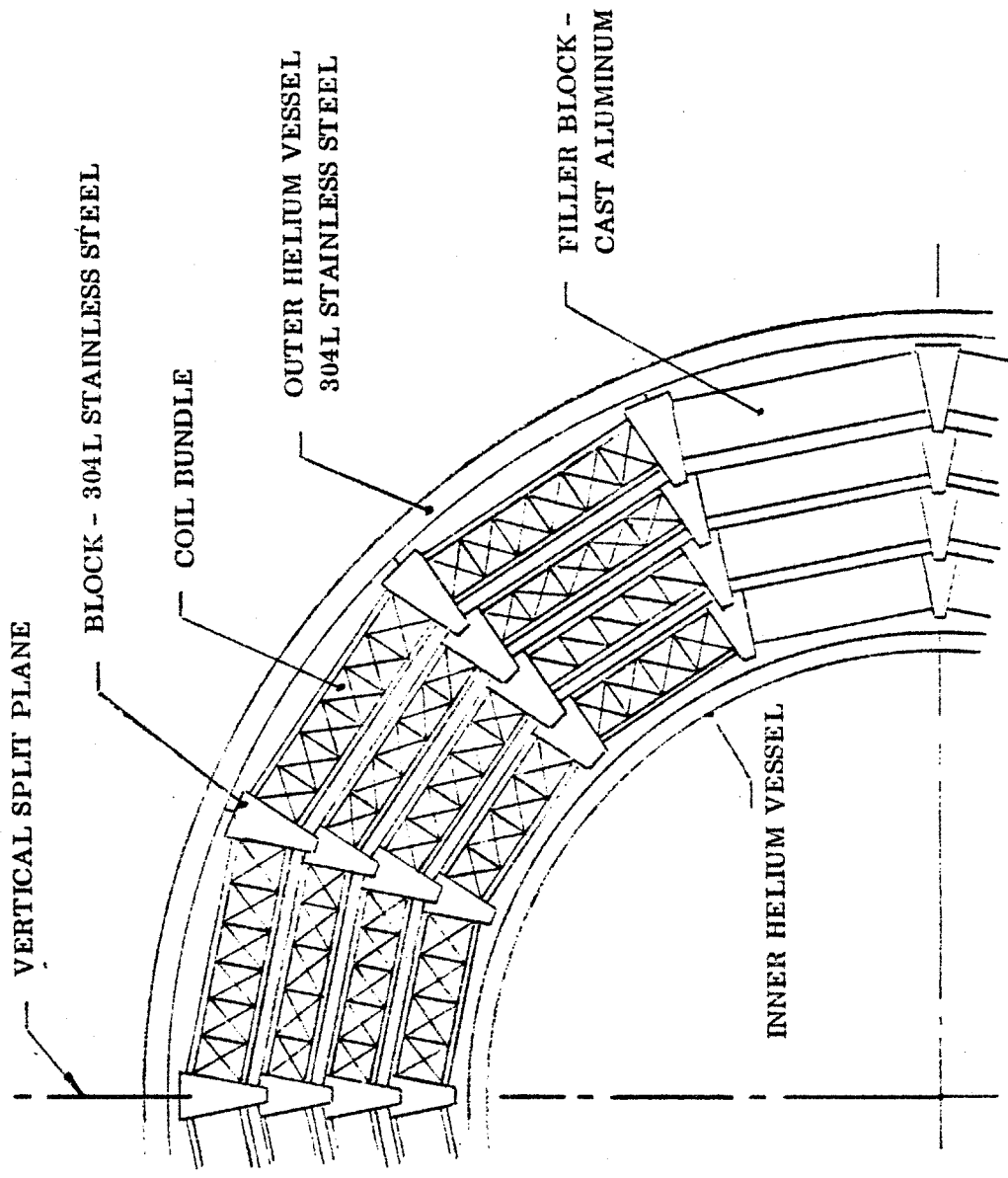
In the proposed manufacturing plan, coil components (substrate sections, conductor), substructure components (staves, blocks) and Dewar components are shipped to the plant site in relatively small pieces. The largest factory-fabricated components are the superstructure girth ring halves (Figure 4.2.5J) which are up to 8.6 m long by 5.1 m high by 1.3 m wide. Coils, substructure and helium vessel are assembled at the plant site with



4.2.5G Diagram of Winding Configuration, CASK Baseload MHD Magnet

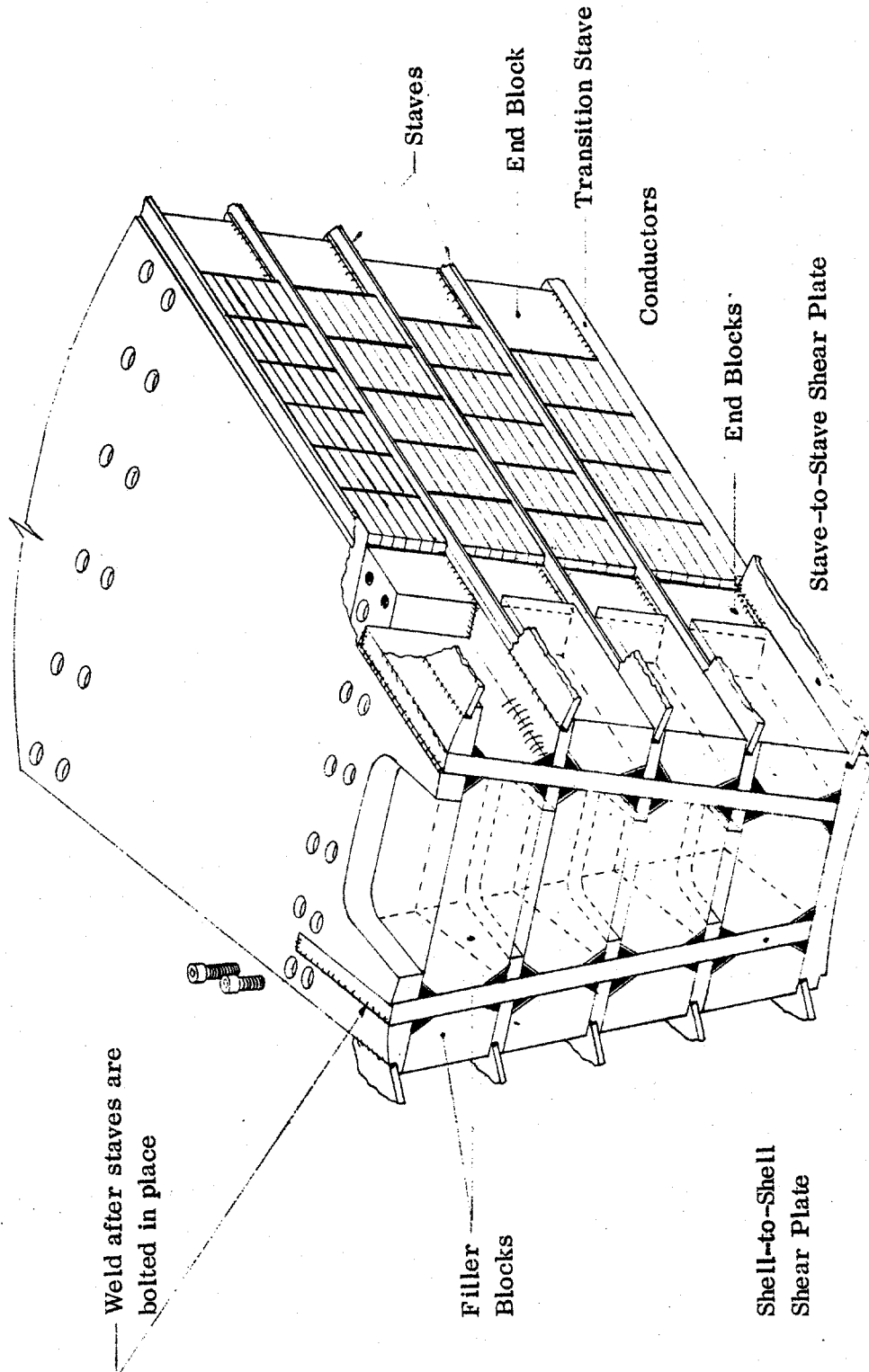


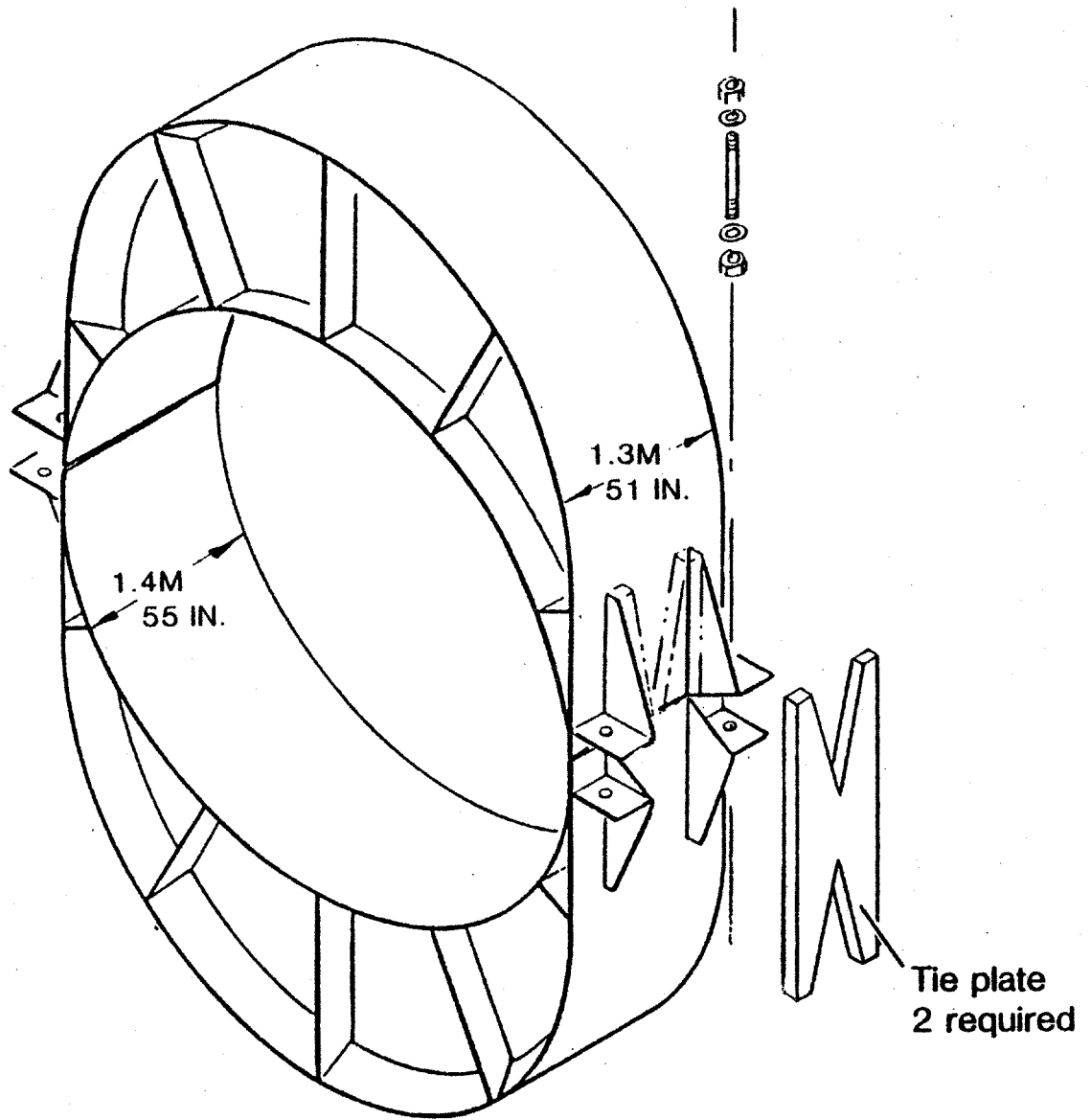




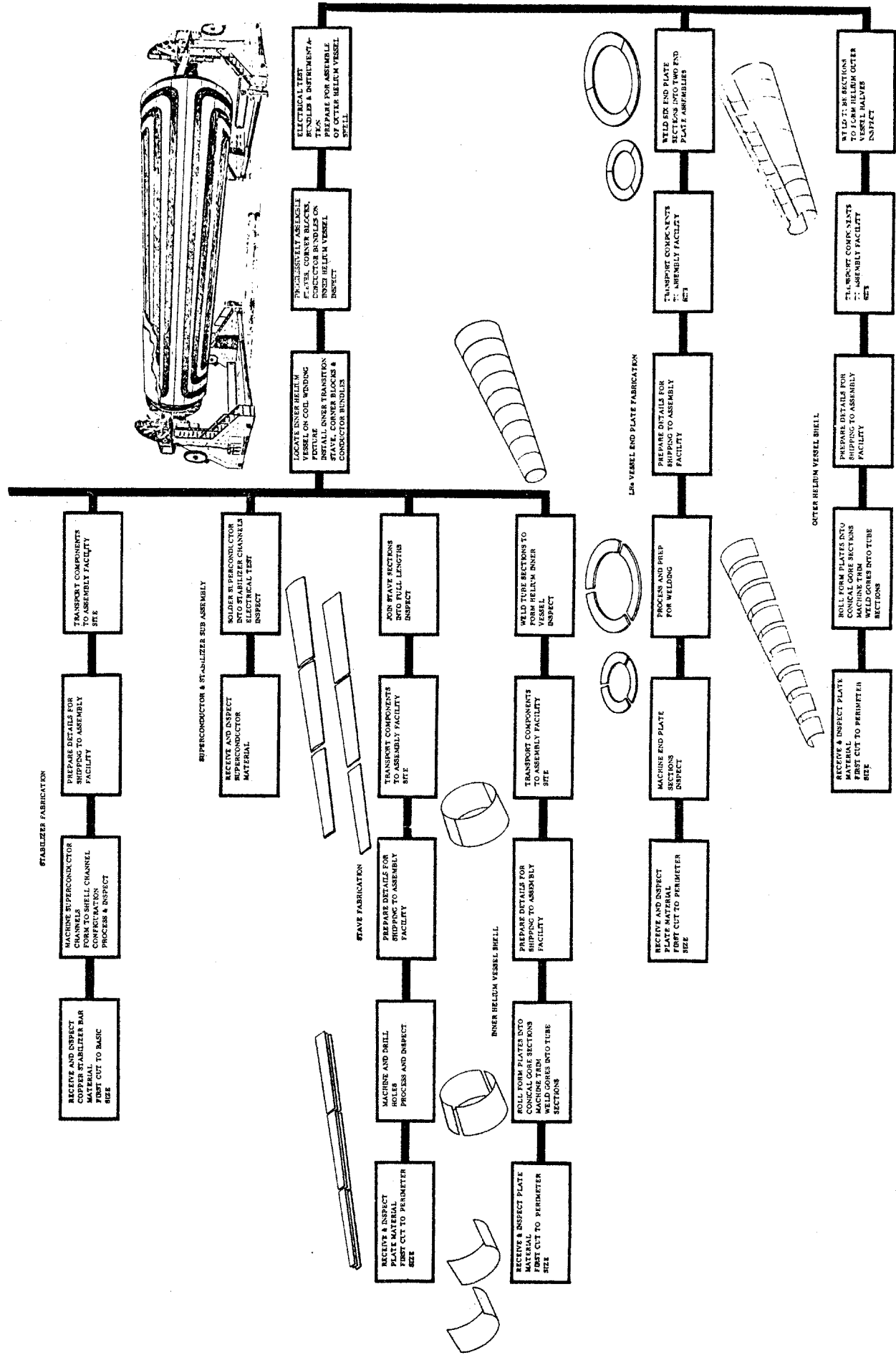
4.2.5H Sketch Showing Midplane Cross Section of Winding of CASK Magnet

4.2.5J Cutaway View of Winding/Substructure Assembly Showing End Block and Shell-to-Shell Shear Plate, CASK Baseload MHD Magnet





4.2.5K Sketch, Crescent Girder Superstructure, CASK Baseload MHD Magnet



the aid of the rotating assembly fixture shown in Figure 4.2.5M.

It was GD's conclusion that the CASK design magnet would be easier to build and would cost less than either the AVCO BL6-P1 design or the AVCO BL6-P2 design (see Sections 4.2.3 and 4.2.4).

More detailed information on the CASK design and manufacturing study is contained in Reference 30.

In November 1979, a subcontract was placed with GD for a cost estimate including a work breakdown structure for the CASK magnet. This work was completed in March 1980.

Detailed work breakdown sheets were prepared for costs of a five-phase program including conceptual design, detail design, component manufacture, on-site assembly and acceptance testing.

An exploded view of the winding, substructure and superstructure, made in connection with cost estimating is shown in Figure 4.2.5N. Typical work breakdown sheets (WBS Input LV3220-Substructure) are shown in Table 4.2.5-III. Estimated total costs and prices (including fee and contingency) for the first unit and the average for units # 2 through 10 are given in Table 4.2.5-IV. The estimated cost for the first unit, not including fee and contingency, is  $\$66 \times 10^6$ . Costs and prices do not include costs of accessory subsystems (cryogenic system, power supply, etc) because estimating these was not a part of GD's task.

An estimated schedule for design and construction of the first unit, amounting to 4.5 years total elapsed time, is shown in Figure 4.2.5P.

More complete information on the CASK cost estimating work is contained in Reference 45.

#### **4.2.6 Commercial-Scale MHD Magnet Design by MIT, 60° Rectangular Saddle, CSM**

It will be informative to introduce first a brief description of the Component Development and Integration Facility Superconducting Magnet (CDIF/SM). This is because of its relationship to the large commercial-scale studies, all of which identified the need for a load-bearing substructure to reduce the cumulative Lorentz load on conductors and insulation. Although such a load-bearing substructure is not a necessity at CDIF scale, it was decided to implement a design concept which would be suitable for commercial scale application and thus gain experience with and demonstrate the concept. The CSM design concept developed at MIT thus incorporated the special features of the CDIF/SM magnet design (see Section 4.3.1) for evaluation and comparison with other commercial-scale alternatives (see Sections 4.2.2, 4.2.3, 4.2.4, 4.2.5).

The CDIF/SM magnet is an intermediate-size MHD test facility magnet (MHD power 2 to 4 MWe) under construction by GE based on a conceptual design originally developed by MIT starting in 1977. The design includes the following special features: 1) 45° rectangular saddle configuration, 2) individual support of winding turns in modular glass-reinforced plastic substructure, and 3) rectangular cross section bore for maximum utilization of high field volume, features which were not incorporated in previous MHD magnet designs but are considered advantageous, particularly for commercial-scale magnets (see Section 4.3.1 for a more complete description of CDIF/SM).

The CSM magnet design in its current version embodies the salient features of the CDIF/SM, but incorporates certain modifications in those features, dictated by scale and by manufacturing considerations. The CSM rectangular saddle ends turn up more sharply than those of the CDIF/SM (60° instead of 45°) in order to provide a steeper field rise and fall at the ends and to shorten overall magnet length. The CSM substructure, which gives individual turn support, is in the form of multiple molded glass-reinforced polyester segments adapted to low-cost production, instead of G-10 plates with machined grooves used in the CDIF/SM. The CSM conductor is a circular cross section, flexible cable for ease of plant-site winding, instead of the square cross section built-up (bar-type) conductor used in the CDIF/SM. The CSM liquid helium containment means consists of containment vessels surrounding each coil half and closely following the coil shape, thus minimizing

Table 4.2.5-III Sheet 1 of 2  
 Typical Work Breakdown Sheets Used in Estimating Costs of CASK Magnet<sup>a</sup>

Cost Elements	Hours or Base \$	Effective Rate \$ or Pct	Estimated Cost	Total Estimated Cost
<b>Direct Material</b>				
Raw Material				
Tooling Material	—	—	62300	—
Mfg Raw Material	—	—	4735807	—
Subtotal Raw Material	—	—	—	<u>4798107</u>
<b>Total Direct Material</b>	—	—	—	<b>4798107</b>
<b>Direct Labor</b>				
Manufacturing Labor				
Mfg Engineering (Tooling)				
Tool Manufacturing	<u>8900</u>	9.220	<u>82058</u>	—
Subtotal Mfg Engr	8900	—	82058	—
Factory				
Experimental	<u>29769</u>	9.020	<u>268516</u>	—
Subtotal Factory	29769	—	268516	—
Manufacturing Support				
Plant Engineering	<u>4420</u>	8.860	<u>39161</u>	—
Subtotal Mfg Support	4420	—	39161	—
Mfg Quality Assurance				
Qual Assur Services	693	9.251	6411	—
Procmnt Qual Assur	576	10.300	5933	—
Receive & Ship Insp	587	8.440	4954	—
Quality Control	<u>3422</u>	8.870	<u>30353</u>	—
Subtotal Mfg Qual Assur	5278	—	47651	—
<b>Total Manufacturing Labor</b>	<b>48367</b>	<b>9.043</b>	—	<b>437386</b>
<b>Support Labor</b>				
Procmnt Qual Verif	<u>576</u>	10.300	5933	—
<b>Total Support Labor</b>	<b>576</b>	<b>10.300</b>	—	<b>5933</b>
<b>Total Direct Labor</b>	<b>48943</b>	—	—	<b>443319</b>

<sup>a</sup> one unit basis

Table 4.2.5-III Sheet 2 of 2

Cost Elements	Hours or Base \$	Effective Rate \$ or Pct	Estimated Cost	Total Estimated Cost
<b>Labor Overhead</b>				
Manufacturing Overhead	437386	121.00	529236	—
Support Overhead	5933	26.01	1543	—
<b>Total Labor Overhead</b>	—	—	—	<b>530779</b>
<b>Travel</b>				
Transportation & Per Diem	—	—	—	14400
<b>Other Direct Costs</b>				
Dir Fringe Benefits	443319	44.90	199049	—
Allocations	—	—	57762	—
Labor Premium Amount	—	—	8866	—
Graphic Services	—	—	13215	—
<b>Total Other Direct Costs</b>	—	—	—	<b><u>278892</u></b>
<b>Subtotal Dir Costs &amp; Overhead</b>	—	—	—	<b>6065497</b>
General & Admin Expense	443319	55.20	—	<b><u>244714</u></b>
<b>Total Estimated Cost</b>	—	—	—	<b>6310211</b>

Table 4.2.5-IV

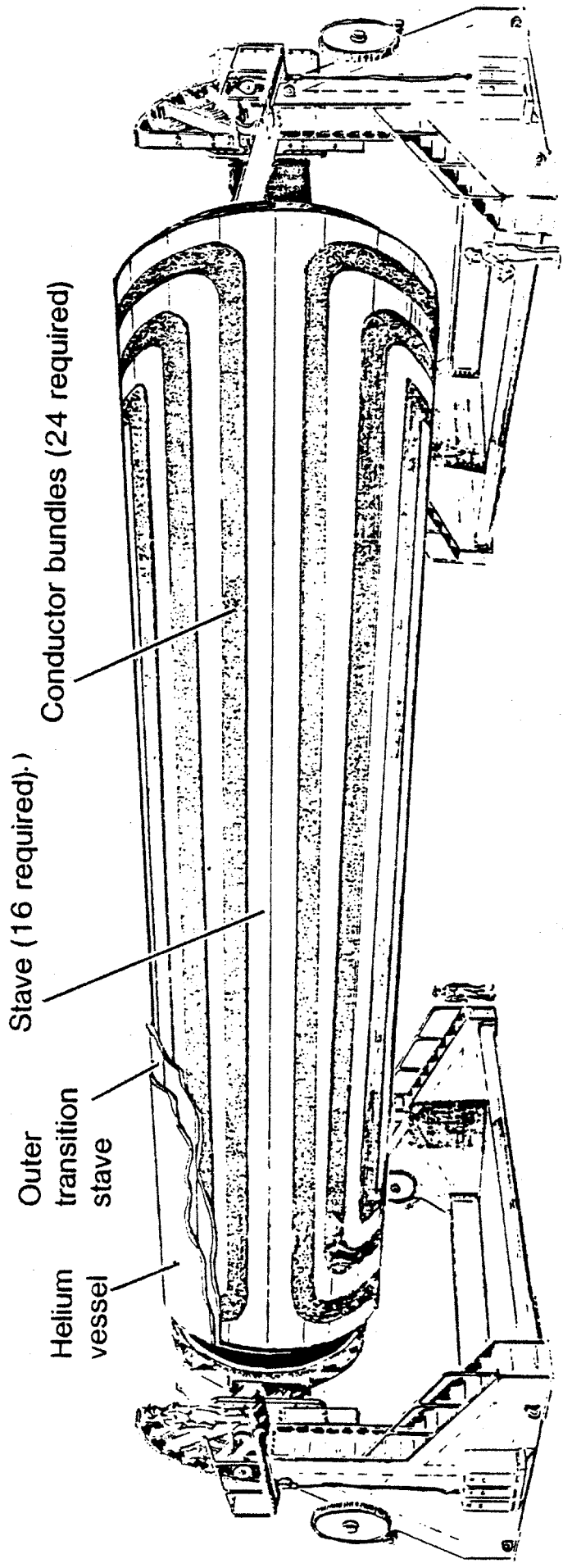
Commercial Scale MHD Magnet Design CASK (GD)  
Cost Estimates

Type of Estimate: Budgetary & Planning

Period of Performance: 4-1/2 yrs. - Unit #1  
 7-1/2 yrs. - Units #2-10

	<u>Unit #1</u>	<u>Units #2-10</u>	<u>TOTAL</u>
Estimated Cost	\$65,888,902	\$421,388,407	\$487,277,309
Fee & Contingency 25%	<u>16,472,226</u>	<u>105,347,102</u>	<u>121,819,328</u>
Price	\$82,361,128	\$526,735,509	\$609,096,637
Avg. Cost/Unit	\$65,888,902	\$46,820,934	\$48,727,731





Conductor bundles (24 required)

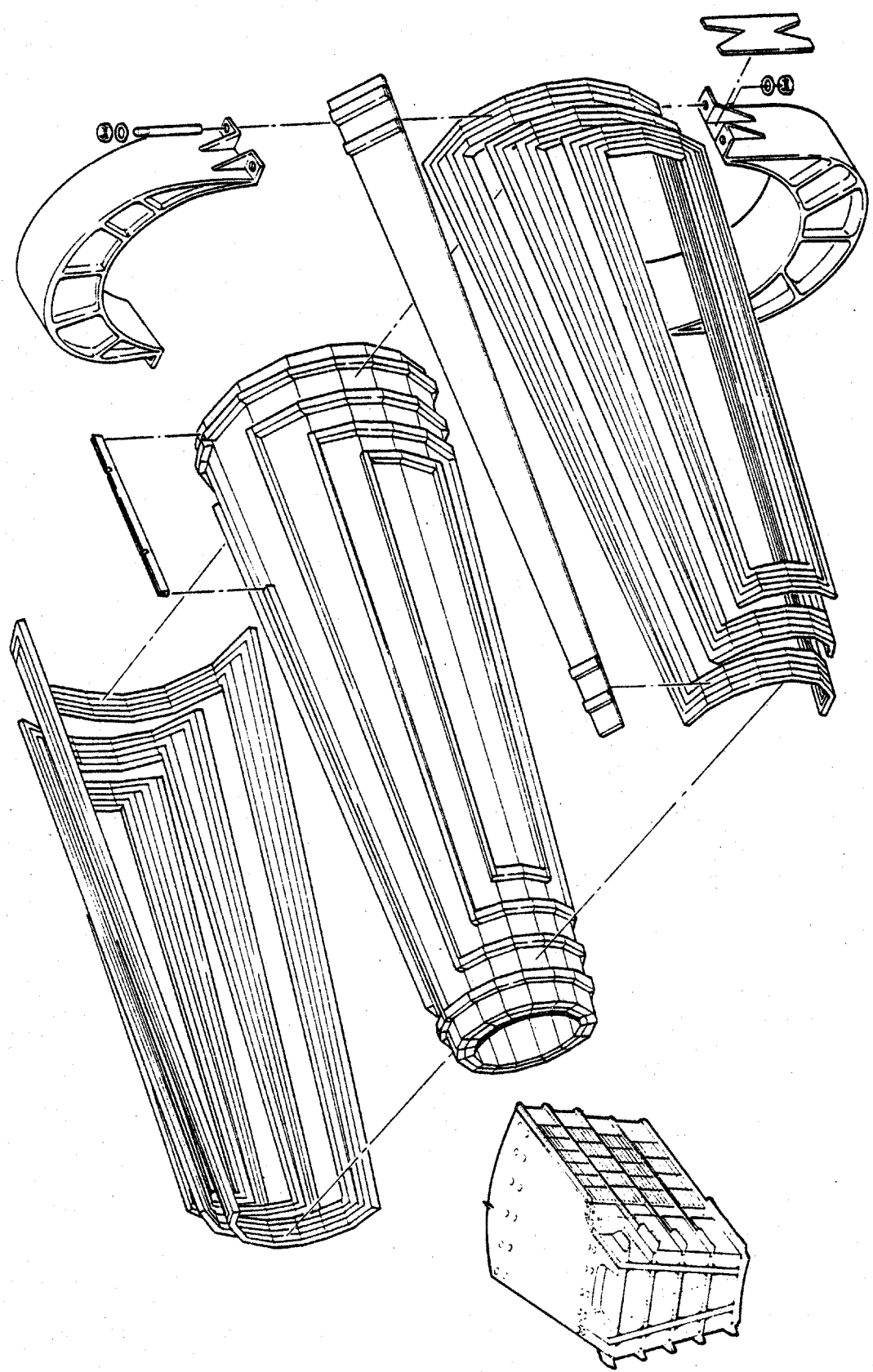
Stave (16 required)

Outer transition stave

Helium vessel

4.2.5M Sketch of Assembly Fixture, CASK Baseload MHD Magnet

4.2.5N Exploded View of Winding, Substructure and Superstructure, CASK Baseload MHD Magnet



MONTHS AFTER GO-AHEAD

1 2 3 4 5 6 7 8 9 10 11 12 13 14 15 16 17 18 19 20 21 22 23 24 27 30 33 36 39 42 45 48 50 51 52 53 54

CONCEPTUAL DESIGN

PH. I

DETAIL OF DESIGN

PH. II

MANUFACTURING

PH. III

ASSEMBLY & INSTL.

PH. IV

ACCEPTANCE TESTING

PH. V

DENOTES PGM MGR, CHIEF ENGINEER, AND  
OPS. MGR. WHO MUST REMAIN ON THE PROGRAM  
AT GDC DURING PH. IV AND PH. V

WORK IN BUTTE, MONTANA.

4.2.5P Estimated Schedule, Design and Construction of CASK Magnet

the volume of excess liquid helium. The CSM main force containment structure (superstructure) is formed by the coil containment vessels themselves in combination with a system of beams, tension-plates and stiffeners that are welded on the outside of the containment assembly. This is in contrast to the CDIF/SM design in which the superstructure is attached directly around the winding and substructure assembly and the helium containment means is a single large vessel surrounding both winding and superstructure.

The design criteria used as a starting point for the CSM design were the same as those used for the CASK design (see Table 4.2.5-I). The CSM warm bore cross sections at channel inlet and exit planes were initially established as square apertures of the same areas as the corresponding circular apertures specified in Table 4.2.5-I. Later, as the design progressed, the apertures were changed to rectangles retaining the same heights (perpendicular to field) as the squares but with width increased to provide an aspect ratio (width/height) approaching 1.2. This change was advantageous because it provided more room inside the warm bore at the sides for channel cooling pipes and power cables, without requiring any increase in magnet winding size (and cost) except for the small increment associated with spreading the end turns to clear the wider bore.

It is expected that channel designers can, in most cases, take advantage of the rectangular shape by using more of the central, high field portion of the bore for power generation and thus obtain a higher power output with a given size magnet.

The CSM conceptual design with its 60° rectangular saddle winding and rectangular warm bore is shown in cold mass assembly drawings, Figures 4.2.6A, 4.2.6B and 4.2.6C and vacuum vessel drawing, Figure 4.2.6D. Design characteristics are listed in Table 4.2.6-I. The calculated field profile is shown in Figure 4.2.6E.

The design incorporates a 52.2 kA twisted cable conductor having a circular envelope of 4.44 cm diameter. The conductor is composed of 427 strands, each 16.3 mm in diameter. There are two grades of conductor used in the winding. Grade A, used in the high field region, contains 252 composite NbTi/Cu strands and 175 plain copper strands. Grade B, used in the low field region, contains 162 strands of composite and 265 strands of copper. The Grade A conductor configuration is shown in Figure 4.2.6F.

In the winding assembly, the conductor turns are individually supported in an insulating substructure, as shown in Figure 4.2.6G. The substructure segments (elements) are made of molded glass-reinforced polyester with notches to hold the turns. Gaps between segments provide passages for coolant circulation. The magnetic load on each turn is transmitted directly to the substructure and the accumulated loading from the winding bundle is transmitted through the substructure to the surrounding coil containment vessel and superstructure. Therefore, no accumulated loading is applied to individual conductor turns.

The overall coil configuration is shown in Figure 4.2.6H. Each half consists of a saddle-shaped coil bundle of rectangular cross section, containing 360 turns. A midplane cross section of the coil bundle of one winding half is shown in Figure 4.2.6J. There are 24 layers of conductor in each coil bundle, with 15 conductors in each layer. Along the length of the magnet, toward the exit end, the coil bundles diverge from each other in both horizontal and vertical planes, following roughly the divergence of the warm bore. The desired sloping field profile is the natural result of this coil divergence.

Two winding and helium containment vessels of welded stainless steel (type 304LN) enclose the two saddle coils and follow closely the contours of the coils. The vessels are mounted on either side of the centerline of the magnet and are joined structurally along the vertical plane through the magnet centerline to form a single coil container weldment as shown in Figure 4.2.6K. Cross-connecting manifolds are provided to distribute liquid helium between the vessels and to maintain equal pressures within them. Stiffeners are welded to the outer walls of the coil container weldment to provide structural support against magnetic forces. The containment vessel outer walls and stiffeners, together with tension plates and special beams which are attached after the windings are installed, combine to form the main force containment structure (superstructure) of the magnet, as

Table 4.2.6-1 Sheet 1 of 3

Design Characteristics  
 Commercial-Scale MHD Magnet Design CSM  
MIT

Date of design		1980
MHD power train data		
MHD power output (estimated)	(MWe)	250 <sup>a</sup>
Magnet data		
Magnet type	—	60° rect. sad.
Warm bore liner?	—	No
Magnetic field:		
Peak on-axis field	(T)	6.0
Active field length	(m)	14.5
Field at start of active length	(T)	4.8
Field at end of active length	(T)	3.6
Field uniformity at end of active length <sup>b</sup>	(%)	+9 —5
Peak field in winding	(T)	7.2
Dimensions:		
Aperture, warm bore inlet <sup>c</sup>	(m)	2.2×2.8
Aperture, start of active length <sup>c</sup>	(m)	2.2×2.8
Aperture, end of active length <sup>c</sup>	(m)	4.0×4.2
Aperture, warm bore exit <sup>c</sup>	(m)	—
Aperture area, start of active length <sup>c</sup>	(m <sup>2</sup> )	—
Aperture area, end of active length <sup>c</sup>	(m <sup>2</sup> )	16.8
Distance, bore inlet to start of active length	(m)	—
Warm bore liner wall thick. & clearance	(m)	0.07
Warm bore length	(m)	19.2
Vacuum vessel overall length	(m)	21.0
Vacuum vessel outside dia.	(m)	12.0
Warm bore volume, active <sup>c</sup>	(m <sup>3</sup> )	162

<sup>a</sup> Magnet bore is sized very conservatively for 250 MWe channel. With careful channel packaging, magnet should accommodate 500 MWe channel.

<sup>b</sup> Field uniformity is + and - variation from on-axis field, central 50% of warm bore cross section

<sup>c</sup> Dimensions inside warm bore, without liner

Table 4.2.6-I Sheet 2 of 3

Winding characteristics:		
Build, winding cross section	(m)	1.08
Number of winding modules (or layers) per half	—	24
Design current, I	(kA)	52.2
Winding current density, average, $J\lambda^a$	( $10^7 \text{ A/cm}^2$ )	1.15
Packing factor, $\lambda^a$	—	0.2
Conductor current density, $J^a$	( $10^7 \text{ A/cm}^2$ )	5.7
Total number of turns, N	—	720
Total length of conductor	(km)	35.4
Ampere turns, NI	( $10^6 \text{ A}$ )	37.6
Ampere meters	( $10^8 \text{ Am}$ )	18.5
Inductance	(H)	5.3
Stored energy	(MJ)	7200
Conductor type	—	Cable
Conductor materials	—	NbTi-Cu
Conductor dimensions <sup>a</sup>	(cm)	4.44 dia.
Copper-to-superconductor ratio <sup>a</sup>	—	7.7
LHe to conductor ratio (vol.) <sup>a</sup>	—	0.4
Heat flux <sup>a,b</sup>	( $\text{W/cm}^2$ )	0.07
Weights:		
Conductor	(tonnes)	300
Insulation	(tonnes)	incl. below
Substructure	(tonnes)	155
Superstructure	(tonnes)	930
Liquid He vessel	(tonnes)	incl. above
Total cold mass	(tonnes)	1385
Thermal shield, cold mass supports, etc	(tonnes)	65
Vacuum vessel	(tonnes)	400
Miscellaneous	(tonnes)	0
Total magnet weight	(tonnes)	1850

<sup>a</sup> Where graded winding is incorporated, values listed are for high field region of winding.

<sup>b</sup> Assumes all strands in cable 100% surface cooled.

Table 4.2.6-I Sheet 3 of 3

Cryogenic data:

Operating temperature at winding	(K)	4.5
Operating temperature, thermal shield	(K)	80
Coolant, thermal shield	—	LN <sub>2</sub>

Materials of construction:

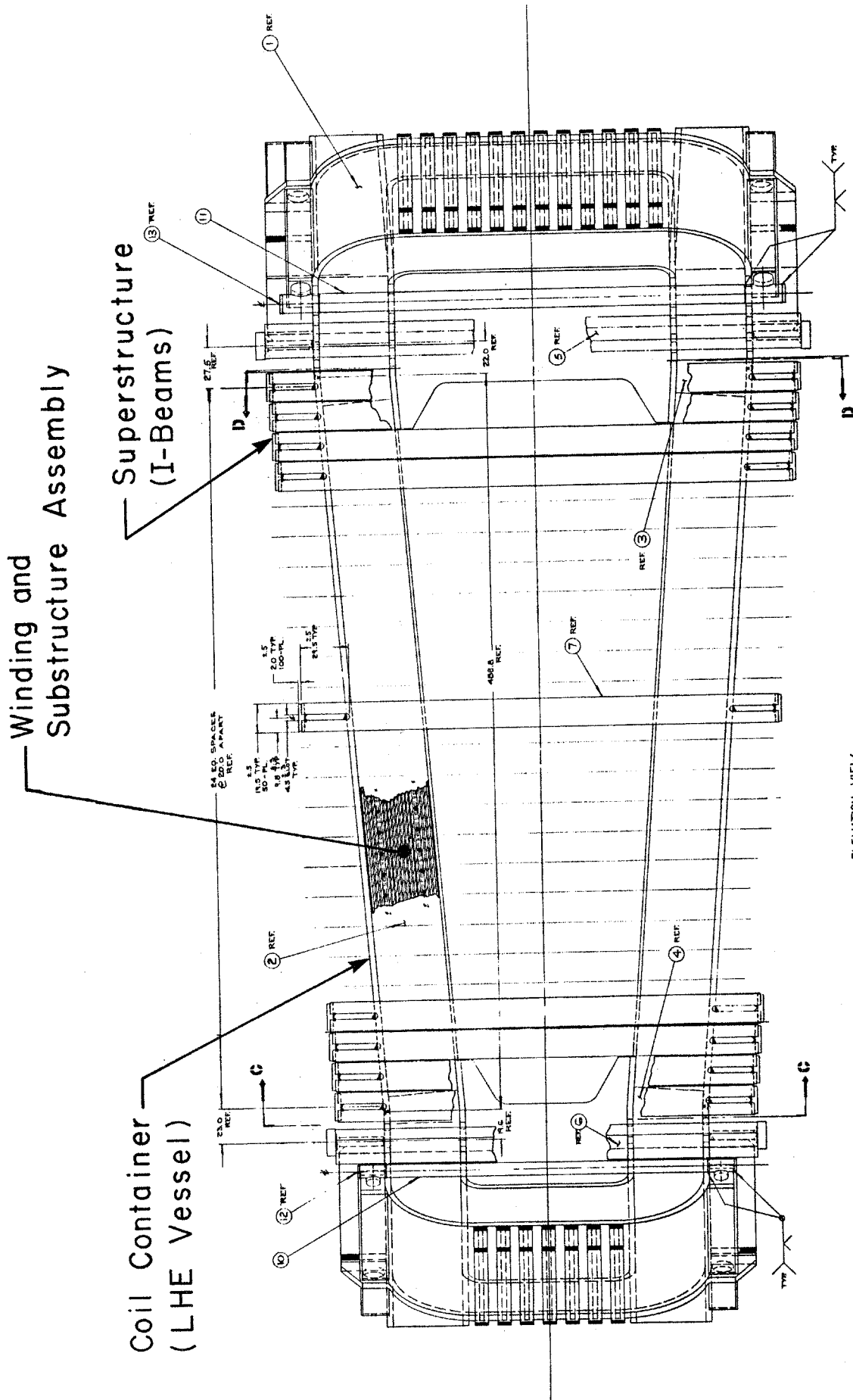
Winding substructure	—	Glass/polyester
Insulation	—	Above and G-10
Superstructure	—	SS 304 LN
Liquid helium vessel	—	SS 304 LN
Thermal shield	—	Al 6061
Vacuum vessel	—	SS 304 L

Design stresses:

Superstructure (bending)	(MPa)	414
--------------------------	-------	-----

Pressure rating

Liquid helium vessel		
Normal operating	(atm)	1.3



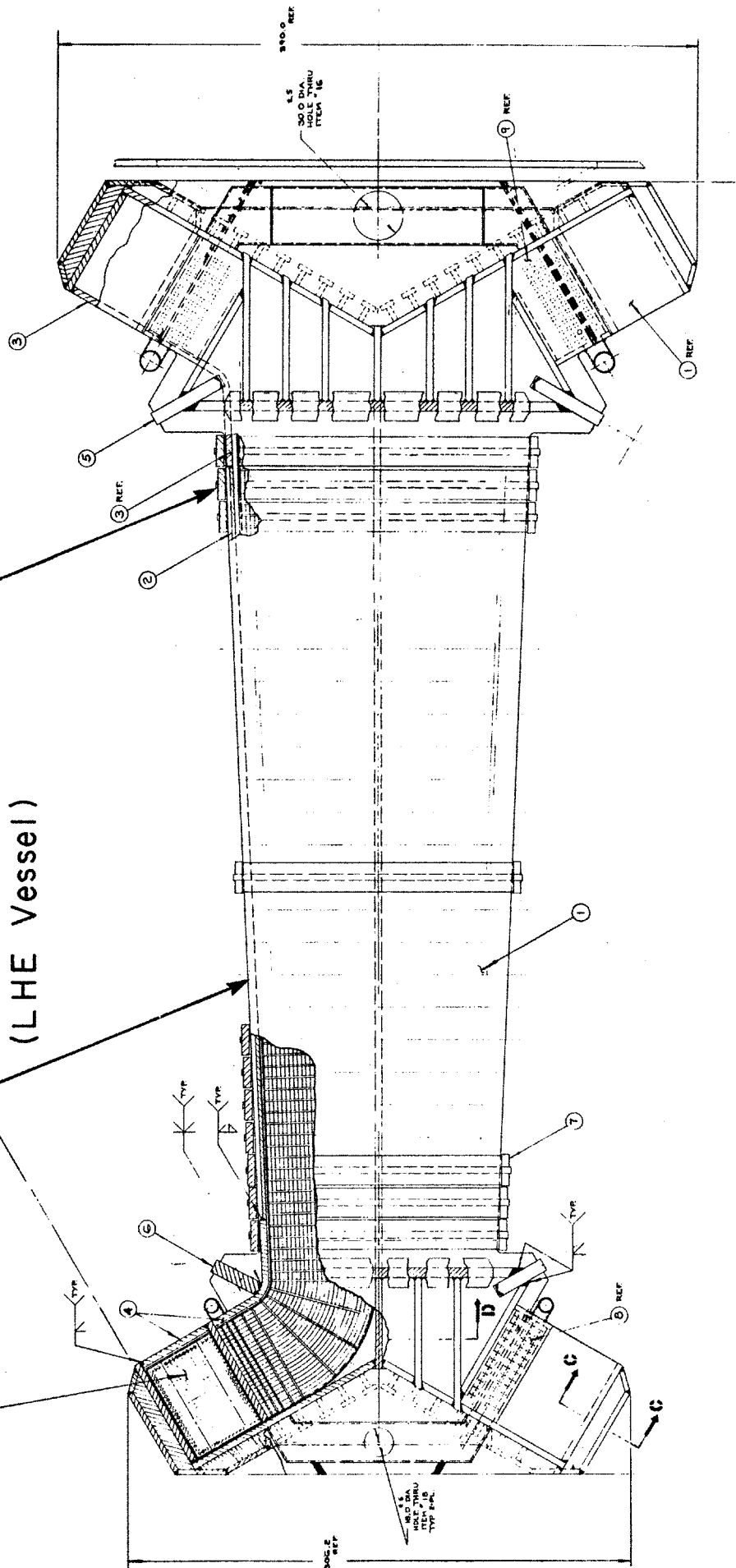
ELEVATION VIEW



Superstructure  
(Tension Straps)

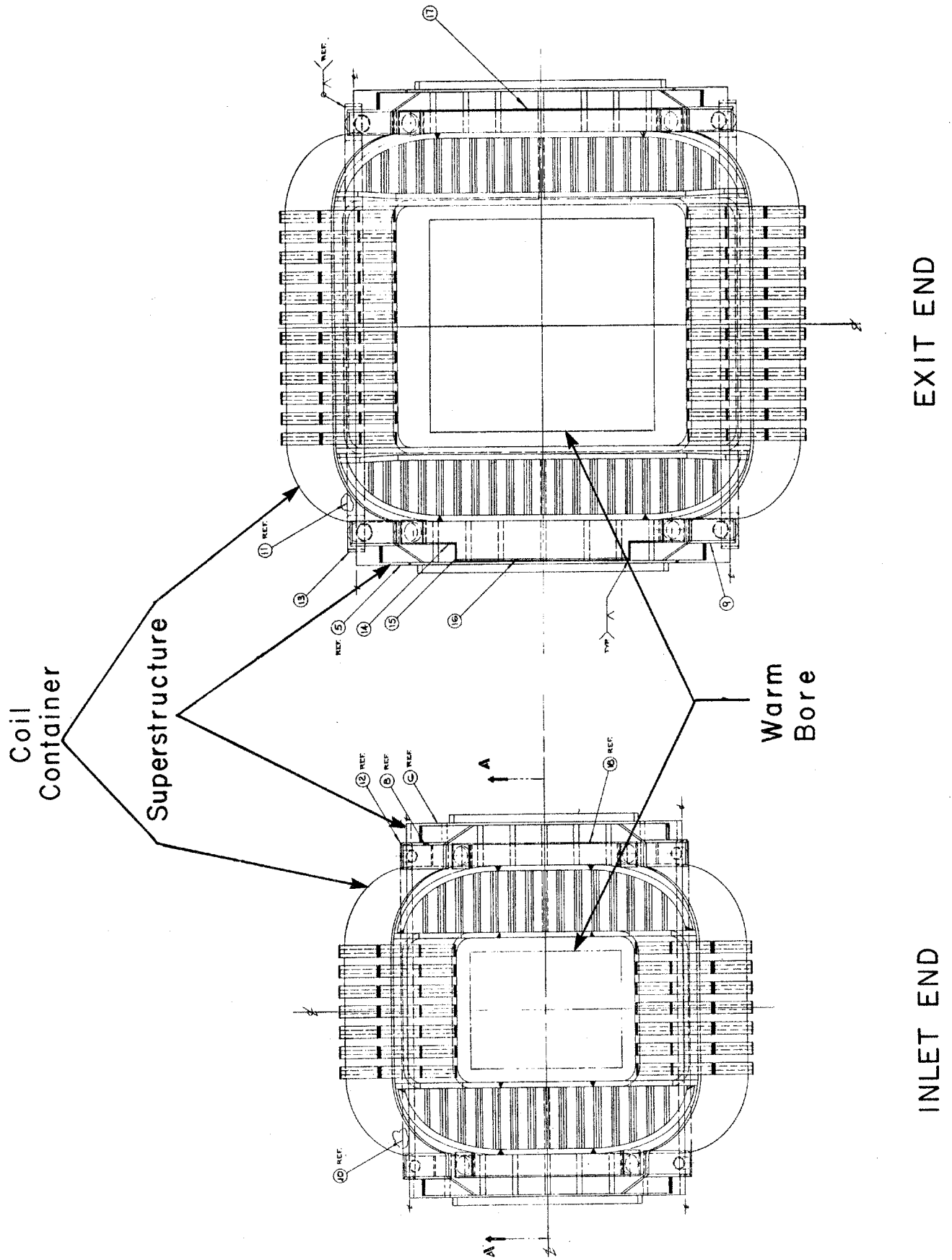
Coil Container  
(LHE Vessel)

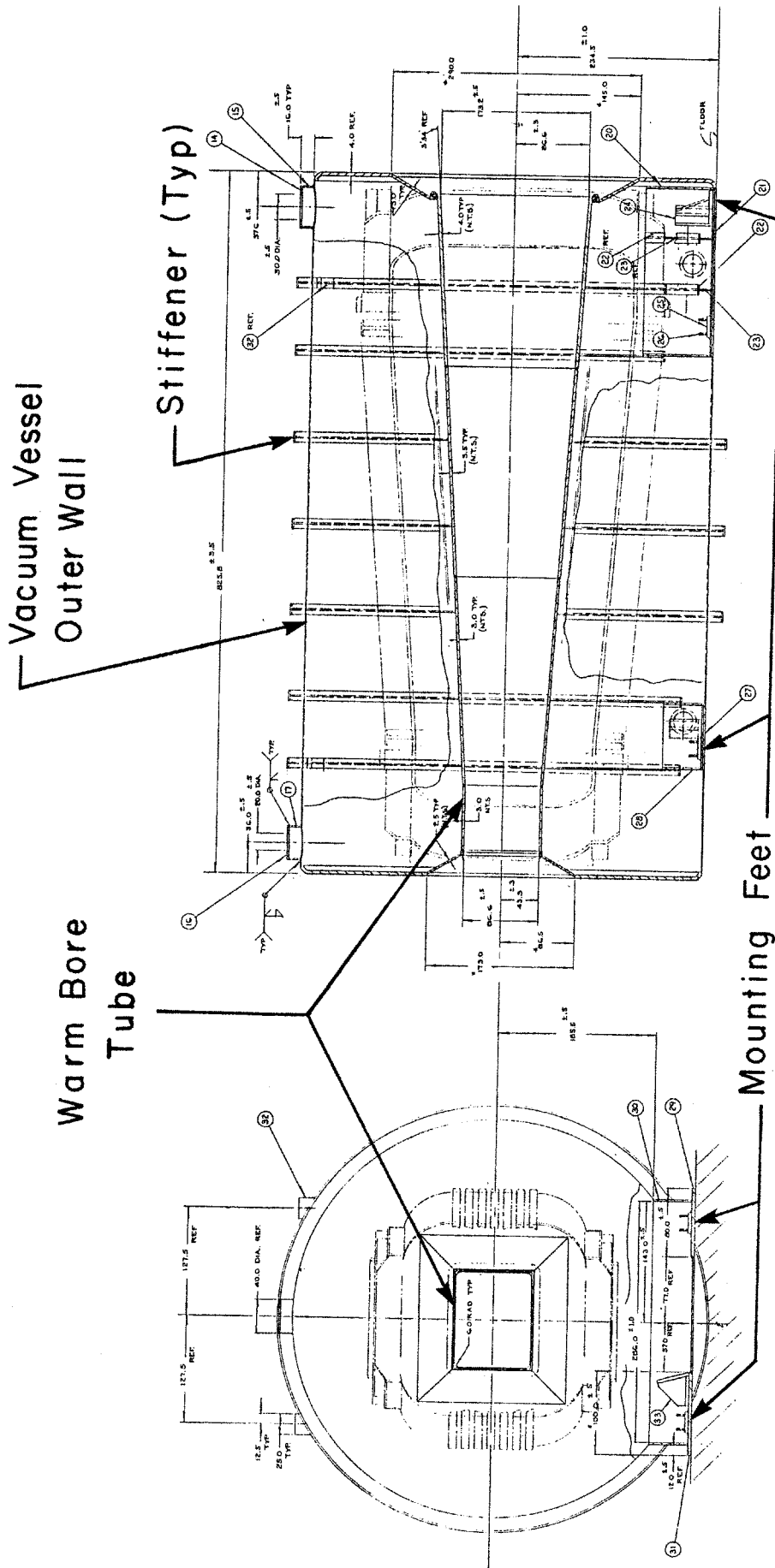
WINDING & SUB-STRUCTURE ASS'Y



4.2.6B Plan View of Magnet Assembly, CSM Design

4.2.6C. Inlet and Exit Views of Magnet Assembly, CSM Design



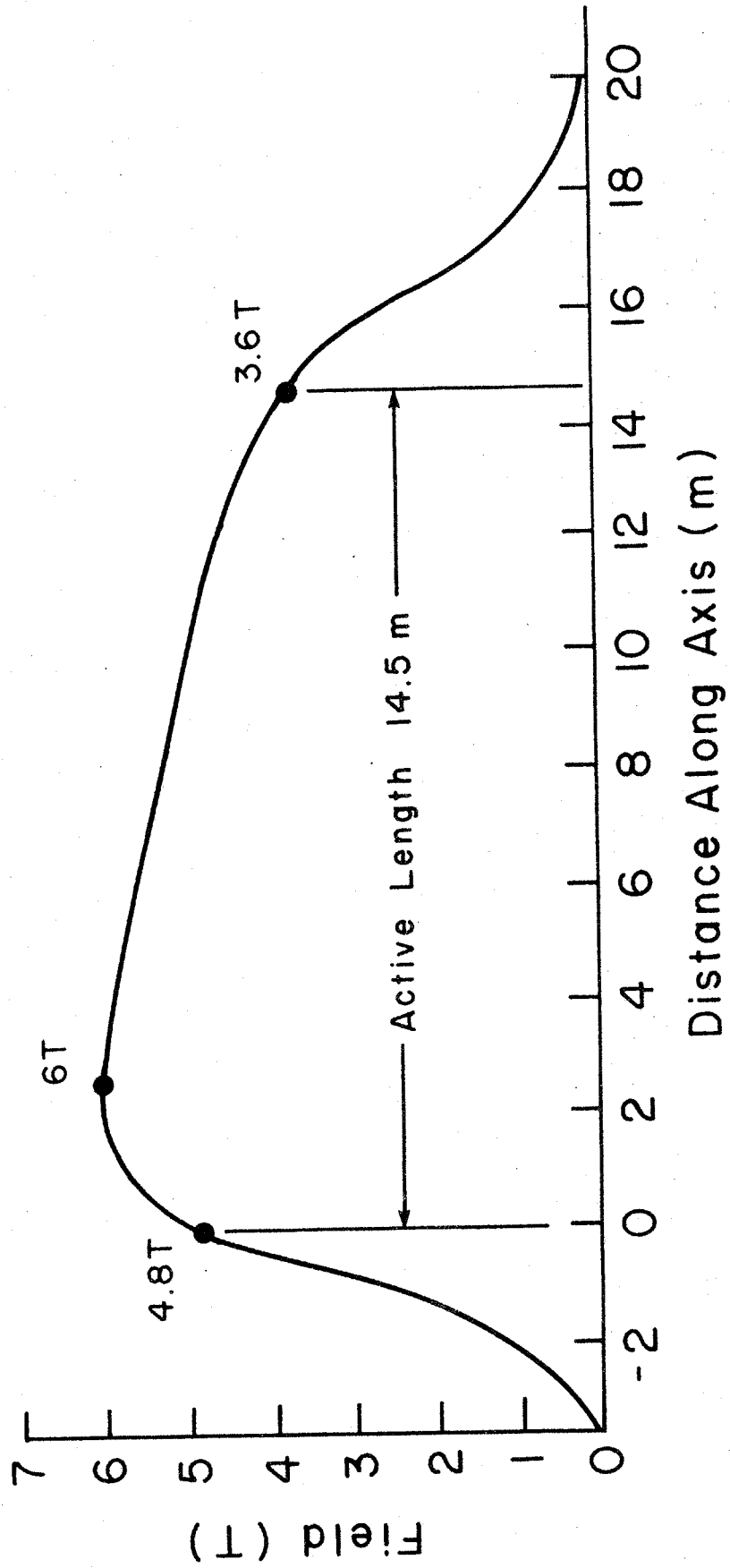


INLET END VIEW

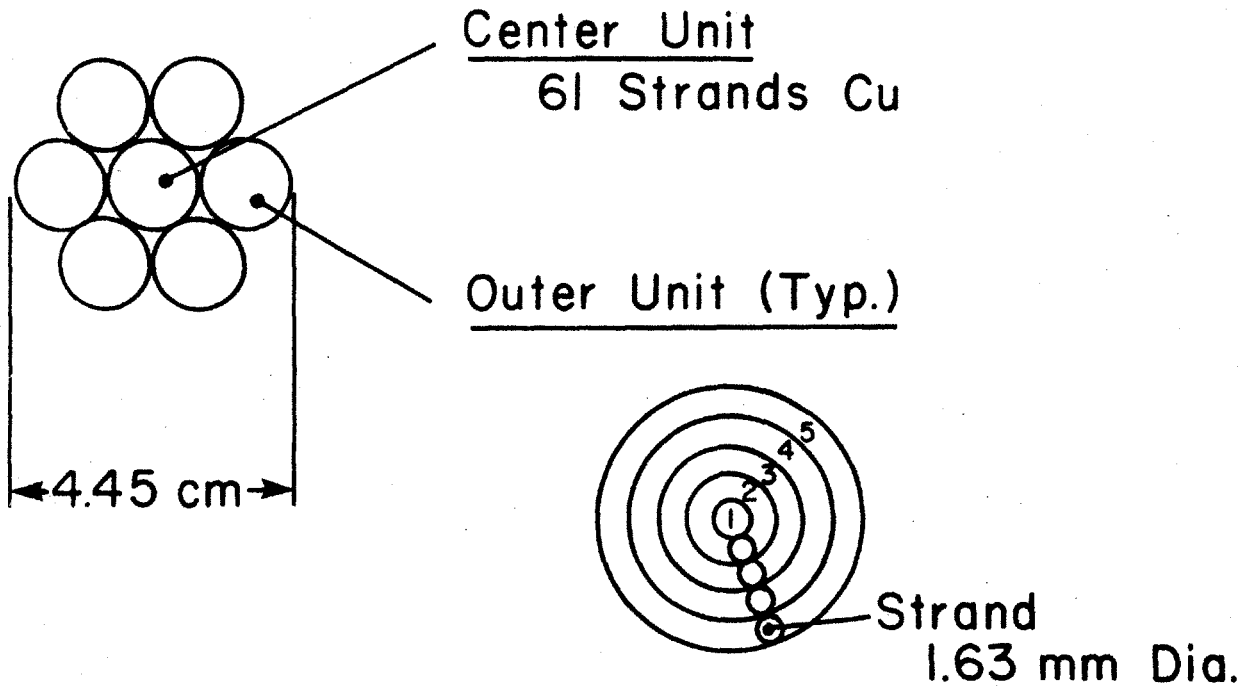
ELEVATION

4.2.6D Elevation and End View of Vacuum Vessel, CSM Design

4.2.6E Curve of On-Axis Field vs Distance Along Axis for CSM Design



Cable (Grade A)



Layer	No. Strands	Mat'l.
1 Core	1	Cu
2	6	Cu
3	12	Cu
4	18	NbTi/Cu
5	<u>24</u>	NbTi/Cu
	61	

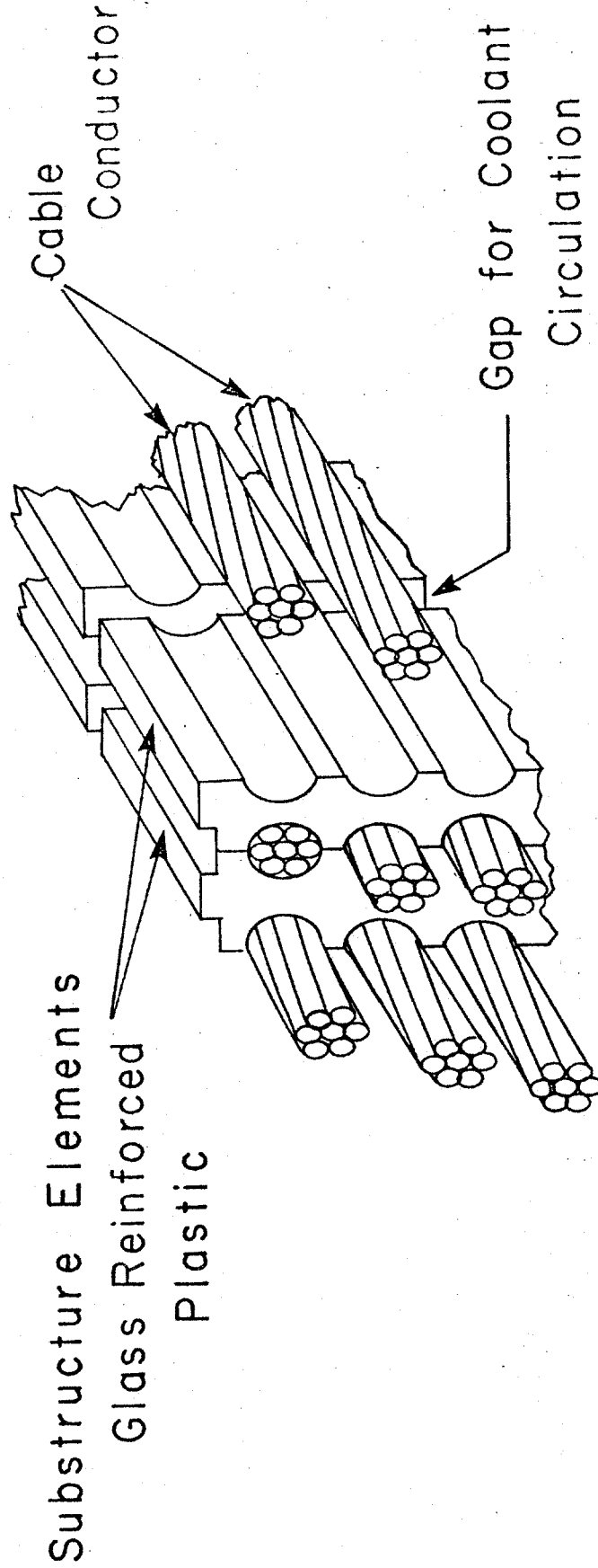
Cable Overall: 175 Strands Cu  
252 Strands NbTi/Cu  
427 Strands Total

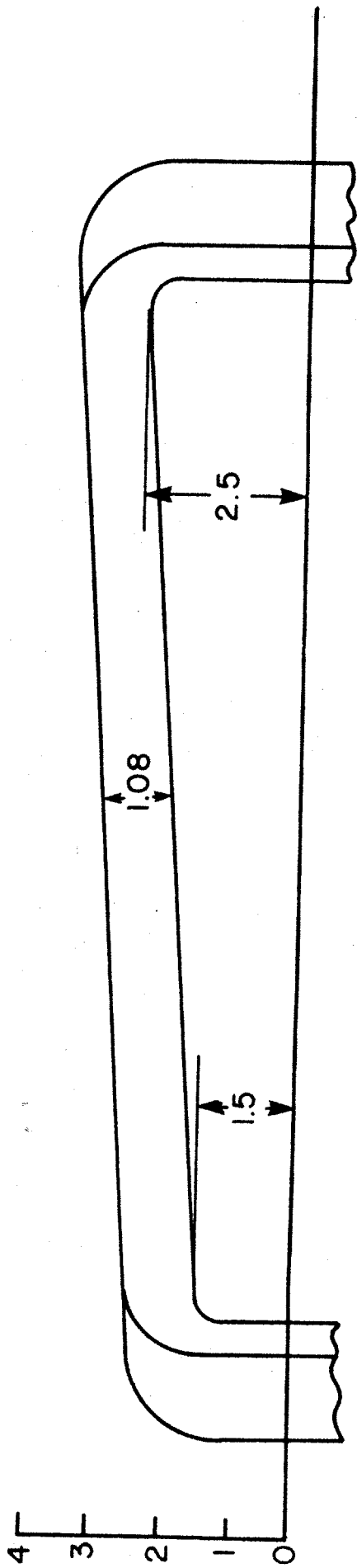
Design Current 52.5 kA

Design Current Density  $5.86 \times 10^7$  A/m<sup>2</sup>

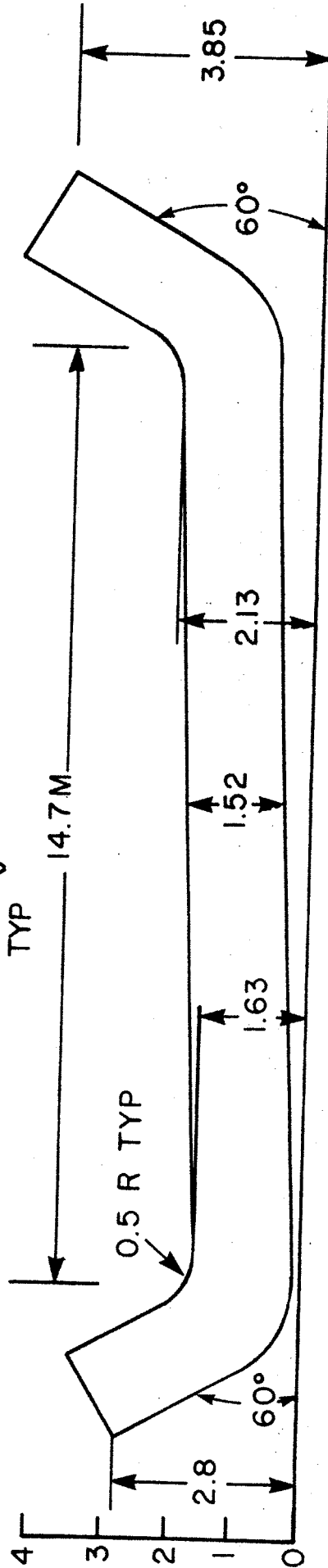
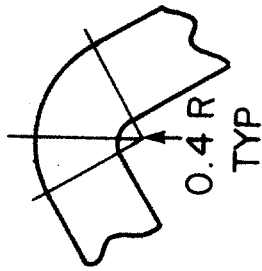
4.2.6F Diagram Showing Conductor Configuration for SM Design (Grade A)

4.2.6G Sketch Showing Cable Conductor Turns Individually Supported in Insulating Substructure, CSM



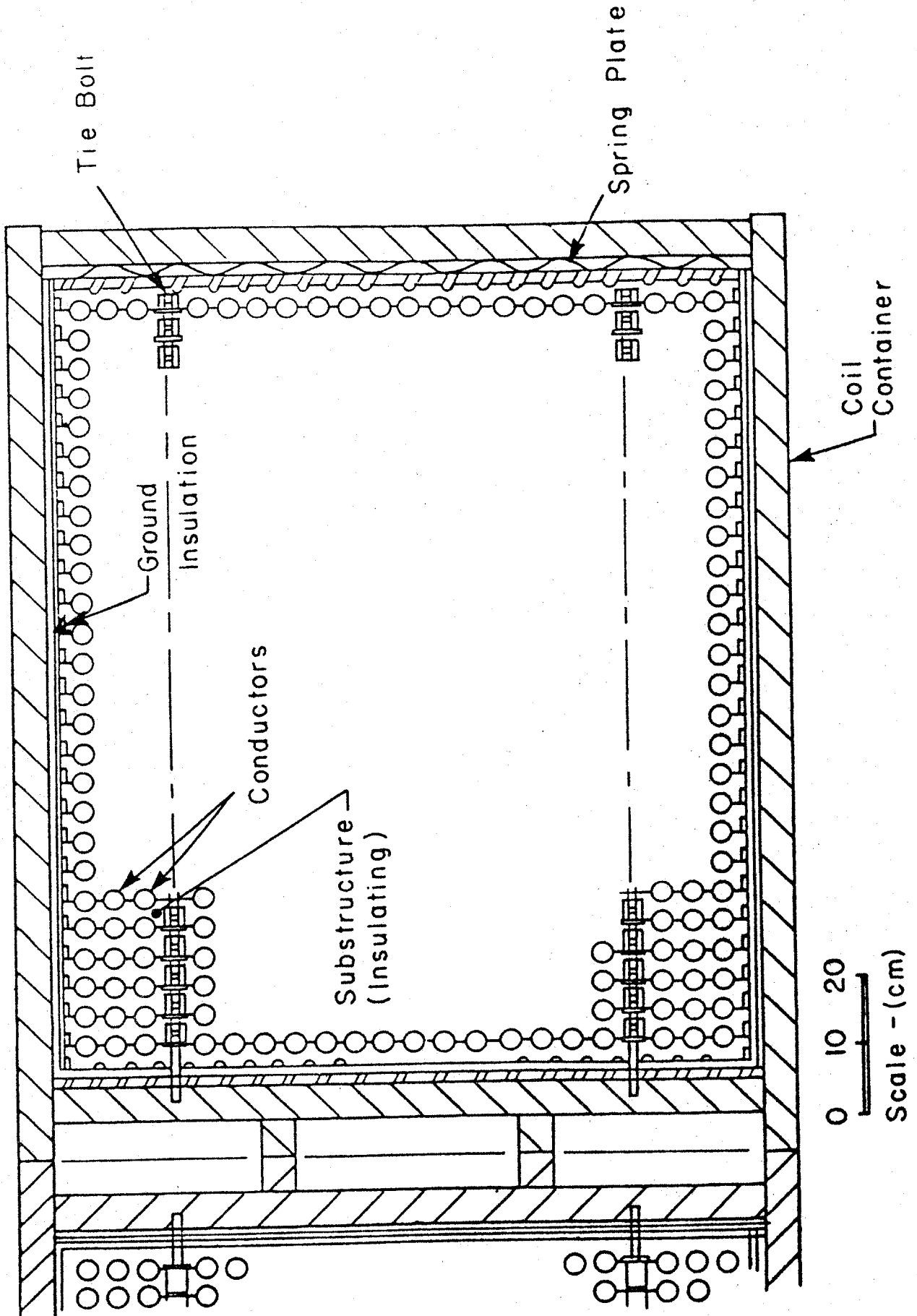


Dimensions in Meters

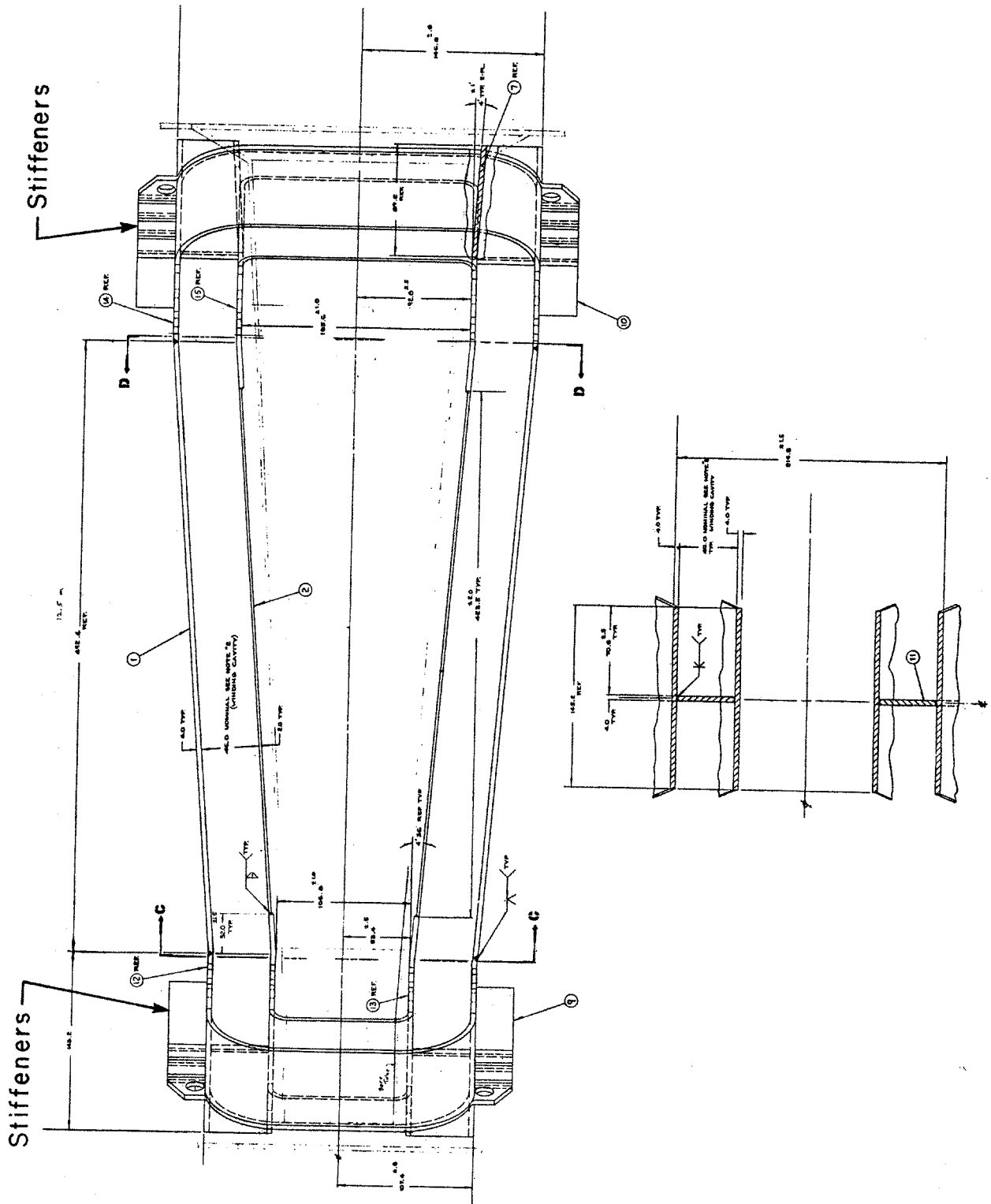


4.2.6H Diagram Showing Overall Winding Configuration, One Half CSM Design

4.2.6J Layout Showing Cross Section of Coil Bundle of One Winding Half, CSM Design







Stiffeners

Stiffeners

SECTION C-C

4.2.6K Layout Drawing of Coil Container Weldment, CSM

described later herein.

The main functions of the vessels are to maintain the windings in a bath of liquid helium and to serve, in combination with tie plates and special beams, as structural support for the coils. The coil containment vessels are located inside a vacuum vessel and are designed for a maximum internal pressure of 3 atmospheres with an external vacuum. The containers are designed to carry the entire longitudinal magnetic force produced by the coil-ends.

A large plenum chamber is incorporated as a part of the coil containment vessels just above the exit end turns. The chamber and associated manifolds cross-connect the two containment vessels, provide a reservoir for liquid helium above the level of the windings and provide access to the windings for power leads, coolant connections, vents and instrumentation. A plenum chamber is also incorporated above the inlet end turns. This chamber, smaller than the exit-end chamber, provides access to the windings for emergency venting and instrumentation.

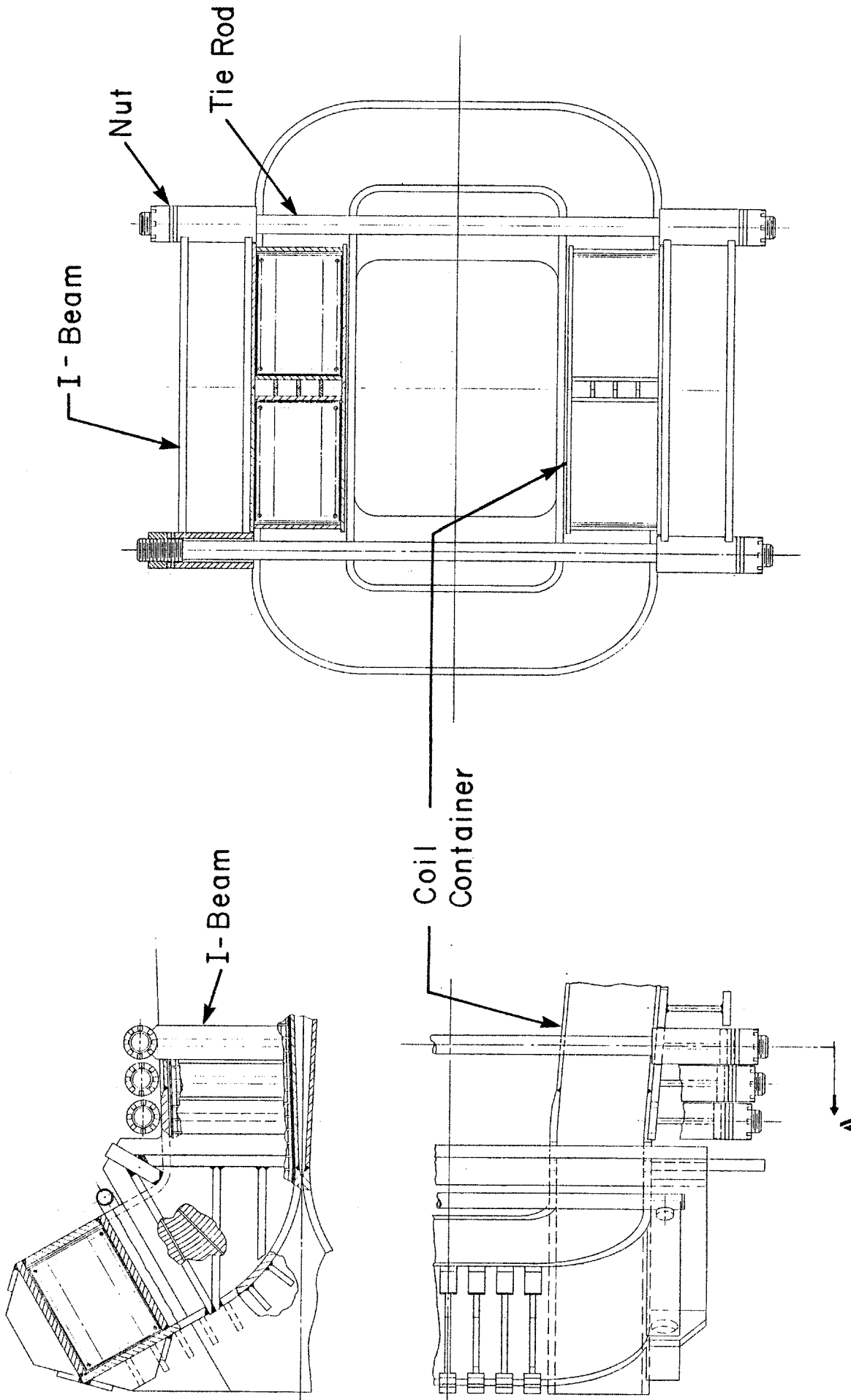
The main force containment system consists of rectangular frames, made up of I-beams and tension plates supporting the middle (straight) portion of the coils, and thick-walled, stiffener-reinforced containment structures surrounding the end turns. All parts are of 304LN stainless steel. The design of the containment system is shown in assembly drawings, Figures 4.2.6A and 4.2.6B. The system represents an integration of the winding containment vessels with stiffeners, special beams and tension plates to form an all-welded structure in which structural material is used efficiently.

An alternative main force containment system was investigated as a part of a manufacturing study described later herein. In the alternative system, support for the middle "straight" portion of the coils is provided by separate I-beams clamped around the coil containers with threaded tie-rods and nuts instead of by I-beams integral with coil container walls, held together with welded-on tension plates. The alternative system is shown in Figure 4.2.6L. Although the separate beam and threaded tie-rod system requires more material than the original all-welded system (see discussion under manufacturing study reported later in this section), the alternative system is considered to be superior and more cost effective overall. It is planned that the CSM design will be modified to incorporate the alternative structural system as a part of future work on evaluation and selection of magnet designs.

The Dewar consists of a liquid-nitrogen-cooled aluminum alloy thermal radiation shield, multilayer insulation blankets and a 304L stainless steel cylindrical outer vacuum vessel, rectangular-cross-section warm bore tube and dished heads. The cold mass of the magnet is supported by a system of low-heat-leak tubular struts of G-10, including four vertical struts to support the gravity load of the cold mass, a transverse strut to restrain sideways motion at the inlet end and a pair of diagonal struts to restrain sideways and longitudinal motion at the exit end.

Accessory subsystems (cryogenic support system, power supply system, etc.) have not yet been designed for the CSM magnet.

Manufacturing studies were carried out with assistance from vendors. Samples of production electrical cables (all copper) were obtained from Phelps-Dodge. One of these cables, 4.44 cm in diameter, was used as a basis for the design of the superconducting cable conductor for the CSM magnet. Several manufacturers of reinforced plastic parts were contacted for recommendations on materials and processes for substructure elements. The molded glass-reinforced polyester substructure element design evolved from these recommendations. Layout drawings of the coil container weldment and of the container/superstructure assembly were transmitted to Pittsburgh-DesMoines Steel Co. (PDM) for their review and recommendations. The manufacturing plan outlined in collaboration with PDM involved breaking down the coil container weldment into conveniently shippable modules. The modules could be factory fabricated and then shipped to the plant site



SECTION A-A

4.2.6L Layout Drawing Showing Alternative Main Structural Support System, CSM Design

where they would be welded together to form the complete assembly. A number of design improvements were recommended by PDM, a major one being the change to separate I-beams and threaded tie-rods with nuts. This alternative superstructure system was considered advantageous because 1) it avoided the excessive distortion that would have occurred in the coil container weldment during manufacture with the original design integral I-beams, 2) it reduced the amount of field (plant site) welding required, replacing it with factory welding on smaller pieces (separate I-beams) more adaptable to automatic processing and 3) it provided for easy field assembly and better controlled prestressing of support frames around the magnet winding.

When final evaluations are made, these advantages must be traded off against the added material required in the alternative design because the I-beam flanges toward the coils are no longer integral with coil containers and therefore represent extra material, and the bolted joint design requires more material than the original all-welded tie-plate design.

An ROM cost estimate of  $\$35 \times 10^6$  (1980 \$) was made by PDM on the alternative design coil container and structure assembly, including field erection and closing of the container around the windings (but not including installation of substructure and winding itself). Information was obtained from Owens Corning Fiberglass Co. indicating that the cost of molded glass-reinforced polyester substructure elements (finished parts), produced in the quantity required for one CSM magnet, should be less than the cost of G-10 sheets (unmachined raw stock), on a cost per pound basis.

A complete cost estimate for the CSM magnet has not yet been prepared.

It should be noted that the CSM design was scaled down to ETF size and used as a basis for the MHD ETF magnet design described in Section 4.2.12. Cost studies made on this design by MIT with the assistance of Combustion Engineering indicate that the overall design is cost effective and should compare favorably with other design alternatives.

#### **4.2.7 Commercial-Scale MHD Magnet, Advanced 45° Rectangular Saddle Design with Internally-Cooled Cable Superconduct**

The commercial-scale 6 T MHD magnet advanced conceptual design was developed at MIT in parallel with the CSM design (see Section 4.2.6), starting in 1979. The objective was to develop a design alternative incorporating special features somewhat beyond the present state of the art, for evaluation and comparison with CSM and other commercial-scale alternatives (see Sections 4.2.2, 4.2.3, 4.2.4, 4.2.5, 4.2.6).

Advanced features incorporated in the design include the use of internally-cooled cable superconductor (ICCS) in the winding and the use of a tension-band type (momentless) main force containment structure.

Expected advantages of the ICCS winding include 1) simplification of the overall magnet design by eliminating the need for a liquid helium containment vessel and 2) reduction of the amount of superstructure required by allowing the stainless steel jacket (conduit) of the internally-cooled conductor to carry in tension most of the longitudinal magnetic forces acting on the winding crossovers. Expected advantages of the tension-band main structure are simplification of overall structure by eliminating the need for built-up structural I-beams or girth rings and a reduction in structure weight (and cost) by making more effective use of structural material.

Internally-cooled cable superconductor has been under development at MIT for several years (see Section 4.1.6). The momentless main force containment structure concept has also been the subject of special investigations (see Section 4.1.7).

The design criteria used as a basis for the advanced design magnet were the same as those used for the CASK and CSM designs (see Table 4.2.5-1). The warm bore cross sections at channel inlet and exit planes are square apertures of the same areas as the corresponding circular apertures specified in Table 4.2.5-1.

The advanced design magnet, with its 45° rectangular saddle winding, square bore and tension-band superstructure, is shown in cutaway view, Figure 4.2.7A and in assembly views, Figures 4.2.7B, 4.2.7C and 4.2.7D. Design characteristics are listed in Table 4.2.7-I. The calculated field profile is shown in Figure 4.2.7E. The conductor-insulation arrangement is shown diagrammatically in Figure 4.2.7F.

More detailed information on the advanced design is contained in Reference 31.

#### 4.2.8 Summary of ETF Magnet Designs

ETF magnet designs prepared and/or investigated during the past five years are as follows:

<u>Type</u>	<u>Designer</u>	<u>Remarks</u>
Rectangular Saddle and Racetrack (6 T)	MCA	Report June 1977 [57] Scaledown of BL-MCA commercial-scale design
Circular Saddle Conical-Shell (6 T)	AVCO	Report June 1977 [58] Scaledown of BL6-P1 commercial-scale design
90° Rectangular Saddle (6 T)	AVCO	Report June 1977 [58] Scaledown of BL6-P2 commercial-scale design
45° Rectangular Saddle and Racetrack (6 T)	AVCO	Report April 1979 [78] Original design, part of AVCO 1978 ETF system design
60° Rectangular Saddle (6 T)	MIT	Report Nov. 1981 [38] Scaledown of CSM commercial-scale design. Design developed by MIT under DOE/NASA LeRC ETF program
60° Rectangular Saddle (4 T)	MIT	Report Nov. 1981 [73] Scaled from above 6 T design Design developed by MIT under DOE/NASA LeRC ETF program

The major characteristics of the six designs are listed in Table 4.2.8-I.

The fifth and sixth designs (CSM scaledown) were prepared by MIT under subcontract to NASA LeRC as a part of the overall DOE/NASA LeRC ETF conceptual design program. As explained in Section 4.2, tentative

Table 4.2.7-1 Sheet 1 of 3

Design Characteristics  
Commercial-Scale MHD Magnet Advanced Design<sup>(a)</sup> with ICCS  
MIT/FBNML

Date of design		1980
MHD power train data		
MHD power output <sup>b</sup> (estimated)	(MWe)	250
Magnet data		
Magnet type <sup>a</sup>	—	45° rect. sad.
Warm bore liner?	—	No
Magnetic field:		
Peak on-axis field	(T)	6.0
Active field length	(m)	14.5
Field at start of active length	(T)	4.8
Field at end of active length	(T)	3.6
Field uniformity at end of active length <sup>c</sup>	(%)	+5    -5
Peak field in winding	(T)	7.1
Dimensions:		
Aperture, warm bore inlet <sup>d</sup>	(m)	2.2×2.2
Aperture, start of active length <sup>d</sup>	(m)	2.2×2.2
Aperture, end of active length <sup>d</sup>	(m)	4.4×4.4
Aperture, warm bore exit <sup>d</sup>	(m)	4.4×4.4
Aperture area, start of active length <sup>d</sup>	(m <sup>2</sup> )	4.84
Aperture area, end of active length <sup>d</sup>	(m <sup>2</sup> )	16.0
Vacuum vessel overall length	(m)	25.2
Vacuum vessel outside dia.	(m)	12.3
Warm bore volume, active <sup>d</sup>	(m <sup>3</sup> )	143

*a* Advanced features include internally-cooled conductor, self-supporting end turns and tension band (momentless) superstructure.

*b* Magnet bore is sized very conservatively for 250 MWe channel. With careful channel packaging, magnet should accommodate 500 MWe channel.

*c* Field uniformity is + and - variation from on-axis field, central 50% of warm bore cross section

*d* Dimensions inside warm bore, without liner

Table 4.2.7-I Sheet 2 of 3

<b>Winding characteristics:</b>		
Build, winding cross section	(m)	1.03 max
Number of winding modules (or layers) per half	—	4
Design current, I	(kA)	20
Winding current density, average, $J\lambda^a$	( $10^7$ A/cm <sup>2</sup> )	1.3
Packing factor, $\lambda^a$	—	0.21
Conductor current density, $J^a$	( $10^7$ A/cm <sup>2</sup> )	6.06
Total number of turns, N	—	1660
Total length of conductor	(km)	84.2
Ampere turns, NI	( $10^6$ A)	33.2
Ampere meters	( $10^8$ Am)	16.8
Inductance	(H)	29.0
Stored energy	(MJ)	5800
Conductor type	—	Int. cooled cable
Conductor materials	—	NbTi, Cu, SS sheath
Conductor dimensions <sup>a</sup>	(cm)	3.14 × 3.14
Copper-to-superconductor ratio <sup>a</sup>	—	9.93
LHe to conductor ratio (vol.) <sup>a</sup>	—	0.54
<b>Weights:</b>		
Conductor	(tonnes)	555
Insulation	(tonnes)	177
Substructure <sup>b</sup>	(tonnes)	100
Superstructure	(tonnes)	269
Thermal shield, inner	(tonnes)	28
<b>Total cold mass</b>	(tonnes)	<b>1129</b>
Thermal shield, outer, cold mass supports, etc	(tonnes)	63
Vacuum vessel	(tonnes)	362
Miscellaneous	(tonnes)	67
<b>Total magnet weight</b>	(tonnes)	<b>1621</b>

<sup>a</sup> Where graded winding is incorporated, values listed are for high field region of winding.

<sup>b</sup> Substructure consists of filler wedges and plates (Al alloy and G-10)

Table 4.2.7-I Sheet 3 of 3

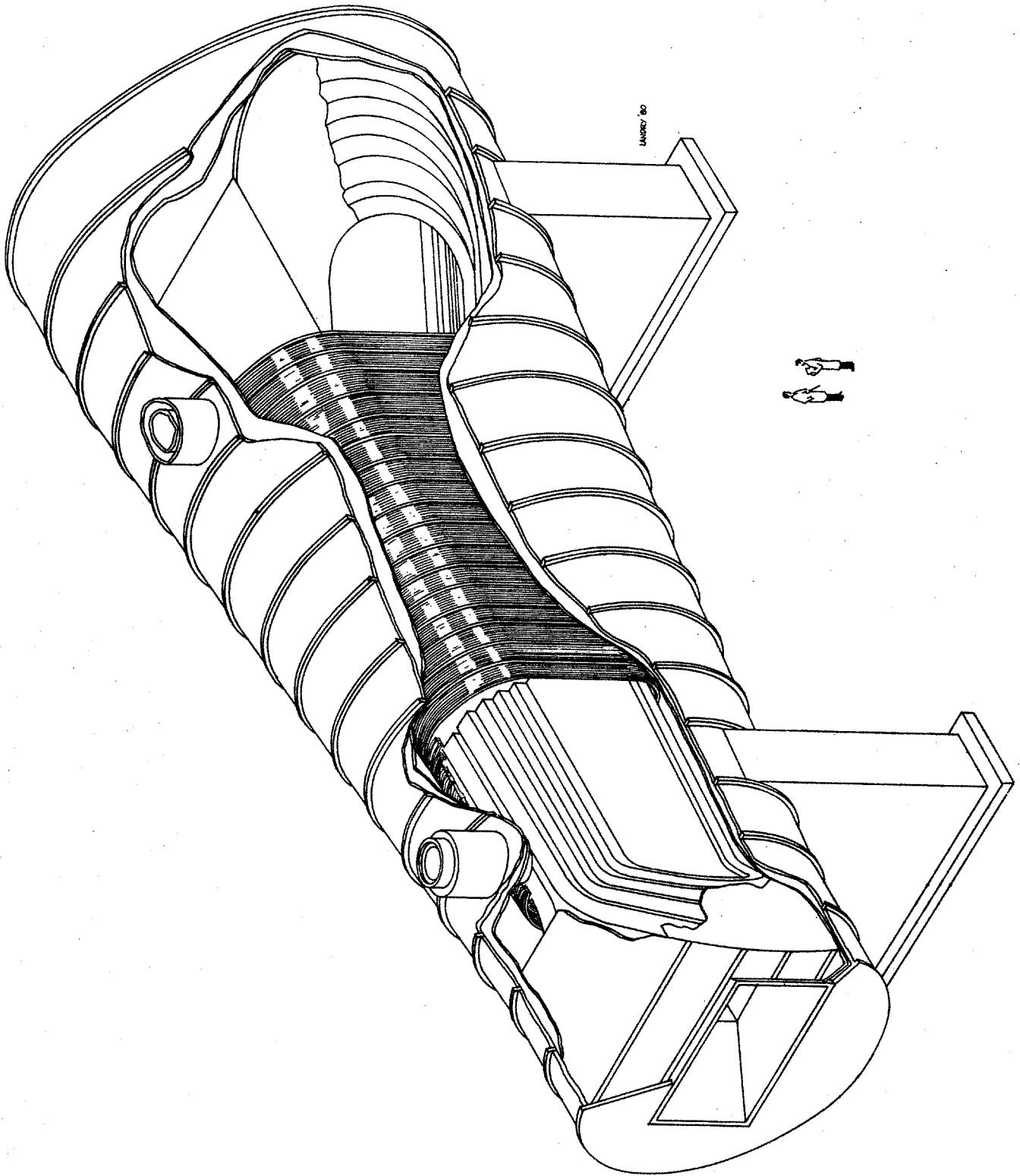
**Materials of construction:**

Winding substructure	—	Al alloy & G-10
Insulation	—	G-10
Superstructure	—	SS 304 LN
Conductor sheath	—	SS 304 LN
Thermal shield	—	SS 304 LN
Vacuum vessel	—	SS 304 LN

**Design stresses:**

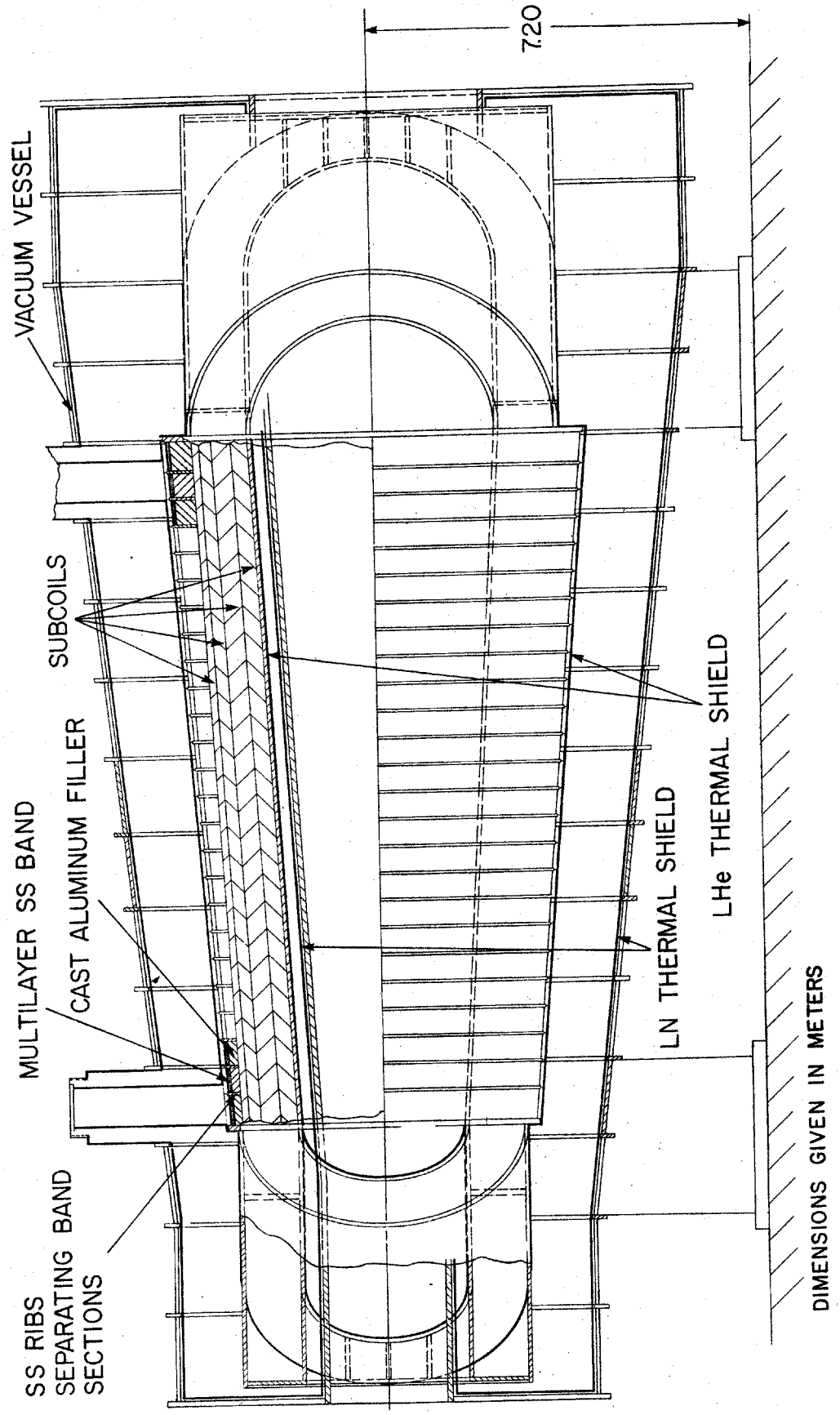
Superstructure (tension)	(MPa)	414
--------------------------	-------	-----

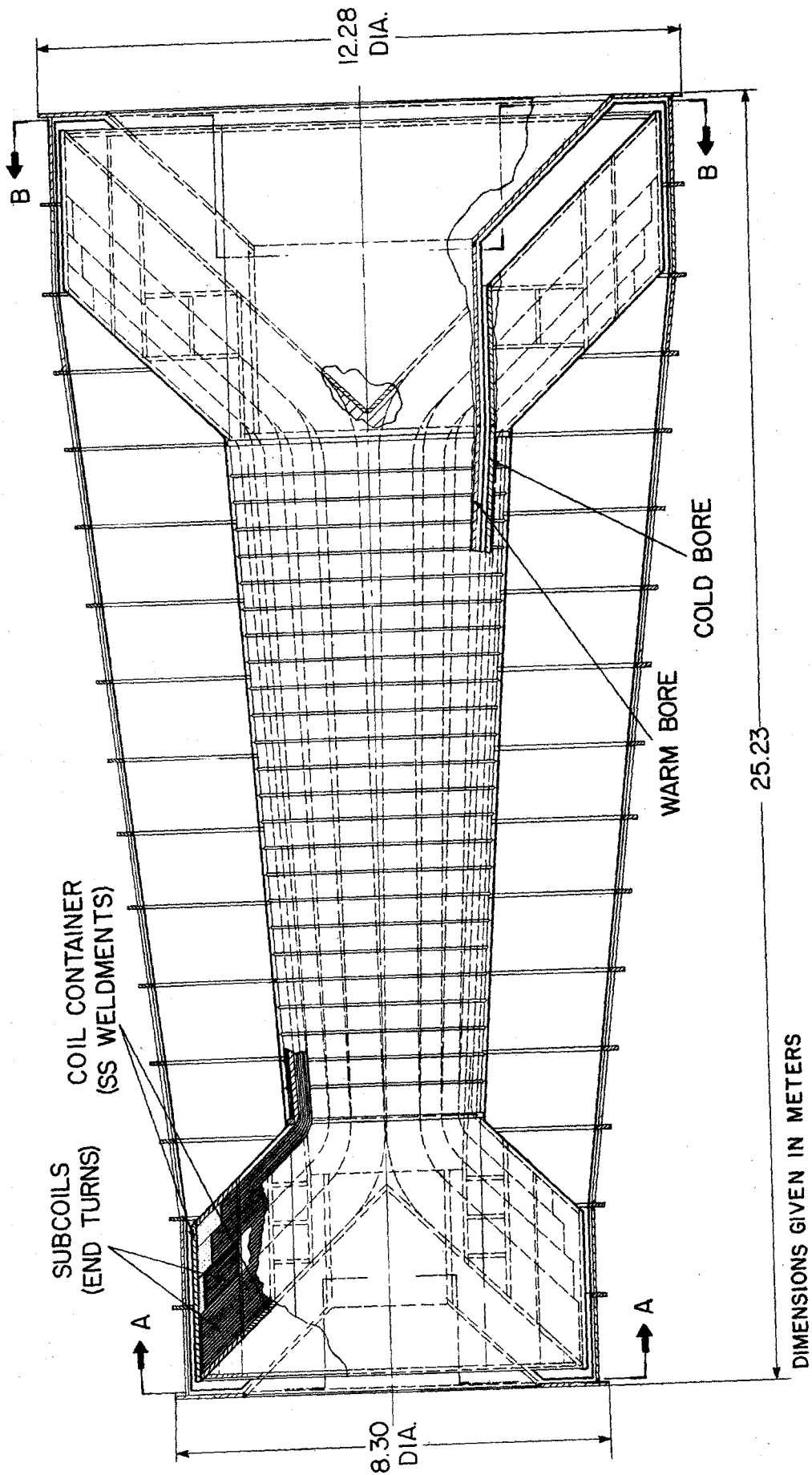




4.2.7A Cutaway View of Advanced Design Commercial Size MHD Magnet, ICCS/SM

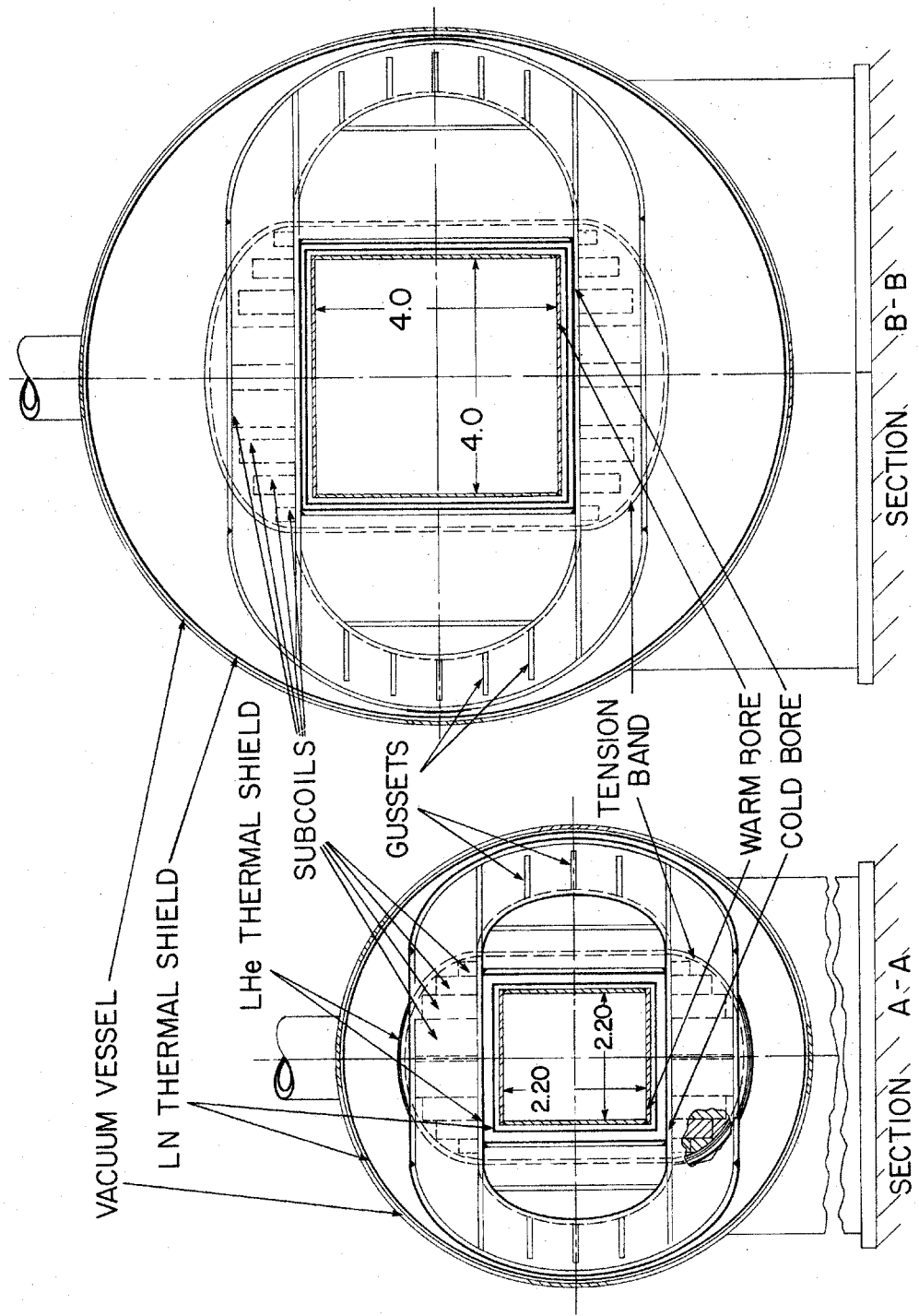
4.2.7B Elevation View of Advanced Design Magnet Assembly, ICCS/SM



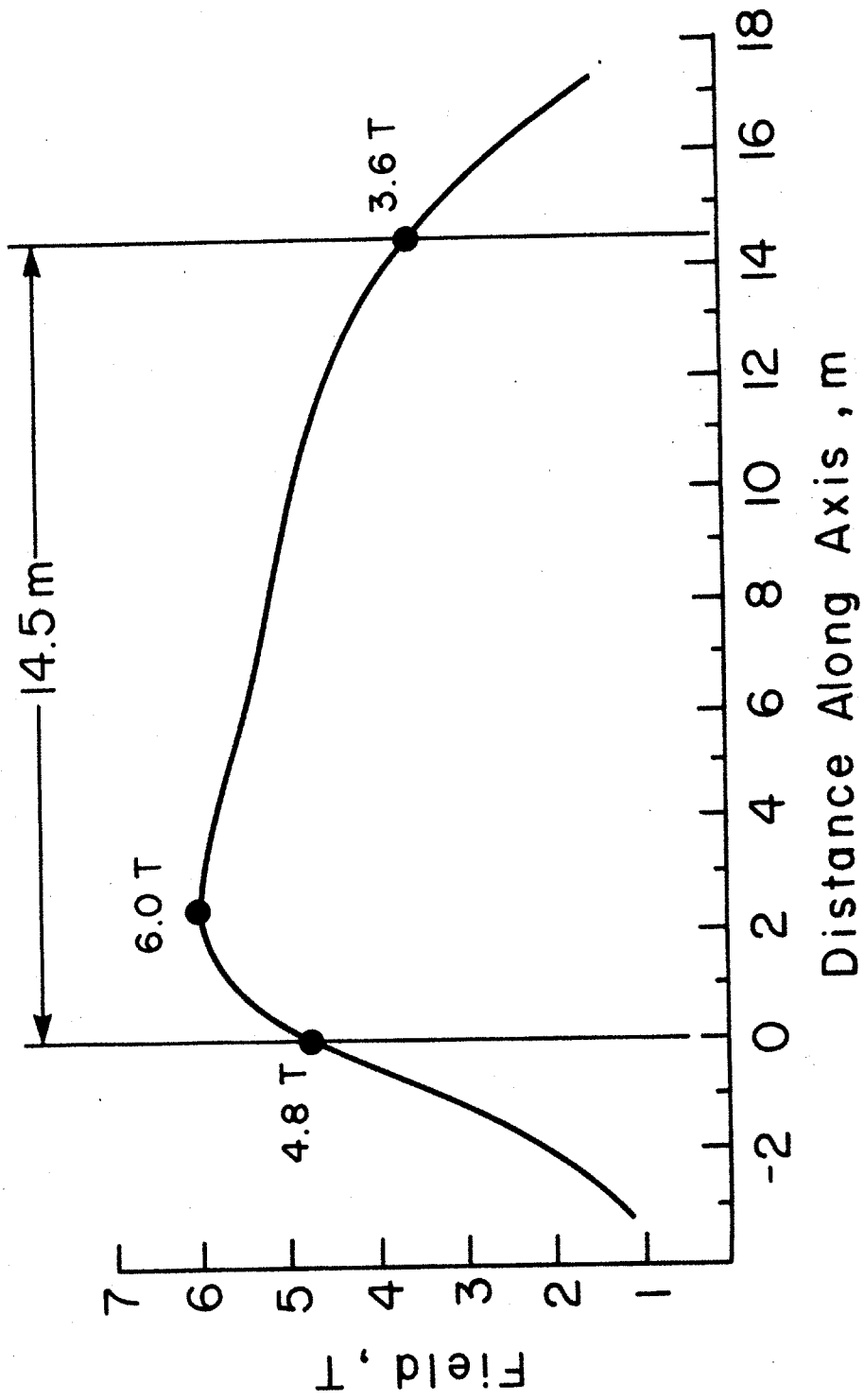


4.2.7C Plan View of Advanced Design Magnet Assembly, ICCS/SM

4.2.7D Inlet and Outlet Views of Advanced Design Magnet, ICCS/SM



DIMENSIONS GIVEN IN METERS



4.2.7E Curve of On-Axis Field vs Distance Along Axis for Advanced Design Magnet, ICCS/SM

4.2.7F Conductor-Insulation Arrangement in Winding, ICCS/SM

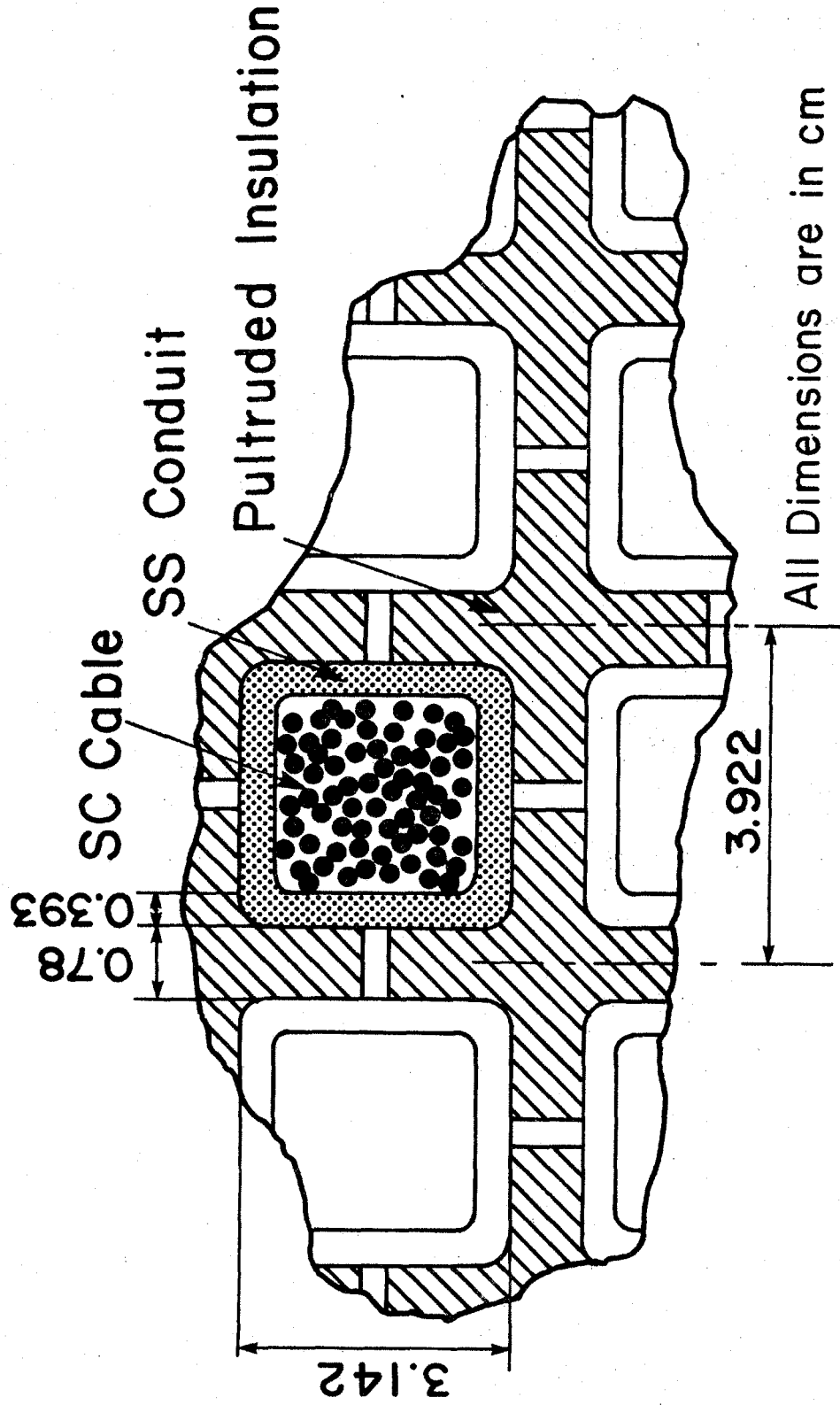


Table 4.2.8-1 Sheet 1 of 2  
Major Characteristics of ETF-Scale Magnet Reference and Conceptual Designs

Magnet designation	ETF-MCA	ETF6-P1	ETF6-2	AVCO-3	ETF6-NAS	ETF4-NAS
Designer	MCA	AVCO	AVCO	AVCO	MIT	MIT
Date of Design	1977	1977	1977	1979	1981	1981
Magnet type	90° rect. sad. + racetr.	Circ. sad.	90° rect. sad.	45° rect. sad. + racetr.	60° rect. sad.	60° rect. sad.
Peak on-axis field (T)	6.0	6.0	6.0	6.0	6.0	4.0
Active field length (m) <sup>a</sup>	7.0(8.0)	7.0(8.0)	7.0(8.0)	8.9	12.1	12.1
Field at start of active length (T) <sup>a</sup>	6.0(4.8)	6.0(4.8)	6.0(4.8)	4.0	4.0	2.7
Field at end of active length (T)	4.0	4.0	4.0	4.0	3.5	2.3
Peak field in winding (T)	—	6.6	6.7	6.5	7.6	5.3
Aperture, start of active length, dimensions (m)	0.64 sq. <sup>b</sup>	0.90 dia <sup>b</sup>	0.8 sq. <sup>b</sup>	1.5 sq. <sup>b</sup>	1.4×1.8 <sup>c</sup>	1.4×1.8 <sup>c</sup>
Aperture, start of active length, area (m <sup>2</sup> )	0.41	0.64	0.64	2.25	2.52	2.52
Aperture, end of active length, dimensions (m)	1.24 sq. <sup>b</sup>	1.75 dia <sup>b</sup>	1.6 sq. <sup>b</sup>	2.28 sq. <sup>b</sup>	2.06×2.69 <sup>c</sup>	2.06×2.69 <sup>c</sup>
Aperture, end of active length, area (m <sup>2</sup> )	1.54	2.4	2.56	5.18	5.54	5.54
Warm bore (active) volume (m <sup>3</sup> ) <sup>a</sup>	6.4(7.3)	10.0(11.4)	10.5(12.0)	32.2	47.6	47.6
Vacuum vessel overall length (m)	13	12	12.1	14.9	16.6	16.6
Vacuum vessel outside dimensions (m)	6.0 dia	6.6 dia	5.8×6.6	10.2×10.5	8.4 dia	7.9 dia
Conductor type <sup>d</sup>	Built-up	Built-up	Built-up	Built-up	Cable	Cable

<sup>a</sup> Values in parentheses are adjusted values based on definition of active length as starting at 80% of peak field. Field profile is unchanged. After 1977, design characteristics for most large MHD magnet designs were consistent with this definition.

<sup>b</sup> Dimensions inside warm bore, without liner

<sup>c</sup> Dimensions inside warm bore liner

<sup>d</sup> All conductors are NbTi/Cu composite

Table 4.2.8-I Sheet 2 of 2

Magnet Designation	ETF-MCA	ETF6-P1	ETF6-2	AVCO-3	ETF6-NAS	ETF4-NAS
Design current (kA)	20	5.5	5.5	13.5	24.4	25
Winding current density, average (J $\lambda$ )(10 <sup>7</sup> A/m <sup>2</sup> )	2.39	1.5	1.2	1.44	1.42	1.40
Conductor current density, (J)(10 <sup>7</sup> A/m <sup>2</sup> )	4.0	—	—	3.6	8.16 <sup>e</sup>	—
Copper-to-superconductor ratio, high field region	—	—	—	12	6.0	12.0
Heat flux (W/cm <sup>2</sup> )	1.0	—	—	0.4	<0.15 <sup>f</sup>	<0.15
Ampere turns (10 <sup>6</sup> NI)	16.0	19.2	18.7	26.6	27.9	18.0
Ampere meters (10 <sup>8</sup> Am)	4.0	4.4	—	8.8	10.8	6.9
Inductance (H)	5.8	54	—	19.8	9.9	4.2
Stored energy (MJ)	1160	820	684	1700	2900	1300
Weight: conductor (tonnes)	83	86	124	215	102	—
substructure and insulation (tonnes)	incl. below	140	incl. below	215	90	—
superstructure (tonnes)	221	238	255	344	incl. above	—
helium vessel (tonnes)	incl. above	37	incl. above	330	incl. above	—
thermal shield, cold mass supports, etc (tonnes)	incl. above	7	incl. above	33	30	—
vacuum vessel (tonnes)	72	27	70	327	157	—
miscellaneous (tonnes)	0	0	0	21	30	—
total magnet (tonnes)	376	535	449	1485	909	565
Superstructure material	SS 310S	Al 6061	Al 6061	Al & SS	SS 304 LN	SS 304 LN
Design stress (MPa)	379	179	—	251 & 359	414	414

<sup>e</sup> Current density in metal cross section

<sup>f</sup> Assumes all strands in cable 100% surface cooled



selection of the CSM as the preferred basic design alternative was made by MIT in 1980, in order that a suitable ETF magnet design would be available to meet the schedule date of September 1981 for issuing the final NASA LeRC report [38]. However, evaluation of design alternatives and magnet design features has not yet been completed and therefore the ETF design contained in the NASA LeRC report [38] should be regarded as a tentative selection only, subject to change as further evaluation and comparison of basic designs proceeds.

Descriptions of each of the designs summarized above and of other ETF magnet designs reviewed, together with cost estimates where applicable, are contained in the following sections.

#### **4.2.9 ETF Magnet Design by MCA, Rectangular Saddle and Racetracks**

The ETF magnet reference design described below was prepared in 1976 and 1977 as a part of the same ERDA-sponsored program at MCA that developed the baseload magnet reference design described in Section 4.2.2. The ETF design is a scaled-down version of the baseload design.

The design criteria established by ERDA for this ETF reference design are listed in Table 4.2.9-I. The same criteria were used for the AVCO ETF magnet designs described in Sections 4.2.10 and 4.2.11.

The MCA ETF magnet design incorporates a 20 kA copper-stabilized NbTi "built-up" conductor similar to that used in the MCA baseload design. The winding consists of a total of six coils, four of racetrack configuration and two of 90° saddle configuration. As in the baseload design, the sides of the coils diverge to produce the required tapered field profile, the coils are enclosed in individual stainless steel containers which serve also as helium containment vessels, and the major force containment structure which is made of stainless steel is external to the helium containment vessels. Winding and structure details are similar to those of the MCA baseload design, Section 4.2.2.

The Dewar, similar in concept to that of the baseload design, consists of a helium gas-cooled thermal radiation shield surrounding the cold mass (coils and structure), a cylindrical outer vacuum shell, dished end covers and a square cross section room temperature bore tube, all of aluminum alloy. The cold mass of the magnet is carried on four low heat leak columns which transmit the load to the magnet foundation.

The characteristics of the MCA ETF magnet design are listed in Table 4.2.9-II. The calculated axial field profile is shown in Figure 4.2.9A and the coil configuration is shown in Figure 4.2.9B. The magnet assembly is shown in Figures 4.2.9C and 4.2.9D.

In comparing the MCA ETF magnet design with the AVCO ETF designs described in Sections 4.2.10 and 4.2.11, it should be kept in mind that the MCA (square) bore cross section is smaller than both AVCO square and circular bore cross sections by a factor of 0.64. The same situation exists with respect to the MCA and AVCO baseload designs described in Sections 4.2.2, 4.2.3 and 4.2.4. The MCA magnet is therefore smaller in terms of MHD power generation capability than the AVCO magnet.

The major accessory subsystems for the MCA ETF magnet are a cryogenic system for magnet cooldown, steady state operation and warmup and a power supply system for magnet charging and discharging. These subsystems, shown diagrammatically in Figure 4.2.9E, are similar in design and operation to those for the MCA baseload magnet described in Section 4.2.2.

The fabrication plan for the ETF magnet components is similar to that for the MCA baseload magnet components outlined in Section 4.2.2. However, the assembly plan is different in that all assembly will be accomplished off-site. The completed ETF magnet and Dewar assembly will be shipped as a unit from the assembly facility to the power plant site.

Table 4.2.9-I

Design Criteria For an ETF-Scale MHD Magnet:  
Estimated MHD Power, 40 MWe

Channel Inside Dimensions

Inlet 0.5 m × 0.5 m

Exit 1.0 m × 1.0 m

Active length 7.0 m

Magnetic Field

Inlet, Active Length 6.0 T

Exit, Active Length 4.0 T

Magnet Field Uniformity ±5% across duct &  
deviation from linear taper

Warm Bore Dimensions

Inlet 0.9 m dia

Exit 1.75 m dia

Operating Temperature 4.5 K

Table 4.2.9-II Sheet 1 of 3

Design Characteristics  
ETF MHD Magnet Design ETF-MCA  
Magnetic Corporation of America

Date of design		1977
MHD power train data		
MHD power output (estimated)	(MWe)	40
Magnet data		
Magnet type	—	90° rect. sad. & racetracks
Warm bore liner?	—	No
Magnetic field:		
Peak on-axis field	(T)	6.0
Active field length <sup>a</sup>	(m)	7.0 (8.0)
Field at start of active length <sup>a</sup>	(T)	6.0 (4.8)
Field at end of active length	(T)	4.0
Field uniformity at end of active length <sup>b</sup>	(%)	+7.3    -0
Dimensions:		
Aperture, warm bore inlet <sup>c</sup>	(m)	0.64 sq.
Aperture, start of active length <sup>c</sup>	(m)	0.64 sq.
Aperture, end of active length <sup>c</sup>	(m)	1.24 sq.
Aperture, warm bore exit <sup>c</sup>	(m)	1.24 sq.
Aperture area, start of active length <sup>c</sup>	(m <sup>2</sup> )	0.41
Aperture area, end of active length <sup>c</sup>	(m <sup>2</sup> )	1.54
Vacuum vessel overall length	(m)	13
Vacuum vessel outside dia.	(m)	6
Warm bore volume, active <sup>a,c</sup>	(m <sup>3</sup> )	6.4 (7.3)

<sup>a</sup> Values in parentheses are adjusted values based on definition of active length as starting at 80% of peak field. Field profile is unchanged. After 1977, design characteristics for most large MHD magnet designs were consistent with this definition.

<sup>b</sup> Field uniformity is + and - variation from on-axis field, central 50% of warm bore cross section

<sup>c</sup> Dimensions inside warm bore, without liner

Table 4.2.9-II Sheet 2 of 3

Winding characteristics:

Number of winding modules (or layers) per half	—	3 (1 sad, 2 r.t.)
Design current, I	(kA)	20
Winding current density, average, $J\lambda^a$	( $10^7$ A/cm <sup>2</sup> )	2.39
Packing factor, $\lambda^a$	—	—
Conductor current density, $J^a$	( $10^7$ A/cm <sup>2</sup> )	4.0
Total number of turns, N	—	792
Total length of conductor	(km)	19.9
Ampere turns, NI	( $10^6$ A)	16.0
Ampere meters	( $10^8$ Am)	4.0
Inductance	(H)	5.8
Stored energy	(MJ)	1160
Conductor type	—	Built-up
Conductor materials	—	NbTi Cu
Conductor dimensions <sup>a</sup>	(cm)	2.54 × 2.17
LHe to conductor ratio (vol.) <sup>a</sup>	—	0.26
Heat flux <sup>a</sup>	(W/cm <sup>2</sup> )	1.0
<b>Weights:</b>		
Conductor	(tonnes)	83
Insulation	(tonnes)	incl. in struct.
Substructure	(tonnes)	incl. in struct.
Superstructure	(tonnes)	221
Liquid He vessel	(tonnes)	incl.
Thermal shield, cold mass supports, etc	(tonnes)	incl. in vac. jack.
Vacuum vessel	(tonnes)	72
Miscellaneous	(tonnes)	0
<b>Total magnet weight</b>	<b>(tonnes)</b>	<b>376</b>

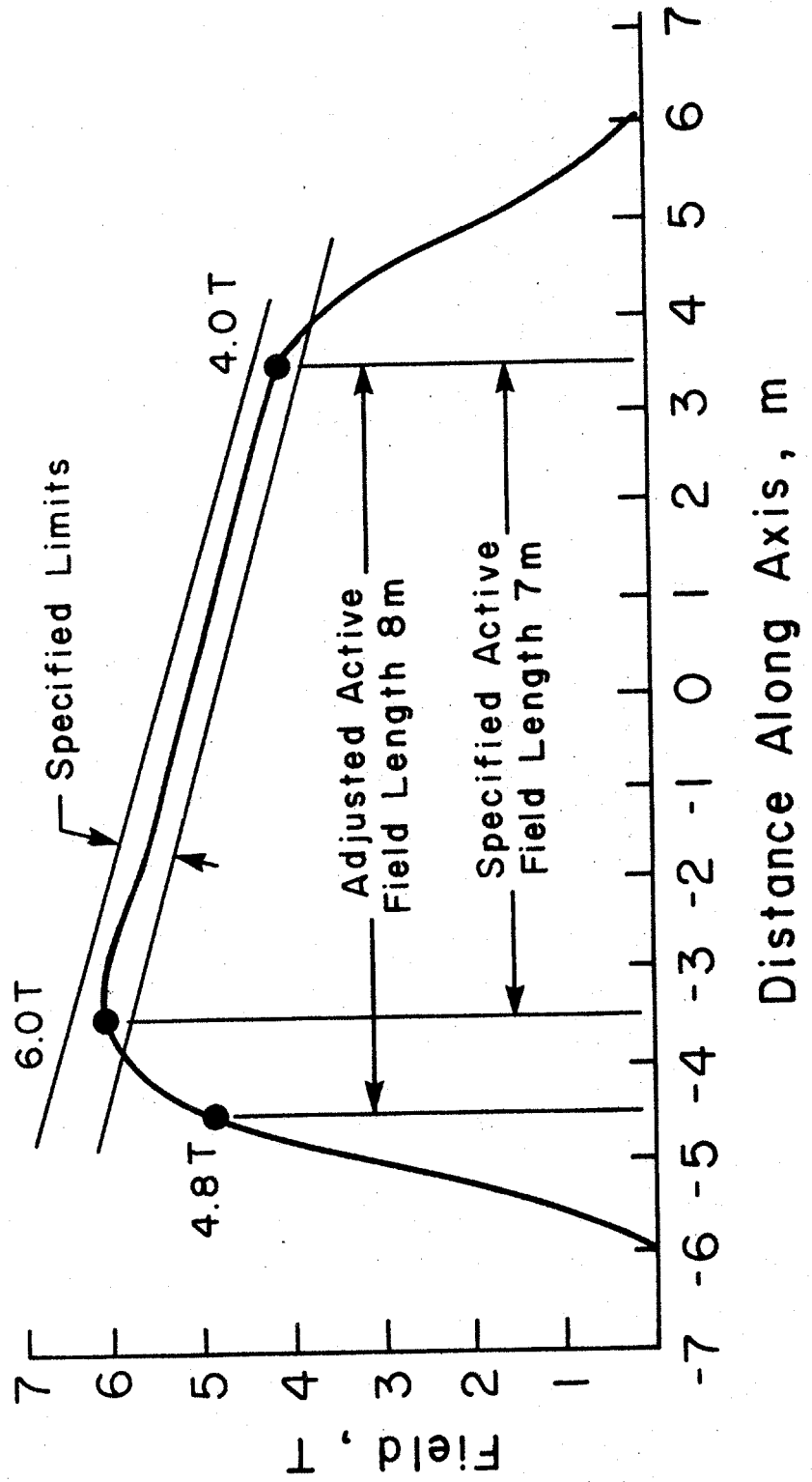
<sup>a</sup> Where graded winding is incorporated, values listed are for high field region of winding.

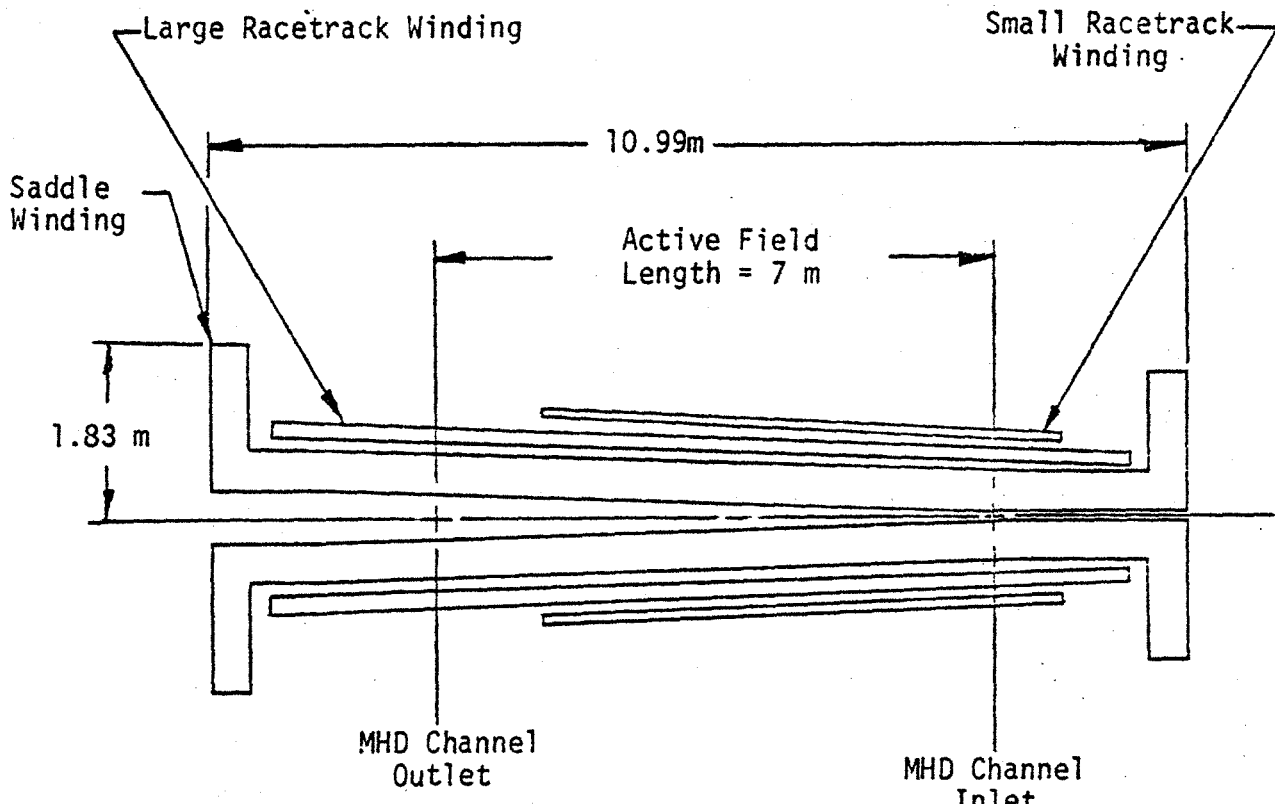
Table 4.2.9-II Sheet 3 of 3

Cryogenic data:		
Operating temperature at winding	(K)	4.5
Operating temperature, thermal shield	(K)	102
Coolant, thermal shield	—	He gas
Heat loads LHe region, not incl. leads	(W)	39 <sup>a</sup>
LHe for lead cooling at design current	(ℓ/hr)	60
Materials of construction:		
Winding substructure	—	SS 310 S
Insulation	—	Epoxy/glass
Superstructure	—	SS 310 S
Liquid helium vessel	—	SS 310 S
Thermal shield	—	Al 5083
Vacuum vessel	—	Al 5083
Design stresses:		
Winding substructure	(MPa)	379
Superstructure (tension)	(MPa)	379
Superstructure (bending)		379
Pressure rating		
Liquid helium vessel		
Normal operating	(atm)	1.3

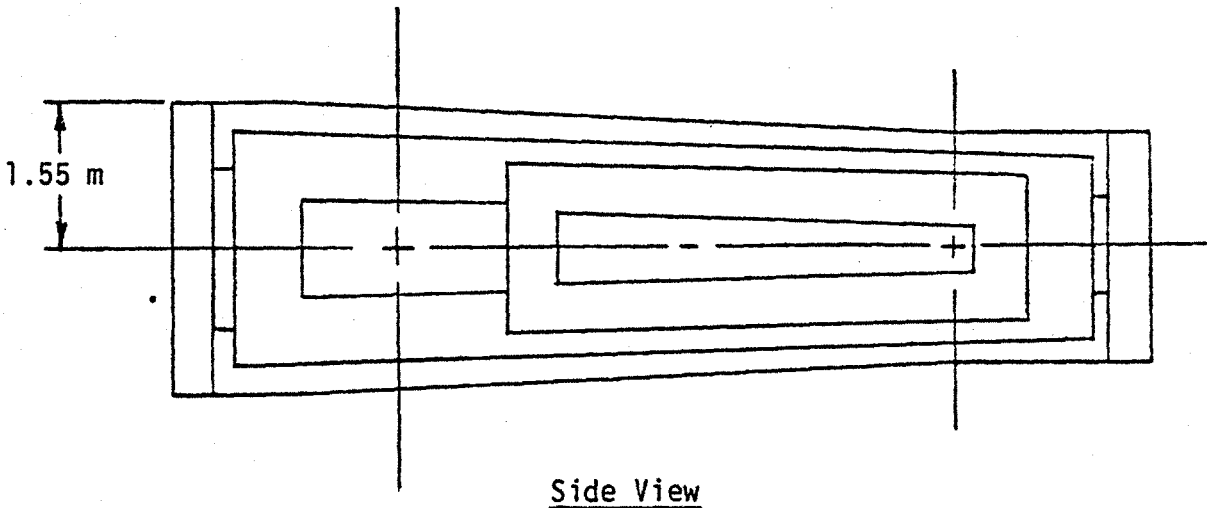
<sup>a</sup> Not including conductor splice loss.

4.2.9A Curve of On-Axis Field vs Distance Along Axis for MCA ETF Magnet Design





Top View

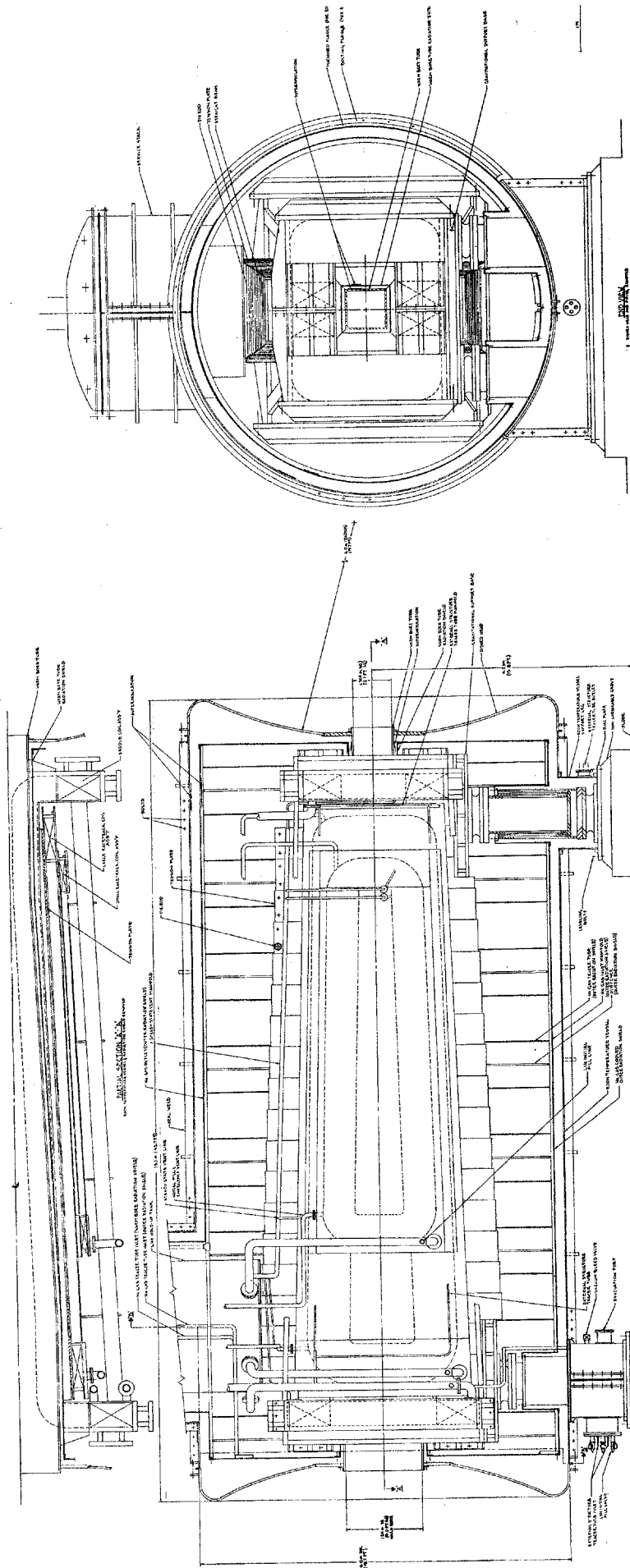


Side View

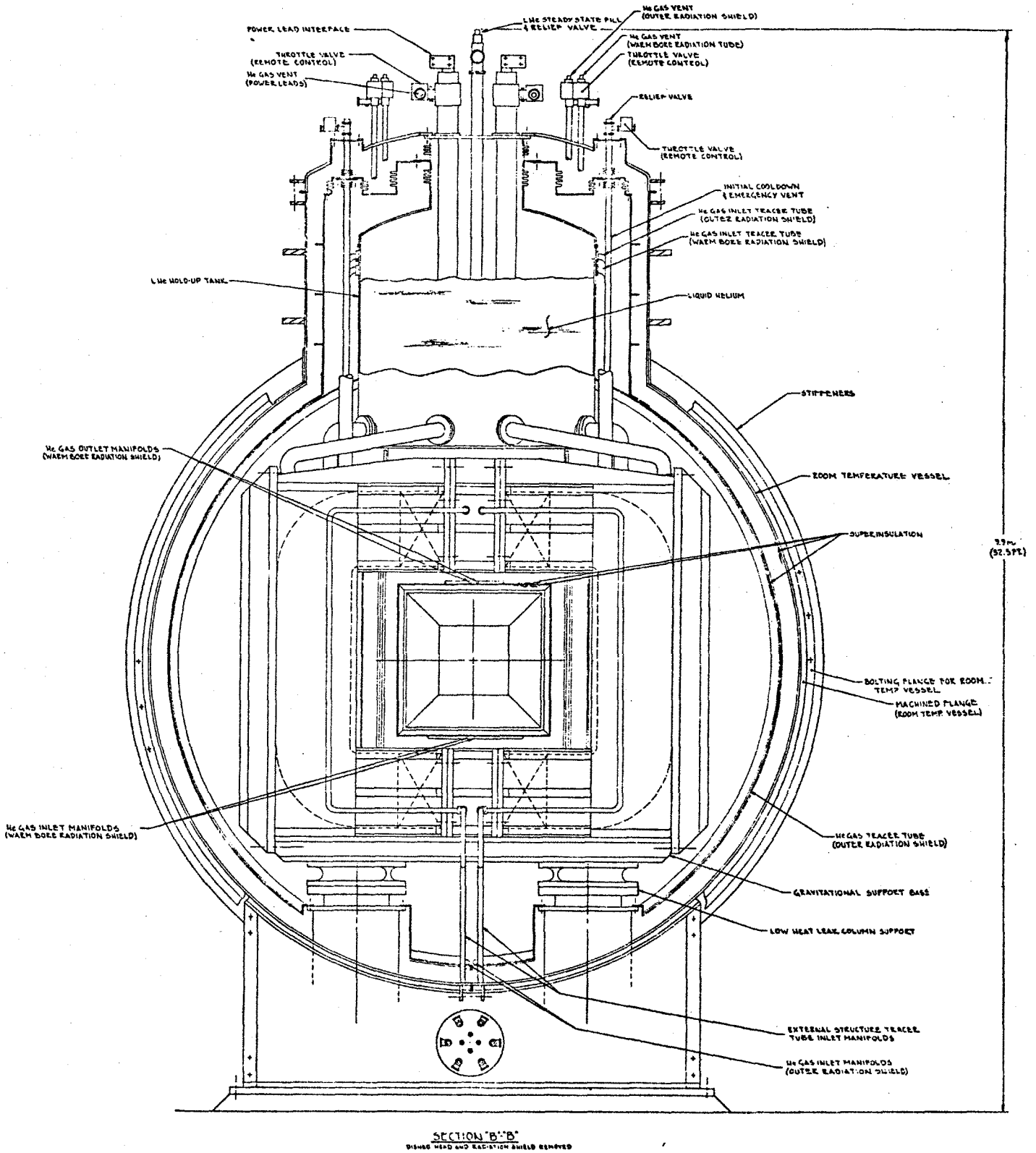
1 meter

4.2.9B Diagram Showing Magnet Winding Configuration, MCA ETF Magnet Design

4.2.9C Elevation View, MCA ETF Magnet Assembly

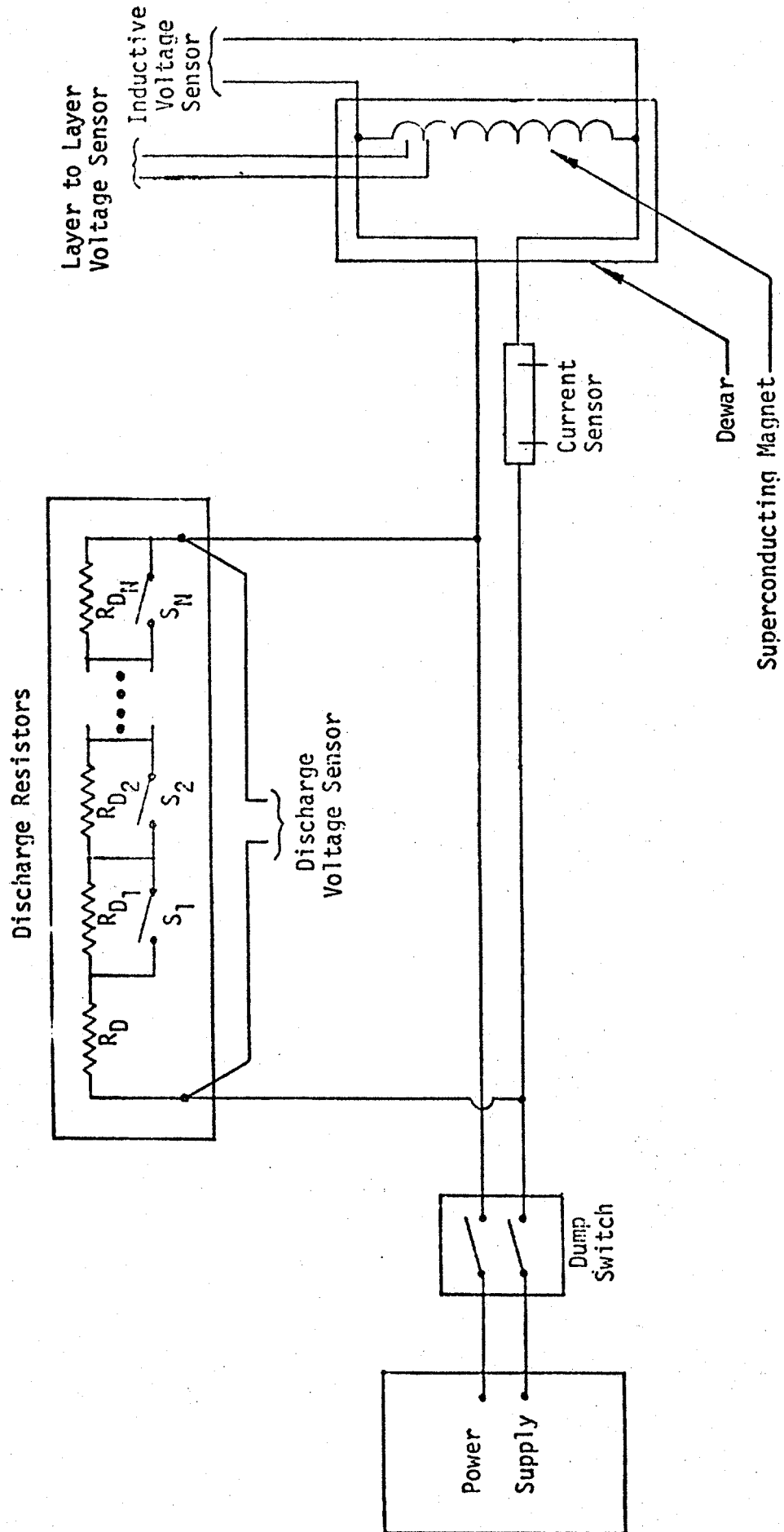






4.2.9C

Elevation View, MCA ETF Magnet Assembly



The total weight of the ETF magnet assembly,  $3.76 \times 10^5$  kg, is less than that of the saddle coil assembly of the baseload magnet,  $5.01 \times 10^5$  kg. The overall length and height of the ETF magnet, 13 m and 6 m respectively, are less than the corresponding dimensions of the baseload saddle coil, 23.3 m and 6.2 m. Therefore, shipment of the ETF magnet assembly can be accomplished using transportation arrangements similar to those proposed for shipping the baseload saddle coil assembly from the coil assembly facility to the plant site.

The estimated costs for one ETF magnet system are shown in Table 4.2.9-III. The total estimated installed cost is  $\$16 \times 10^6$ . The estimated schedule shows a three year program including an initial 12 months of preliminary design and development. Completion of the magnet system occurs 24 months after start of the final (Title II) design.

More detailed information on the MCA ETF magnet design is contained in Reference 57.

#### 4.2.10 ETF Magnet Design by AVCO, Circular Saddle, ETF6-P1

The ETF 6 T magnet reference design described below was developed in 1976 and 1977 as a part of the ERDA-sponsored program at AVCO that developed the baseload magnet reference designs described in Sections 4.2.3 and 4.2.4. The ETF design is a scaled-down version of the baseload design, BL6-P1. MEA and IGC, under subcontract to AVCO, assisted in the preparation of this design.

The design criteria established by ERDA for this ETF reference design are listed in Table 4.2.9-I. The same criteria were used for the MCA ETF magnet design described in Section 4.2.9.

The AVCO ETF magnet design ETF6-P1 is a circular-saddle-coil magnet design with a circular-cross-section warm bore. It incorporates a 5500 ampere built-up copper and NbTi composite conductor, consisting of a rectangular-cross-section copper substrate with a spiral wrapping of NbTi/Cu composite wire soldered in place. The conductor components are readily available items. The winding is modular, with saddle-shaped winding layers installed in grooves in conical aluminum alloy structural shells which are stacked concentrically around a central core tube to make up the winding assembly. The shells form a substructure which supports groups of conductors and prevents the accumulation of magnetic loading on the conductor bundle as a whole. The shells themselves carry the axial magnetic load; they transmit radially-outward loads to the surrounding superstructure.

The substructure shells are conical, so that the winding layers diverge from the magnet axis going toward the channel exit end, thus producing the desired tapered field profile. There are ten structural shells in each coil half, with two layers of conductor in each shell. The liquid helium containment vessel consists of a conical outer shell wrapped around the winding and substructure, a pair of end plates and the core tube which forms the inner wall of the vessel. The entire vessel is of welded aluminum alloy construction. The major force containment structure (superstructure) is a series of aluminum alloy ring girders with bolted joints assembled around the outer envelope of the winding assembly liquid helium containment vessel.

The Dewar includes an aluminum alloy thermal radiation shield cooled by tracer tubes supplied with cold helium gas, and an aluminum alloy room temperature vacuum jacket consisting of a conical outer shell, dished heads and a conical warm bore tube, all of welded construction. The cold mass of the magnet is supported by a system of low-heat-leak tubular struts of titanium alloy including four vertical struts, two transverse struts and one longitudinal strut.

The characteristics of the AVCO ETF (ETF6-P1) circular saddle reference design are listed in Table 4.2.10-I. The calculated axial field profile is shown in Figure 4.2.10A, the coil configuration in Figure 4.2.10B, upper view, typical winding cross section in Figure 4.2.10C and the magnet assembly in Figure 4.2.10D.

Table 4.2.9-III

ETF Magnet System Cost Estimates - (ETF MCA)  
Magnetic Corporation of America

Material Costs (\$10<sup>6</sup>)

Conductor	4.98
Structure	2.19
Dewar	0.52
Tooling	1.08
Misc. and Shipping	<u>1.32</u>
<b>Subtotal</b>	<b>10.1</b>
Administrative Expenses	<u>3.0</u>
<b>Subtotal</b>	<b>13.1</b>
Labor for Design and Fabrication (\$ × 10 <sup>6</sup> )	<u>2.9</u>
<b>TOTAL</b>	<b>16.0</b>

Table 4.2.10-1 Sheet 1 of 3

Design Characteristics  
 ETF MHD Magnet Design ETF6-P1  
AVCO Everett Research Laboratory Inc.

Date of design		1977
MHD power train data		
MHD power output (estimated)	(MWe)	40
Magnet data		
Magnet type	—	circ. sad.
Warm bore liner?	—	No
Magnetic field:		
Peak on-axis field	(T)	6.0
Active field length <sup>a</sup>	(m)	7.0(8.0)
Field at start of active length <sup>a</sup>	(T)	6.0(4.8)
Field at end of active length	(T)	4.0
Dimensions:		
Aperture, warm bore inlet <sup>b</sup>	(m)	0.9
Aperture, start of active length <sup>b</sup>	(m)	0.9
Aperture, end of active length <sup>b</sup>	(m)	1.75
Aperture, warm bore exit <sup>b</sup>	(m)	1.75
Aperture area, start of active length <sup>b</sup>	(m <sup>2</sup> )	0.64
Aperture area, end of active length <sup>b</sup>	(m <sup>2</sup> )	2.4
Vacuum vessel overall length	(m)	12
Vacuum vessel outside dia.	(m)	6.6
Warm bore volume, active <sup>a,b</sup>	(m <sup>3</sup> )	10(11.4)

<sup>a</sup> Values in parentheses are adjusted values based on definition of active length as starting at 80% of peak field. Field profile is unchanged. After 1977, design characteristics for most large MHD magnet designs were consistent with this definition.

<sup>b</sup> Dimensions inside warm bore, without liner

Table 4.2.10-1 Sheet 2 of 3

## Winding characteristics:

Number of winding modules (or layers) per half	—	36
Design current, I	(kA)	5.5
Winding current density, average, $J\lambda^a$	( $10^7$ A/cm <sup>2</sup> )	1.5
Packing factor, $\lambda^a$	—	0.345
Conductor current density, $J^a$	( $10^7$ A/cm <sup>2</sup> )	4.52
Total number of turns, N	—	3490
Total length of conductor	(km)	80
Ampere turns, NI	( $10^6$ A)	19.2
Ampere meters	( $10^8$ Am)	4.4
Inductance	(H)	54
Stored energy	(MJ)	820
Conductor type	—	Built-up
Conductor materials	—	NbTi Cu
Conductor dimensions <sup>a</sup>	(cm)	$1.52 \times 0.89$
Copper- to-superconductor ratio <sup>a</sup>	—	18
LHe to conductor ratio (vol.) <sup>a</sup>	—	0.5
Heat flux <sup>a</sup>	(W/cm <sup>2</sup> )	0.45
Weights:		
Conductor	(tonnes)	86
Insulation and misc.	(tonnes)	9
Substructure	(tonnes)	131
Superstructure	(tonnes)	238
Liquid He vessel	(tonnes)	37
Total cold mass	(tonnes)	501
Thermal shield, cold mass supports, etc	(tonnes)	7
Vacuum vessel	(tonnes)	27
Miscellaneous	(tonnes)	0
Total magnet weight	(tonnes)	535

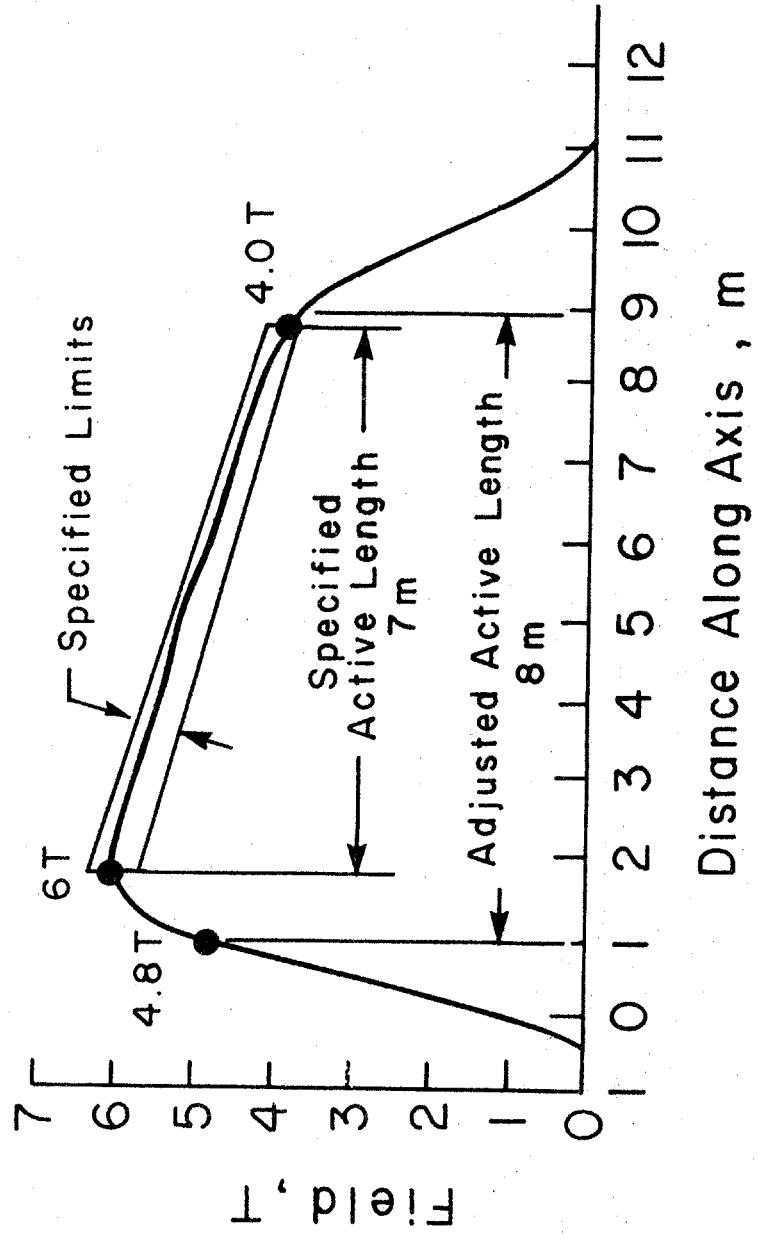
<sup>a</sup> Where graded winding is incorporated, values listed are for high field region of winding.

Table 4.2.10-1 Sheet 3 of 3

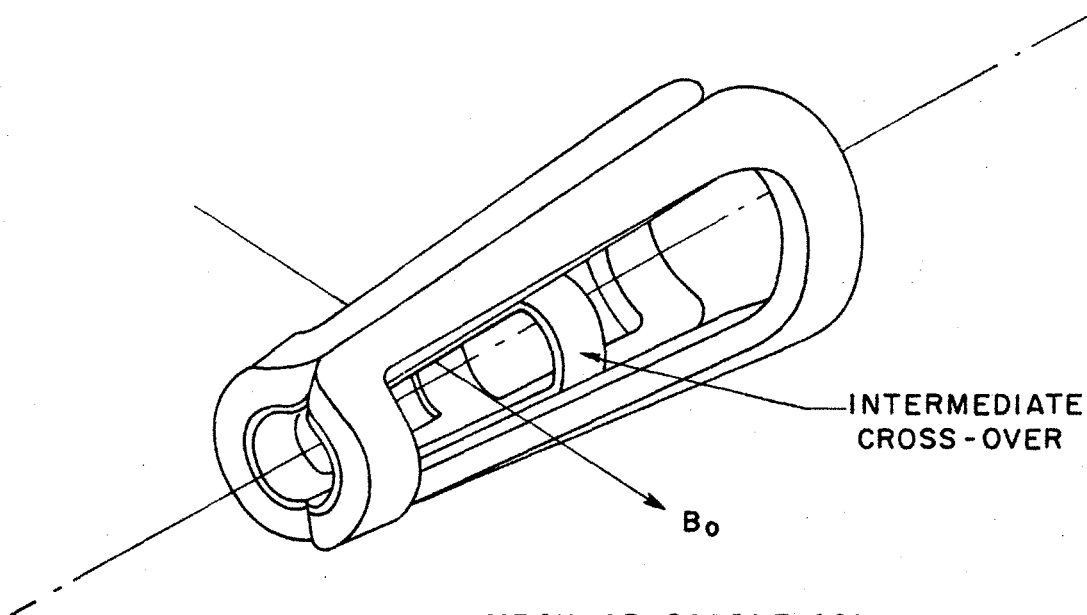
<b>Cryogenic data:</b>		
Operating temperature at winding	(K)	4.5
Operating temperature, thermal shield	(K)	80
Coolant, thermal shield	—	He gas
Heat loads LHe region, not incl. leads <sup>a</sup>	(W)	100
LHe for lead cooling at design current	(ℓ/hr)	16.5
<b>Power supply and discharge data:</b>		
Number of current leads	—	2
Rated voltage, power supply	(V)	20
Minimum charge time	(hrs)	4
Resistance, emergency dump resistor	(Ω)	0.11
Maximum discharge voltage, terminal	(V)	610
<b>Materials of construction:</b>		
Winding substructure	—	Al 5083
Insulation	—	G-10
Superstructure	—	Al 6061
Liquid helium vessel	—	Al 5083
Thermal shield	—	Al 6061
Vacuum vessel	—	Al 5083
<b>Design stresses:</b>		
Superstructure (bending)	(MPa)	179
<b>Pressure rating</b>		
Liquid helium vessel		
Normal operating	(atm)	1.3

<sup>a</sup> Not including conductor splice loss.

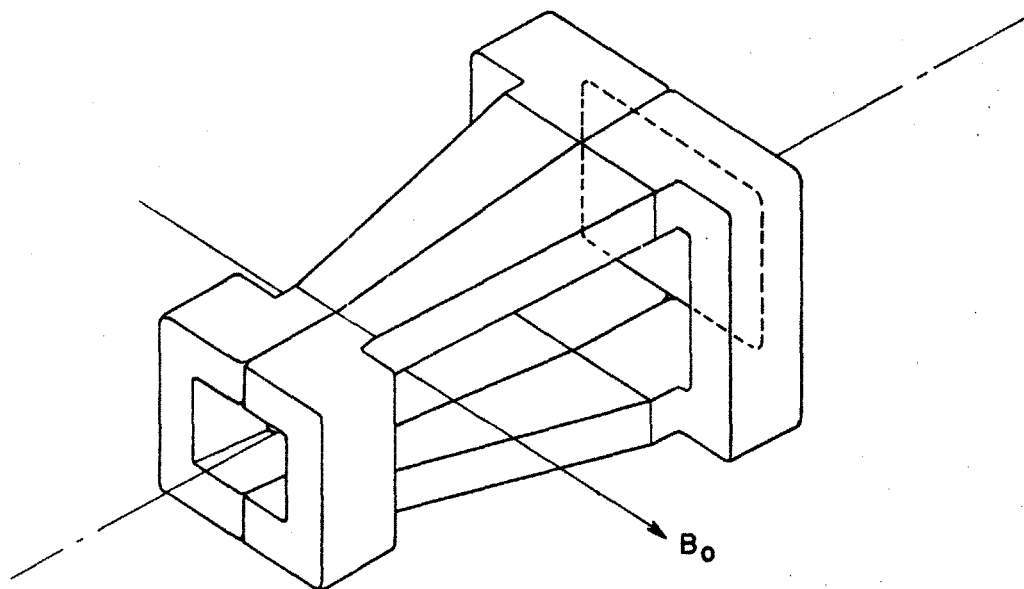
4.2.10A Curve of On-Axis Field vs Distance Along Axis for AVCO EIF Magnet, ETF6-P1







CIRCULAR SADDLE COIL  
 TAPERED, WITH INTERMEDIATE CROSS-OVER  
 (ETF6-P1)



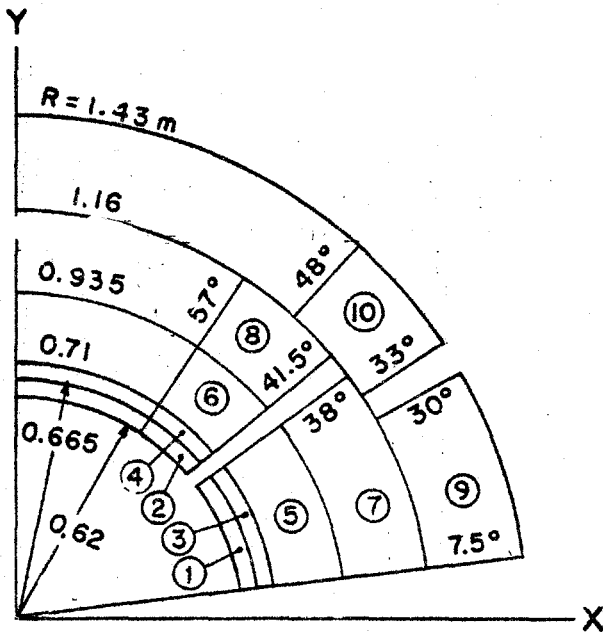
RECTANGULAR SADDLE COIL  
 TAPERED  
 (ETF6-P2)

4.2.10B Diagram Showing Coil Configuration, AVCO ETF Magnet, ETF6-P1 (circular saddle) and ETF6-P2 (rectangular saddle)

NOTES:

1. AREAS DENOTED BY NUMBERS IN CIRCLES, (X), ARE
1. AREAS WHERE CONDUCTOR BUNDLES ARE LOCATED (CALLED "SHELLS" IN COMPUTER PROGRAM)
2. WINDING ROTATED 90° IN MAGNET

TAPER HALF-ANGLE 2.9°  
 INTERMEDIATE CROSS-OVERS,  
 SHELLS 1, 2, 3, 4  
 DESIGN CURRENT DENSITY 1560 A/cm<sup>2</sup>

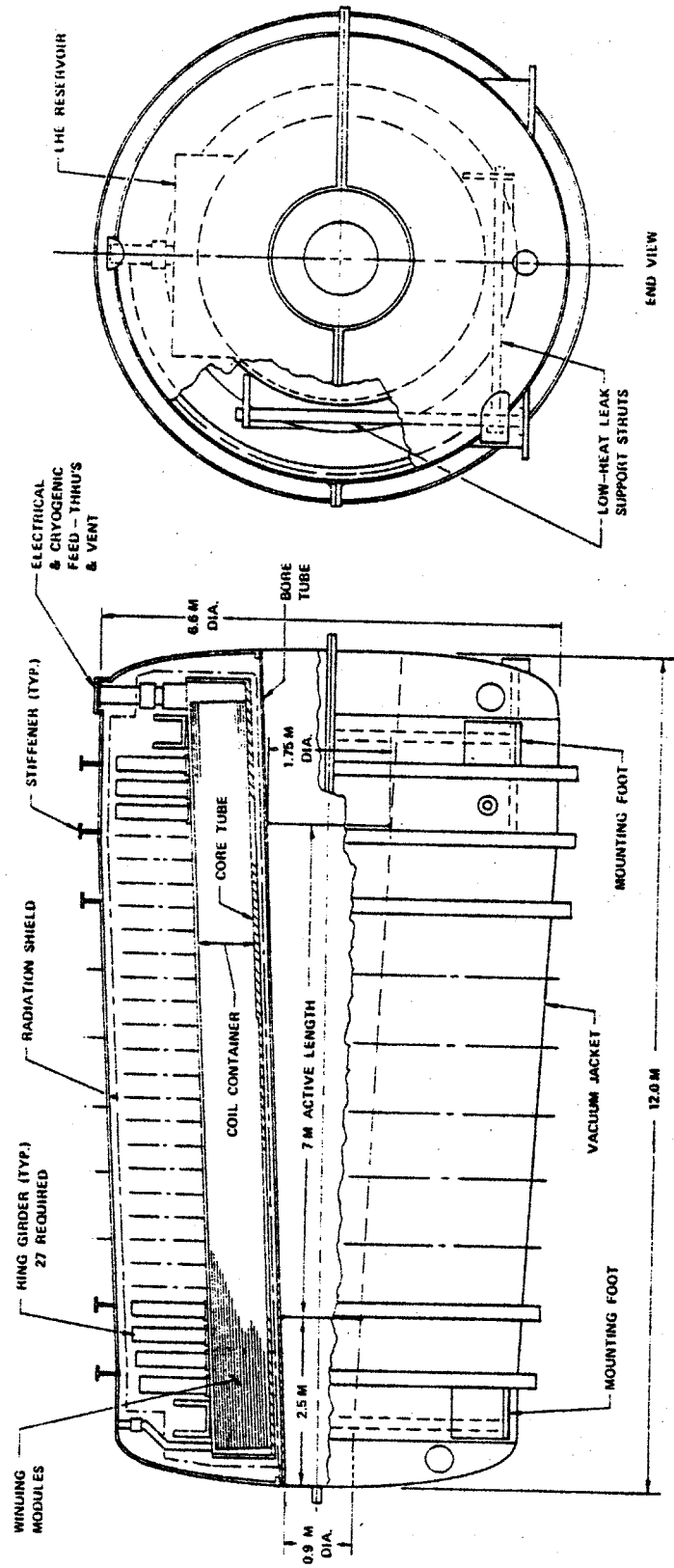


SHELL LENGTHS AND SHELL STARTING ANGLES AT REFERENCE PLANE Z = 8.7 m

SHELL NO.	LENGTH O. A.	STARTING ANGLE AT 8.7 m
1	6.0	7.5°
2		47.0°
3	8.0	7.5°
4		47.0°
5	10.3	7.5°
6		47.0°
7	10.3	7.5°
8		47.0°
9	10.3	7.5°
10		39.0°

4.2.10C Typical Winding Cross Section (One Quadrant) AVCO ETF Magnet, ETF6-P1

4.2.10D Elevation and End View of Magnet Assembly, AVCO EIF Magnet, ETF6-PI



The AVCO design anticipates that a cryogenic system, including a closed-loop helium refrigerator of a type currently available, would be used to cool down the magnet and maintain it at operating temperature. A power supply subsystem is proposed as shown in Figure 4.2.10E. A single rectifier power supply unit is connected to the magnet coils through two vapor-cooled leads. A system of discharge resistors and switches (circuit breakers) provide for both routine and emergency (fast) discharge of the magnet coils. A fault detecting system is installed, similar to that of the baseload magnet described in Section 4.2.3.

In the manufacturing plan proposed by AVCO, the conductor will be shipped fully assembled from the superconductor manufacturer to the coil fabrication and assembly facility where it will be wound into grooves in the structural shells to form winding and substructure modules. The modules will then be assembled on the core tube. The outer wall of the helium containment vessel will be installed around the winding assembly and the end covers will be welded in place. The assembled coils and container will then be shipped to the power plant site. Main structural components and Dewar components will be prefabricated at manufacturing facilities and shipped to the plant site where they will be assembled with the coil and container assembly to constitute the complete magnet.

The costs for one ETF magnet, design ETF6-P1, as estimated by AVCO, are shown in Table 4.2.10-II. The total estimated installed cost, including design and engineering, accessory equipment and other cost items not included in Table 4.2.10-II is  $\$15.1 \times 10^6$ . The total cost includes the AVCO estimate of  $\$5.5 \times 10^6$  for components plus MIT estimates for other costs as listed in Table 4.2.10-III.

A schedule for manufacture and assembly was not included in AVCO's report. More detailed information on the AVCO ETF circular-saddle magnet design ETF6-P1 is contained in Reference 58.

#### **4.2.11 ETF Magnet Design by AVCO, Rectangular Saddle, ETF6-2**

The ETF 6 T magnet reference design described below was developed in 1976 and 1977 as a part of the ERDA-sponsored program at AVCO that developed the baseload and ETF magnet reference designs described in Sections 4.2.3, 4.2.4 and 4.2.10. The design ETF6-2 is similar in concept to the baseload design BL6-P2. MEA and IGC, under subcontract to AVCO, assisted in the preparation of this design.

The design criteria established by ERDA for this design are listed in Table 4.2.9-I.

The AVCO ETF magnet design ETF6-2 is a rectangular saddle coil magnet with a square-cross-section warm bore. The dimensions of the bore are such that the cross-sectional areas are the same as those of the circular-cross-section bore specified in the design criteria, Table 4.2.9-I.

The ETF6-2 conceptual design was developed in the first phase of the AVCO program. Work on this design was discontinued in the second phase of the AVCO program because of AVCO's (tentative) decision to concentrate effort on the circular-saddle design as a more promising concept. As a result, the ETF6-2 design is in an earlier stage of development than other ETF designs reported on, and cost estimates for this design were not prepared.

The AVCO ETF6-2 conceptual design incorporates 90° saddle coils wound with built-up copper and NbTi conductor consisting of a rectangular-cross-section copper substrate with a spiral wrapping of composite wire soldered in place. The winding is modular. Conductor bundles are installed in grooves in flat plate substructure members made of aluminum alloy turned up at the ends to form saddle-shaped modules, which are then stacked to form the two winding halves. Winding module taper, structural support arrangement, helium containment vessel configuration and vacuum jacket design are similar in material and design to those of the rectangular saddle baseload design BL6-P2.

Table 4.2.10-II  
 Summary - Estimated Component Costs and Assembly Labor  
 6 T ETF-Size Circular-Saddle Magnet Design - ETF6-P1  
 Avco Everett Research Laboratory, Inc.

<u>Components</u>	<u>Estimated</u>		<u>Total Cost</u> \$ × 10 <sup>3</sup>
	<u>Weight</u> 10 <sup>3</sup> kg	<u>Cost/kg</u> \$/kg	
Conductor (graded winding)	90 <sup>a</sup>	19.00	<u>1710</u>
Insulating spacers, etc.	9 <sup>a</sup>	10.00	90
Winding support shells	131	9.45	1240
Coil container (core tube, outer shells, end plates, etc.)	37	8.40	310
Ring girders	238	7.70	<u>1830</u>
Total cold structure			3470
Radiation shield	5	8.40	40
Vacuum jacket	27	8.60	230
Support struts, thermal insulaton and miscellaneous	2	20.00	<u>40</u>
Total, radiation shield, vacuum jacket, etc.			<u>310</u>
Total components (f.o.b. factory)			5490
Miscellaneous materials and supplies	—	—	<u>30</u>
Total component and material cost	—	—	5520
	<u>Labor</u>		<u>Man Weeks</u>
	Coil winding and module assembly (factory)		3000
	Assembly of magnet (partial at factory, final on-site)		2100

*a* includes 5% margin over calculated weight

Notes:

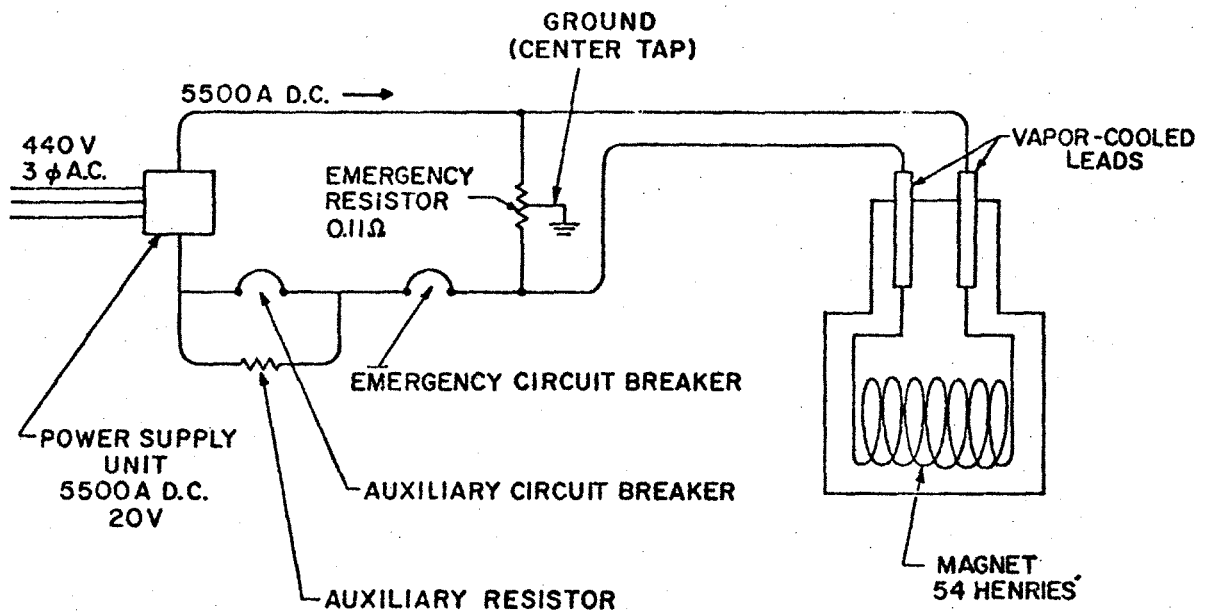
(1) Special tools and fixtures, rough estimate 10% to 20% of total cost of assembled magnet, or \$1,000,000 to \$2,000,000.

(2) The above cost estimate does not include development, design engineering, tool design, costs related to buildings, foundations, etc., transportation costs, refrigeration and power supply system, shakedown test and similar items.

**Table 4.2.10-III**  
**Summary, Estimated Cost of Installed Magnet System**  
**6 T ETF-Size Circular-Saddle Magnet Design, ETF6-P1 (AVCO)**

	<b>\$ × 10<sup>3</sup> (1977)</b>
Total, components and materials	5500
Coil winding module assembly, etc. (factory)	
3000 man weeks at \$1000/wk <sup>a</sup>	3000
Magnet system assembly and installation (on site)	
2100 man weeks at \$1040/wk <sup>a</sup>	2200
Supervision, QA, etc.	Incl. in above
Tooling, facility modifications and other	1000 <sup>a</sup>
Accessory subsystems	1500 <sup>a</sup>
Design, analysis, engineering	<u>1900<sup>a</sup></u>
<b>Total</b>	<b>15100</b>

<sup>a</sup> MIT estimate



4.2.10E Diagram. Electrical System, AVCO ETF Magnet, ETF6-P1

The characteristics of the AVCO ETF6-2 rectangular saddle conceptual design are listed in Table 4.2.11-I. The coil configuration is shown in Figure 4.2.10B, lower view. The calculated axial field profile is shown in Figure 4.2.11A and the magnet assembly in Figure 4.2.11B.

Designs for accessory subsystems were not developed for the ETF6-2 magnet, nor were any specific cost estimates, manufacturing plans or schedules prepared.

More detailed information on the AVCO ETF rectangular saddle magnet design ETF6-2 is contained in Reference 58.

#### 4.2.12 Alternative ETF Magnet Design by AVCO

An ETF 6 T magnet design with a much larger bore than that of the designs described in Sections 4.2.10 and 4.2.11 was developed by AVCO in 1977 and 1978, as a part of AVCO's MHD ETF Power Plant Conceptual Design Program for DOE (DOE Contract EF-77-C-01-264). The warm bore inlet area was increased by a factor of 4, and the active length by 1.3. In MIT's initial review, it was concluded that this design represented a new approach, with certain advantageous features which could facilitate fabrication, assembly and inspection and lead to reasonable overall costs. However, the design was not sufficiently developed to permit verification of the potential advantages.

A subcontract was placed with AVCO in 1978 for engineering work aimed at developing a better definition of portions of the design and providing more credible cost estimates. The work was completed and a report issued by AVCO in April 1979. The report clarified some design features and provided backup for costs of portions of the design. The general concepts of coil support, mechanically-joined structure and easy access to the magnet via covers on the vacuum jacket remained attractive for carrying into future designs. However, the feasibility of constructing the windings according to the detailed design shown remained in doubt.

The description and cost data which follow are based on the design as modified by the April 1979 AVCO report [78].

The AVCO ETF alternative magnet design, referred to as AVCO-3, incorporates a modular winding made up of 45° rectangular saddle coils and racetrack coils surrounding a square-cross-section warm bore. The conductor, operating at about 13 kA, is a built-up copper and NbTi composite consisting of a multifilament monolith or cable superconductor soldered into a slot in a rectangular-cross-section copper substrate.

Each winding half consists of a racetrack coil and a series of 45° saddle coils nested together to form a rectangular cross section bundle. Each coil is enclosed in a thick-walled stainless steel container, which serves as a substructure to carry the magnetic force of the conductor bundles to the external superstructure without subjecting the bundles to accumulated loading from other bundles.

A stainless steel liquid helium container surrounds each coil half. The superstructure in the "straight" (central) region of the winding consists of aluminum alloy I-beams and tension plates clamped around the helium containers. Plate-to-beam joints are mechanical, with bolts and load-bearing teeth. To support the end turns of the magnet against longitudinal magnetic forces, a horizontal stainless steel tension plate is provided to connect inlet-end to outlet-end on each coil half.

The assembly of coils, containers and superstructure (cold mass) is supported on low-heat-leak columns which carry the load to the base of the vacuum jacket.

The vacuum jacket outer shell is cylindrical. Large removable covers on each side are intended to make possible the assembly and disassembly of the magnet within the remaining portion of the vacuum jacket. At the inlet end, the vacuum jacket end-plate is recessed so that the combustor can project within the end envelope of the magnet, thus shortening the distance between the combustor and start of the active channel, to minimize



Table 4.2.11-1 Sheet 1 of 3

Design Characteristics  
 ETF MHD Magnet Design ETF6-2  
 AVCO Everett Research Laboratory Inc.

Date of design		1977
MHD power train data		
MHD power output (estimated)	(MWe)	40
Magnet data		
Magnet type	—	Rect. sad.
Warm bore liner?	—	No
Magnetic field:		
Peak on-axis field	(T)	6.0
Active field length <sup>a</sup>	(m)	7.0(8.0)
Field at start of active length <sup>a</sup>	(T)	6.0(4.8)
Field at end of active length	(T)	4.0
Peak field in winding	(T)	6.7
Dimensions:		
Aperture, warm bore inlet <sup>b</sup>	(m)	0.8 sq.
Aperture, start of active length <sup>b</sup>	(m)	0.8 sq.
Aperture, end of active length <sup>b</sup>	(m)	1.6 sq.
Aperture, warm bore exit <sup>b</sup>	(m)	1.6 sq.
Aperture area, start of active length <sup>b</sup>	(m <sup>2</sup> )	0.64
Aperture area, end of active length <sup>b</sup>	(m <sup>2</sup> )	2.56
Vacuum vessel overall length	(m)	12.1
Vacuum vessel outside height and width	(m)	5.8 × 6.0
Warm bore volume, active <sup>a,b</sup>	(m <sup>3</sup> )	10.5(12.0)

<sup>a</sup> Values in parentheses are adjusted values based on definition of active length as starting at 80% of peak field. Field profile is unchanged. After 1977, design characteristics for most large MHD magnet designs were consistent with this definition.

<sup>b</sup> Dimensions inside warm bore, without liner

Table 4.2.11-1 Sheet 2 of 3

**Winding characteristics:**

Build, winding cross section	(m)	0.8
Design current, I	(kA)	5.5
Winding current density, average, $J\lambda^a$	( $10^7$ A/cm <sup>2</sup> )	1.2
Ampere turns, NI	( $10^6$ A)	18.7
Stored energy	(MJ)	684
Conductor type	—	Built-up
Conductor materials	—	NbTi Cu

**Weights:**

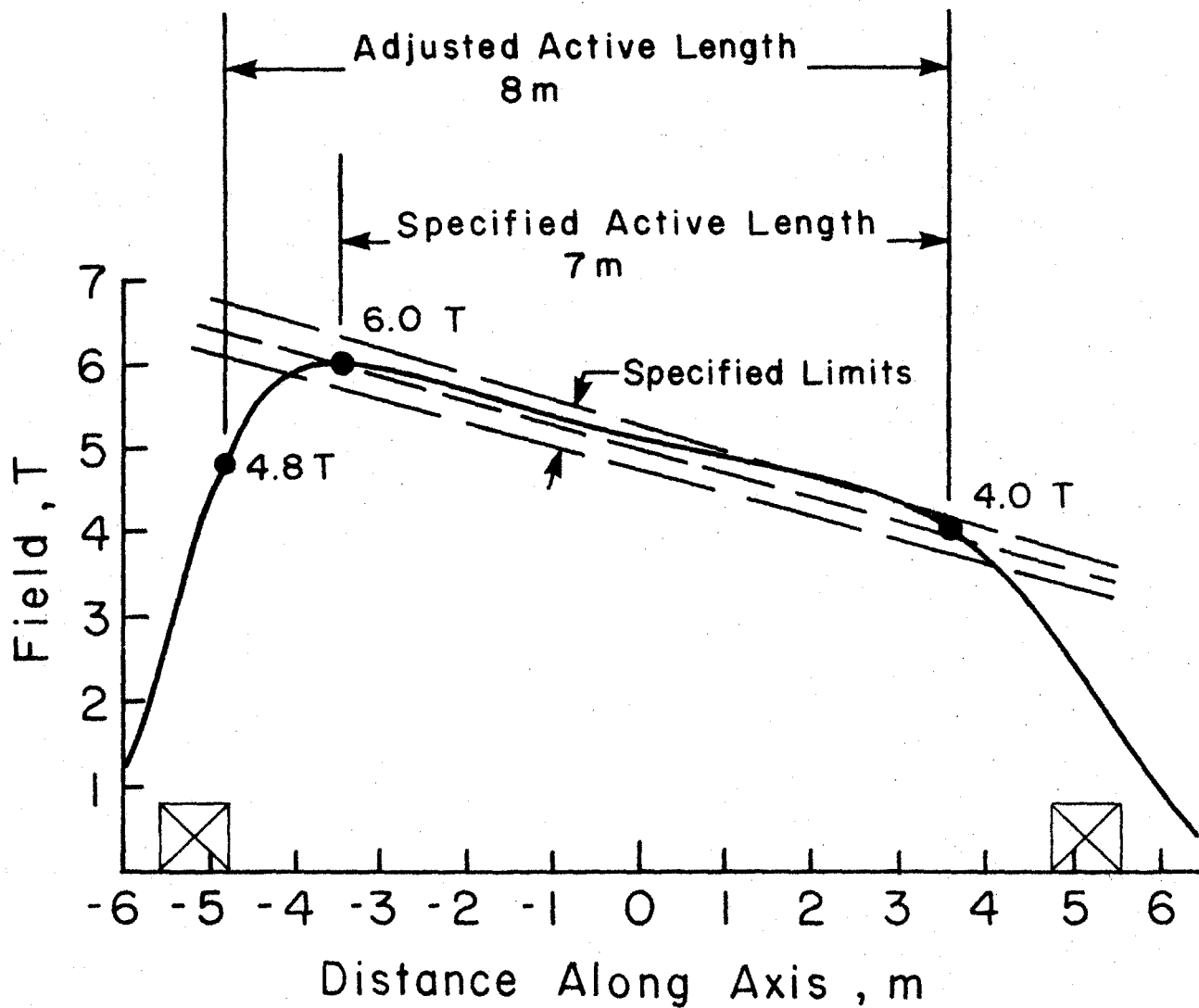
Conductor	(tonnes)	124
Insulation	(tonnes)	incl. below
Substructure	(tonnes)	incl. below
Superstructure	(tonnes)	255
Liquid He vessel	(tonnes)	incl. above
Total cold mass	(tonnes)	379
Thermal shield, cold mass supports, etc	(tonnes)	incl. below
Vacuum vessel	(tonnes)	70
Miscellaneous	(tonnes)	0
Total magnet weight	(tonnes)	449

<sup>a</sup> Where graded winding is incorporated, values listed are for high field region of winding.

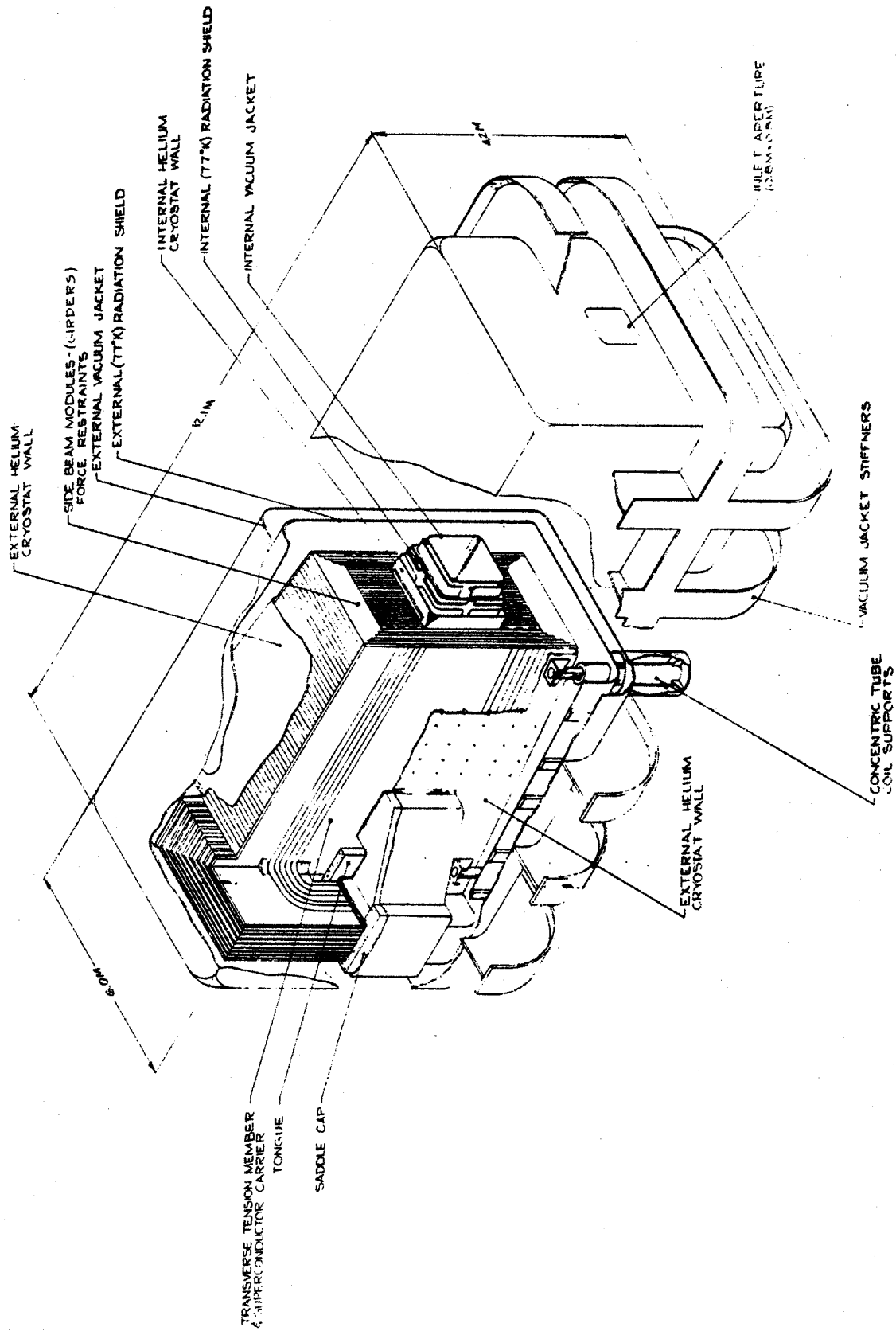
Table 4.2.11-1 Sheet 3 of 3

<b>Cryogenic data:</b>		
Operating temperature at winding	(K)	4.5
Operating temperature, thermal shield	(K)	80
Coolant, thermal shield	—	He gas
Heat loads LHe region, not incl. leads <sup>a</sup>	(W)	—
LHe for lead cooling at design current	(ℓ/hr)	16.5
<b>Materials of construction:</b>		
Winding substructure	—	Al 5083
Insulation	—	G-10
Superstructure	—	Al 6061
Liquid helium vessel	—	Al 5083
Thermal shield	—	Al 6061
Vacuum vessel	—	Al 5083
<b>Design stresses:</b>		
Superstructure (bending)	(MPa)	179
<b>Pressure rating</b>		
Liquid helium vessel		
Normal operating	(atm)	1.3

<sup>a</sup> Not including conductor splice loss.



4.2.11A Curve of On-Axis Field vs Distance Along Axis for AVCO ETF Magnet Assembly, ETF6-2



4.2.11B Cutaway View of AVCO ETF Magnet Assembly, ETF6-2

heat loss. The warm bore tube is a tapered, square-cross-section duct which is inserted from the exit end of the vacuum jacket. The vacuum jacket and warm bore tube are of stainless steel. A thermal shield operating at liquid nitrogen temperature and blankets of multilayer insulation are interposed between the cold mass and the warm surfaces of the vacuum jacket and bore tube.

The characteristics of the AVCO ETF alternative design are listed in Table 4.2.12-I. The calculated axial field profile is shown in Figure 4.2.12A, the coil configuration in Figure 4.2.12B, a typical winding cross section in Figure 4.2.12C and the magnet assembly in Figures 4.2.12D and 4.2.12E.

A cryogenic subsystem, including refrigerator, compressor package, liquid and gaseous helium storage and liquid nitrogen storage is a part of the overall magnet system. A power supply unit, discharge resistors, circuit breakers, instrumentation, controls and vacuum pumping subsystem are also part of the overall system.

The manufacturing plan calls for the assembled (built-up) conductor and the prefabricated U-shaped support submodules to be shipped from their respective manufacturing sites to a coil winding and assembly facility where the conductor and insulation will be installed in the submodules, the submodules nested together to form coil assemblies and these assemblies enclosed in the coil containment vessel. The coil and containment vessel assemblies will then be shipped to the plant site.

Superstructure components and Dewar modules will be shipped from their manufacturing sites to the plant site, where they will be assembled with the coils to form the complete magnet.

The costs estimated by AVCO for the alternative ETF magnet system are shown in Table 4.2.12-II.

More detailed information on the AVCO alternative ETF magnet design is contained in Reference 78.

#### **4.2.13 ETF Magnet Designs Developed by MIT for a 200 MWe Power Plant**

The ETF 6 T and 4 T designs described below were developed in 1980 and 1981 as a part of the overall conceptual design study of the MHD/ETF 200 MWe Power Plant for which NASA Lewis Research Center had management responsibility. The MIT magnet design work was done under a grant from NASA LeRC (NAS-G-100).

Assistance in preparing the designs and associated manufacturing studies and cost estimates was obtained from MEPPSCO, Combustion Engineering, Inc., Cryogenic Consultants, Inc., Alexander Kusko, Inc. and Pittsburgh Des Moines Steel Co., the first four through subcontracts.

Two designs were developed. The principal design was for a 6 T magnet for use with a subsonic MHD generator. The second (alternative) design was for a 4 T magnet for use with a supersonic generator. The latter design has the same bore size and active length as the 6 T design. Its configuration and construction are similar to those of the 6 T magnet, but the winding, structure and Dewar are scaled down in size and weight as appropriate to the lower field strength required.

The principal (6 T) ETF magnet design is a 60° rectangular-coil saddle magnet with a rectangular-cross-section warm bore. It incorporates a 24.4 kA flexible, circular-cross-section, twisted cable-type conductor consisting partly of copper strands and partly of NbTi/Cu composite strands. The conductor is supported in a substructure consisting of a multiplicity of grooved segments (short plates) of glass-reinforced plastic which serve both as turn-to-turn insulation and as structural means to support conductors against gravity and magnetic forces. The plates, with conductors installed in the grooves, are stacked in layers in two saddle-shaped stainless steel coil containers, one for each half of the magnet winding. Forces on conductors are carried through the substructure plates to the walls of the coil containers and thence to the superstructure surrounding the containers. This arrangement provides individual support for each conductor and prevents the accumulation of loads on conductors. There are 26 layers of conductors in each winding half. After the windings are installed, covers

Table 4.2.12-1 Sheet 1 of 3

Design Characteristics  
Alternative ETF MHD Magnet Design AVCO-3  
AVCO Everett Research Laboratory

Date of design		1978
Magnet type	—	45° rect sad & racetrack
Warm bore liner?	—	No
Magnetic field:		
Peak on-axis field	(T)	6.0
Active field length	(m)	8.9
Field at start of active length	(T)	4.0
Field at end of active length	(T)	4.0
Field uniformity at end of active length <sup>a</sup>	(%)	+3 -3
Peak field in winding	(T)	6.5
Dipole moment	(Am <sup>2</sup> )	9.1 × 10 <sup>8</sup>
Dimensions:		
Aperture, warm bore inlet <sup>b</sup>	(m)	1.5 × 1.5
Aperture, start of active length <sup>b</sup>	(m)	1.5 × 1.5
Aperture, end of active length <sup>b</sup>	(m)	2.275 × 2.275
Aperture, warm bore exit <sup>b</sup>	(m)	2.275 × 2.275
Aperture area, start of active length <sup>b</sup>	(m <sup>2</sup> )	2.25
Aperture area, end of active length <sup>b</sup>	(m <sup>2</sup> )	5.18
Distance, bore inlet to start of active length	(m)	1.6
Warm bore length	(m)	13.9
Vacuum vessel overall length	(m)	14.9
Vacuum vessel outside dia. (or h and w)	m)	10.2 × 10.5
Warm bore volume, active <sup>b</sup>	(m <sup>3</sup> )	32.2

<sup>a</sup> Field uniformity is + and - variation from on-axis field, central 50% of warm bore cross section

<sup>b</sup> Dimensions inside warm bore liner, if liner incorporated

Table 4.2.12-I Sheet 2 of 3

<b>Winding characteristics:</b>		
Build, winding cross section	(m)	0.87
Number of winding modules (or layers) per half	—	15
Design current, I	(kA)	13.5
Winding current density, average, $J\lambda^a$	( $10^7$ A/cm <sup>2</sup> )	1.44
Packing factor, $\lambda^a$	—	0.40
Conductor current density, $J^a$	( $10^7$ A/cm <sup>2</sup> )	3.6
Total number of turns, N	—	2100
Total length of conductor	(km)	71.4
Ampere turns, NI	( $10^8$ A)	26.6
Ampere meters	( $10^8$ Am)	8.8
Inductance	(H)	19.8
Stored energy	(MJ)	1700
Conductor type	—	Built-up
Conductor materials	—	NbTi Cu
Conductor dimensions <sup>a</sup>	(cm)	3.3 × 1.1
Copper-to-superconductor ratio <sup>a</sup>	—	12
LHe to conductor ratio (vol.) <sup>a</sup>	—	0.21
Heat flux <sup>a</sup>	(W/cm <sup>2</sup> )	0.4
<b>Weights:</b>		
Conductor	(tonnes)	215
Substructure	(tonnes)	215
Superstructure	(tonnes)	344
Liquid He vessel	(tonnes)	330
Total cold mass	(tonnes)	1104
Thermal shield, cold mass supports, etc	(tonnes)	33
Vacuum vessel	(tonnes)	327
Miscellaneous	(tonnes)	21
Total magnet weight	(tonnes)	1485

<sup>a</sup> Where graded winding is incorporated, values listed are for high field region of winding.



Table 4.2.12-I Sheet 3 of 3

**Cryogenic data:**

Operating temperature at winding	(K)	4.7
Operating temperature, thermal shield	(K)	80
Coolant, thermal shield coolant	—	—
Heat loads LHe region, not incl. leads <sup>a</sup>	(W)	48
LHe for lead cooling at design current	(ℓ/hr)	60

**Materials of construction:**

Winding substructure	—	SS 310
Insulation	—	Polymer
Superstructure	—	AL + SS
Liquid helium vessel	—	SS 310
Thermal shield	—	SS
Vacuum vessel	—	SS

**Design stresses:**

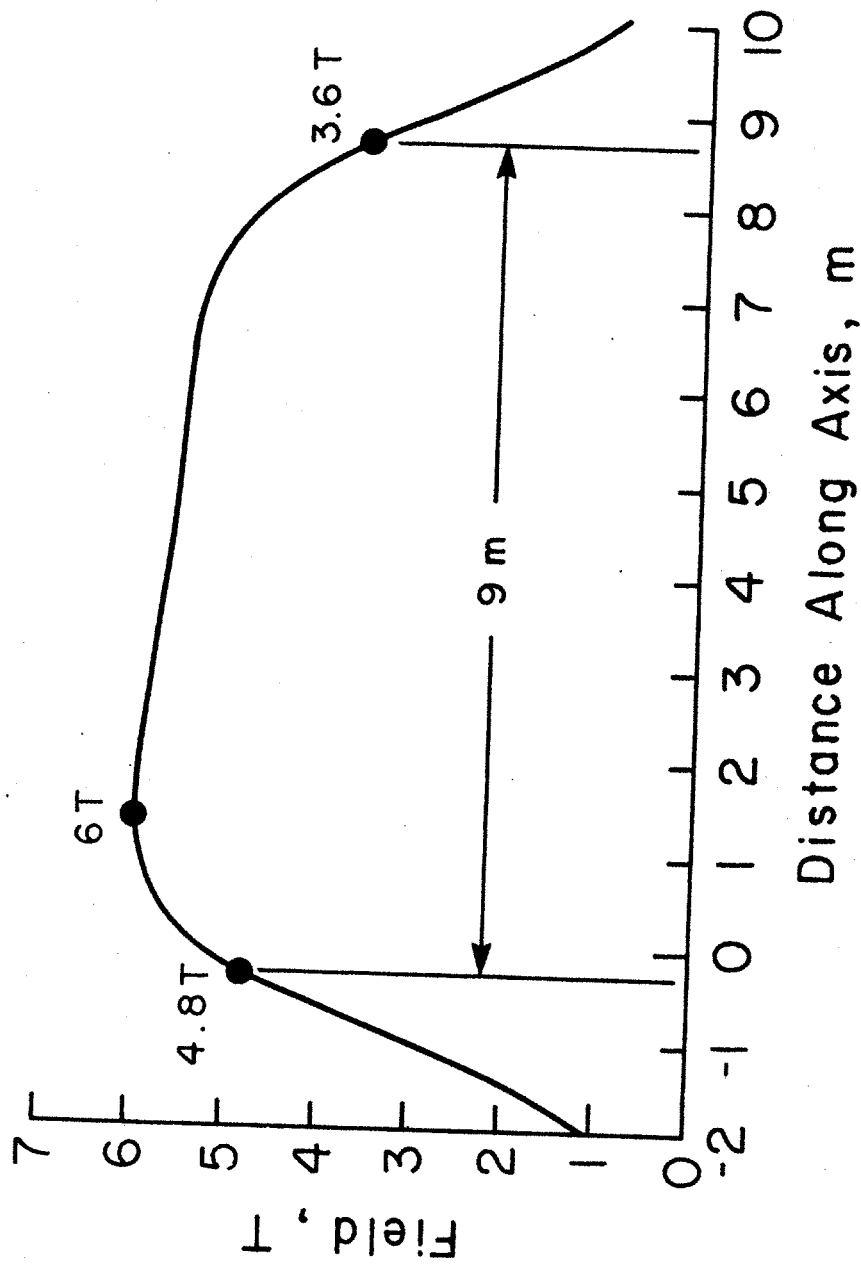
Winding substructure	(MPa)	359
Insulation (compression)	(MPa)	69
Superstructure (bending and tension)	(MPa)	Al 241 SS 359

<sup>a</sup> Not including splice losses.

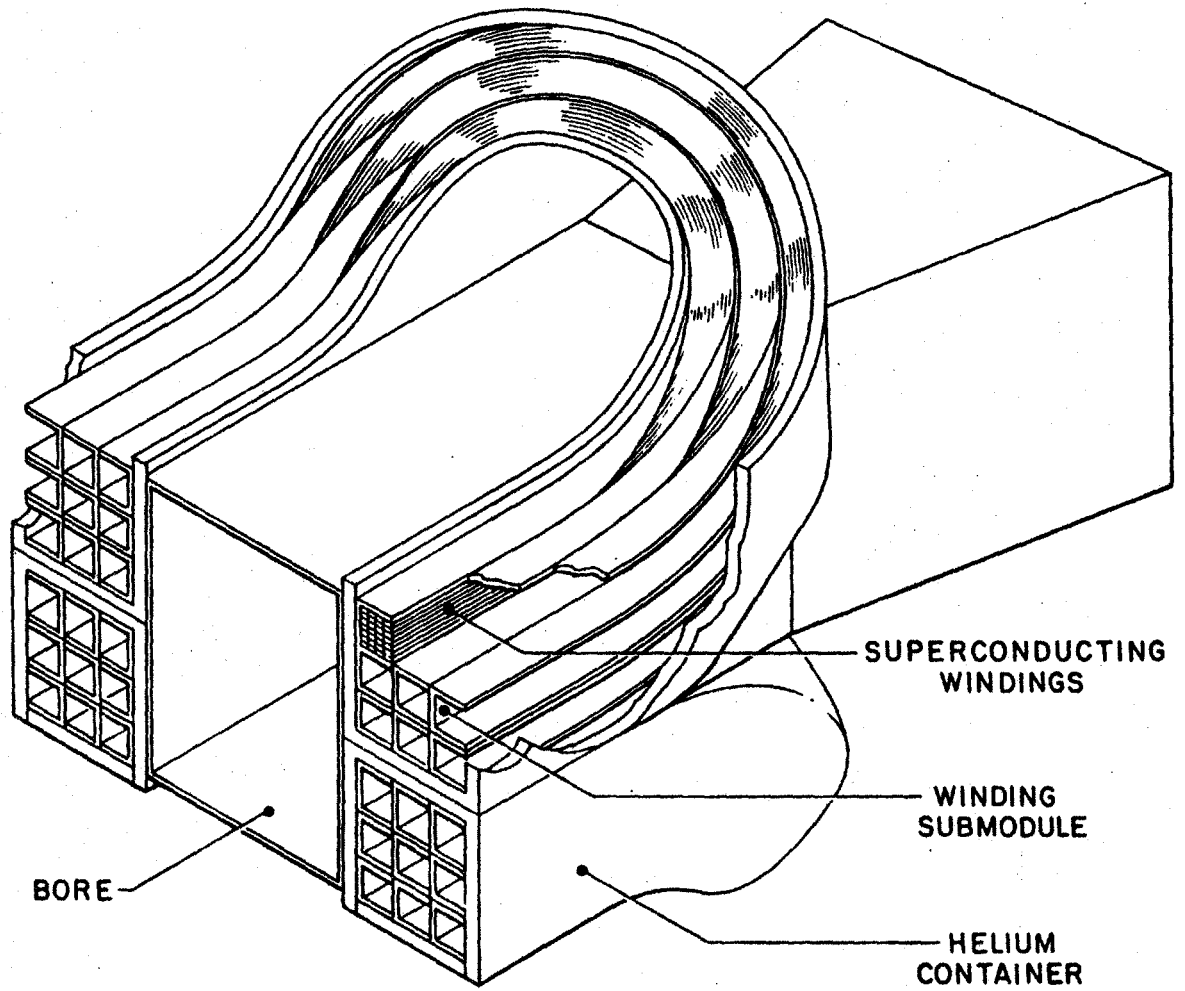
Table 4.2.12-II  
 Summary, Estimated Cost of Installed Magnet System (k\$)  
 Alternative ETF 6 T Magnet Design, AVCO-3

<u>Description</u>	<u>Component Cost</u>	<u>Install. Cost</u>	<u>Indirect Cost</u>	<u>Contin- gency</u>	<u>Total</u>
Winding Assembly	2086	48	24	642	2782
Structure	8280	10	5	2488	10784
Dewar	4192	20	10	1267	5489
Refrigeration system	1015	15	8	311	1349
Power supply, instrum. and controls	<u>583</u>	<u>134</u>	<u>67</u>	<u>235</u>	<u>1019</u>
<b>Total magnet system</b>	<b>16138</b>	<b>227</b>	<b>114</b>	<b>4943</b>	<b>21422</b>

Note: Analysis and design, project management, quality assurance, and tooling are included in the above.

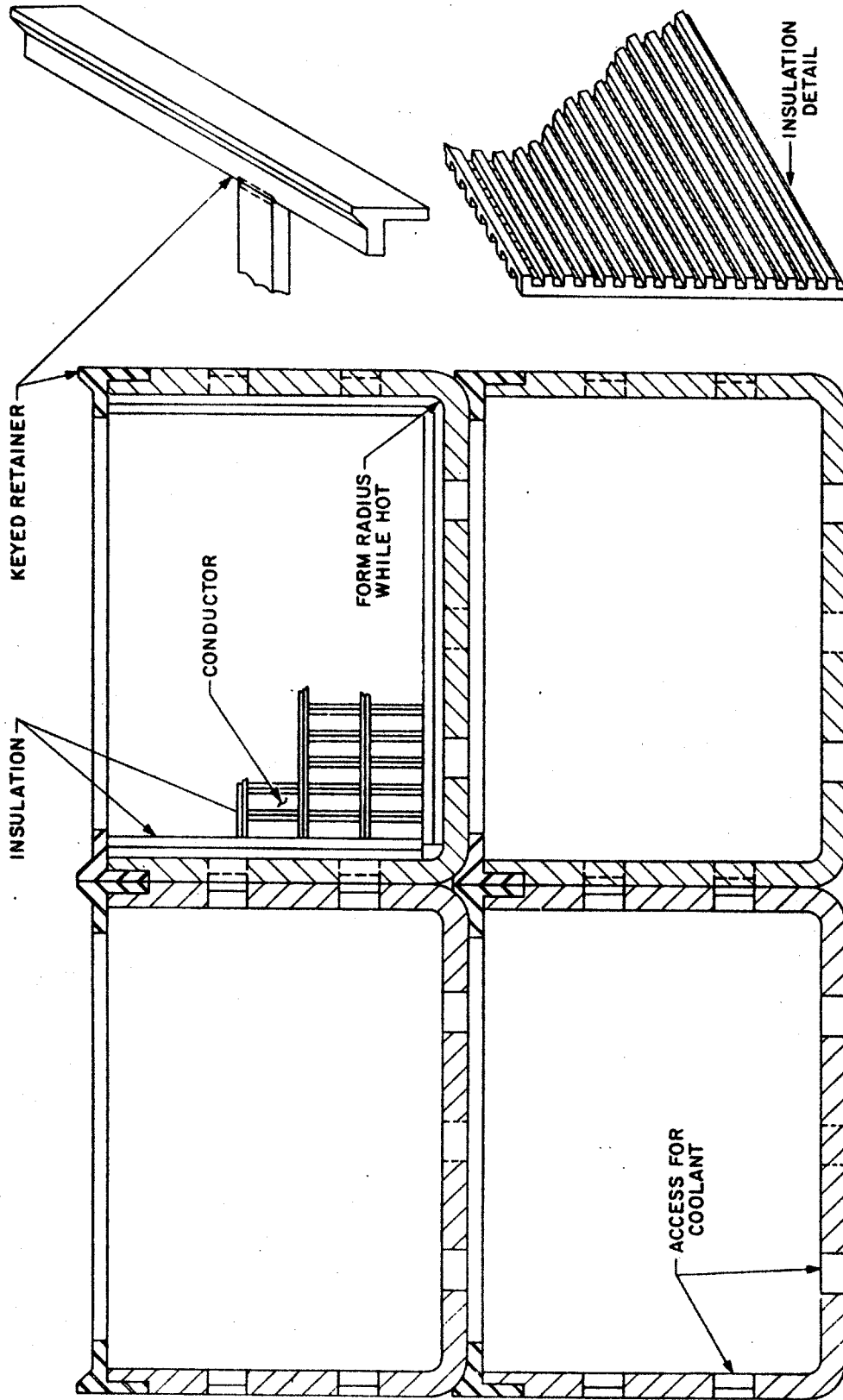


4.2.12A Curve of On-Axis Field vs Distance Along Axis for AVCO ETF Alternative Design Magnet

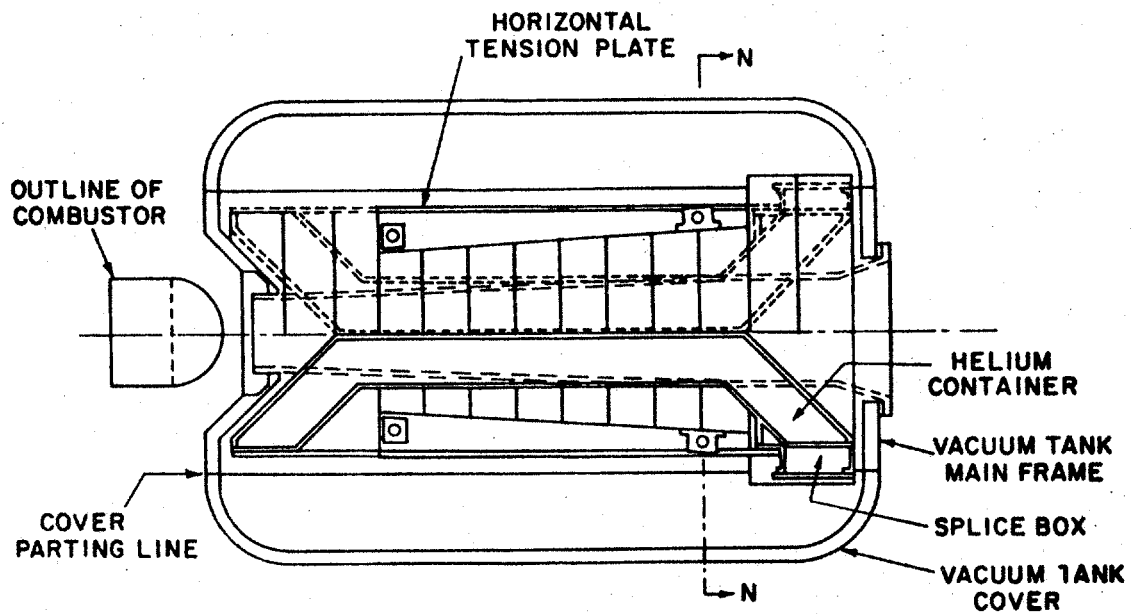


4.2.12B Sketch Showing Winding Configuration in End Turn Region, AVCO ETF Alternative Design Magnet

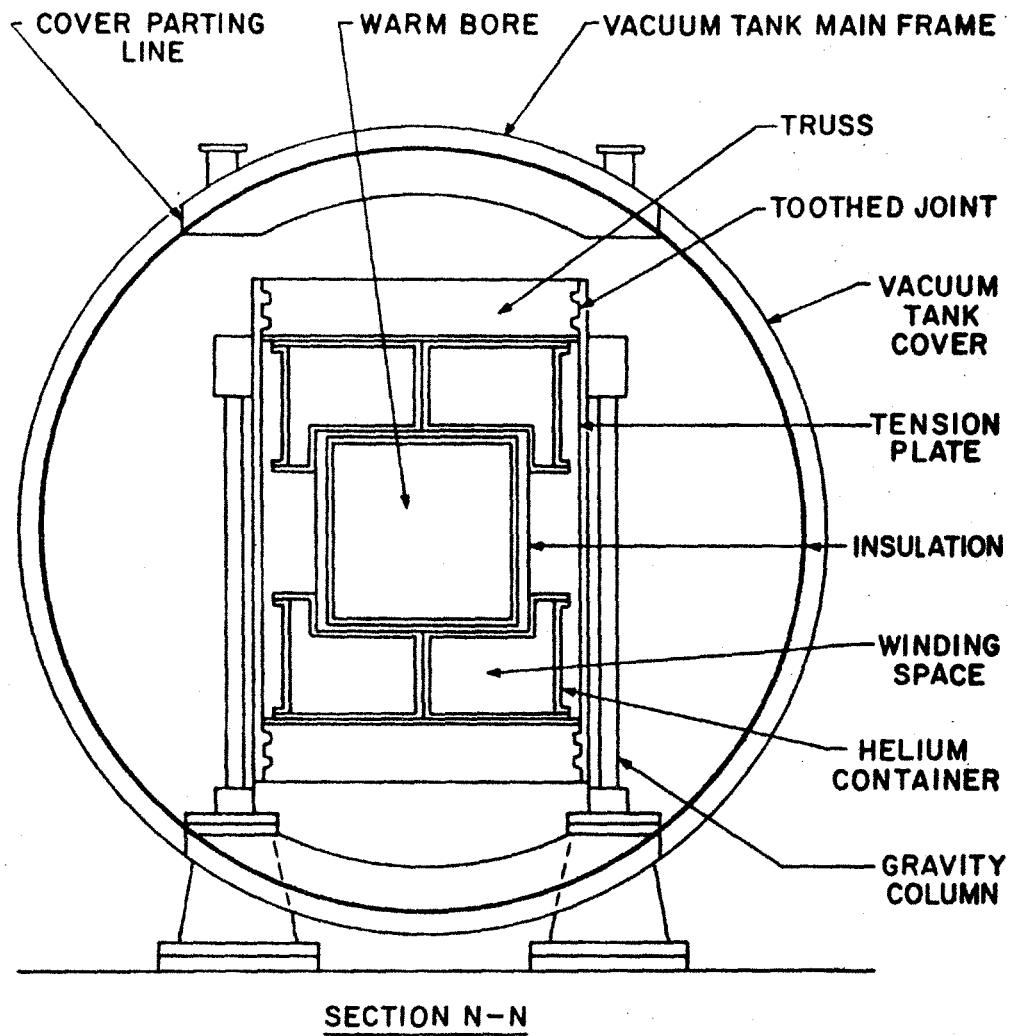
WINDING SUBMODULES FOR ETF MHD MAGNET



4.2.12C Sketch of Typical Winding Cross Section Showing Modular Construction, AVCO ETF Alternative Design Magnet



4.2.12D Plan View of Magnet Assembly, AVCO ETF Alternative Design Magnet



4.2.12E Cross Section View of Magnet Assembly, AVCO ETF Alternative Design Magnet

are welded in place to close the coil containers and make them suitable to serve as liquid helium containment vessels.

The major force containment structure (superstructure) supporting the "straight" (central) section of the windings against outward magnetic forces consists of stainless steel I-beams and tension rods assembled around the coil containment vessels. The tension rod ends are threaded, inserted in collars on the I-beams ends and fitted with large nuts to facilitate assembly and clamping at the power plant site.

The force containment structure supporting the end turn crossovers against longitudinal magnetic forces consists of the coil containment vessel walls combined with a series of stiffeners and tension plates welded in place around the end turns.

The Dewar includes an aluminum alloy thermal radiation shield cooled by tracer tubes supplied with liquid nitrogen, a stainless steel vacuum jacket consisting of a cylindrical outer shell, flat heads recessed to provide extra access at warm bore inlet and exit and a tapered, rectangular-cross-section warm bore tube. The cold mass of the magnet is supported by a system of low-heat-leak tubular struts of glass-reinforced epoxy, including four vertical struts, two angled horizontal struts and one transverse strut.

The MIT alternative (4 T) ETF magnet design is the same in concept and construction as the principal (6 T) design and the above description is applicable to the alternative design as well as the principal design.

The characteristics of the MIT principal and alternative ETF magnet designs are listed in Table 4.2.13-I. The calculated axial field profiles of the principal and alternative designs are shown in Figures 4.2.13A and 4.2.13B, respectively. The cable conductor cross section for the principal design is shown in Figure 4.2.13C, a typical winding cross section is shown in Figure 4.2.13D and the winding configuration is shown in Figure 4.2.13E. Outline and assembly drawings of the principal design are shown in Figures 4.2.13F, 4.2.13G, 4.2.13H and 4.2.13J, respectively. An outline drawing of the alternative design is shown in Figure 4.2.13K.

These ETF magnet systems include water-cooled warm bore liners, provisions for rolling the magnets aside to facilitate channel changeout, cryogenic support subsystems, power supply and discharge subsystems and vacuum pumping subsystems. Plan and elevation views of the principal design magnet installation, including accessory subsystems, is shown in Figure 4.2.13L. The principal magnet design helium (cryogenic) system is shown in Figure 4.2.13M, its nitrogen (cryogenic) system in Figure 4.2.13N and its electrical power supply and discharge system in Figure 4.2.13P.

The manufacturing plan calls for factory fabrication of a separate coil container for each winding half, after which the installation of the substructure plates and cable conductor in the containers will take place at a coil assembly facility. The two assembled coils, sealed in their containers, will be shipped to the power plant site where they will be mated on a special assembly stand. Superstructure and Dewar components, factory prefabricated in modules, will be shipped to the plant site and assembled around the coils and coil containers.

The coil and container assemblies, two per magnet, are the largest single assemblies to be shipped from an off-site facility to the plant site. Each of these assemblies will be approximately 3.5 m wide by 5.5 m high by 16 m long and will weigh approximately 200 tonnes. It is planned that shipment to the power plant site will be accomplished part way by barge and part way by special truck.

Rough budgetary estimates of costs for the principal (6 T) and alternative (4 T) ETF magnet systems are listed in Tables 4.2.13-II and 4.2.13-III, respectively.

More detailed information on the MIT ETF 200 MWe Power Plant magnet designs is contained in References 38 and 73.



Table 4.2.13-I Sheet 1 of 3

Design Characteristics  
ETF MHD Magnet Designs CSM Scaledown

MIT

(magnets for NASA LeRC Conceptual Design MHD ETF 200 MWe Power Plant)

		6 T		4 T	
		Principal Design		Alternative Design	
Date of design		1981		1981	
MHD power train data					
Thermal power train input	(MWt)	540		540	
MHD power output (estimated)	(MWe)	≈ 87		—	
Channel inlet dimensions	(m)	0.62		—	
Channel exit dimensions	(m)	1.42		—	
Magnet data					
Magnet type	—	60° rect. sad.		60° rect. sad.	
Warm bore liner?	—	Yes		Yes	
Magnetic field:					
Peak on-axis field	(T)	6.0		4.0	
Active field length	(m)	12.1		12.1	
Field at start of active length	(T)	4.0		2.7	
Field at end of active length	(T)	3.5		2.3	
Field uniformity at end of active length <sup>a</sup>	(%)	+2	-2	+2	-2
Area ratio, plasma c.s./warm bore, end of active length	—	0.36		0.36	
Peak field in winding	(T)	7.6		5.3	
Dipole moment	(Am <sup>2</sup> )	13.8 × 10 <sup>8</sup>		—	
Dimensions:					
Aperture, warm bore inlet <sup>b</sup>	(m)	1.40 × 1.80		1.40 × 1.80	
Aperture, start of active length <sup>b</sup>	(m)	1.40 × 1.80		1.40 × 1.80	
Aperture, end of active length <sup>b</sup>	(m)	2.06 × 2.69		2.06 × 2.69	
Aperture, warm bore exit <sup>b</sup>	(m)	2.16 × 2.82		2.16 × 2.82	
Aperture area, start of active length <sup>b</sup>	(m <sup>2</sup> )	2.52		2.52	
Aperture area, end of active length <sup>b</sup>	(m <sup>2</sup> )	5.54		5.54	
distance, bore inlet to start of active length	(m)	1.07		1.07	
Warm bore liner wall thick. incl. & clearance	(m)	0.065		0.065	
Warm bore length	(m)	15.2		15.2	
Vacuum vessel overall length	(m)	16.6		16.6	
Vacuum vessel outside dia.	(m)	8.4		7.9	
Warm bore volume, active <sup>b</sup>	(m <sup>3</sup> )	47.6		47.6	
MVU <sup>c</sup>		0.28		0.28	

<sup>a</sup> Field uniformity is + and - variation from on-axis field, central 50% of warm bore cross section

<sup>b</sup> Dimensions inside warm bore liner

<sup>c</sup> Ratio of channel volume to warm bore volume (inside liner)

Table 4.2.13-I Sheet 2 of 3

		6 T Principal Design	4 T Alternative Design
<b>Winding characteristics:</b>			
Build, winding cross section	(m)	0.52	0.35
Chord, winding cross section, one quadrant	(m)	1.032	1.032
Winding volume, total	(m <sup>3</sup> )	75.64	—
Number of winding modules (or layers) per half	—	26	16
Design current, I	(kA)	24.4	25
Winding current density, average, $J\lambda^a$	(10 <sup>7</sup> A/cm <sup>2</sup> )	1.42	1.40
Packing factor, $\lambda^a$	—	0.17	—
Conductor current density, $J^{a,b}$	(10 <sup>7</sup> A/cm <sup>2</sup> )	8.16	—
Total number of turns, N	—	1144	—
Total length of conductor	(km)	42.68	—
Ampere turns, NI	(10 <sup>6</sup> A)	27.9	18.0
Ampere meters	(10 <sup>8</sup> Am)	10.76	—
Inductance	(H)	9.7	4.2
Stored energy	(MJ)	2900	1300
Conductor type	—	Cable	—
Conductor materials	—	NbTi Cu	—
Conductor dimensions <sup>a</sup>	(cm)	2.54 dia.	—
Copper-to-superconductor ratio <sup>a</sup>	—	6.0	12.0
LHe to conductor ratio (vol.) <sup>a</sup>	—	0.8	0.8
Heat flux	(W/cm <sup>2</sup> )	<0.15	—
<b>Weights:</b>			
Conductor	(tonnes)	102	—
Insulation	(tonnes)	incl. below	—
Substructure	(tonnes)	90	—
Superstructure	(tonnes)	500	—
Liquid He vessel	(tonnes)	incl. above	—
<b>Total cold mass</b>	(tonnes)	<b>692</b>	—
Thermal shield, cold mass supports, etc	(tonnes)	30	—
Vacuum vessel	(tonnes)	157	—
Miscellaneous	(tonnes)	30	—
<b>Total magnet weight</b>	(tonnes)	<b>909</b>	<b>568</b>

<sup>a</sup> Where graded winding is incorporated, values listed are for high field region of winding.

<sup>b</sup> Conductor current density is current density in conductor metal cross section

Table 4.2.13-I Sheet 3 of 3

		6 T <u>Principal Design</u>	4 T <u>Alternative Design</u>
<b>Cryogenic data:</b>			
Operating temperature at winding	(K)	4.5	4.5
Operating temperature, thermal shield	(K)	80	80
Coolant, thermal shield	—	LN <sub>2</sub>	LN <sub>2</sub>
Heat loads LHe region, not incl. leads	(W)	180	—
LHe for lead cooling at design current	(ℓ/hr)	75	75
<b>Power supply and discharge data:</b>			
Number of current leads	—	2	2
Rated voltage, power supply	(V)	108	—
Minimum charge time	(hrs)	0.75	—
Resistance, emergency dump resistor	(Ω)	0.41	—
Emergency discharge time constant	(min)	3.86	—
Maximum discharge voltage, terminal	(V)	1000	—
<b>Materials of construction:</b>			
Winding substructure	—	Glass/polyester	Glass/polyester
Insulation	—	—	—
Superstructure	—	SS 304 LN	SS 304 LN
Liquid helium vessel	—	SS 304 LN	SS 304 LN
Thermal shield	—	Al 6061	Al 6061
Vacuum vessel	—	SS 304 L	SS 304 L
<b>Design stresses:</b>			
Winding substructure (compression)	(MPa)	77	77
Superstructure (bending)	(MPa)	414	414
<b>Pressure rating</b>			
Liquid helium vessel			
Normal operating	(atm)	1.3	1.3
Maximum design	(atm)	3.1	3.1

Table 4.2.13-II Sheet 1 of 2  
 Summary, Estimated Cost of Installed Magnet System <sup>1,7</sup>  
 6 T Magnet Design, MIT, Magnet for MHD ETF 200 MWe Power Plant

Account Description	Quan	Design & Anal	Matl & Mfg	Shop Eng	Pack & Ship	Material Mjr Comp	Cost <sup>2</sup> BOA
Magnet Assembly	—	—	—	—	—	—	—
On-site tools	—	—	—	—	—	2070	—
Roll-aside track	—	—	—	—	—	621	—
Wind. contain vessels <sup>3</sup>	—	—	—	—	—	15,870	—
Main structure	—	—	—	—	—	5244	—
Cold mass supp. struts	—	—	—	—	—	621	—
Therm. rad. shield	—	—	—	—	—	1518	—
Vacuum vessel	—	—	—	—	—	3036	—
Warm bore liner	—	—	—	—	—	621	—
Total magnet assembly	1	5363	21,450	2145	643	29,601	—
Support subsystems	—	—	—	—	—	—	—
Hydro. actuator sys.	—	—	—	—	—	128	—
Cryogenic supp. system	—	—	—	—	—	1536	—
Power supply & dis. sys.	—	—	—	—	—	1152	—
Main vacuum pump sys.	—	—	—	—	—	256	—
Utility boom, contr., misc.	—	—	—	—	—	640	—
Total support system	1 set	725	2900	—	87	3712	—
Magnet shakedown test	—	150 <sup>4</sup>	60	20	2	232 <sup>4</sup>	80 <sup>5</sup>
Total	—	—	—	—	—	33,446	80
Engineering services	—	—	—	—	—	—	—
Other cost	—	—	—	—	—	—	—
TOTAL	—	—	—	—	—	—	—

<sup>1</sup> This estimate does not include foundations

<sup>2</sup> Material cost is FOB site

<sup>3</sup> This item includes conductor, coil winding (in shop) and shop assembly

<sup>4</sup> Includes 100 K\$ eng. test supervision and analysis

<sup>5</sup> Includes liquid nitrogen and liquid helium

<sup>6</sup> On-site technician labor cost

<sup>7</sup> Costs are K\$; mid 1981

<sup>8</sup> Field engineering

Table 4.2.13-II Sheet 2 of 2

Account Description	Inst Cost	Indir Cost	Eng Serv <sup>8</sup>	Other Cost	Contin	TOTAL COST
Magnet Assembly	—	—	—	—	—	—
On-site tools	400	—	—	—	—	—
Roll-aside track	150	—	—	—	—	—
Wind. contain vessels <sup>3</sup>	1800	—	—	—	—	—
Main structure	800	—	—	—	—	—
Cold mass supp. struts	150	—	—	—	—	—
Therm. rad. shield	900	—	—	—	—	—
Vacuum vessel	1200	—	—	—	—	—
Warm bore liner	80	—	—	—	—	—
Total magnet assembly	5600	560	(2861)	(966)	10,728	46,439
Support subsystems	—	—	—	—	—	—
Hydro. actuator sys.	30	—	—	—	—	—
Cryogenic supp. system	250	—	—	—	—	—
Power supply & dis. sys.	150	—	—	—	—	—
Main vacuum pump sys.	70	—	—	—	—	—
Utility boom, contr., misc.	100	—	—	—	—	—
Total support system	600	60	(350)	(118)	874	5246
Magnet shakedown test	300 <sup>6</sup>	30	(51)	(17)	193	835
<b>Total</b>	<b>6500</b>	<b>650</b>	<b>—</b>	<b>—</b>	<b>11,766</b>	<b>52442</b>
Engineering services	—	—	3254	—	651	3905
Other cost	—	—	—	1099	220	1319
<b>TOTAL</b>	<b>—</b>	<b>—</b>	<b>—</b>	<b>—</b>	<b>—</b>	<b>57,666</b>

<sup>3</sup> This item includes conductor, coil winding (in shop) and shop assembly

<sup>6</sup> On-site technician labor cost

<sup>8</sup> Field engineering

Table 4.2.13-III Sheet 1 of 2  
 Summary, Estimated Cost of Installed Magnet System (k\$)  
 4 T Magnet Design, MIT, Magnet for MHD ETF 200 MWe Power Plant

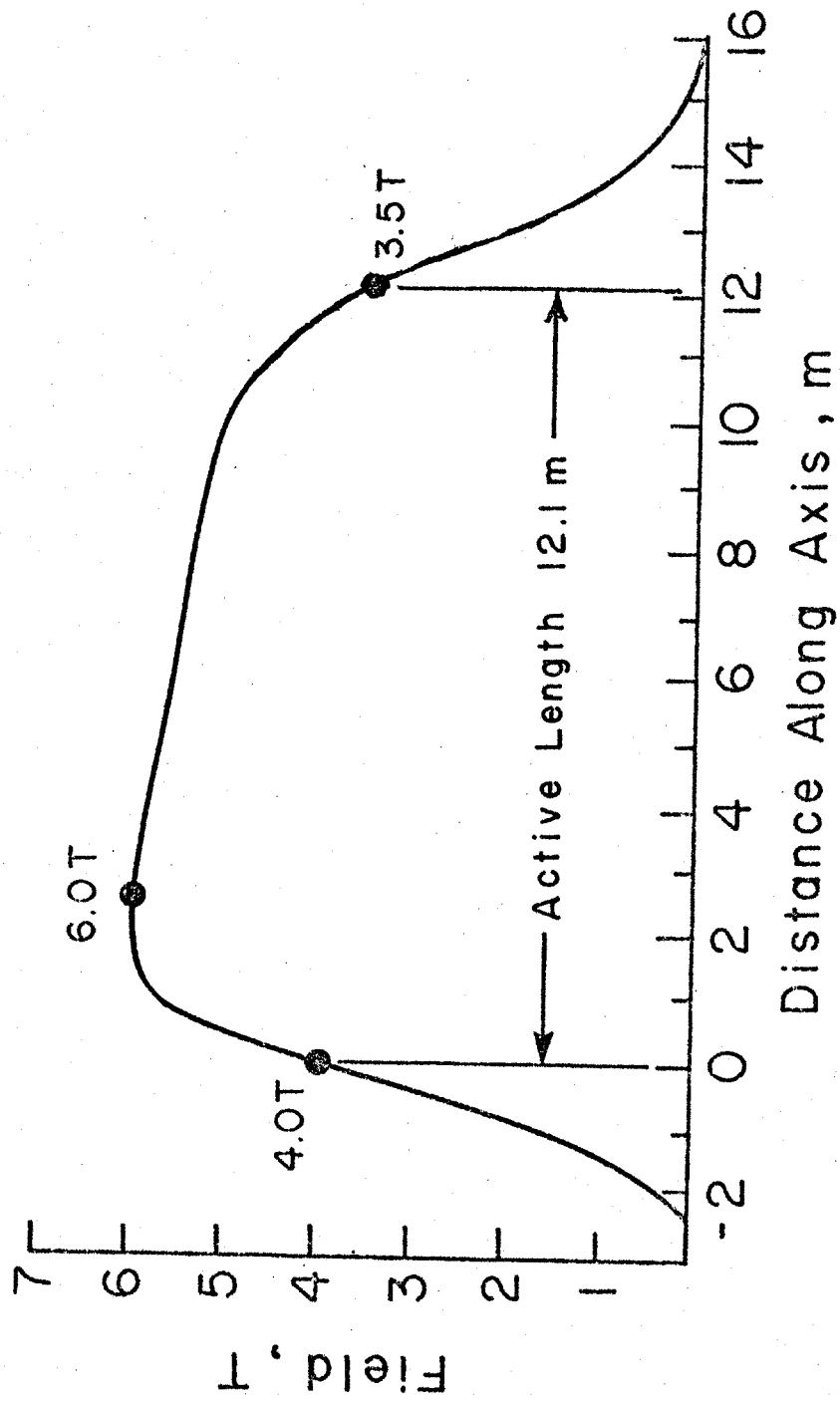
	Total Component at Factory <sup>1</sup>	Pack and Ship	Total Components at Site	Assemble and Install	Indirect
On-site tools	1829	—	—	—	—
Conductor	4862	—	—	—	—
Substructure	866	—	—	—	—
Instrum, piping, etc	136	—	—	—	—
Coil containers	3155	—	—	—	—
Wind & assemble coils	1224	—	—	—	—
Superstructure	2570	—	—	—	—
Thermal shield	1666	—	—	—	—
Cold mass supports	456	—	—	—	—
Vacuum vessel	<u>3129</u>	—	—	—	—
<b>Total</b>	<b>19,893</b>	<b>7759</b>	<b>20,689</b>	<b>4950</b>	<b>495</b>
Roll-aside system	1396	50	1440	280	28
Warm bore liner	921	15	936	80	8
Accessory subsystems	2608	95	2703	470	47
Instruments and controls	298	5	303	100	10
Shakedown test, etc	390	1	391	300	30
<b>Total</b>	<b>25,440</b>	<b>985</b>	<b>26,359</b>	<b>6180</b>	<b>618</b>
Eng services, total	—	—	—	—	—
Other, total	—	—	—	—	—
<b>Total</b>	<b>—</b>	<b>—</b>	<b>—</b>	<b>—</b>	<b>—</b>

1. Includes design and analysis, shop engineering

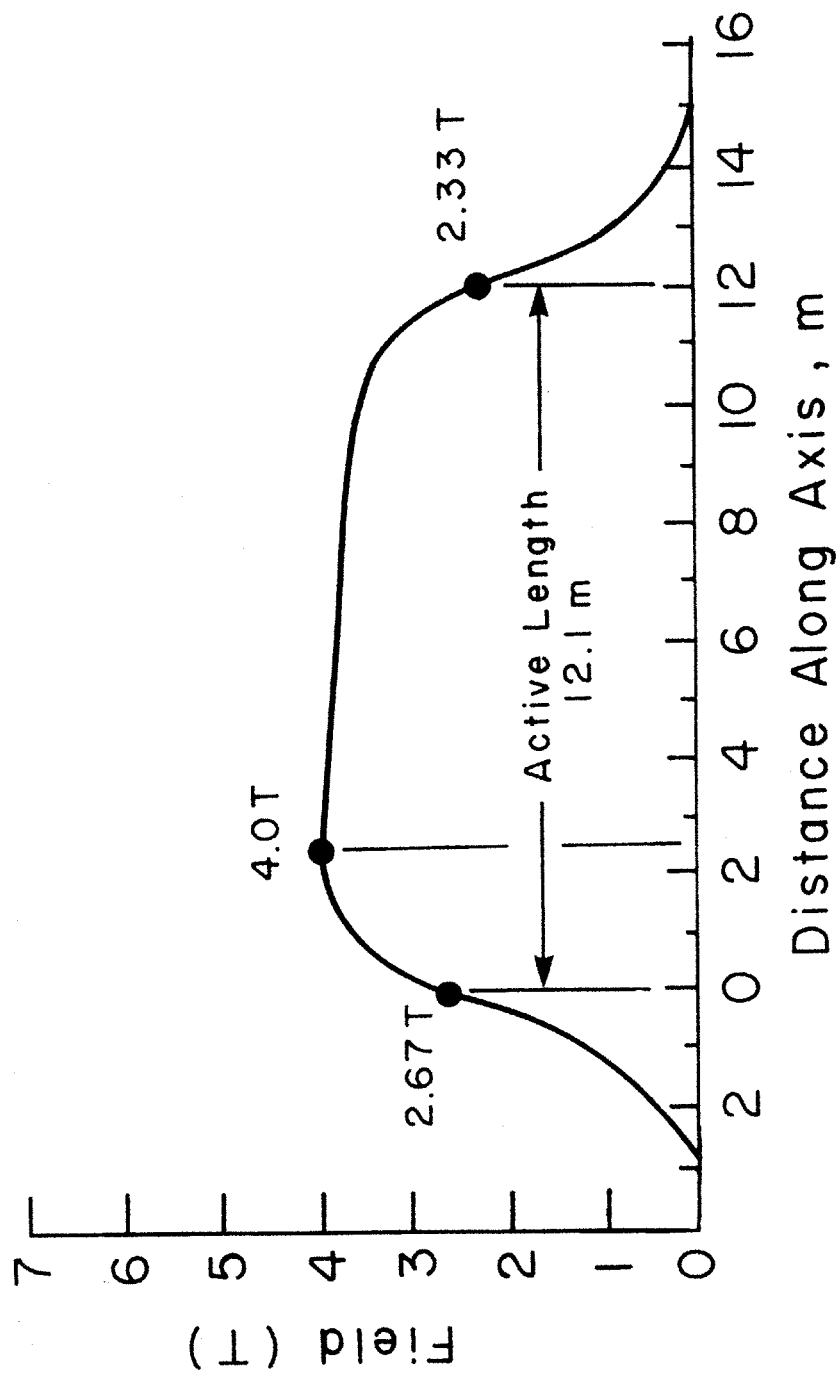
Table 4.2.13-III Sheet 2 of 2

	Eng Serv	Other	Contingency	Total
On-site tools	—	—	—	—
Conductor	—	—	—	—
Substructure	—	—	—	—
Instrum, piping, etc	—	—	—	—
Coil containers	—	—	—	—
Wind & assemble coils	—	—	—	—
Superstructure	—	—	—	—
Thermal shield	—	—	—	—
Cold mass supports	—	—	—	—
Vacuum vessel	—	—	—	—
<b>Total</b>	—	—	<b>7124</b>	<b>33,258</b>
Roll-aside system	—	—	350	2098
Warm bore liner	—	—	309	1333
Accessory subsystems	—	—	644	3864
Instruments and controls	—	—	83	496
Shakedown test, etc	—	—	216	937
<b>Total</b>	—	—	—	—
Eng services, total	2653	—	530	3183
Other, total	—	900	180	<u>1080</u>
<b>Total</b>	—	—	<b>10,120</b>	<b>46,249</b>

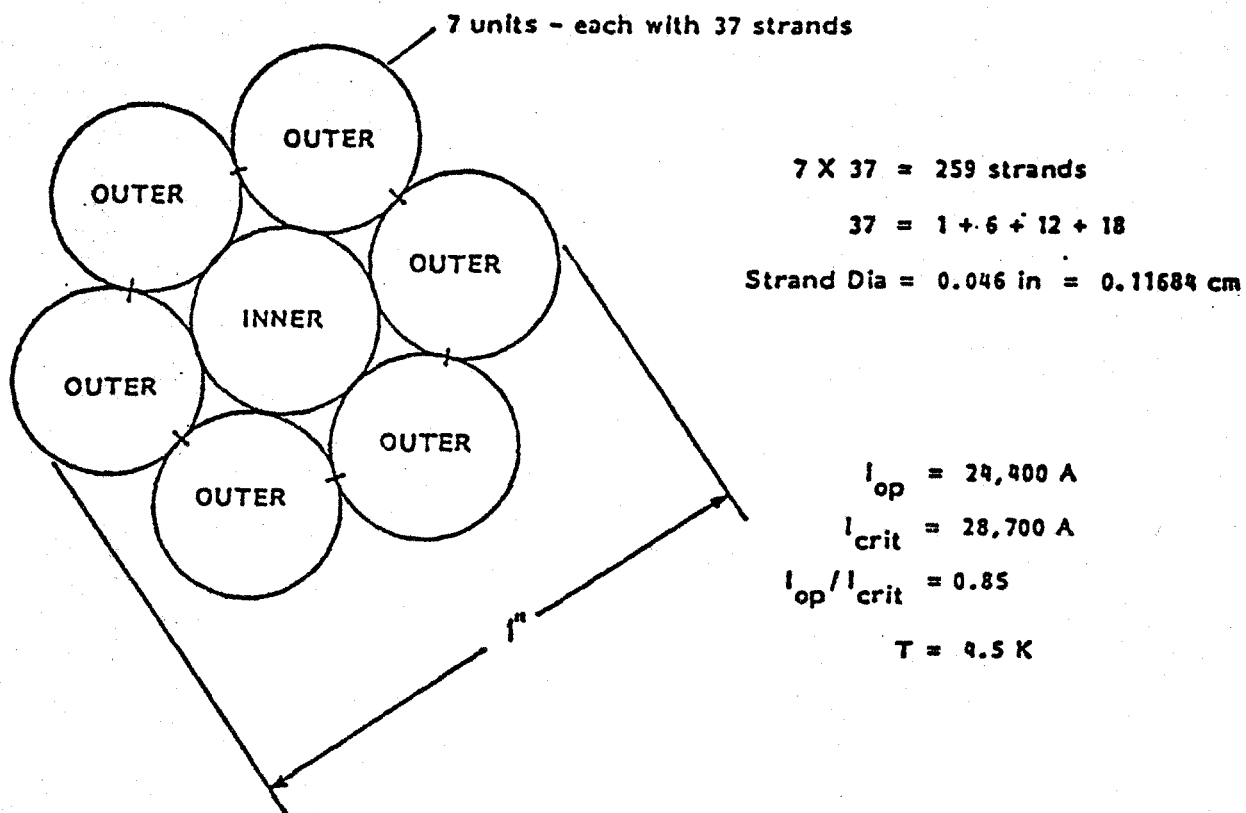
4.2.13A Curve of On-Axis Field vs Distance Along Axis for MIT ETF 6 T Magnet (Principal Design)



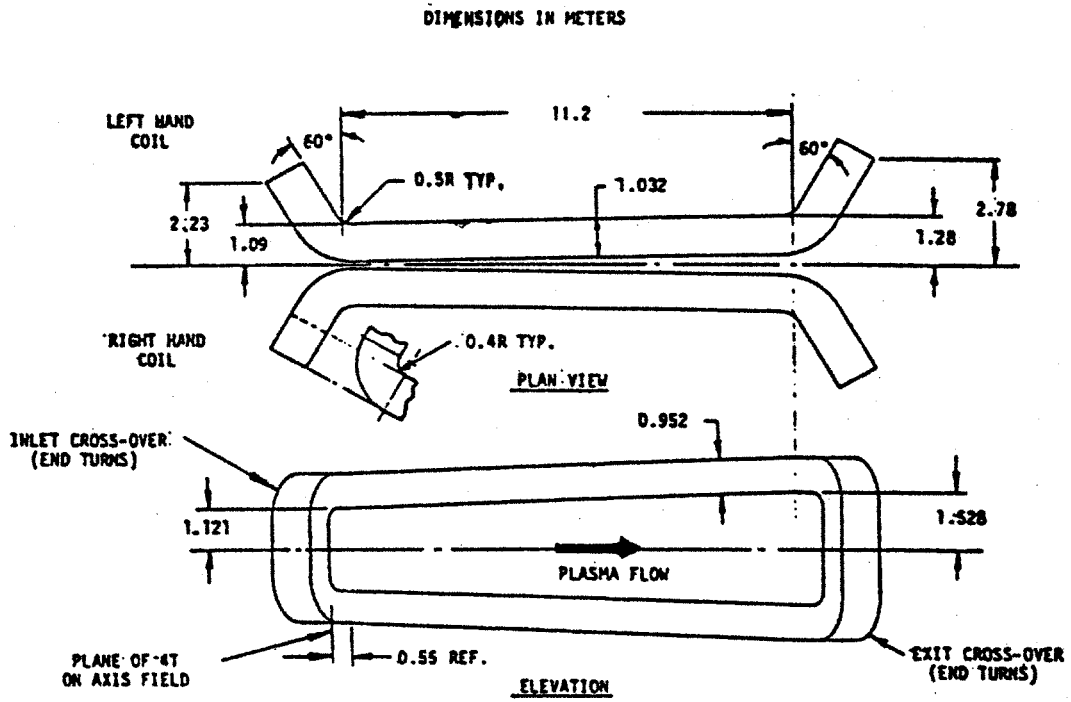




4.2.13B Curve of On-Axis Field vs Distance Along Axis for MIT E1F 4 T Magnet (Alternative Design)

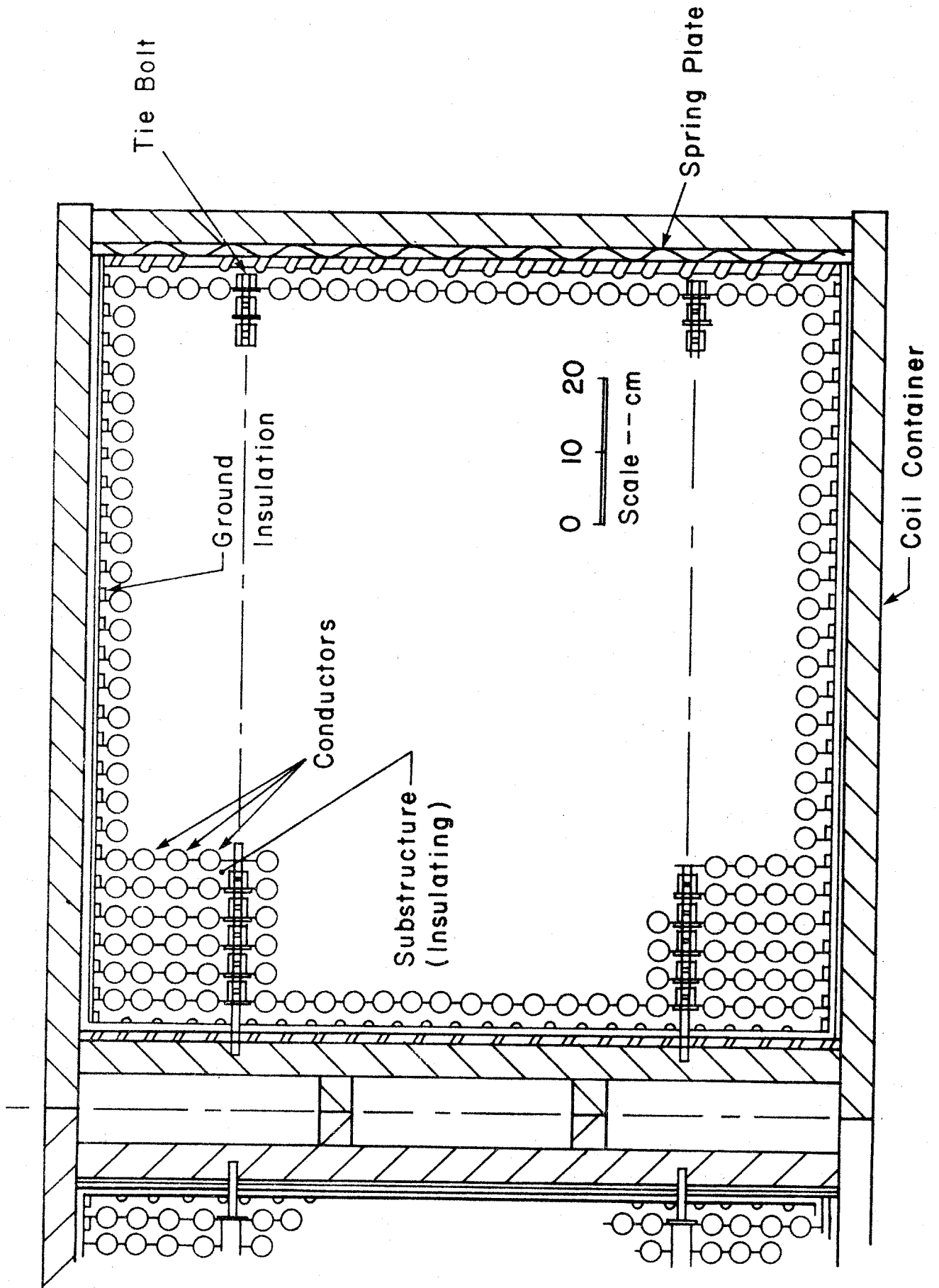


4.2.13C Diagram Showing Cable Conductor Cross Section for MIT ETF 6 T Magnet (Principal Design)

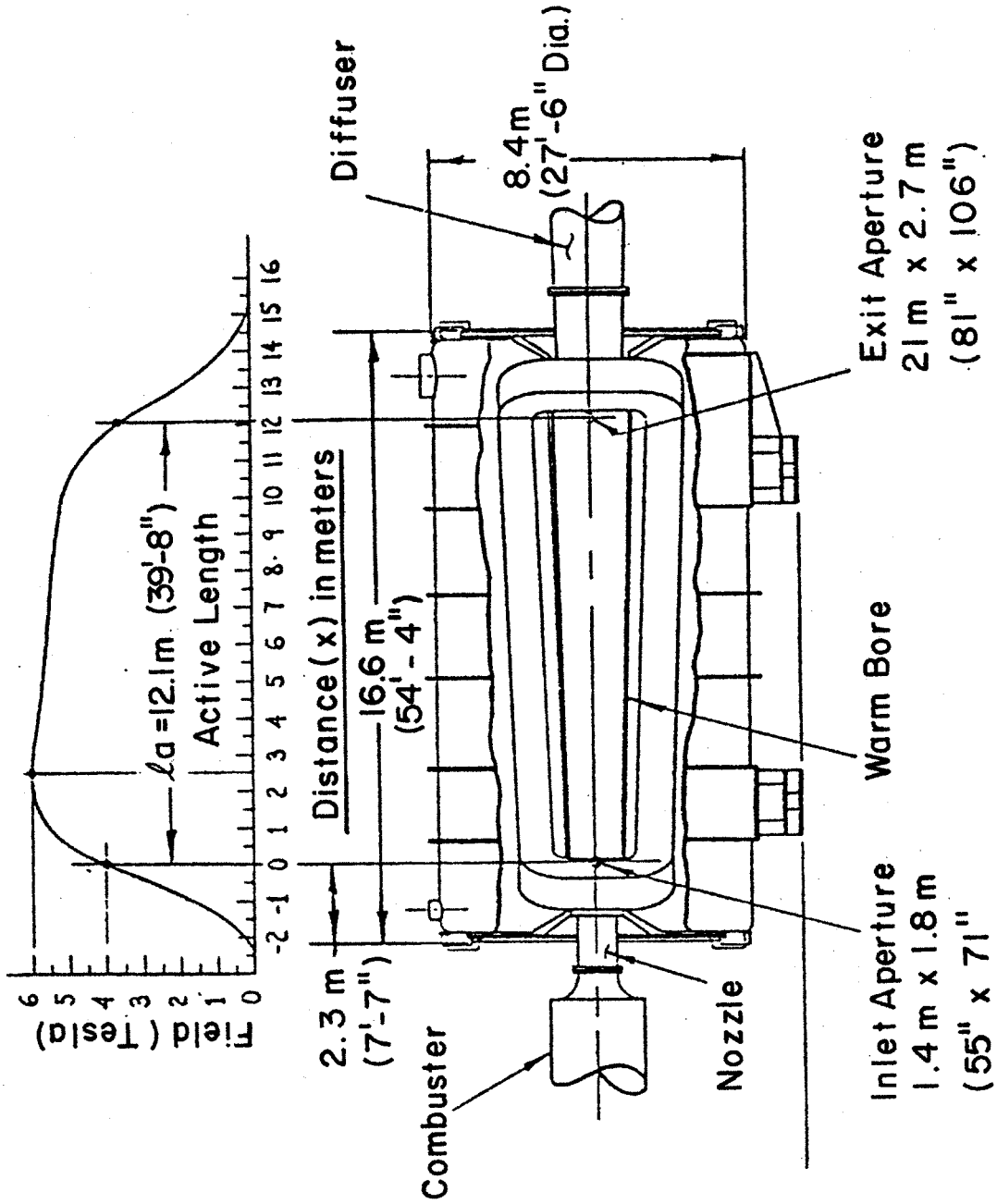


4.2.13D Diagram Showing Winding Configuration, MIT ETF 6 T Magnet (Principal Design)

4.2.13E Sketch Showing Typical Winding Cross Section for MIT ETF 6 T Magnet (Principal Design)

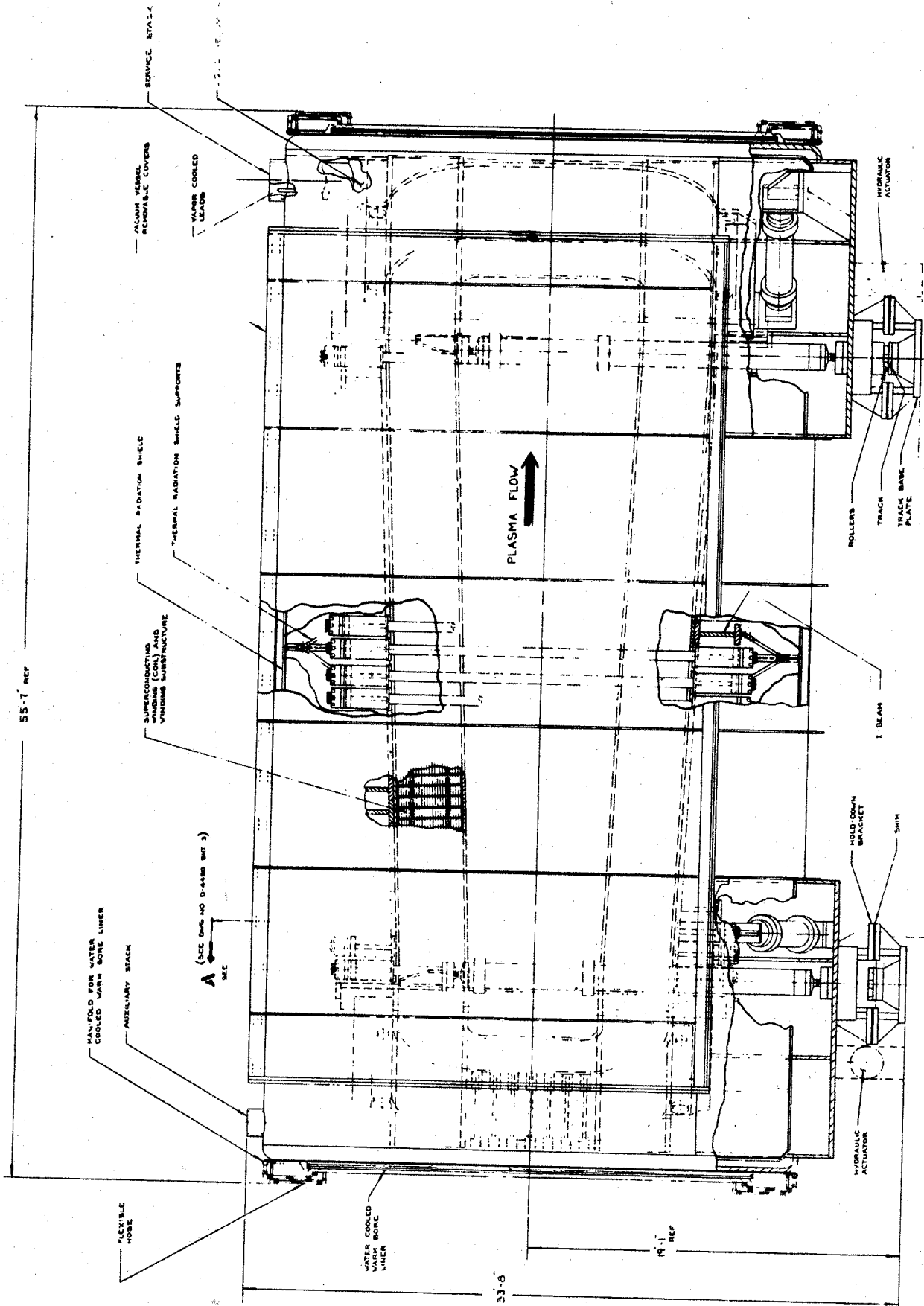


# FIELD PROFILE



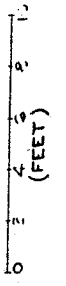
4.2.13F Outline Drawing of MIT ERF 6 T Magnet (Principal Design)

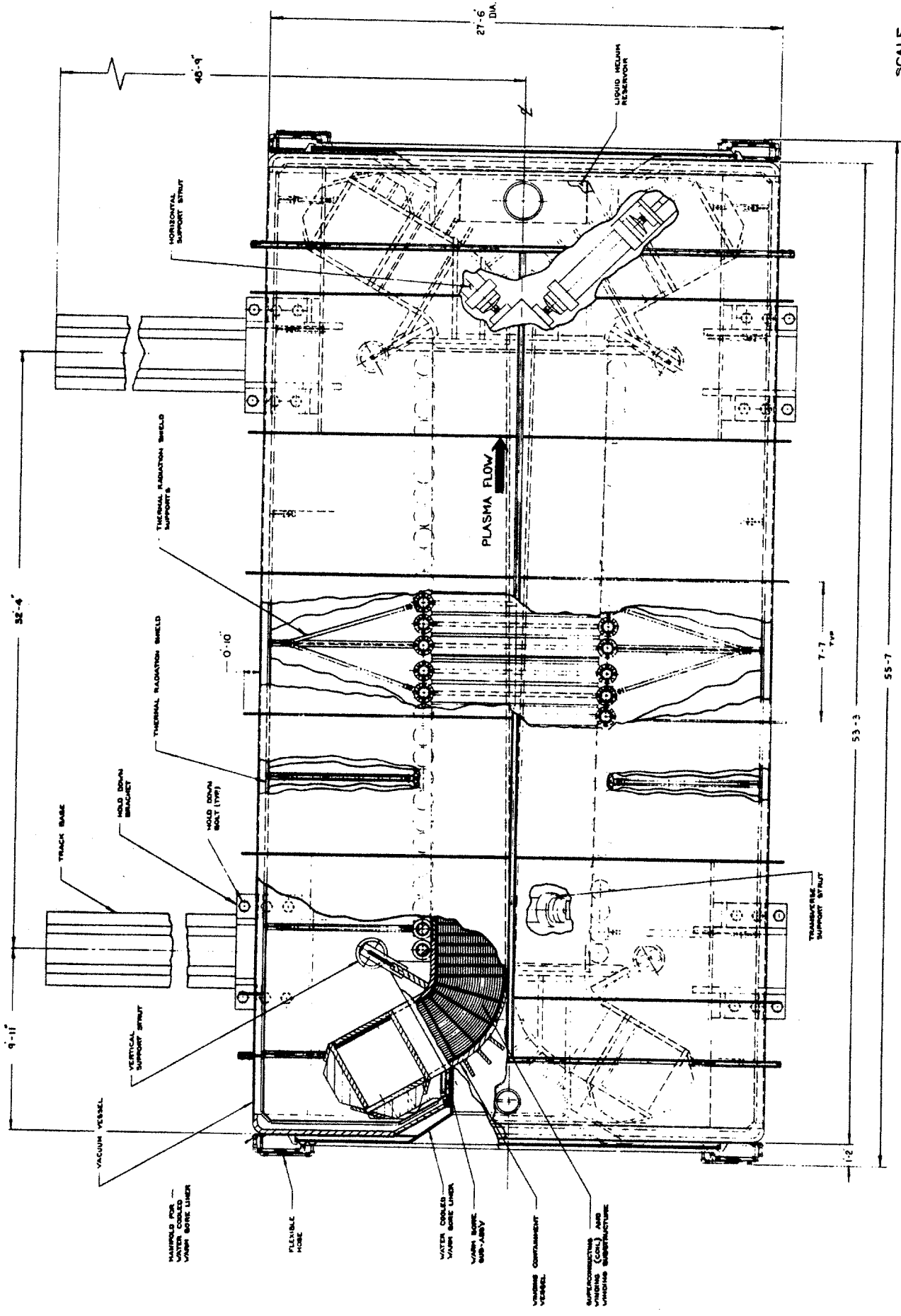
4.2.13G Elevation View, Magnet Assembly, MIT ETF 6 T Magnet (Principal Design)



ELEVATION VIEW

SCALE





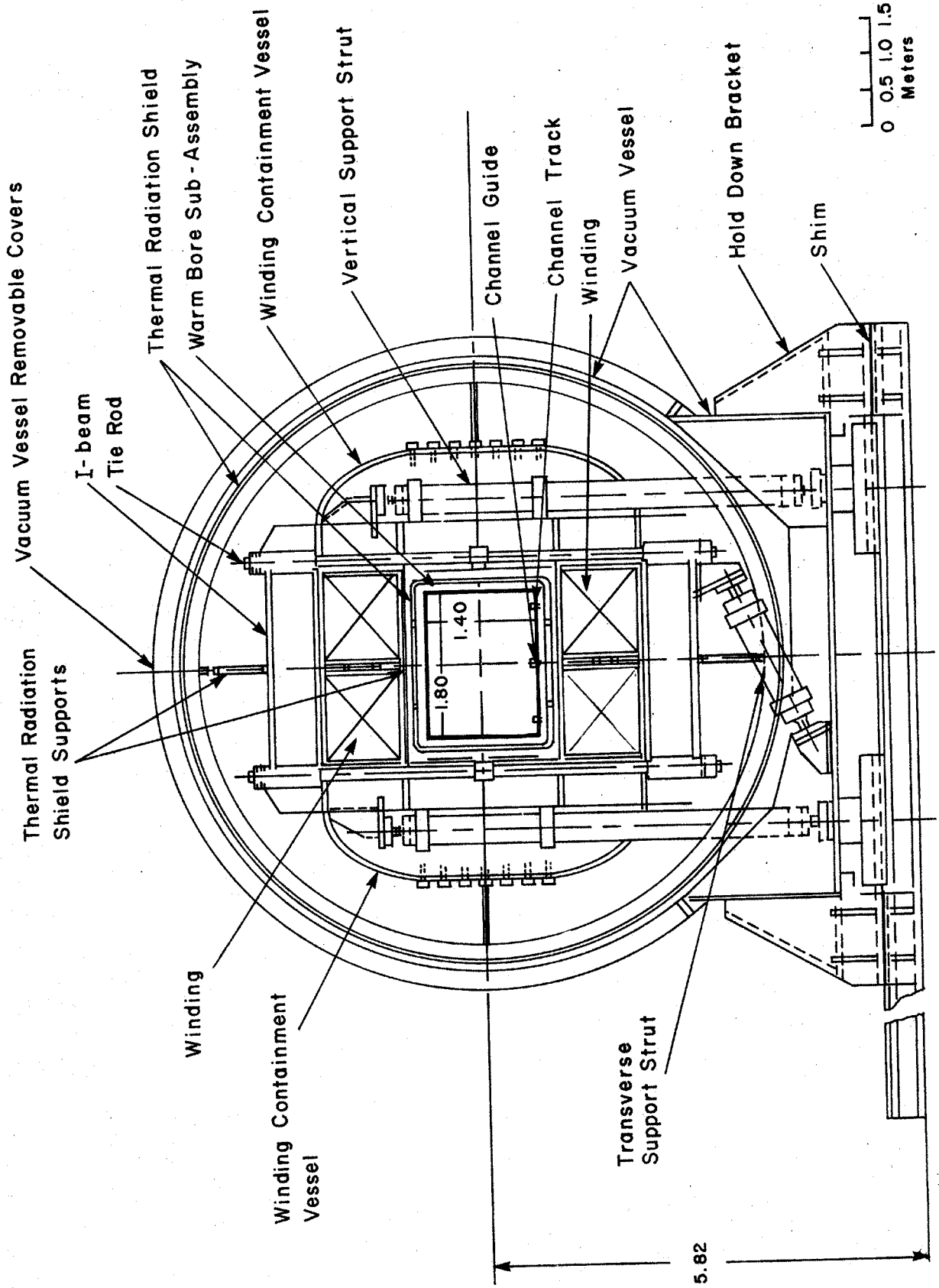
SCALE



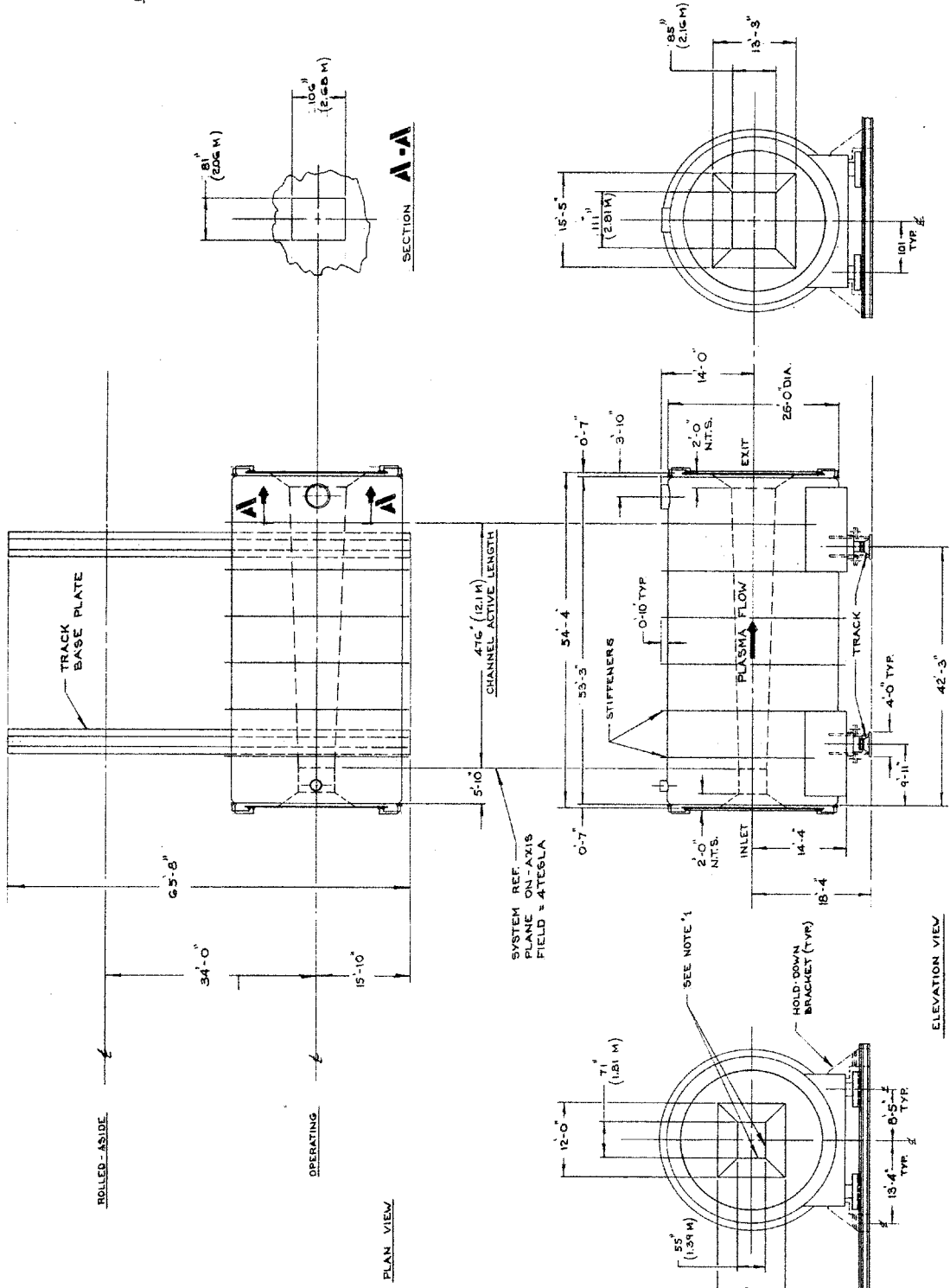
PLAN VIEW

4.2.13H Plan View, Magnet Assembly, MIT EIF 6 T Magnet (Principal Design)

4.2.13J End View, Magnet Assembly, MIT EIF 6 T Magnet (Principal Design)



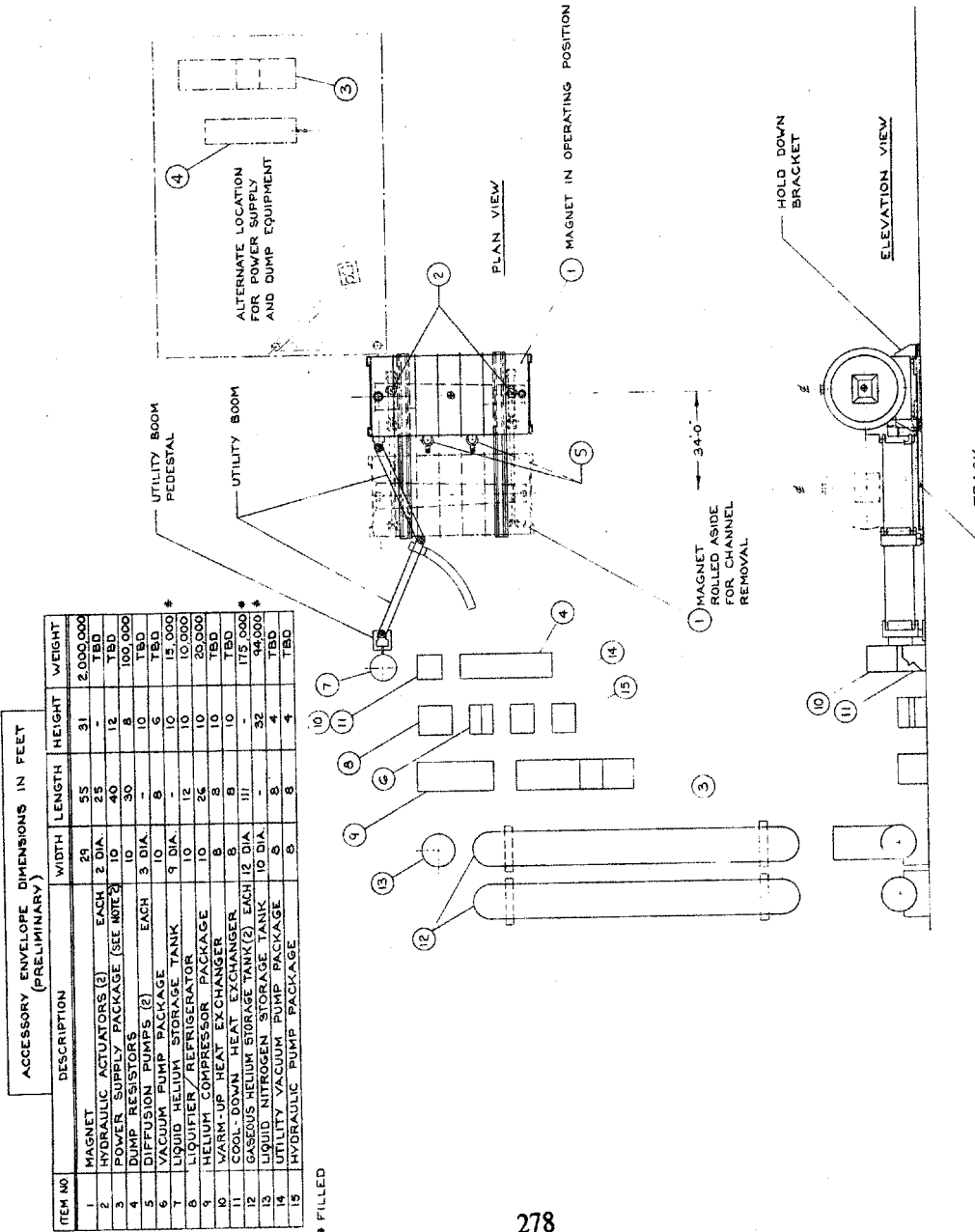




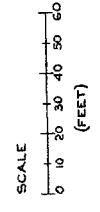
**NOTE:**

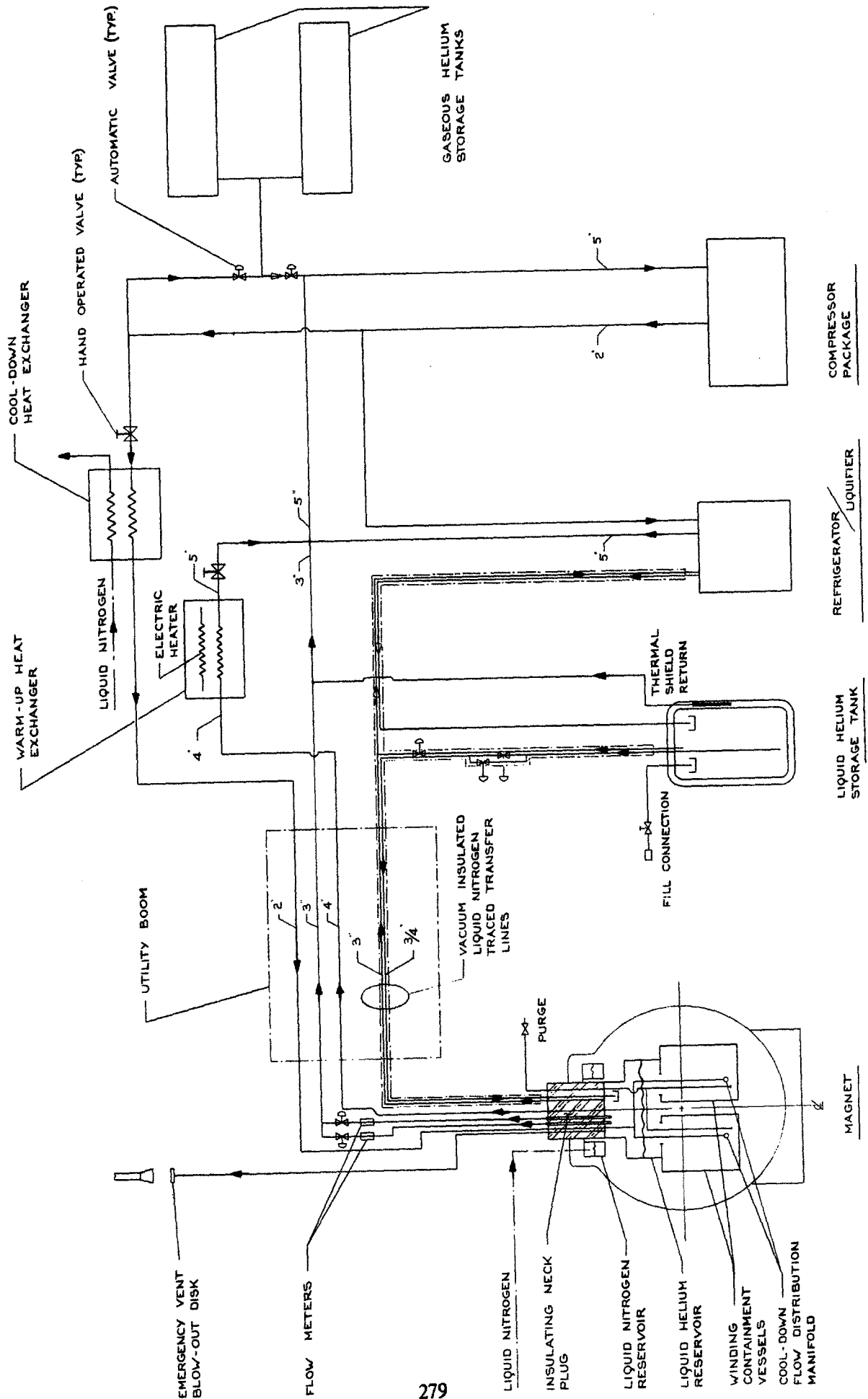
1. BORE CROSS-SECTION DIMENSIONS ARE INSIDE WARM BORE LINER DIMENSIONS ARE IN FEET.
2. EXCEPT WHERE OTHERWISE NOTED HOLD-DOWN BRACKETS ARE DESIGNED TO HOLD MAGNET FIRMLY IN PLACE IN "OPERATING" POSITION. THEY WILL BE DISENGAGED WHEN MAGNET IS TO BE ROLLED ASIDE

4.2.13L Plan and Elevation Views of Magnet System Including Accessories,  
MIT ETF 6 T Magnet (Principal Design)



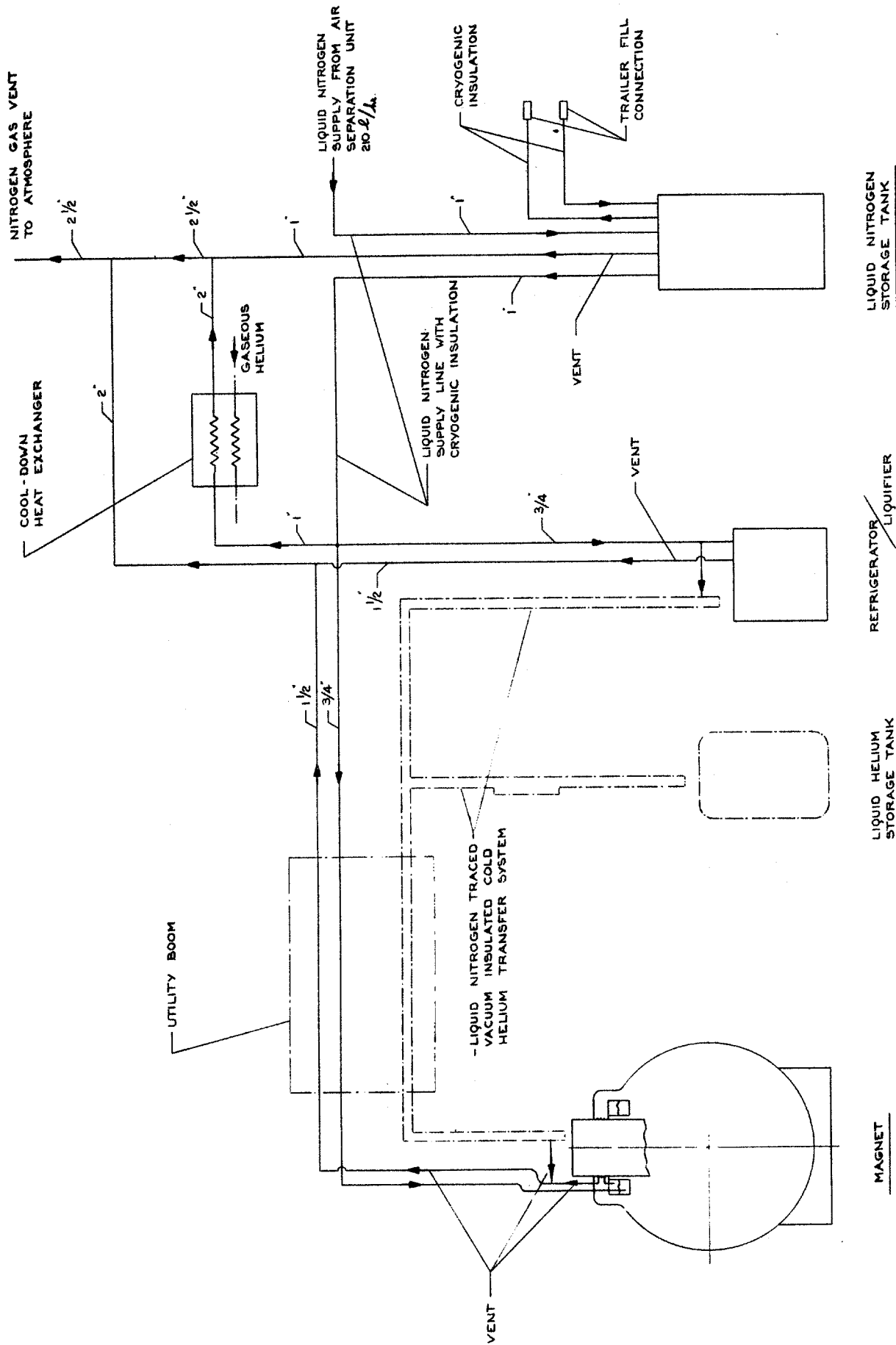
- NOTES:
- EQUIPMENT MAY BE REARRANGED PROVIDED FOLLOWING CONSTRAINTS ARE OBSERVED:  
ITEMS 3, 5, 8, 9, 14, 15 MUST BE NOT LESS THAN 100'-0" FROM MAGNET CENTERLINE, (MAGNETIC EFFECTS).  
ITEMS 3, 4, 7, 8, 9, 10, 11, 13, 14, 15 MUST BE SO LOCATED THAT LENGTH OF PIPING AND ELECTRICAL CABLES TO UTILITY BOOM PEDESTAL WILL BE AS SHORT AS PRACTICAL, CONSISTENT WITH NOTE 1 ABOVE.
  - ITEMS 12, 13 MAY BE LOCATED OUTDOORS. ALL OTHER ITEMS ARE INTENDED TO BE LOCATED INDOORS (SHELTERED FROM WEATHER AND SUB-FREEZING TEMPERATURE).  
POWER SUPPLY PACKAGE (3) INCLUDES RECTIFIER, CIRCUIT BREAKERS, TRANSFORMERS AND CONTROLS



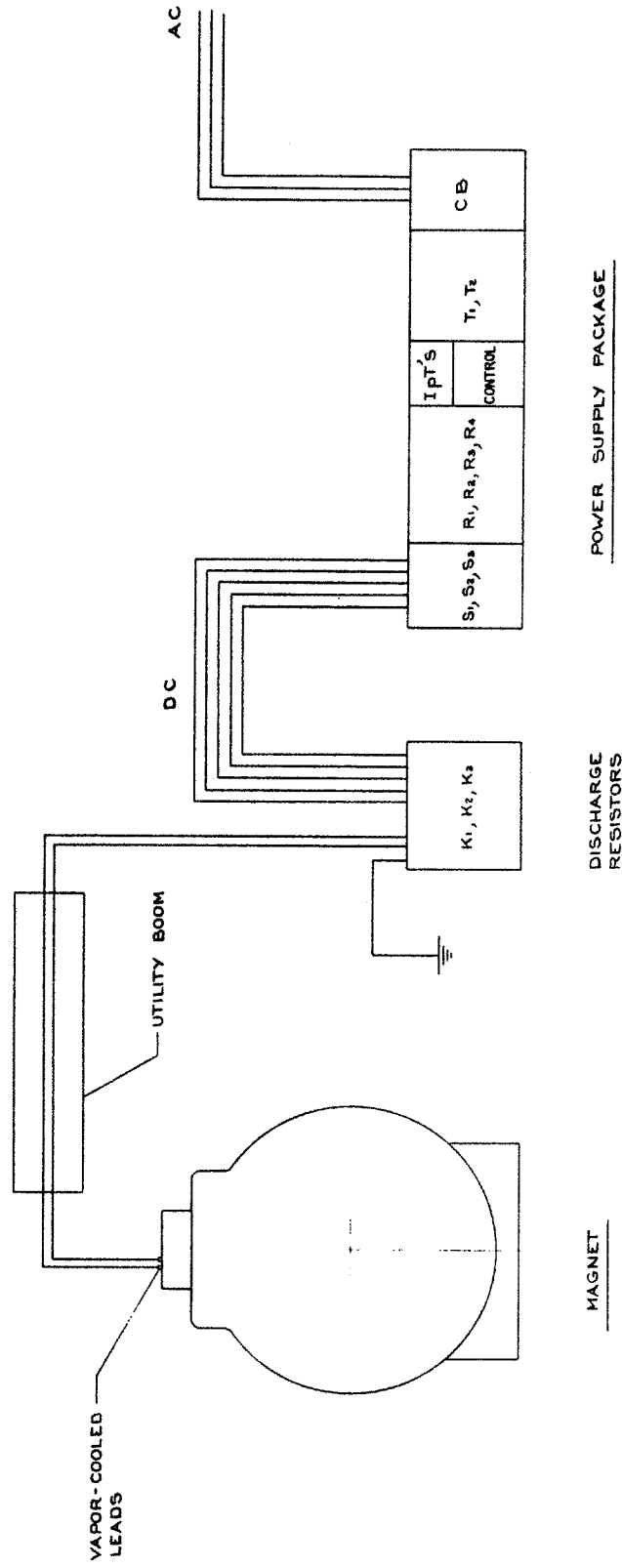
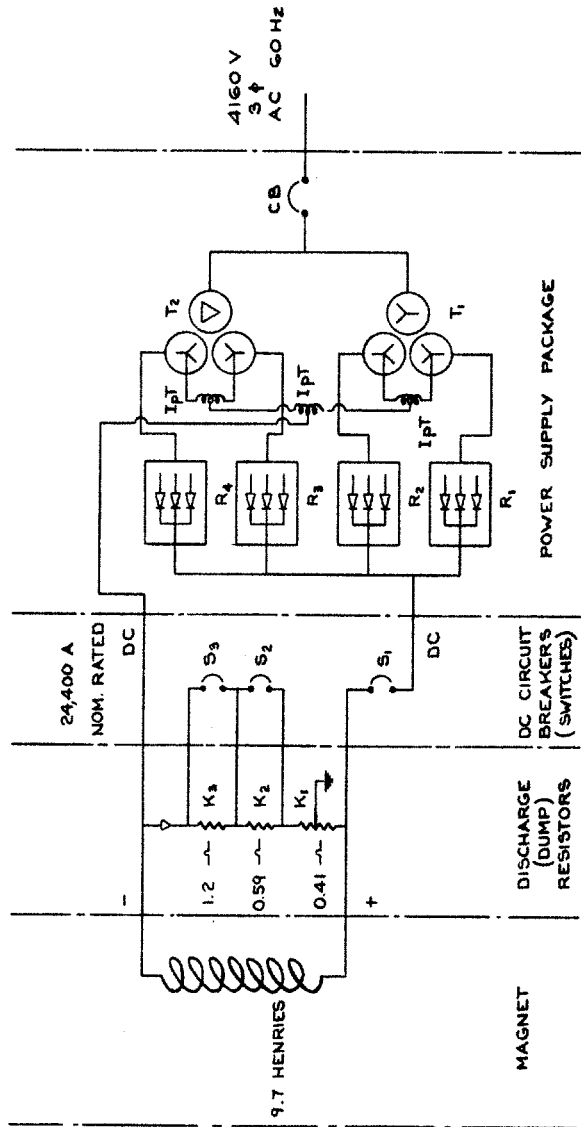


4.2.13M Diagram of Helium (Cryogenic) System, MIT ETF 6 T Magnet

4.2.13N Diagram of Nitrogen (Cryogenic) System, MIT ETF 6 T Magnet



- T = TRANSFORMER
- I<sub>PT</sub> = INTERPHASE TRANSFORMER
- R = RECTIFIER
- CB = AC CIRCUIT BREAKER
- S = DC CIRCUIT BREAKER
- K = DISCHARGE (DUMP) RESISTOR



4.2.13P Diagram of Electrical System, MIT ETF 6 T Magnet

#### 4.2.14 Disk Generator Magnet Studies

Several studies of commercial-scale disk generator magnets were made by MIT during the report period. The work was done in conjunction with DOE sponsored research and development on disk-type MHD generators by the Westinghouse Advanced Energy Systems Division.

A single coil solenoid disk magnet design was developed which permits the operation of one channel on each magnet face. Installing a channel on each side of the solenoid doubles the MHD power output compared to a single-side system, without increasing magnet cost. The magnet system concept, shown in an artist's conceptual sketch, Figure 4.2.14A, was designed for a 1000 MWe channel with 20 m<sup>3</sup> of active volume and a 5.21 m outer radius. The magnet provides 7 T axial field to the direct-fired MHD disk channel.

This design effort also included the development of approximate scaling laws for single coil disk magnet dimensions, stresses and costs in terms of channel dimensions and channel power. Single solenoid disk magnets were also compared with split-pair disk magnets. Figure 4.2.14B shows in outline the two systems. The split pair magnet requires much more complex structural and cryogenic designs and the separation structure must penetrate the channel thereby diminishing accessibility. However, the split-pair does use less conductor and has only a minimal radial field component in the channel region.

If only one channel is used with the single disk magnet the cost is comparable to that of a split-pair magnet. However, if a double channel is used, for the same 1000 MWe the single solenoid disk magnet is considerably less expensive.

Further information on these studies is contained in Reference 80, pages 2-127 to 2-141..

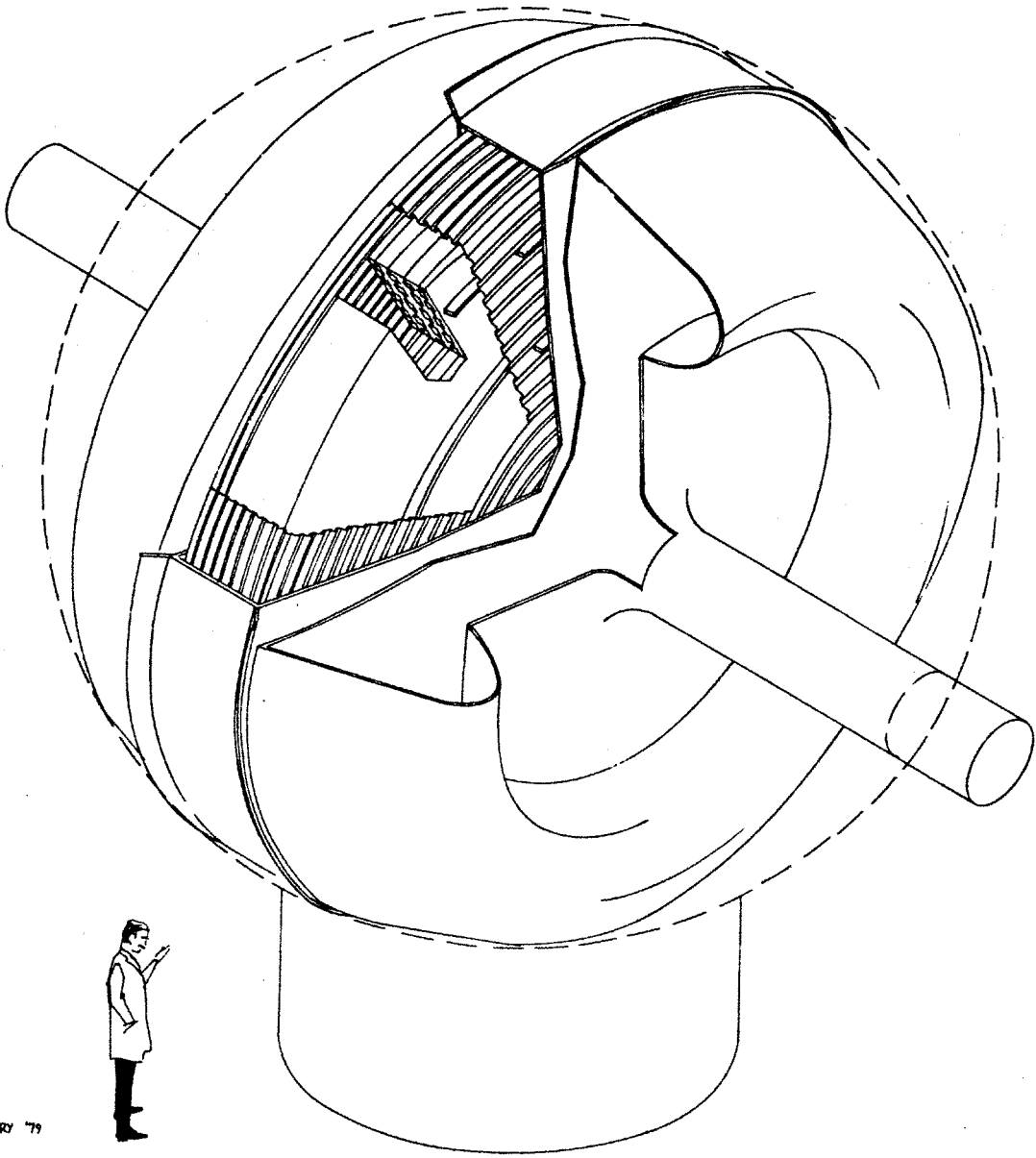
#### 4.2.15 Magnet Design Variations Study by AVCO

As a part of the conceptual design phase leading to the development of the 6 T baseload magnet reference designs described in Sections 4.2.3 and 4.2.4, AVCO investigated several design variations including the following:

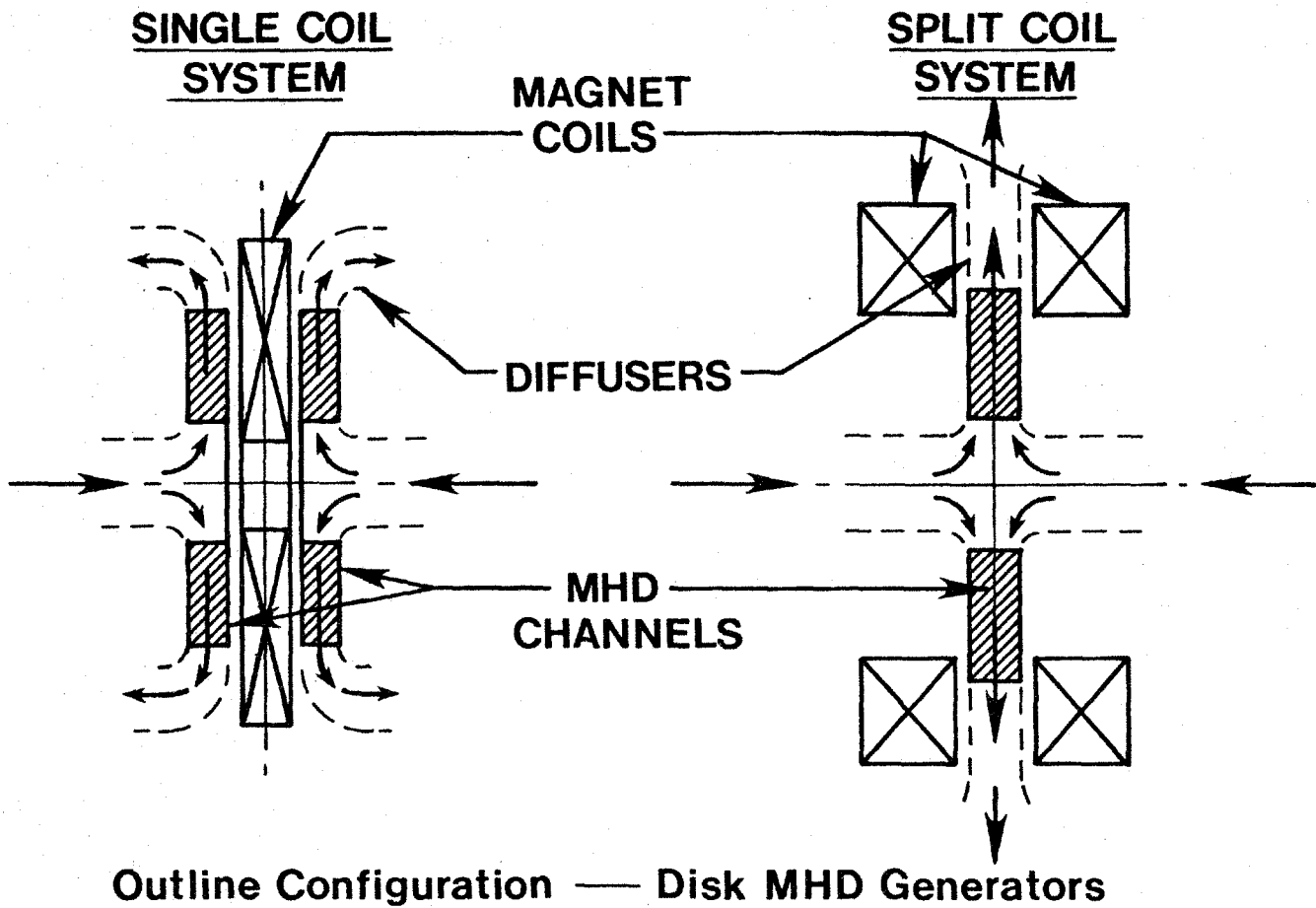
1. 6 T circular saddle baseload magnet with solid ring girder superstructure (instead of I-beam girders).  
Comment: Use of solid girders results in smaller structure and Dewar outside diameter, but greater girder weight. The purpose of the study was to determine how the overall weight of this design compares with that of other designs.
2. 5 T circular saddle baseload magnet (I-beam girders), same bore size as 6 T design.
3. 7 T circular saddle baseload magnet (I-beam girders), same bore size as 6 T design.  
Comment: The purpose of investigating 5 T and 7 T designs was to determine how overall magnet size and weight vary with variation in design field strength, keeping bore size constant.

Conceptual designs of the 6 T baseload magnets (circular and rectangular saddles) and the magnets with variations were developed in parallel. These designs are shown in Figures 4.2.15 through E. Total weight and stored magnetic energies were estimated. Total weights and stored magnetic energies are plotted vs field strength in Figure 4.2.15F. Normalized weights of components are compared in the bar chart in Figure 4.2.15G. Significant results of the studies are as follows:

1. The total weight of the solid girder circular-saddle design is substantially greater than the weight of either the I-beam girder circular-saddle or the rectangular-saddle designs (all 6 T field strength). Cost reductions resulting from simpler construction and the slight reduction in vacuum jacket size are more than offset by

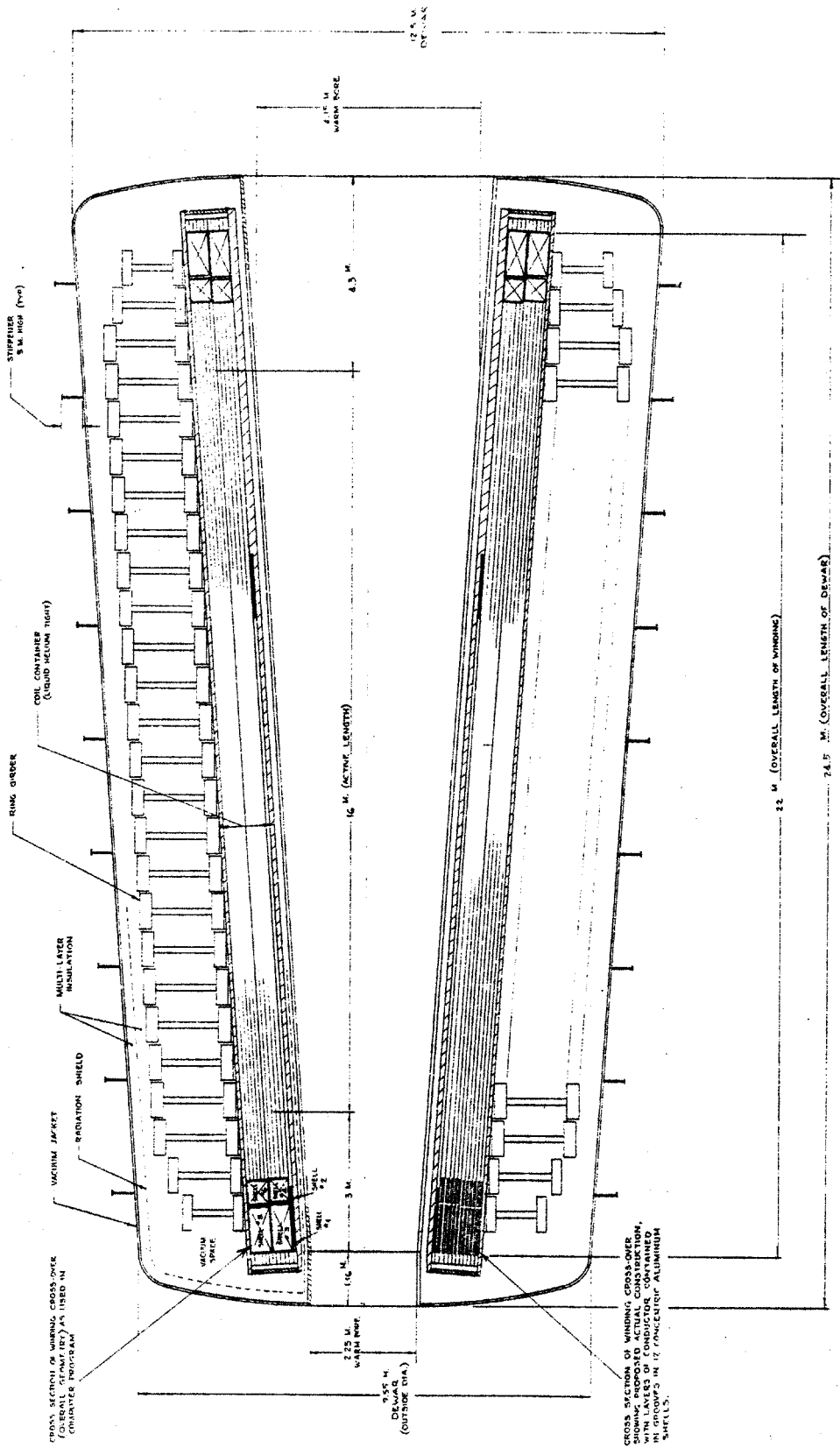


4.2.14A Artist's Conception of Single Coil Solenoid Disk Magnet Design



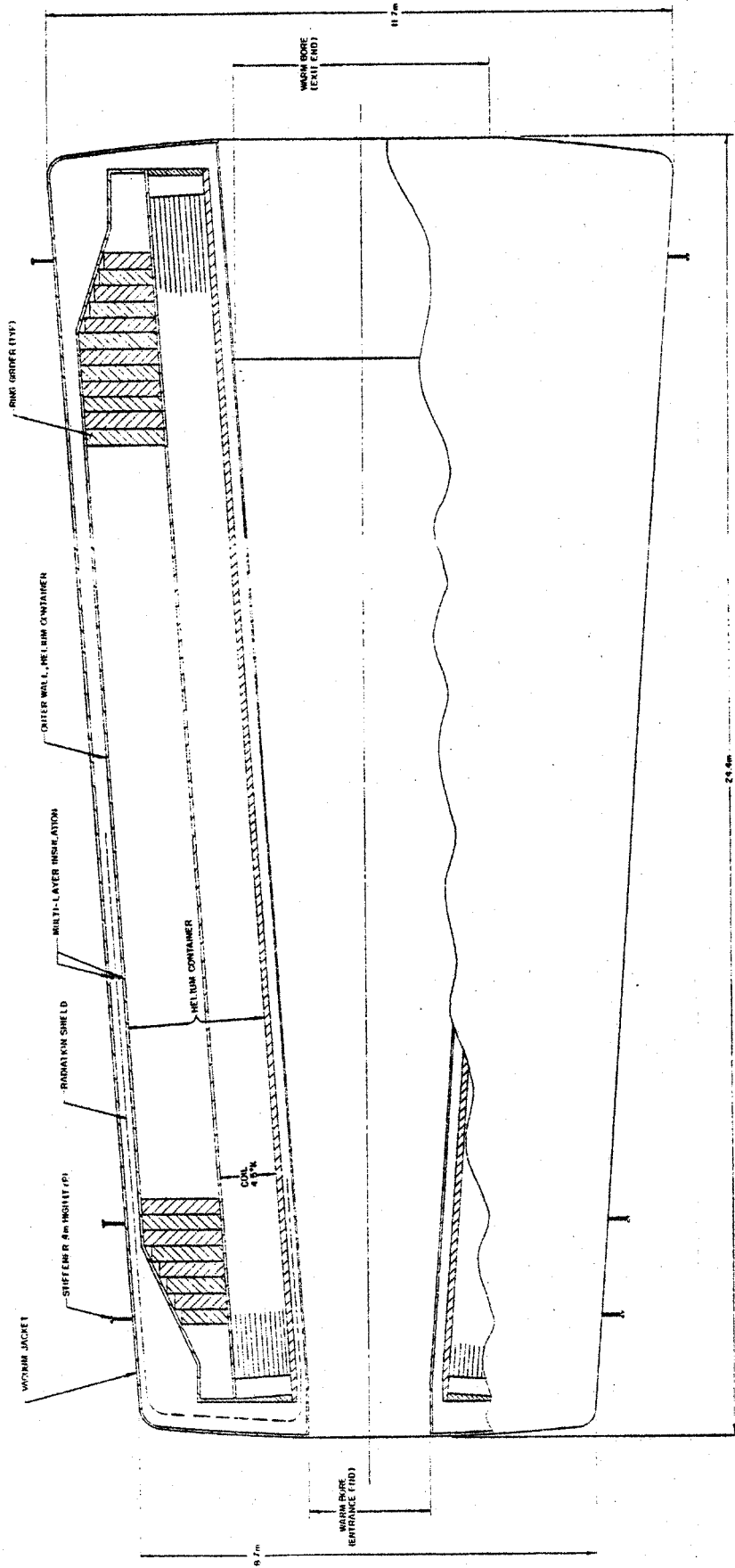
4.2.14B Diagram Showing Single Solenoid Disk Magnets and Split Pair Magnets Compared

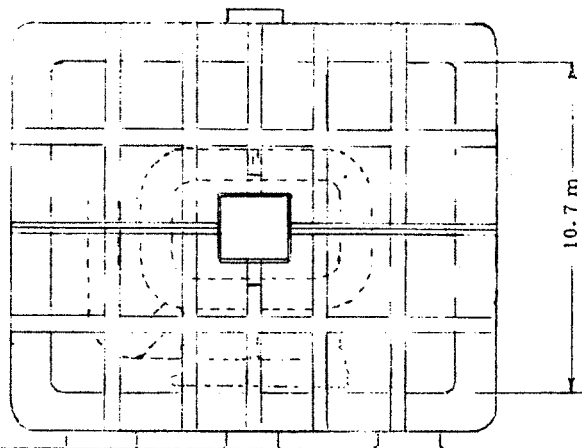
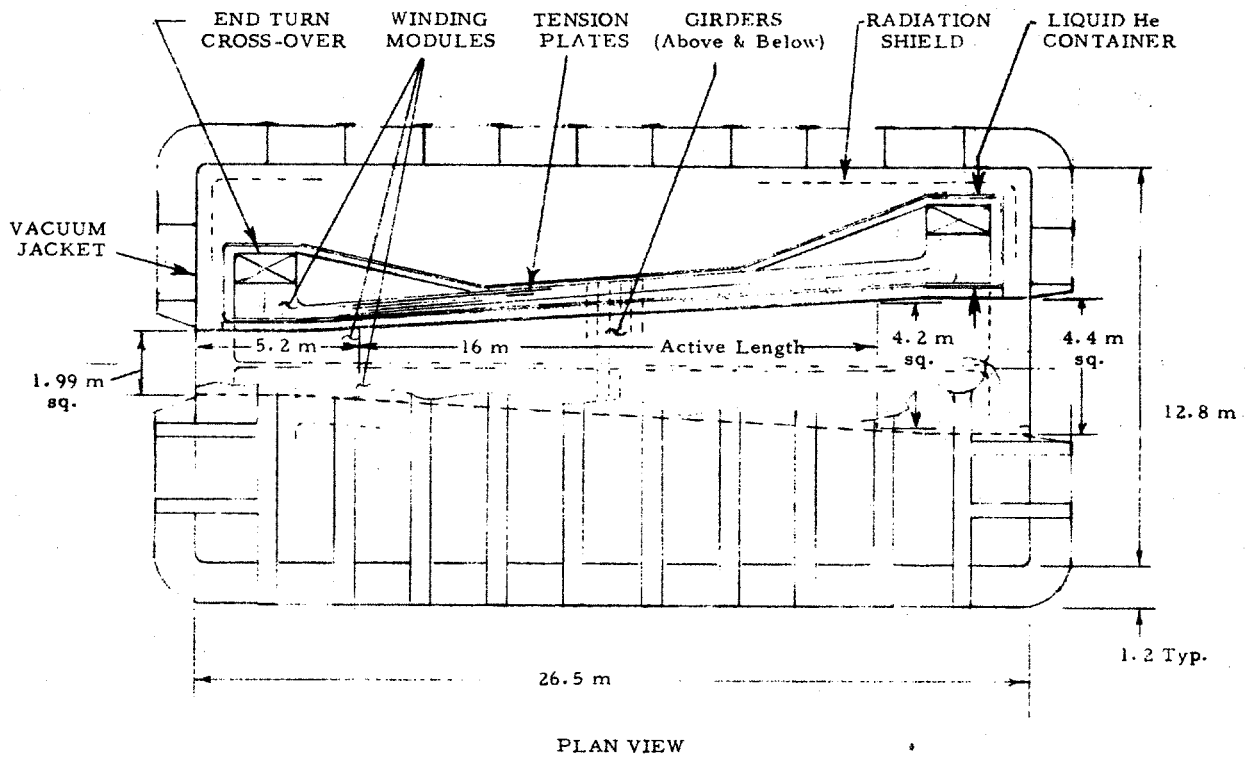




4.2.15A Cutaway Plan View (Conceptual) of Baseload Size 6 T Circular Saddle Magnet with I-Beam Ring Girders, Design BL6-1

4.2.15B Cutaway Plan View (Conceptual) of Baseload Size 6 T Circular Saddle Magnet  
with Solid Ring Girders, Design BL6-2

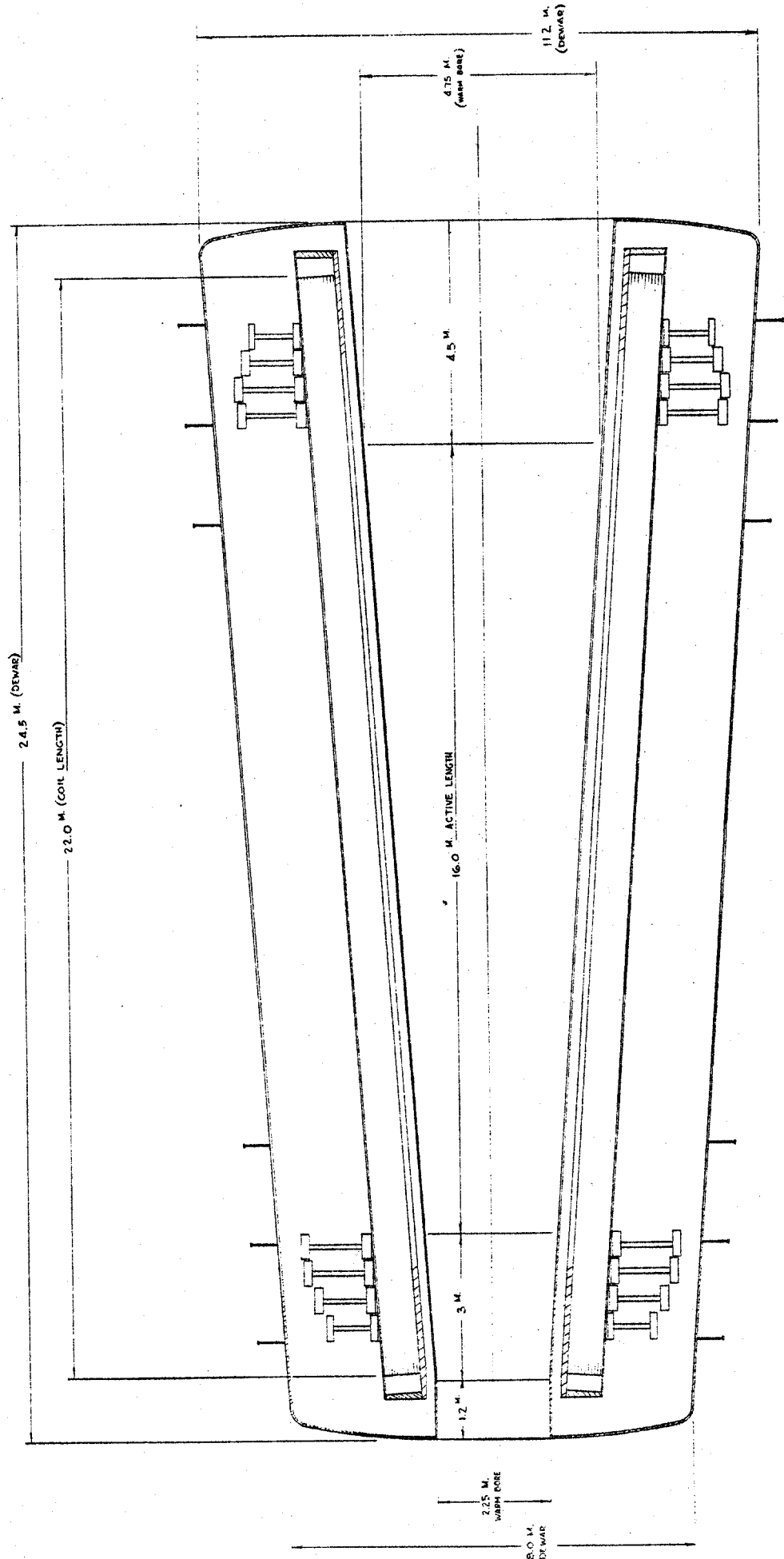


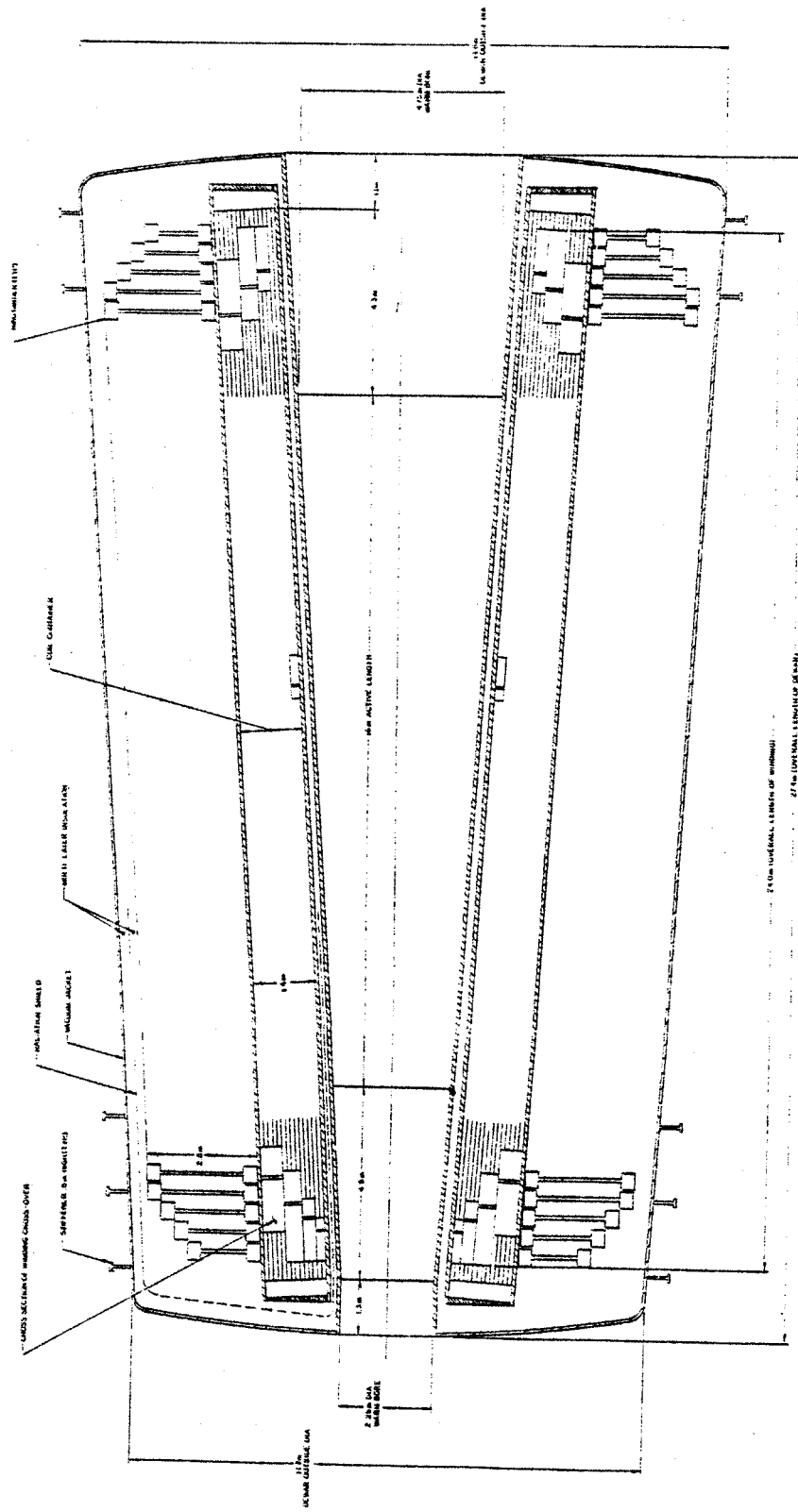


END VIEW (Inlet End)

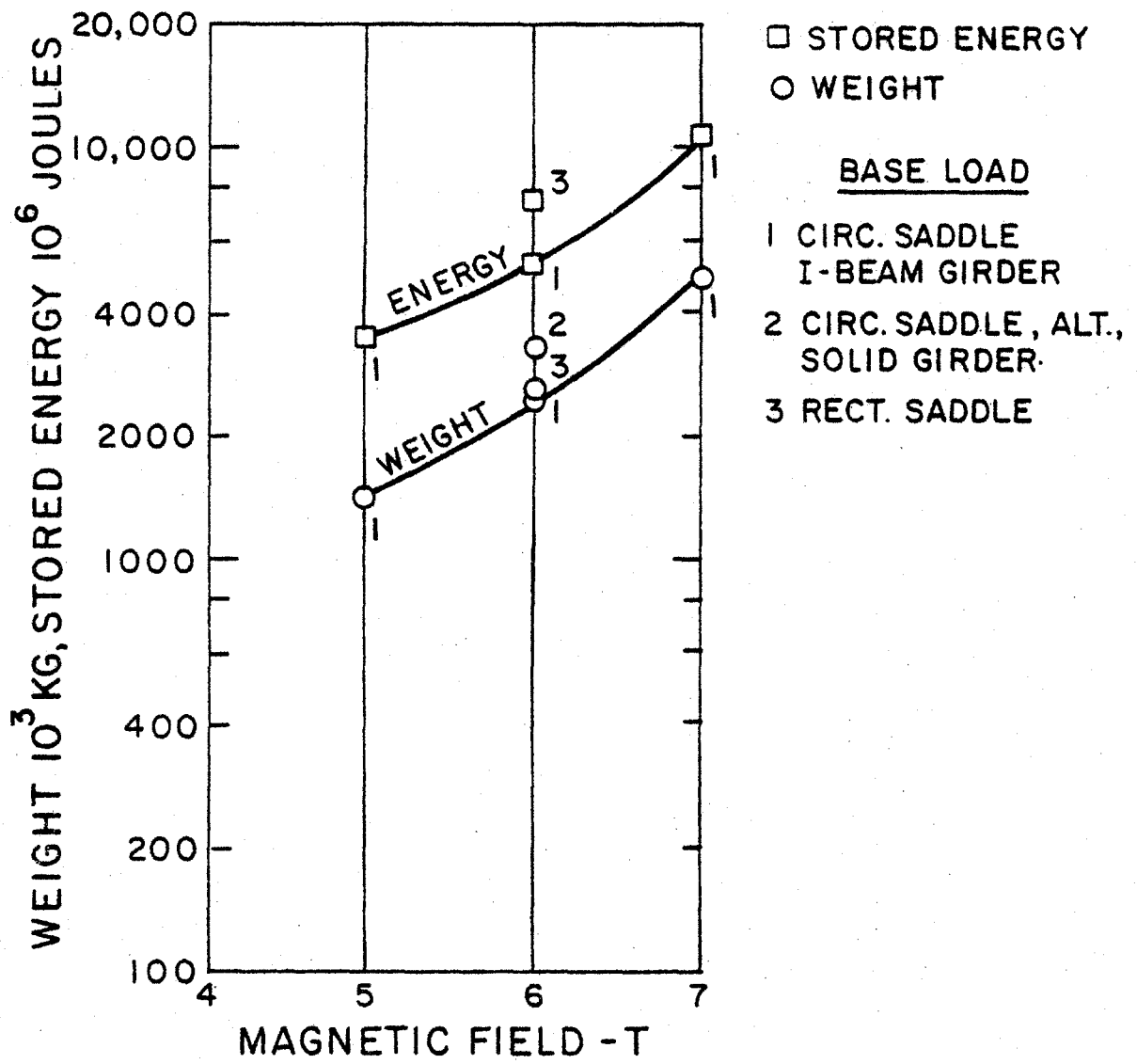
4.2.15C    Cutaway Plan View and End View (Conceptual) of Baseload Size 6 T Rectangular Saddle Magnet, Design BL6-3

4.2.15D Cutaway Plan View (Conceptual) of Baseload Size 5 T Circular Saddle Magnet, Design BL5-1

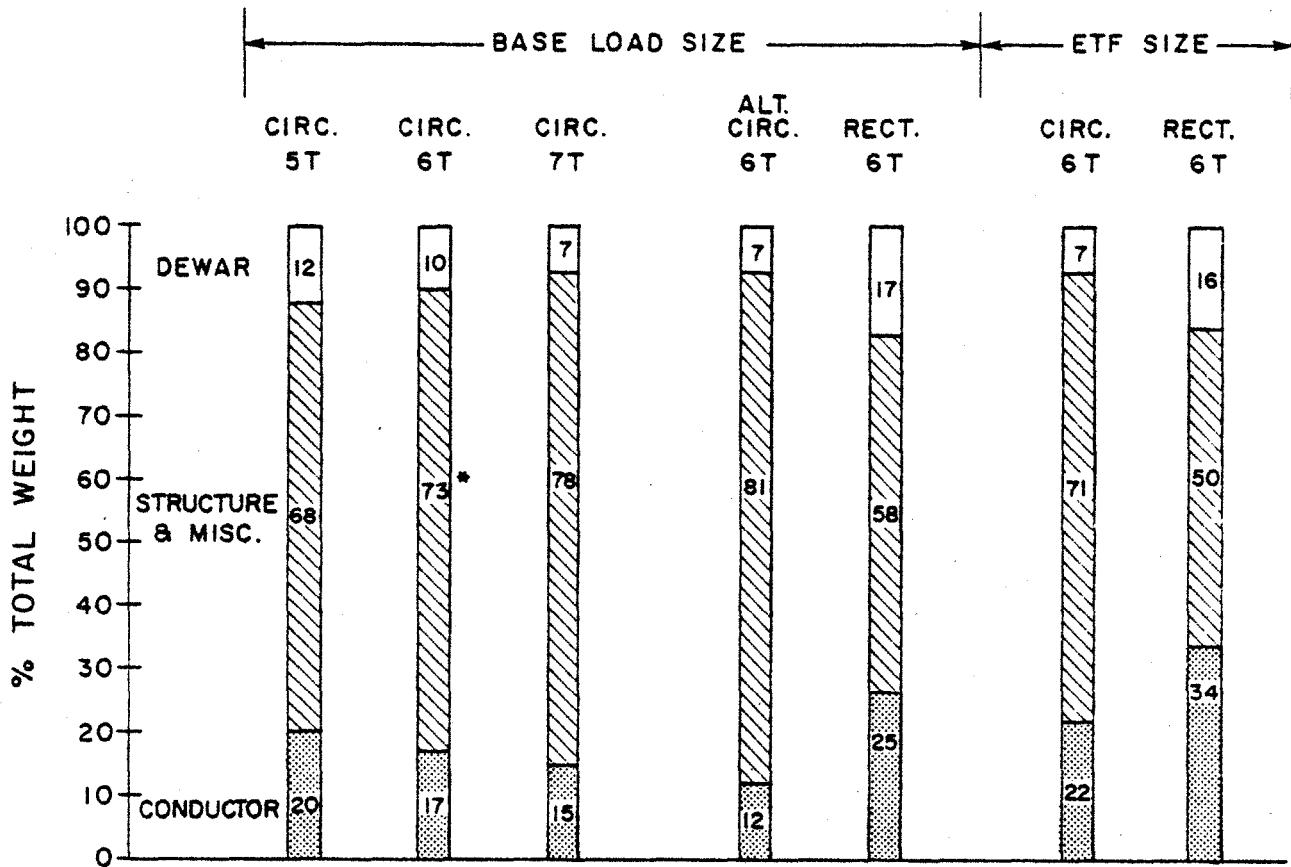




4.2.15E Cutaway Plan View (Conceptual) of Baseload Size 7 T Circular Saddle Magnet, Design BL7-1



4.2.15F Graph of Estimated Weights and Stored Energies of Conceptual Design Magnets



\* STRUCTURE WEIGHT OF 73% INCLUDES RING GIRDERS, 41%, AND OTHER STRUCTURAL PARTS, INSULATION, ETC. 32%.

G5615

4.2.15G Bar Chart - Normalized Weights of Major Components of Conceptual Design Magnets

the greater material cost. Therefore, the solid girder design is considered less attractive than the others and does not merit further attention.

2. The size, weight and stored energy of the circular saddle magnet design rises moderately going from 5 T to 6 T and rapidly from 6 T to 7 T (see Figure 4.2.16F). The study showed that the 7 T design was approaching the limit, with regard to peak-on-axis field, of practical magnet design using NbTi conductor. Further information on these studies is contained in Reference 58.

#### **4.2.16 Special Magnet System Design Studies, Roll-Aside and Roll-Apart**

Several schemes to facilitate channel changout in MHD magnet and flow train systems were discussed in the Workshop on Magnet-Channel Interfacing held at MIT on November 18, 1980. The changout schemes and other subjects discussed at the Workshop are covered in Section 4.1.20. The changout schemes are illustrated in Figures 4.1.20B, C, D and E of that section.

Two of these schemes, magnet roll-aside and roll-apart were investigated in some detail by MIT, as reported in the following subsections.

All magnet system reference and conceptual designs described in Section 4 incorporated one piece, stationary magnets, except for the two ETF designs described in Subsection 4.2.13 where roll-aside provisions were incorporated so that the magnets could be moved to facilitate channel changout. With the one piece, stationary magnets, it was assumed that channel changout would be accomplished by moving the diffuser and then withdrawing the channel into the space vacated by the diffuser.

Schemes which provide for channel changout without moving the diffuser are considered advantageous by some in the MHD community and were therefore studied by MIT, as reported in Sections 4.2.16.1 and 4.2.16.2 below.

##### **4.2.16.1 Roll-Aside Scheme Evaluation**

The magnet system for the ETF 200 MWe Power Plant, described in Section 4.2.13, incorporates a roll-aside arrangement to facilitate channel changout. Tracks, rollers and hydraulic actuators are provided so that the magnet can be rolled sideways a distance of 34 feet. A swinging utility boom carries flexible jointed piping and power buss so that it is not necessary to disconnect these utilities when the magnet is moved. The roll-aside arrangement was incorporated by direction from NASA LeRC. (See Figure 4.2.13L)

This arrangement was selected by NASA in lieu of the alternative arrangement involving moving the diffuser, because the problems of interfacing with other equipment appeared at the time to be easier to handle if only the magnet moved. It was agreed that the decision was subject to review in the future, but the system incorporating the magnet roll-aside provision was frozen for the ETF Conceptual Design Program.

To evaluate the impact of the roll-aside arrangement on the magnet system cost and integrity, an investigation was made at NASA LeRC's request, in October 1980. Magnet rotation (turntable scheme) as an alternative to roll-aside was included in the investigation. The conclusions derived by MIT from the investigation were that the roll-aside or turntable features would add to the complexity of the magnet system, would have a slight adverse effect on system reliability and would increase overall system costs up to  $\$1 \times 10^6$ .

It was felt that moving the diffuser to one side (with magnet stationary) would be a more practical and cost effective way to facilitate channel changout.



It was recommended that the final decision on whether or not to provide magnet roll-aside capability should not be made until a thorough investigation of alternative channel changeout provisions is made and various arrangements are compared and evaluated.

Additional information concerning the investigation of the roll-aside arrangement is contained in Attachment E to Reference 73.

#### 4.2.16.2 Roll-Apart Scheme Studies

Another possible arrangement to facilitate channel changeout and to provide easier access to the channel for repair is to design the magnet so that the two halves can be rolled apart. (See Figure 4.1.20E)

With halves rolled apart, excellent access to channel connections is provided and after disconnecting the channel from the combustor/nozzle and the diffuser, the channel can be removed either upward (by crane) or sideways (by dolly). A number of water-cooled, iron yoke MHD test facility magnets now in use are of the roll-apart design. However, no superconducting MHD magnets of roll-apart design have ever been built.

Incorporating the roll-apart feature in a superconducting MHD magnet involves extensive redesign of the structure and Dewar. The structure tends to become heavier and the Dewar more complicated and not as reliable.

An early, brief review by MIT of the general concept of a roll-apart superconducting magnet indicated that for a given size bore, structure weight would probably be double the structure weight of a conventional one piece superconducting magnet, and heat leakage to the cold regions would be substantially higher. The cost of the roll-apart magnet would therefore be expected to be considerably higher. For these reasons, further work on roll-apart designs was not pursued. Within the time and funding limitations existing, it was necessary to restrict effort to higher priority items.

In 1980, further consideration was given to roll-apart designs in connection with magnet-channel packaging studies conducted by MIT and MEPPSCO (Reference 76) as reported in Section 4.1.20, and in connection with conceptual designs developed by AVCO and reviewed by MIT.

The packaging studies showed that the roll-apart design is advantageous because channel cooling water piping and power wiring can be brought out along the magnet split-line, instead of only at the ends. For the type of channel which requires a large number of power take-offs, considerable space can be saved by using the split-line access, and the overall size of the warm bore can be made smaller. This means that windings and structure can be smaller and the cost of the magnet reduced.

The AVCO designs reviewed incorporated (proprietary) ideas which may be useful in working toward an optimum structure for a roll-apart superconducting magnet. By very tight packaging of the channel and its structure inside the bore, and by special structural design, AVCO suggested that the roll-apart system might have cost advantages compared to the one piece magnet system.

The review concluded that there is not yet sufficient evidence to permit a meaningful evaluation of the roll-apart magnet in comparison with one piece magnets, but the roll-apart concept shows sufficient promise to justify future, in-depth investigation.

#### **4.2.17 Framework for Design Selection**

A systematic approach (framework) was developed by MIT to serve as a guide in the commercial-scale magnet system design effort and the supporting investigations.

A network diagram, Figure 4.2.17A, was prepared showing the relationships of the various elements which influence magnet system design, and the sequence of events which occur in a logical program of design development, evaluation and final selection. The network diagram includes, but is not limited to, the following items:

System design requirements

(user requirements, facility constraints, code restrictions)

Magnet configuration options

(circular saddle, rectangular saddle, saddle plus racetrack, circular bore, square bore, rectangular bore)

Rated current options

(20 kA, 50 kA, 100 kA)

Component design options

(type and materials of conductor, substructure, helium vessel, superstructure, thermal shield)

Ratings of subsystems

(power supply and discharge, cryogenic support)

Evaluation criteria

(cost, risk, schedule, interfacing characteristics)

A second network diagram, Figure 4.2.17B, shows the kinds and sequences of supporting investigations that are required in conjunction with the magnet system design and selection program depicted in Figure 4.2.17A.

Since the network approach was instituted in 1978, a number of magnet design options have been explored and supporting investigations have been conducted. However, because some reference designs are still in process, the network approach has not yet been applied systematically to make design selections. The network diagrams have not yet been updated to reflect the results of work done to date and to revise scheduling to agree with most recent MHD program target extensions. These steps should be taken at such time as a positive future direction of the overall MHD magnet program is resolved.

More detailed information on the framework plan and proposed implementation is contained in Reference 81.

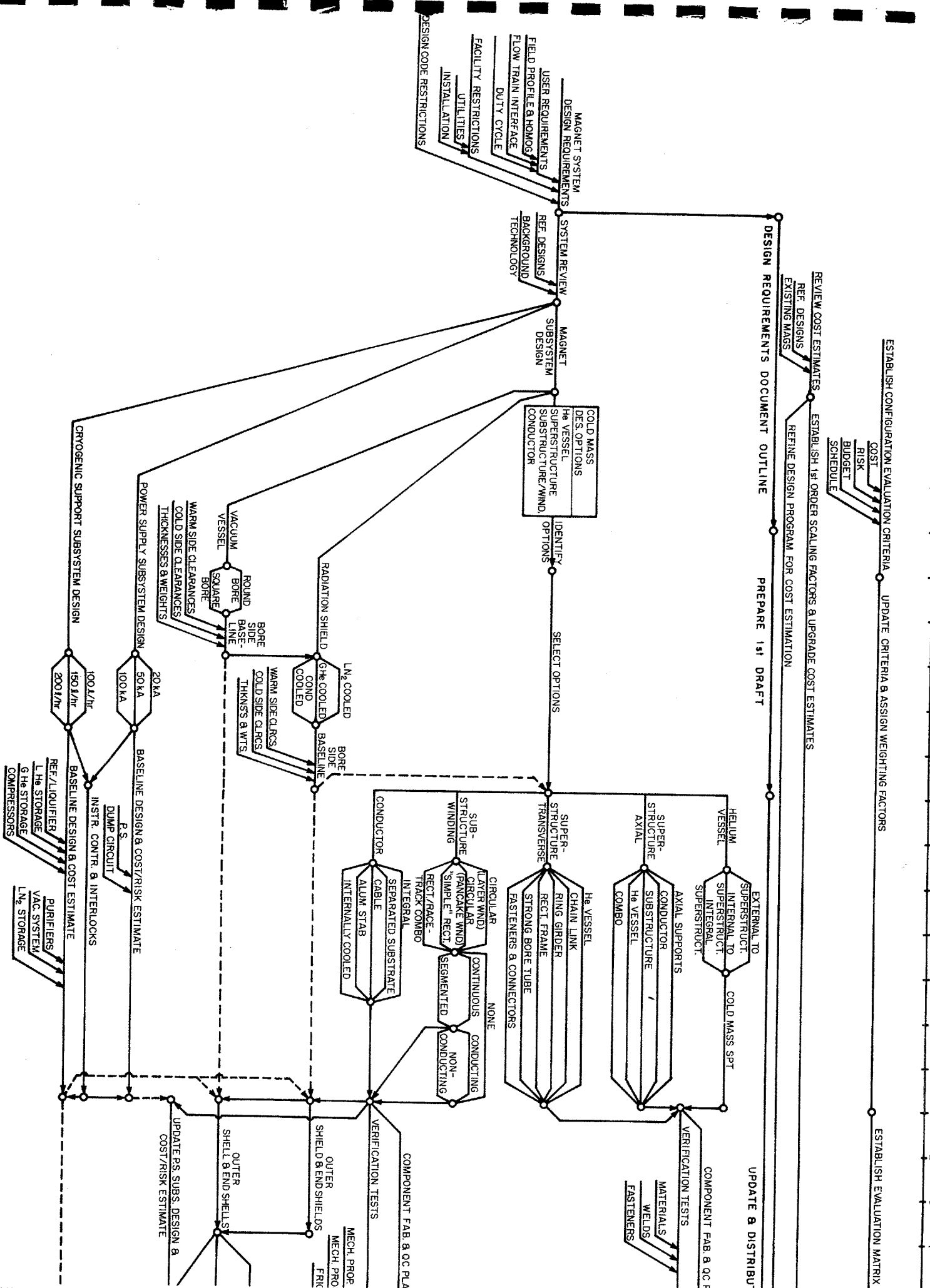
#### **4.3 Design and Construction Supervision of Magnets for Government-Sponsored MHD Test Facilities**

Responsibility for developing conceptual designs and for managing detail design and construction by industry rested with MIT for two large test facility superconducting magnets, one for DOE's MHD Component Development and Integration Facility (CDIF) and the other for the Stanford High Temperature Gasdynamics Laboratory MHD test facility. MIT was also responsible for design and procurement of conventional water-cooled MHD magnets for the CDIF and for the AVCO MHD test facility. In addition, MIT provided assistance to DOE in reviewing designs and performing special investigations relative to two additional superconducting MHD magnet programs, namely the superconducting magnet for the USSR U25 Bypass MHD test facility (U.S. SCMS) and for the Coal-Fired Flow Facility (CFFF). The work done on these programs is summarized in the following paragraphs.

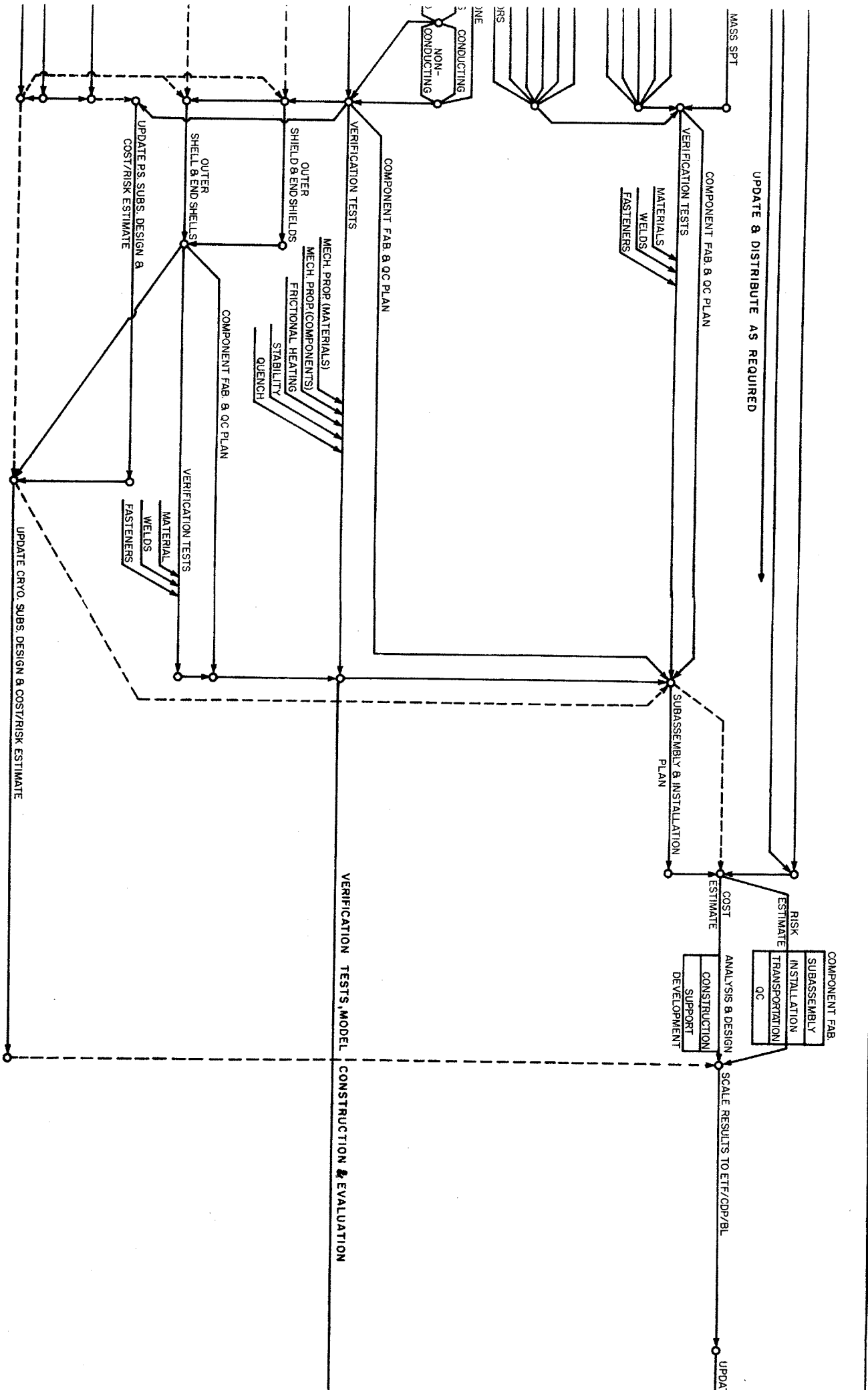
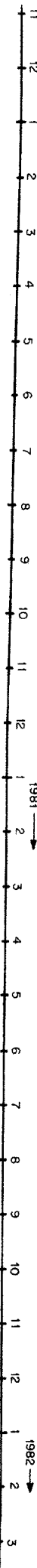
1978 →

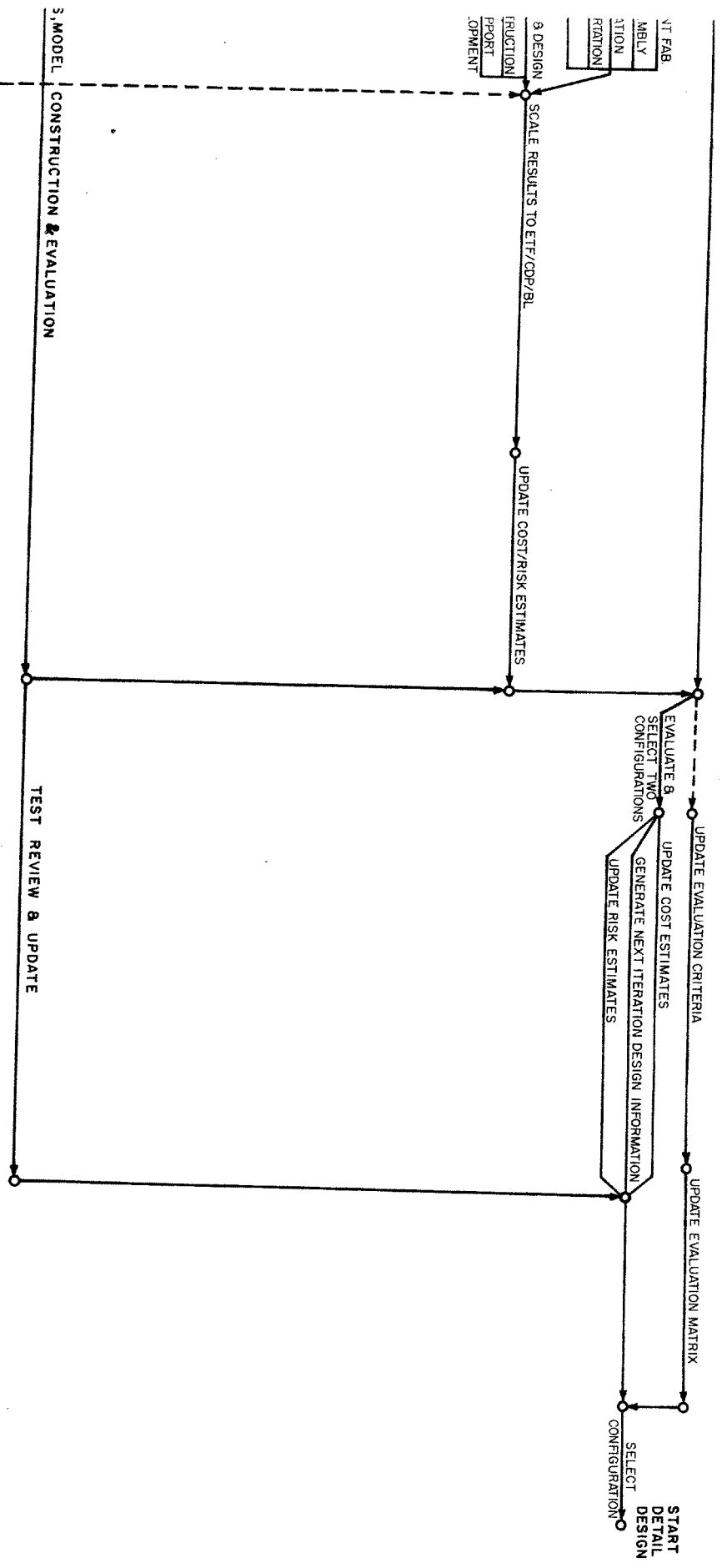
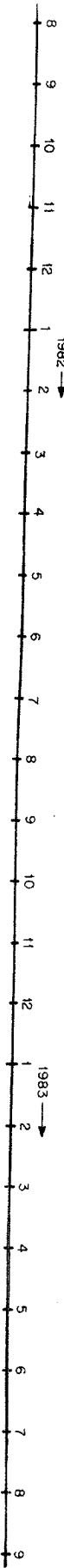
1979 →

1980 →



ESTABLISH EVALUATION MATRIX (UPDATE AS REQUIRED)





VT FAB.  
 ASSEMBLY  
 ACTION  
 RATION

3. DESIGN  
 INSTRUCTION  
 REPORT  
 COMMENT

3. MODEL CONSTRUCTION & EVALUATION

TEST REVIEW & UPDATE

START  
 DETAIL  
 DESIGN

SELECT  
 CONFIGURATION

EVALUATE &  
 SELECT TWO  
 CONFIGURATIONS

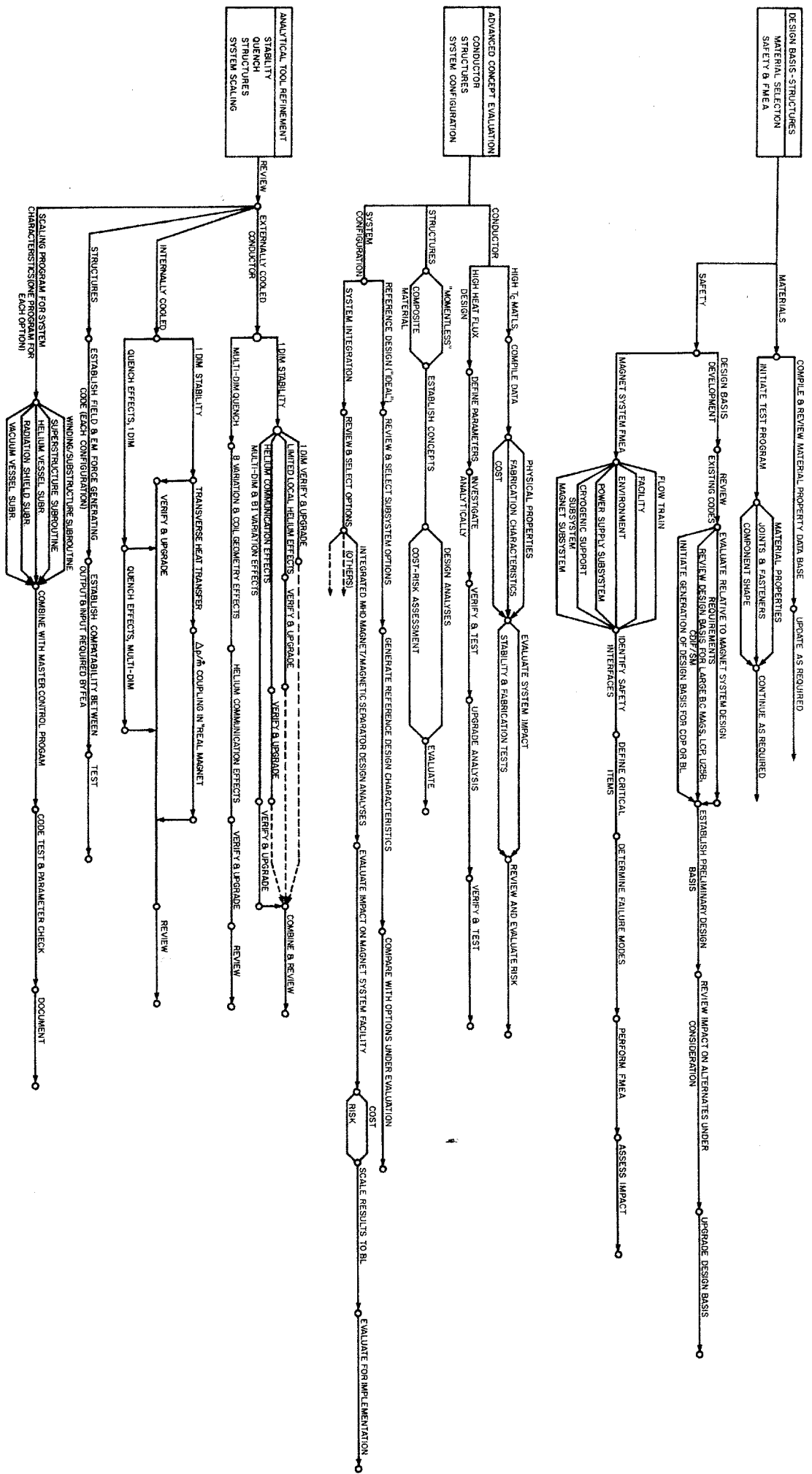
UPDATE COST ESTIMATES  
 GENERATE NEXT ITERATION DESIGN INFORMATION  
 UPDATE RISK ESTIMATES

UPDATE EVALUATION CRITERIA

UPDATE EVALUATION MATRIX

UPDATE COST/RISK ESTIMATES

SCALE RESULTS TO ETF/CDP/BL



4.2.17B Network Diagram, Commercial-Scale MHD Magnet Supporting Investigations

## 4.3.1 Component Development and Integration Test Facility Superconducting Magnet (CDIF/SM)

### 4.3.1.1 Summary

The CDIF 6 T superconducting magnet was intended for installation in the DOE-sponsored Component Development and Integration Test Facility at Butte, Montana. It was intended to be used in connection with the testing of developmental MHD flow trains of ratings up to 50 MW<sub>t</sub>. The design criteria established by ERDA are listed in Table 4.3.1-1.

A conceptual design for the CDIF superconducting MHD magnet was developed by MIT at the beginning of the report period (Reference 53). A 45° rectangular saddle coil was depicted, with conductors individually supported in a grooved substructure and accumulated magnetic forces supported by a tension-band superstructure. An RFP was issued, bids received and evaluated and a contract placed with GE for detail design and construction of a magnet based on the MIT concept. During the detail design process carried out by GE, the design was modified to incorporate a nonmetallic (G-10) substructure and the more conventional I-beam and tension-strap superstructure, instead of the tension band scheme.

The design was completed in June, 1979 and construction was initiated. At the end of calendar year 1981, manufacture of the conductor was substantially completed, substructure and superstructure components were manufactured and on hand at GE, and winding had been started. Delays in completion of detail design, delays in component manufacture, particularly conductor manufacture, and in DOE's providing funding beyond original estimates, combined to cause a delay beyond the original estimated program schedule of 24 months. As of the date of this report, the contract with GE was in the process of termination and disposition of components of the unfinished magnet was being determined.

### 4.3.1.2 Description

The CDIF/SM is a 6 T 45° rectangular-saddle-coil magnet with a warm bore of rectangular-cross-section at the inlet and square-cross-section at the exit. The conductor used in the coils is a 6130 ampere built-up copper and NbTi composite conductor. It consists of a round, multifilamentary NbTi/Cu composite monolith, soldered into a groove in a square cross section copper substrate which is spirally wrapped with copper wire soldered in place. The winding is modular, with conductor installed in grooves in saddle-shaped support plates (substructure) made of G-10 epoxy-glass laminate. There are 40 support plates, each carrying one layer of conductor, in each half of the magnet winding. Each turn of conductor is individually supported in the grooved substructure, and magnetic loads exerted on the conductors are carried through the substructure to the main structure without any accumulated load acting on individual conductors. The G-10 substructure serves as electrical insulation for the winding and contains a system of passages which supply liquid helium to the winding for cooling.

The conductor grooves in the substructure plate sections on each side of the magnet warm bore diverge slightly toward the exit end of the magnet, thus producing the desired tapered field profile.

The major force containment structure (superstructure) consists of a central spool piece of stainless steel, and a system of I-beams and tension plates of stainless steel assembled around the winding modules and fastened together by welding. Outward magnetic forces on the central portion of the winding are supported by the main I-beams and tension plates. Longitudinal forces on the end turns are supported by the smaller I-beams located across the ends in combination with the central spool piece, and outside tension plates.

**Table 4.3.1-I**

**Design Criteria  
CDIF Superconducting Magnet**

**Aperture dimensions (room temperature)**

<b>Inlet end</b>	<b>(m)</b>	<b>0.7 × 0.7</b>
<b>Exit end</b>	<b>(m)</b>	<b>0.9 × 0.9</b>
<b>Active field length</b>	<b>(m)</b>	<b>3.0</b>
<b>Peak on-axis field</b>	<b>(T)</b>	<b>6.0</b>



The liquid helium containment vessel consists of a stainless steel shell which surrounds the main structure and is welded at the ends to the central spool piece, which forms the inner wall of the vessel.

The Dewar consists of a liquid nitrogen-cooled stainless steel and copper thermal shield located in vacuum space and surrounding the liquid helium containment vessel, multilayer insulation blankets and a cylindrical vacuum jacket with conical, recessed heads and a rectangular-cross-section warm bore duct, all of welded stainless steel.

The cold mass of the magnet is supported on eight low-heat-leak tension links of filament-wound epoxy fiberglass. The inner ends of the links are connected to lugs welded to the magnet cold structure. The outer ends of the links are connected to bosses on ring girders built into the outer wall of the vacuum jacket. The links are angled to provide support in all three planes.

The characteristics of the CDIF/SM design are listed in Table 4.3.1-II. The calculated axial field profile is shown in Figure 4.3.1A. The coil configuration is shown in Figure 4.3.1B, a typical winding cross section in Figure 4.3.1C and the conductor in Figure 4.3.1D. The cold mass assembly is shown in Figure 4.3.1E and a cutaway view of the magnet and vacuum jacket assembly in Figure 4.3.1F.

The CDIF/SM system includes a water-cooled warm bore liner, a cryogenic support subsystem, a power supply and discharge subsystem, vacuum pumping equipment, instruments and controls. The cryogenic subsystem and power supply subsystem are shown diagrammatically in Figure 4.3.1G.

The manufacturing plan calls for shipment of all major (subcontracted) components from manufacturers to the magnet assembly site at Schenectady, N.Y. Substructure plate sections, premachined, are then joined to form complete saddle-shaped subplates. The conductor is installed and plates are stacked to form complete windings. Structure and Dewar are assembled around the winding. Plans called for shipment of the completed assembly from Schenectady to the plant site, Butte, Montana, on special rail car.

More detailed information on the CDIF/SM design is contained in References 19 and 82.

### **4.3.2 Stanford Test Facility Superconducting Magnet (SSM)**

#### **4.3.2.1 Summary**

The Stanford 7 T superconducting magnet was intended for installation in the Stanford University High Temperature Gasdynamics Laboratory. The magnet was designed to be enclosed in a 500 ton low carbon steel magnetic shield.

The design criteria for the magnet are listed in Table 4.3.2-I. Work on the conceptual design of the Stanford superconducting magnet was initiated by MIT early in the report period. Alternate concepts, a racetrack split-pair, and a circular-saddle were investigated. An RFP was issued by MIT, bids were received and evaluated in 1978, and a contract placed with GD for detail design and construction of a 7 T circular saddle magnet.

GD proceeded with preliminary and detail design based on the MIT conceptual design in which the windings are installed in machined grooves in cylindrical shells (substructures) of aluminum alloy. The detail design was substantially completed in early 1980. Funds for construction were delayed, and the program was redirected in April 1980 to address redesign of the SSM to incorporate the CASK concept, an alternative design for circular saddle magnets developed earlier by GD for a commercial-scale MHD magnet as described in Section 4.2.5. The change to the CASK design was considered advantageous because that design was expected to be less expensive to manufacture, to require less time in manufacture and to embody equal or better

Table 4.3.1-II Sheet 1 of 3

Design Characteristics  
CDIF Superconducting Magnet (CDIF/SM)

Date of design		1978
MHD power train data		
Thermal power train input	(MWt)	50
MHD power output	(MWe)	1 to 5
Magnet data		
Magnet type	—	45° rect. saddle
Warm bore liner?	—	Yes
Magnetic field:		
Peak on-axis field	(T)	6.0
Active field length	(m)	3.0
Field at start of active length	(T)	4.8
Field at end of active length	(T)	4.8
Peak field in winding	(T)	6.94
Dimensions:		
Aperture, warm bore inlet <sup>a</sup>	(m)	0.776 × 0.976
Aperture, start of active length <sup>a</sup>	(m)	0.776 × 0.976
Aperture, end of active length <sup>a</sup>	(m)	0.976 × 0.976
Aperture, warm bore exit <sup>a</sup>	(m)	0.976 × 0.976
Aperture area, start of active length <sup>a</sup>	(m <sup>2</sup> )	0.757
Aperture area, end of active length <sup>a</sup>	(m <sup>2</sup> )	0.953
Warm bore liner wall (incl. clearance)	(m)	0.038
Vacuum vessel overall length	(m)	6.452
Vacuum vessel outside dia.	(m)	4.110
Warm bore volume, active <sup>a</sup>	(m <sup>3</sup> )	2.57

<sup>a</sup> Dimensions inside warm bore, without liner

Table 4.3.1-II Sheet 2 of 3

## Winding characteristics:

Build, winding cross section	(m)	0.622
Number of winding modules (or layers) per half	—	40
Design current, I	(kA)	6.13
Winding current density, average, $J\lambda^a$	( $10^7$ A/cm <sup>2</sup> )	1.87
Packing factor, $\lambda^a$	—	0.30
Conductor current density, $J^a$	( $10^7$ A/cm <sup>2</sup> )	65.2
Total number of turns, N	—	2320
Total length of conductor	(km)	30.8
Ampere turns, NI	( $10^6$ A)	14.22
Ampere meters	( $10^8$ Am)	1.89
Inductance	(H)	12.8
Stored energy	(MJ)	240
Conductor type	—	Built-up
Conductor materials	—	NbTi-Cu
Conductor dimensions, overall <sup>a</sup>	(cm)	1.28 × 1.28
Copper-to-superconductor ratio <sup>a</sup>	—	11.1
LHe to conductor ratio (vol.) <sup>a</sup>	—	0.19
Heat flux <sup>a</sup>	(W/cm <sup>2</sup> )	0.4

## Weights:

Conductor	(tonnes)	35.9
Insulation	(tonnes)	incl. below
Substructure	(tonnes)	7.7
Superstructure	(tonnes)	45.7
Liquid He vessel	(tonnes)	24.5
Total cold mass	(tonnes)	113.8
Thermal shield, cold mass supports, etc	(tonnes)	4.2
Vacuum vessel	(tonnes)	24.5
Miscellaneous	(tonnes)	1.8
Total magnet weight	(tonnes)	144.3

<sup>a</sup> Where graded winding is incorporated, values listed are for high field region of winding.

Table 4.3.1-II Sheet 3 of 3

**Cryogenic data:**

Operating temperature at winding	(K)	4.5
Operating temperature, thermal shield	(K)	77
Thermal shield coolant	—	LN <sub>2</sub>
Heat load, LHe region, not incl. leads	(W)	38.7
LHe for lead cooling at design current	(ℓ/hr)	20.0
Refrigerator/liqefier capacity	(ℓ/hr)	35
Cool-down time	(hrs)	624

**Power supply and discharge data:**

Number of current leads	—	2
Rated voltage, power supply	(V)	10
Minimum charge time	(hrs)	2
Resistance, emergency dump resistor	(Ω)	0.16
Emergency discharge time constant	(sec)	60
Maximum discharge voltage, terminal	(V)	1000

**Materials of construction:**

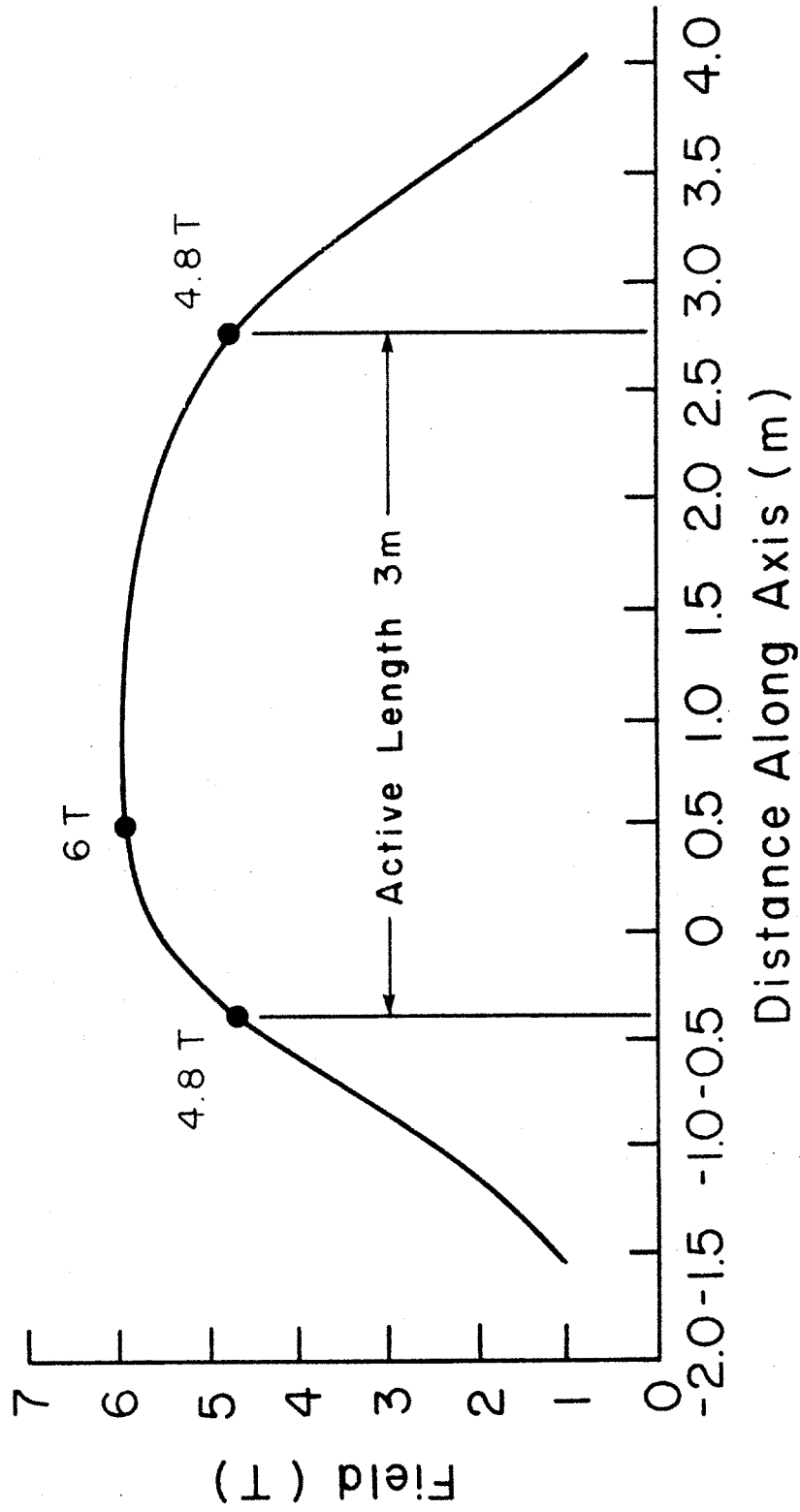
Winding substructure	—	G-10
Superstructure	—	SS 304 LN
Liquid helium vessel	—	SS 304 LN
Thermal shield	—	SS 304L & Cu
Vacuum vessel	—	SS 304

**Design stresses:**

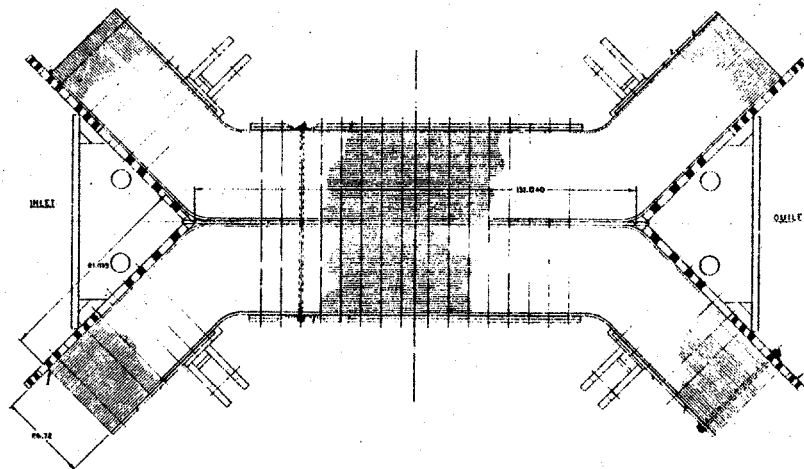
Conductor (compressive)	(MPa)	69
Winding substructure (compressive)	(MPa)	184
Superstructure (bending)	(MPa)	460

**Pressure rating**

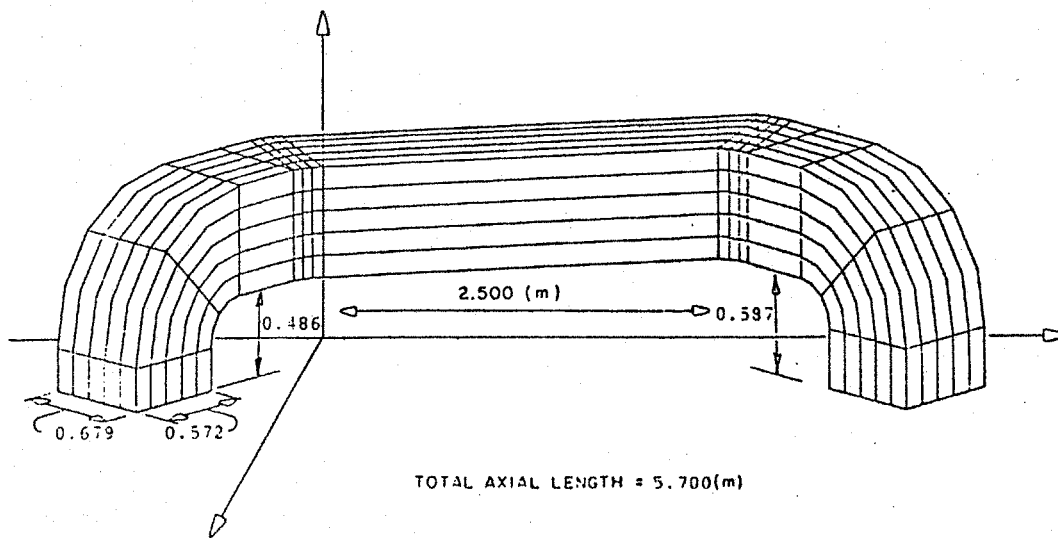
Liquid helium vessel		
Normal operating	(atm)	1.3
Maximum design	(atm)	4



4.3.1A Curve of On-Axis Field vs Distance Along Axis for CDIF Superconducting Magnet (CDIF/SM)

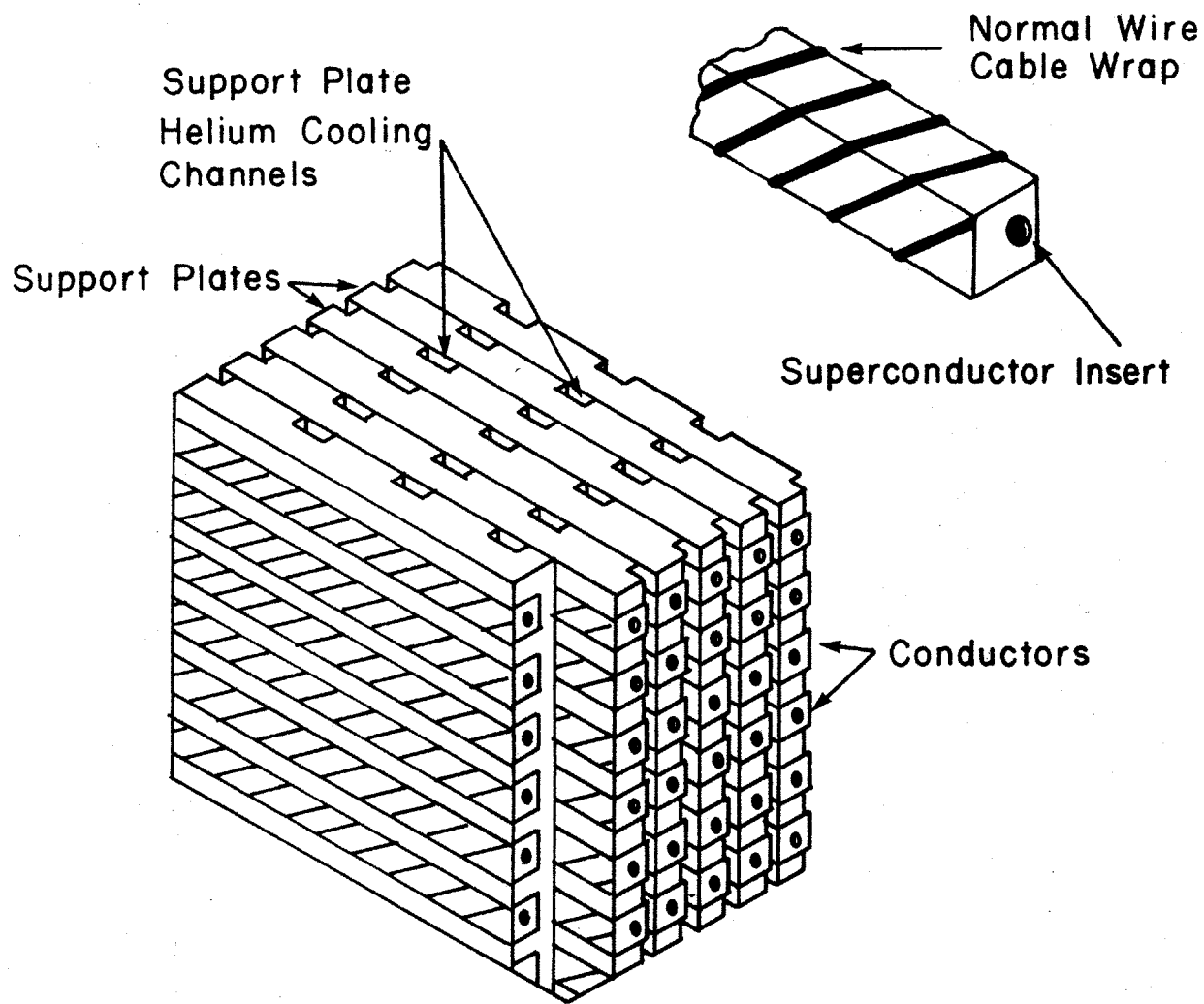


TOP VIEW - COIL ASSEMBLY



VIEW OF ONE QUADRANT (ELEVATION)  
SHOWING MAJOR DIMENSIONS

4.3.1B Diagram Showing Coil Configuration, CDIF Superconducting Magnet (CDIF/SM)

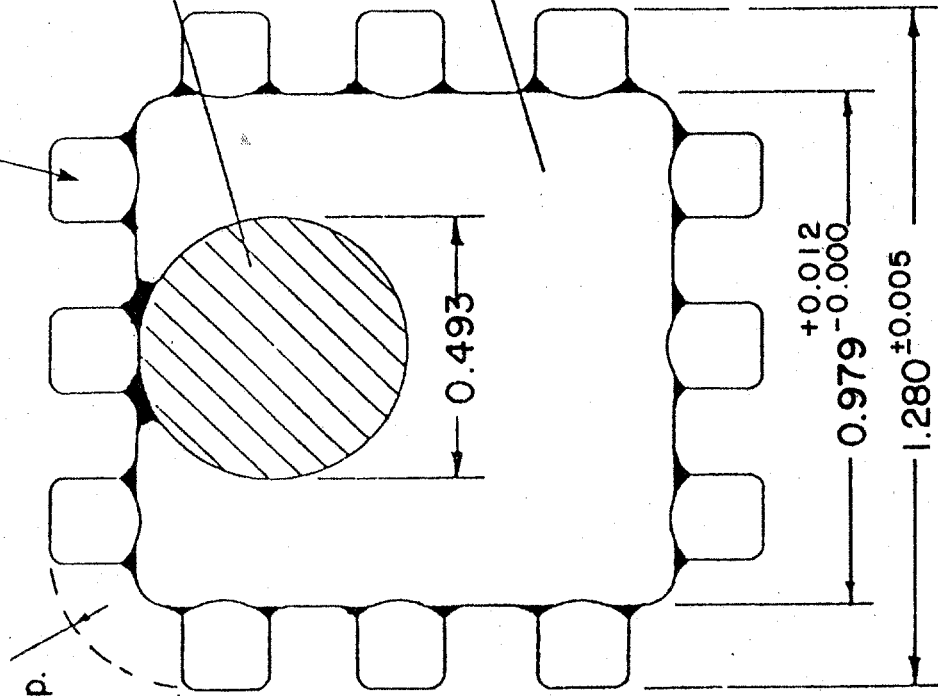


4.3.1C Sketch Showing Typical Winding Cross Section, CDIF Superconducting Magnet (CDIF/SM)

4.3.1D Sketch Showing Conductor, CDIF Superconducting Magnet (CDIF/SM)

External Overwrap Strands  
 $0.1636 \text{ cm} \begin{matrix} +4\% \\ -1\% \end{matrix}$  Dia. Equivalent Round

.254 cm  
 Min. Rad. Typ.



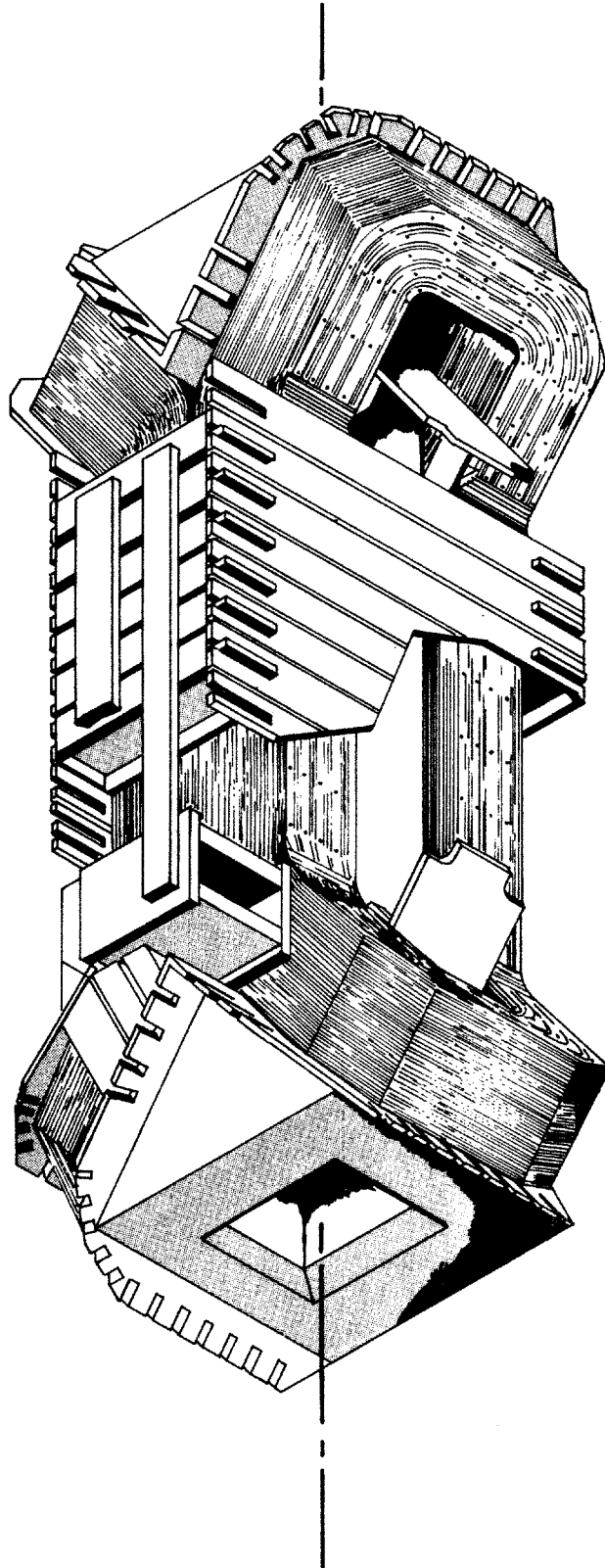
Superconductor Element  $+0.025$   
 Equivalent Round:  $0.493 \text{ cm} \begin{matrix} -0.000 \end{matrix}$

Minimum Distance Between Overwrap Strands  
 (Helium Channels) : 0.100 cm  
 Cable Pitch of Overwrap Strands about  
 Core Element :  $17^\circ \pm 3^\circ$

Copper Stabilizer Core

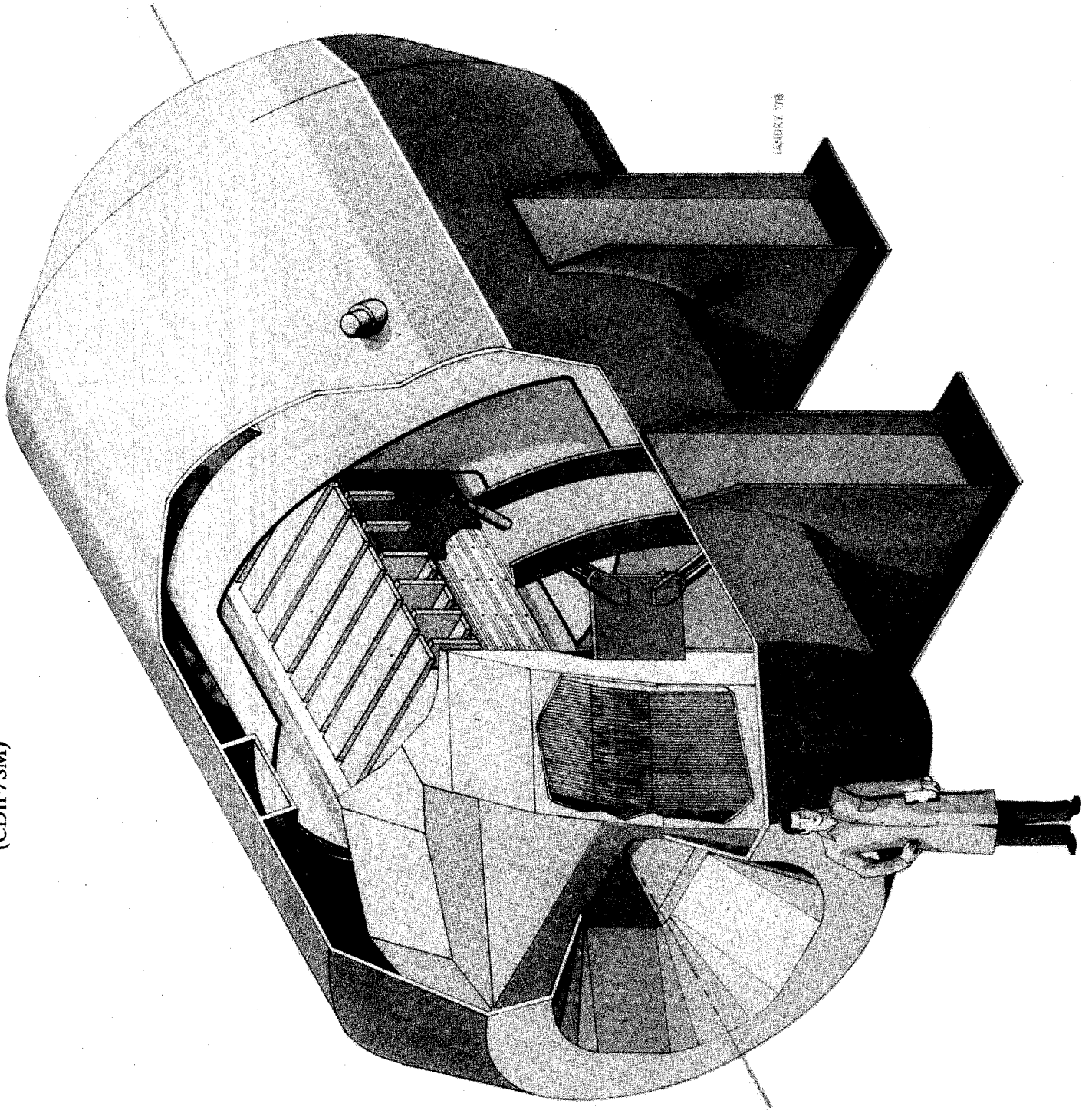
All Dimensions are in cm

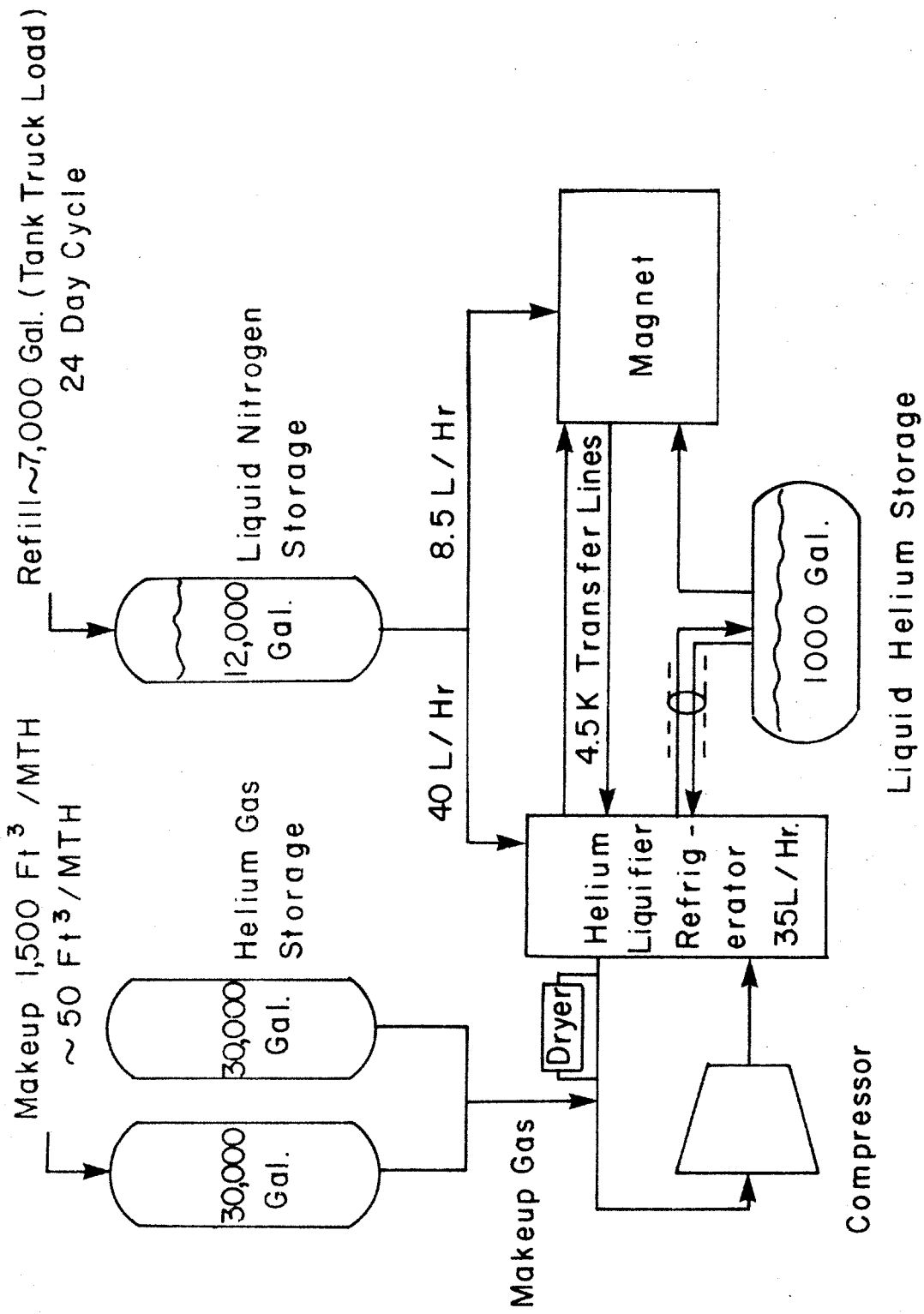




4.3.1E Layout Showing Cold Mass Assembly, CDIF Superconducting Magnet (CDIF/SM)

4.3.1F Cutaway View of Magnet and Vacuum Jacket Assembly, CDIF Superconducting Magnet (CDIF/SM)





4.3.1G Diagram, Cryogenic Subsystem and Power Supply Subsystem, CDIF Superconducting Magnet (CDIF/SM)

Table 4.3.2-I

Design Criteria for Stanford  
Superconducting MHD Magnet (SSM)

Active Volume (m)	0.14 × 0.30 × 1.50
Magnetic field in active volume (T)	7.0 minimum
Maximum field variation in active volume	± 2.5%
Magnetic field outside shield <sup>a</sup> (G)	100 maximum

<sup>a</sup> Shield is an iron enclosure surrounding the magnet and dimensioned to provide working space around the magnet inside the shield.

reliability features as compared to the cylindrical shell design. The Stanford alternative design was designated CASK Magnet Prototype System (CMPS) because the Stanford magnet with CASK features would serve as a prototype for commercial-scale magnets of similar design. Work on the CMPS design continued through 1980 and detail design was nearly complete early in 1981. Due to funding constraints, a stop work order was issued to GD in April 1981. Since then, the program has been on hold and no further design effort has been expended.

#### 4.3.2.2 Description

The Stanford superconducting magnet design is specified to be of the circular saddle type, with a circular cross section warm bore. Unlike other designs described in Section 4.3, the Stanford magnet bore is of constant cross section (no taper), its field profile is without taper and the winding side bundles are parallel (no divergence). Design criteria for the Stanford superconducting magnet (SSM) are listed in Table 4.3.2-I.

Both the initial design (cylindrical shell substructure) and the alternative design (CMPS) are described below. They are similar in external appearance and substantially the same in performance. The characteristics of the two designs are listed in Table 4.3.2-II. The field profiles produced by the two designs are substantially the same; the common field profile is shown in Figure 4.3.2A.

The initial (cylindrical shell) design incorporates a winding consisting of rectangular-cross-section built-up conductor with 5000 A design current, supported in machined grooves in cylindrical, aluminum alloy shells (subplates). There are 15 concentric shells split into 180° segments with a total of 155 channels containing 1181 conductor turns in each winding half. The split is on the vertical axis. The number of conductors per groove varies from 5 to 12. In the middle portion of the winding, magnetic force acting on the conductor bundle in each groove is transmitted through the substructure to the main force containment structure (superstructure) surrounding the winding, without any accumulated loading on the individual bundles. The superstructure consists of stacks of continuous rings of aluminum alloy fitted tightly around the winding and substructure with the aid of wedges. In the end regions of the winding, longitudinal magnetic forces are supported by the substructure alone.

The helium containment vessel consists of an aluminum outer shell, core tube and end plates welded in place around the winding and superstructure. The cryostat consists of a liquid-nitrogen-cooled aluminum alloy thermal radiation shield surrounding the cold mass of the magnet, multilayer insulation blankets, fiberglass tension support straps for the cold mass and a stainless steel vacuum vessel comprised of cylindrical outer shell, concave heads and a cylindrical warm bore tube.

The winding configuration of the cylindrical shell magnet design is shown in Figure 4.3.2B, the conductor configuration in Figure 4.3.2C and the magnet assembly in Figure 4.3.2D.

The alternative design (CMPS) incorporates a winding consisting of a rectangular-cross-section built-up conductor similar in configuration to that of the initial design but with 7400 A design current, supported in a stainless steel substructure of the CASK configuration. The winding is modular. Each half consists of six concentric tiers of two-layer conductor bundles, each bundle supported individually in the stainless steel substructure. Magnetic forces acting on the bundles are transmitted through the substructure to the main force containment structure (ring girders) surrounding the winding, without any accumulated loading on the individual bundles. Turn-to-turn and layer-to-layer electrical insulation consists of strips of G-10 fiberglass laminate, slotted to permit access of liquid helium coolant to the conductor surfaces.

The substructure consists of a system of longitudinal staves, corner blocks and end blocks, assembled with the winding bundles around a cylindrical core tube. Longitudinal magnetic forces on the end turns are supported by the end blocks and staves of the substructure.

Table 4.3.2-II Sheet 1 of 3

Design Characteristics  
Stanford 7 T Superconducting Magnet (SSM)

		<u>Original Design</u>	<u>Alternative Design</u>
		SSM	CMPS
Date of design		1978	1980
Magnet data			
Magnet type	—	Circ. Saddle	CASK
Warm bore liner?	—	No	No
Magnetic field:			
Peak on-axis field	(T)	7.3	7.3
Active field length	(m)	1.5	1.5
Field at start of active length	(T)	7.0	7.0
Field at end of active length	(T)	7.0	7.0
Field uniformity at end of active length <sup>a</sup>	(%)	2.5	2.5
Peak field in winding	(T)	8.1	8.1
Dimensions:			
Aperture, warm bore inlet <sup>b</sup>	(m)	0.55 dia.	0.55 dia.
Aperture, start of active length <sup>b</sup>	(m)	0.55 dia.	0.55 dia.
Aperture, end of active length <sup>b</sup>	(m)	0.55 dia.	0.55 dia.
Aperture, warm bore exit <sup>b</sup>	(m)	0.55 dia.	0.55 dia.
Aperture area, start of active length <sup>b</sup>	(m <sup>2</sup> )	0.24	0.24
Aperture area, end of active length <sup>b</sup>	(m <sup>2</sup> )	0.24	0.24
Vacuum vessel overall length	(m)	4.8	5.0
Vacuum vessel outside dia.	(m)	3.0	3.1

<sup>a</sup> Field uniformity is + and - variation from on-axis field, central portion of warm bore cross section, 0.14 m × 0.3 m

<sup>b</sup> Dimensions inside warm bore, without liner

Table 4.3.2-II Sheet 2 of 3

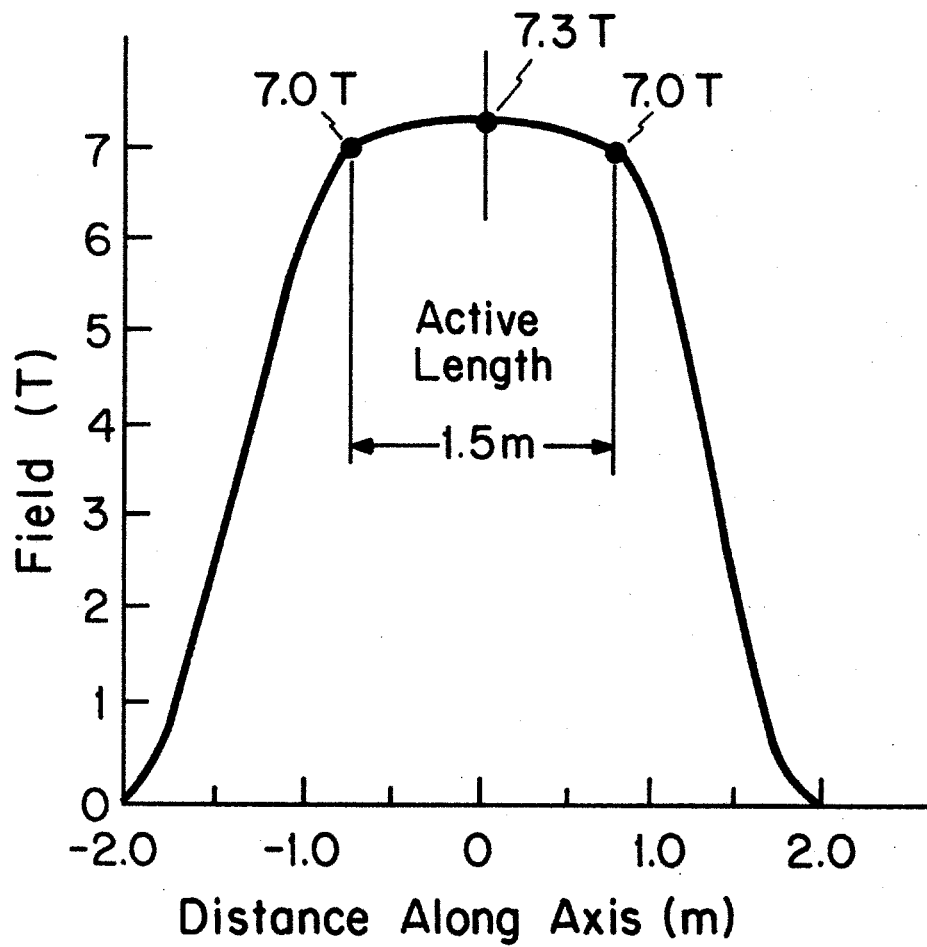
		SSM	CMPS
<b>Winding characteristics:</b>			
Build, winding cross section	(m)	0.47	0.50
Number of winding modules (or layers) per half	—	15	6 (12 layers)
Design current, I	(kA)	5.117	7400
Winding current density, average, $J\lambda^a$	( $10^7$ A/cm <sup>2</sup> )	2.0	2.0
Packing factor, $\lambda^a$	—	0.26	—
Conductor current density, $J^a$	( $10^7$ A/cm <sup>2</sup> )	7.7	—
Total number of turns, N	—	2362	1658
Ampere turns, NI	( $10^6$ A)	12.1	12.3
Inductance	(H)	7.14	3.5
Stored energy	(MJ)	93	96
Conductor type	—	Built-up	Built-up
Conductor materials	—	NbTi-Cu	NbTi-Cu
Conductor dimensions <sup>a</sup>	(cm)	4.59 × 0.86	—
Copper-to-superconductor ratio <sup>a</sup>	—	5.6	—
LHe to conductor ratio (vol.) <sup>a</sup>	—	0.25	—
Heat flux <sup>a</sup>	(W/cm <sup>2</sup> )	<0.75	—
<b>Weights:</b>			
Total cold mass	(tonnes)	51.7	
Total magnet weight	(tonnes)	81.6	

<sup>a</sup> Where graded winding is incorporated, values listed are for high field region of winding.

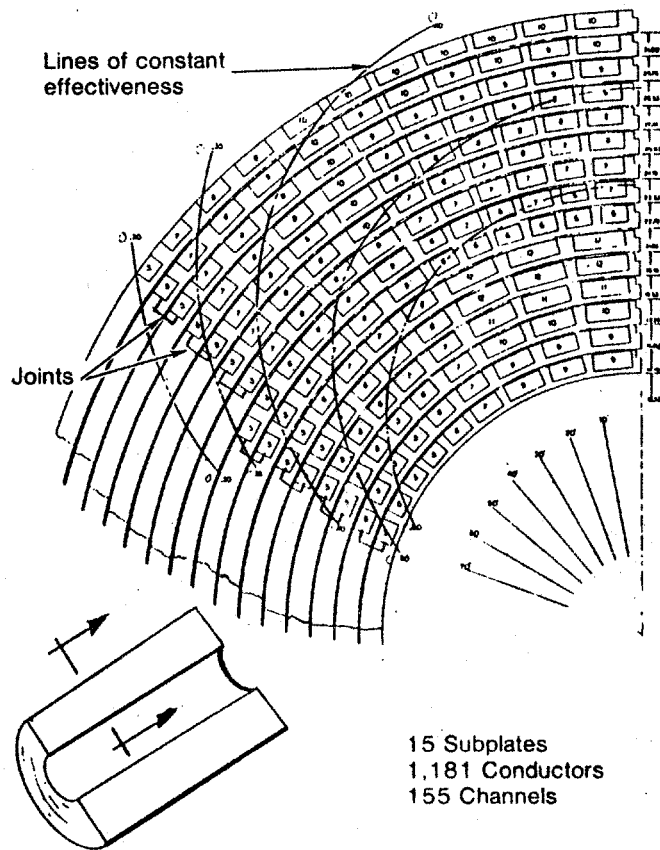
Table 4.3.2-II Sheet 3 of 3

		SSM	CMPS
<b>Cryogenic data:</b>			
Operating temperature at winding	(K)	4.45	4.45
Operating temperature, thermal shield	(K)	77	77
Thermal shield coolant	—	LN <sub>2</sub>	LN <sub>2</sub>
Heat load, LHe region, not incl. leads	(W)	17.5	17.5
LHe for lead cooling at design current	(ℓ/hr)	14	—
Refrigerator/liquefier capacity	(ℓ/hr)	34.6	—
Cool-down time	(hrs)	1000	—
<b>Power supply and discharge data:</b>			
Number of current leads	—	2	2
Rated voltage, power supply	(V)	10	—
Minimum charge time	(hrs)	1.8	—
Resistance, emergency dump resistor	(Ω)	0.176	—
Emergency discharge time constant	(sec)	42	—
Maximum discharge voltage, terminal	(V)	900	—
<b>Materials of construction:</b>			
Winding substructure	—	Al 2219 T87	SS 304 LN
Insulation	—	Epoxy/glass	G-10 CR
Superstructure	—	Al 2219 T87	SS 304 LN
Liquid helium vessel	—	Al 5083	SS 304 LN
Thermal shield	—	Al 6061 T6	Al 6061 T6
Vacuum vessel	—	SS 304 L	SS 304 L
<b>Design stresses:</b>			
Conductor (tensile)	(MPa)	46	—
Winding substructure	(MPa)	241	—
Superstructure	(MPa)	241	—
<b>Pressure rating</b>			
Liquid helium vessel			
Normal operating	(atm)	1.25	1.25

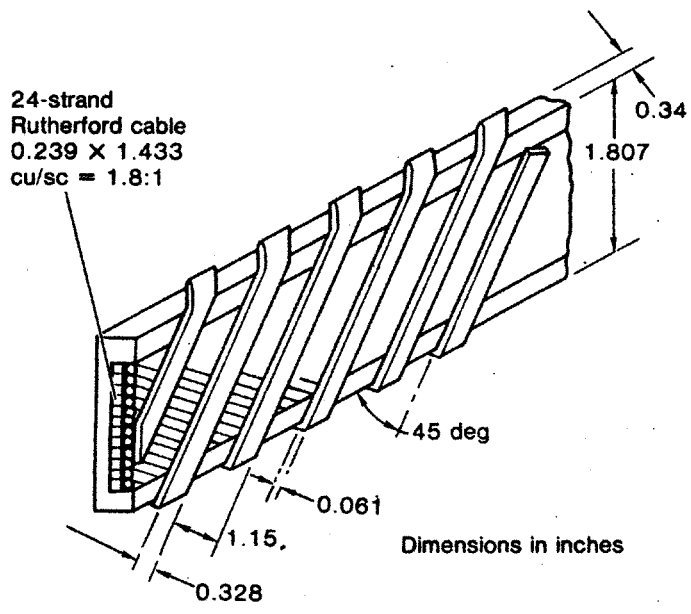




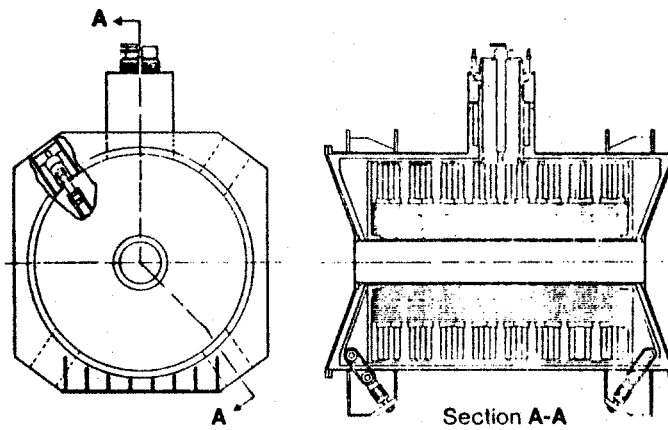
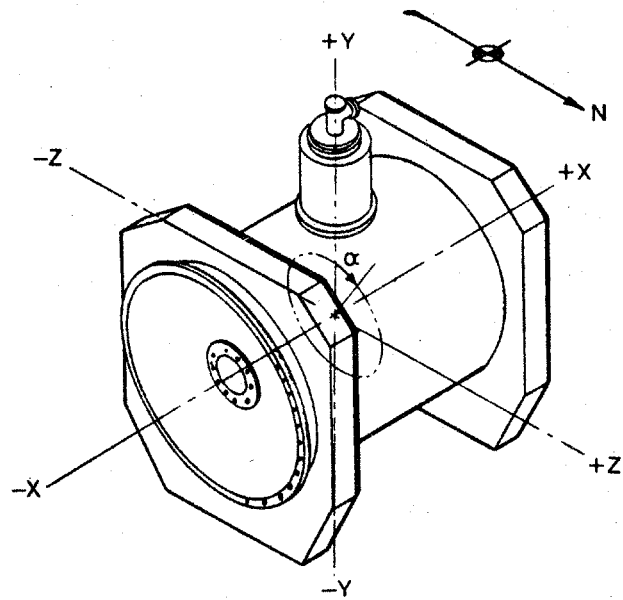
4.3.2A Curve of On-Axis Field vs Distance Along Axis for Stanford Superconducting Magnet



4.3.2B Diagram Showing Winding Configuration, Stanford Superconducting Magnet



4.3.2C Sketch of Conductor, Stanford Superconducting Magnet



4.3.2D Elevation and End Views of Magnet Assembly, Stanford Superconducting Magnet

The liquid helium containment vessel consists of a cylindrical shell assembled around the outside of the winding and substructure, a pair of flat heads and the core tube. These components, all of stainless steel, are welded together around the winding to form a helium-tight enclosure. The main force containment structure consists of a series of ring girders of welded stainless steel construction, clamped around the outside of the helium containment vessel.

The cryostat consists of a liquid-nitrogen-cooled thermal radiation shield of aluminum alloy surrounding the cold mass of the magnet, multilayer insulation blankets and a stainless steel vacuum jacket which consists of a cylindrical outer shell, concave heads and a cylindrical warm bore tube. The cold mass of the magnet is supported on low-heat-leak links of laminated fiberglass-epoxy material.

A typical cross section of the CMPS winding and substructure is shown in Figure 4.3.2E. The ring girder design is shown in Figure 4.3.2F and the conductor design is shown in Figure 4.3.2G. The cold mass support links of the CMPS design are shown in Figure 4.3.2H and a cutaway view of the magnet assembly is shown in Figure 4.3.2J.

The accessories for both the original SSM and the CMPS include a cryogenic support system, a power supply and discharge system, vacuum pumping equipment, instrumentation and controls and a steel magnetic shield in the form of a rectangular enclosure around the magnet.

The manufacturing plans for both designs call for assembly of the magnet at GD and shipment of the completed assembly to Stanford by special truck.

More detailed information on the Stanford magnet design is contained in Reference 18.

### 4.3.3 U-25B Superconducting MHD Magnet, U.S. SCMS

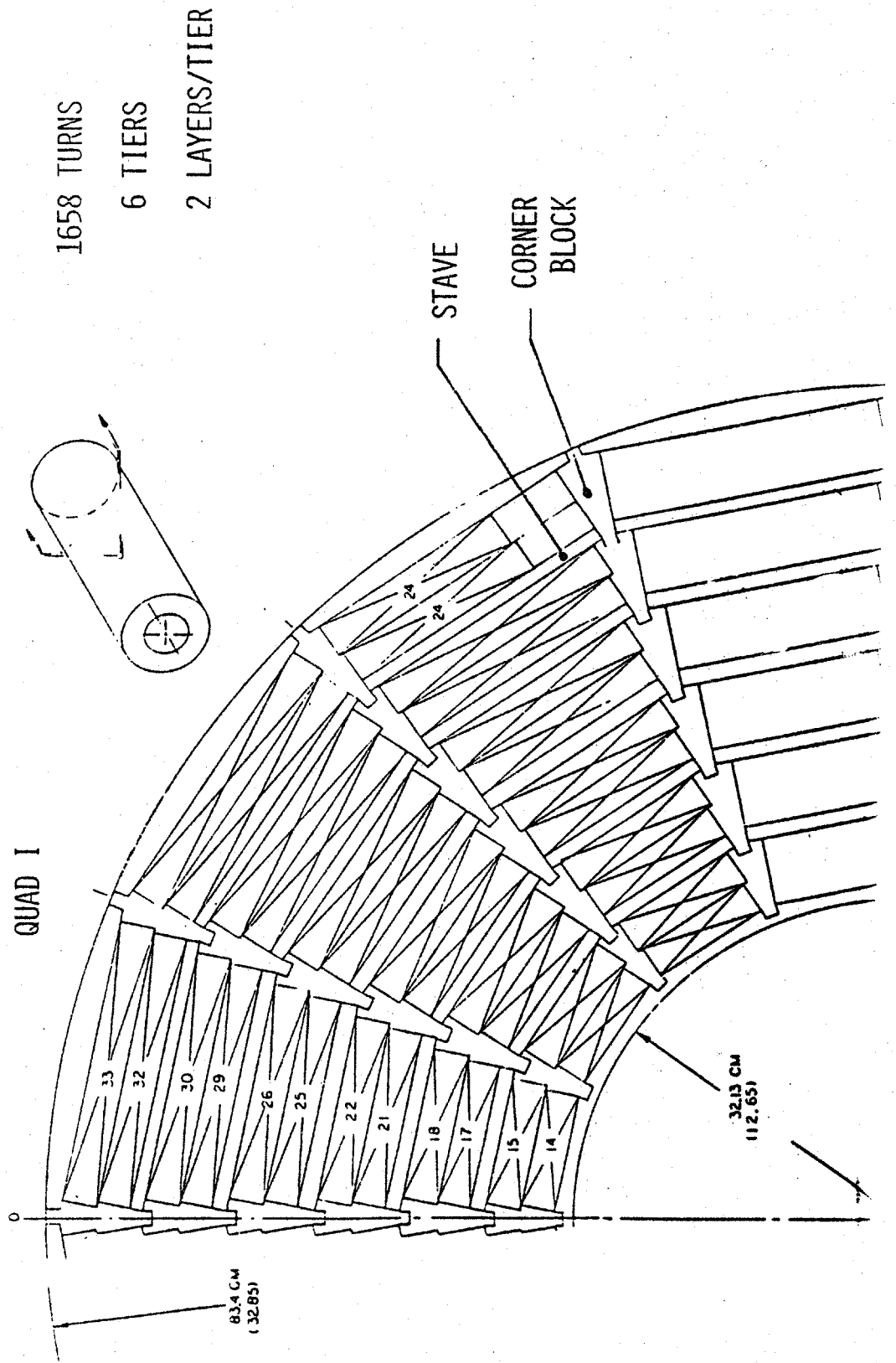
#### 4.3.3.1 Summary

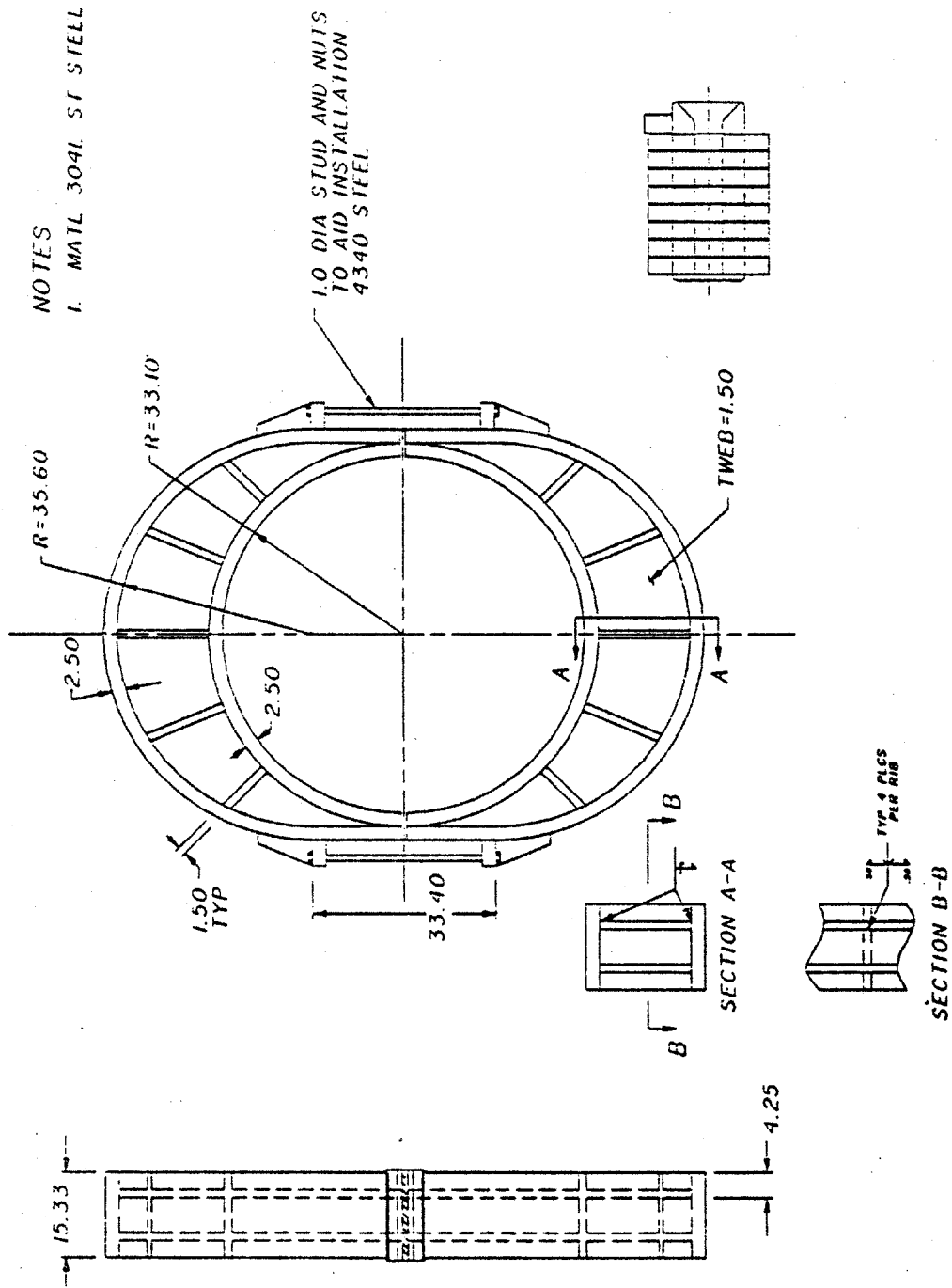
The U-25B superconducting MHD magnet is a 5 T test facility magnet, designed and constructed at Argonne National Laboratory under the sponsorship of ERDA, and delivered to the Institute for High Temperature, Moscow, U.S.S.R., as part of a joint research project within the framework of the U.S./U.S.S.R. Program of Scientific and Technical Cooperation.

During the design, construction and testing of the magnet at Argonne, MIT participated in design reviews and observed construction and testing. In addition, MIT performed stability analyses of the winding, stress analyses of structure and tests of samples of conductor.

The magnet was completed and tested at Argonne early in 1977, delivered to the Institute for High Temperature in June, 1977 and tested to design field strength of 5 T at the Institute in September of that year. It has since been in operation in connection with MHD flow train testing in the bypass loop of the U-25 MHD test facility.

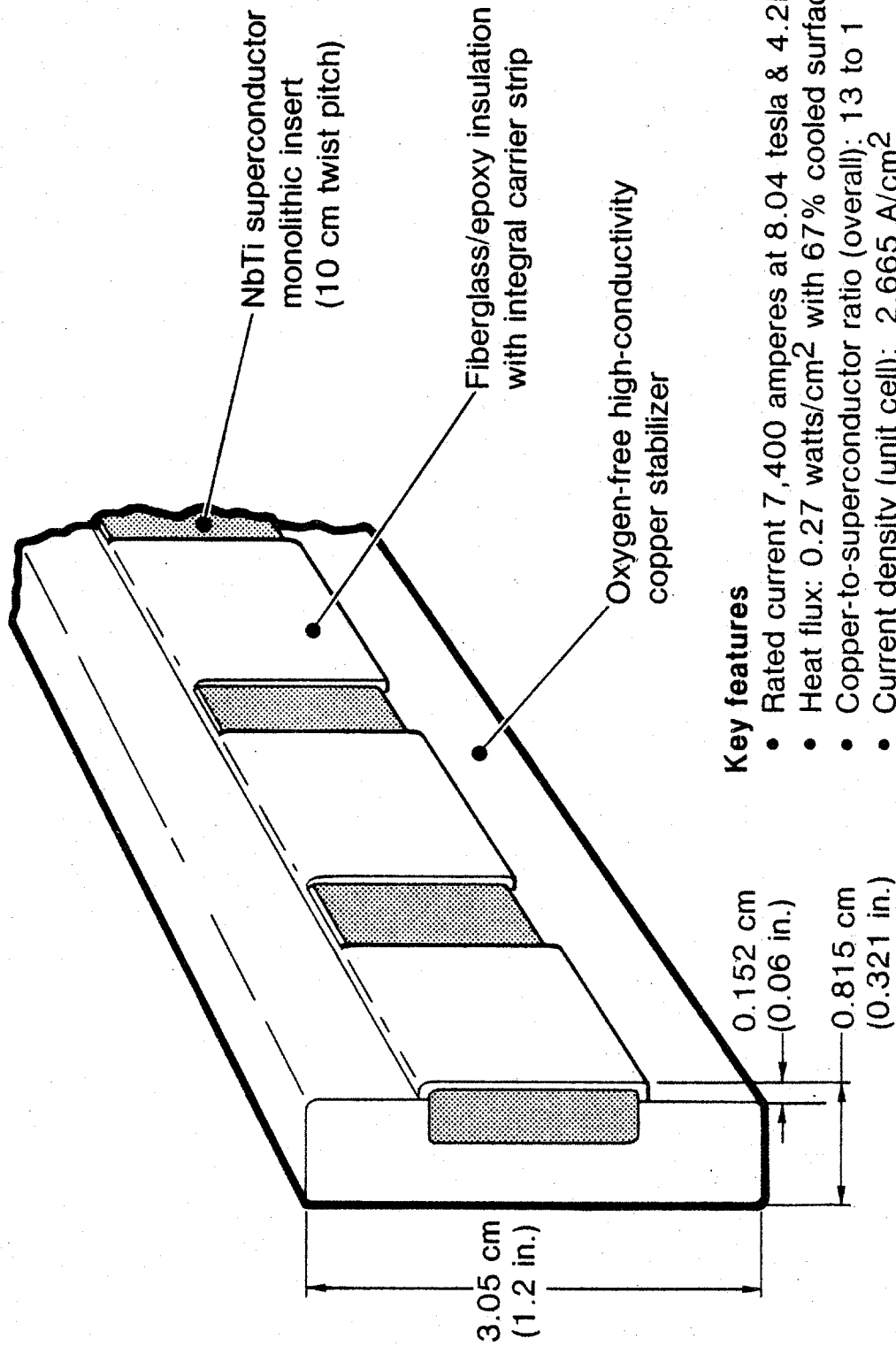
4.3.2E Cross Section of Stanford Alternative Design (CMPS) Magnet Winding and Substructure





4.3.2F Layout of Ring Girder for Stanford Alternative Design (CMPS) Magnet

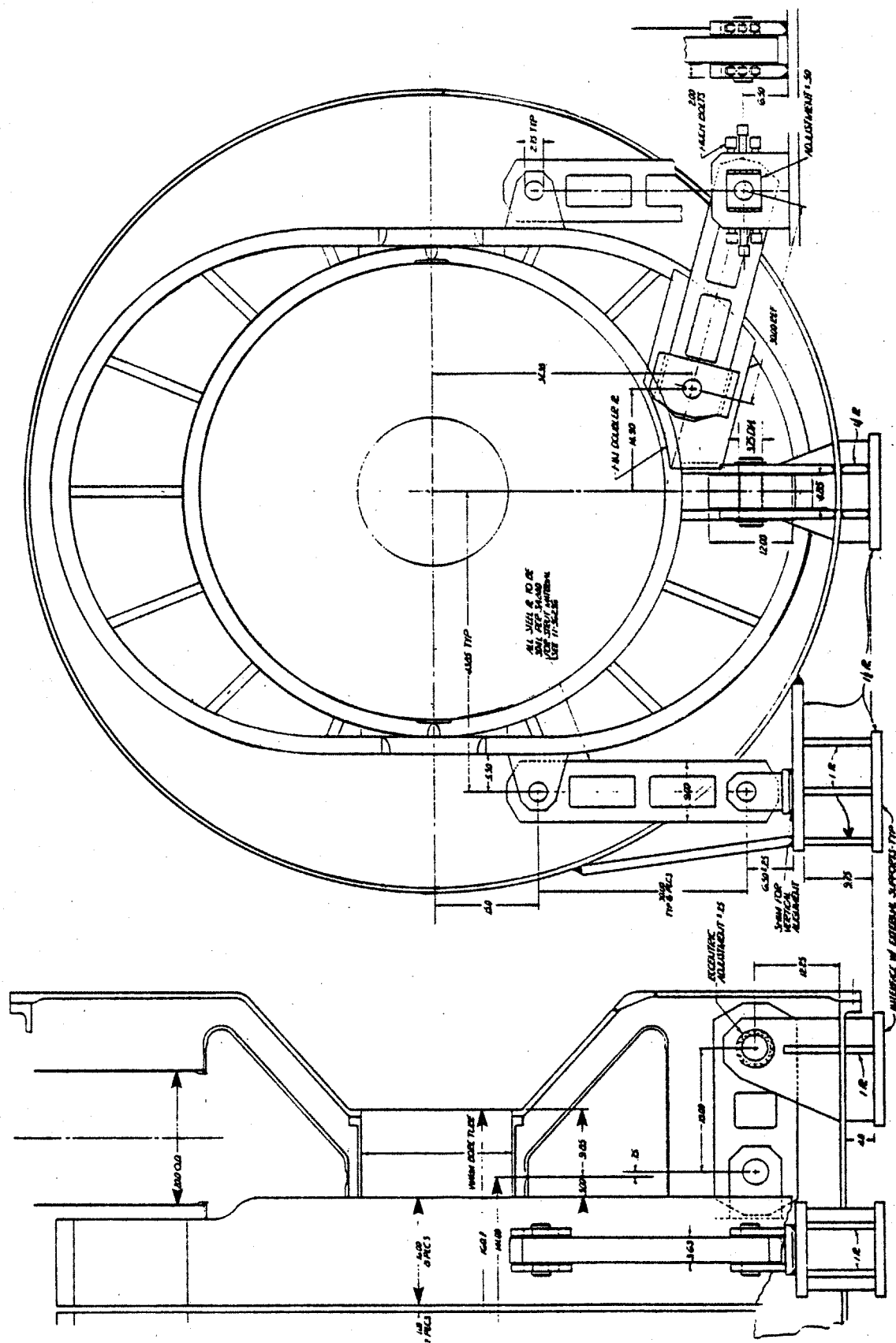
4.3.2G Sketch of Conductor for Stanford Alternative Design (CMPS) Magnet



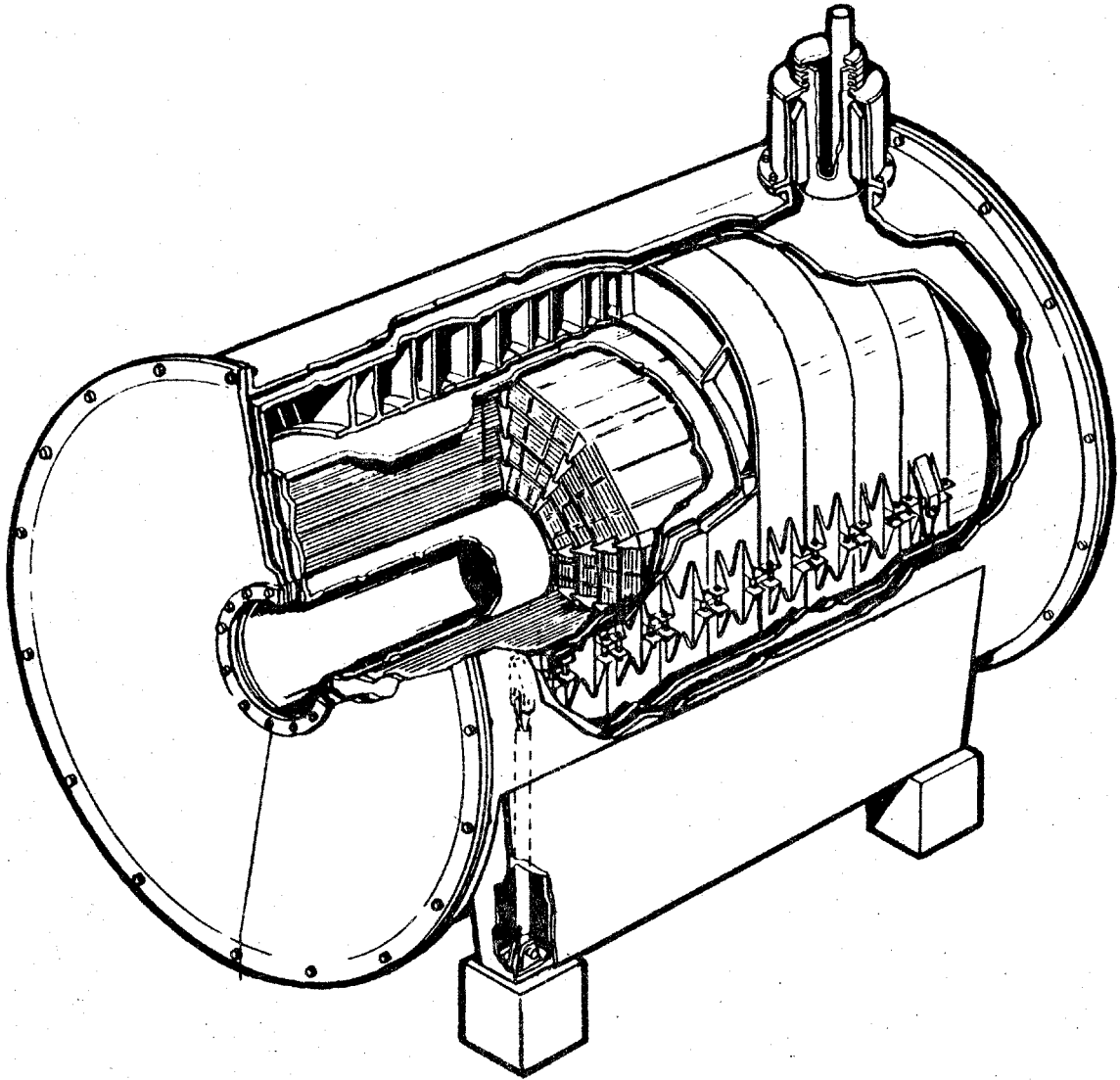
**Key features**

- Rated current 7,400 amperes at 8.04 tesla & 4.2K He bath
- Heat flux: 0.27 watts/cm<sup>2</sup> with 67% cooled surface
- Copper-to-superconductor ratio (overall): 13 to 1
- Current density (unit cell): 2,665 A/cm<sup>2</sup>
- Length: 11,905m (39,056 ft)
- Weight: 21,720 Kg (47,800 lb)





4.3.2H Layout Showing Cold Mass Support Links for Stanford Alternative Design (CMPS) Magnet



4.3.2J Cutaway View of Stanford Alternative Design (CMPS) Magnet Assembly

#### 4.3.3.2 Description

The design criteria established by ERDA for the magnet were a peak on-axis field of 5 T, an active length of 2.5 m (4 T to 3.2 T) and warm bore diameters of 0.4 m at start of active length and 0.6 m at end of active length.

The magnet is of the circular saddle coil type with a warm bore of circular cross section. It incorporates an 890 ampere built-up copper and NbTi composite conductor, consisting of a rectangular, multifilamentary composite monolith, soldered into a groove in a rectangular-cross-section copper substrate. The winding is modular, with cylindrical, saddle-shaped winding layers. The layers were form-wound and then nested around a central core tube with insulated stainless steel banding separating the layers. There are 23 winding layers in each winding half. The inner layers are shorter, extending from the inlet end only part of the way toward the exit end, resulting in the tapered field profile desired for MHD channel operation.

The main force containment structure consists of the thick stainless steel core tube, the core tube end flanges and the stainless steel banding between layers and around the outside of the winding. Outward magnetic forces are supported by the banding in tension. Because outward forces are not uniformly distributed around the circumference, there will be a reaction from the banding, tending to distort the core tube into an oval cross section. The core tube is designed to have sufficient strength to withstand this bending load. The conductor is subjected to accumulated compressive load due to magnetic forces on the winding. Turn-to-turn and layer-to-layer insulation have sufficient compressive strength to withstand this loading.

The liquid helium vessel outer portion consists of a cylindrical stainless steel shell surrounding the winding, and structural banding. This shell is welded to flanges on the core tube at each end, so that the flanges and core tube serve as the ends and inner portion of the container.

The Dewar includes a liquid nitrogen-cooled stainless steel thermal radiation shield, multilayer insulation blankets and a stainless steel vacuum jacket with recessed ends and a tapered warm bore tube. The cold mass is supported by eight low-heat-leak tension links of filament-wound glass epoxy connected between the cold structure at the ends of the magnet, and bosses located in reinforced end rings on the vacuum jacket.

The characteristics of the U.S. SCMS design are listed in Table 4.3.3-I. The on-axis field profile and the cryostat cross section are shown in Figure 4.3.3A and the magnet and cryostat cross section in Figure 4.3.3B. A cryogenic subsystem and a power supply and discharge subsystem are included with the magnet. The cryogenic subsystem is shown diagrammatically in Figure 4.3.3C. A photograph of the completed magnet is shown in Figure 4.3.3D. More detailed information on the U-25B (U.S. SCMS) magnet is contained in References 46, 83 and 84.

Table 4.3.3-1 Sheet 1 of 3

Design Characteristics  
U-25B Superconducting Magnet (U.S. SCSM)

Date of design		1975
<b>Magnet data</b>		
Magnet type	—	Circ. Saddle
Warm bore liner?	—	No
<b>Magnetic field:</b>		
Peak on-axis field	(T)	5.0
Active field length	(m)	2.56
Field at start of active length	(T)	4.0
Field at end of active length	(T)	3.2
Field uniformity at end of active length <sup>a</sup>	(%)	< 5%
Peak field in winding	(T)	6.0
<b>Dimensions:</b>		
Aperture, warm bore inlet <sup>b</sup>	(m)	0.40
Aperture, start of active length <sup>b</sup>	(m)	0.40
Aperture, end of active length <sup>b</sup>	(m)	0.60
Aperture, warm bore exit <sup>b</sup>	(m)	0.67
Aperture area, start of active length <sup>b</sup>	(m <sup>2</sup> )	0.16
Aperture area, end of active length <sup>b</sup>	(m <sup>2</sup> )	0.36
Distance, bore inlet to start of active length	(m)	0.72
Vacuum vessel overall length	(m)	4.20
vacuum vessel outside dia.	(m)	2.29

<sup>a</sup> Field uniformity is + and - variation from on-axis field, central 50% of warm bore cross section

<sup>b</sup> Dimensions inside warm bore, without liner

Table 4.3.3-1 Sheet 2 of 3

## Winding characteristics:

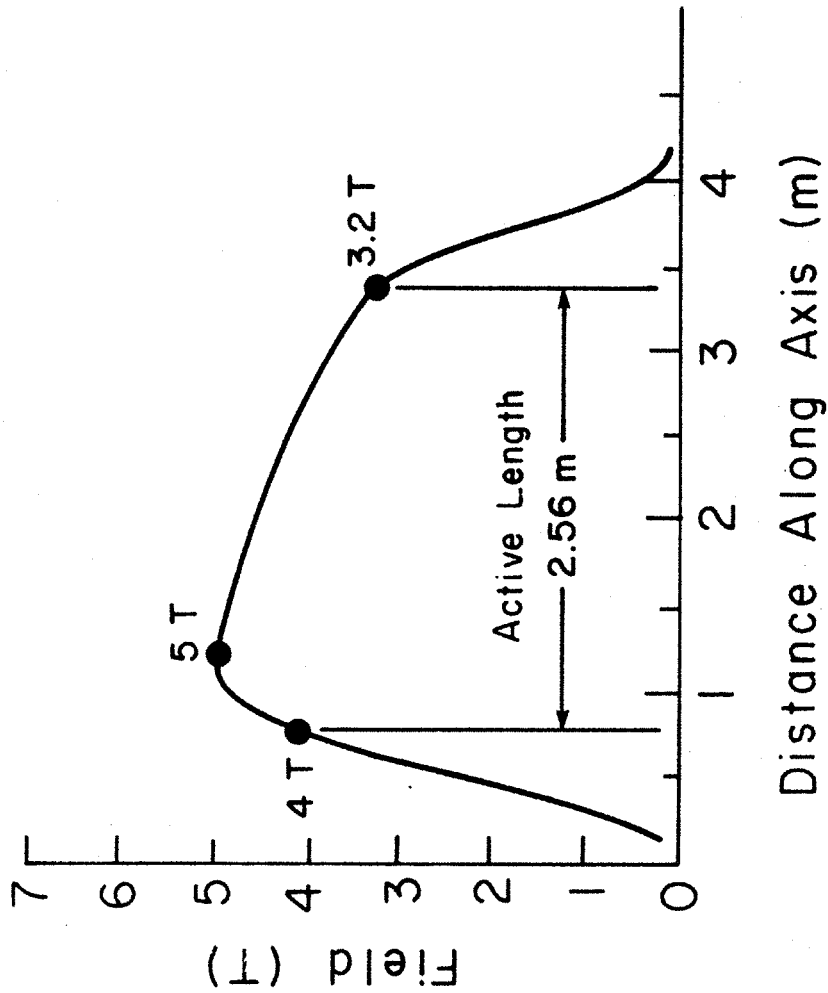
Build, winding cross section	(m)	0.37
Number of winding modules (or layers) per half	—	23
Operating current, I	(kA)	0.892
Winding current density, average, $J\lambda^a$	( $10^7$ A/cm <sup>2</sup> )	2.82
Packing factor, $\lambda^a$	—	0.56
Conductor current density, $J^a$	( $10^7$ A/cm <sup>2</sup> )	4.5
Total number of turns, N	—	7620
Total length of conductor	(km)	57.8
Ampere turns, NI	( $10^6$ A)	6.8
Ampere meters	( $10^8$ Am)	0.49
Inductance	(H)	85
Stored energy	(MJ)	36
Conductor type	—	Built-up
Conductor materials	—	NbTi-Cu
Conductor dimensions <sup>a</sup>	(cm)	0.2 × 1.0
Copper-to-superconductor ratio <sup>a</sup>	—	15
Heat flux <sup>a</sup>	(W/cm <sup>2</sup> )	0.7
Weights:		
Conductor	(tonnes)	10.0
Insulation	(tonnes)	incl. below
Substructure	(tonnes)	2.1
Superstructure	(tonnes)	12.0
Liquid He vessel	(tonnes)	3.6
Total cold mass	(tonnes)	27.7
Thermal shield, cold mass supports, etc	(tonnes)	3.1
Vacuum vessel	(tonnes)	9.0
Miscellaneous	(tonnes)	0.1
Total magnet weight	(tonnes)	39.9

<sup>a</sup> Where graded winding is incorporated, values listed are for high field region of winding.

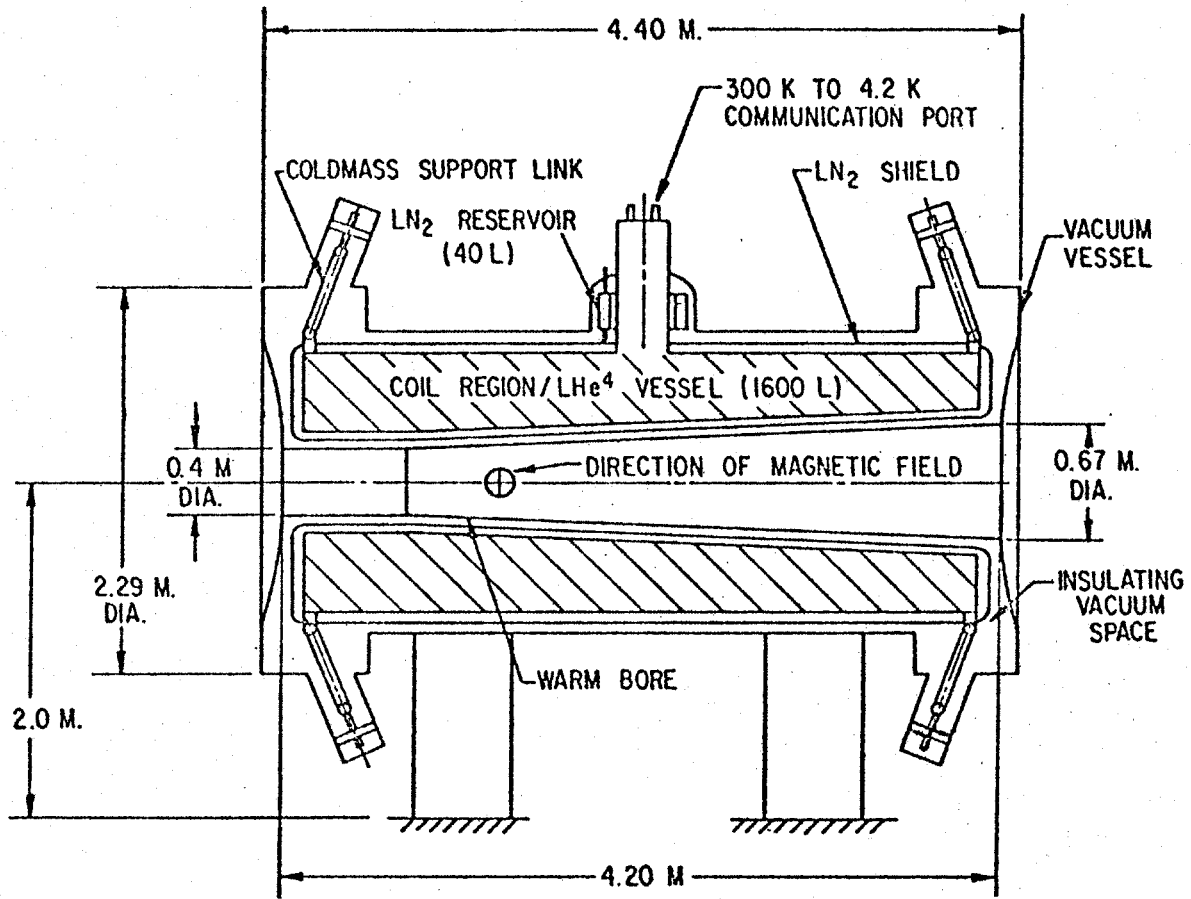
Table 4.3.3-I Sheet 3 of 3

Cryogenic data:		
Operating temperature at winding	(K)	4.2
Operating temperature, thermal shield	(K)	80
Thermal shield coolant	—	LN <sub>2</sub>
Heat load, LHe region, not incl. leads	(W)	4.8
LHe for lead cooling at design current	(ℓ/hr)	4.2
Refrigerator/liquefier capacity	(ℓ/hr)	22 <sup>a</sup>
Cool-down time	(hrs)	530
Power supply and discharge data:		
Number of current leads	—	2
Rated voltage, power supply	(V)	20
Minimum charge time	(hrs)	1.1
Resistance, emergency dump resistor	(Ω)	0.12
Emergency discharge time constant	(min)	12
Maximum discharge voltage, terminal	(V)	118
Materials of construction:		
Winding substructure	—	SS 310 (bands)
Insulation	—	G-10 & Mylar
Superstructure	—	SS 316 cast (core tube)
Liquid helium vessel	—	SS 304
Thermal shield	—	SS 304
Vacuum vessel	—	SS 304
Design stresses:		
Superstructure	(MPa)	419 (core tube)
Pressure rating		
Liquid helium vessel		
Normal operating	(atm)	1.0
Maximum design	(atm)	4.4

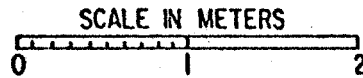
<sup>a</sup> One liquefier unit with 2 compressors



4.3.3A Curve of On-Axis Field vs Distance Along Axis for U25 Superconducting Magnet (U.S. SCM)

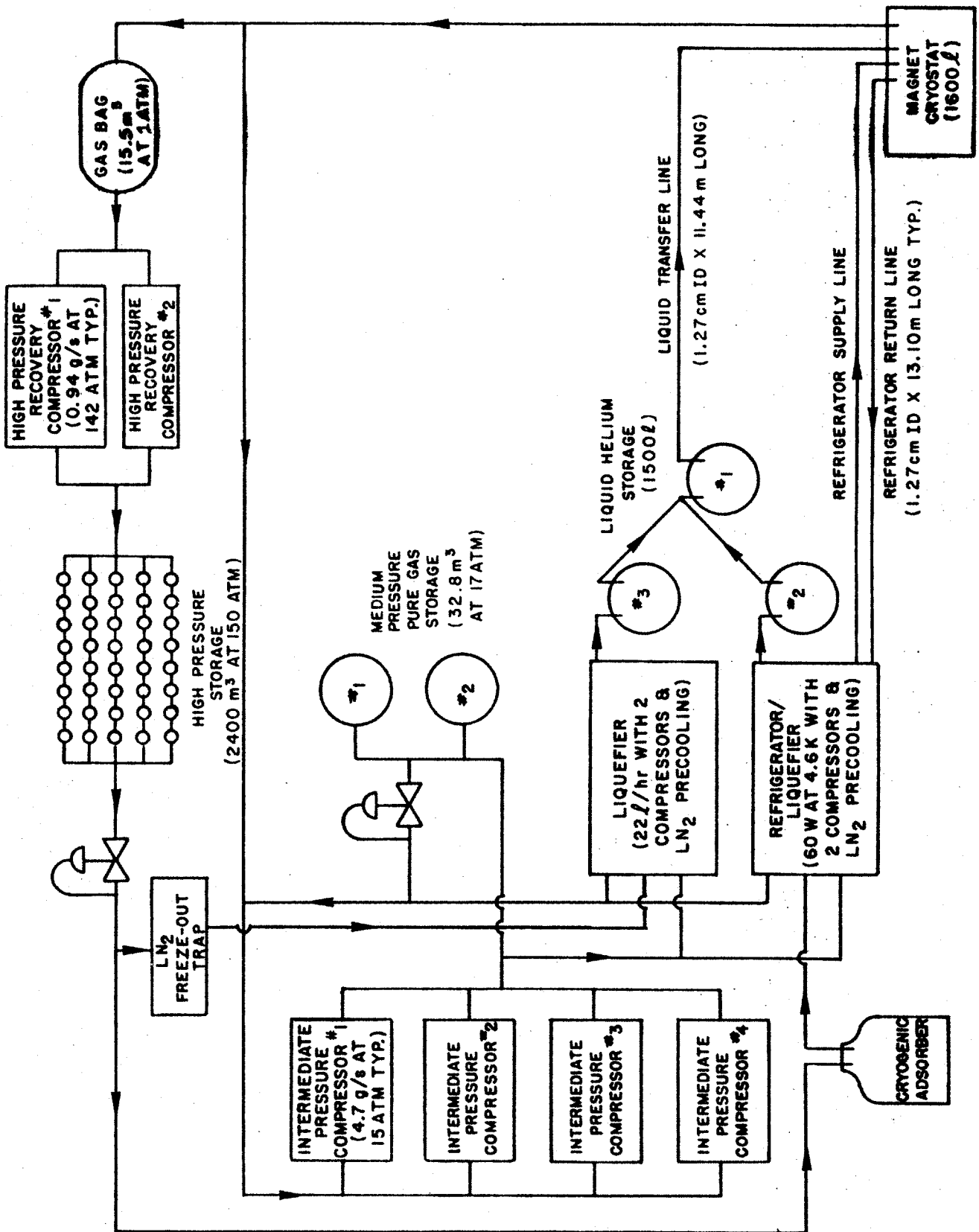


TOTAL WEIGHT = 36,800 Kg.



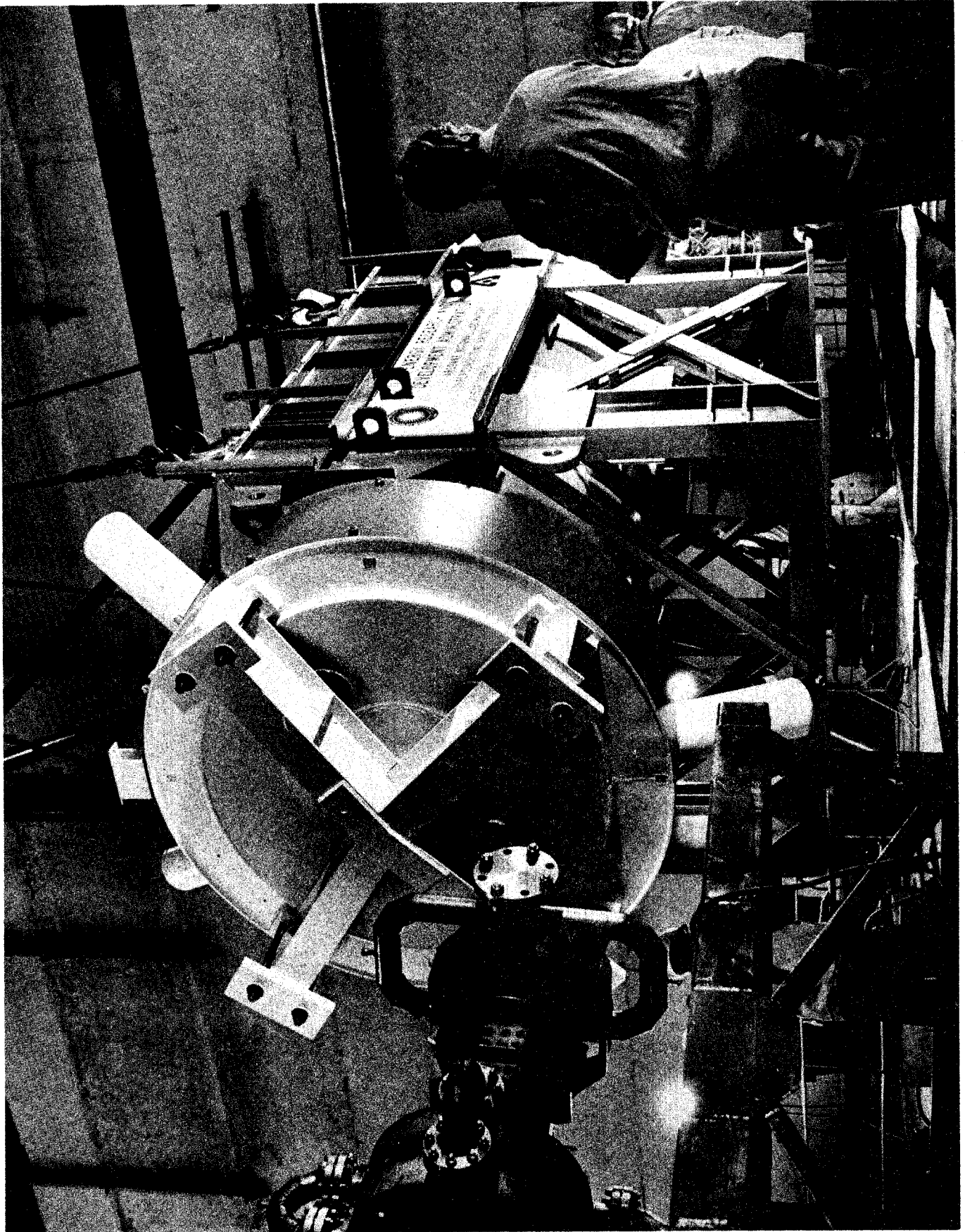
4.3.3B Cutaway View of Magnet and Cryostat, U25 Superconducting Magnet (U.S. SCM)





4.3.3C Diagram of Cryogenic Subsystem, U25 Superconducting Magnet (U.S. SCM)

4.3.3D Photograph of U25 Superconducting Magnet (U.S. SCM)



## 4.3.4 Coal-Fired Flow Facility Superconducting Magnet CFFF/SM

### 4.3.4.1 Summary

The Coal-Fired Flow Facility superconducting magnet is a 6 T test facility magnet, designed and constructed at Argonne National Laboratory under the sponsorship of DOE and intended for installation in the MHD facility operated by the University of Tennessee Space Institute at Tullahoma, TN.

During the design and construction of the magnet, MIT participated in design reviews and observed construction and testing.

The magnet was completed and tested to design field strength at Argonne in 1981. As of the date of this report, it is stored at Argonne awaiting DOE disposition.

### 4.3.4.2 Description

The design criteria established by DOE for the magnet were a peak field of 6 T, a high field region length of 3.0 m (4.8 T to 4.8 T) and warm bore diameters of 0.80 m at bore inlet and 1.0 m at exit end of the high field region.

The magnet is of the circular saddle type with a warm bore of circular cross section, diverging from inlet to exit. It incorporates a 3675 ampere built-up conductor consisting of a cable (insert) of multiple wires of NbTi-copper composite transposed around a copper strip with a strand pitch of 0.2 turn/cm and soldered into a longitudinal groove in a rectangular-cross-section copper stabilizer (substrate).

The winding is similar in design to that of the U.S. SCMS magnet described in Section 4.3.3. It is modular, with cylindrical saddle-shaped winding layers form-wound and then nested around a central core tube with spiral-wound pultruded fiberglass banding separating the layers. There are 14 layers in each winding half. The inner layers are shorter, extending from the inlet end only part way toward the exit end, resulting in a tapered field profile.

The main force containment structure consists of a stainless steel core tube with integral, reinforced end flanges (to resist longitudinal magnetic forces) and a series of girder rings clamped around the outside of the winding (to resist radially outward forces). Each main girder ring consists of two 130° cast stainless steel segments pinned to six (three per side) aluminum tie plates.

The liquid helium vessel outer portion consists of a cylindrical stainless steel shell surrounding the winding and girder rings. The shell is welded to flanges on the core tube at each end, so that the flanges and core tube serve as the ends and inner wall of the vessel.

The Dewar includes a liquid nitrogen-cooled stainless steel thermal radiation shield, multilayer insulation blankets and a stainless steel vacuum jacket with a recessed inlet end and a tapered warm bore tube. The cold mass is supported by eight low heat leak tension links, four of stainless steel and four of fiberglass, connected between the cold structure at the ends of the magnet and bosses located in reinforced end rings on the vacuum jacket.

The characteristics of the CFFF/SM design are listed in Table 4.3.4-I. The on-axis field profile is shown in Figure 4.3.4A. The winding configuration and the conductor and insulation system are shown in Figure 4.3.4B. The main structural components including the core tube, end flanges and girder ring assemblies are shown in Figure 4.3.4C. A cutaway view showing the magnet and cryostat assembly is contained in Figure 4.3.4D.

A cryogenic subsystem and a power supply and discharge subsystem are included with the magnet. The cryogenic subsystem is shown diagrammatically in Figure 4.3.4E.

Table 4.3.4-I Sheet 1 of 3

Design Characteristics  
Coal-Fired Flow Facility Superconducting Magnet (CFFF/SM)  
Argonne National Laboratory

Date of design		1978
Magnet data		
Magnet type	—	Circ. saddle
Warm bore liner?	—	No
Magnetic field:		
Peak on-axis field	(T)	6.0
Active field length	(m)	3.0 (3.2)
Field at start of active length	(T)	4.8
Field at end of active length	(T)	4.8 (4.0)
Field uniformity at end of active length <sup>a</sup>	(%)	5.0
Peak field in winding	(T)	6.9
Dimensions:		
Aperture, warm bore inlet <sup>b</sup>	(m)	0.80
Aperture, start of active length <sup>b</sup>	(m)	0.85
Aperture, end of active length <sup>b</sup>	(m)	1.00
Aperture, warm bore exit <sup>b</sup>	(m)	1.09
Aperture area, start of active length <sup>b</sup>	(m <sup>2</sup> )	0.57
Aperture area, end of active length <sup>b</sup>	(m <sup>2</sup> )	0.79
Distance, bore inlet to start of active length	(m)	1.67
Warm bore length	(m)	5.62
Vacuum vessel overall length	(m)	6.40
Vacuum vessel outside dia.	(m)	3.66
Warm bore volume, active	(m <sup>3</sup> )	2.02

<sup>a</sup> Field uniformity is + and - variation from on-axis field, central 50% of warm bore cross section

<sup>b</sup> Dimensions inside warm bore, without liner

Table 4.3.4-I Sheet 2 of 3

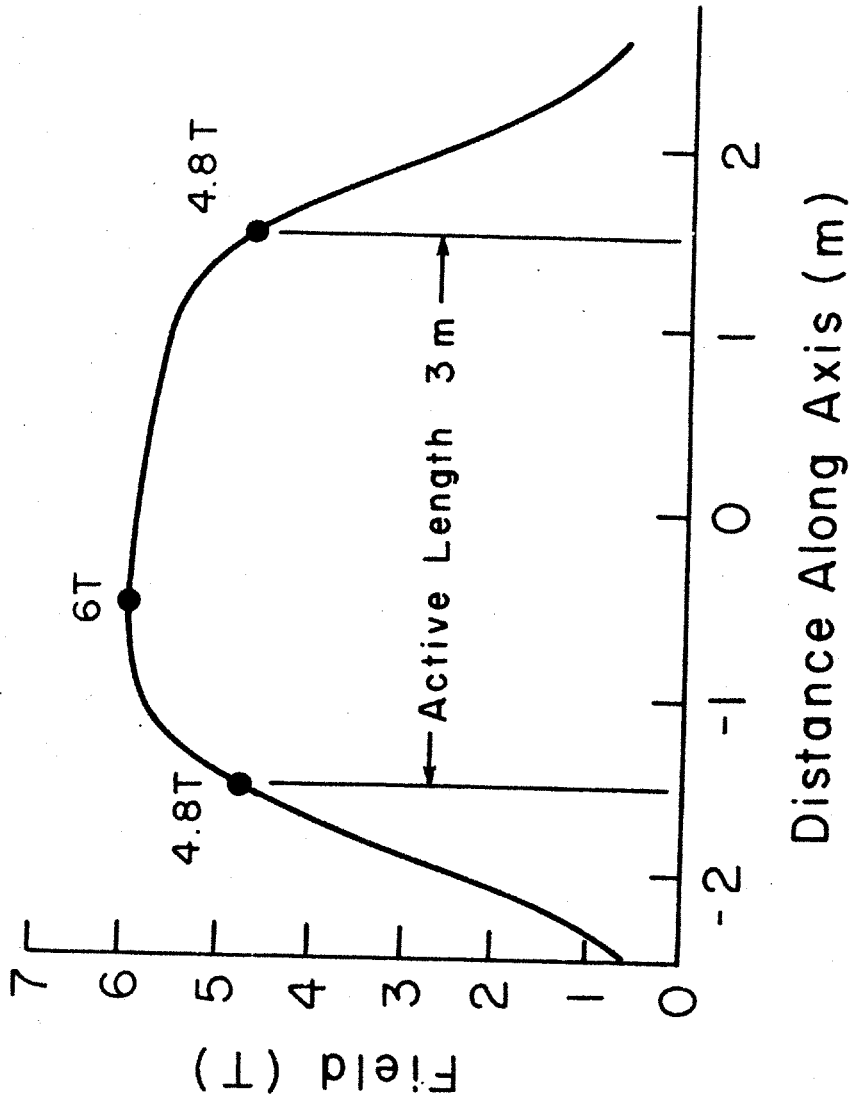
## Winding characteristics:

Build, winding cross section	(m)	0.53
Number of winding modules (or layers) per half	—	14
Operating current, I	(kA)	3.675
Winding current density, average, $J\lambda^a$	( $10^7$ A/cm <sup>2</sup> )	2.00
Packing factor, $\lambda^a$	—	0.76
Conductor current density, $J^a$	( $10^7$ A/cm <sup>2</sup> )	2.63
Total number of turns, N	—	3728
Total length of conductor	(km)	39.5
Ampere turns, NI	( $10^6$ A)	13.7
Ampere meters	( $10^8$ Am)	1.45
Inductance	(H)	32
Stored energy	(MJ)	216
Conductor type	—	Built-up
Conductor materials	—	NbTi-Cu
Conductor dimensions <sup>a</sup>	(cm)	$3.1 \times 0.47$
Copper-to-superconductor ratio <sup>a</sup>	—	21
Heat flux <sup>a</sup>	(W/cm <sup>2</sup> )	0.16
Weights:		
Conductor	(tonnes)	48
Superstructure, liquid He vessel, etc.	(tonnes)	83
Total cold mass	(tonnes)	131
Thermal shield, cold mass supports, etc	(tonnes)	3
Vacuum vessel	(tonnes)	38
Miscellaneous	(tonnes)	incl. above
Total magnet weight	(tonnes)	172

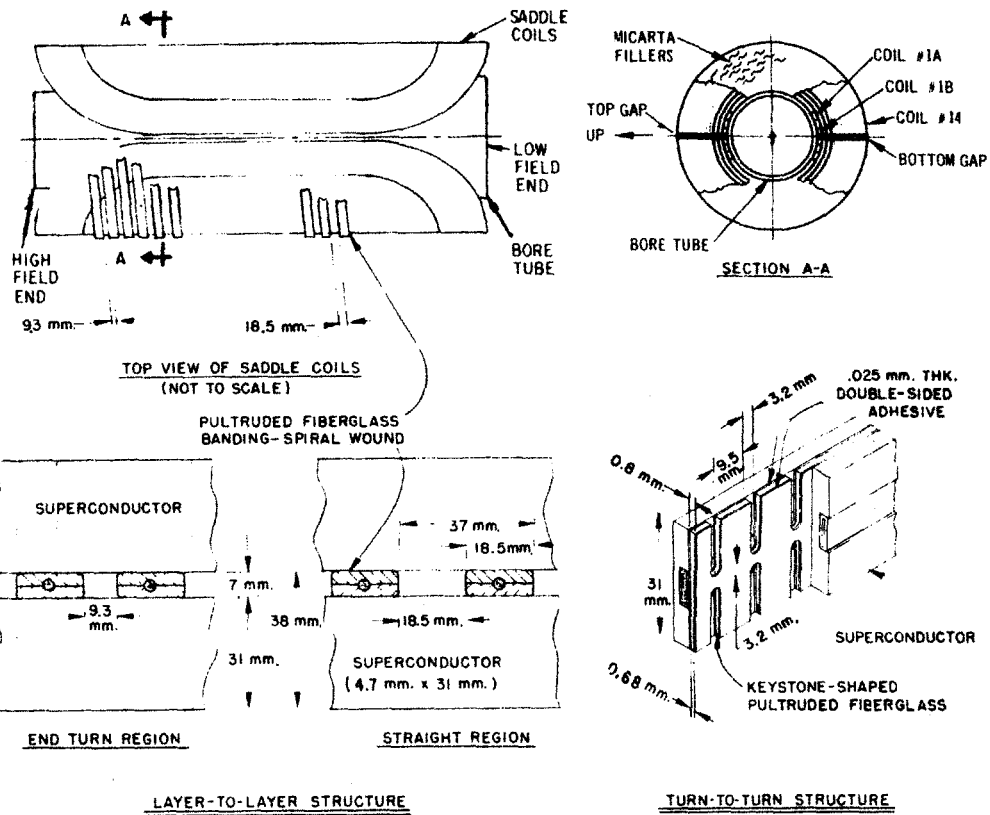
<sup>a</sup> Where graded winding is incorporated, values listed are for high field region of winding.

Table 4.3.4-1 Sheet 3 of 3

<b>Cryogenic data:</b>		
Operating temperature at winding	(K)	4.5
Operating temperature, thermal shield	(K)	80
Thermal shield coolant	—	LN <sub>2</sub>
Heat load, LHe region, not incl. leads	(W)	14
LHe for lead cooling at design current	(ℓ/hr)	11
Refrigerator/liquefier capacity	(ℓ/hr)	50
Cool-down time	(days)	28
<b>Power supply and discharge data:</b>		
Number of current leads	—	2
Rated voltage, power supply	(V)	20
Minimum charge time	(min)	70
Resistance, emergency dump resistor	(Ω)	0.05
Emergency discharge time constant	(min)	11
Maximum discharge voltage, terminal	(V)	200
<b>Materials of construction:</b>		
Winding substructure	—	Epoxy/glass
Insulation	—	Epoxy/glass
Superstructure	—	SS 316 L/A1 2219 T87
Liquid helium vessel	—	SS 316
Thermal shield	—	SS 304/Cu
Vacuum vessel	—	SS 304
<b>Design stresses:</b>		
Superstructure, SS girder (tension)	(MPa)	234
<b>Pressure rating</b>		
Liquid helium vessel		
Normal operating	(atm)	1.3
Maximum design	(atm)	3.33

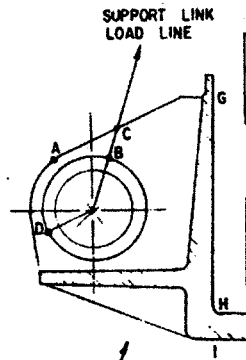
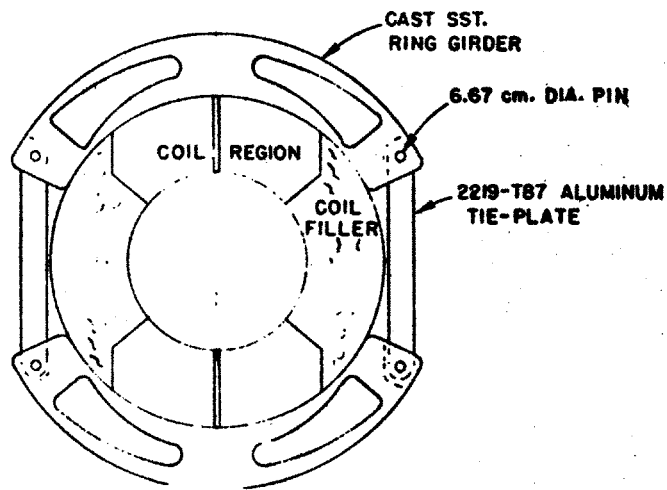


4.3.4A Curve of On-Axis Field vs Distance Along Axis, Coal-Fired Flow Facility Magnet (CFFF/SM)



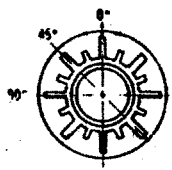
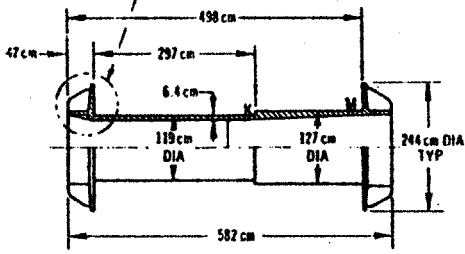
4.3.4B Diagram Showing Winding Configuration and Conductor and Insulation System for Coal-Fired Flow Facility Magnet (CFFF/SM)





LOADING	A	B	D
VERTICAL ( $\frac{kg}{cm^2}$ )	210	186	172
AXIAL ( $\frac{kg}{cm^2}$ )	252	223	207
SHIPPING			

LOADING	G	H	I	K	M
AXIAL ( $\frac{kg}{cm^2}$ )	-	339	290	88	140
AZIMUTHAL ( $\frac{kg}{cm^2}$ )	33	147	29.6	14	62
MAGNETIC LOADING PLUS HELIUM PRESSURE					

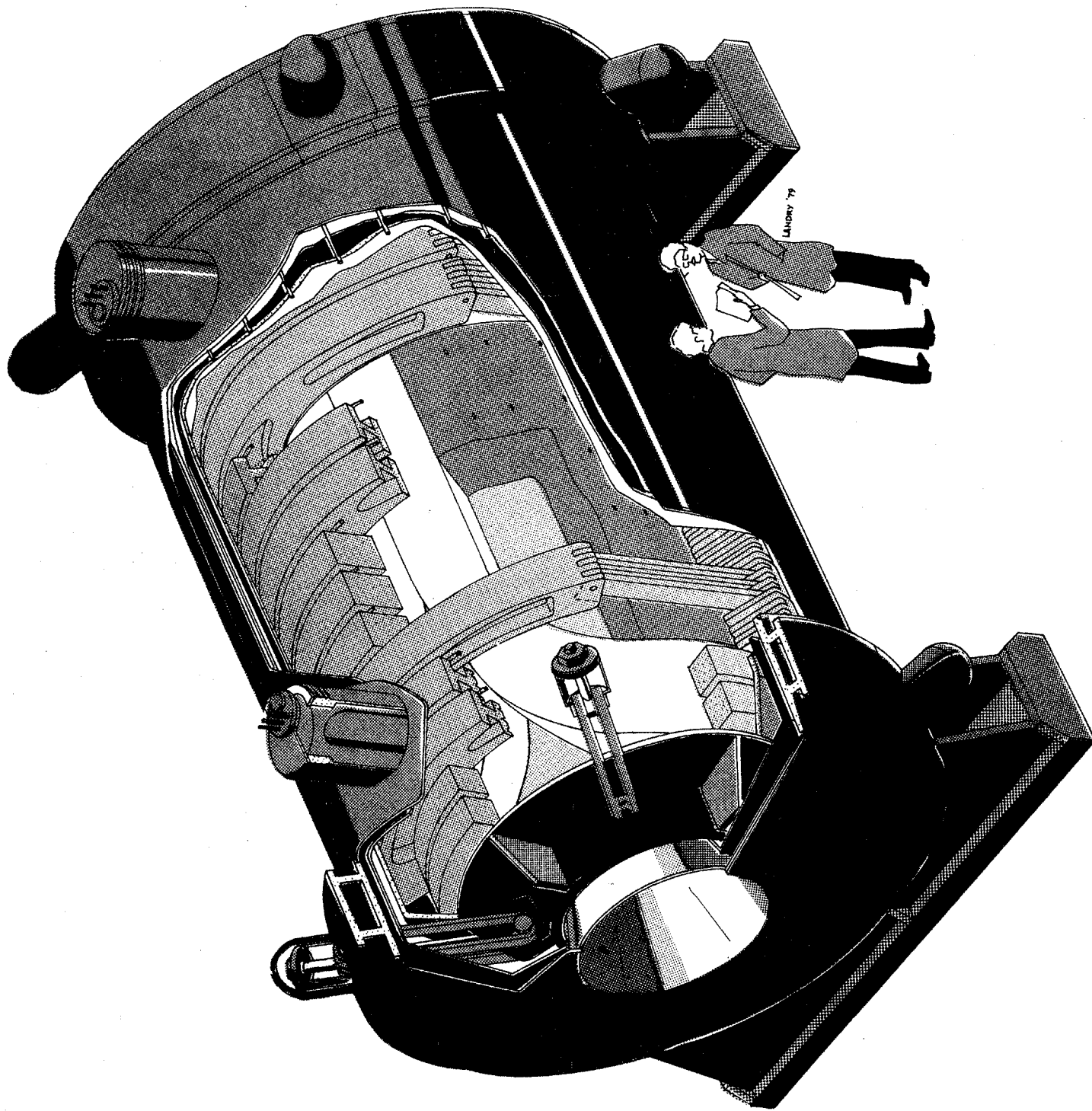


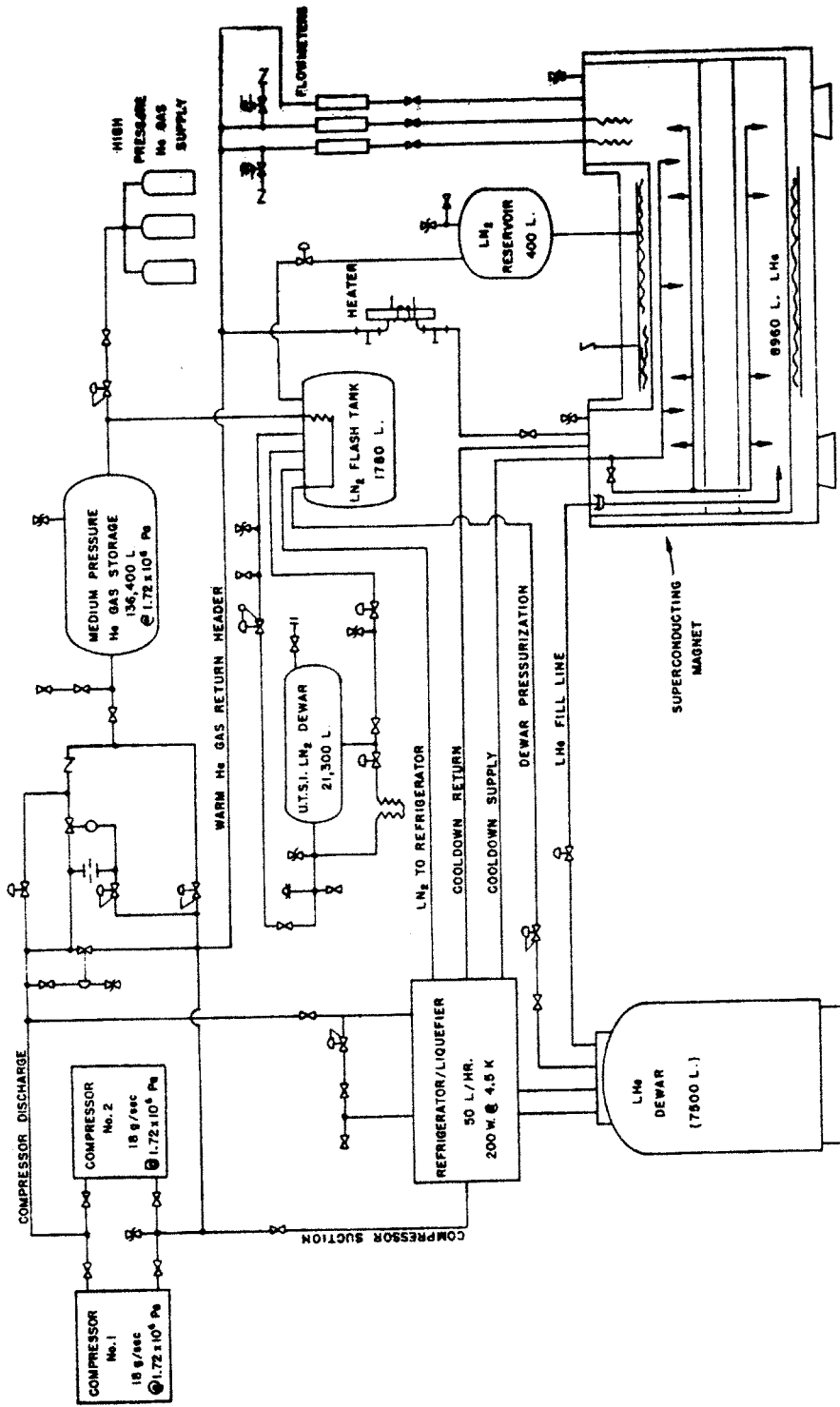
**BORE TUBE & END FLANGES**

4.3.4C

Sketch Showing Structural Core Tube and Cross Section of Winding and Main Structure Consisting of Ring Girders and Tie Plates, Coal-Fired Flow Facility Magnet (CFFF/SM)

4.3.4D Cutaway View of Magnet and Cryostat Assembly, Coal-Fired Flow Facility Magnet (CFFF/SM)





4.3.4E Diagram of Cryogenic Subsystem, Coal-Fired Flow Facility Magnet (CFFF/SM)

More detailed information on the CFFF/SM magnet is contained in Reference 17.

### **4.3.5 The CDIF Conventional Water-Cooled Magnet, CDIF/CM**

#### **4.3.5.1 Summary**

The CDIF conventional magnet (CDIF/CM) is a nominal 3 T MHD magnet which was procured by MIT under DOE auspices and is now installed and operating in one of the two test bays of the CDIF in Butte, Montana. The other test bay is intended to house the 6 T superconducting magnet (CDIF/SM) described in Section 4.3.1.

The CDIF/CM conceptual design was developed by MIT in 1977. Following competitive bidding, magnet detail design and manufacture were subcontracted to Magnetic Corporation of America (MCA), Waltham, MA, on a fixed price basis. Coils were wound at the MCA Waltham facility. Steel fabrication and magnet assembly were accomplished by Combustion Engineering in their Wellsville, NY facility under subcontract to MCA. The magnet was delivered to the CDIF site in January, 1980. Installation and checkout of the magnet system was completed early in 1981 and testing of an MHD test train in the magnet was started in the latter part of 1981.

#### **4.3.5.2 Description**

The CDIF/CM produces a horizontal magnetic field with a tapered profile in a rectangular cross section bore 0.4 m wide by 0.7 m high at the inlet end, diverging in width to 0.72 m at the exit end. The magnet is built in two halves which can be rolled apart to provide easy access to the channel.

The magnet windings consist of two rectangular saddle-shaped coils of hollow copper conductors, one coil in each half. The coils are untapered; the field profile taper is achieved by tapering the pole pieces. Turn-to-turn insulation and ground insulation are woven polyester tape with flexible epoxy. Each coil half was vacuum-bag impregnated. Iron (low carbon steel) pole pieces and flux return frames are provided, the latter serving also as supports for the central portions of the coils. Steel plates structurally tied to the return frames support the ends of the coils against longitudinal magnetic forces.

An insulating aperture liner is provided, consisting of an ablative teflon inner wall backed by a fiberglass outer shell.

The characteristics of the CDIF/CM are listed in Table 4.3.5-I. Performance data shown are for a peak on-axis field of 3.0 T, consistent with the present facility capability. However, the coils and coil support structure are designed to operate at a peak field of 4.0 T, with the associated increases in power and cooling requirements.

The on-axis field profile of the CDIF/CM is shown in Figure 4.3.5A. An exploded view of the magnet is shown in Figure 4.3.5B, assembly views in Figure 4.3.5C, the coil outline in Figure 4.3.5D, an artist's sketch of the magnet assembly in Figure 4.2.5E and a photograph of the completed magnet in Figure 4.3.5F.

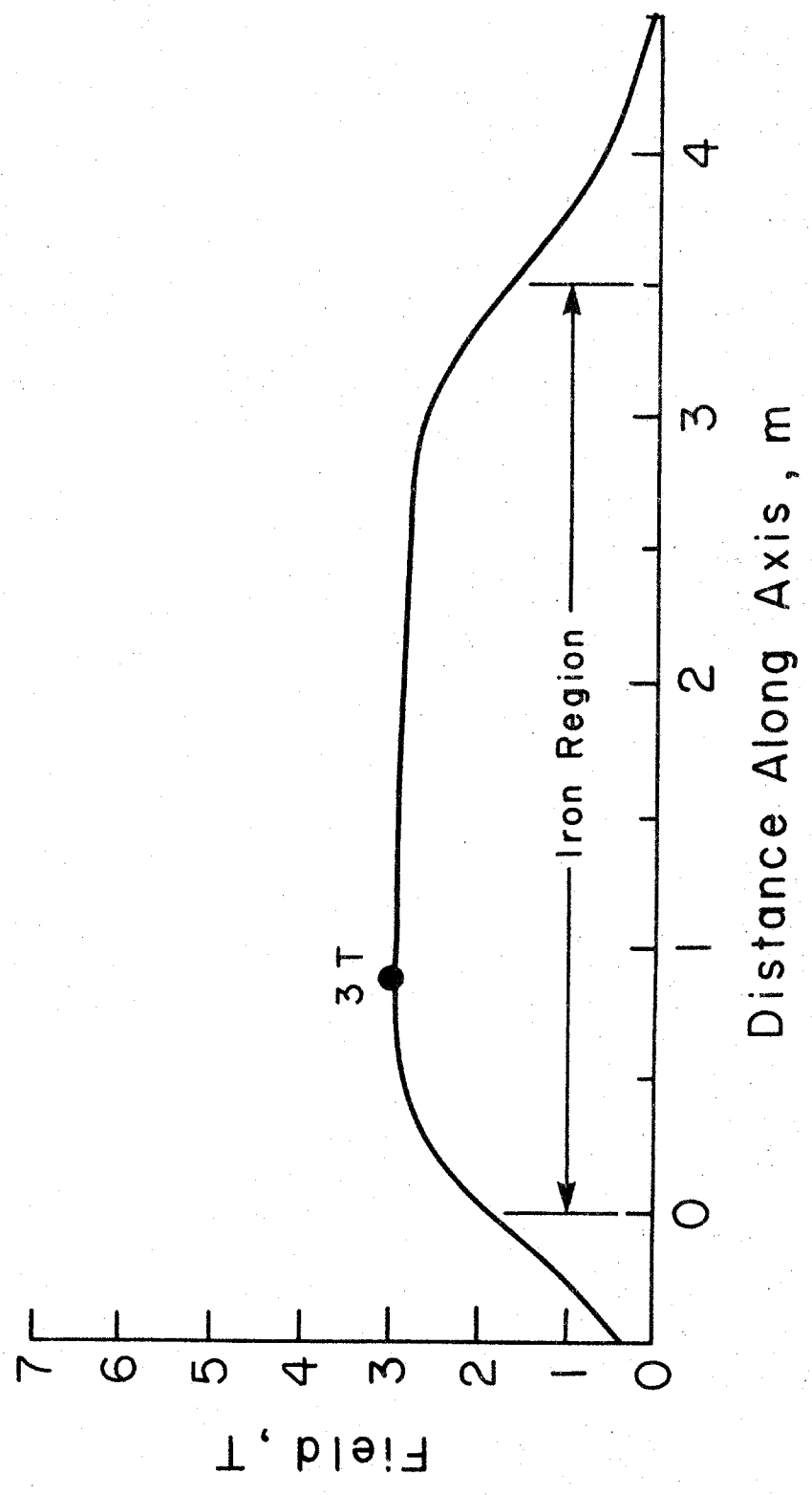
More detailed information on the magnet is contained in References 16 and 85.

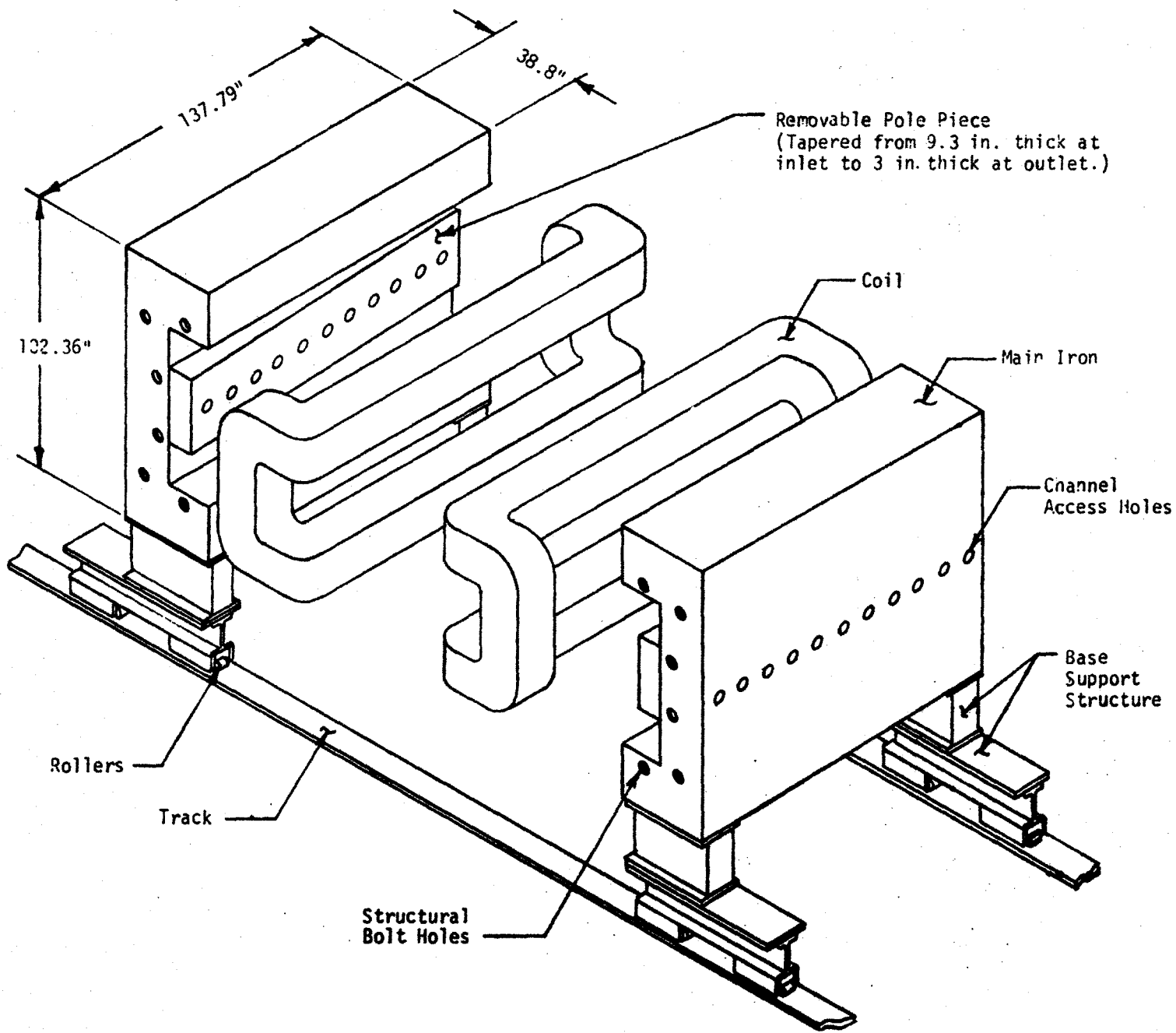
Table 4.3.5-1

Magnet System Characteristics  
CDIF/CM

Peak on-axis field	(T)	3.0
Active field length (pole length)	(m)	3.5
Inlet bore width	(m)	0.40
Inlet bore height	(m)	0.70
Exit bore width	(m)	0.72
Exit bore height	(m)	0.70
Iron frame length	(m)	3.50
Iron frame width	(m)	2.00
Iron frame height	(m)	2.60
Overall magnet length	(m)	4.90
Winding build	(m)	0.40
Winding current density	( $10^7$ A/m <sup>2</sup> )	0.69
Winding packing factor	—	0.75
Conductor copper current density	( $10^7$ A/m <sup>2</sup> )	0.92
Ampere turns	( $10^6$ A)	2.4
Design current	(kA)	8.25
Design voltage	(V)	648
Design power	(MW)	5.34
Conductor outside dimensions	(cm)	3.15 sq.
Conductor hole diameter	(cm)	1.11
Number of coil modules	—	2
Total number of turns	—	288
Mean turn length	(m)	12
Insulation type	—	Polyester
Insulation thickness, turn-to-turn	(mm)	1.5
Insulation thickness, layer	(mm)	4.5
Insulation thickness, ground	(mm)	5.3
Coil average temperature	(C)	60
Cooling water flow	(kg/s)	38
Cooling water inlet temperature, max	(C)	29
Pressure drop	(MPa)	0.7
Pressure rating	(MPa)	4.1
Weight, coils	(tonnes)	27
Weight, poles & return frame	(tonnes)	104
Weight, structure & miscellaneous	(tonnes)	21
Weight, magnet total	(tonnes)	152

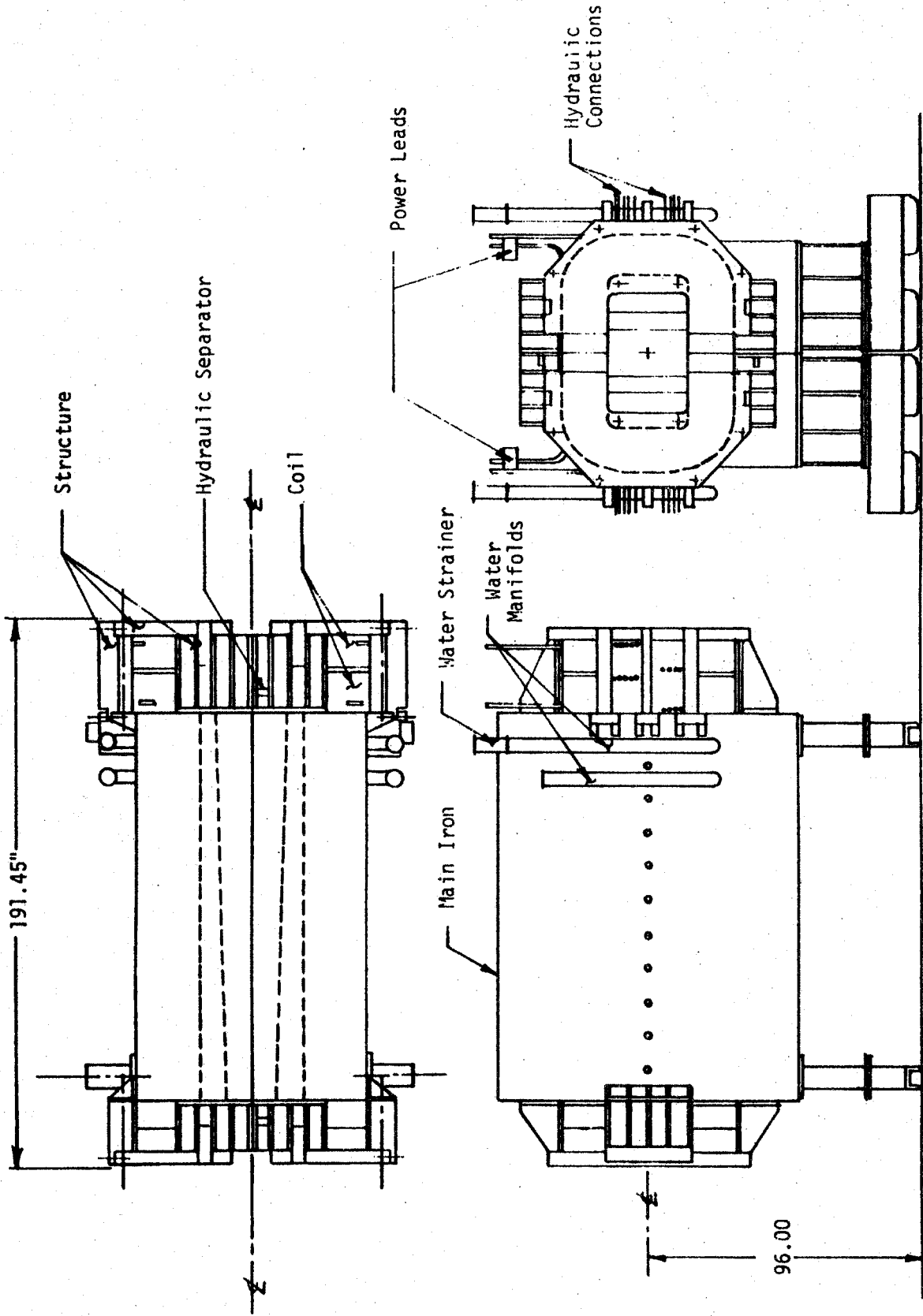
4.3.5A Curve of On-Axis Field vs Distance Along Axis, CDJF Conventional Magnet (CDJF/CM)



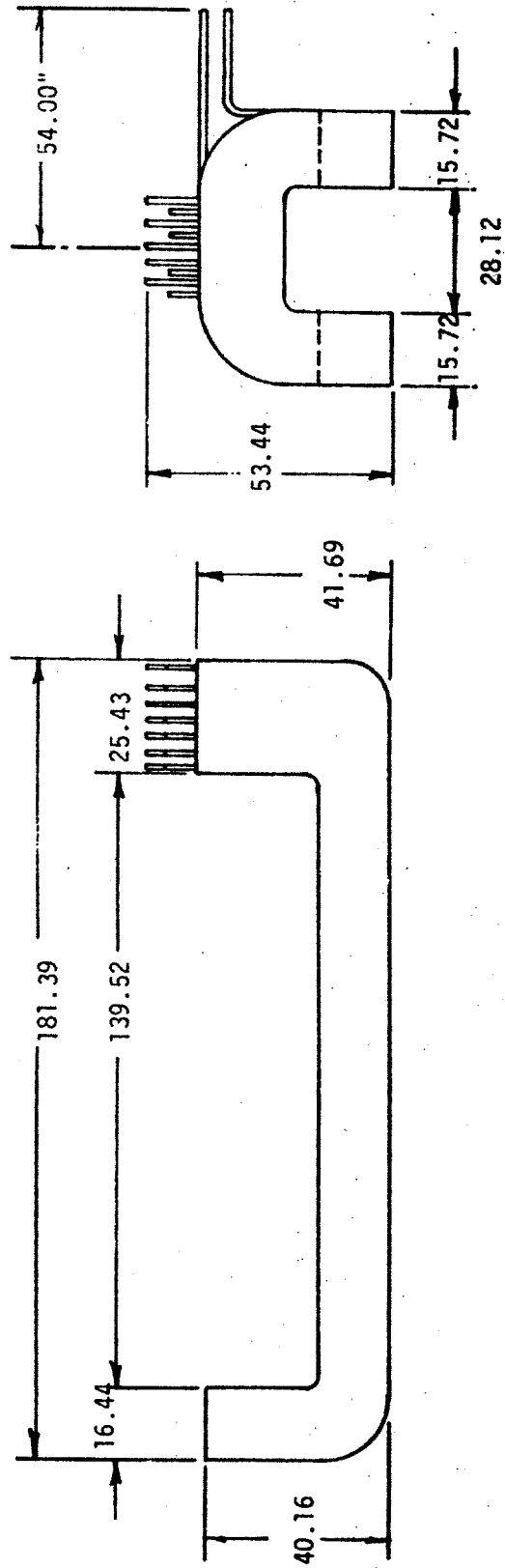
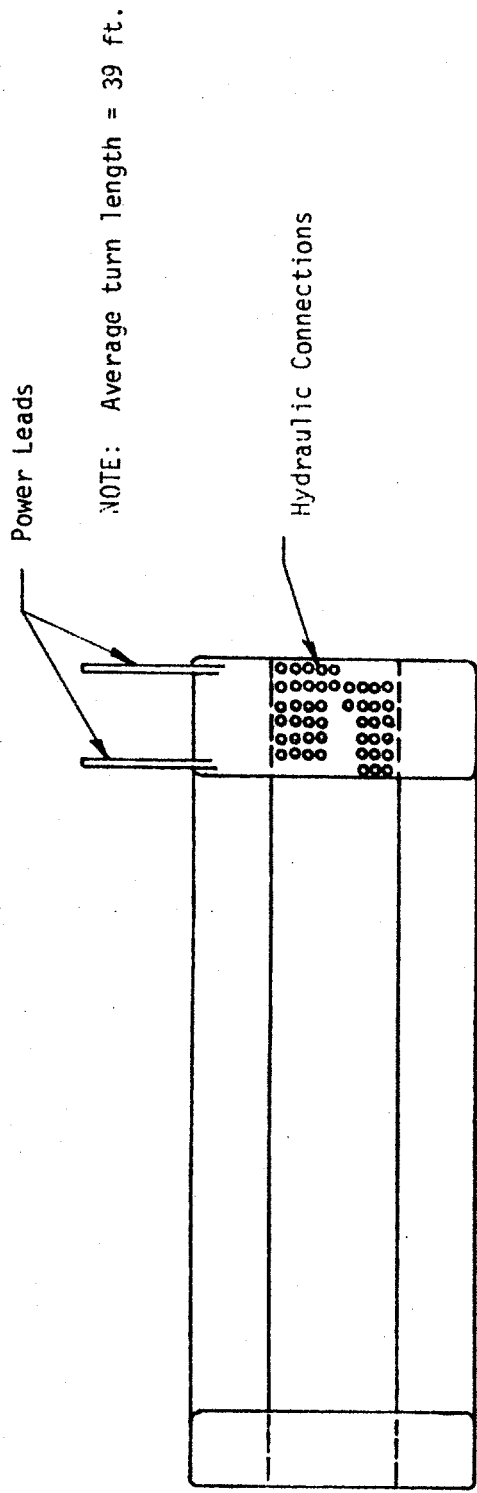


4.3.5B Exploded View of CDIF Conventional Magnet Coils, Yokes and Pole Pieces (CDIF/CM)

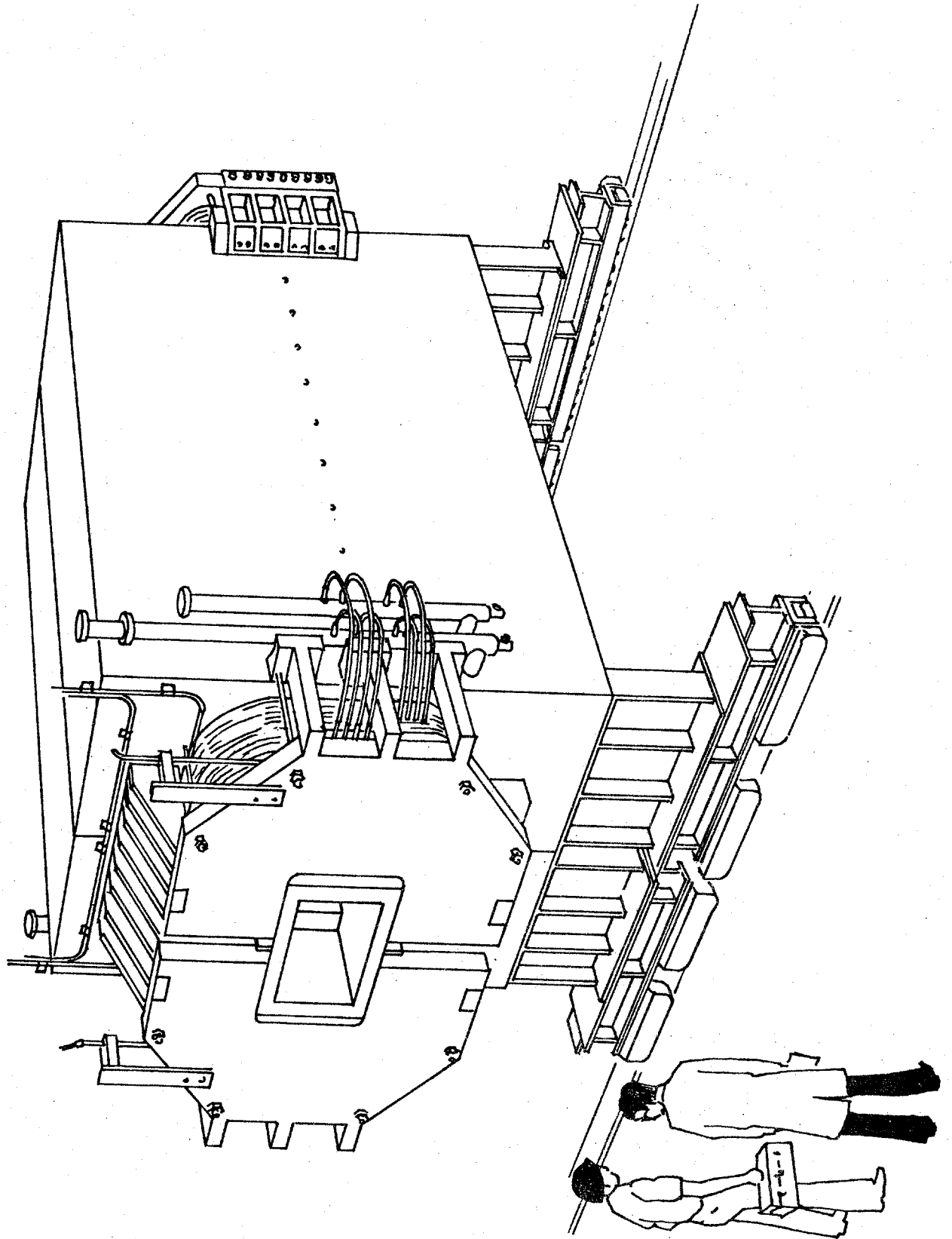
4.3.5C Elevation, Plan and End Views of CDIF Conventional Magnet (CDIF/CM)

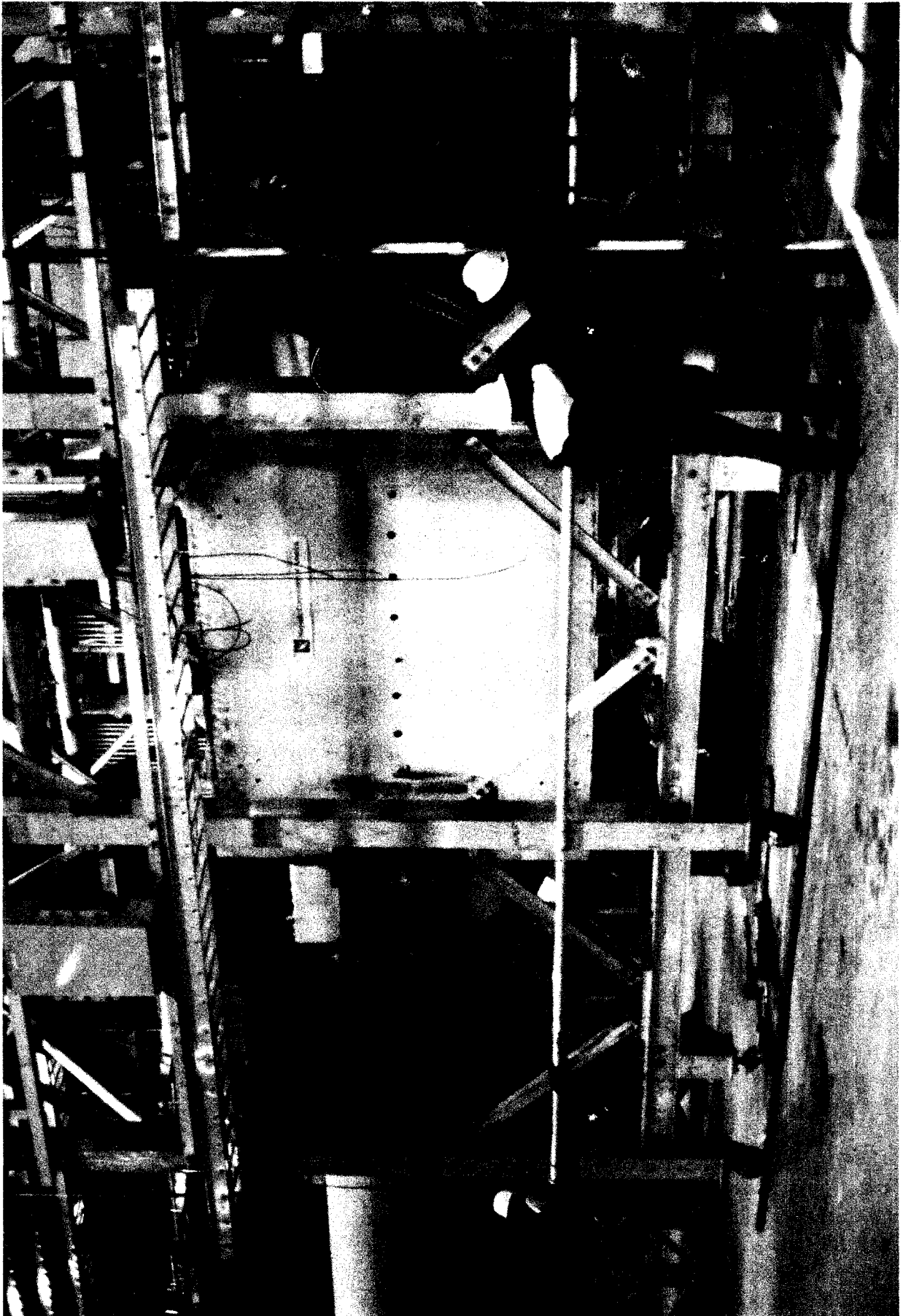






4.3.5E Artist's Sketch of CDIF Conventional Magnet Assembly





4.3.5F Photograph of Completed CDIF Conventional Magnet (CDIF/CM)

### 4.3.5.3 Comparative Evaluation, CDIF/CM and AVCO/CM

The CDIF/CM and the other conventional MHD magnet procured during the same period, the AVCO/CM (described in Section 4.3.6) appear similar in design and construction when viewed externally. However, fundamental differences in the basic design and manufacturing philosophies exist. Based on these differences, the CDIF/CM approach may be termed high risk/low cost because of greater coil strain sensitivity and more limited access for coil repair. The AVCO/CM approach may be termed low risk/high cost because its modular coil construction contributes to lower strain sensitivity and greater access for repair. However, it should be noted that the ratio of cost to weight of the completed magnets actually turned out to be slightly lower for the AVCO/CM. Comparative evaluation of the two designs is further discussed in Reference 16.

### 4.3.6 The AVCO Mk VI-II Conventional Water-Cooled Magnet, AVCO/CM

#### 4.3.6.1 Summary

The AVCO Mk VI-II conventional magnet (AVCO/CM) is a 4 T MHD magnet which was designed and procured by MIT under DOE auspices and is now installed and operational in the Mk VI test facility at AVCO Everett Research Laboratory (AVCO), in Everett, MA.

The preliminary design of the AVCO/CM was developed by Magnetic Engineering Associates (MEA) early in 1977. Coil fabrication was subcontracted to the Everson Electric Co., Bethlehem, PA, in January, 1978. Fabrication of return frame and support structure was subcontracted to the Bethlehem Corp., Easton, PA. After testing, coils were shipped from Everson to Bethlehem Corp., where the magnet was assembled and tested.

The magnet was delivered to the AVCO Everett site in February, 1980 and installation was completed in April, 1980. During preliminary checkout, a coil-to-ground fault occurred which required magnet disassembly, coil repair and reassembly. Checkout and magnet performance testing were completed in July, 1980. Since that date, the magnet has been in use testing MHD power train equipment.

#### 4.3.6.2 Description

The AVCO/CM produces a horizontal magnetic field with a tapered profile in a rectangular cross section bore 0.40 m wide by 0.44 m high at the inlet end, diverging to 0.60 m wide by 0.50 m high at the exit end. The magnet is built in two halves which can be rolled apart to provide easy access to the channel.

The magnet windings consist of ten rectangular, saddle-shaped coil modules of hollow copper conductor, five of which are nested in each half of the magnet. The coil modules are tapered, diverging toward the exit end. The coil shape, in conjunction with the taper of the iron components, produces the desired tapered field profile. Turn-to-turn insulation and module overwrap are fiberglass tape. Each coil module was impregnated in a metal mold. Coil-to-ground insulation is provided by G-10 and polypropylene shims.

Iron (low carbon steel) pole pieces and flux return frames are provided, the latter serving also as support for the central portions of the coils. Steel end plates, structurally tied to the return frames, support the ends of the coils against longitudinal magnetic forces.

The characteristics of the AVCO/CM are listed in Table 4.3.6-I. The on-axis field profile is shown in Figure 4.3.6A, assembly views in Figure 4.3.6B, the coil outline in Figure 4.3.6C and a photograph of the completed magnet in Figure 4.3.6D.

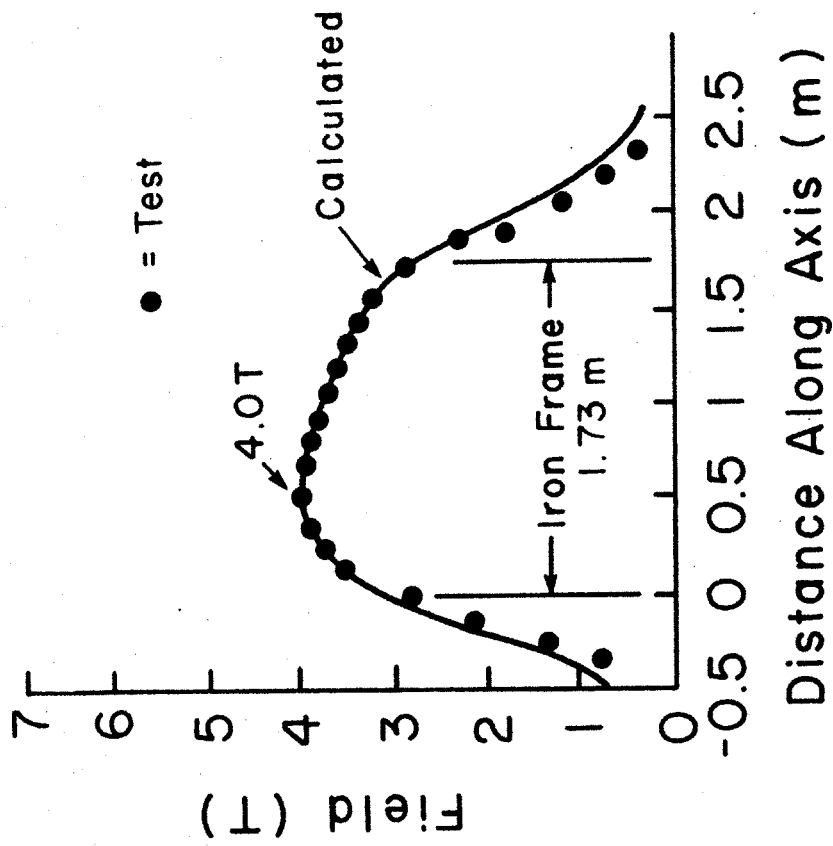
More detailed information on the magnet is contained in Reference 16.

A comparative evaluation of the AVCO/CM and the externally similar CDIF/CM is contained in Section 4.3.5.3.

Table 4.3.6-I

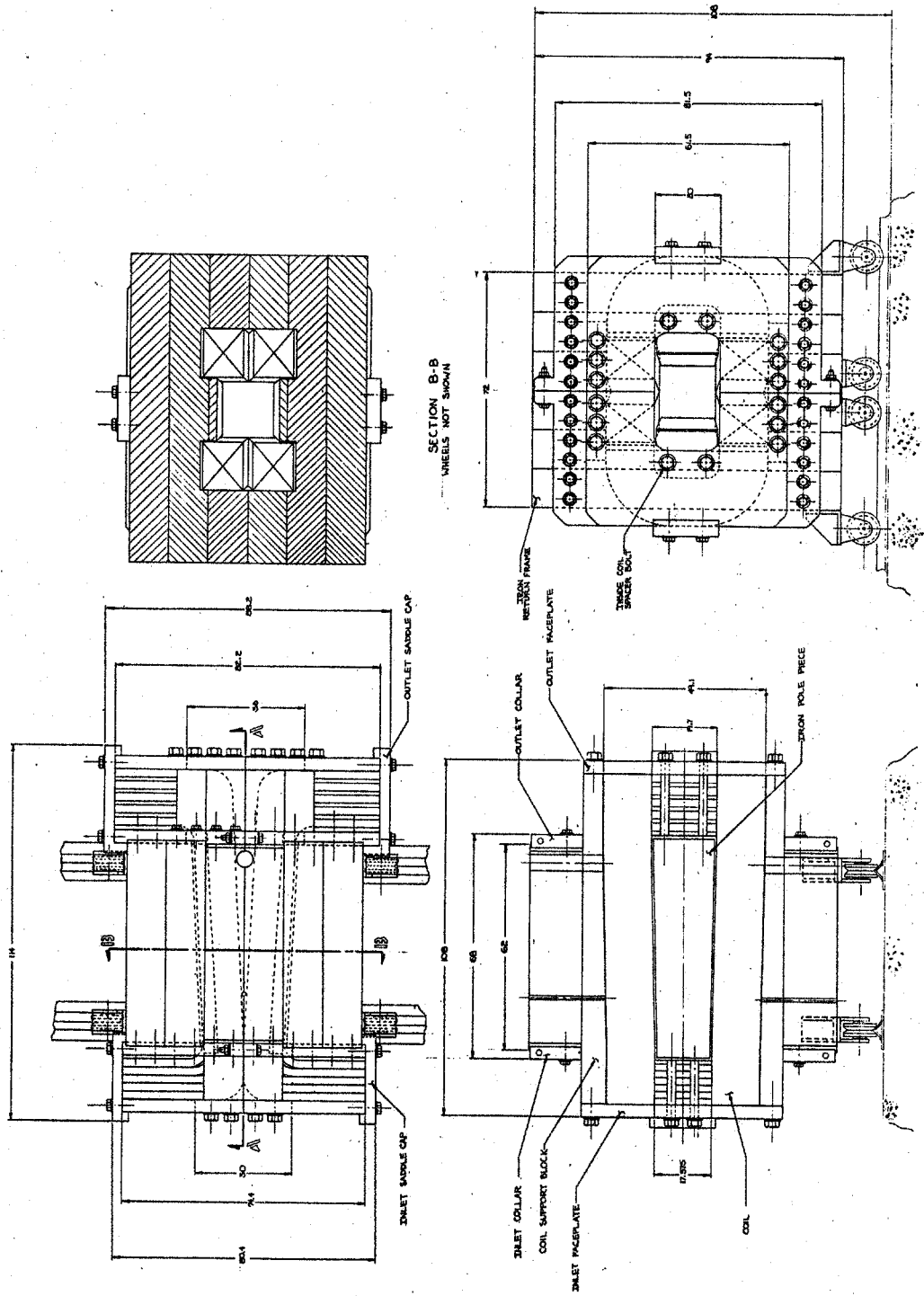
Magnet System Characteristics  
AVCO/CM

Peak on-axis field	(T)	4.0
Active field length (pole length)	(m)	1.73
Inlet bore width	(m)	0.40
Inlet bore height	(m)	0.44
Exit bore width	(m)	0.60
Exit bore height	(m)	0.50
Iron frame length	(m)	1.73
Iron frame width	(m)	1.83
Iron frame height	(m)	2.43
Overall magnet length	(m)	2.94
Winding build	(m)	0.37
Winding current density	( $10^7$ A/m <sup>2</sup> )	1.06
Winding packing factor	—	0.75
Conductor copper current density	( $10^7$ A/m <sup>2</sup> )	1.41
Ampere turns	( $10^6$ A)	2.86
Design current	(kA)	11
Design voltage	(V)	600
Design power	(MW)	6.6
Conductor outside dimensions	(cm)	3.0 sq.
Conductor hole diameter	(cm)	1.22
Number of coil modules	—	10
Total number of turns	—	260
Mean turn length	(m)	7.9
Insulation type	—	Fiberglass
Insulation thickness, turn-to-turn	(mm)	1.0
Insulation thickness, layer (pancake)	(mm)	5.1
Insulation thickness, ground	(mm)	—
Coil average temperature	(C)	58
Cooling water flow	(kg/s)	44
Cooling water inlet temperature, max	(C)	27
Pressure drop	(MPa)	1.0
Pressure rating	(MPa)	—
Weight, coils	(tonnes)	14
Weight, poles & return frame	(tonnes)	54
Weight, structure & miscellaneous	(tonnes)	14
Weight, magnet total	(tonnes)	82



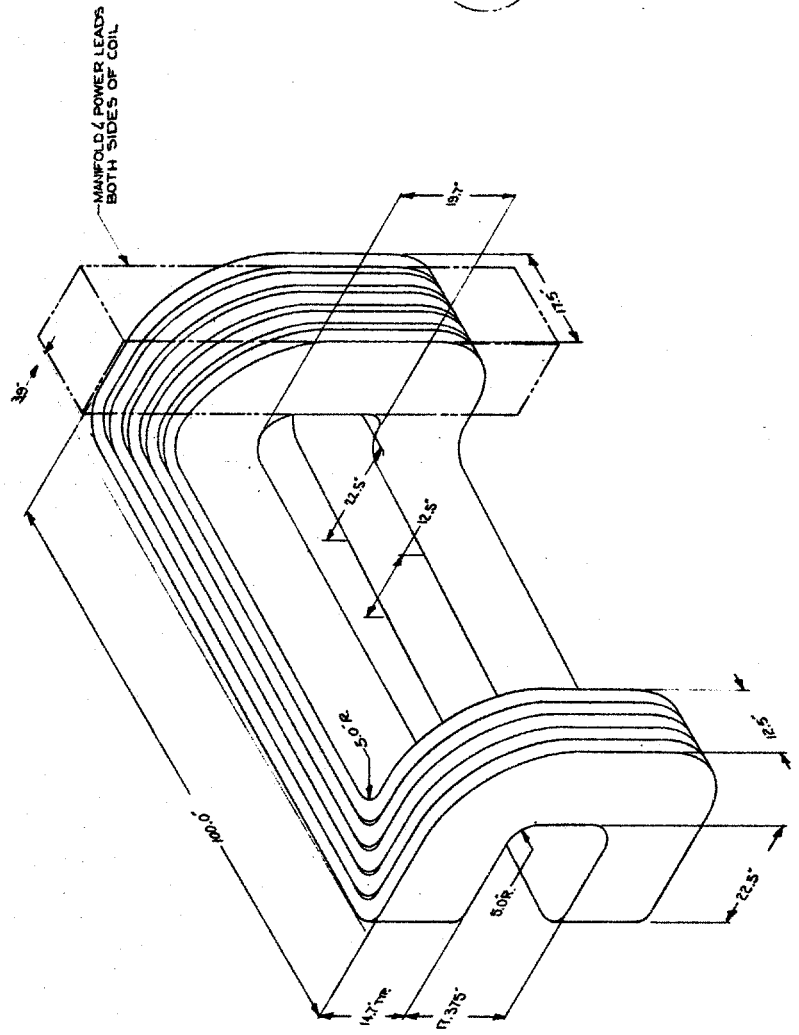
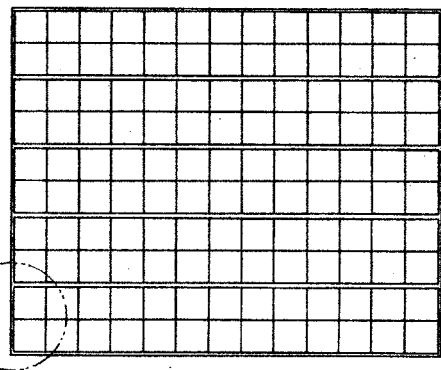
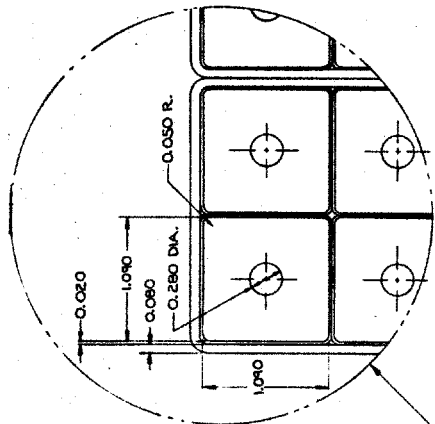
4.3.6A Curve of On-Axis Field vs Distance Along Axis, A VCO Conventional Magnet (AVCO/CM)

4.3.6B Elevation, Plan and End Views of AVCO Conventional Magnet (AVCO/CM)



ALL DIMENSIONS IN INCHES

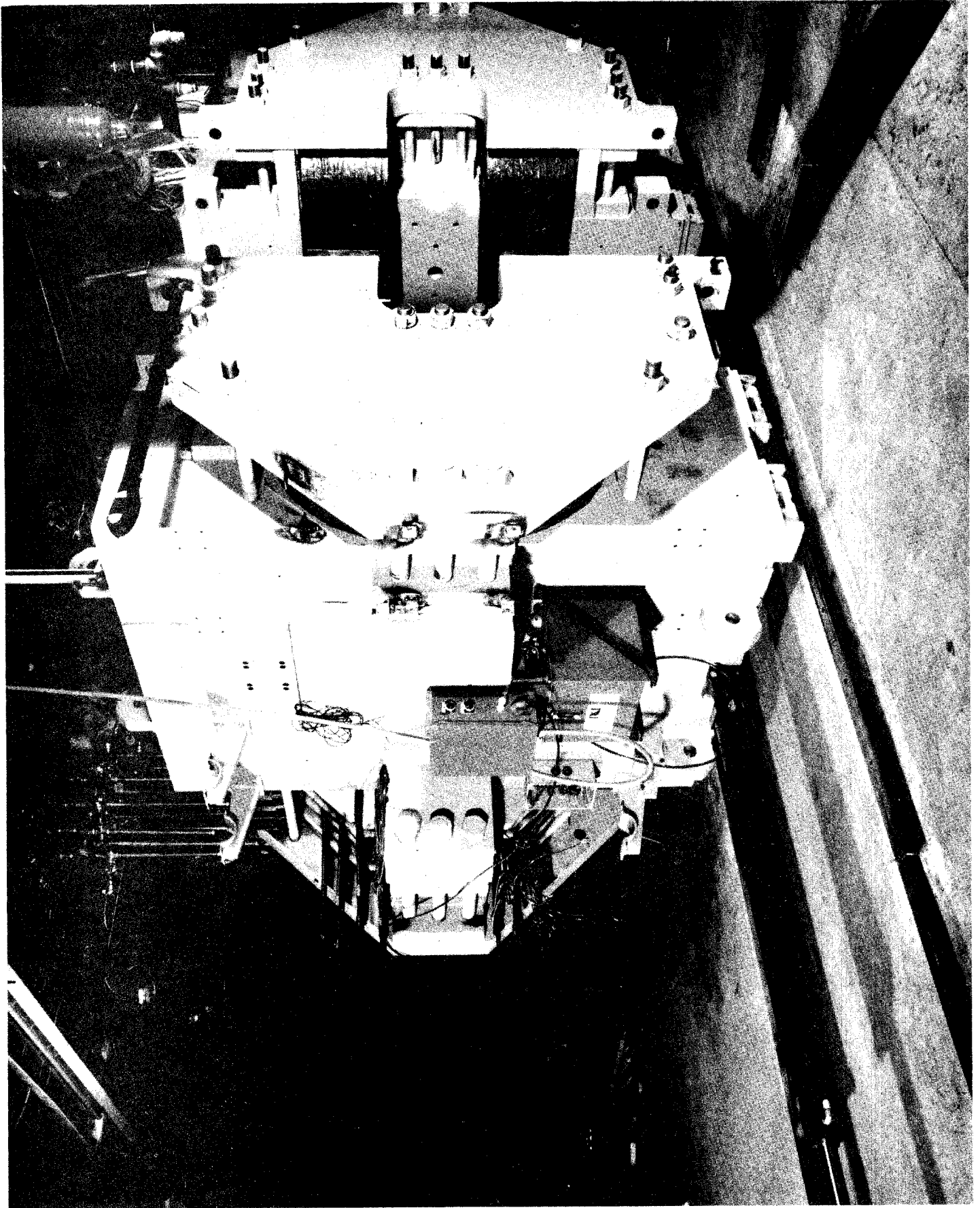




ALL DIMENSIONS IN INCHES

4.3.6C Sketch Showing Coil Outline (One Half of Winding), and Coil Cross Section, AVCO Conventional Magnet (AVCO/CM)

4.3.6D Photograph of Completed AVCO Conventional Magnet (AVCO/CM)



## 5.0 References

1. Montgomery, D.B., et al., Superconducting Magnets for Baseload MHD Generators, 6th International Symposium on MHD, June 1975.
2. Montgomery, D.B., et al. (MIT) and Zenkevich, V. (HTI-USSR) Joint U.S.-U.S.S.R. Status Report, Superconducting Magnets, December 1976.
3. Montgomery, D.B., et al., The Technology Base for Large MHD Superconducting Magnets, 15th Symposium, Engineering Aspects of MHD, 1976.
4. Williams, J.E.C., Montgomery, D.B. (MIT) and Rudins, G. (DOE), Superconducting Magnet Development for the MHD Program, 16th Symposium, Engineering Aspects of MHD, Pittsburgh, June 1977.
5. Montgomery, D.B., and Zenkevich, V.B., "Superconducting Magnets," Chapter 7, pp. 229-274, in Open-Cycle Magnetohydrodynamic Electrical Power Generation, M. Petrick and B. Ya. Shumyatskaj, eds., Argonne National Laboratory, Argonne, IL, 1978.
6. Marston, P.G., Superconducting Magnets for Magnetohydrodynamic Power Generation, presented at the Annual Meeting of the Electrochemical Society, Boston, May 1979.
7. Montgomery, D.B., Magnet Program Overview, Technology Construction Interactions, Proc. 1978 Superconducting MHD Magnet Design Conf., pp. 69-74, MIT, May 1979.
8. Williams, J.E.C., The Superconducting MHD Magnet Technology Development Program, Proc. 1978 Superconducting MHD Magnet Design Conf., pp. 75-102, MIT, May 1979.
9. Marston, P.G., Montgomery, D.B., Williams, J.E.C., and Dawson, A.M., Superconducting MHD Magnets: Technology Development, Procurement and the Path to Commercial Scale, Proc, 18th Symp. Eng. Aspects of MHD, Butte, MT, June 1979.
10. Wilson, M.N., Large Superconducting Magnets for New Energy Technologies, Advances in Cryogenic Engineering, Vol. 24, pp.1-15, Plenum Press, New York (Proc. 2nd Int. Cryo. Materials Conf., 1977)
11. Marston, P.G., and Thome, R.J., Strategy of the U.S. MHD Magnet Program, Proc. 7th Int. MHD Conf., Vol. II, pp. 450-458, June 1980.
12. Marston, P.G., and Thome, R.J., Strategy of the U.S. MHD Magnet Program, 1980 Superconducting MHD Magnet Design Conf., pp. 1-9, MIT, March 1980.
13. Marston, P.G., Dawson, A.M., Montgomery, D.B., and Williams, J.E.C., Superconducting MHD Magnet Engineering Program, Advances in Cryogenic Engineering, Vol. 25, pp. 1-11, Plenum Press, New York, 1978 (Proc. 1977 CEC).

14. Dawson, A.M., Marston, P.G., Thome, R.J., Iwasa, Y., and Tarrh, J.M., The United States Superconducting Magnet Technology Development Program IEEE Trans. Mag., MAG-17(5): 1966-1069, 1981. (MT7-Karlsruhe)
15. Marston, P.G., and Dawson, A.M., Status of MHD Technology, 16th IECEC, Vol. 2, pp. 1477-1482, 1981.
16. Tarrh, J.M., Two Conventional MHD Magnets, 1980 Superconducting MHD Magnet Design Conf., pp. 51-54, MIT, March 1980.
17. Wang, S.T. et al., The Fabrication Experiences and Performance Test of the Coal-Fired Flow Facility Superconducting Dipole Magnet, 19th Symposium on Engineering Aspects of MHD, Tullahoma, TN, June 1981.
18. General Dynamics Convair Division, Report GDC-107-SSM-80-103, Stanford Superconducting Magnet (SSM) Program, Phase II Detail Design Status Report, prepared under MIT PO ML 67270, March 1980.
19. Rhodenizer, R.L., General Electric Co., The Superconducting CDIF Magnet, Proc. 1978 Superconducting MHD Magnet Design Conf., pp. 167-189, MIT, May 1979.
20. Iwasa, Y., Thome, R.J., Leupold, M.J., Maguire, J.F., Montgomery, A.G., Olmstead, M.M., Rabasco, A.D., Sinclair, M.W., Sliski, D.J., and Thompson, J.B., The MHD Component Test Facility at the Francis Bitter National Magnet Laboratory, IEEE Trans. Mag., MAG-17(1): 498-501, 1981.
21. Wilson, M.N., and Iwasa, Y., Stability of Superconductors against Localized Disturbances of Limited Magnitude, Cryogenics, 18(1): 17-21, 1978
22. Dawson, A.M., Design of High Current Superconductor for MHD Magnets, MIT/FBNML Report, November 1977.
23. Hoenig, M.O., Internally-Cooled Cable Superconductors, Cryogenics, July 1980, pp. 373-389 and August 1980, pp. 427-434.
24. Stekly, Z.J.J. et al., Magnetic Corporation of America, Magnet Protection for MHD Systems, Final Report, Phase I, prepared for MIT/FBNML, September 1981.
25. Erez, E.A., Update on Properties of Glass Reinforced Plastics at Cryogenic Temperatures, CDIF Verification Tests, 1980 Superconducting MHD Magnet Design Conf., pp. 110-117, MIT, March 1980.
26. Iwasa, Y., and Sinclair, M.W., Acoustic Emission in Superconductors and Superconducting Magnets and its Diagnostic Potential, in Mechanics of Superconducting Structures, F.C. Moon, ed., AMD - Vol 41, pp. 109-134, ASME, New York, 1980.
27. Tarrh, J.M., Computational Techniques for MHD Magnet Design, Proc. of 1978 Superconducting MHD Magnet Design Conference, pp. 513-524, MIT, May 1979.

28. Bobrov, E.S., ETF Magnet Design Alternatives, Proc. of 1980 Superconducting MHD Magnet Design Conference, pp. 37-45, MIT, March 1980.
29. Marston, P.G., The CDIF Superconducting Magnet, MIT/FBNML Report, March 1977.
30. General Dynamics Convair Division Report No. CASK-GDC-031, Cask Commercial Demo Plant MHD Superconducting Magnet Systems: Conceptual Design Final Report, prepared under MIT PO ML 67466, December 1979.
31. Bobrov, E.S., Marston, P.G., and Kuznetsov, E.N., Theoretical and Engineering Aspects of Momentless Structures and Coil End-Turns in Superconducting MHD Magnets, Advances in Cryogenic Engineering Vol. 27, pp. 47-56, Plenum Press, New York, 1982 (Proc. 1981 CEC).
32. Becker, H., Development of a Structural Design Code for MHD Magnets, Interim Report, MIT/FBNML, October 1979.
33. Marston, P.G., Hatch, A.M., Dawson, A.M. and Brogan, T.R., Magnet-Flowtrain Interface Considerations, 19th Symposium, Engineering Aspects of MHD, Tullahoma, TN, June 1981.
34. Belding Corporation, An Investigation of Current Heavy Equipment Transportation Methods, MHD Plant Components, report prepared for MIT/FBNML, June 1979.
35. Cryogenic Consultants, Inc., (Allentown, PA) Cryogenic Support Systems for Large Scale MHD Magnets, report prepared under MIT PO ML 111122, May 1979.
36. Kusko, A., (Alexander Kusko, Inc.) Power Supplies for Superconducting MHD Magnets, 1980 Superconducting MHD Magnet Design Conf., pp. 160-163, MIT, March 1980.
37. Hatch, A.M., MHD Magnet Cost Analysis and Estimation (Course Notes) MIT/FBNML July 27, 1980.
38. NASA/LeRC Conceptual Design Engineering Report - MHD Engineering Test Facility 200 MWe Power Plant, prepared for NASA/LeRC for DOE by Gilbert/Commonwealth, DOE/NASA/0224-1 Vol. I-V, September 1981.
39. Iwasa, Y., Experimental Activities at Francis Bitter National Magnet Laboratory, 1980 Superconducting MHD Magnet Design Conf., pp. 75-81, MIT, March 1980.
40. Iwasa, Y., et al., Operation of the MHD Component Test Facility and First Experimental Results, Advances in Cryogenic Engineering, Vol. 27, pp. 29-36, Plenum Press, New York, 1982 (Proc. 1981 CEC).
41. Iwasa, Y., A Critical Current Margin Design Criterion for High Performance Magnet Stability, Cryogenics, 19(12): 705-714, 1979.

42. Thome, R.J., et al., Magnetic Corporation of America, Impact of High Current Operation on the Cost of Superconducting Magnets for Large Scale Magnetohydrodynamic (MHD) Application, prepared under MIT PO ML 67150, June 1978.
43. Ibid. Appendix C. Extension of Results to the Range 10 kA to 250 kA Operating Current, prepared under MIT PO ML 67726, September 1978.
44. Ibid. Appendix D. Impact of Shell Type Substructures, prepared under MIT PO ML 67437 by B.O. Pedersen, December 1978.
45. General Dynamics Convair Division Report No. PIN78-182 Cask Commercial Demo Plant MHD Magnet: Budgetary (Cost Estimate) and Planning, Final Report, prepared under MIT PO ML 68221, February 1980.
46. Niemann, R. et al., Superconducting Magnet System - U25 MHD Facility, IEEE Trans. Mag., MAG 13(1): 632-635, 1977.
47. Batzer, T.H., The Technology of Mirror Machines - LLL Facilities for Magnetic Mirror Fusion Experiments, 7th Symposium on Engineering Problems of Fusion Research, IEEE Pub. No. 77CH1267-4-NPS, 1977.
48. McWilliams, M.D., Stability Margin of Cabled Superconductors Wound into Channeled Subplates, M.S. Thesis, MIT, June 1981.
49. Morpurgo, M., The Design of the Superconducting Magnet for the 'Omega' Project, Particle Accelerators, Gordon and Breach Science Publishers, Ltd 1 (1970).
50. Bobrov, E.S., Force Containment Structure Design Considerations, Proc. 1978 Superconducting MHD Magnet Design Conf., pp. 339-372, MIT, May 1979.
51. Bobrov, E.S., ETF Magnet Design Alternatives, 1980 Superconducting MHD Magnet Design Conf., pp. 37-45, MIT, March 1980.
52. Williams, J.E.C., A 7 Tesla Superconducting Magnet for MHD Studies at Stanford University, Final Report, MIT/FBNML June 1977.
53. Marston, P.G., Consultant, A Superconducting Magnet for CDIF, Stanford-CDIF Trade-off Study, #1 Monthly Report, MIT/FBNML, June 1976.
54. Hatch, A.M. et al., Design of Superconducting Magnets for Full Scale MHD Generators, Cryogenics, February 1978.
55. Becker, H., An Exploratory Study of MHD Magnet Structural Optimization, internal report, MIT Francis Bitter National Magnet Laboratory, MHD Magnet Technology Group, March 1979.

56. Kuznetsov, E.N., Battelle Columbus Laboratories, Analysis and Development of Isotension Superstructure for MHD Magnets, report prepared for MIT/FBNML, June 1979.
57. Thome, R.J. et al, Magnetic Corporation of America, Design of Superconducting Magnets for Magneto-hydrodynamic (MHD) Applications, Final Technical Report, prepared for DOE (ERDA), June 1977.
58. Hatch, A.M., et al., AVCO Everett Research Laboratory, Inc., Design of Superconducting Magnets for MHD Applications, Final Technical Report, prepared for DOE (ERDA) June 1977.
59. Thome, R.J., Magnetic Corporation of America, Preliminary Design of a Winding Model for Baseload MHD Magnets, Winding Model Magnet (WMM) Program Technical Report Phase I, prepared for MIT/FBNML, April 1978.
60. General Dynamics Convair Division and Magnetic Engineering Assoc., Superconducting Winding Model Magnet (WMM) Program Technical Report CASD - MIT - 78-001 Final Report, Phase I, prepared for MIT/FBNML, April 1978.
- 60A. Maddock, B.J., James, G.B. and Norris, W.T., Superconductive Composites: Heat Transfer and Steady State Stabilization, Cryogenics, 9: 261, 1969.
- 60B. Wipf, S.L. and Martinelli, A.P., Investigation of Cryogenic Stability and Reliability of Operation of Nb<sub>3</sub>Sn Coils in Helium Gas Environment, Proceedings of the 1972 Applied Superconductivity Conference, IEEE Pub. No. 72CH0682-5-TABSC, p. 331, 1973.
61. Willig, R.L., Magnetic Engineering Associates, Stability in High Current Superconductors, Proc. 1978 Superconducting MHD Magnet Design Conf., pp. 249-274, MIT, May 1979.
62. Willig, R.L., Coughlin, J.M., and Tarrh, J.M., Magnetic Engineering Associates, Inc., Cambridge, MA, Conductor Analysis for Large Scale Superconducting Magnets, Prepared under MIT PO ML 62351, March 1979.
63. Hilal, M.A., Michigan Technological University, Persistent Resistive Regions in Composite Conductors, report prepared for MIT/FBNML, December 16, 1980.
64. Ibid. Evaluation of MHD Conductors, December 16, 1980.
65. Ibid. Effect of Electric and Thermal Contact Resistance on Cryogenic Stability of MHD Conductors, December 16, 1980.
66. Whipple, T.A., Results of Testing of Two 316L Submerged Arc Welds, letter report, National Bureau of Standards, Boulder, CO, April 10, 1980.
- 66A. Becker, H., memorandum, Preliminary Shear Tests on CDIF Welds, June 27, 1980.

- 66B. Kasen, M.B., Mechanical and Thermal Properties of Filamentary-Reinforced Structural Composites at Cryogenic Temperatures, Cryogenics, 15: 327-351, 1975.
67. Reed, R.P., et al., National Bureau of Standards, Boulder, CO, Materials for Superconducting Magnets for MHD Power Systems: A Usage Survey and a Proposed Research Program, report prepared for MIT/FBNML, June 1979.
68. Becker H., Structural Design Basis for Superconducting Magnets, MIT/FBNML, February 1980.
69. Dawson, A.M., ed., Proc. Structural Standards Workshop, MIT, 1981.
70. Fickett, F.R. and Clark, A.F., National Bureau of Standards, Boulder, CO, Development of Standards for Superconductors, Annual Report FY79 under DOE and MIT PO ML 112876, December 1979.
71. Fickett, F.R., Goodrich, L.F. and Clark, A.F., National Bureau of Standards, Development of Standards for Superconductors, Annual Report FY80, Report NBSIR 80-1642, December 1980.
72. Underground Power Corporation, Quench Protection of Baseload Scale Magnets: Insulation and Voltage Breakdown Levels, Phase I Report, prepared for MIT/FBNML, October 1978.
73. MHD Magnet Technology Group, MIT, Conceptual Design of Superconducting Magnet System for MHD ETF 200 MWe Power Plant, Final Report, November 1981.
74. Alexander Kusko, Inc., Report MI31, Power Supply Subsystem for MHD Generator Superconducting Magnet, Baseline Power Supply Designs and Costs, prepared for MIT/FBNML, April 1981.
75. Hatch, A.M. (MIT) and Brogan, T.R. (MEPPSCO), MHD Channel Packaging Study, Interim Report, MIT/FBNML, July 1980.
76. Brogan, T.R., MEPPSCO, MHD Generator Superconducting Magnet Packaging Study, prepared for MIT/FBNML under MIT PO ML 162789, August 1981.
77. Hatch, A.M., MHD Magnet Flow Train Interfacing Meeting, November 18, 1980 (summary), MIT/FBNML, December 3, 1980.
78. Zar, J.L., AVCO Everett Research Laboratory, Inc., Design and Cost for the Superconducting Magnet for the ETF MHD Generator, report prepared for MIT/FBNML, April 1979.
79. Bobrov, E.S., Marston, P.G., (MIT) and Kuznetsov, E.N., (Battelle), Theoretical and Engineering Aspects of Momentless Structures for MHD Magnets, 1980 Superconducting MHD Magnet Design Conf. pp. 90-102, MIT, March 1980.
80. Proposal, Disk MHD Generator Study, BH901501, prepared by Westinghouse Electric Corp. for NASA/LeRC, February 1979.



81. Thome, R.J., Magnetic Corporation of America, Framework for Selection of Superconducting MHD Magnet System Configuration (ETF Scale or Larger), prepared for MIT/FBNML, December 1978.
82. General Electric Co., Design Summary Report, Phase II, Detailed Design, Manufacture, Installation and Test of a Superconducting MHD Magnet (for CDIF), prepared for MIT/FBNML, PO ML65100, June 1979.
83. Wang, S.T. et al., Fabrication Experiences and Operating Characteristics of the U.S. SCMS Superconducting Dipole Magnet for MHD Research, Advances in Cryogenic Engineering, Vol. 23, pp. 17-27, Plenum Press, New York, 1978 (Proc. 1977 CEC).
84. Niemann, R.C. et al., Cryogenic Aspects of the U.S. SCMS Superconducting Dipole Magnet for MHD Research, Advances in Cryogenic Engineering, Vol. 23, pp. 9-16, Plenum Press, New York, 1978 (Proc. 1977 CEC).
85. Stekly, Z.J.J. and Smith, B.A., CDIF Conventional Magnet, Proc. 1978 Superconducting MHD Magnet Conference, pp. 153-165, MIT, May 1979.

## 6.0 Supplementary Bibliography

- Agatsuma, K., Maguire, J.F., Montgomery, A.G., and Iwasa, Y., Investigation of Quench Propagation and Stability Margin in a Sample, Internally-Cooled, Cabled Superconductor (ICCS), IEEE Trans. Mag., MAG-17(1): 1076-1078, 1981.
- Arp, V.D., National Bureau of Standards, Boulder, CO, Stability and Thermal Quenches in Force-Cooled Superconducting Cables, prepared under MIT PO ML 62592, published in proceedings of 1980 Superconducting MHD Magnet Design Conf., pp. 142-157, MIT, March 1980.
- Becker, H., and Erez, E.A., A Study of Interlaminar Shear Strength at Cryogenic Temperatures, Adv. Cryogenic Eng., 26:259-267, 1980.
- Becker, H., Evaluation of Materials Test Programs and Methods, Proc. 1980 Superconducting MHD Magnet Design Conf., pp. 118-122, MIT, March 1980.
- Becker, H., An Exploratory Study of MHD Magnet Structural Optimization, report, MIT/FBNML, March 1979.
- Becker, H., Some Structural Aspects of Internally-Cooled Conductors, internal report, MIT Francis Bitter National Magnet Laboratory, MHD Technology Group, April 1979.
- Becker, H., Preliminary Shear Tests on CDIF Welds, memorandum, MIT/FBNML, June 27, 1980.
- Bents, D.J. et al., Conceptual Design of the MHD Engineering Test Facility, 19th Symposium on Engineering Aspects of MHD, Tullahoma, TN, June 1981.
- Bobrov, E.S., and Marston, P.G., Theoretical and Engineering Aspects of Momentless Structures, Proc. 1980 Superconducting MHD Magnet Design Conf., pp. 90-102, MIT, March 1980.
- Bobrov, E.S., and Williams, J.E.C., Stresses in Superconducting Solenoids, Mechanics of Superconducting Structures, F.C. Moon, ed., AMD-Vol 41, pp. 13-42, ASME, New York, 1980.
- Bobrov, E.S., Williams, J.E.C., Sinclair, M.W., and Iwasa, Y., Mechanical Training of Impregnated Superconducting Solenoids, IEEE Trans. Mag., MAG-17(1): 736-737, 1981.
- Bobrov, E.S., and Williams, J.E.C., Direct Optimization of the Winding Process for Superconducting Solenoid Magnets (Linear Programming Approach), IEEE Trans. Mag., MAG-17(1): 1981.
- Brogan, T.R., MEPPSCO, MHD Magnet Warm Bore Liners, Proc. 1980 Superconducting MHD Magnet Design Conf., pp. 168-171, MIT, March 1980.
- Combustion Engineering, Inc., Manufacturability Report, MHD ETF 200 MWe Power Plant Magnet System Conceptual Design, prepared under MIT PO ML 211446, September 1981.

- Cooper, W.E., Teledyne, Cold Mass Design Criteria Standardization, Letter Report, prepared for MIT/FBNML, October 1979.
- Ibid. Annual Report, FY80.
- Dawson, A.M., Montgomery, D.B., and Marston, P.G., Superconducting Magnets for MHD and Fusion: Common Problems - Joint Solutions? Proc. 8th Symposium on Engineering Problems of Fusion Research, pp. 734-738, 1979. (IEEE Pub. No. 79CH1441-SNPS)
- Dawson, A.M., The Francis Bitter National Magnet Laboratory: Cryogenic Research Facilities, Cryogenics, 21(8): 451-459, 1981.
- Dawson, A.M. ed., Proc. 1978 Superconducting MHD Magnet Design Conf., 581 pp., MIT, May 1979.
- Dawson, A.M. and Overlan, D., eds., Proc. 7th Int. Conference on MHD Electrical Power Generation, 3 Volumes, Cambridge, MA, June 1980.
- Dawson, A.M., ed., Proc. Internally-Cooled, Cabled Superconductor Workshop, MIT, 1981.
- Dawson, A.M. ed., Proc. 1980 Superconducting MHD Magnet Design Conf., 319 pp., MIT, March 1980.
- Design of High Current Superconductor for MHD Magnets - Independent Reports by Magnetic Corporation of America; Intermagnetics General Corporation; Supercon, Incorporated; AIRCO; September 1977.
- Erez, E.A., et al., Some Mechanical Properties of G-10 GRP at Lower Temperatures, NBS-DOE Workshop, Material at Low Temperature, Vail, CO, October 1978.
- Erez, E.A., and Becker, H.D., Evaluation of Materials for Internally-Cooled, Cabled Superconductor Jackets, (invited paper) KD-2, International Cryogenic Materials Conf., San Diego, CA, 1981.
- General Electric Co., Energy Systems Programs Department, Winding Model Magnet Detailed Design, Fabrication and Delivery, report prepared for MIT Francis Bitter National Magnet Laboratory, MIT PO ML 63841, May 1978.
- Ibid. Phase I, Preliminary Design Report, June 1978.
- Ibid. Design, Manufacture, Installation and Test of a Superconducting Magnetohydrodynamic Magnet (for CDIF), Phase II - Detailed Design, MIT PO ML 65100, June 1979.
- Ibid. Phase II Report, March 1979.
- Ibid. Plan for Experimental Evaluation of Voltage Breakdown Characteristics of Baseload Conductors and Insulators, July 1979.

- Hatch, A.M., Comparison of Sizes and Costs for MHD Magnets, MHD Magnet Group, report, MIT Francis Bitter National Magnet Laboratory, April 1978.
- Hatch, A.M., Interim Report, MIT/FBNML, Cost Analysis Techniques for Superconducting Magnets, September 1979.
- Hatch, A.M. et al., Design of Superconducting Magnets for Full Scale MHD Generators, Adv. Cryo. Eng., 23: 37-47, 1977.
- Hatch, A.M., Characteristics of Superconducting Magnets for Large MHD Generators, 14th Symposium, Engineering Aspects of MHD, Washington DC, 1975
- Hilal, M.A., (Michigan Technological University) and Marston, P.G. and Thome, R.J., (MIT), High Current Conductors for Baseload MHD Superconducting Magnets, presented at Specialists Meeting on Coal Fired MHD Power Generation, Sydney, Australia, November 1981.
- Hilal, M.A., Willig, R.L. and Thome, R.J., Persistent Normal Regions in Large Conductors, IEEE Trans. Mag., MAG-17: 1040, 1981.
- Hilal, M.A., Stability of Large Conductors, Madison, WI: Workshop in Energy Storage, Sponsored by the NSF and Japanese Council on Science and Technology, October 1981.
- Hilal, M.A., Thermal Contact Resistance and Cryogenic Stability of Large Conductors, Advances in Cryogenic Engineering, Vol. 27, 255-263, 1981.
- Hilal, M.A., Persistent Resistive Regions and Cryogenic Stability of Composite Conductors: Effect of Cooling Spacers, Proc. 9th Symposium on Engineering Problems in Fusion Research, Chicago, November 1981.
- Hoenig, M.O., Force-Flow-Cooled Superconductors, Proc. 1978 Superconducting MHD Magnet Design Conf., pp. 381-394, MIT, May 1979.
- Hoenig, M.O., Lue, J.W. and Montgomery, D.B., Force-Cooled Cabled Superconductors, Proc. Sixth International Conf. on Magnet Technology, (MT-6) pp. 1021-1027, Bratislava, Czech., 1977.
- Hoenig, M.O. et al., Cryostability in Force-Cooled Superconducting Cables, Applied Superconductivity Conf., Madison, WI, September 1978, IEEE Trans. Mag., MAG-15, 1979.
- Iwasa, Y., Hoenig, M.O., and Montgomery, D.B., Cryostability of a Small Superconducting Coil Wound with Cabled Hollow Conductor, IEEE Trans. Mag., MAG-13, 1977.
- Iwasa, Y., Leupold, M.J., and Williams, J.E.C., Stabilization of Large Superconducting Magnets: Experimental Models, IEEE Trans. Mag., MAG-13: 20-23, 1977.

- Iwasa, Y., and Apgar, B.A., Transient Heat Transfer to Liquid Helium from Bare Copper Surfaces in a Vertical Orientation - 1: Film Boiling Regime, Cryogenics, 18(5): 267-275, 1978.
- Iwasa, Y., Kensley, R.S., and Williams, J.E.C., Frictional Properties of Metal-Insulator Interfaces, IEEE Trans. Mag., MAG-15: 36, 1979.
- Iwasa, Y., A Critical-Current-Margin Design Criterion for High-Performance Magnet Stability, Cryogenics, 19(12): 705-714, 1979.
- Iwasa, Y., The National Magnet Laboratory's Program to Assess Superconductor Stability, Proc. 1978 Superconducting MHD Magnet Design Conf., pp. 219-238, MIT, May, 1979.
- Iwasa, Y., Maguire, J.F., and Williams, J.E.C., The Effect on Stability of Frictional Decoupling for a Composite Superconductor, Proc. 8th Symp. on Eng. Problems of Fusion Research, pp. 1407-1411, (IEEE Pub. NO. 79CH1441-SNPS), 1979.
- Iwasa, Y., and Sinclair, M.W., Protection of Large Superconducting Magnets: Maximum Permissible Undetected Quench Voltage, Cryogenics, 20 (12): 711-714, 1980.
- Iwasa, Y., CCM Theory and Experimental Results, Proc. 1980 Superconducting MHD Magnet Design Conf., pp. 75-81, MIT, March 1980.
- Iwasa, Y., Maguire, J.F., Sinclair, M.W., Tsukamoto, O., Sliiski, D.J., Thome R.J., and Thompson, J.B., Operation of the MHD Component Test Facility and First Experimental Results, Advances in Cryogenic Engineering, Vol. 27, pp. 29-35, Plenum Press, New York, 1981 (Proc. CEC 1980).
- Iwasa, Y., Conductor Motion in the Superconducting Magnet - A Review, Presented at the Workshop on the Stability of Superconductors in He I and II, Saclay, Nov., 1981.
- Iwasa, Y., Diagnostic Requirements and Mechanical Disturbances in Superconducting Magnets, ICEC9, ICMC, Kobe, May 1982.
- Iwasa, Y. and Leupold, M.J., Critical Current Data of NbTi Conductors at Sub-4.2 K Temperatures and High Fields, Cryogenics, 22(9): 472-476, 1982.
- Iwasa, Y. and Montgomery, D.B., Threshold Currents of Large Cross Section Superconductors, J. Appl. Phys., 42: 1040, 1971.
- Kensley, R.S., and Iwasa, Y., Frictional Properties of Metal-Insulator Surfaces at Cryogenic Temperatures, Cryogenics, 20 (1): 25-36, 1980.
- Kensley, R.S., Maeda, H., and Iwasa, Y., Frictional Disturbances in Superconducting Magnets, IEEE Trans. Mag., MAG-17(1): 1068-1071, 1981.

- Kensley, R.S., Maeda, H., and Iwasa, Y., Transient Step Behavior of Metal/Insulator Pairs at 4.2 K, Cryogenics, 21(8): 479-490, 1981.
- Lanell, P.T., et al., Magnetic Engineering Associates, Inc., Preliminary Design of the AVCO MK VI-II MHD Magnet, prepared for MIT/FBNML, May 1977.
- Leupold, M.J., Weggel, R.J. and Iwasa, Y., Design and Operation of 25.4 and 30.1 T Hybrid Magnet Systems, Proc. Sixth International Conf. on Magnet Technology, (MT-6) pp. 400-405, Bratislava, Czech., 1977.
- Maeda, H., Tsukamoto, O., and Iwasa, Y., The Mechanism of Frictional Motion and its Effects at 4.2 K in Superconducting Magnet Winding Models, Cryogenics, 22: 2871, 1982.
- Maeda, H. and Iwasa, Y., Heat Generation from Epoxy Cracks and Bond Failures, Cryogenics, 22(9):469-472, 1982.
- Maguire, J.F., Iwasa, Y., and Thome, R.J., Techniques for Quality Assurance, Critical-Current, and Stability Measurements for CDIF Conductor, IEEE Trans. Mag., MAG-17(1): 474-477, 1981.
- Markiewicz, W.D. and Stuart, R.W., Intermagnetics General Corp., Guilderland, NY, The Use of Force-Cooled Superconductors in MHD Magnets, report prepared for MIT/FBNML April 1979.
- Marston, P.G., Thome, R.J., Bobrov, E.S., and Dawson, A.M., ETF Magnet Design Alternatives for the National MHD Program, IEEE Trans. Mag., MAG-17(1): 352, 1981.
- Marston, P.G., Iwasa, Y., Thome, R.J., and Hoenig, M.O., The "Football" Test Coil: A Simulated Service Test of Internally-Cooled, Cabled Superconductors, IEEE Trans. Mag., MAG-17(5): 2217-2221, 1981.
- Marston, P.G., Hatch, A.M., Thome, R.J., and Dawson, A.M., Conceptual Design of a Superconducting Magnet for a 200 MWe Engineering Test Facility, International MHD Specialists' Meeting, Sydney, Australia, November 1981.
- Marston, P.G., Hatch, A.M., Thome, R.J., Dawson, A.M., Conceptual Design of 4 T and 6 T Superconducting Magnets for a 200 MWe MHD Engineering Test Facility, 20th Symp. Eng. Asp. MHD, June 1982.
- Marston, P.G., CDIF Conventional Magnet Basic Data, report, MIT/FBNML, March 1977.
- Marston, P.G. et al., Cryogenic and Mechanical Design of Large Six Tesla Dipole Magnet, Advances in Cryogenic Engineering, Vol. 23, pp. 17-27, Plenum Press, N.Y., 1977 (Proc. CEC 1976).
- MEPPSCO, Inc., Fabrication and Testing of a Warm Bore Liner for the Superconducting Magnet at the Component Development and Integration Facility (CDIF), Butte, Montana, report prepared for

MIT/FBNML, 1979.

- MHD Magnet Technology Group, Review of ETF Superconducting Magnet Conceptual Designs, internal report, MIT Francis Bitter National Magnet Laboratory, July 1978.
- Montgomery, A.G. and Hoenig, M.O., Multifilamentary Nb<sub>3</sub>Sn or Multistrand Cable Performance Using Supercritical Helium, Applied Superconductivity Conf., Madison, WI, September 1978, IEEE Trans. Mag., MAG-15, January 1979.
- Montgomery, D.B., Common Problems in MHD and Fusion, Proc. 1980 Superconducting MHD Magnet Design Conf., pp. 10-14, MIT, March 1980.
- Montgomery, D.B., Large Magnets: Where We Are, and Where We Must Go, IEEE Trans. Mag., MAG-17(5): 1541-1550, 1981.
- Montgomery, D.B., Superconducting Magnets: Where Did We Go Wrong? Sixth Symposium on Engineering Problems of Fusion Research, pp. 122-127, San Diego, CA, November 1975.
- Nomura, H., Sinclair, M.W., and Iwasa, Y., Acoustic Emission in a Composite Copper NbTi Conductor, Cryogenics, 20 (5): 283-289, 1980.
- Nomura, H., Sinclair, M.W., and Iwasa, Y., Acoustic Signals and Quench Precursors in a Superconducting Magnet, unpublished.
- Pillsbury, Jr., R.D., NMLMAP - A Two-Dimensional Finite Element Program for Transient or Static, Linear or Nonlinear Magnetic Field Problems, Compumag, Chicago, IL, September 1981.
- Shanfield, S.R., Agatsuma, K., Montgomery, A.G., and Hoenig, M.O., Transient Cooling in Internally-Cooled, Cabled Superconductors (ICCS), IEEE Trans. Mag., MAG-17(5): 2019-2023, 1981.
- Sinclair, M., and Iwasa, Y., Transient Resistive Zones in NbTi Composites, IEEE Trans. Mag., MAG-15: 347-350, 1979.
- Sinclair, M.W., Tsukamoto, O., and Iwasa, Y., Acoustic Emission from Superconducting Magnets and Superconductors, IEEE Trans. Mag., MAG-17(1): 1064-1067, 1981.
- Stekly, Z.J.J. et al., A Large Experimental Superconducting Magnet for MHD Power Generation, AVCO Everett Research Laboratory, internal report AMP210, October 1966.
- Stitt, Susan S. and Reed, F. Everett, Littleton Research and Engineering Corp., LRSADMAG - Saddle Magnet Interactive Computer Modeling, Program for Field Strength Calculations, report prepared under MIT PO ML 68141, May 1979.
- Tarrh, J.M., Failure Mode and Effects Analysis, Proc. 1980 Superconducting MHD Magnet Design Conf.,

pp. 164-167, MIT, March 1980.

- Taylor, W.D., Williams, J.E.C., and Sinclair, M.W., Pool Boiling Liquid Helium Heat Transfer in an MHD Conductor Pack, Advances in Cryogenic Engineering, Vol. 27, pp. 349-356, Plenum Press, New York, 1981 (Proc. CEC 1980).
- Thome, R.J., et al., Impact of High Current Operation on the Cost of Superconducting Magnet System for Large-Scale MHD Applications, Advances in Cryogenic Engineering, Vol. 25, pp. 12-18, 1979, Plenum Press, New York, (Proc. of CEC, 1978).
- Thome, R.J., The Football Experiment - Simulation of ICCS Operation in a Large-Scale Magnet, Proc. 1980 Superconducting MHD Magnet Design Conf., pp. 70-74, MIT, March 1980.
- Thome, R.J., Pillsbury, R.D., Segal, H.R., and Pedersen, B.O., Impact of High-Current Operation on the Cost of Superconducting Magnet Systems for Large-Scale MHD Operation, Advances in Cryogenic Engineering Vol. 25, pp. 12-18, Plenum Press, New York, 1981 (Proc. CEC 1980).
- Thome, R.J., Langton, W.G., and Pillsbury, Jr., R.D., PF Coil Current Sheets for Circular Section Tori to Produce Specified Internal Fields, 9th Symposium, Engineering Aspects of Fusion Research, Chicago, IL, 1982.
- Thome, R.J., Pillsbury, Jr., R.D., and Langton, W.G., Eddy Current Load Estimation for Toroidal Shells as a Result of Plasma Disruption, 9th Symposium, Engineering Aspects of Fusion Research, Chicago, IL, 1981.
- Thome, R.J., and Tarrh, J.M., MHD and Fusion Magnets: Field and Force Design Concepts, John Wiley and Sons, Inc., New York, Spring, 1982.
- Thome, R.J., et al., PF Coil Current Sheets for Circular Section Tori to Produce Specified Internal Fields, 9th Conference on Engineering Problems in Fusion Research, Chicago, November 1981.
- Thome, R.J., et al., Eddy Current Load Estimation for Toroidal Shells as a Result of Plasma Disruptions, 9th Conference on Engineering Problems in Fusion Research, Chicago, 1981.
- Thome, R.J. and Tarrh, J.M., Far Field Interaction with Small Magnetically Permeable Bodies, report, MHD Technology Group, MIT Francis Bitter National Magnet Laboratory, June 1980.
- Thome, R.J., et al., Safety and Protection for Large Scale Superconducting Magnets, FY'81 Report, MIT/FBNML, October 1981.
- Tsukamoto, O., and Iwasa, Y., An Acoustic Emission Technique to Localize Mechanical Disturbances in Superconducting Magnets - A Review, Presented at the Workshop on the Stability of Superconductors in He I and II, Saclay, Nov., 1981.



- Tsukamoto, O., Steinhoff, M.F., and Iwasa, Y., Acoustic Emission Triangulation of Disturbances and Quenches in a Superconductor and a Superconducting Magnet, Appl. Phys. Lett., 40: 538-540, 1982.
- Whipple, T.A., National Bureau of Standards, Boulder, CO, Letter Report, Results of Testing of Two 316L Submerged Arc Welds, April 10, 1980.
- Williams, J.E.C., Superconducting Magnet Development for the MHD Program, 16th Symposium, Engineering Aspects of MHD, 1977.
- Willig, R.L., Magnetic Engineering Associates, Inc., Conductor Analysis for Large Scale Superconducting MHD Magnets, report prepared for MIT/FBNML, April 1979.



## Appendix A

### Lists of Major Subcontractors and Bidders, MHD Magnet Technology Development

Major subcontractors are listed in Appendix A, Sheets 1 - 7, together with contract numbers and starting dates.

Bidders (including unsuccessful bidders) on major RFP's issued by MIT are listed in Appendix A, Sheet 8.

Appendix A Sheet 1  
List of Major Subcontractors  
MHD Magnet Technology Development

Subcontractor	Subject	Contract PO No.	Start Date	End Date	Report
Aluminum Co. of America Air Reduction Co., Inc.	Manufacture Aluminum Stabilized Superconductor	ML59342	Nov 76	—	—
	Manufacture Aluminum Stabilized Superconductor	ML57245	Nov 76	—	—
	Set-up for Conductor Processing	ML60014 ML277475	Feb 77 Feb 82	Aug 78 —	— —
Alexander Kusko, Inc.	Consulting Services on Power Supply CDIF/SM	ML69417	Dec 78	Mar 80	—
	Power Supply Systems for MHD Magnets, Baseline Designs and Costs	ML66020 ML68501	May 78 Nov 78	— Apr 81	MI-31
	Consulting Services on Power Supply, Stanford	ML66641	Jun 78	Mar 79	—
	Consulting Services on Power Supply, ETF Magnet	ML243477	May 81	—	—
American Magnetics Inc.	Vapor-Cooled Leads, 1 Pair, for CDIF/SM	ML277475	—	Feb 82	—
Avco Everett Research Lab, Inc.	Design of Superconducting Magnets for MHD Applications (Large Scale Reference Designs)	E(49-18)2285*	Mar 76	Jun 77	FE-2285-19 (Jun 77)
	ETF Magnet Design and Cost Study	ML66986	Jul 78	Aug 81	Apr 79
Battelle-Columbus Laboratories	Development of Isotension Structure	ML111759	Mar 79	Oct 79	6/30/79

\* Direct ERDA contract

Appendix A Sheet 2

Subcontractor	Subject	Contract PO No.	Start Date	End Date	Report
Belding Corp.	Transportation Study Large MHD Magnets and Components	ML112274	Apr 79	July 79	1979
Bethlehem Corp.	Steel Magnet Frame for CDIF/CM	ML141230	Aug 79	—	—
C-E Power Systems	Manufacturing and Cost Study, ETF Magnet	ML211446	Sept 81	—	yes
Cryogenic Consultants, Inc.	Baseline Design for Cryogenic System for Large MHD Magnets	ML111122	May 79	—	5/31/79
	Technical Support for Stanford and CDIF/SM Magnet and Test Facility at MIT (Cryogenic)	ML61152	May 78	Feb 79	—
	New Type Vapor-Cooled Leads (1 Pair)	ML112168	Mar 79	—	—
CTI Cryogenics, Div. Helix Tech. Corp.	Technical Support for Stanford MHD Magnet (Cryogenic)	ML243094	Jul 81	—	—
	Cryogenic Equipment for CDIF/SM	ML113311	Jun 79	—	—

Appendix A Sheet 3

Subcontractor	Subject	Contract PO No.	Start Date	End Date	Report
Everson Electric Co.	Wind "Football" Test Coil	ML211224	Feb 81		—
	Wind Dummy Racetrack Coil Pancake	ML63100	Oct 77	Oct 78	—
	Wind Coils for AVCO/CM Magnet	ML67128	Jul 78		—
General Dynamics Convair Div.	Winding Model Magnet Design Study	ML63842	Nov 77	Mar 79	yes
	CASK CDP Magnet Design	ML67466	Nov 78	Oct 80	GDC031
	CASK CDP Magnet Cost Estimate	ML68821	Nov 79	Aug 80	PIN78-182
	Design and Manufacture of Stanford MHD Magnet	ML67270	Aug 78		yes
General Electric Co.	Winding Model Magnet Design Study	ML63841	Mar 78	Apr 79	yes
	Design and Manufacture of CDIF/SM	ML65100 null	Feb 78		CDIF-DD-F79-003 (Jun 79)
Hilal, M.A.	Analysis of Performance Characteristics and Stability of MHD Magnet Conductors	ML162725	Jan 80		12/16/80
		ML243769	Apr 81	Jul 81	
Intermagnetics General Inc.	Design and Fabrication of Conductor for MHD Magnet	ML59244	Nov 76	Jun 77	—
	Study of Use of Forced Flow Cooled Conductors in Baseload MHD Magnets	ML62598	Jan 78	Jul 78	yes

Appendix A Sheet 4

Subcontractor	Subject	Contract PO No.	Start Date	End Date	Report
Littleton Research & Engineering Corp.	Review and Development of Computer Programs for Design and Analysis of Magnets	ML68141	Oct 78	Jan 80	—
Magnetic Corporation of America	Design of Superconducting Magnets for MHD Applications (Large- Scale Reference Designs)	E(49-18)2217*	Feb 76	May 77	FE2217-15 (Jun 77)
	Design Study of High Current Conductors	ML59330 ML59243	Dec 76 Nov 76	Jan 78	
	Winding Model Magnet Design Study	ML63843	Nov 77	May 78	MIT 18
	Study of Impact of Operating Current Level (50-100 kA) on Cost and Reliability of Baseload Magnets	ML62834	Oct 77	Aug 78	MIT 14
	Study of Impact of Shell-Type Substructure on Cost and Reliability	ML67437	Aug 78	Nov 78	MIT 27
	Study of Impact of Operating Current Level (10-25 kA) on Cost and Reliability of Baseload Magnets	ML67726	Aug 78	Oct 78	MIT 27
	Make Sample Winding Stack	ML65431	Mar 78	—	—
	Perform Saddle Coil Winding Exercise	ML61499	Jun 77	—	—
	Study of Magnet MHD Protection	ML209345	Jul 80	Sept 81	MIT 40

\* Direct ERDA contract

Appendix A Sheet 5

Subcontractor	Subject	Contract PO No.	Start Date	End Date	Report
Magnetic Corporation of America	Technical Support in Large MHD Magnet Design & Analysis	ML61154	Sept 77	—	—
	Sample Conductors	ML69287	Dec 78	—	—
		ML69288	Dec 78	—	—
	Design & Manufacture of CDIF/CM	ML64100	May 78	—	—
Manlabs Inc.	Materials Testing and Specimen Preparation	ML112461	Mar 79	—	—
		ML164885	May 80	—	
		ML210708	Oct 80	—	
		ML210990	Oct 80	—	
		ML211729	Oct 80	—	
		ML212050	Dec 80	—	
		ML212143	Dec 80	—	
Magnetic Engineering Associates	Design and Analysis of Conventional Magnet for CDIF (CDIF/CM)	ML58922	Oct 76	Apr 77	yes
	Analysis and Design of Conductor for Large Superconducting MHD Magnet	ML62351	Oct 77	Feb 79	FE2295



Appendix A Sheet 6

Subcontractor	Subject	Contract PO No.	Start Date	End Date	Report
Modern Electric Power Products and Service Co. (MEPPSCO Inc.)	Magnet/Channel Packaging Study and Consulting on Interfacing, ETF	ML162789	Jan 80	Aug 81	yes
	Consulting on Interfacing, CDIF/SM Magnet	ML61153	Jun 77	—	—
	Design and Manufacture of Warm Bore Liner for CDIF/SM				—
National Bureau of Standards, Boulder	Computer Analysis of Quench Transients in Forced Flow Conductor for Large MHD Magnets	ML62597	Dec 77	sept 80	yes
	Assessment of Materials Research Needs for SC Baseload Magnets & Their Structural Support Systems	ML112877	May 79	Oct 79	yes
	Development of	ML112876	Sept 78	—	NBSIR80-162
	Superconductor	ML162265		—	NBSIR80-163
	Standards	ML212300	Jan 81	—	NBSIR80-167

Appendix A Sheet 7

Subcontractor	Subject	Contract PO No.	Start Date	End Date	Report
Supercon, Inc.	Study of Design and Fabrication of Composite Conductor for MHD Magnets Cable Conductor for Use in Development Tests	ML59241	Nov 76	Jul 77	—
		ML61046	May 77	—	—
		ML61260	May 77	—	—
		ML64829	Feb 78	—	—
		ML64830	Feb 78	—	—
		ML161547	Oct 79	—	—
		ML161477	Oct 79	—	—
		ML162809	Jan 80	—	—
		ML162841	Jan 80	—	—
Underground Power Corp.	Study of Electrical Insulation of SC Magnet Windings Plan for Experimental Evaluation of Voltage Breakdown in Baseload Magnet Conductor and Insulation Experimental Investigation of Force Distribution Around Rectangular Circuit	ML164862	May 80	—	—
		ML67725	Aug 78	—	yes
		ML113310	May 79	—	yes
		ML113962	Jul 79	Dec 79	yes

Appendix A Sheet 8  
List of Bidders on Major RFP's  
MHD Magnet Technology Development

Subject	Bidders	RFP Date	Award
Studies of Major Load Containment Structures for Superconducting MHD Magnets	CBI	8/31/78	no contract awarded*
	Beechcraft	8/31/78	no contract awarded*
	General Atomics	8/31/78	no contract awarded*
	CE	8/31/78	no contract awarded*
	MCA	8/31/78	no contract awarded*
	Westinghouse	8/31/78	no contract awarded*
	MEA	8/31/78	no contract awarded*
	AVCO	8/31/78	no contract awarded*
	Littleton Research	8/31/78	no contract awarded*
CDIF Superconducting Magnet Design and Construction	GE/IGC	7/26/77	yes
	AVCO/MEA	7/26/77	no
	GD/MCA	7/26/77	no
	Westinghouse	7/26/77	no
Stanford Superconducting Magnet Design and Construction	GD	3/20/78	yes
	GA	3/20/78	no

\* Lack of program funds prevented awarding of any contracts



## Appendix B

### Data Tables, Large Magnet Systems from Other Programs

Data on magnet design characteristics and costs obtained from published reports, conference papers and other sources are given in the attached tables as listed below:

#### Table No.

B1	PSPEC MHD Magnets Designed by GE and AVCO, 1979
B2	USAF MHD Magnet Designed and Built by MCA
B3	Early MHD ETF Magnets Designed by GE/GD, Westinghouse and AVCO, 1977
B4	ECAS MHD Magnet Proposed by AVCO, 1977
B5	AEDC Cryogenic MHD Magnet and AVCO Mk VI Water-Cooled MHD Magnets Designed by MEA and Built by ARO and AVCO, Respectively
B6	12" Model Saddle Coil MHD Magnet Designed and Built by AVCO, 1966
B7	Hydrogen Bubble Chamber Magnets at ANL, BNL, CERN, RHEL and NAL

Design techniques and experience with the above magnets were reviewed by MIT and served as a base for further technology development and reference design work carried out.

Table B1

## Magnet Design Characteristics and Costs

Magnet Identification		PSPEC	PSPEC
Contractor		GE	AVCO
Date of design		1979	1979
MHD power	MWe	460	495
Magnet type	—	circ sad	45° rect sad
Peak on-axis field	T	6.0	6.0
Active length	m	—	16.6
Field at start of active length	T	—	4.8
Field at end of active length	T	—	3.5
Aperture, start of active length	m	2.45 dia	1.92 sq
Aperture, end of active length	m	5.4 dia	3.5 sq
Stored energy	MJ	—	7800
Weight, Conductor	tonnes	865	—
Cold structure	tonnes	6080	—
Cryostat	tonnes	375	—
Total	tonnes	7320	4000
Cost: Conductor	k\$	17300	—
Cold structure	k\$	60800	—
Cryostat	k\$	6000	—
Coil wind & assem	k\$	10000	—
Magnet assem & install	k\$	10000	—
Accessories, proj mgt, etc	k\$	12000	—
Other	k\$	in above	—
Total	k\$	116100	50700
Cost/weight	\$/kg	15.86	12.68
Cost/stored energy	\$/kJ	—	6.50

Table B2

Magnet Design Characteristics and Costs

Magnet Identification		USAF MHD Coil
Contractor		MCA
Date of design		1979
Magnet type	—	circ sad
Peak on-axis field	T	4.0
Active length	m	1.04
Aperture, start of active length	m	0.29 dia
Aperture, end of active length	m	0.53 dia
Vacuum vessel overall length	m	2.62
Vacuum vessel outside diameter	m	1.7
Winding current density, average	$10^7 \text{ A/m}^2$	8.4
Stored energy	MJ	3.1
Weight, Total	tonnes	2.0

Table B3 Sheet 1 of 2

## Magnet Design Characteristics and Costs

Early ETF Designs

## Magnet Identification

Contractor		GE/GD	Westghse	AVCO
Date of design		1977	1977	1977
MHD power	MWe	—	—	45
Magnet type	—	circ sad	circ sad	45° rect sad
Peak on-axis field	T	6.0	6.0	6.0
Active length	m	7.8	9.0	9.0
Field at start of active length	T	4.8	6.0	—
Field at end of active length	T	4.0	5.0	—
Aperture, start of active length	m	0.9	2.6	1.5
Aperture, end of active length	m	1.75	2.6	2.3
Vacuum vessel overall length	m	11.5	13.5	15
Vacuum vessel outside diameter	m	6.6	6.6	10 × 10
Winding build	m	0.8	0.6	—
Design current	kA	9	10	—
Winding current density, average	10 <sup>7</sup> A/m <sup>2</sup>	1.5	2.0	—
Packing factor	—	0.4	0.31	—
Conductor current density	10 <sup>7</sup> A/m <sup>2</sup>	4.0	6.4	—
Total number of turns	—	—	—	—
Ampere turns	10 <sup>6</sup> A	—	35	—
Ampere meters	10 <sup>8</sup> Am	4.4	—	—
Inductance	H	20	68	—
Stored energy	MJ	820	3400	—
Conductor dimensions	cm	1 × 2.4	1.25 × 1.25	—
Heat flux	W/cm <sup>2</sup>	—	—	—
Weight, Conductor	tonnes	97	—	—
Cold structure	tonnes	312	—	—
Cryostat	tonnes	28	—	—
Total	tonnes	437	535	—
Materials: Substructure	—	Al	—	—
Superstructure	—	Al	Al	—
Helium vessel	—	Al	SS	—
Thermal shield	—	Al	Cu	—
Vacuum jacket	—	Al	SS	—



Table B3 Sheet 2 of 2

Early ETF Designs

Magnet Identification			GE/GD	Westghse	AVCO
Contractor					
Cost: Conductor	k\$	4200	730	—	
Cold structure	k\$	4950	938	—	
Cryostat	k\$	—	2802	—	
Coil wind & assem	k\$	10400 <sup>a</sup>	14540	—	
Magnet assem & install	k\$	11030	in above	—	
Accessories, proj mgt, etc	k\$	2050	4800	—	
Other	k\$	1250	in above	—	
Total	k\$	42080	30440	—	
Cost/weight	\$/kg	78.65	56.90	—	
Cost/stored energy	\$/kJ	51.32	8.95	—	

<sup>a</sup> incl. substructure

Table B4

Magnet Design Characteristics and Costs

Magnet Identification		ECAS
Contractor		AVCO
Date of design		1977
MHD power	MWe	≈1000
Magnet type	—	Circ. sad.
Peak on-axis field	T	6.0
Active length	m	25
Aperture, start of active length	m	2.87
Aperture, end of active length	m	6.5
Cost, Total	k\$	(130000)

Table B5

Magnet Design Characteristics and Costs

Magnet Identification		AEDC	AVCO Mk VI
Contractor		MEA/ARO	MEA/AVCO
Date of design		1976	1969
Notes		cryogenic	water-cooled
Magnet type	—	90° rect sad	90° rect sad
Peak on-axis field	T	6.7	3.0
Active length	m	7.1	1.3
Aperture, start of active length	m	0.71 × 0.89	0.36 × 0.23
Aperture, end of active length	m	1.17 × 1.40	0.46 × 0.36
Conductor dimensions	cm	2.5 × 2.5	—
Weight, Conductor	tonnes	83.5	—
Cold structure	tonnes	54.1	—
Materials: Superstructure	—	Al alloy 2219	—
Cost: Design	k\$	529	—
Conductor	k\$	334	—
Cold structure	k\$	327	—
Cryostat	k\$	380	—
Coil wind & assem	k\$	997	—
Magnet assem & install	k\$	587	—
Accessories, proj mgt, etc	k\$	618	—
Other	k\$	635	—
Total	k\$	4417	100

Table B6

## Magnet Design Characteristics and Costs

Magnet Identification		12" Model MHD Coil
Contractor		AVCO
Date of design		1966
Magnet type	—	circ sad
Peak on-axis field	T	4.0
Active length	m	1.5
Field at start of active length	T	3.5
Field at end of active length	T	3.5
Peak field in winding	T	4.6
Aperture, start of active length <sup>a</sup>	m	0.305
Aperture, end of active length <sup>a</sup>	m	0.305
Vacuum vessel overall length	m	4.8
Vacuum vessel outside diameter	m	1.8
Winding build	m	0.25
Design current	kA	0.785
Ampere turns	10 <sup>6</sup> A	3.49
Ampere meters	10 <sup>8</sup> Am	0.16
Inductance	H	15
Stored energy	MJ	4.6
Conductor dimensions	cm	0.1 × 1.27
Heat flux	W/cm <sup>2</sup>	≈1.0
Weight, Conductor	tonnes	2.18
<b>Total<sup>b</sup></b>	tonnes	7.14
Materials: Substructure	—	Al
Superstructure	—	Al
Helium vessel	—	SS
Vacuum jacket	—	SS
<b>Cost: Total</b>	k\$	≈1000
Cost/weight	\$/kg	140
Cost/stored energy	\$/kJ	67

<sup>a</sup> Coil inside diameter (warm bore not provided)

<sup>b</sup> Cold mass only

Table B7

## Design Characteristics and Costs - Hydrogen Bubble Chamber Magnets

Location		ANL(1)	BNL(2)	CERN(3)	RHEL(4)	NAL(5)
Bubble chamber dia		3.7	2.1	3.7	1.5	3.7
Coil inside dia	(m)	4.8	—	—	—	—
Central field	(T)	1.8	3.0	3.5	7.0	3.0
Design current	(kA)	1.9	6.0	5.7	7.5	5.0
Inductance	(H)	40	4	50	11	30
Stored energy	(MJ)	80	72	800	300	375
Average current density	( $10^7$ A/m <sup>2</sup> )	0.7	2.7	1.0	1.8	2.0
Refrigeration at 4.2 K	(W)	400	240	1500	700	400
Superconductor type	—	monolith strip	monolith strip	monolith strip	twisted filament	twisted filament
Iron yoke	—	Yes	No	No(6)	No(6)	No
Weight	(tonnes)	1600	—	200	100	—
Magnet cost	(M\$)	2.4	—	4.6	2.4	—
Completion date		1969	1969	1972	—	1972

(1) Argonne National Laboratory, Argonne, Ill.

(2) Brookhaven National Laboratory, Upton, N.Y.

(3) CERN, Geneva, Switzerland

(4) Rutherford High Energy Laboratory, Berkshire, England

(5) National Accelerator Laboratory, Batavia, Ill.

(6) Iron for flux shielding only



**Appendix C**

**Method of Calculating Magnet Size Index,  $VB^2$**

## Method of Calculating Magnet Size Index, $VB^2$

In investigating costs of MHD magnets, it is important to determine how magnet system cost varies with magnet size. For example, a curve of magnet cost vs. size based on cost data available for smaller magnets can be extrapolated to indicate the expected costs for larger magnets.

The magnet size index,  $VB^2$ , is a convenient measure of magnet size for use in examining cost vs. size effects. The V is a nominal warm bore volume and the B is peak on-axis magnetic field. These terms are defined in Figure C1. (It should be noted that the volume, V, as defined in Figure C1 is not the actual volume of the warm bore, but is only a "characteristic" volume, which is the product of the bore cross-sectional area at the inlet and the active length.)

This index is appropriate because the power generated in an MHD duct is theoretically proportional to the duct volume and to the square of the magnetic field. It is an easy value to calculate because peak on-axis field, active length and bore area at plane of channel inlet are generally readily available, even for preliminary magnet designs.

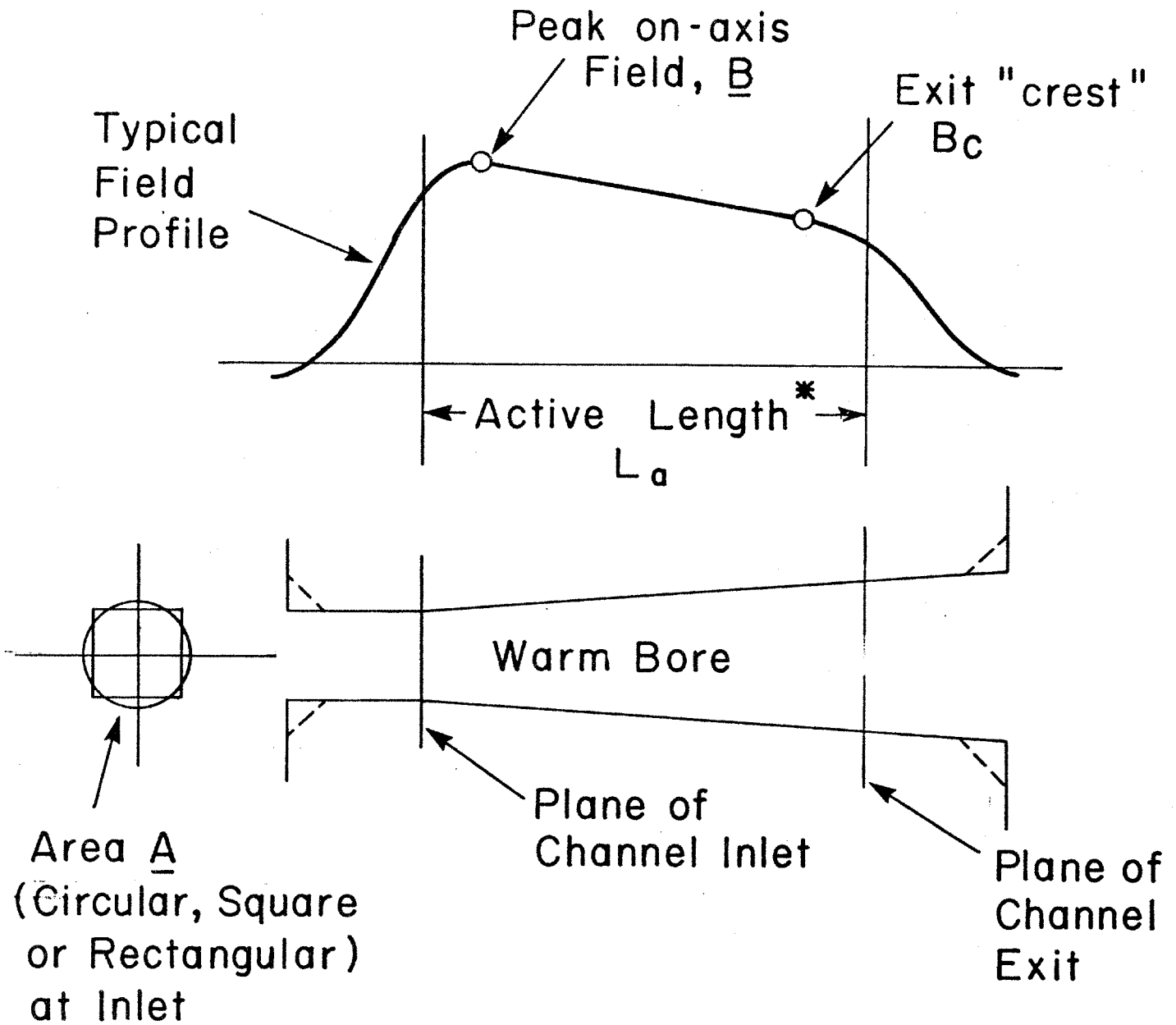
A more rigorous size index would be that given below:

$$\text{Size Index} = \int_{\ell=0}^{\ell=L_a} b^2 a d\ell$$

where  $\ell$  is the distance along axis from channel inlet, a and b are the warm bore area and on-axis field, respectively, at distance  $\ell$  and  $L_a$  is the active length. However, experience has shown that the two methods of determining the index give results that are in reasonably close agreement and the method shown in Figure C1 is more convenient, particularly for preliminary studies where exact field profiles are not determined.

In actual cases, the power generated in particular MHD channel/magnet combinations may not always be proportional to the magnet size indices. Power will vary with the effectiveness of packaging of the channel in the bore (how much of the available bore volume is actually utilized for plasma) and with the specific design of the channel itself. These factors are discussed in Section 4.1.20, Interfacing (Packaging) Study.





Characteristic Volume,  $V = A \times L_a \text{ (m}^3\text{)}$   
 Magnetic Size Index =  $VB^2 \text{ (m}^3 \text{T}^2\text{)}$

\* For purposes of magnet comparison, active length is taken as the distance along the channel axis from the point where inlet field is  $0.8 B$  to where exit field is  $0.8 B_c$ .

Fig. C-1 Method of Calculating Magnet Size Index,  $VB^2$



## **Appendix D**

### **Interim Criteria for Personnel and Equipment Exposure to Magnetic Fields**

**This Appendix consists of MIT/FBNML Specification No. A4442 Rev. D, Issue Date Dec. 11, 1980, Revision Date March 3, 1981.**

**The specification was prepared by MIT under subcontract from NASA LeRC (Grant NAS-G-100) as a part of the DOE-sponsored conceptual design of an MHD Engineering Test Facility 200 MWe Power Plant.**


Note: This "Interim Criteria" is not an approved document. It has been issued for review and comments only.

- Entire Specification Attached
- Revision Sheets Only Attached

SPECIFICATION TITLE SHEET

THIS SHEET IS A RECORD OF EACH ISSUE OR REVISION TO THE SUBJECT SPECIFICATION. EACH TIME THE SPECIFICATION IS CHANGED ONLY THE NEW OR REVISED SHEETS NEED TO BE ISSUED.

THE EXACT SHEETS CHANGED AND THE NATURE OF THE CHANGE SHOULD BE NOTED UNDER REMARKS. THESE REMARKS ARE NOT A PART OF THE SPECIFICATION. THE REVISED SHEETS BECOME PART OF THE ORIGINAL SPECIFICATION AND SHALL BE COMPLIED WITH IN THEIR ENTIRETY.

REVISIONS	REV.	DATE	BY	APP'D	REMARKS
	A	12/16/80	AmH		Sheets 2 and 3 - minor rewording to clarify
	B	2/5/81	AmH		All sheets rewritten. Max. Field for 8 hr exposure changed from 0.03 T to 0.01 T
	C	2/18/81	AmH		Sheets 1-4 revised. Limit for un authorized personnel changed from 0.005 T to 0.0005 T. In table on Sheet 4, 0.03 T changed to 0.05 T
	D	3/3/81	AmH		Rewritten. Section 5 revised; Sec. 6 and Fig. 2-4 deleted
ISSUED		DATE	BY	APP'D	TITLE:
 <p>FRANCIS BITTER NATIONAL MAGNET LABORATORY MASSACHUSETTS INSTITUTE OF TECHNOLOGY</p>		12/11/80	AmH		MHD-ETF 200 MWe POWER PLANT MAGNET SYSTEM
		SH	OF	SPECIFICATION NO.	REV.
		1	7	A4442	D

## 1. Purpose

The purpose of this document is to define interim criteria to serve as guidelines in providing for the protection of personnel and equipment from adverse effects of magnetic (fringe) fields in the ETF.

## 2. Introduction

The (unshielded) superconducting magnet in the ETF will, when charged, produce relatively high DC magnetic fringe fields in the region around it. Specifically, fields between 1 and 2 tesla will exist close to the outer surface of the magnet enclosure and fields of 0.0005 tesla (8.3 times the earth's magnetic field) will exist at a distance of 270 feet from the magnet. The field decreases exponentially as one moves away from the magnet, dropping off approximately as the reciprocal of the distance cubed in regions remote from the magnet.

The use of shielding to reduce fringe fields of large magnets has been investigated. Results indicate that shielding of the entire magnet assembly to reduce fringe fields to very low levels is prohibitively expensive.

With the magnet not shielded, relatively large forces will be produced by the interaction of fringe fields with magnetic material located near the magnet. Objects of such material, not adequately secured, will be accelerated toward the magnet and may become dangerous missiles. The functioning of many types of equipment will be adversely affected by the near fringe fields. This specification establishes interim exposure limits for personnel, guidelines for the location of electrical accessory equipment in relation to the magnet, and procedures for determining the magnetic force interaction between ferromagnetic structures and the magnet.

The most practical and economical means of coping with fringe fields appears to be the separation of personnel and sensitive equipment from the magnet by appropriate distances, as specified later herein. The use of local shielding, for example around a particular item of equipment or a control station, may be appropriate in cases where remote location is impossible or has serious disadvantages.

## 3. Personnel Exposure Limits

In the past, personnel exposure to DC magnetic fields equivalent to the ETF fringe fields has occurred on many occasions with no observed adverse effects. However, there has not yet been sufficient experience and medical investigation to serve as the basis for any final personnel exposure criteria.

The interim standards presented below are based on recommended standards included in a letter from Dr. Edward L. Alpen, University of California, to Dr. Kenneth R. Baker, ERDA, dated July 23, 1979. They are intended to serve as preliminary guidelines during the ETF conceptual design stage and are subject to change as more information and experience are accumulated.

FRANCIS BITTER NATIONAL MAGNET LABORATORY MASSACHUSETTS INSTITUTE OF TECHNOLOGY	SH	OF	SPECIFICATION NO.	REV.
	2	7	A4442	D

The standards are limited to constant DC fields because the rate of change of field during charging and discharging of the magnet is so slow that it is not a significant factor affecting personnel or equipment. Rapidly cycling magnetic fields cannot be produced by the ETF magnet system.

Interim Standards for Personnel Exposure to Magnetic Fields (ETF)

a. Limits for Approved Personnel

	<u>Magnetic Field</u> <u>Not Exceeding</u> (tesla)
Exposure for entire work-days (8 hour work-days, 5 days per week)	0.01
Exposure for 1 hours or less per work-day	0.1
Exposure for 10 minutes or less per work-day	0.5

b. Limits for Others

Unapproved personnel shall be limited to areas where magnetic field is less than 0.0005 tesla (no time limit).

c. Fringe Field Zones

Estimated boundaries of 0.5 T, 0.1 T, 0.01 T and 0.0005 T zones around the installed ETF magnet are shown on Dwg. D4444.

d. Approved Personnel

Prior to the initial charging of the magnet, all facility personnel and others who may be expected to approach the charged magnet closer than the 0.0005 tesla perimeter shall be given a medical examination to determine that they are in good health and do not have any implanted devices (pacemakers or other such devices) that may be adversely affected by magnetic fields. Approval for exposure to fields between 0.0005 tesla and 0.01 tesla and for exposure to higher fields within the limits of Section (a) above, shall be based on that examination, and on reexaminations at appropriate intervals.

e. Use of Tools and Equipment by Personnel

Hand tools and portable equipment for use inside the 0.01 tesla perimeter shall be only such items as are specifically approved by the facility supervisor for such use (non-magnetic and/or determined to be suitable for use in the presence of high fields).

FRANCIS BITTER NATIONAL MAGNET LABORATORY MASSACHUSETTS INSTITUTE OF TECHNOLOGY	SH	OF	SPECIFICATION NO.	REV.
	3	7	A4442	D

## Implementation

The facility in the vicinity of the magnet shall have appropriate caution signs, rope barriers, colored lines and/or other means permanently installed to identify areas where fields above 0.0005 tesla, 0.01 tesla, 0.1 tesla and 0.5 tesla will exist when the magnet is charged.

### 4. Effect on Equipment Function

DC magnetic fields such as will exist around the ETF magnet may have serious adverse effects on the functions of equipment with moving parts, electrical devices, instruments and controls. In most cases, the maximum field in which any particular item will operate without suffering adverse effects can be determined only by test and/or experience. When equipment is purchased, the equipment suppliers should be requested to specify the maximum field in which the equipment can be operated safely and without adverse effect on performance. However, very little experience or test data is available to date and suppliers may be unable to specify environmental field limits.

The table below is intended to provide general guidelines for initial planning or the ETF facility with respect to environmental field limits for equipment.

Tentative Guidelines  
Environmental Magnetic  
Field Limits for Equipment  
Instruments, etc.

	<u>Environmental Field Limits</u> (tesla)	
	<u>Maximum</u> (functional)	<u>Recommended</u> (to allow for personnel access)
LHe storage tank	Note 1	0.05
Liquefier/refrigerator	0.05	0.01
Refrigerator compressor package	0.05	0.01
Liquid nitrogen storage tank	Note 1	0.05
Gaseous helium storage tank	Note 1	Note 2
Cool-down heat exchanger	Note 1	0.05
Warm-up heat exchanger	Note 1	0.05
Mechanical vacuum pump	0.05	0.01
Diffusion pump	Note 1	Note 2
Dump resistor	Note 1	0.05
Circuit breakers	T.B.D.	0.01
Rectifiers and diodes	T.B.D.	0.01
Transformers	T.B.D.	0.01

FRANCIS BITTER NATIONAL MAGNET LABORATORY MASSACHUSETTS INSTITUTE OF TECHNOLOGY	SH	OF	SPECIFICATION NO.	REV.
	4	7	A4442	D

Power supply controls	T.B.D.	T.B.D.
Ammeters	T.B.D.	-
Volt meters	T.B.D.	-
Flow-meters (float type)	T.B.D.	-
Transducers, pressure	T.B.D.	-
Transducers, linear	T.B.D.	-
Thermocouples	No limit	-
Strain Gages	Note 3	-
Recorders	T.B.D.	-

Note 1 No limit on environmental field from functional standpoint. However, forces on ferromagnetic parts must be considered (See Section 5).

Note 2 It is not expected that personnel access will be required when magnet is charged.

Note 3 Strain gage systems may require compensation.

## 5. Magnetic Force Interactions

Magnetic force interactions between the charged magnet and magnetic materials close to the magnet will be quite large. For example, a one cubic foot sphere of steel located beside the magnet and 20 ft. from its centerline would be attracted to the magnet by a force of over 2 short tons. By rough approximation, this force drops off inversely as the fourth power of the distance from the magnet. At 40 ft., the magnetic force on the sphere of steel will be about equal to its weight. (490 lbs.) The estimated maximum attractive force on a mild steel block (expressed as ratio of magnetic force to gravity) versus distance from the ETF magnet center is shown by the curve on Figure 1.

Guidelines for equipment and structure close to the magnet are as follows:

### a. Flow-Train Components

The combustor, nozzle, channel, diffuser and associated piping and structure should be made of non-magnetic material.

### b. Coal, Slag and Seed Systems; Heat Recovery System, Piping, etc.

Components of coal, slag and seed systems, heat recovery system and other items of equipment that are less than 70 ft., from the magnet centerline (i.e. - in zone of 0.1 "g" or greater) and are of ferromagnetic material should be designed to take account of magnetic loading in addition to other types of loading.

### c. Structure

Facility structure and other facility items including overhead crane components, etc. that are less than 70 ft. from the magnet centerline should

FRANCIS BITTER NATIONAL MAGNET LABORATORY MASSACHUSETTS INSTITUTE OF TECHNOLOGY	SH	OF	SPECIFICATION NO.	REV.
	5	7	A4442	D

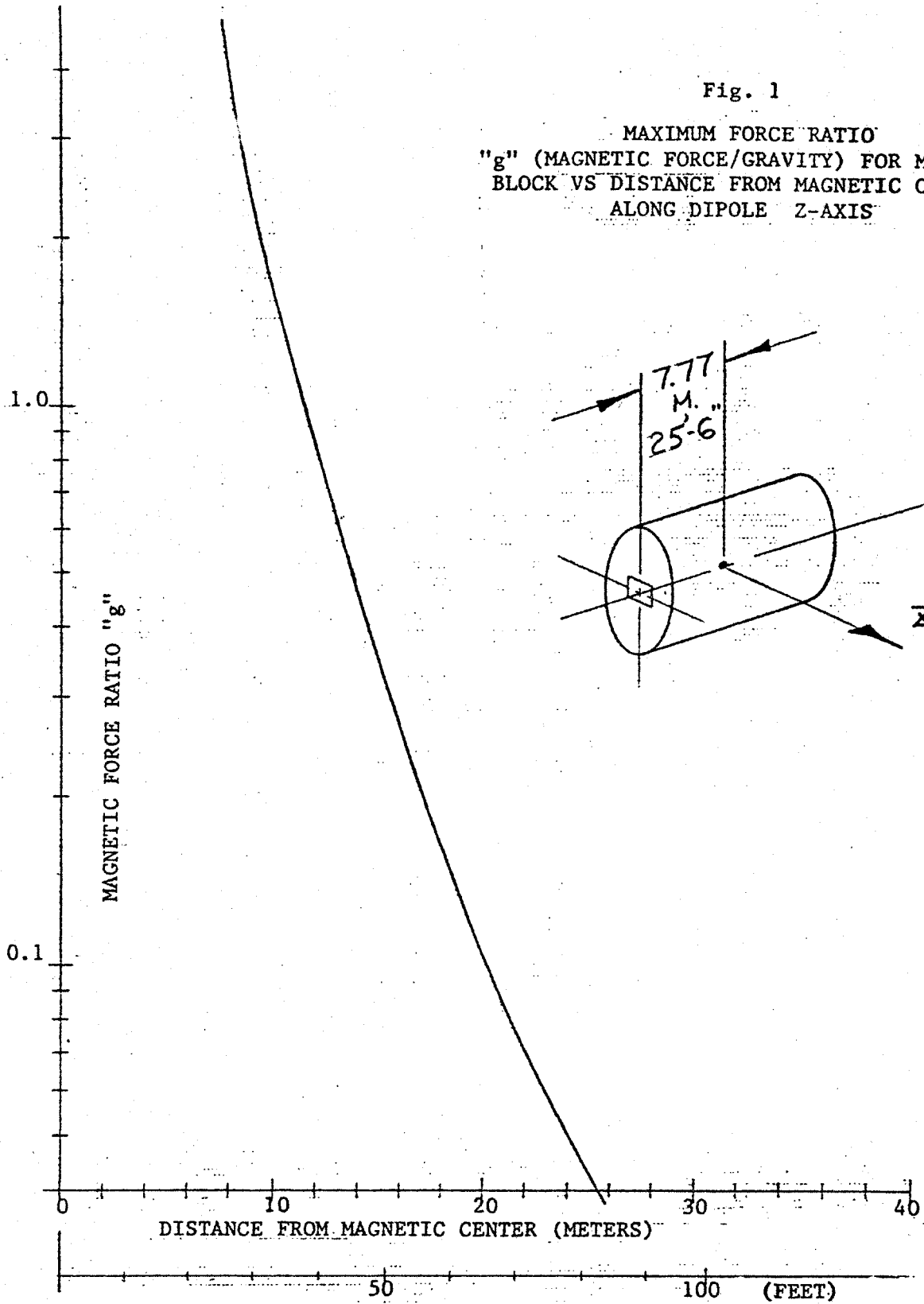


be designed to take account of magnetic loading. Rough estimates of the maximum attractive force on small magnetic objects (< 500 lbs) located well away from the magnet (> 70 feet) may be made using the curve on Figure 1. For larger and/or closer objects, more accurate means for load determination are generally necessary, considering both force and torque interactions and taking into account the magnetization characteristics and geometry of the object. In such cases, the MHD Magnet Group, Francis Bitter National Magnet Laboratory, Massachusetts Institute of Technology should be contacted.

FRANCIS BITTER NATIONAL MAGNET LABORATORY MASSACHUSETTS INSTITUTE OF TECHNOLOGY	SH	OF	SPECIFICATION NO.	REV.
	6	7	A4442	D

Fig. 1

MAXIMUM FORCE RATIO  
 "g" (MAGNETIC FORCE/GRAVITY) FOR MILD STEEL  
 BLOCK VS DISTANCE FROM MAGNETIC CENTER,  
 ALONG DIPOLE Z-AXIS



FRANCIS BITTER NATIONAL MAGNET LABORATORY MASSACHUSETTS INSTITUTE OF TECHNOLOGY	SH	OF	SPECIFICATION NO.	REV.
	7	7	A4442	D